TESIS DE LA UNIVERSIDAD DE ZARAGOZA

2023

60

Cristina Sequero López

Facies evolution of a latest Kimmeridgian shallow carbonate ramp (Higueruelas Fm, north-central Iberian Basin): sedimentary models and controlling factors

Director/es

Aurell Cardona, Marcos
Bádenas Lago, Beatriz

ISSN 2254-7606

Prensas de la Universidad
Universidad Zaragoza

ISSN 2254-7606

Tesis Doctoral

FACIES EVOLUTION OF A LATEST KIMMERIDGIAN SHALLOW CARBONATE RAMP (HIGUERUELAS FM, NORTH-CENTRAL IBERIAN BASIN): SEDIMENTARY MODELS AND CONTROLLING FACTORS

Autor

Cristina Sequero López

Director/es

Aurell Cardona, Marcos
Bádenas Lago, Beatriz

UNIVERSIDAD DE ZARAGOZA
Escuela de Doctorado

Programa de Doctorado en Geología

2021

Universidad Zaragoza

1542

Facies evolution of a latest Kimmeridgian shallow carbonate ramp (Higueruelas Fm, north-central Iberian Basin): sedimentary models and controlling factors

PhD Thesis

Cristina Sequero López

Zaragoza, 2021

FACIES EVOLUTION OF A LATEST KIMMERIDGIAN SHALLOW CARBONATE RAMP (HIGUERUELAS FM, NORTH-CENTRAL IBERIAN BASIN): SEDIMENTARY MODELS AND CONTROLLING FACTORS

Author:

Cristina SEQUERO LÓPEZ

A Thesis submitted to the University of Zaragoza in the fulfilment of the requirements for the degree of Doctor in Geology

University of Zaragoza – 2021

Supervisors:

Dr. Marcos Aurell Cardona (Univ. Zaragoza)

Dr. Beatriz Bádenas Lago (Univ. Zaragoza)

LIST OF SCIENTIFIC PAPERS

This PhD Thesis compiles the results published in five scientific papers, four of them belonging to international journals included in the Scientific Citation Index (SCI): *Facies*, *Marine and Petroleum Geology*, *Sedimentary Geology* and *Cretaceous Research*. The fifth remaining paper has been published in a peer-reviewed book of extended abstracts from the *1st Springer Conference of the Arabian Journal of Geosciences (CAJG-1)*.

Four of these contributions develop a common objective, which is the facies analysis of the uppermost Kimmeridgian (Late Jurassic) shallow carbonate ramp succession of the Higueruelas Formation, which is widely exposed south of the city of Zaragoza, in the north-central part of the Iberian Chain (NE Spain). Additionally, the age calibration of the Higueruelas Formation in the study area has been obtained, being this result part of an updated chronostratigraphic review of the Late Jurassic-Early Cretaceous in the central part of the Iberian Basin published in the journal *Cretaceous Research*. The ultimate contributions of this Thesis are included in two additional chapters: a not-published manuscript, which concerns evaluating the carbon and oxygen stable isotope composition on these shallow-marine carbonate deposits; and a concluding chapter, which incorporates a comparative analysis with several Mesozoic carbonate ramp systems within the Tethyan realm.

The publications included in this PhD Thesis are listed below in chronological order:

Sequero, C., Bádenas, B., Aurell, M., 2018. Facies mosaic in the inner areas of a shallow carbonate ramp (Upper Jurassic, Higueruelas Fm, NE Spain). Facies 64 (9).

JOURNAL IMPACT FACTOR (2018): 1.719 (Q2: 14/47)

Contribution: Main author, conducting the bulk of fieldwork and laboratory analyses, and coordinating the interpretation of the results.

Sequero, C., Bádenas, B., Aurell, M., 2019. Factors controlling oncoid distribution in the inner areas of a late Kimmeridgian carbonate ramp (northeast Spain). In: Boughdiri, M., Bádenas, B., Selden, P., Jaillard, E., Bengtson, P., Granier, B.R.C. (Eds), Paleodiversity and Tectono-Sedimentary Records in the Mediterranean Tethys and Related Eastern Areas. Proceedings of the 1st Arabian Journal of Geosciences (CAJG-1), Tunisia, Springer, pp. 171-174.

Contribution: Main author, conducting the bulk of fieldwork and laboratory analyses, and coordinating the interpretation of the results.

Sequero, C., Aurell, M., Bádenas, B., 2019. Sedimentary evolution of a shallow carbonate ramp (Kimmeridgian, NE Spain): Unravelling controlling factors for facies heterogeneities at reservoir scale. Marine and Petroleum Geology 109, 145-174.

JOURNAL IMPACT FACTOR (2019): 3.79 (Q1: 31/200)

Contribution: Main author, conducting the bulk of fieldwork and laboratory analyses, and coordinating the interpretation of the results.

Aurell, M., Bádenas, B., Canudo, J.I., Castanera, D., García-Penas, A., Gasca, J.M., Martín-Closas, C., Moliner, L., Moreno-Azanza, M., Rosales, I., Santas, L., **Sequero, C.**, Val, J., 2019. Kimmeridgian-Berriasian stratigraphy and sedimentary evolution of the central Iberian Rift System (NE Spain). Cretaceous Research 103, 104153.

JOURNAL IMPACT FACTOR (2019): 1.854 (Q2: 13/47)

Contribution: Contributor along with the main author (M. Aurell), conducting the strontium isotope analyses and biostratigraphic record of larger benthic foraminifera (i.e. lituolids) for the age calibration of the Higueruelas Formation.

Sequero, C., Aurell, M., Bádenas, B., 2020. Oncoid distribution in the shallow domains of a Kimmeridgian carbonate ramp (Late Jurassic, NE Spain). Sedimentary Geology 398, 105585.

JOURNAL IMPACT FACTOR (2019): 2.728 (Q1: 8/47)

Contribution: Main author, conducting the bulk of fieldwork and laboratory analyses, and coordinating the interpretation of the results.

In addition, some of the preliminary results were shared in national and international scientific meetings through poster and oral communications, listed below in chronological order:

Sequero, C., Bádenas, B., Aurell, M., 2018. Facies mosaic distribution of the inner areas of a shallow carbonate ramp (Upper Jurassic, Higueruelas Fm, NE Spain). 33rd IAS International Meeting of Sedimentology (Toulouse, France). Poster contribution.

Sequero, C., Bádenas, B., Aurell, M., 2018. Distribución de facies en mosaico en las zonas internas de una rampa carbonatada somera (Jurásico Superior, Fm. Higueruelas, NE de España). V Jornadas del Instituto Universitario de Investigación en Ciencias Ambientales de Aragón, IUCA (Zaragoza, Spain). Poster contribution.

Sequero, C., Bádenas, B., Aurell, M., 2018. Factors controlling oncoid distribution in the inner areas of a late Kimmeridgian carbonate ramp (northeast Spain). 1st Springer Conference of the Arabian Journal of Geosciences, CAJG-1 (Hammamet, Tunisia). Poster contribution.

Sequero, C., Val, J., Aurell, M., Bádenas, B., Rosales, I., 2018. The Kimmeridgian-Tithonian boundary in the Central Iberian Basin (Spain): new stratigraphic information. JK2018: International Meeting around the Jurassic-Cretaceous Boundary (Geneva, Switzerland). Poster contribution.

Sequero, C., Aurell, M., Bádenas, B., 2019. Sedimentary evolution in a shallow carbonate ramp (Kimmeridgian, NE Spain): factors controlling facies heterogeneities. 34th International Meeting of Sedimentology (Rome, Italy). Oral contribution.

ACKNOWLEDGEMENTS/ AGRADECIMIENTOS

Intentar plasmar en estas palabras la enorme gratitud que siento hacia todas aquellas personas que han hecho posible que haya llegado hasta aquí se hace difícil, pues es tanto el apoyo y cariño que he recibido que las palabras se quedan bastante cortas.

Quiero agradecer en primer lugar la excelente labor por parte de mis directores de tesis, Marcos Aurell y Beatriz Bádenas, que tanto me han enseñado y guiado en esta complicada pero apasionante etapa, y que sin ellos no hubiera sido posible la realización de esta tesis doctoral. Su dedicación, trabajo constante e incansable pasión por la geología son una verdadera inspiración, enseñándome que la perseverancia y el positivismo son las mejores armas frente a cualquier adversidad. Desde que decidí sumergirme de lleno con ellos en el mundo de la Estratigrafía y Sedimentología en la Universidad de Zaragoza, pese a las dificultades que sin duda son inevitables y acompañan a todo investigador, en mí permanece intacta, o incuso ha ido creciendo, mi pasión por esta profesión y mis ganas de seguir aprendiendo y maravillándome con esta ciencia que, desde muy pequeña, despertó en mí una gran curiosidad. Donde quiera que vaya, me llevo conmigo el afecto y la admiración hacia estas dos personas que tanto me han enseñado tanto en lo personal como en lo profesional, y que han sido como mi segunda familia en Zaragoza.

Mi más sincero agradecimiento también a todos aquellos revisores que, con sus sugerencias y comentarios, han contribuido a mejorar la calidad científica de los artículos indexados que incluye esta tesis doctoral por compendio: Michele Morsilli, Maurice Tucker y un revisor anónimo por su revisión del manuscrito enviado a la revista *Facies*; Andreas Strasser y Laura Tomassetti, que revisaron el manuscrito presentado a la revista *Marine and Petroleum Geology*; Alberto Pérez López y un revisor anónimo por su revisión del manuscrito enviado a *Sedimentary Geology*; y finalmente Bruno Granier y de nuevo Andreas Strasser, que revisaron el manuscrito presentado a *Cretaceous Research*. Gracias también a Laura Tomassetti por sus indicaciones y sugerencias en el volumen de la tesis en su labor de revisora externa, para optar a la mención de doctorado internacional.

I am so grateful to Giovanna Della Porta for assisting me during my three-months stay at the Earth Sciences Department *Ardito Desio* at the University of Milan (Italy). It was an enriching and positive experience where I was able to learn a lot from an excellent person, who was always willing to help me and made me feel truly welcomed. I would also like to thank you for your time and effort dedicated to preparing the isotopic analyses for this Thesis, especially in times as complicated as those that have occurred this year. Thanks also to those PhD students that I met during my stay, Mattia and Mario, with whom I shared many great talks and moments. I wish you all the best and I hope to meet you again in the future.

Quiero mostrar mi gratitud a aquellas personas que han contribuido también en la elaboración del material necesario para realizar esta tesis. Gracias al personal del Servicio de preparación de rocas y materiales duros de la Universidad de Zaragoza, Felipe y Manolo, por su enorme paciencia y excelente labor en la preparación de las láminas delgadas, material esencial en esta tesis. Gracias también a Idoia Rosales, investigadora en el IGME en Madrid, por su dedicación e implicación en lo referente a los análisis de isótopos de estroncio, cuyos resultados han sido de gran relevancia en esta investigación.

Agradezco también al Instituto Universitario de Ciencias Ambientales de Aragón (IUCA), del cual he formado parte estos cuatro años, en especial al servicio de prensa y radio, pues me ha permitido aparecer en la prensa escrita, radio y televisión, en un ejercicio muy gratificante de divulgación científica y visibilidad de la ciencia. En este sentido, agradezco también el haber podido formar parte de las actividades de divulgación científica organizadas por el Departamento de Ciencias de la Tierra, como son las jornadas del *Geolodía* o las *Olimpiadas Geológicas*, donde detrás hay un esfuerzo encomiable por parte de aquellas personas que toman las riendas en la preparación de dichas actividades.

Me gustaría hacer también una mención a mis profesores que me impartieron el Grado de Geología en la Universidad de Granada, con los que di mis primeros pasos en este mundillo y a los que les agradezco que me inculcasen las bases necesarias para afrontar futuros retos. También agradecer a los profesores que me impartieron las asignaturas del máster *Geología: Técnicas y Aplicaciones*, siendo mi primer contacto con la geología en Zaragoza.

Qué decir que una travesía como ésta ha requerido también el apoyo de otras personas maravillosas que he tenido el placer de conocer. Por un lado, mi familia geológica en Zaragoza, Alicia, Ángel, Javi, Leticia, Úrbez, Elisa, Manu, Fer, Diego, Álvaro, Ivan, Lope, Nerea, Roi, Marcos, Calvín… con algunos sólo coincidí al inicio de la tesis, otros me han acompañado casi toda la travesía, pero todos habéis dejado huella en mí, especialmente mis habituales compañeros de comidas, Alicia, Ángel y Úrbez, y por supuesto mis compañeros de área con los que he coincidido más tiempo, Javi y Leticia, con los que tantas charlas y cafés he compartido. Gracias Javi también por tu paciencia y tu ayuda en determinados momentos de la tesis, por tantas buenas charlas que hemos tenido y, por supuesto, esos buenos ratos cinéfilos los viernes tarde. No me olvido por supuesto de mi otra familia Zaragozana no geóloga, Viky y Chechu; qué decir, no hubiera sido lo mismo sin vosotros, sin las risas, los momentos y el haber compartido nuestra pasión por el baile. Y mil gracias también a mis amigos de Granada, en especial Mar, Javi, Lucía, Carlos y Diego. La distancia ha hecho que hayan sido pocos los momentos que hemos podido compartir en estos últimos cuatro años, pero siempre os recuerdo con cariño y espero que la vida siempre os depare lo mejor.

Por supuesto, gracias a mi familia, mis padres y mi hermana, que tanto me han aguantado y se han preocupado por mí, apoyándome siempre en todas las decisiones que he tomado. Y qué decir de mi marido…Nacho, no encuentro palabras para expresar lo afortunada que me siento de tenerte. Pese a la enorme distancia que nos ha separado, jamás has dejado de estar a mi lado. Eres mi mayor apoyo, mi mejor amigo y el mejor compañero de vida que se puede tener. Gracias por tu infinita paciencia y por ser una luz en mi vida. 你在哪里，我家在哪里。 我爱你

A todos vosotros, y a los que no alcanzo a nombrar, ¡mil gracias de corazón!

Esta tesis doctoral ha sido financiada por un contrato de Formación de Personal Universitario (FPU) (FPU15/02327) del Ministerio Español de Educación, Cultura y Deporte (MECD), y por los proyectos CGL 2017-85038-P y Grupo E18 (Aragosaurus: Recursos Geológicos y Paleoambientales), siendo éstos subvencionados por el Ministerio Español de Ciencia e Innovación, el Fondo Europeo de Desarrollo Regional y el Gobierno de Aragón. Agradecer también la ayuda económica por parte de la *International Association of Sedimentologists (IAS)*, en su programa de concesión de becas para investigación (*IAS Postgraduate Grant Scheme*).

No podemos elegir los tiempos en los que nos toca vivir, lo único que podemos hacer es decidir qué hacer con el tiempo que se nos ha dado.

J. R. R. Tolkien

Esta tesis se la dedico a mis padres, a mi hermana y a mi marido, pilares básicos en mi vida.

INDEX

ABSTRACT

This PhD Thesis is focused on the characterization of the facies evolution of the Upper Jurassic (uppermost Kimmeridgian) shallow carbonate ramp deposits of the Higueruelas Formation that developed in the north-central part of the Iberian Basin (NE Spain). The main objectives are: 1) to reconstruct accurate sedimentary ramp models, showing the along-strike and down-dip distribution of the different components and facies, and 2) to unravel the factors controlling the facies distribution and sedimentary evolution of the platform. The unit has been studied in a 20 x 30 km area located south of the city of Zaragoza (NE Spain), through extensive field analysis on 35 closely-spaced sedimentary logs, including facies mapping in continuous outcrops, and the recognition of continuous, km-scale well-marked sedimentary discontinuities for log correlation. Additionally, stable isotope analyses have been performed with two purposes: 1) strontium isotope analyses in combination with biostratigraphic data from key marker lituolids, to obtain the age calibration of the Higueruelas Formation in the study area; and 2) carbon and oxygen stable isotope analyses, to evaluate if these data are reflecting palaeoenvironmental conditions or the influence of post-depositional diagenetic processes.

In the study area, the Higueruelas Formation is latest Kimmeridgian (i.e. upper *eudoxus* and *beckeri* zones) in age, and has 40 to 80 m in thickness. The unit is characterized by a wide variety of facies and components, in particular non-skeletal grains. Analysis of the lateral and vertical facies relationships within the nine high-frequency sequences identified in the unit, allowed the reconstruction of the transition from inner-ramp subenvironments (i.e. intertidal, lagoon, backshoal, shoal-sand blanket) to the mid-ramp foreshoal and offshore domains. Two ramp models are proposed for the sequences 1-4 and 5-9, respectively. The *oncolitic-peloidal-oolitic-dominated ramp* (sequences 1 to 4) includes a peloidal intertidal belt, a low-energy oncolitic sheltered lagoon with a mosaic of stromatoporoid carpets, and peloidal-oolitic backshoal, shoal-sand blanket and foreshoal areas with along-strike oncolitic-dominated carbonates and local intertidal patches, as well as washover deposits and stromatoporoid carpets in the backshoal domain. These inner-ramp domains grade offshore into mid-ramp peloidal-bioclastic packstones to mudstones with mosaics of chaetetid-stromatoporoid-coral buildups, surrounded by oncolitic-stromatoporoid facies. The *oolitic-peloidal-dominated ramp* (sequences 5 to 9) is, in turn, characterized by a wide restricted peloidal-bioclastic-oolitic lagoon without stromatoporoid carpets, grading into a backshoal area dominated by peloids and storm-related intraclastic-peloidal deposits. Oncolitic-dominated facies are mostly constrained to some areas of the backshoal and foreshoal domains.

The distribution and abundance of the different types of oncoids present on the *oncolitic-peloidal-oolitic-dominated ramp* is examined in detail. Six types of oncoids are recorded, based on the internal structure of the cortex. Type I oncoids are well rounded and micrite-dominated, and occur in all the subenvironments in low proportions. Type II oncoids, with rounded morphology, are also micrite-dominated but with discontinuous organism-bearing laminae of mostly *Bacinella irregularis*, and are ubiquitous in the oncolitic-dominated shoal-sand blankets. Type III oncoids are irregular to well rounded, and show alternating micritic and organism-bearing laminae of mostly *Bacinella irregularis-Lithocodium aggregatum* association. Two varieties are distinguished: type IIIa oncoids (micritic and organism-bearing laminae of similar thickness) characterize the oncolitic backshoal and foreshoal domains, particularly abundant in the latter; type IIIb oncoids (with thinner micritic laminae) form in the sheltered lagoon. Type IV oncoids are irregular and microbial-dominated, and encompass type IVa oncoids (*Bacinella-Lithocodium* meshworks), which occur abundantly in the lagoon; and less abundant type IVb oncoids (continuous organism-bearing laminae of *Lithocodium*), which are found in the mid-ramp domain.

The combined role of external and internal factors controlled the along-strike and down-dip facies heterogeneities and the sedimentary evolution of the carbonate ramp. In the *oncolitic-peloidal-oolitic -dominated ramp*, low siliciclastic input and low-energy conditions in the inner ramp due to the barrier effect of the shoal-sand blankets, favoured the development of a low-energy sheltered lagoon, where large and irregular microbial-dominated type IIIb and IVa oncoids generated. Alternating higher- and lower-energy conditions in the backshoal and foreshoal domains determined the along-strike lateral variation from peloidal-oolitic to oncolitic-dominated facies, with the predominance of micrite-microbial-dominated type IIIa oncoids particularly in the foreshoal domain. The along-strike lateral variation to oncolitic-dominated facies within the shoal body reveals an irregular depositional topography for this facies belt, where small and well-rounded micrite-dominated type II oncoids occurred in possible depressions/protected areas. Regarding the stromatoporoid-bearing facies, the higher tolerance of stromatoporoids to water energy enabled their colonization from lagoon to backshoal domains with a patchy distribution, in contrast to the chaetetid-stromatoporoid-coral buildups which grew offshore below the fair-weather wave base in specific areas of the proximal middle ramp. The transition to the *oolitic-peloidal-dominated ramp* is determined by the long-term fall in relative sea level occurring at the end of the Jurassic at basin scale, leading to more restricted conditions and an increase of the siliciclastic input in proximal domains, combined with an increment in water energy (i.e. storm-related beds).

The outcrop characterization of the lateral and vertical facies distribution in the Higueruelas Formation presented in this Thesis, helps to better understand and predict the interwell-scale internal facies heterogeneities in carbonate reservoirs of similar age and composition. In particular, the Higueruelas Formation reveals a complex stratigraphic facies architecture, where the dimension of the sedimentary (facies) bodies is highly variable, showing from tens of km to hundreds of m in lateral extent (e.g. shoal-sand blanket or stromatoporoid-rich facies, respectively), but only from few dm to several m in thickness. The observed complex facies architecture is determined by the combined effect of the depositional facies heterogeneities (and their complex controlling factors), and the reduced accommodation space created by both the long-term regional fall in relative sea level and the higher-order sea-level fluctuations (i.e. high-frequency sequences), probably induced by short -eccentricity climate variations. However, carbon and oxygen stable isotope analyses performed in two selected sections did not provide criteria for further palaeoenvironmental interpretations, but in turn highlighted the strong influence of the diagenesis on the isotopic composition, in particular two distinctive diagenetic imprints related to the different post-depositional diagenetic evolution of the unit in each selected sector (i.e. burial vs meteoric alteration), and a possible link between the facies type and the magnitude of diagenetic alteration.

RESUMEN

Esta tesis doctoral se centra en la caracterización de la evolución de facies de los depósitos de rampa carbonatada somera de la Formación Higueruelas, de edad Jurásico Superior (Kimmeridgiense superior), y cuyo depósito tuvo lugar en la zona marginal situada al norte de la Cuenca Ibérica (noreste de España). Los principales objetivos son: 1) la reconstrucción precisa de modelos de rampa, mostrando la distribución de los diferentes componentes y facies tanto en una dirección perpendicular a la línea de pendiente (*along strike*) como pendiente abajo (*down dip*), y 2) la determinación de los factores que han controlado dicha distribución de facies y la evolución sedimentaria de la plataforma. La unidad ha sido estudiada en un área de 20 x 30 km situada al sur de la ciudad de Zaragoza (noreste de España). Para ello se ha realizado el análisis exhaustivo de 35 perfiles sedimentarios cercanos entre sí, incluyendo la cartografía de facies en afloramientos continuos y la identificación de discontinuidades sedimentarias bien marcadas, continuas a escala kilométrica, para la correlación de los perfiles. De manera adicional, se han llevado a cabo análisis de isótopos estables: 1) análisis de isótopos de estroncio en combinación con datos bioestratigráficos de lituólidos clave, para determinar la edad de la Formación Higueruelas en el área de estudio, y 2) isótopos estables de carbono y oxígeno, para evaluar si estos datos isotópicos están reflejando las condiciones paleoambientales o bien la influencia de los procesos diagenéticos post-deposicionales.

En el área de estudio, la Formación Higueruelas se ha datado como Kimmeridgiense superior (*i.e.* la parte superior de la biozona *eudoxus* y la biozona *beckeri*), y presenta entre 40 a 80 m de espesor. Esta unidad se caracteriza por mostrar una gran variedad de facies y componentes, en particular granos no esqueletales. El análisis de las relaciones laterales y verticales de las facies establecidas en las nueve secuencias de alto orden identificadas en la unidad, permitió la reconstrucción de varios subambientes de rampa interna (*i.e.* intermareal, *lagoon*, *backshoal*, *shoal-sand blanket*) que dan paso lateralmente a dominios de rampa media de *foreshoal* y *offshore*. Se han propuesto dos modelos de rampa para las secuencias 1 a 4 y para las secuencias 5 a 9. La *rampa dominada por oncoides, peloides y ooides* (secuencias 1 a 4) incluye un cinturón intermareal dominado por peloides, un *lagoon* protegido de baja energía con predominio de oncoides que desarrolla mosaicos de praderas de estromatopóridos, y zonas de *backshoal*, *shoal-sand blanket* y *foreshoal* dominadas por peloides y ooides. Los dominios de *backshoal* a *foreshoal* dominados por peloides y ooides dan paso lateralmente (*along strike*) a carbonatos dominados por oncoides, así como el desarrollo de parches locales intermareales, y depósitos de *washover* y praderas de estromatopóridos en la zona de *backshoal*. Los dominios de rampa media presentan facies *packstone* a *mudstone* de peloides y bioclastos, y el desarrollo de bioconstrucciones dominadas por chaetétidos, estromatopóridos y corales que dan paso lateralmente a facies de mezcla de oncoides y estromatopóridos, mostrando una distribución en mosaico. En cambio, la *rampa dominada por ooides y peloides* (secuencias 5 a 9) se caracteriza por el desarrollo de un amplio *lagoon* restringido dominado por peloides, ooides y bioclastos, con ausencia de estromatopóridos, que da paso a una zona de *backshoal* dominada por depósitos intraclásticos y peloidales relacionados con tormentas. Las facies oncolíticas quedan reducidas fundamentalmente a algunas zonas de los dominios del *backshoal* y del *foreshoal*.

Se ha examinado en detalle la distribución y abundancia de los diferentes tipos de oncoides presentes en la *rampa dominada por oncoides, peloides y ooides*, donde se han reconocido seis tipos en base a la estructura interna de la corteza. Los oncoides de tipo I son aquellos que presentan un buen redondeamiento y están dominados por micrita, encontrándose en escasa proporción en todos los subambientes. Los oncoides de tipo II, de morfología redondeada, muestran también predominio de micrita, pero en este caso incorporando laminaciones microbiales discontinuas, principalmente de *Bacinella irregularis*, y predominan en los *shoal-sand blankets* oncolíticos. Los oncoides de tipo III muestran una morfología irregular a bien redondeada, y se caracterizan por presentar una alternancia de láminas micríticas y microbiales, principalmente de la asociación *Bacinella irregularis*-

Lithocodium aggregatum. Estos oncoides se subdividen en dos tipos: los oncoides de tipo IIIa (ambas laminaciones presentan el mismo espesor) que caracterizan los dominios de *backshoal* y *foreshoal* oncolíticos, particularmente este último, y los oncoides de tipo IIIb (con laminaciones micríticas de menor espesor) que se forman en el *lagoon* protegido. Los oncoides de tipo IV, de morfología irregular, son aquellos dominados por crecimientos microbiales, y comprenden los de tipo IVa (entramado de *Bacinella-Lithocodium*) que predominan en el *lagoon* y, en menor abundancia, los oncoides de tipo IVb (laminaciones microbiales continuas de *Lithocodium*) que aparecen en la zona de rampa media.

La acción combinada de una serie de factores, tanto externos como internos a la rampa, controlaron las heterogeneidades de las facies de la plataforma (*along strike* y *down dip*), así como su evolución sedimentaria. En la *rampa dominada por oncoides, peloides y ooides*, existe un bajo aporte de terrígenos y unas condiciones de baja energía en la zona interna de dicha rampa, en este último caso debido al efecto barrera de los *shoal-sand blankets*. Estas condiciones favorecieron el desarrollo de un *lagoon* protegido de baja energía, donde se generaron oncoides microbiales de tipo IIIb y IVa de gran tamaño y morfología irregular. La alternancia de condiciones más y menos energéticas en los dominios de *backshoal* y *foreshoal* dieron lugar a cambios laterales (*along strike*) de facies peloidales y oolíticas a facies oncolíticas, donde los oncoides microbiales-micríticos de tipo IIIa predominan particularmente en el dominio de *foreshoal*. En los *shoal-sand blankets*, la variación lateral (*along strike*) de facies peloidales y oolíticas a facies oncolíticas revela una topografía deposicional irregular para este cinturón de facies, donde la existencia de posibles zonas deprimidas o protegidas permitió el desarrollo de los oncoides micríticos de tipo II. En cuanto a las facies que contienen estromatopóridos, la adaptabilidad de dichos organismos a condiciones energéticas variables permitió que éstos pudiesen colonizar desde el dominio del *lagoon* hasta el *backshoal* con una distribución en mosaico, al contrario que las bioconstrucciones dominadas por chaetétidos, estromatopóridos y corales que sólo pudieron desarrollarse en zonas específicas de la rampa media proximal, por debajo del nivel de base del oleaje de buen tiempo. Finalmente, la transición a la *rampa dominada por ooides y peloides* estuvo marcada por una caída relativa prolongada del nivel del mar que ocurrió a escala de cuenca al final del Jurásico, que dio lugar a condiciones más restringidas y a un aumento del aporte siliciclástico en dominios proximales, combinado con un incremento en la energía del agua (*i.e.* capas de tormenta).

La caracterización de la distribución de facies en la lateral y vertical en los afloramientos de la Formación Higueruelas llevada a cabo en esta tesis, ayuda a comprender mejor y a predecir las heterogeneidades internas de facies entre perfiles/sondeos separados varios kilómetros entre sí en reservorios carbonatados de edad y composición similar. En particular, la Formación Higueruelas revela una arquitectura de facies compleja, donde la dimension de los cuerpos sedimentarios (facies) es muy variable: desde decenas de kilómetros hasta centenares de metros de extensión lateral (como es el caso de los *shoal-sand blankets* o las facies ricas en estromatopóridos, respectivamente), pero sólo desde pocos decímetros hasta varios metros de espesor en la vertical. Esta compleja arquitectura sedimentaria es el resultado de las heterogeneidades de facies descritas en el medio de depósito (y los complejos factores que las controlan), y de una reducción del espacio de acomodación originada tanto por el contexto regresivo prolongado a escala de cuenca como por variaciones relativas del nivel del mar de alto orden (*i.e.* secuencias de alto orden), estas últimas probablemente relacionadas con ciclos de excentricidad de corto término. Sin embargo, los análisis de isótopos estables de carbono y oxígeno, realizados en dos secciones seleccionadas, no aportaron criterios para profundizar en las interpretaciones paleoambientales, pero en cambio destacaron la fuerte influencia de la diagénesis en la composición isotópica. En concreto, dichos análisis revelaron dos patrones distintivos en la impronta diagenética, que están en relación con la diferente evolución diagenética post-deposicional de la unidad en cada sector seleccionado (diagénesis meteórica o por enterramiento), así como un posible vínculo entre el tipo de facies y la magnitud de la alteración diagenética.

1. INTEREST, OBJECTIVES AND OUTLINE OF THE THESIS

C H A P T E R

1

INTEREST, OBJECTIVES AND OUTLINE OF THE THESIS

1.1. INTEREST AND OBJECTIVES

This PhD Thesis is focused on the facies analysis of the Oncolitic limestones of the Higueruelas Formation (formally defined by Gómez and Goy, 1979), after the study of a set of well-exposed outcrops located south of the city of Zaragoza (NE Spain).

The studied Higueruelas Fm represents deposition in the shallow areas of a wide carbonate ramp that developed in the north-central part of the Iberian Basin during the latest Kimmeridgian (Late Jurassic). The characterization of the internal facies architecture in ancient shallow carbonate ramp successions is a difficult task which requires a control of the lateral (both along-strike and down-dip directions) and vertical facies relationships as detail as possible, because of the multiple palaeoenvironmental factors controlling the spatial facies distribution and sedimentary evolution of the platform (e.g. Burchette and Wright, 1992; Bádenas and Aurell, 2010; Bádenas et al., 2010; Pomar, 2018). In fact, as reported in other ancient and modern shallow carbonate platforms (e.g. Strasser and Védrine, 2009; Bádenas et al., 2010; Rankey, 2016), as a result of the several controlling factors, complex patterns of depositional subenvironments can occur in specific areas of the carbonate ramp (i.e. facies mosaics), thus resulting in complex internal facies distributions.

In this PhD Thesis, the characterization of the uppermost Kimmeridgian shallow carbonate ramp succession has been performed by investigating the lateral (along strike and down dip) and vertical facies heterogeneities of the Higueruelas Fm outcropping in an area of 20 x 30 km in extent. This characterization has followed two specific aims:

- Reconstructing accurate sedimentary models for these shallow domains of the carbonate ramp, showing the along-strike and down-dip distribution of the different components and facies which constitute the depositional subenvironments, therefore improving the knowledge of the palaeoenvironmental processes controlling carbonate production and accumulation. This reconstruction has been performed at different outcropping scales, considering the variable complexity in the internal facies heterogeneities documented by previous works in specific sectors of the platform (e.g. Ipas, 2003; Ipas et al., 2004). This objective has been carried out through the detailed facies description and interpretation in numerous closely-spaced sedimentary logs, whose correlation allowed the characterization of the lateral and vertical facies relationships.

- ❖ Analysing the different types of oncoids recognized in the Higueruelas Fm, since their wide variability in size, shape and internal structure provides valuable information about the physico-chemical parameters of the depositional subenvironment in which they formed, as reported in previous works (e.g. Dahanayake et al., 1985; Tucker and Wright, 1990; Flügel, 2004; Védrine et al., 2007; Bádenas and Aurell, 2010). This task has involved the evaluation of the petrographic characteristics of the different types of oncoids as well as their distribution across the shallow carbonate ramp, and therefore obtaining a classification following previous nomenclatures (i.e. Dahanayake, 1977).

In addition, this sedimentological characterization of the Higueruelas Fm is complemented by stable isotope analyses with two purposes:

- ❖ Obtaining the age calibration of the Higueruelas Fm in the study area, in order to contribute to provide an updated chronostratigraphic distribution of the sedimentary successions deposited during the Kimmeridgian-Berriasian in the central part of the Iberian Basin. This purpose has been accomplished by the combination of strontium isotope analyses performed in thick calcitic bivalve and brachiopod shells collected from selected intervals, combined with biostratigraphic data from larger benthic foraminifera (i.e. lituolids).

- ❖ Evaluating if the carbon and oxygen stable isotope analyses performed on these shallow-marine carbonates are reflecting palaeoenvironmental conditions or the influence of post-depositional diagenetic processes. Two sections have been selected for this purpose, representing sedimentation in the proximal and relatively distal areas of the carbonate ramp.

The along-strike and down-dip facies distribution revealed in the carbonate ramp models obtained in this Thesis, can be applied to the interpretation of shallow carbonate platforms showing similar components. In particular, this sedimentological analysis has important implications in reservoir characterization, as the Higueruelas Fm is considered as potential analogue of well-known Middle-East hydrocarbon carbonate reservoirs of similar age and composition, as it is the case of the upper Kimmeridgian shallow carbonate ramp deposits of the Arab-D Formation in Saudi Arabia (Al-Awwad and Collins, 2013). Because of the limited knowledge provided by subsurface data, outcrop analogue studies become essential for predictability of the facies architecture at interwell scale, and particularly the lateral (along strike and down dip) and vertical characterization of facies heterogeneities performed in this Thesis, can provide the key guidelines concerning the interpretation of facies distributions and factors controlling the stratigraphic facies architecture in carbonate reservoirs. On the other hand, the results concerning the carbon and oxygen stable isotope composition recorded in the Higueruelas Fm, provide interesting insights for interpreting such isotopic signatures in ancient shallow-marine carbonate successions.

1.2. OUTLINE OF THE THESIS

This PhD Thesis includes 9 chapters. After this brief introduction (Chapter 1), Chapter 2 comprises an overview based on the published information, concerning the sediment production in carbonate platforms, their geometry, and factors controlling carbonate accumulation, accommodation and sequence development. A review of the previous information available for the studied carbonate ramp is also provided, indicating which aspects of this carbonate ramp are already known versus those characteristics that are still to be known, both regarding the facies distribution on the platform and the facies architecture of the unit. Chapter 3 describes the different methodologies used in this work. Chapter 4 explains the geological and stratigraphic context of the studied outcrops, including an updated chronostratigraphic review for the Late Jurassic-Early Cretaceous in central areas of the Iberian Basin presented as a peer-reviewed scientific paper (Aurell et al., 2019b), in which part of the results of this PhD Thesis (i.e. biostratigraphic and strontium isotope data performed on the Higueruelas Fm) have been included.

The main contributions of the Thesis are presented in chapters 5 to 7, being those of the chapters 5 and 6 following the results presented in 4 peer-reviewed scientific papers:

- ❖ Reconstructing the along-strike and down-dip distribution of the different facies types constituting the shallow domains of the carbonate ramp, and so as the factors controlling the facies distribution and the sedimentary evolution of the platform. These results are presented in Chapter 5, based on Sequero et al. (2018) and Sequero et al. (2019b).

- ❖ Characterization of the factors controlling the distribution of the different types of oncoids recorded in the Higueruelas Fm. A revised classification for marine carbonate oncoids of that reported by Dahanayake (1977) is provided in this work, based on their petrographic features and distribution along these shallow domains of the platform. These results are presented in Chapter 6, based on Sequero et al. (2019a) and Sequero et al. (2020).

- ❖ Evaluating if the carbon and oxygen stable isotope analyses performed on these shallow-marine carbonates are reflecting palaeoenvironmental conditions or the influence of post-depositional diagenetic processes. These results are presented in Chapter 7, which constitute a draft of a scientific paper which will be sent for revision and possible publication on a SCI international journal.

Chapter 8 includes a summary of the results obtained in this Thesis, together with a comparative analysis with similar carbonate ramp systems concerning the spatial facies arrangement and stratigraphic architecture, and proposals for the forward stepping on further investigations. Final concluding remarks of Chapter 9 synthesize the key results obtained in this Thesis.

Four Annexes are attached at the end of the manuscript. Annexe 1 contains the database of the sedimentological work, including field pictures of the Higueruelas Fm in each studied sector, detailed sedimentological information of the studied logs, the mapping of facies, units and key surfaces in continuous outcrops, and the location of the collected samples for petrographic descriptions. Annexe 2 illustrates macro-scale polished slabs and microphotographs under binocular microscope in thin sections for all the facies defined in this work. Annexe 3 shows petrographic and cathodoluminescence characteristics of the selected samples for the carbon and oxygen stable isotope analyses. Finally, Annexe 4 includes tables gathering the chemostratigraphic data from the stable isotope analyses.

2. CONCEPTUAL FRAME OF THE STUDIED LATEST KIMMERIDGIAN RAMP

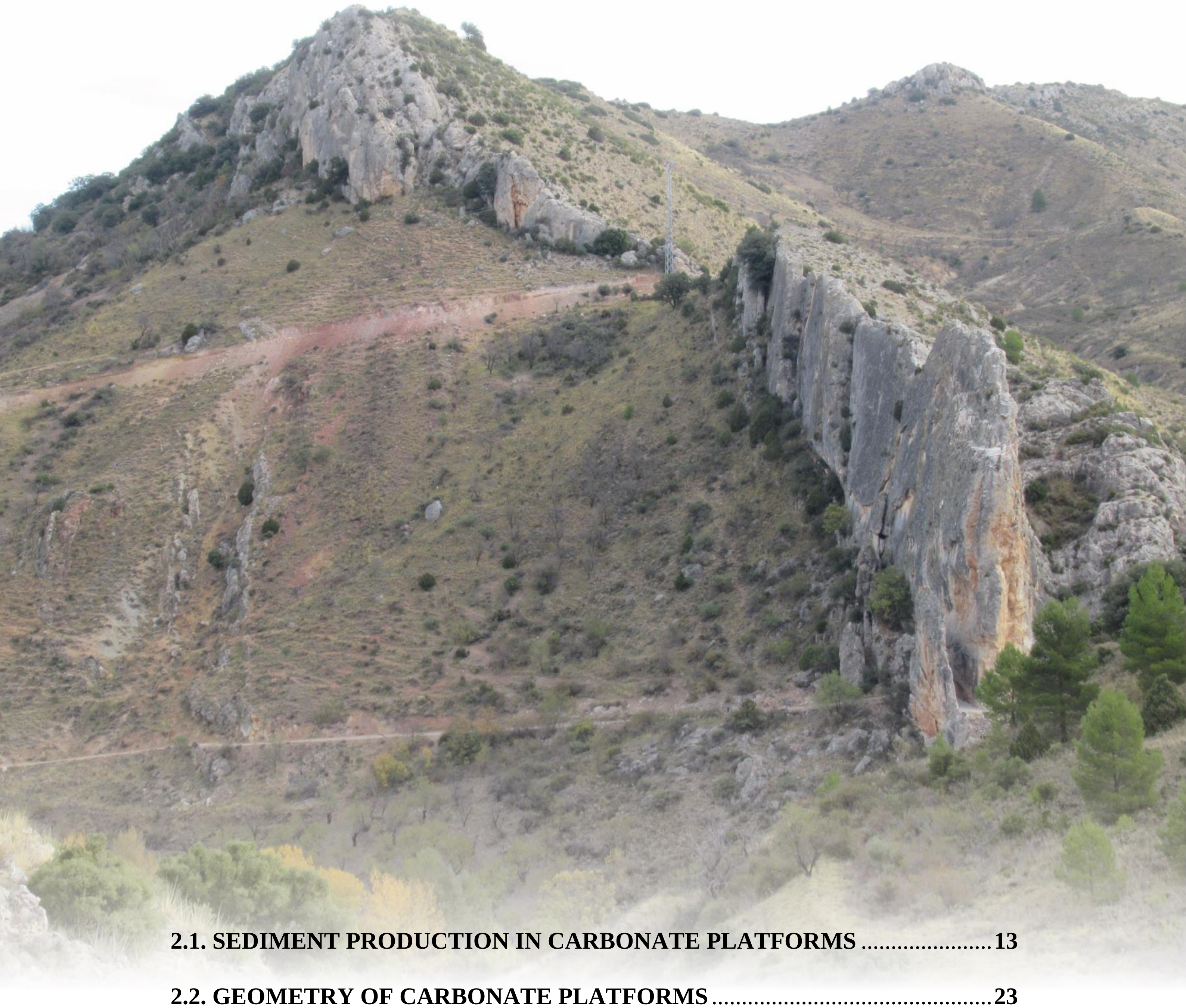

C H A P T E R

2

CONCEPTUAL FRAME OF THE STUDIED LATEST KIMMERIDGIAN RAMP

2.1. SEDIMENT PRODUCTION IN CARBONATE PLATFORMS

2.1.1. Carbonate factories

Understanding the shallow-marine carbonate sedimentation from coastal settings to open shelves has been one of the key targets in Sedimentology through decades, as regards the complex factors involved in the precipitation and generation of carbonate sediments, both carbonate mud, skeletal and non-skeletal grains and bioconstructions. Mechanisms involved in carbonate precipitation are divided into abiotic, biotically induced (mainly microbial precipitates) and biotically controlled (skeletal), in some cases occurring simultaneously (Schlager, 2003). Therefore, organism communities living in carbonate systems play an essential role in carbonate production, so that there is a link between the specific palaeoenvironmental conditions required for the suitable development of biota and carbonate production.

Modern carbonate platform systems such as the Bahamas, South China Sea, eastern Red Sea, South Florida or Western and Southern Australia have been examined by many authors (e.g. Ginsburg, 1956, 1975; Shinn et al., 1969; Logan et al., 1970; James and Bone, 1994; Rankey, 2004, 2016; Rankey and Reeder, 2010; James et al., 2013; Purkis et al., 2015), in order to improve the knowledge about the ecological parameters involved in biotically induced and biotically controlled carbonate sedimentation and their distribution, which can be applied to the geological record by associating the observed sedimentary features (Purkis et al., 2015). However, numerous studies on ancient carbonate settings show that characteristics of carbonate factories have varied through space and time, from the Precambrian to present (e.g. Walsh, 1996; Taylor and Allison, 1998; Kiessling et al., 2000, 2003; Pomar, 2018) (Fig. 2.1). Thus, compiling information of past carbonate platforms from the geological record is essential to comprehend their characteristics and evolution.

Carbonate production depends, among other factors, on the characteristics of the biota community, which strongly influences the type and amount of carbonate production. In addition, the evolution of carbonate-producing organisms throughout the Phanerozoic is another factor that determines the amount and spatial distribution of carbonate productivity, which therefore influences the depositional architecture of carbonate platforms (e.g. predominance of crinoids and bryozoans during the Early Carboniferous, in contrast to the prolific contribution of reefs at Jurassic times; e.g. Chatellier, 1988; Aurell et al., 1995; Brandley and Krause, 1997; Kiessling et al., 2000, 2003). This situation differs from siliciclastic-dominated shelves, where sediment production and accumulation

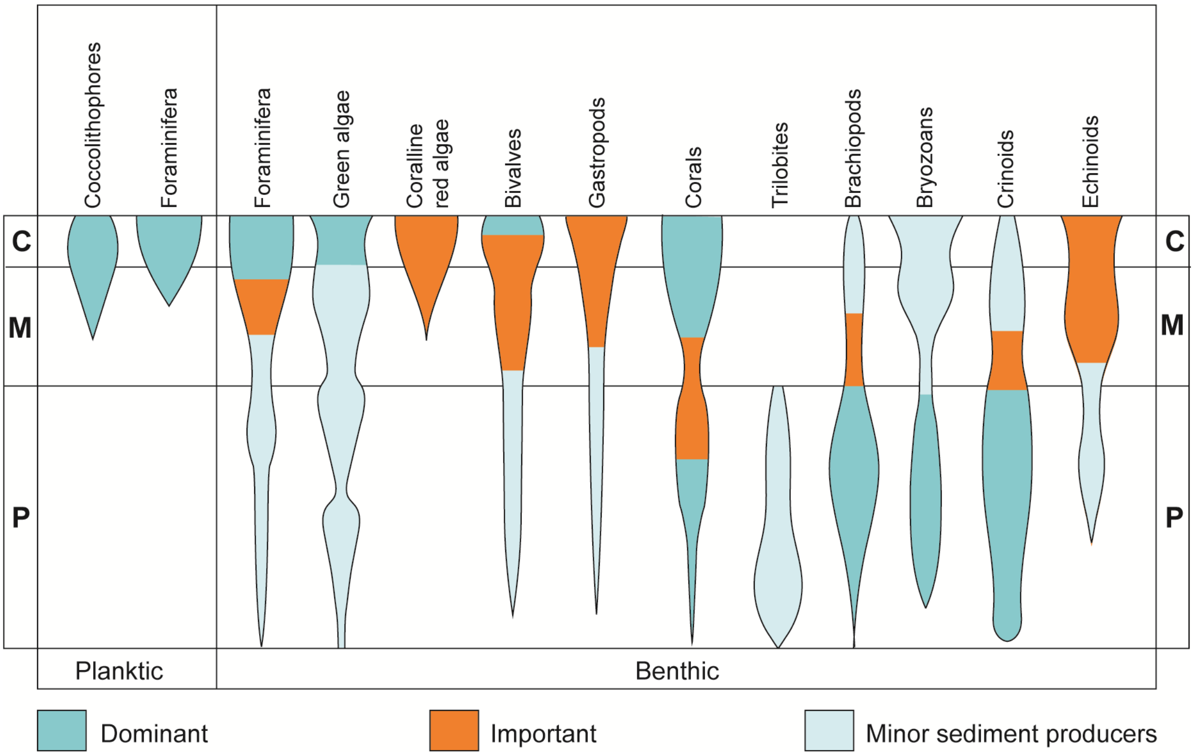

Fig. 2.1. Contribution of calcareous marine organisms to carbonate sedimentation through time; P: Palaeozoic; M: Mesozoic; C: Cenozoic (extracted from Hanken et al., 2015 after Wilkinson, 1979).

have a predominant hydrodynamic control. Furthermore, carbonate sedimentation can occur at variable production rates in localized areas, in contrast to siliciclastic systems where detrital sediment comes from external sources, which in some cases are situated far apart from the depositional sites (Wright and Burgess, 2005).

Carbonate sedimentation in shallow-marine domains is classified in terms of carbonate factories. The carbonate factory is defined as a high-productivity area with a limited lateral extent, which is characterized on the basis of the ecosystem, in-situ sedimentation and early modification of the sediment (e.g. Schlager, 2000; 2003; Wright and Burgess, 2005; Pomar and Hallock, 2008; James and Jones, 2015; Michel et al., 2019). Schlager (2000, 2003) defined three types of benthic carbonate factories (Fig. 2.2a): the tropical factory (T-factory), where precipitation occurs through biota living in the photic zone (both photoautotroph organisms and those living in symbiosis with them); the cool -water factory (C-factory), with heterotrophic carbonate-producing organisms; and the mud-mound factory (M-factory), where carbonate production is biotically induced by microbial activity (e.g. Betzler et al., 1997; Schlager, 2000, 2003; Pomar and Hallock, 2008). Following the Schlager's classification, Reijmer (2014) included a fourth category of carbonate factory, i.e. the cold-water coral reefs (first described by Teichert, 1958), which share characteristics with the T-factory regarding the type of dominant skeletal builder (i.e. scleractinian corals), and with the C-factory in the carbonate production mode.

Optimum carbonate productivity associated to these carbonate factories depends of different factors, according to the type of biota community (Fig. 2.2b). For the T-factory, light and temperature are the main controlling factors, so that high production rates locate in shallow warm waters (e.g. Wilson, 1975; Schlager, 2005), particularly those areas of the photic zone above 20 m deep with normal salinity (mean value of 3.5 ppt), and decrease along the water column until the base of the photic zone (around 100 m in depth). The specific ecological requirements of certain photoautotroph organisms may in turn constrain the range of maximum carbonate precipitation, such as zooxanthellate corals, which are well developed in seawaters warmer than 18ºC (Veron, 1995; Kleypas et al., 1999), or even the extinct stromatoporoids, which better proliferated under moderate

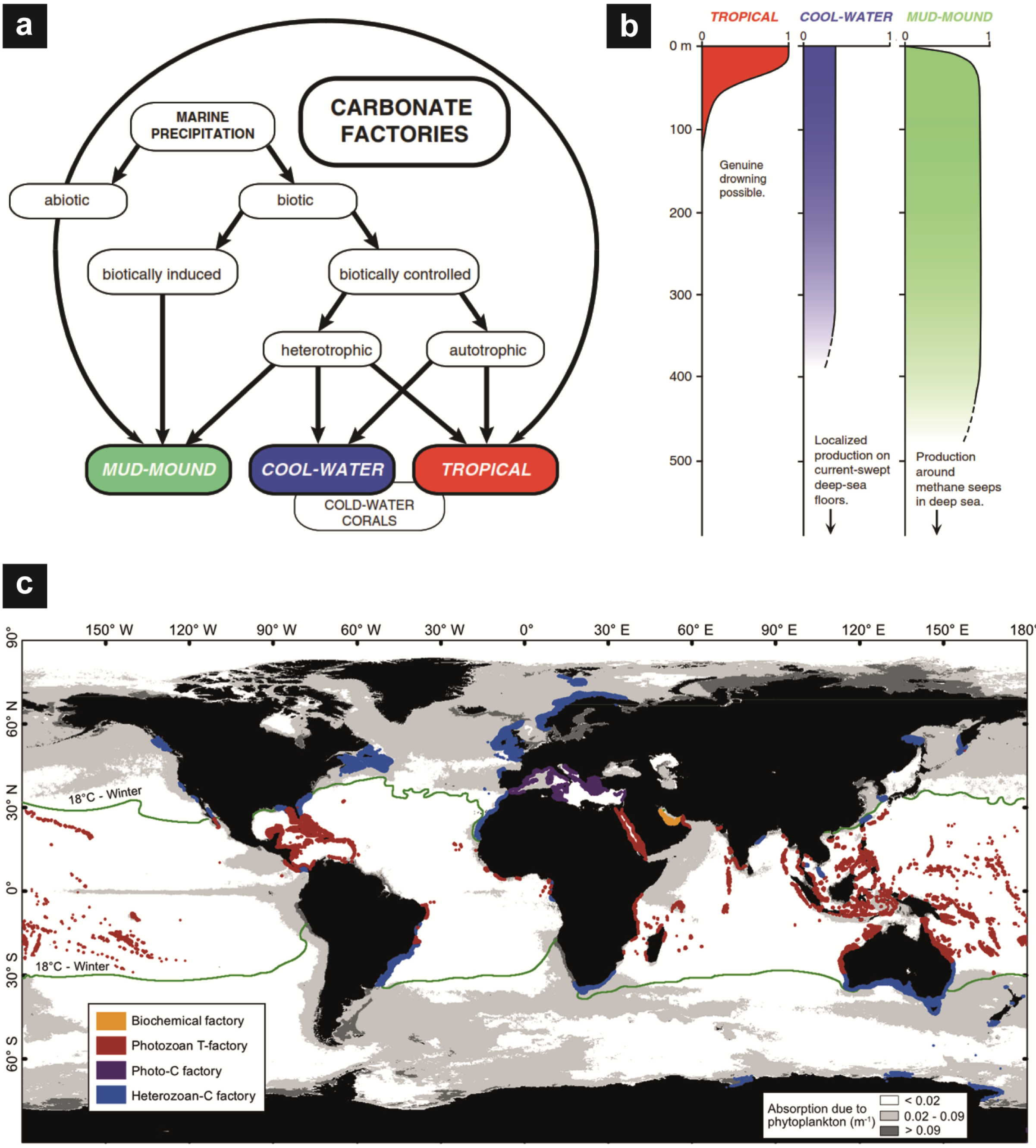

Fig. 2.2. *a) Types of carbonate factories regarding their precipitation modes. b) Production rates for the different types of carbonate factories and depth distribution (a, b: extracted from Reijmer, 2014 after Schlager, 2003). c) Global distribution of modern carbonate factories (extracted from Michel et al., 2019).*

high-energy conditions in detriment of corals (e.g. Leinfelder et al., 2005). At present times, T-factories are situated between 30ºN and 30ºS (Fig. 2.2c), in areas without large terrigenous input. In this regard, the excess of nutrients derives in negative consequences for carbonate productivity, particularly for those organisms which require oligotrophic conditions to thrive (e.g. sponges, corals, green algae), or even originates blooms of planktonic species that may inhibit the light penetration in the photic zone (e.g. Michel et al., 2019). Detrital input in shallow areas can also affect to the substrate characteristics, and so as the capability of benthic communities for colonizing the seafloor.

Carbonate production for the other factories extends hundreds of metres, as their biota communities are largely light-independent (Fig. 2.2b). Low-temperature waters and nutrients availability are the main factors controlling carbonate production of the C-factory (e.g. Reijmer, 2014), and so as for the cold-water corals system, with higher carbonate production rates in water temperatures lower than 10ºC. Accordingly, the C-water factory is situated at higher latitudes than the T-factory, northward 30ºN and southward 30ºS, but also in upwelling areas or in cooler deep waters below the thermocline (Fig. 2.2c). The M-mound factory was well developed during the late Proterozoic and Palaeozoic, for example forming shallow-water stromatolites and mound buildups in deep waters (e.g. Lees and Miller, 1995; Wendt et al., 1997). At present times, microbially induced carbonate precipitation includes for example shallow-water stromatolites and peritidal carbonates (biochemical factory in Michel et al., 2019; Fig. 2.2c).

2.1.2. The Higueruelas Formation: a tropical factory dominated by non-skeletal grains

The latest Kimmeridgian shallow carbonate ramp represented by the Higueruelas Fm in the northern Iberian Basin, located at tropical latitudes (30-35ºN) under greenhouse conditions (Fig. 2.3), and was characterized by a T-factory as indicated by the association of light-dependent fossil organisms. The most common skeletal carbonate grains identified by previous authors (e.g. Aurell and Meléndez, 1987; Aurell, 1990; Ipas et al., 2004) in these shallow-marine deposits are dasyclad green algae, benthic foraminifera (mainly miliolids, lituolids and textulariids), bivalves, brachiopods, gastropods, echinoderms, serpulids, stromatoporoids, chaetetids and corals, as well as several encrusting organisms (mainly *Cayeuxia-Ortonella* and *Bacinella irregularis*).

Analysis of the abundance and distribution of these skeletal components provides information about the characteristics of the depositional subenvironments (Fig. 2.4). Dasyclad green algae are representative of well-oxygenated and protected normal-marine waters, i.e. sheltered lagoons (Flügel, 1977), and commonly appear in association with a high diversity of skeletal grains (e.g. Colombié and Strasser, 2005; Védrine and Strasser, 2009; Bádenas and Aurell, 2010; Al-Awwad and Collins, 2013; Alnazghah et al., 2013). Similar to dasyclad green algae, the occurrence of encrusting organisms such as *Cayeuxia-Ortonella* or *Bacinella irregularis*, which are attributed to the group of cyanobacteria (Leinfelder et al., 1993; Dupraz and Strasser, 1999), thrive under normal-marine waters in moderate- to low-energy subenvironments, both in protected lagoons or in open-marine settings, in some cases as part of reefal microbial crusts (e.g. Dahanayake, 1978; Schmid, 1996; Shiraishi and Kano, 2004; Védrine et al., 2007; Bádenas and Aurell, 2010; Rameil et al., 2010). The record of benthic foraminifera is another key palaeoenvironmental indicator, being miliolids and textulariids a frequent association in inner shallow waters, whereas lituolids show a wider distribution (e.g. Flügel, 1977; Pélissié et al., 1984; Hughes, 2004, 2005; Rameil, 2005; Reolid et al., 2008). In addition, certain specimens of these benthic foraminifera are diagnostic for a particular subenvironment, as explained in Chapter 5. Bivalves, brachiopods, echinoderms, gastropods and

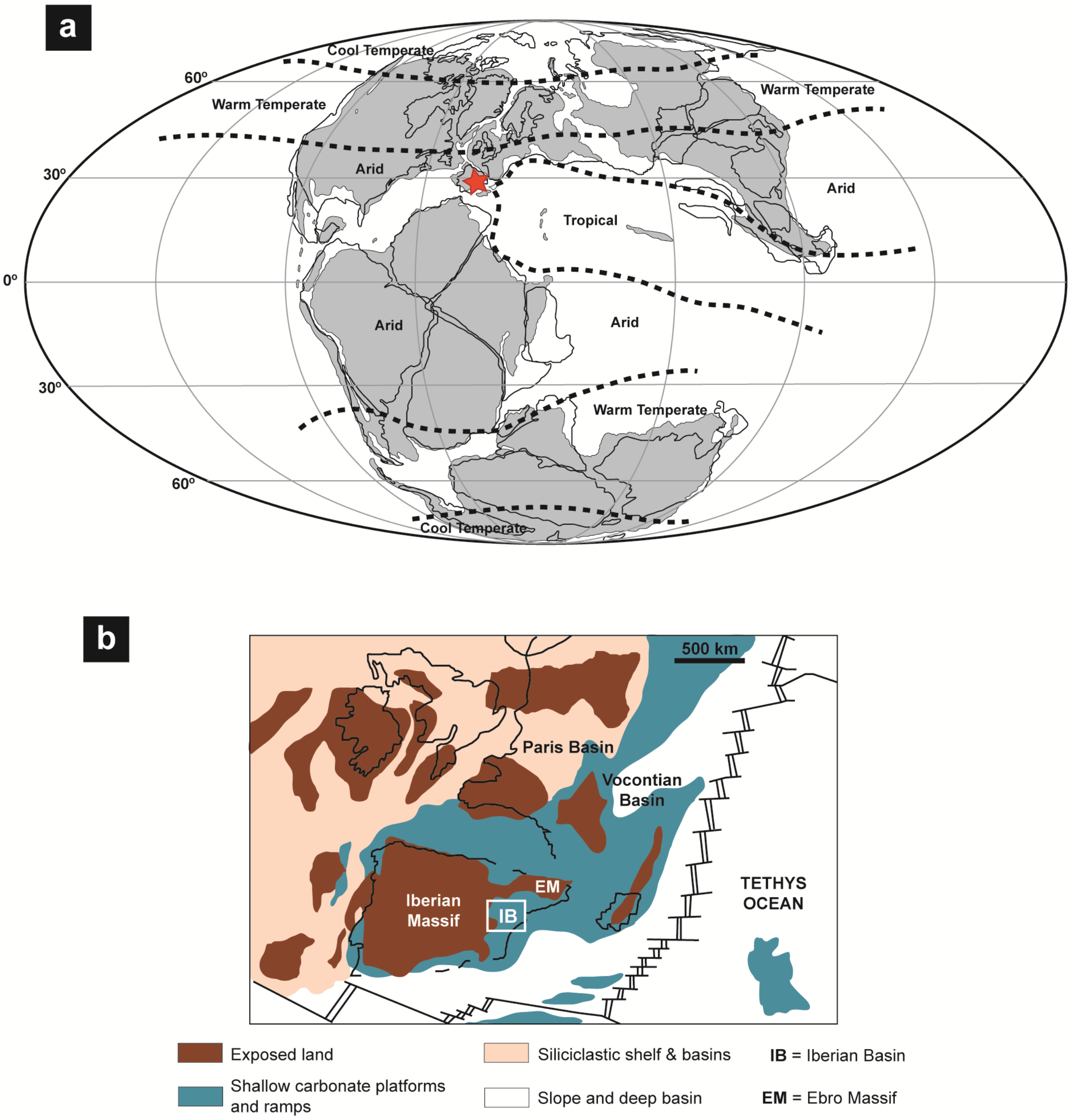

Fig. 2.3. *a) Global palaeogeographic map for the Late Jurassic (150 Ma) with the location of the climatic bands. The red star indicates the location of Iberia (modified from Rees et al., 2000 and Scotese, 2014). b) Palaeogeography of western Tethys during the late Kimmeridgian and location of the Iberian Basin (IB) (modified from Dercourt et al., 1993).*

serpulids have a wide distribution on these shallow domains, although they are generally more abundant in open-marine settings, excepting bivalves, gastropods and serpulids, which can also tolerate more restricted conditions (i.e. restricted lagoons; e.g. James and Dalrymple, 2010; Fig. 2.4).

Regarding the stromatoporoids, chaetetids and corals, these organisms were the predominant reef builders during the Late Jurassic, together with siliceous sponges and microbial communities (e.g. Leinfelder et al., 1994; Schmid, 1996; Leinfelder, 2001; Olivier et al., 2011; Alnazghah et al., 2013; Pomar and Haq, 2016; Tomás et al., 2019). They can be arranged in a variety of structures according to the characteristics of the environment (e.g. wave energy, substrate stability, sedimentation rates), from rigid frameworks (e.g. reef barriers, mounds) to meadows in protected inner platform domains

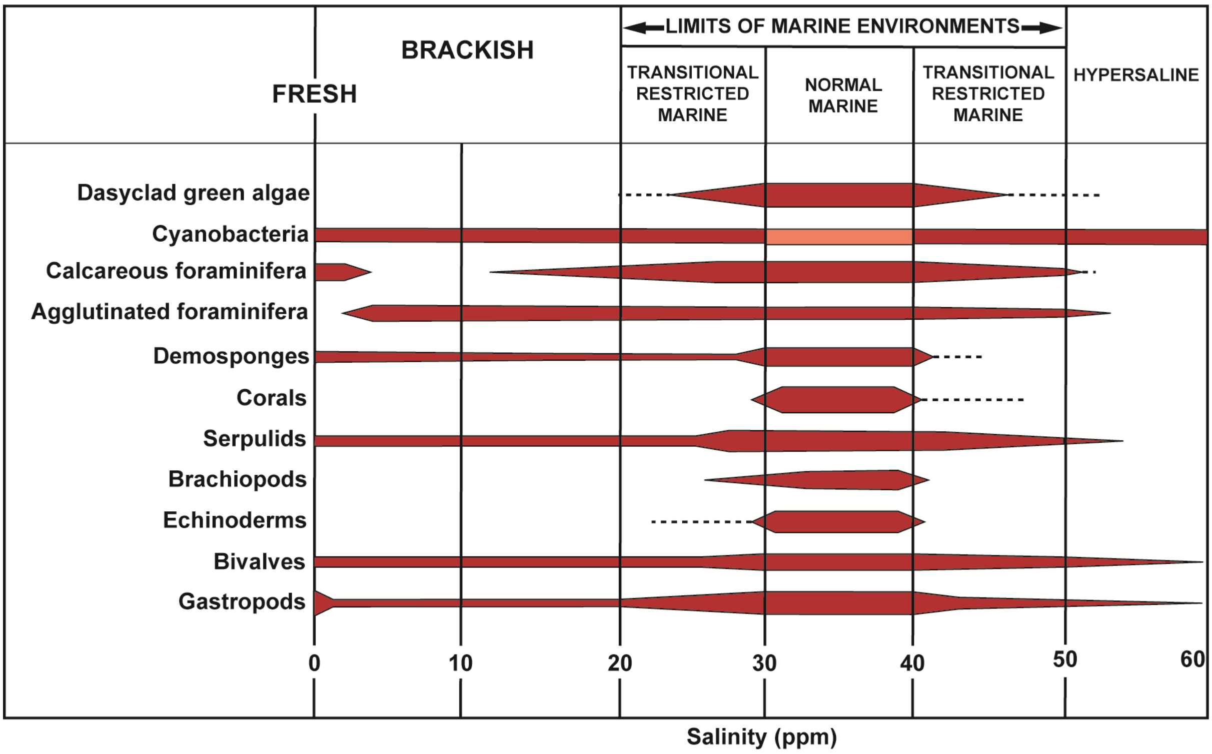

Fig. 2.4. Distribution of some carbonate-producing organisms according to salinity (extracted from James and Dalrymple, 2010). Light-red colour in cyanobacteria refers to distribution of Bacinella irregularis *and* Cayeuxia-Ortonella.

(e.g. Leinfelder, 1993; Kiessling and Flügel, 2002; Leinfelder et al., 2005; Kiessling, 2009; Al-Awwad and Collins, 2013). In the Higueruelas Fm, up to 8 m-high bioconstructions of stromatoporoids, chaetetids and corals have been described in relatively distal areas of the carbonate platform (e.g. Aurell and Meléndez, 1987; Ipas, 2003; Bádenas and Aurell, 2003; Ipas et al., 2004). Corals are the predominant reef-builder component, with microbial crusts and encrusting organisms (mainly cyanobacteria) constituting the rigid frame. However, these reefal structures are scarce within the Higueruelas Fm. Stromatoporoids, chaetetids and corals are also reported in shallower and protected domains of this platform (i.e. lagoon), including stromatoporoids as main component, forming dm- to m-thick bioherms with a limited lateral extent (Aurell and Meléndez, 1987; Ipas, 2003; Ipas et al., 2004; Aurell et al., 2012). The common presence of stromatoporoids in lagoonal settings has been highlighted by several authors (e.g. Flügel, 1974; Turnsek et al., 1981; Leinfelder et al., 2005), being the predominance of stromatoporoids over corals result of their capability to thrive under moderate water-energy and oligotrophic conditions (e.g. Leinfelder et al., 2005).

Despite of the wide variability of carbonate-producing organisms recognized in the Higueruelas Fm, the most significant contribution to carbonate sedimentation corresponds to non-skeletal grains. The most common are oncoids, ooids, peloids and in minor proportion intraclasts and aggregate grains. Analysis of these non-skeletal grains can provide valuable information about palaeoenvironmental conditions. Particularly oncoids and ooids can record a wide spectrum of sizes, shapes and internal structures that chiefly reflect the characteristics of the depositional environment in which they formed (e.g. Peryt, 1981; Strasser, 1986; Flügel, 2004; Shi and Chen, 2006; Bádenas and Aurell, 2010; Olivier et al., 2011).

Oncoids are one of the main non-skeletal components of the Higueruelas Fm, and in fact this type of grain is included in the formal definition of the unit (i.e. Oncolitic limestones of the Higueruelas Fm; Gómez and Goy, 1979). Oncoids are traditionally described as coated grains larger than 2 mm in diameter, constituted by irregular or concentric laminae surrounding a skeletal or non-skeletal nucleus (e.g. Tucker and Wright, 1990; Flügel, 2004; Zhang et al., 2015). Oncoids can have a wide variability in size, shape and internal structure, being these parameters controlled by many different biological and physical factors (e.g. Dahanayake, 1978; Flügel, 2004; Védrine et al., 2007; Olivier et al., 2011). The nomenclature proposed for marine oncoids by Dahanayake (1977) is based on the internal characteristics of the cortex, in particular on the proportion of two types of laminae, i.e. micritic and organism-bearing laminae, the latter constituted by different types of encrusting microorganisms (mainly cyanobacteria). In particular, Dahanayake (1977) recognized four types of oncoids (Fig. 2.5a): spherical to elliptical type I oncoids, smaller in size (< 10 mm in diameter), showing concentric micritic laminae; elliptical type II oncoids (0.5–3 cm in size), constituted by micritic laminae with discontinuous organism-bearing laminae; spherical to subspherical type III oncoids (1–3 cm in size), with alternating micritic and organism-bearing laminae; and irregular type IV oncoids (< 4 cm in size), entirely composed by a microbial meshwork (without lamination), with a simple nucleus (IVS) or integrating several oncoids in the structure (IVC). These types of oncoids are related to a particular hydrodynamic regime, hence being useful in palaeoenvironmental interpretations (Dahanayake, 1978): rounded morphology and well-defined micritic laminae (i.e. type I and II oncoids) are indicative of turbulent waters, whereas lower-energy conditions are suitable for microbial encrustations and the generation of irregular shapes (i.e. type III and IV oncoids). In addition, the analysis of the light-dependent micro-encruster association in the organism-bearing laminae or the microbial meshwork provides information about the palaeoecological conditions (e.g. water transparency, salinity). In the Higueruelas Fm, the four types of oncoids described above have been recognized in previous works (Ipas, 2003; Bádenas and Aurell, 2003; Ipas et al., 2004), ranging from few millimetres to up to 9 cm in diameter. The most common micro-encruster organisms identified are *Bacinella irregularis* and *Lithocodium aggregatum*, also *Thaumatoporella parvovesiculifera* and occasionally *Girvanella*, indicating well-oxygenated, shallow normal-marine waters and oligotrophic conditions (e.g. Leinfelder et al., 1993).

Ooids are spherical to elliptical coated grains generally lower than 2 mm in diameter, composed by concentric micritic and/or sparitic laminae forming on a nucleus of variable nature (Flügel, 1982; Strasser, 1986; Tucker and Wright, 1990). Ooids are characteristic of shallow-water domains, and display different internal compositions related to the characteristics of the depositional environment. For shallow-marine environments, Strasser (1986) proposes a classification of ooids in five types based on the type of cortex, which are indicative of variable energy and salinity conditions (Fig. 2.5b). Micrite-dominated type 1 and 2 ooids, the latter representing a transitional mode to micritic type I oncoids, are constituted by concentric or irregular thin micritic laminae, respectively. Type 1 ooids represent deposition in high-energy domains (i.e. sand bars), whereas type 2 ooids form in low-energy lagoons, both under normal-marine water conditions. The fibrous-radial type 3 and 4 ooids are constituted by thin (type 3) and thicker (type 4) concentric sparitic laminae, and represent deposition in moderate- to relatively high-energy conditions (sand bars to lagoon), under normal to relatively fluctuating salinity. Finally, the fibrous-radial type 5 ooids, composed by a single thick sparitic laminae, represent deposition under calm conditions and fluctuating salinity. In the Higueruelas Fm, mainly type 3 and 4 ooids have been documented in previous works (Ipas, 2003; Ipas et al., 2004). They are less abundant than oncoids and peloids, and record deposition from high-energy shoals (type 3 ooids) to restricted lagoon in inner domains (type 4 ooids).

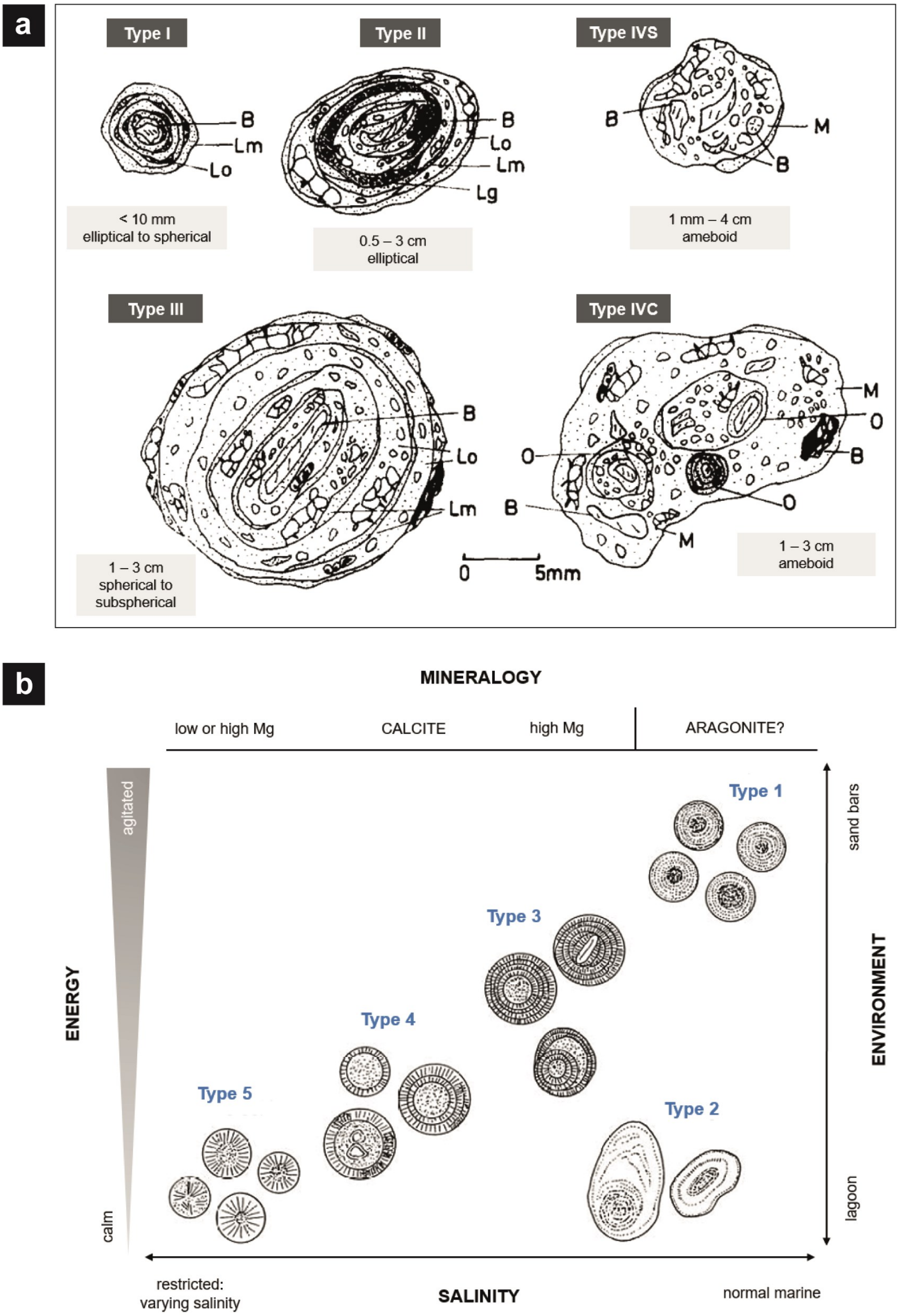

Fig. 2.5. *a) Different types of marine oncoids sensu Dahanayake (1977) classification according to the internal structure of the cortex (i.e. type of laminae and presence of encrusting organisms). Lm: micritic laminae; Lo: organism-bearing laminae; Lg: discontinuous organism-bearing laminae; B: bioclast; M: micrite; O: oncoid. b) Classification of ooids sensu Strasser (1986) nomenclature, including their palaeoenvironmental interpretation (water energy, salinity and depositional environment).*

Peloids are defined as rounded to well-rounded micritic grains less than 600 µm in diameter, without internal structure. The origin of peloids is variable, distinguishing from biogenic peloids (i.e. fecal pellets, microbial peloids), peloids formed by micritization of other components (e.g. bioclasts; also called *bahamite* peloids, locally with relicts of the primary microstructure), or those which derive from reworking of carbonate mud sediments (i.e. lithic peloids) (Fig. 2.6) (Tucker and Wright, 1990; Flügel, 2004). Peloids, together with oncoids, have been described as the most significant non-skeletal grains in the Higueruelas Fm, even constituting in some cases the total rock volume (Ipas, 2003; Ipas et al., 2004). Lithic and microbial peloids are the main types recognized (locally fecal pellets), showing well-rounded shapes and 100 µm in mean diameter (microbial peloids) or variable sizes and shapes (lithic peloids, 0.5–1 mm in size).

Intraclasts consist of fragments of consolidate and/or cemented sediment which has been eroded and redeposited, showing variable shapes and sizes (Folk, 1959). They are commonly found in shallow-marine environments, but can also be transported offshore. The generation of intraclasts can be associated to high-current velocities (i.e. storms), which rework and redistribute cemented sediment fragments from different subenvironments; other processes such as bioturbation, desiccation of carbonate muds in supratidal environments, brecciation and resedimentation of cemented subtidal sediments within the vadose zone, or local sliding (seismic events), can contribute to intraclast generation (e.g. Folk, 1959; Ainardi and Champetier, 1976; Leinfelder, 1987; Whisonant, 1987; Flügel, 2004). **Aggregate grains** are in turn produced by cementation of grains by microbial filaments, encrusting organisms (e.g. foraminifera, calcareous algae, serpulids) and aragonite or Mg-calcite carbonate cements (Winland and Matthews, 1974; Tucker and Wright, 1990; Flügel, 2004), being indicative of low to moderate water-energy conditions. Both intraclasts and aggregate grains have

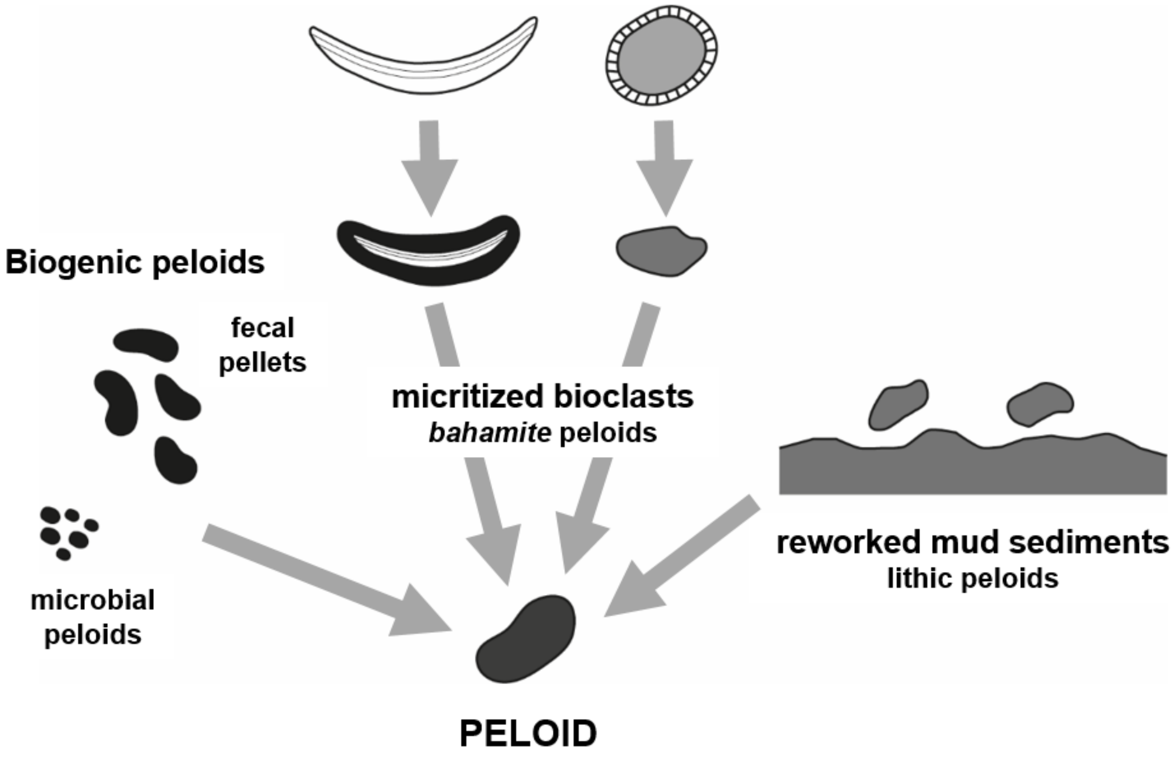

Fig. 2.6. *Different types of peloids according to their origin (modified from Rameil, 2005 after Tucker and Wright, 1990).*

been recognized in the Higueruelas Fm. Intraclasts are a usual component in these shallow-marine deposits, but generally representing a less significant proportion of the total volume of the non-skeletal components recorded. They have been attributed to fragments of mud- to grain-supported sediment (Ipas, 2003). Presence of aggregate grains is occasional.

In this Thesis, the detailed analysis of the types and distribution of both skeletal and non-skeletal carbonate components recorded in the Higueruelas Fm, has provided key information about the lateral and vertical extent of the sedimentary bodies, in particular of the grain-supported sedimentary bodies dominated by non-skeletal grains, and of their palaeoenvironmental factors. This has potential interest for certain subsurface hydrocarbon reservoirs (e.g. the Arab-D Formation in Persian Gulf, or the Smackover Formation in the USA East Gulf; Benson, 1988; Grötsch et al., 2003). These carbonate systems represent shallow platform domains, which record a wide range of carbonate grains, including groups of non-skeletal, grain-supported facies of particular interest due to their high interparticle porosity associated (e.g. Wender et al., 1998; Grötsch et al., 2003; Hughes, 2004; Lindsay et al., 2006). According to similarities in age and composition, the characterization of the dimension of the different types of non-skeletal, grain-supported sedimentary bodies in the shallow-carbonate ramp successions of the Higueruelas Fm, would provide a potential sedimentary analogue for the Upper Jurassic Arab-D Formation, the major hydrocarbon carbonate reservoir in the Middle East (Grötsch et al., 2003; Al-Awwad and Collins, 2013).

2.2. GEOMETRY OF CARBONATE PLATFORMS

2.2.1. Types of carbonate platform profiles

During the Mesozoic, volume of carbonate sedimentation on carbonate platforms was higher than present, due to the larger extension of platforms linked to high sea level in the Mesozoic greenhouse world. Consequently, the contribution of these ancient shallow-marine deposits to the geological record is notorious, representing thick outcropping stratigraphic successions. A wide spectrum of types of carbonate platforms with different depositional profiles occurred in ancient marine environments. Most of these carbonate platform types have analogues in present times, so some of the processes controlling the ancient counterparts can be inferred from the observation of present examples. However, this comparison has to be done with caution, taking into account the differences in biological and geological factors.

According to morphological characteristics (i.e. size, depositional profile or attachment-detachment to landmass), three main types of carbonate platforms are distinguished: carbonate ramps, flat-topped shelves (rimmed or non-rimmed) and isolated platforms (Pomar, 2001a; Fig. 2.7). Regarding the carbonate ramps and flat-topped shelves, one of the key factors controlling the geometry is the hydrodynamic regime governing dispersal of sediments (Fig. 2.8) (Pomar, 2001a; Pomar and Kendall, 2008), which in turn also depends on the characteristics of the carbonate grains

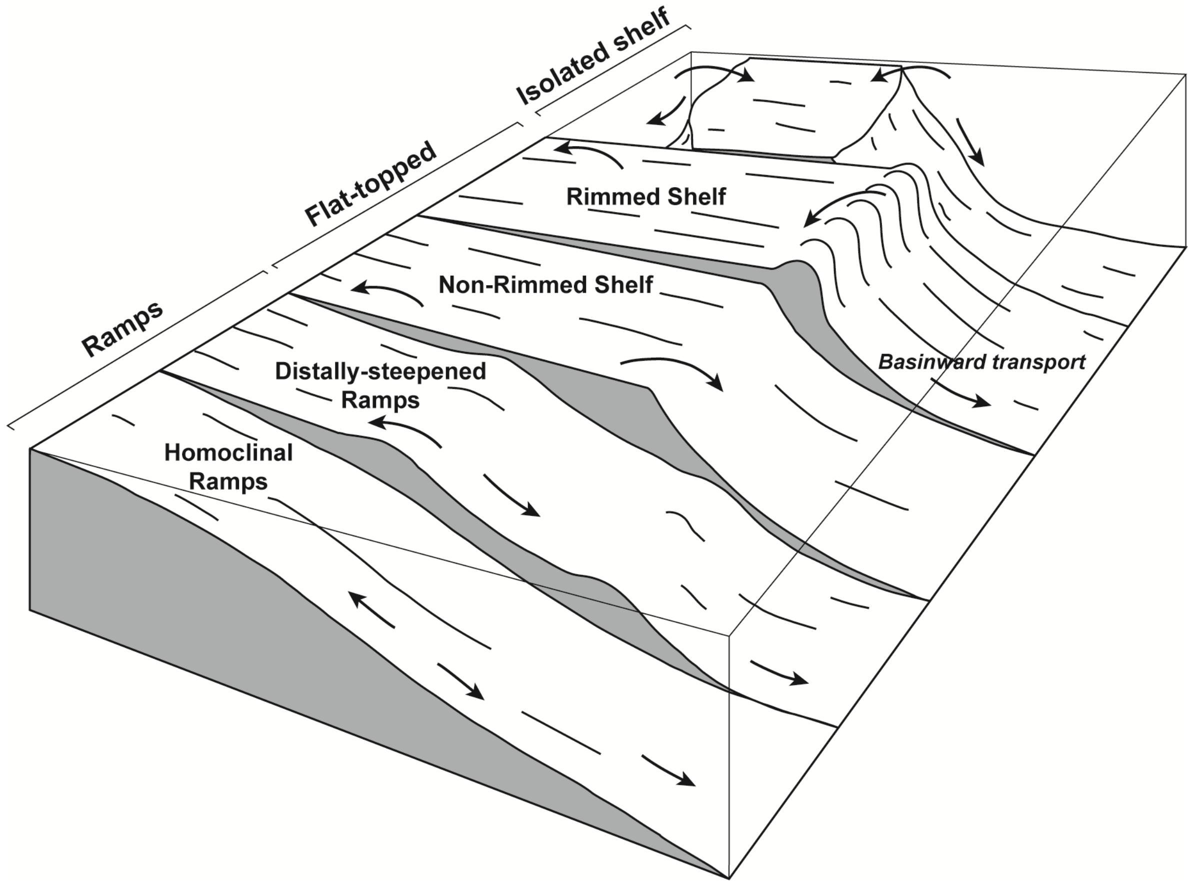

Fig. 2.7. *Types of carbonate platforms (extracted from Val, 2019 after Pomar, 2001a).*

(size, relative density, shape), framework building or syn-depositional cementation (Ginsburg and Lowenstam, 1958; Pomar and Kendall, 2008). Regarding rimmed and isolated shelves, carbonate production rates much higher in shallow-water settings compared to deeper domains are responsible for the characteristic steepened-margin geometry (e.g. Schlager, 1981; Kendall and Schlager, 1981; Bosence et al., 1994; Aurell et al., 1998). On one hand, this significant difference in carbonate production can derive from the enhanced capacity of carbonate-producing organisms to build up the base level (in particular, above the shelf equilibrium profile defined by Swift and Thorne, 1991; Pomar and Kendall, 2008), generating a depositional relief in the shallow-water high-energy zone (e.g. the Llucmajor reef of Mallorca, in the western Mediterranean; Pomar and Ward, 1994, 1999; Bosence et al., 1994; Pomar and Kendall, 2008) (Fig. 2.8). These biogenic frameworks can resist the erosion of waves and storms, whereas uncemented finer-grained sediment is in turn shed off the reef and accumulated in the backreef area or down dip the platform (Li et al., 1997; Pomar, 2001a). On the other hand, the steepened-margin geometry that characterizes rimmed and isolated shelves can also be originated by the formation of sand shoal bodies in the high-energy domain, commonly associated to reefal structures conforming the barrier (e.g. oolitic sand belts from the Late Tithonian-Valanginian carbonate rimmed shelf in NW Sicily; Basilone and Sulli, 2016).

Flat-topped non-rimmed shelves (or open shelves; Fig. 2.8) generate when the carbonate system is dominated by large (gravel-sized) skeletons produced by soft-substrate dwelling metazoans, living in the euphotic high-energy zone, which can remain in-situ on the platform top and/or be accumulated by waves and storms. Hydrodynamic baffling and wave-energy dissipation at the platform margin exerted by these skeletons favour the generation of a flatter platform top, also determining the characteristics of the sediment accumulated in the inner platform (Pomar, 2001a; Pomar and Kendall, 2008). Examples of this type of carbonate platforms are recorded in the Late Cretaceous in the southern Central Pyrenees of Spain, where rudists and corals build a storm-wave resistant rim, or the Middle Miocene in the Mut basin of south-central Turkey, with corals constituting discrete bioherms in association with red algae and microbial crusts (e.g. Bassant, 1999; Bassant et al., 2005; Pomar et al., 2005; Pomar and Kendall, 2008).

Carbonate ramps are originally defined as platforms with a low-angle depositional profile (< 1º), which does not show a slope break from the shallow areas to the oceanic domains (Ahr, 1973) (Fig. 2.8). Ramp geometries can be the result of less strongly differentiated carbonate production rates between the shallower areas and deeper domains (see production curves in Fig. 2.8), or the result of contrasting carbonate production rates and/or intense redistribution. In particular, contrasting carbonate production rates between shallow waters (high productivity) and deep waters, and coeval offshore transport of fine-grained sediment from shallow-water domains, have been highlighted by several authors as responsible for the existence and maintenance of ramp geometry through time (e.g. Aigner, 1985; Einsele, 1985; Burchette and Wright, 1992; Aurell et al., 1995, 1998; Bádenas, 1999; Bádenas and Aurell, 2001b). This is the case of the Late Jurassic carbonate platforms developed in northeastern Iberia (Aurell et al., 1995), some of them dominated by oolitic shoals and coral patch reefs in their shallow domains. Offshore resedimentation by waves and storms on these carbonate ramps was controlled by their windward orientation with respect to the winter winds and hurricanes (Bádenas and Aurell, 2001b, based on circulation model simulations of Marsaglia and Klein, 1983; Price et al., 1995), and is evidenced by the occurrence of storm beds in mid-ramp settings (e.g. Bádenas et al., 2005). In addition, ramp geometries have been also described for cool-water carbonate systems, as a result of the increased carbonate production rate from inshore to offshore areas (e.g. high crinoidal production in deeper domains in Early Carboniferous carbonate systems: Wright and Faulkner, 1990; or bryozoan-dominated communities in the Eocene to Miocene high-energy ramp of southern Australia: James and Bone, 1994).

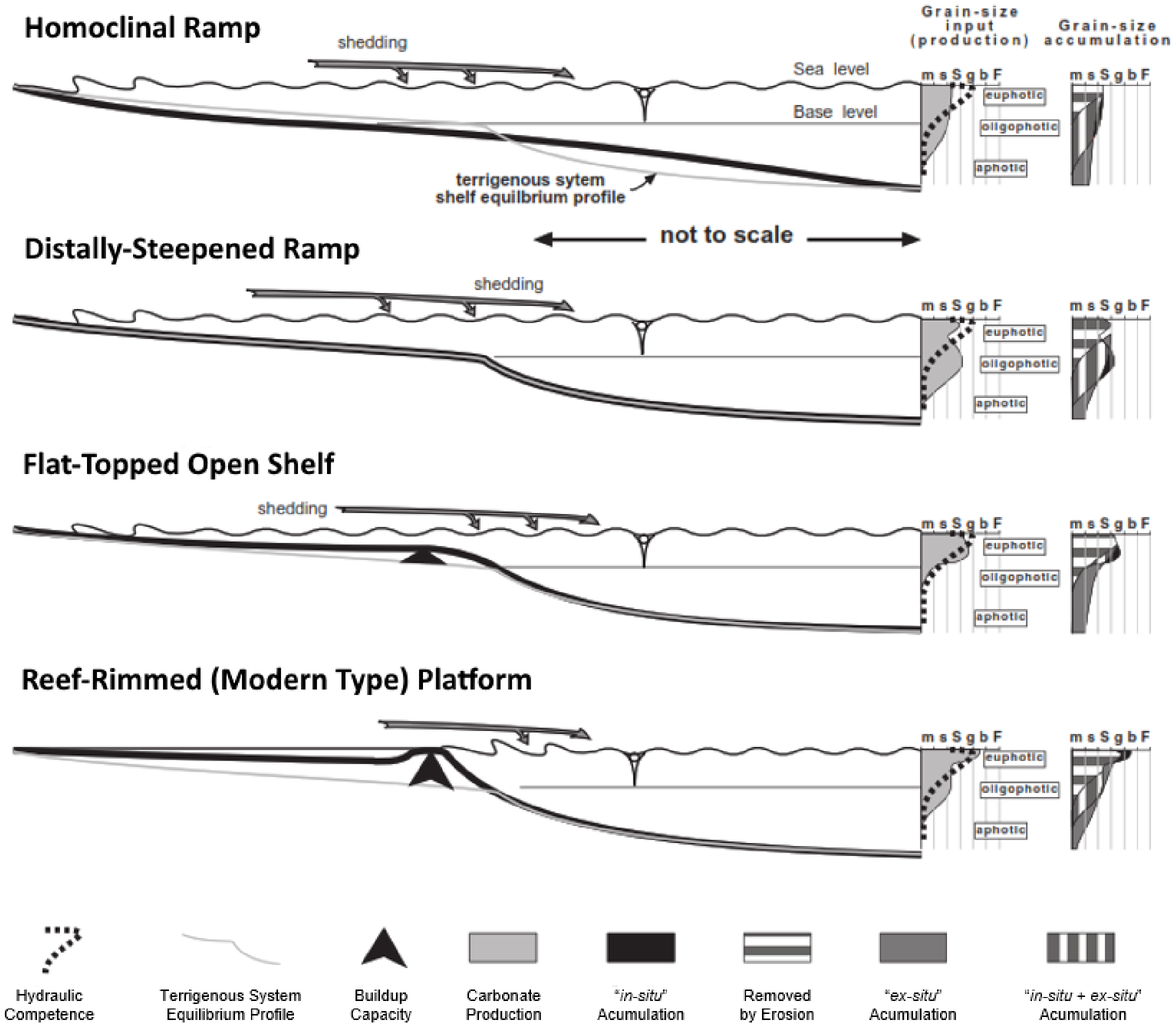

Fig. 2.8. *Depositional profiles for carbonate platforms in response to carbonate production and dispersal modes. Part of the finer-grained carbonate sediment which is produced in shallower areas is removed by erosion and accumulated down dip ("ex-situ" accumulation). Coarser sediment in agitated zones can instead be accumulated in-situ and build a depositional relief above the "theorical" shelf equilibrium profile (i.e. terrigenous system equilibrium profile) (modified from Pomar and Kendall, 2008). m: mud; s: silt; S: sand; g: gravel; b: boulder; F: framestone.*

Several classifications have been proposed for carbonate ramps, including homoclinal and distally -steepened ramps (e.g. Read, 1985; Handford and Loucks, 1993) (Fig. 2.8). In homoclinal ramps, the low-angle depositional profile derives from the homogeneous accumulation of the sediment, which can be the result of resedimentation from high-productivity shallow-water domains (e.g. Jurassic carbonate ramps of northeastern Iberia; Aurell et al., 1998; Bádenas and Aurell, 2001b), or in-situ offshore production and accumulation (e.g. Early Carboniferous carbonate ramps; e.g. Wright and Faulkner, 1990). Distally-steepened ramps are in turn formed when an increased sediment accumulation occurs at certain water depths, due to both in-situ carbonate production and ex-situ accumulation of fine sediment being swept from shallower areas (e.g. Late Miocene carbonate platform in the Balearic Islands of Spain; Pomar, 2001b; Pomar et al., 2002, 2004; Pomar and Kendall, 2008).

Depositional domains on a carbonate ramp are defined according to the influence exerted by wave energy and currents on the seafloor, reflecting a strong hydrodynamic control (similar to wave-dominated siliciclastic systems). In ramps, the hydrodynamic regime controls both carbonate production, redistribution and accumulation. Accordingly, fair-weather wave base (FWWB) and the storm wave base (SWB) delimit three main domains in carbonate ramps (Fig. 2.9; Burchette and Wright, 1992): inner- mid- and outer-ramp domains. The inner ramp corresponds to those areas situated above the FWWB, which represent the more agitated areas (i.e. continuous action of waves and currents), so usually include shoals, sand-blankets or barrier-islands. These high-energy belts can protect lagoons and low-energy coasts (e.g. tidal flats, low-energy beaches, etc). The mid-ramp domain is situated between the FWWB and SWB, and represents the ramp area that only undergoes high-energy conditions during storms, due to the action of storm-related waves and currents. As a result, this domain is characterized by alternating storm-generated deposits (tempestites, some of them with preserved hummocky cross-stratification) and low-energy (fair weather) mud-dominated sediments (e.g. Bádenas and Aurell, 2001b; Pérez-López and Pérez-Valera, 2012). A down-dip gradation of frequency, thickness and grain size of storm-related deposits is usually recorded from proximal to distal mid-ramp domains (e.g. Bádenas and Aurell, 2001b). Finally, the outer-ramp domain, which extents up to the pycnocline, usually records lime mud (commonly pelagic and/or derived from shallow areas) and clay, and occasional distal tempestites during exceptional storms (e.g. Burchette and Wright, 1992; Mohseni and Al-Aasm, 2004).

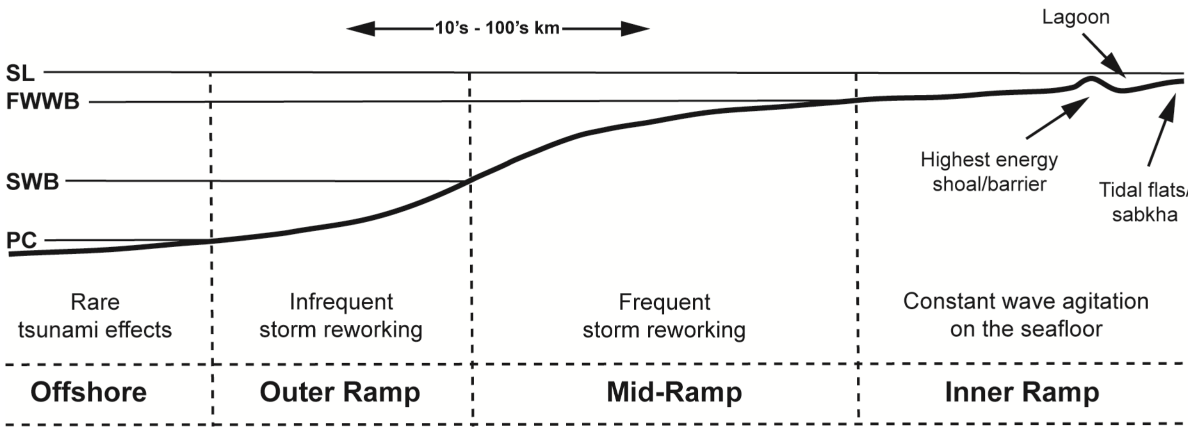

Fig. 2.9. *Depositional domains and sedimentary processes of a carbonate ramp in relation to the position of the hydrodynamic levels (after Burchette and Wright, 1992). SL: sea level; FWWB: fair-weather wave base; SWB: storm wave base; PC: pycnocline.*

2.2.2. The Higueruelas Formation: the shallow domains of a ramp-type platform

In the study area, the Higueruelas Fm represents the shallow-carbonate succession of the latest Kimmeridgian carbonate ramp developed in the north-central part of the Iberian Basin (e.g. Aurell et al., 2003, 2010, 2012). Stratigraphic and sedimentological analyses have been performed in the Higueruelas Fm over the last decades (Gómez, 1979; Aurell and Meléndez, 1986, 1987; Ipas, 2003; Bádenas and Aurell, 2003; Ipas et al., 2004). The palaeoenvironmental reconstruction represented in Ipas (2003) is shown in Fig. 2.10. The inner-ramp areas include a peloidal-oolitic-bioclastic restricted lagoon, oolitic and peloidal bars with bioclasts, and a protected lagoon characterized by peloidal, oncolitic and bioclastic facies with calcareous algae and stromatoporoid-rich patches. In the proximal mid-ramp, a high-energy oncolitic-dominated belt allowed the generation of this protected lagoon. Offshore, intraclastic-peloidal grain-supported facies grade down dip into open-marine mud-supported deposits with the local development of coral-stromatoporoid-microbial buildups.

The previous palaeoenvironmental reconstructions of the latest Kimmeridgian ramp were based on the analysis of a limited number of widely-spaced outcrops of the Higueruelas Fm, with an average separation distance of tens of kilometres. However, due to the fact that shallow-water ramp domains are usually characterized by complex facies heterogeneities, their sedimentological characterization requires a control of the lateral and vertical facies relationships as detailed as possible, in both strike and down-dip directions (e.g. Bádenas and Aurell, 2010; Bádenas et al., 2010). Accordingly, in order to improve the knowledge about the sedimentological characterization of this latest Kimmeridgian shallow carbonate ramp, the stratigraphic and sedimentological study performed in this Thesis has included the detailed analysis of the Higueruelas Fm in numerous closely-spaced logs (mean distance between logs of 5 km) and facies mapping in selected continuous outcrops when possible. This analysis has allowed to further determining both the strike- and down-dip distribution of the different types of components and facies identified in these deposits, and factors controlling this facies distribution and the sedimentary evolution of the platform.

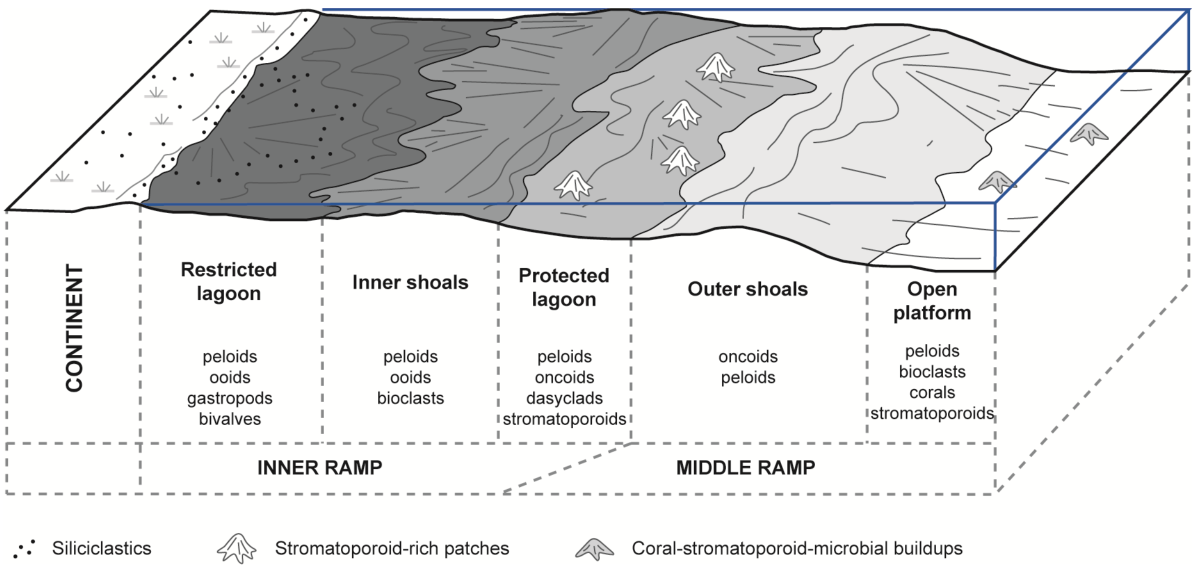

Fig. 2.10. *Sedimentary model for the latest Kimmeridgian shallow carbonate ramp proposed by Ipas (2003). Main skeletal and non-skeletal components for each subenvironment are indicated.*

2.3. CARBONATE ACCUMULATION, ACCOMMODATION AND SEQUENCE DEVELOPMENT

2.3.1. Stratigraphic facies architecture

The sedimentary evolution of ancient carbonate platforms is recorded in the vertical and lateral stacking of facies, and is the response of the depositional system through time to external factors (tectonics and climate). These factors ultimately control the accommodation space, changes in carbonate accumulation and variations in sedimentary production – even in the carbonate factory type – and redistribution, due for instance to changes in palaeoceanographic conditions influencing the hydrodynamic processes that redistribute the sediments (e.g. Vail et al., 1991; Posamentier and James, 1993; Pomar and Kendall, 2008). To unravel the facies stacking and deduce the controlling processes, there are different approaches depending on the scales of the studied successions: for example, sequence stratigraphy, analysis and correlation of high-frequency depositional sequences, and 2D and 3D computer modelling to reproduce the stratigraphic architecture (filling the gaps in areas without outcrop control) and to quantify the factors controlling the origin and evolution of carbonate production and accumulation (e.g. Aurell et al., 1995, 1998).

In marine sedimentary systems, the accommodation space is defined as the space available for sediment accumulation below the sea level (e.g. Jervey, 1988), although in detail wave or tide energy levels have also a strong control on sedimentation (i.e. hydrodynamic levels; e.g. Pomar and Kendall, 2008; Pomar and Haq, 2016). The accommodation space is in turn controlled by the combined effect of tectonics (i.e. subsidence/uplift of the seafloor) and eustacy (controlled by climate). Because of the difficulties in interpreting the tectonic vs eustatic origin of accommodation variations in the sedimentary record, the term "variation in relative sea level" is usually used (e.g. Kendall and Schlager, 1981). In addition, throughout deposition, the accommodation space is not only controlled by relative sea-level variations, but also by the amount of sediment accumulated.

Climate and tectonics are also prime controls on sediment accumulation. As shown above, carbonate production is directly influenced by the ecological requirements of the carbonate factory (i.e. water transparency, nutrients, temperature, salinity, etc), which are ultimately linked to climate and tectonics (e.g. palaeoceanography, global temperature gradients, ocean and atmospheric chemistry; e.g. Pomar and Kendall, 2008; Pomar and Haq, 2016). In addition, sediment production by a defined carbonate factory may be influenced by the relative sea-level variations, as they may dramatically alter the loci of carbonate production, particularly for those organisms with a strong depth-dependence to thrive (i.e. light-dependent tropical factory). For example, a relatively small drop in relative sea level may eliminate part or most of the sediment production zone in the shallow area of the carbonate platform, being the loci of production displaced down shelf. In an opposite scenario, a gradual relative sea-level rise may favour the efficiency of the carbonate factory, by sustaining the space available for the optimal development of biota (e.g. Pomar, 2001a). Tectonics and climate also control the rate of detrital sediment which is eroded and transported from the hinterland to the platform, which influences in carbonate productivity. Accordingly, an increase in detrital input may derive in negative consequences for the biota community, being carbonate production reduced or prevented. In addition, the effect of waves and currents on the seafloor (i.e. the hydrodynamic regime), which determine the amount of carbonate sediment that is in-situ accumulated or redistributed, is also influenced by climate and tectonics (e.g. palaeogeographical changes).

The stratigraphic facies architecture in carbonate platforms is the result of the dual control of carbonate accumulation and changes in accommodation (e.g. Mitchum and Van Wagoner, 1991). The balance between accumulation rates and accommodation results in three different lateral and vertical facies evolutions: progradation (shallowing-upward), aggradation and retrogradation (deepening-upward). A sedimentary sequence is defined as a genetically-related facies succession delimited by distinct surfaces, and reflects a particular vertical distribution (i.e. deepening-upward, deepening-shallowing, shallowing-upward or aggradational), in response to variations in relative sea level (e.g. Strasser et al., 1999; Hillgärtner and Strasser, 2003; Strasser, 2018). The sequences are classified according to their duration in different ranges or orders (e.g. Einsele, 1985). The more useful sequences to unravel the facies architecture at outcrop analysis scale are the high-frequency sequences (4th to 6th –order sequences).

The study and correlation of high-frequency sequences from different stratigraphic sections have been revealed as a useful approach to decipher the stratigraphic facies architecture and controlling factors in carbonate platforms. The facies stacking pattern observed within high-frequency sequences is the result of the balance between relative sea-level changes controlling accommodation, and carbonate accumulation (e.g. Mitchum and Van Wagoner, 1991; Strasser et al., 1999; Aurell and Bádenas, 2004; Bádenas et al., 2004, 2010; Fischer et al., 2004; Colombié and Strasser, 2005; Pomar and Hallock, 2008; Strasser and Védrine, 2009; Amour et al., 2011; Alnazghah et al., 2013; Brandando et al., 2015; Bádenas and Aurell, 2018). The different controlling factors in sequence development include orbitally-controlled sea-level changes (climate changes within the Milankovitch frequency band), high-frequency accommodation changes due to synsedimentary tectonics, and also intrabasinal factors (i.e. lateral migration of sedimentary bodies, or changes in carbonate production rate and accumulation under continuous subsidence) (e.g. Ginsburg, 1971; Védrine and Strasser, 2009; Bosence et al., 2009; Strasser, 2018).

In shallow-water successions, with high carbonate production rates, the high-frequency sequences of external origin (orbitally-induced sea-level changes, tectonically controlled sequences) usually record shallowing-upward vertical facies trends (e.g. Osleger, 1991; Hofmann et al., 2004), but deepening-upward, deepening-shallowing or aggradational facies trends can also be present depending on the interaction between accommodation and carbonate accumulation (e.g. Strasser et al., 1999; Colombié and Strasser, 2005; Spencer and Tucker, 2007; Bosence et al., 2009; Strasser, 2018; Bádenas and Aurell, 2018) (Fig. 2.11). Meter-scale peritidal cycles, i.e. those which end with subaerial exposure levels (Fig. 2.11b), represent the basic genetic unit described in many carbonate platforms (e.g. Wilson, 1975; James, 1984; Hardie and Shinn, 1986; Hillgärtner and Strasser, 2003; Brandano et al., 2015), but also purely subtidal cycles (i.e. those in which facies do not shallow to inter-supratidal conditions; Fig. 2.11a, c) have also been largely described for shallow-water successions (e.g. Lohmann, 1976; Markello and Read, 1982; Aigner, 1985; Osleger, 1991; Osleger and Read, 1991; Hillgärtner and Strasser, 2003; Strasser and Védrine, 2009; Bádenas et al., 2010), being reported as the dominant cycle type on carbonate ramps (Fig. 2.11a; Osleger, 1991).

Facies stacking patterns within high-frequency sequences originated from external factors do not exclusively reflect the accommodation-accumulation interaction, but also the intrinsic dynamics of the carbonate platforms can also have a great influence in the sedimentary record, giving rise into an “autocyclic” signal. In fact, local environmental changes (e.g. variations in carbonate production rates, lateral migration of facies bodies, sediment transport by waves and currents) may be overprinted to the internal facies architecture induced by external mechanisms. In addition, the particular facies depositional arrangements (i.e. facies mosaics and/or facies belts) also represent a determinant factor controlling lateral and vertical facies stacking patterns within high-frequency sequences (e.g. Ginsburg, 1971; Pratt and James, 1986; Strasser et al., 1999; Strasser and Védrine, 2009; Bádenas, 2019), thus complicating the predictability of vertical facies trends especially in facies mosaic distributions. Therefore, the analysis of ancient shallow-water carbonate platforms requires to analyse and understand at once both, the stratigraphic architecture from high-resolution sequential analysis, and the original internal facies heterogeneities.

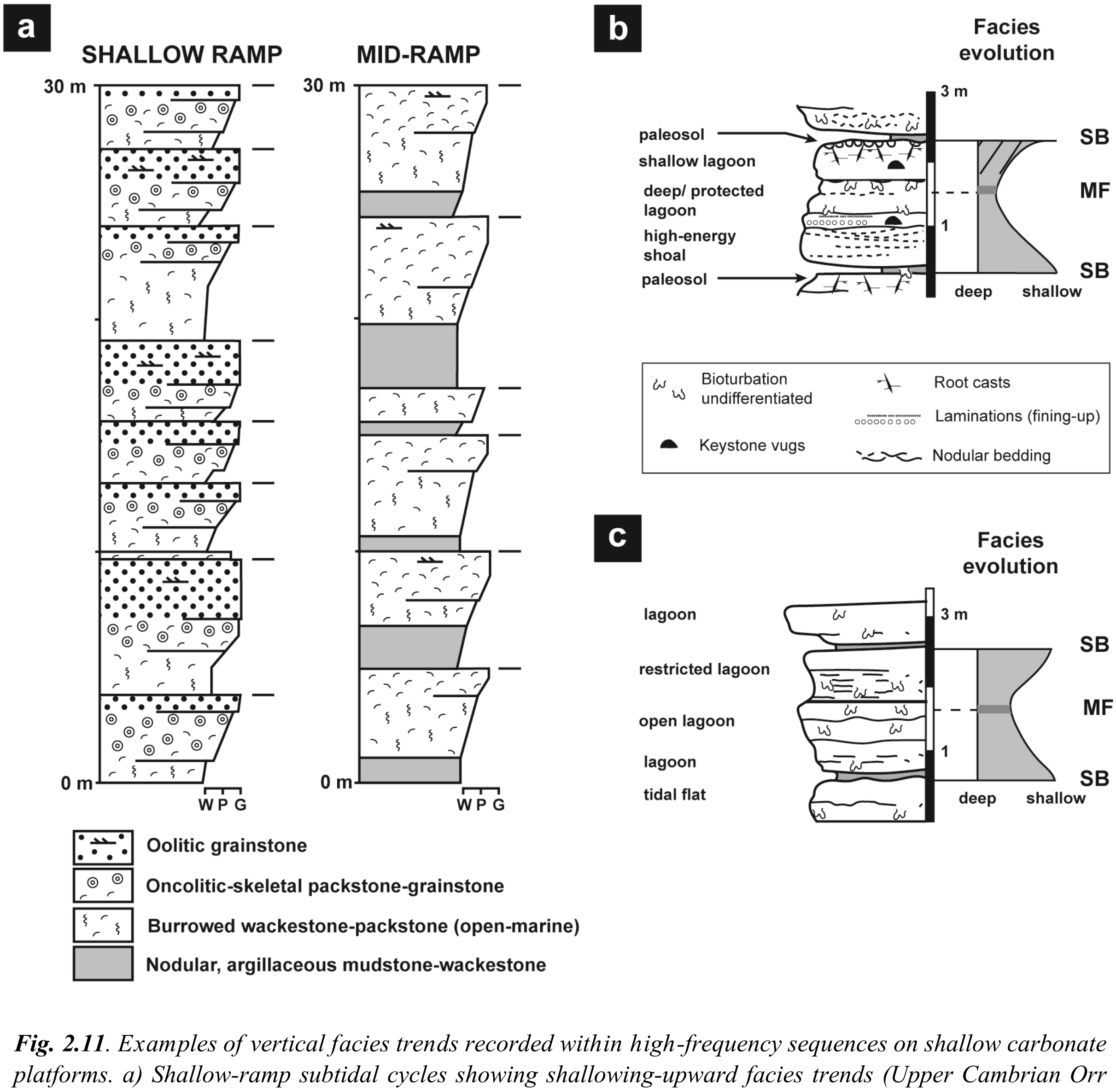

***Fig. 2.11**. Examples of vertical facies trends recorded within high-frequency sequences on shallow carbonate platforms. a) Shallow-ramp subtidal cycles showing shallowing-upward facies trends (Upper Cambrian Orr and Notch Peak formations of House Range, Utah; modified from Osleger, 1991). b, c) Deepening-shallowing facies evolutions in peritidal (b) and subtidal (c) cycles (Early Cretaceous French Jura Platform; modified from Hillgärtner and Strasser, 2003). MF: maximum flooding; SB: sequence boundary.*

2.3.2. The Higueruelas Formation: keys for unravelling a complex stratigraphic facies architecture

In the study area, the Higueruelas Fm represents one of the three third-order depositional sequences recognized for the Kimmeridgian sedimentary succession in the north-central part of the Iberian Basin (i.e. sequence Ki3, see Fig. 4.3 in Chapter 4; Bádenas and Aurell, 2001a; Aurell et al., 2010, 2019b). This succession was deposited during the regressive part of a major transgressive-regressive cycle defined for the Late Jurassic (ca. 15 My; Aurell et al., 2003, 2010).

The overall stratigraphic architecture of the Higueruelas Fm in the north-central part of the Iberian Basin has been reported by previous authors (e.g. Ipas et al., 2004; Aurell et al., 2010), by the recognition of a number of high-frequency sequences and their correlation on different stratigraphic sections located south of the city of Zaragoza (i.e. localities of Mezalocha, Aguilón and Lécera; Fig. 2.12). These sequences were tentatively interpreted as formed by orbitally-driven relative sea-level variations (i.e. short-term eccentricity cycles), as they could be correlated in widely-separated outcrops. However, the characterization and interpretation of the internal facies architecture within these high-frequency sequences and the vertical and lateral extent of the facies bodies was not unravelled in previous works, as the mean distance between the studied logs was larger (tens of kilometres) than the usual width of some facies belts in carbonate ramps (e.g. 10 km wide for inner-ramp lagoons, 3 km for backshoal area or 3-10 km wide for shoal and foreshoal subenvironments; Bádenas and Aurell, 2010). An accurate characterization of the facies distribution and stratigraphic architecture of this shallow carbonate ramp requires the analysis of the lateral and vertical facies relationships within high-frequency sequences in closely-spaced sedimentary logs, encompassing both strike and down-dip directions if possible. Accordingly, this kind of high-resolution sequential analysis has been performed in this Thesis as a tool to provide a more accurate sedimentological characterization of the shallow carbonate ramp of the Higueruelas Fm, in order to accurately decipher the stratigraphic facies heterogeneities, and to interpret the factors controlling the facies distribution and sedimentary evolution of the platform.

Fig. 2.12 (Next page). *High-frequency sequences identified in the Higueruelas Fm in three correlated sections orientated from proximal- to outer-ramp areas (modified from Aurell et al., 2010 after Ipas, 2003). The location of the sections and the mean distance between logs are indicated.*

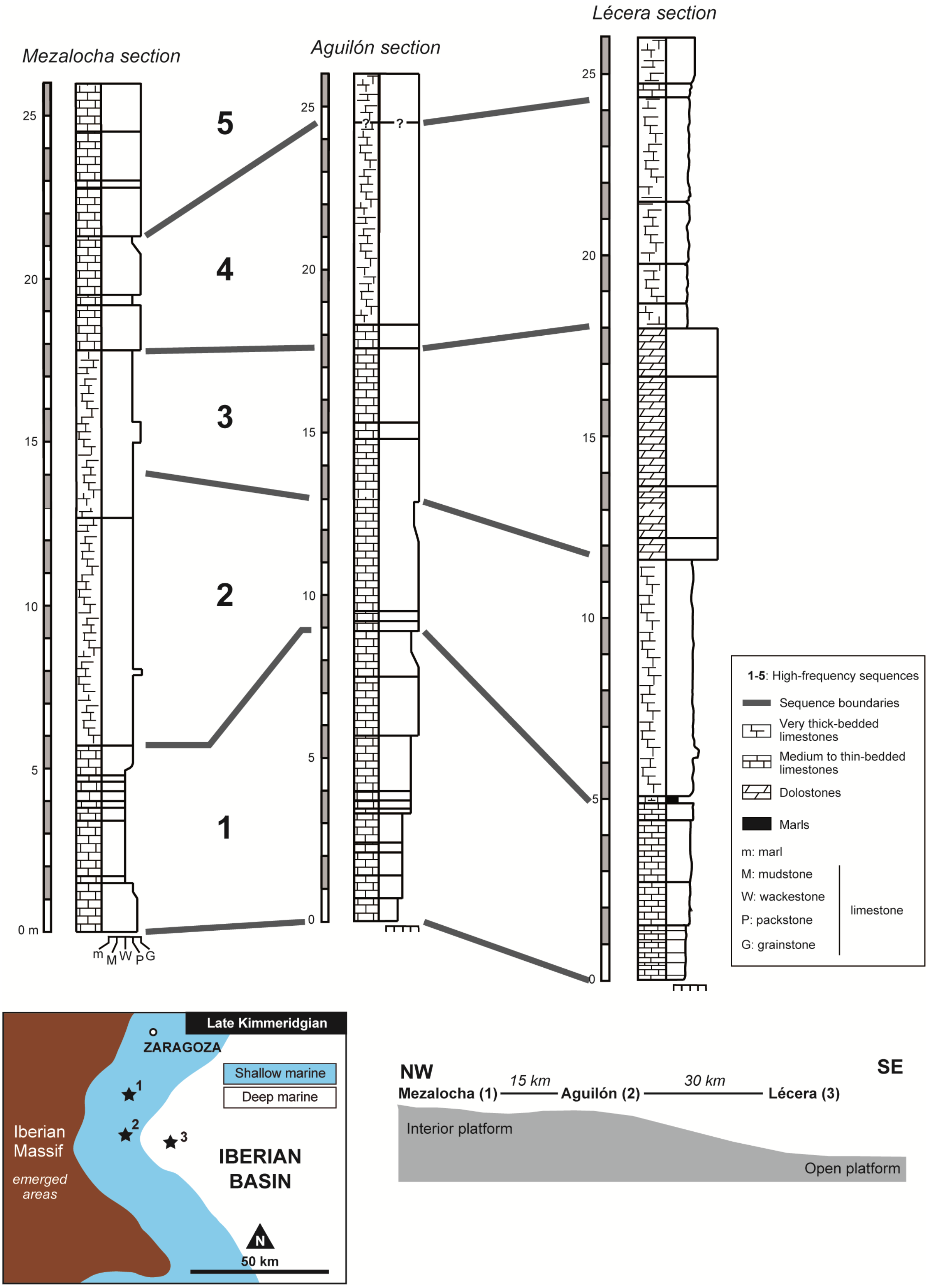
Mezalocha section
Aguilón section
Lécera section
5
4
3
2
1
0 m
m M W P G
1-5: High-frequency sequences
Sequence boundaries
Very thick-bedded limestones
Medium to thin-bedded limestones
Dolostones
Marls
m: marl
M: mudstone
W: wackestone
P: packstone
G: grainstone
limestone
Late Kimmeridgian
ZARAGOZA
Shallow marine
Deep marine
Iberian Massif
emerged areas
IBERIAN BASIN
N
50 km
NW
SE
Mezalocha (1)
15 km
Aguilón (2)
30 km
Lécera (3)
Interior platform
Open platform

3. METHODS

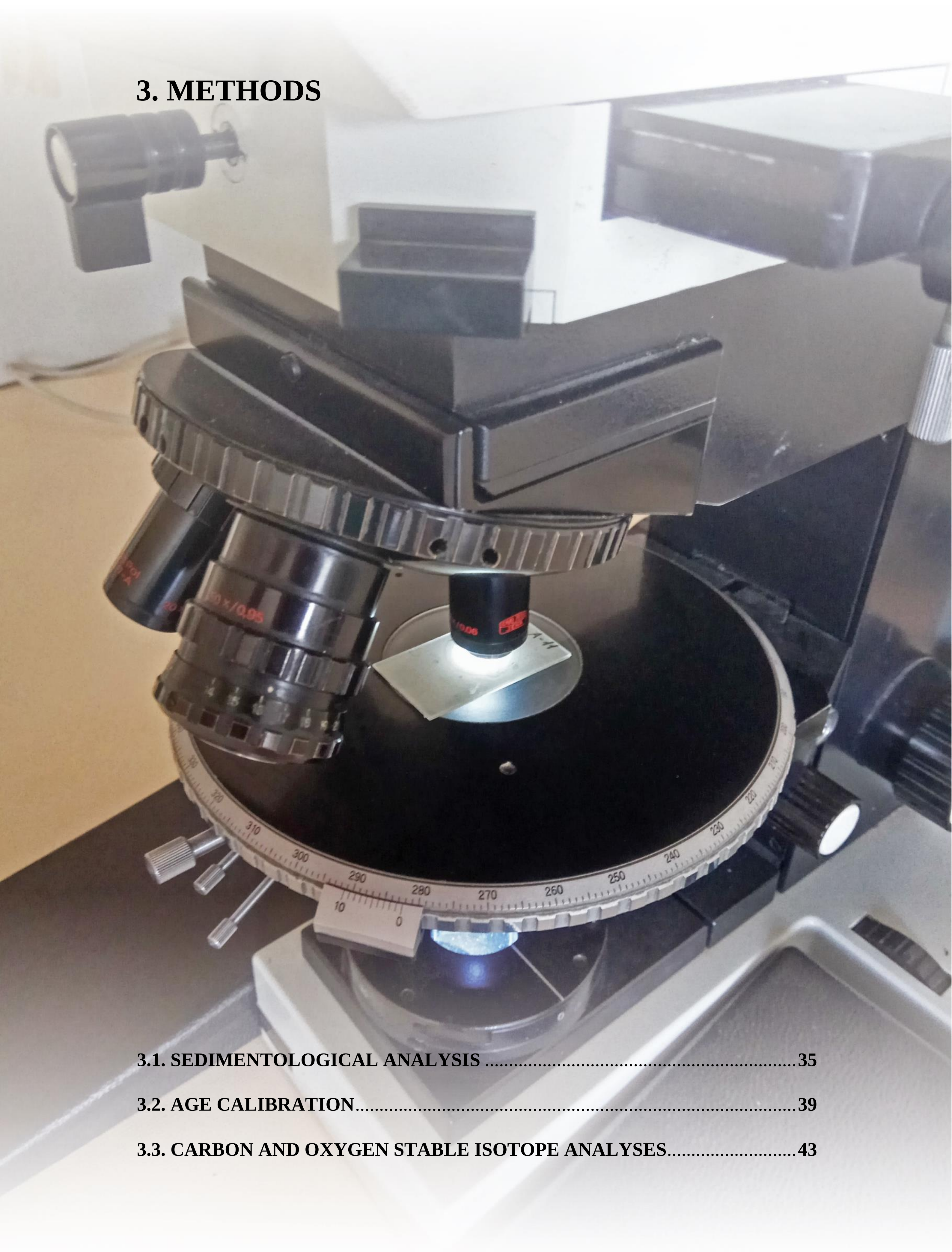

CHAPTER 3

METHODS

3.1. SEDIMENTOLOGICAL ANALYSIS

3.1.1. Field data collection

The shallow-marine carbonate deposits of the Higueruelas Fm are well exposed in north-central areas of the Iberian Range of northeastern Spain (Gómez, 1979; Aurell, 1990; Aurell et al., 2003, 2010). In particular, the Higueruelas Fm outcrops studied in this Thesis locate south of the city of Zaragoza (northeastern Spain), in an area that has 20 x 30 km in extent (Fig. 3.1a). The studied outcrops form part of the system of intraplate fold-and-thrust belts generated during the Alpine Orogeny, and constituted paleo-reliefs during the Cenozoic detrital and evaporitic continental sedimentation (e.g. Guimerà and Álvaro, 1990).

In the study area, the Higueruelas Fm ranges from 40 to 80 m in thickness, and is characterized by dm- to m-thick limestone beds with few marl and sandstone intercalations. The stratigraphic and sedimentological characterization of this carbonate succession was based on the analysis of 35 sedimentary logs and facies mapping in selected outcrops. The studied sections are preferentially situated on the flanks of the E-W and NW-SE orientated anticlines (Fig. 3.1a). The dip angle of these flanks is generally low, between 10 to 30º (locally 80º in the localities of Jaulín and Tosos). The stratigraphic and sedimentological characterization of this shallow-marine succession was accomplished at different outcropping scales. From the 35 stratigraphic sections analysed in this Thesis, 21 logs are distributed throughout the study area from the localities of Muel to Aguilón, with an average separation distance of 5 km (Fig. 3.1a). The selection of these sections was arranged in order to better approach the facies reconstruction of the shallow carbonate ramp in both strike and down-dip directions. In addition, a relatively small window of 1 x 2 km in extent around the locality of Mezalocha, covering well-exposed continuous outcrops, was selected for the detailed analysis of facies distribution and their lateral extent on the inner domains of this carbonate ramp, i.e. the areas with highest facies heterogeneities, as predicted by the ramp models and previous works in the studied unit (Ipas, 2003; Ipas et al., 2004) (see Chapter 2, section 2.2.2). This study was focused on the upper 10 to 16 m thick of the succession outcropping in this area, with the analysis of 14 closely-spaced sedimentary logs (Fig. 3.1b).

The field analysis of the Higueruelas Fm in each of the studied sections consisted on the bed-by-bed description of depositional features, such as bedding thickness and geometry, type of bedding surfaces (planar, irregular, bioturbated, Fe-encrusted, hardground), texture and components

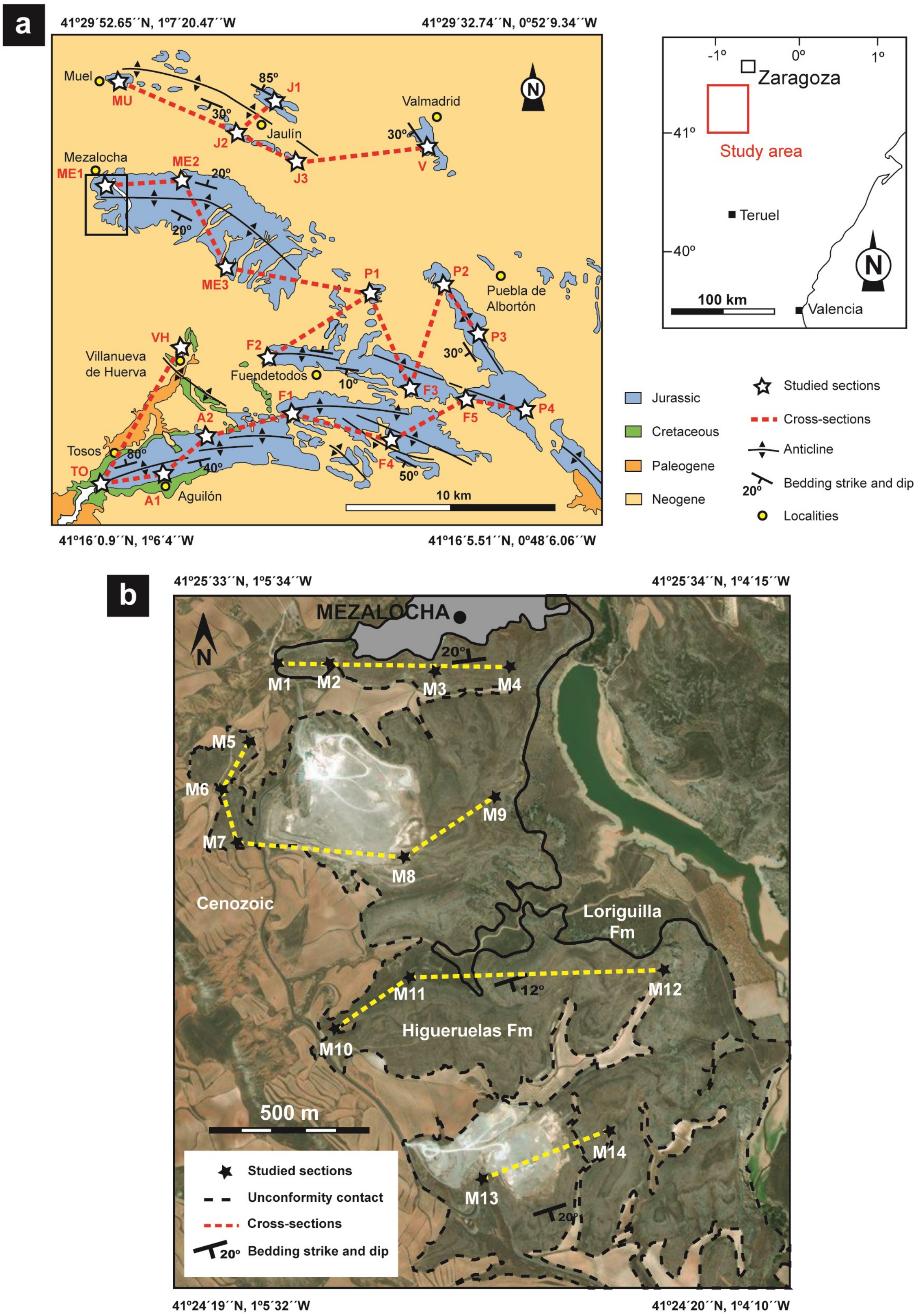

Fig. 3.1. *Jurassic outcrops in the study area (south of the city of Zaragoza; north-central Iberian Chain) and location of the studied sections (stars). The stratigraphic and sedimentological analysis of the Higueruelas Fm was performed on successive W-E cross-sections (dashed lines), orientated from proximal to relatively distal domains of the carbonate ramp. Continuous outcrops around the locality of Mezalocha (see black square in a; modified from Cortés Gracia and Casas Sainz, 1996) were selected for a detailed facies analysis of the inner areas of the carbonate ramp (b).*

(including type, size, abundance of grains) and sedimentary structures. In addition, and exhaustive rock sample collection (1200 samples, an average of two samples/metre) was done to complement the field observations with the petrographic descriptions on polished slabs and thin sections.

3.1.2. Petrographic analysis

Facies analysis was accomplished by the combination of the field observations and petrographic descriptions on rock samples, in particular of 1200 polished slabs and 300 selected thin sections. Facies were differentiated mainly on the basis of the texture and the relative proportion of skeletal and non-skeletal components observed on polished slabs, then precisely determined on thin sections. Texture nomenclature follows Dunham (1962) classification. The semi-quantitative proportion of skeletal and non-skeletal grains was performed by visual estimations using the comparative templates of percentages of constituents in limestones proposed by Baccelle and Bosellini (1965). The main types of non-skeletal grains recognized are oncoids, ooids and peloids, which were classified using the Dahanayake (1977), Strasser (1986) and Flügel (2004) nomenclatures, respectively (see Figs 2.5 and 2.6 in Chapter 2).

Regarding the oncoids, a detailed analysis on abundance and distribution of the different types of oncoids was performed by petrographic descriptions (both on polished slabs and thin sections) on 896 samples selected from the total of the 1200 samples collected in the Higueruelas Fm mentioned above. These samples correspond to the lower 30 to 50 m thick of the unit, where oncoids are more abundant and display a wide variability in size, morphology and internal structure.

3.1.3. Facies correlation and sedimentary models

The correlation of the stratigraphic sections was performed by the identification of continuous well-marked bedding surfaces along cross-sections, both in Mezalocha outcrops (Fig. 3.1b) and at large scale (outcrops from Muel to Aguilón; Fig. 3.1a). The cross-sections are orientated from proximal (i.e. to the west) to distal domains (i.e. to the east), following the palaeogreographic reconstructions for the north-central part of the Iberian Basin during the Late Jurassic times (e.g. Bádenas and Aurell, 2001a; Aurell et al., 2003).

The identification in the field of master bedding surfaces in all the outcrops allowed to recognize a number of correlatable sedimentary units (high-frequency sequences), and led to stablish the lateral and vertical facies relationships for palaeoenvironmental interpretations. The lateral continuity of the studied outcrops located around Mezalocha (Fig. 3.1b) allowed the physical tracing of these sharp bedding planes and facies mapping between sedimentary logs. At large scale (i.e. from Muel to Aguilón; Fig. 3.1a), as no physical tracing between isolated outcrops was possible, correlation of logs was accomplished by the best-fit solution between the recognized master bedding surfaces, also constrained by the lateral and vertical facies distribution observed within the high-frequency sequences identified in individual logs. This large-scale correlation is based on the assumption that these sharp bedding surfaces represent sedimentary discontinuities that can be traced across the entire study area, which is supported by the physical tracing of these sharp bedding planes along the continuous Mezalocha outcrops, but also by previous correlations in other Jurassic shallow carbonate ramp successions of the Iberian Basin, where the km-scale lateral continuity of similar well-defined bedding surfaces is demonstrated (e.g. Bádenas and Aurell, 2010; Bádenas et al., 2010).

Successive palaeogreographic maps were reconstructed for each sedimentary stage (represented in the high-frequency sequences), based on the internal facies architecture observed within the sequences, in order to show the facies distribution and sedimentary evolution of the inner- to mid-ramp areas of the platform. Particularly, the abundance and distribution of the different types of non-skeletal grains identified in the Higueruelas Fm is reported from shallow to deeper domains, with special focus on the types of oncoids in both strike and down-dip directions. The sedimentary features of the facies, combined with their lateral and vertical facies relationships within the sequences, were used as main criteria for interpreting subenvironments, as well as the palaeoenvironmental factors controlling these facies heterogeneities. Finally, the resultant facies models were compared with similar shallow carbonate ramps described in the Kimmeridgian of the Iberian Basin (e.g. Bádenas and Aurell, 2010; San Miguel et al., 2013, 2017a; Pomar et al., 2015), and also with other Late Jurassic shallow marine environments outside the Iberian Basin (e.g. the Kimmeridgian carbonate ramp deposits of the Arab-D Fm, or the Late Oxfordian Swiss Jura Platform; Védrine et al., 2007; Lehmann et al., 2010; Al-Awwad and Collins, 2013).

3.2. AGE CALIBRATION

The age of the Higueruelas Fm has been open to discussion over the years, being traditionally considered as early Tithonian in age up to recent works (e.g. Aurell et al., 1994, 2003, 2010). This age assignment was mainly based on the correlation to the eastern areas of the Iberian Basin, in which the assumed time-equivalent open-marine facies include a rich association of late Kimmeridgian-early Tithonian ammonites (Calanda area, see Fig. 4.3 in Chapter 4) (e.g. Geyer and Pelleduhn, 1979; Atrops and Meléndez, 1984). Because of the absence of ammonites in the shallow-marine successions of the Higueruelas Fm, it becomes challenging to accurate the age of this unit, which must be approached by a combined set of techniques.

In this Thesis, two different methods were used in order to precise the age of the Higueruelas Fm in the study area: 1) biostratigraphy based on key marker benthic foraminifera, and 2) strontium stable isotope analyses.

3.2.1. Biostratigraphic data based on benthic foraminifera

Significant benthic foraminifera were identified in 57 of the total of the 1200 samples studied in the Higueruelas Fm. They correspond to several stratigraphic levels. Particularly for the Late Jurassic in the Tethyan realm, certain species of benthic foraminifera, especially lituolids, are considered key markers for calibration of sedimentary successions because of their constrained stratigraphic ranges. Three species of key marker lituolids are considered (Fig. 3.2a): *Anchispirocyclina lusitanica* (Egger, 1902), *Alveosepta jaccardi* (Schrodt, 1894) and *Redmondellina powersi* (Redmond, 1964). The stratigraphic range for *A. lusitanica* encompasses from early-mid Tithonian to early Berriasian (e.g. Ramalho, 1971, 1981; Ramírez del Pozo, 1971; Septfontaine et al., 1991; Peybernès, 1998; Granier and Bucur, 2011; Taylor et al., 2013; Granier, 2019), whereas *A. jaccardi* and *R. powersi* are found from late Oxfordian to late Kimmeridgian, the latter only recorded in the Kimmeridgian (e.g. Hottinger, 1967; Ramalho, 1981; Septfontaine, 1988; Altiner, 1991; Bassoullet, 1997; Pop and Bucur, 2001; Olszewska, 2010; Taylor et al., 2013; Pleş et al., 2015).

Accordingly, based on scarce but significant records of mid-Kimmeridgian ammonites in the underlying open-marine Loriguilla Fm in the Aguilón area (Bádenas et al., 2003; see Fig. 3.1a for location), the determination of the stratigraphic distribution of the above mentioned key marker lituolids in the studied sedimentary logs allowed to constrain the age of deposition of the Higueruelas Fm in the study area. It is worthy notice that the previous age determination of the unit (early Tithonian) was based on previous proposals of biostratigraphic ranges of these key lituolids (i.e. a late Kimmeridgian to early Tithonian span for *R. powersi*; Hardenbol et al., 1998), which have been improved in the last years.

The micropalaeontological descriptions provided by Hottinger (1967, 2006) and BouDagher-Fadel (2008) for larger benthic foraminifera were followed in order to identity the morphotypes. These descriptions are mainly based on the chamber arrangement and the presence or absence of particular structural elements: *Alveosepta jaccardi* (Schrodt, 1894) is characterized by its finely and complexly alveolar walls with many apertures, and a planispiral-evolute chamber arrangement with a streptospiral early stage (i.e. coiling of chambers occurring in a single or different planes, respectively). The presence of a subepidermal alveolar network in the lateral chamber walls is a diagnostic criterion, which distinguishes this specimen from other contemporaneous genera like

Pseudocyclammina (Yabe and Hanzawa, 1926). *Redmondellina powersi* (Redmond, 1964) differs from *A. jaccardi* in size (larger in *R. powersi*) and in showing pillar-like hypodermal extensions linking alveolar walls. *Anchispirocyclina lusitanica* (Egger, 1902) has in turn a peneropliform growth of the chambers in a late stage, and is characterized by having a central zone with a complex reticulum of densely spaced pillars.

3.2.2. Strontium stable isotopes

Strontium stable isotope analyses were performed on 12 samples corresponding to thick-wall calcitic bivalve shells (i.e. *Trichites*, oysters) and brachiopod shells, in selected intervals of the studied sections.

The strontium stable isotope analyses are based on the marine $^{87}Sr/^{86}Sr$ ratio, whose variations during the Mesozoic reflect the equilibrium between continental radiogenic strontium and non-radiogenic strontium derived from the hydrothermal activity occurring in mid-ocean ridges (e.g. Elderfield, 1986; McArthur, 1994; Jones and Jenkins, 2001; Price and Gröcke., 2002). The $^{87}Sr/^{86}Sr$ ratio in seawater shows worldwide homogeneous values for a particular geologic period, due to the long residence time of this isotope (2-4 My; Hodell et al., 1989, 1990) in relation to the short period involving ocean mixing (ca. 1-2 Ky; Broecker and Peng, 1982). Consequently, the analysis of strontium stable isotopes of non-altered skeletal remains within sedimentary rocks, which have precipitated in isotopic equilibrium with ancient seawater (e.g. Carpenter and Lohmann, 1995; Veizer et al., 1999), constitutes a reliable tool for age calibration. Accordingly, these analyses were performed in the Higueruelas Fm for the age calibration of the unit in the study area, because of the global marine $^{87}Sr/^{86}Sr$ curve defined for the Late Jurassic (Gradstein et al., 2012; McArthur et al., 2012; Wierzbowski et al., 2017) shows regular increasing values (Fig. 3.2b), so that the obtained results, constrained with biostratigraphic data from ammonites and benthic foraminifera, can be correlated.

Concerning the laboratory procedures, the samples were firstly examined under binocular microscope in order to detect and avoid possible diagenetically altered areas of the samples (e.g. dolomite, fractures, external zones in contact with the analysed component, chalky-cloudy areas, stylolites). In addition, cathodoluminescence (CL) microscopy was used in order to identify possible altered zones in function of the absence or presence of luminescence, which depends on the content variations in luminescent activators (mainly Mn^{2+} normally related to reducing late phreatic meteoric or burial fluids in contact with carbonates, but also some REE ions) and/or quenchers (Fe^{2+}, Fe^{3+}, Ni, Co) (e.g. Machel, 1985; Savard et al., 1995; Richter et al., 2003; Hiatt and Pufahl, 2014). The emitted luminescence can be classified as bright or dull, varying from yellow to red-orange colours. Therefore, as far as possible, those parts of the samples showing no luminescence were primarily selected for the analyses. The CL observations were performed with a Technosyn Cold Cathodo Luminiscope at the *Instituto Geológico y Minero de España* (IGME, Spain), operating under 10-12 kV beam potential, 0.5 µA beam current and a 0.05-0.1 Torr pressure.

Regarding the isotopic measurements, those calcites that appeared as translucent under binocular microscope and non-luminescent in CL observations were sampled with a handheld micro-drill. The $^{87}Sr/^{86}Sr$ analyses were determined with a TIMS-Phoenix thermal ionization mass spectrometer at the *CAI Geocronología y Geoquímica Isotópica* of the *Universidad Complutense de Madrid* (Spain). For possible ^{87}Rb interferences, all $^{87}Sr/^{86}Sr$ data were corrected and normalised to a value of 0.1194 for $^{86}Sr/^{88}Sr$. During all the procedure, the standard NBS-987 ($^{87}Sr/^{86}Sr = 0.710246 \pm 0.000014$) was systematically analysed in order to correct the measured values from a possible deviation referred to the standard, giving an average $^{87}Sr/^{86}Sr$ value of 0.710246 ± 0.000014 with an analytical error of 0.01%.

Fig. 3.2 (Next page). *a) The biostratigraphic ranges of the key marker lituolids* Anchispirocyclina lusitanica *(Egger),* Alveosepta jaccardi *(Schrodt) and* Redmondellina powersi *(Redmond) for the Tethyan realm (based on Hottinger, 1967; Ramalho, 1971, 1981; Ramírez del Pozo, 1971; Septfontaine, 1988; Bassoullet, 1997; Pop and Bucur, 2001; Olszewska, 2010; Taylor et al., 2013; Pleş et al., 2015). The images of the foraminifera are extracted from this work (see Chapter 4). Geological Time Scale according to Ogg et al. (2016). b) Strontium isotope variations from the latest Early Jurassic to the Early Cretaceous, based on strontium isotope dataset of well-preserved fossils (extracted from Wierzbowski et al., 2017).*

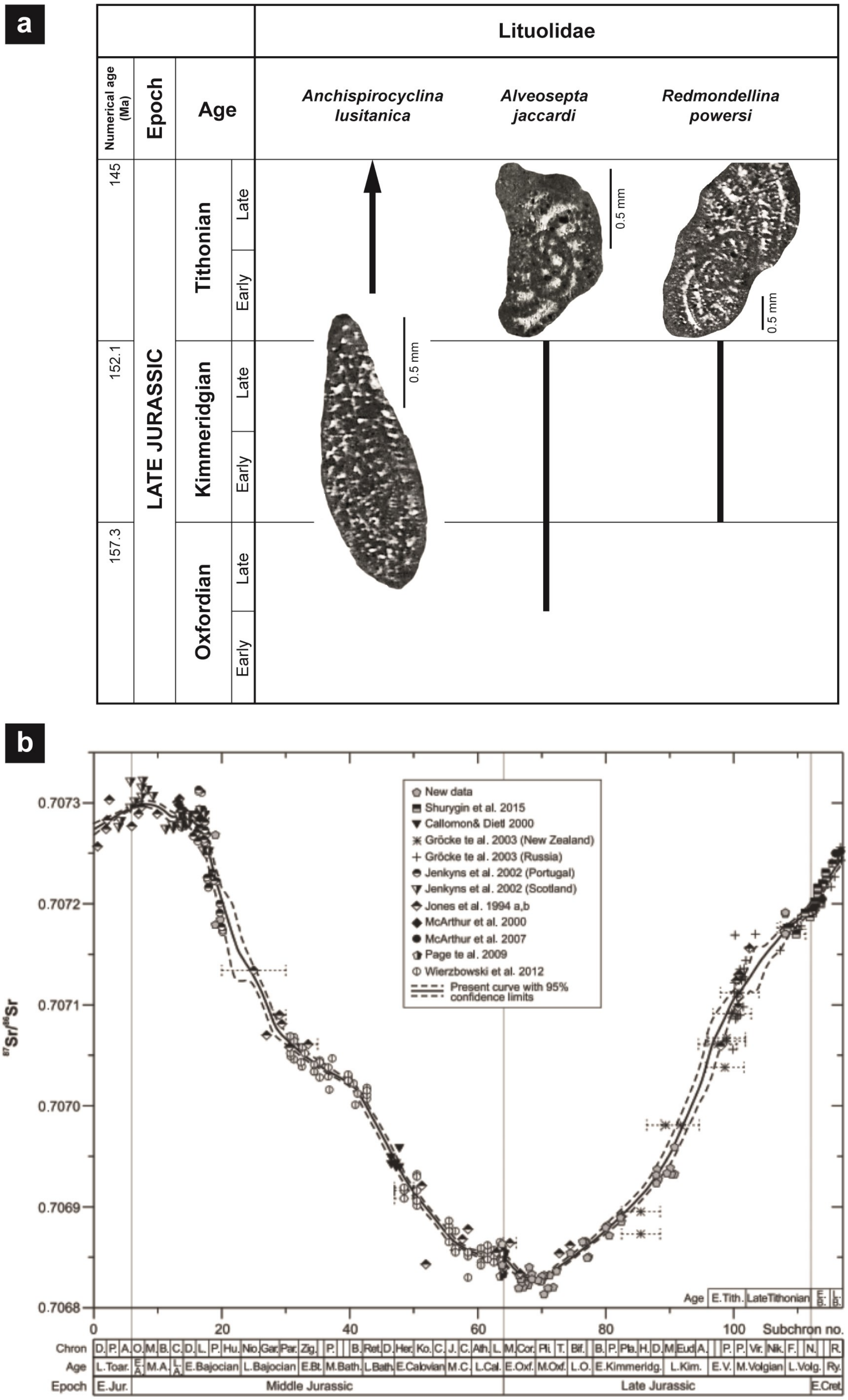
a
Lituolidae
Numerical age (Ma)
Epoch
Age
Anchispirocyclina lusitanica
Alveosepta jaccardi
Redmondellina powersi
145
152.1
157.3
LATE JURASSIC
Tithonian
Kimmeridgian
Oxfordian
Late
Early
0.5 mm
b
New data
Shurygin et al. 2015
Callomon& Dietl 2000
Gröcke te al. 2003 (New Zealand)
Gröcke te al. 2003 (Russia)
Jenkyns et al. 2002 (Portugal)
Jenkyns et al. 2002 (Scotland)
Jones et al. 1994 a,b
McArthur et al. 2000
McArthur et al. 2007
Page te al. 2009
Wierzbowski et al. 2012
Present curve with 95% confidence limits
87Sr/86Sr
0.7073
0.7072
0.7071
0.7070
0.7069
0.7068
0
20
40
60
80
100
Subchron no.
Chron
Age
Epoch
E.Jur.
Middle Jurassic
Late Jurassic
E.Cret.
L.Toar.
M.A.
E.Bajocian
L.Bajocian
M.Bath.
L.Bath.
E.Calovian
M.C.
L.Cal.
E.Oxf.
M.Oxf.
L.O.
E.Kimmeridg.
L.Kim.
E.V.
M.Volgian
L.Volg.
Ry.
E.Tith.
LateTithonian

3.3. CARBON AND OXYGEN STABLE ISOTOPE ANALYSES

The carbon and oxygen stable isotope analyses were performed on 72 bulk-carbonate samples obtained from two selected sections in the localities of Tosos and Fuendetodos (sections TO and F4, respectively; see Fig. 3.1a for location), and on calcitic bivalve shells from 3 specimens of *Trichites* collected in the lower part of the section situated in the locality of Fuendetodos.

The analyses of carbon and oxygen stable isotopes are based on the fractionation of the heavier stable isotopes (^{18}O, ^{13}C) in relation to the lighter stable isotopes (^{16}O, ^{12}C), due to their differences in mass (e.g. O'Neil, 1986; Wieser and Brand, 1999). In carbonate rocks, variations in $^{18}O/^{16}O$ and $^{13}C/^{12}C$ ratios (represented as $\delta^{18}O$ and $\delta^{13}C$, respectively) have been traditionally used for obtaining palaeoenvironmental information during the Phanerozoic (e.g. ocean paleotemperatures, changes in organic matter supply), with a local and/or regional significance (e.g. Urey et al., 1951; Emiliani, 1955; Immenhauser et al., 2003; Wierzbowski, 2004; Lisiecki and Raymo, 2005; Bádenas et al., 2005; Colombié et al., 2011; Zuo et al., 2018). The ^{18}O-enrichment or depletion in ancient seawaters is associated to variations in glacial ice volume, recording glacial-interglacial $\delta^{18}O$ cycles which suitable respond to the orbitally-induced sea-level changes (i.e. Milankovitch cycles) and other relevant climatic events (e.g. Mid-Miocene and Early Eocene climatic optimums; e.g. Zachos et al., 2001), providing a high-resolution isotopic stratigraphy for the Phanerozoic (e.g. Emiliani, 1955; Clarke and Jenkyns, 1999; Veizer et al., 1999; van de Schootbrugge et al., 2000; Zachos et al., 2001; Korte and Hesselbo, 2011; Gradstein et al., 2012). Variations in $^{13}C/^{12}C$ ratios have been, in turn, referred to changes in carbonate production on platforms and pelagic domains, decomposition of organic matter, CO_2 variations in the atmosphere or methane release in seawater (e.g. Kroopnick et al., 1977; Arthur et al., 1985; Jenkyns and Clayton, 1986; Föllmi et al., 1994; Dickens et al., 1995; Weissert and Mohr, 1996; Weissert et al., 1998; Bartolini et al., 2003), reflecting variations in the global carbon cycle through time.

In shallow-marine carbonates, in particular, unravelling the carbon and oxygen stable isotope composition of paleo-seawater becomes more challenging, due to: 1) the multiple factors that control the chemical variability of shallow seawaters (e.g. evaporation, carbon transfer, changes in salinity or water-masses restrictions; Patterson and Walter, 1994; Immenhauser et al., 2003; Colombié et al., 2011; Zuo et al., 2018) (Fig. 3.3a); 2) the potential singular isotopic compositions recorded by their different components (e.g. skeletal remains, coated grains, micrite matrix; Hudson, 1977; Anderson and Arthur, 1983; Jenkyns and Clayton, 1986; McConnaughey, 1989a, b; Nelson and Smith, 1996; Schobben et al., 2015); and 3) the diagenetic processes that can alter the primary isotopic signature, thus complicating the use of these isotopic records as palaeoenvironmental proxies (e.g. Brand and Veizer, 1981; Moore, 1989; Marshall, 1992; Glumac and Walker, 1998; Immenhauser et al., 2002; Coimbra et al., 2014; Huck et al. 2017).

Diagenesis in marine carbonates commonly implies a decrease in $\delta^{18}O$ values by the influence of ^{18}O-depleted meteoric waters and/or relatively high-temperature burial fluids, being the magnitude of such alteration depending on the degree of the fluid-rock interaction (e.g. Hudson, 1977; Brand and Veizer, 1980; Allan and Matthews, 1982; Given and Lohmann, 1985; Plunkett, 1997; van der Kooij et al., 2009; Grotzinger et al., 2011; Madden and Wilson, 2013; Coimbra et al., 2014; Al-Mojel et al., 2018). Post-depositional alteration also generally leads to a decrease in $\delta^{13}C$ values, which is normally attributed to the interaction with meteoric solutions enriched in organic ^{12}C by soil weathering (e.g. Hudson, 1977; Allan and Matthews, 1982; O'Neil, 1987; Lohmann, 1988; Patterson and Walter, 1994; Moore, 2001; Immenhauser et al., 2002; Lavastre et al. 2011; Bahamonde et al.,

2017) (Fig. 3.3b). Consequently, it is important to firstly characterize the type and magnitude of the diagenesis (if present), in order to ensure the reliability of the carbon and oxygen stable isotope signature as a palaeoenvironmental proxy.

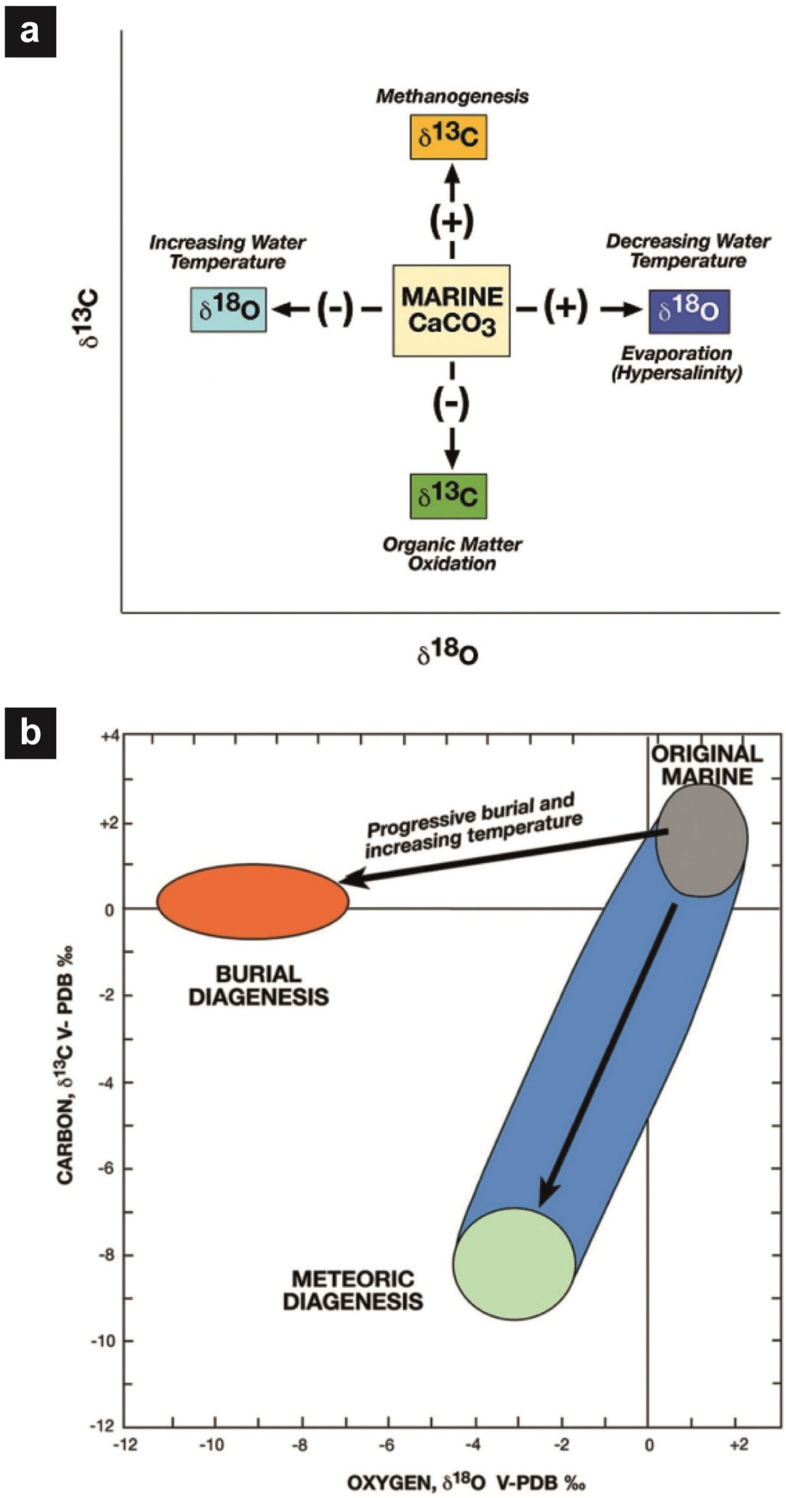

Fig. 3.3. *a) Control of seawater temperature, organic matter oxidation and methanogenesis on the carbon and oxygen stable isotope composition in marine carbonates. b) Isotopic fields of carbonates influenced by burial (i.e. increasing temperature with depth) and meteoric diagenesis (i.e. contact with* ^{12}C*-enriched meteoric fluids), leading to more negative* $\delta^{13}C$ *and* $\delta^{18}O$ *values (after James and Jones, 2015).*

In this Thesis, the initial aim for the carbon and oxygen stable isotope analyses performed on the Higueruelas Fm in the two selected sections was obtaining palaeoenvironmental information with a local and/or regional significance, and thus complementing the knowledge about the factors controlling sedimentation on the latest Kimmeridgian shallow carbonate ramp in the study area. These sections represented the proximal (Tosos) and relatively distal (Fuendetodos) areas of the carbonate ramp, in order to consider the influence of facies and palaeoenvironmental differences on the recorded primary isotopic signature. However, the preliminary results highlighted that diagenesis exerted a strong influence on the isotopic composition, according to the particular post-depositional diagenetic evolution of the Higueruelas Fm in each studied sector (Pérez et al., 1985; Pérez, 1989; Soria et al., 1995). Therefore, these isotopic analyses performed in this work turned into investigating the diagenetic imprint on the carbon and oxygen stable isotope composition.

Concerning the laboratory procedures, since diagenesis usually implies concomitant chemical and textural changes on carbonates (e.g. Brand and Veizer, 1980, 1981; Lavoie and Bourque, 1993; Colombié et al., 2011; Coimbra et al., 2014; Huck et al., 2017), the 72 bulk-carbonate samples were firstly analysed in thin sections under binocular microscope in order to differentiate between primary carbonate components (i.e. micrite matrix and carbonate grains) from diagenetic calcite cements, the latter being classified using the Flügel (2004) nomenclature. This petrographic analysis was complemented by CL microscopy on 21 thin sections for the characterization of both primary carbonate components and diagenetic calcite cements, on the basis of the absence or type of luminescence (see section 3.2.2) (e.g. Machel, 1985; Savard et al., 1995; Richter et al., 2003; Hiatt and Pufahl, 2014). The CL observations were performed with a Technosyn Cold Cathodo Luminiscope at the *Instituto Geológico y Minero de España* (IGME, Spain), operating under 10-14 kV beam potential, 0.5 µA beam current and a 0.05-0.1 Torr pressure.

Regarding the isotopic measurements, carbonate powders from the 72 bulk-carbonate samples were extracted using a handheld micro-drill, avoiding as far as possible the incorporation of diagenetic calcite cements during sampling, but also large bioclastic fragments of corals or stromatoporoids, due to the disequilibrium-isotopic precipitation by organisms (e.g. McConnaughey, 1989a, b). These isotopic measurements also included the analysis of three specimens of *Trichites* collected in the lower part of the Fuendetodos section, as their calcitic bivalve shells have potential to record the original seawater stable isotope composition, as reported by previous authors (e.g. Zuo et al., 2018), so they can be useful for quantifying the magnitude of the diagenetic alteration. A double measure per sample (in both bulk-carbonates and calcitic bivalve shells) was performed in order to ensure the reliability of the carbon and oxygen stable isotope composition in each sample, performing a total of 169 stable isotope analyses. The $\delta^{13}C$ and $\delta^{18}O$ analyses were determined with an automated carbonate preparation device (GasBench II) connected to a Delta V Advantage (Thermo Fisher Scientific Inc.) isotope ratio mass spectrometer at the Earth Sciences Department *Ardito Desio*, University of Milan (Italy). Carbonate powders were reacted with > 99% orthophosphoric acid at 70ºC. The carbon and oxygen stable isotope compositions are expressed in the conventional delta notation calibrated to the Vienna Pee-Dee Belemnite (V-PDB) scale by the international standards IAEA-603 and NBS-18 and an internal laboratory standard. Analytical reproductibility for these analyses, being checked by repeated analyses of the certified carbonate standards and after ten consecutively isotopic measurements, was better than ± 0.1‰ for both $\delta^{13}C$ and $\delta^{18}O$ values.

4. GEOLOGICAL SETTING

CHAPTER

4

GEOLOGICAL SETTING

4.1. TECTONO-SEDIMENTARY EVOLUTION OF THE IBERIAN BASIN

The Iberian Basin, also referred to as the Iberian intra-cratonic Rift System, forms part of the network of rifted basins that developed in the northwestern margin of the Tethyan realm during the Late Permian and Mesozoic (Salas et al., 2001). This basin was situated in the northeastern areas of the Iberian Plate, east of an emerged land-mass of the Iberian Massif, facing the Tethys Ocean to the east (Dercourt et al., 1993) (Fig. 4.1a). During the Late Jurassic, this basin was temporally connected to the north with the Basque-Cantabrian Basin along the Soria Seaway, bounded in northeastern areas by the Ebro Massif (Bulard, 1972).

The sedimentary evolution of the Iberian Basin during the Late Permian and Mesozoic was controlled by two major syn-rift episodes: Late Permian-Triassic and Late Jurassic-Early Cretaceous (Salas et al., 2001), each followed by a period characterized by thermal subsidence (post-rift stage). During the first (Late Permian-Triassic) syn-rift episode, sedimentation was controlled by late-Variscan major faults (Arthaud and Matte, 1977; Esteban and Robles, 1979; Vegas and Banda, 1982), and included from continental red-beds (Permian, Triassic Buntsandstein facies) to coastal-shallow marine carbonates and evaporites (Muschelkalk and Keuper facies) towards the east. This rifting event was followed by a Jurassic post-rift period (Hettangian-Oxfordian), which was characterized by regional thermal subsidence and the establishment of wide carbonate platforms.

The second syn-rift stage (Kimmeridgian–mid-Albian) concurs with the northward propagation of the Central Atlantic rifting and the gradual opening of the Western Tethys (Salas et al., 2001). In the Iberian Basin, this rifting event generated the progressive individualization of several subsiding domains in eastern and southern areas of the basin, i.e. Cameros, Maestrazgo, Columbretes, Valencia and Cuenca basins, which are in turn divided into successive depocentres or sub-basins (Salas and Guimerà. 1996; Aurell et al., 2019b; Liesa et al., 2019), bounded by NW dominant-orientated late- and post-Variscan strike-slip and Triassic normal faults (e.g. Álvaro et al., 1979; Salas and Casas, 1993; Liesa et al., 2006). Two pulses of rapid subsidence are distinguished during this second rifting episode: Late Jurassic-earliest Cretaceous (Kimmeridgian-Berriasian: syn-rift sequence 1 in Liesa et al., 2019; Fig. 4.1b, c) and Early Cretaceous (Valanginian-early Albian: syn-rift sequence 2; Fig. 4.1d, e), interrupted by a period of decelerated subsidence around the Berriasian-Valanginian transition.

During most of the Kimmeridgian, at the onset of the sedimentation of the syn-rift sequence 1, the palaeogeographic reconfiguration of the Iberian Basin together with the transgressive events led to the development of wide carbonate ramps facing the Tethys Ocean eastwards (e.g. Aurell et al., 2003). During the late Kimmeridgian, the oncolitic, peloidal and skeletal carbonates of the Higueruelas Fm formed in the shallow domains of the ramp, including the area studied in this Thesis south of the city of Zaragoza (Fig. 4.1b). The coeval down-dip (i.e. eastwards) successions of the Higueruelas Fm consist of a rhythmic alternation of marls and lime mudstones accumulated in middle- to outer-ramp areas (i.e. Loriguilla Fm; e.g. Aurell et al., 2010).

The Higueruelas Fm is regarded to be deposited during a stage with no significant differential tectonic activity (e.g. Aurell et al., 2010, 2019a), and therefore sedimentation occurred under relatively homogeneous subsidence. An increase in the tectonic activity around the Kimmeridgian-Tithonian transition resulted in the fragmentation of the wide Late Jurassic carbonate ramps by reactivated or newly formed major normal faults, and the development of the Maestrazgo and Valencia basins, and related sub-basins (Aurell et al., 2019a; Liesa et al., 2019) (Fig. 4.1c). As a consequence of a coeval considerable basinward shift of the coastline, related to the uplift and emersion of the western margin of the Iberian Basin, sedimentation became restricted to the Maestrazgo and Valencia basins within coastal to shallow-marine environments (e.g. Aurell et al., 2016, 2019a).

During early stages of the syn-rift sequence 2 (Valanginian-early Albian), structural compartmentalization gave rise to the development of the Cuenca Basin. Continental clastic and carbonate sedimentation dominated in subsiding areas located to the east and northwest of the Maestrazgo and Valencia basins and in the Cuenca Basin (i.e. *Weald* facies; e.g. García-Ramos, 1985; Soria et al., 1995; Soria, 1997; Salas et al., 2001; Liesa et al., 2006; Meléndez et al., 2009; Aurell et al., 2016; Liesa et al., 2019) (Fig. 4.1d). During the late Barremian to mid-Albian, shallow carbonate platforms developed in the Maestrazgo and Valencia basins (i.e. Urgonian facies; e.g. Bover-Arnal et al., 2010; Liesa et al., 2019) (Fig. 4.1e), and siliciclastic-dominated transitional realms occurred to the west, in marginal areas of the Cuenca, Valencia and Maestrazgo basins. This sedimentary evolution reflects a major transgression event which has been associated to large-scale transgressive-regressive cycles (e.g. Salas et al., 2001; Peropadre, 2012; Peropadre et al., 2013).

Sedimentation during the Late Cretaceous post-rift stage in wide areas of the central Iberian Basin is characterized by continental (fluvial, eolian) deposits of the Utrillas Group (e.g. Rodríguez-López et al., 2008, 2012), and the overlying Upper Cretaceous marine carbonate deposits, reflecting a major transgression event. At the end of the Cretaceous, the tectonic regime turned to compressional (Alpine Orogeny; Guimerà, 1984; Guimerà and Álvaro, 1990; Vergés and García-Senz, 2001). As a consequence, the normal faults operating during the Mesozoic extensional phase were reactivated as reverse faults and thrust belts, giving rise to the inversion of the Iberian Basin into the so-called Iberian Range (Álvaro et al., 1979; Cortés Gracia and Casas Sainz, 1996). This deformation lasted from middle Eocene to middle Miocene, with a phase of intense tectonic activity during the late Oligocene (Guimerà and Álvaro, 1990; Capote et al., 2002). The Neogene post-orogenic extension and subsequent erosion of these deformed structures constituted the current configuration of the Iberian Range (Simón, 1989), which is traditionally divided into five major morphostructural domains: Cameros-Demanda Massif, Aragonian Range, Castillian Range, Maestrazgo-Levantine sector and Altomira and Cuenca Ranges (Fig. 4.2).

The Upper Jurassic shallow-marine deposits studied in this Thesis are well exposed in the outcrops located in the Aragonian Range, on the flanks of a system of E-W and NW-SE orientated anticlines (see Fig. 3.1 in Chapter 3). Here, deformed Jurassic rocks constituted paleo-reliefs during the Cenozoic sedimentation, whose erosion contributed in part to the infill of the inter-mountain and marginal depressed areas (e.g. González et al., 1991).

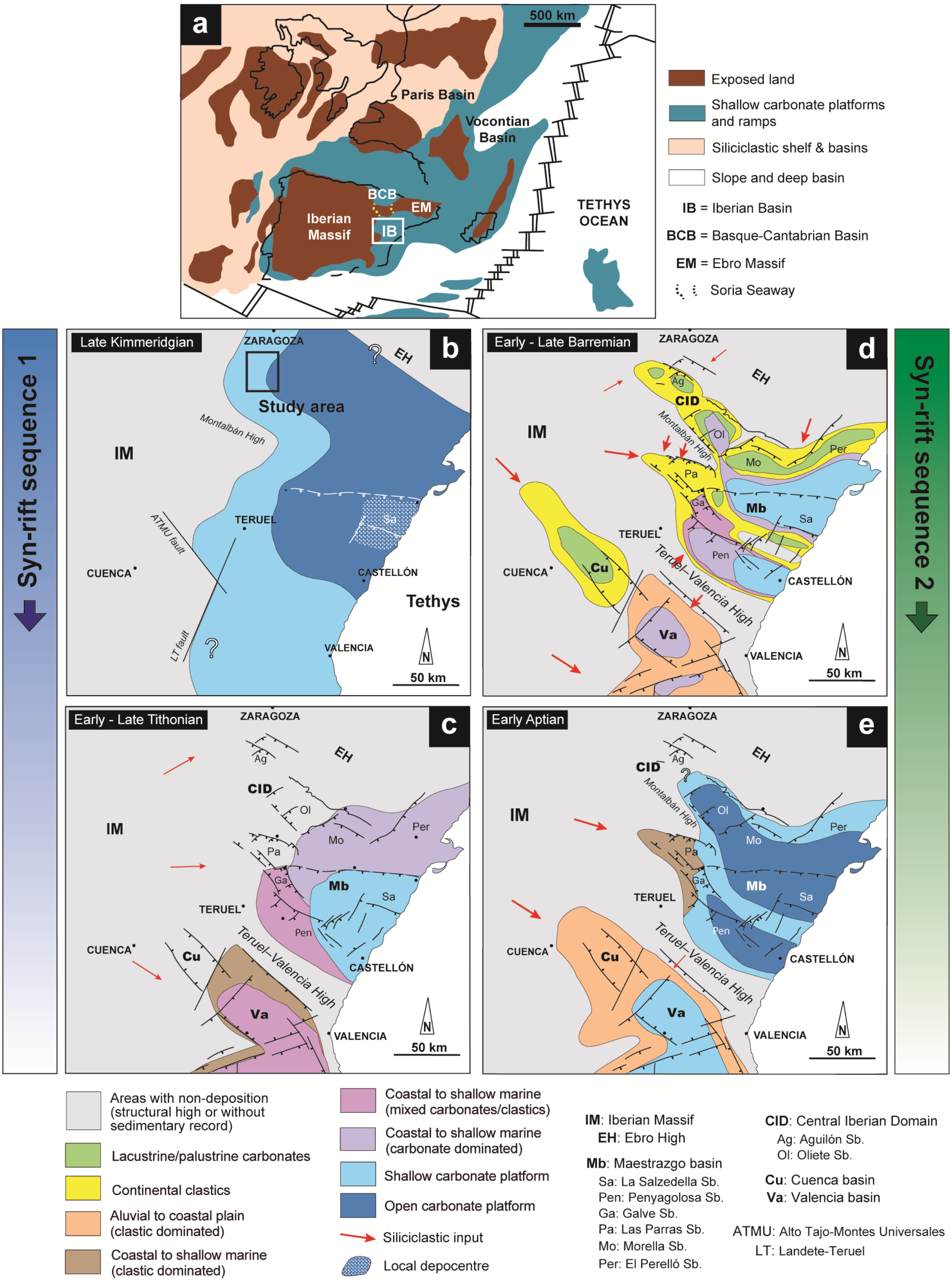

Fig. 4.1. *a) Palaeogeographic reconstruction of western Europe during the Late Jurassic (modified from Dercourt et al., 1993), with the location of the Iberian Basin (IB). b-e) Palaeogeographic maps showing the evolution of the Iberian Basin during the rifting episodes from the late Kimmeridgian to early Aptian times (modified from Liesa et al., 2019). The shallow-marine carbonates studied in this Thesis (see black square in b) were deposited under relatively homogeneous subsidence, prior to the individualization of the Iberian Basin in separated subsiding domains (c-e).*

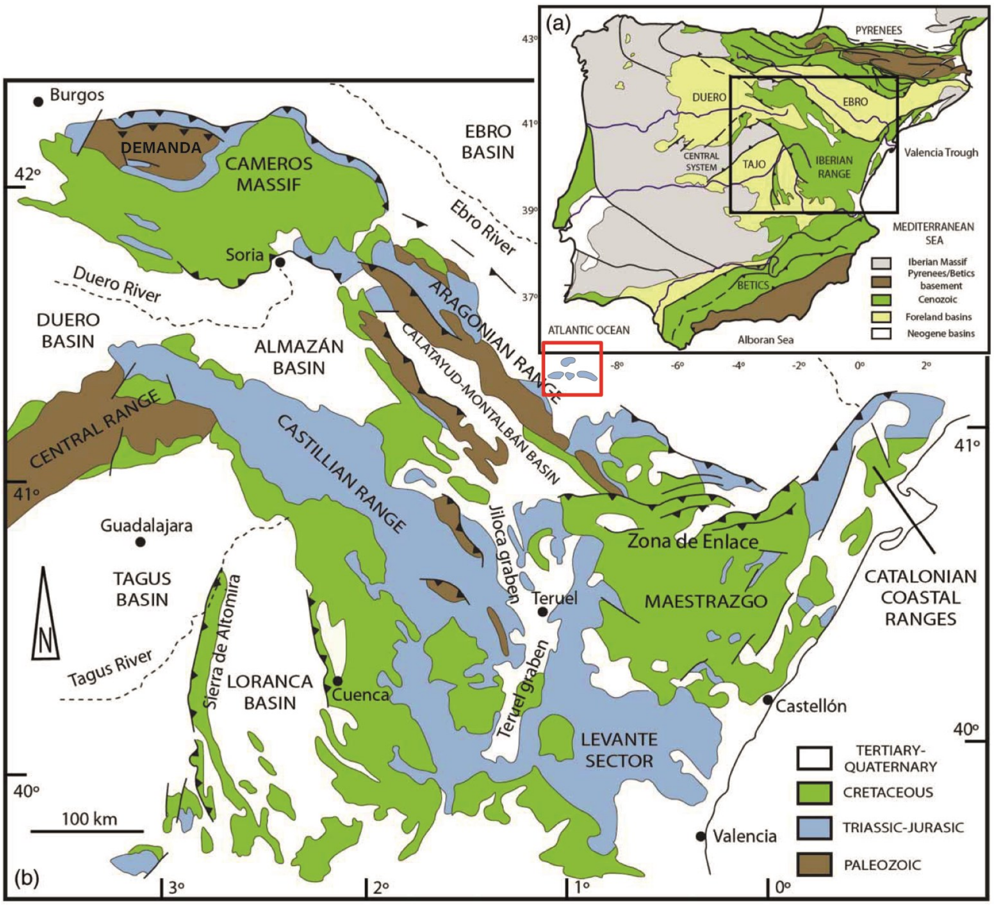

Fig. 4.2. Distribution of main lithological units and morphostructural parts of the Iberian Range: Cameros-Demanda Massif (NW), Aragonian Range (NE), Castillian Range (SW), Maestrazgo-Levantine sector (SE) and Altomira and Cuenca Ranges (SW) (adapted from Pueyo et al., 2015 after Liesa and Simón, 2009). The red square indicates the location of the studied outcrops.

4.2. UPPER JURASSIC SEDIMENTARY SUCCESSIONS IN THE NORTHERN IBERIAN BASIN: AN UPDATED STRATIGRAPHIC FRAMEWORK

The stratigraphy of the Upper Jurassic units outcropping in the northern Iberian Chain has been re -evaluated over the last years. The extensional tectonic deformation operating during the Late Jurassic-Early Cretaceous syn-rift cycle resulted in rapid lateral facies and thickness changes, thus complicating the analysis and correlation of the continental to shallow-marine successions (Aurell et al., 2019a). The improvement in the stratigraphic interpretation and age calibration of the lithostratigraphic units has been favoured by different factors, including: 1) the detailed analyses of a large number of closely-spaced outcrops, obtaining more information about the stratigraphy and sedimentary evolution of the Late Jurassic carbonate ramps from shallow to relatively distal domains; 2) the increasing availability and improved knowledge of the biostratigraphic data, comprising not only outer-ramp ammonites but also charophytes, sporomorphs and ostracods in coastal-continental settings, and some benthic foraminifera such as lituolids in shallow- to relatively distal ramp environments; and 3) recently strontium isotope analyses on calcitic shells of shallow-water organisms (i.e. bivalves and brachiopods).

First interpretations about the distribution of the main Upper Jurassic genetic stratigraphic units of the northern Iberian Basin started with the definition of three depositional sequences bounded by major discontinuity surfaces, which are included in the long-term Upper Jurassic transgressive-regressive cycle (Fig. 4.3a). These were named Oxfordian, Kimmeridgian and Tithonian sequences (Giner, 1980; Salas, 1987; Aurell, 1991; Aurell and Meléndez, 1993). Within these sequences, the open-platform sedimentation is represented by the mid-outer ramp marls and limestones of the Yátova, Sot de Chera and Loriguilla formations, whereas shallow ramp facies are represented by the cross-bedded oolitic-siliciclastic shoals of the Pozuel Fm (also referred as Ricla Mb; e.g. Bádenas and Aurell, 2001a; Bádenas et al., 2005), the oncolitic, peloidal and skeletal facies of the Higueruelas Fm, and the skeletal and oolitic mud- to grain-supported facies of the Bovalar Fm. The Higueruelas Fm was considered as belonging to the Tithonian sequence, laterally equivalent to the Bovalar Fm, and overlapped by the upper Tithonian coastal to shallow-marine carbonate successions of the Villar del Arzobispo and La Pleta formations (e.g. Giner, 1980; Aurell, 1990; Aurell and Meléndez, 1993).

Further sequence stratigraphic work led to the definition of four Upper Jurassic depositional sequences in the northern proximal domains of the Iberian Basin, with the identification of two higher-order sequences, i.e. Kim1 and Kim2, in the Kimmeridgian-early Tithonian sequence or T-R cycle 3.2 in Aurell et al. (2003). In shallower domains, the sequence Kim1 ends with the deposition of the upper Kimmeridgian oolitic-siliciclastic deposits of the Pozuel Fm (Ricla Mb), whereas sequence Kim2 is represented by the upper Kimmeridgian-lower Tithonian reefal facies of the Torrecilla Fm (Fig. 4.3b; Bádenas et al., 1998; Bádenas, 1999; Aurell et al., 2000, 2003; Bádenas and Aurell, 2001a, b).

Subsequent works on sequence stratigraphy (e.g. Ipas et al., 2005; Bádenas and Aurell, 2008; Ramajo and Aurell, 2008; Aurell et al., 2010) resulted in the identification of five second- to third-order depositional sequences within the Upper Jurassic cycle (Fig. 4.3c): Ox, Kim1, Kim2, Ti1 and Ti2, with a mean time span from ca. 1.5 to 6.5 My. In this case, the early Berriasian interval was included within the Upper Jurassic cycle, due to the recognition of the benthic foraminifera *Anchispirocyclina lusitanica* (Egger) in the middle and upper part of the sequence Ti2 (Bovalar and La Pleta formations; Aurell et al., 2010). These five long-term depositional sequences have well-defined retrogradational-progradational facies evolution patterns. In the Oxfordian sequence, shallow siliciclastic-carbonate facies prograded over sponge-rich mid-outer ramp facies of the Yátova Fm, with the local development of peloidal-glauconitic facies in the upper part of the unit. The cross-bedded oolitic shoal facies (Ricla Mb) and the coral-microbial reefs (Torrecilla Fm) which characterize the shallow domains of the Kimmeridgian Kim1 and Kim2 sequences, grade down dip into the mid-outer ramp marls and lime mudstones of the Sot de Chera and Loriguilla formations, and further offshore into the rich-ammonite limestones and marls of the Calanda Mb. The Tithonian-early Berriasian interval includes the Ti1 and Ti2 sequences, with significant differences concerning the geometry and facies architecture (Aurell et al., 2010). The shallow oncolitic, peloidal and skeletal facies of the Higueruelas Fm belong to the lower Tithonian Ti1 sequence, whose thickness slightly increases basinwards, reflecting a relatively homogenous subsidence (e.g. Aurell et al., 2003). In the lower part of the sequence Ti1, the Higueruelas Fm grades laterally into the shallow-marine grain-supported peloidal and skeletal limestones of the Alacón Mb. The onset of the sequence Ti2 (middle Tithonian-early Berriasian), referred to as *Purbeck facies* in previous works (e.g. Canérot, 1974; Meléndez et al., 1979; Gautier, 1980, 1981), is related to a major change in tectonic activity, showing the carbonate successions significant changes in facies and thickness in the eastern areas of the basin. The siliciclastic influence is remarkable at this stage of evolution of the carbonate ramp, with the progradation of coastal to shallow-marine carbonate-siliciclastic deposits (Villar del Arzobispo Fm) and intertidal algal-laminated facies (La Pleta Fm) in proximal areas, grading basinwards into shallow-marine oolitic and skeletal mud- to grain-supported facies (Bovalar Fm) (e.g. Bádenas et al., 2004; Ipas et al., 2005). The uppermost part of the sequence Ti2 (early Berriasian) is characterized by the onset of the lacustrine marl-dominated facies with charophytes of the Ladruñán Mb (e.g. Ipas et al., 2007; Aurell et al., 2010).

The most updated sequence stratigraphic scheme of the Kimmeridgian-Berriasian of the north-central Iberian Chain is that of Aurell et al. (2019b). This updated scheme has been based on the compilation of previous data combined with new data on the sedimentology, biostratigraphy and stable isotopes analyses in the Kimmeridgian-Berriasian successions recorded in four sub-basins of the western part of the central Iberian Rift System (Aguilón, Oliete, Morella and Galve sub-basins; Figs 4.3d and 4.4; see Fig. 4.1 for location). In particular, the age and lateral relationships of the shallow-water units have been constrained by the combination of benthic foraminifera (Ricla Mb, Torrecilla, Higueruelas, La Pleta, Bovalar, Cedrillas and Aguilar del Alfambra formations), charophytes (Ladruñán Mb, Aguilar del Alfambra and Galve formations), ostracods (Aguilar del Alfambra and Galve formations), sporomorphs (Galve Fm) and strontium isotopes (Torrecilla, Higueruelas, Cedrillas and Aguilar del Alfambra formations) (Fig. 4.4). Part of the newly data to achieve this updated stratigraphic scheme comes from the analysis of the Higueruelas Fm of the present Thesis.

Fig. 4.3 (Next page). *Evolution of the stratigraphy for the Late Jurassic in the northern Iberian Basin (adapted from Aurell et al., 2010). First interpretations started with the definition of three main genetic stratigraphic units (a; Oxfordian (1), Kimmeridgian (2) and Tithonian (3) sequences; e.g. Giner, 1980; Aurell and Meléndez, 1993), and were modified in subsequent works by the identification of five second- to third-order depositional sequences (b-c; Ox, Kim1, Kim2, Ti1 and Ti2; e.g. Bádenas, 1999; Aurell et al., 2003, 2010; Ipas et al., 2005; Bádenas and Aurell, 2008). The most updated sequence stratigraphic scheme is that of Aurell et al. (2019b) (d), based on new data from strontium isotopes and distribution of relevant biostratigraphic markers in the continental to shallow-marine units. See key localities in Aurell et al., 2010, 2019b.*

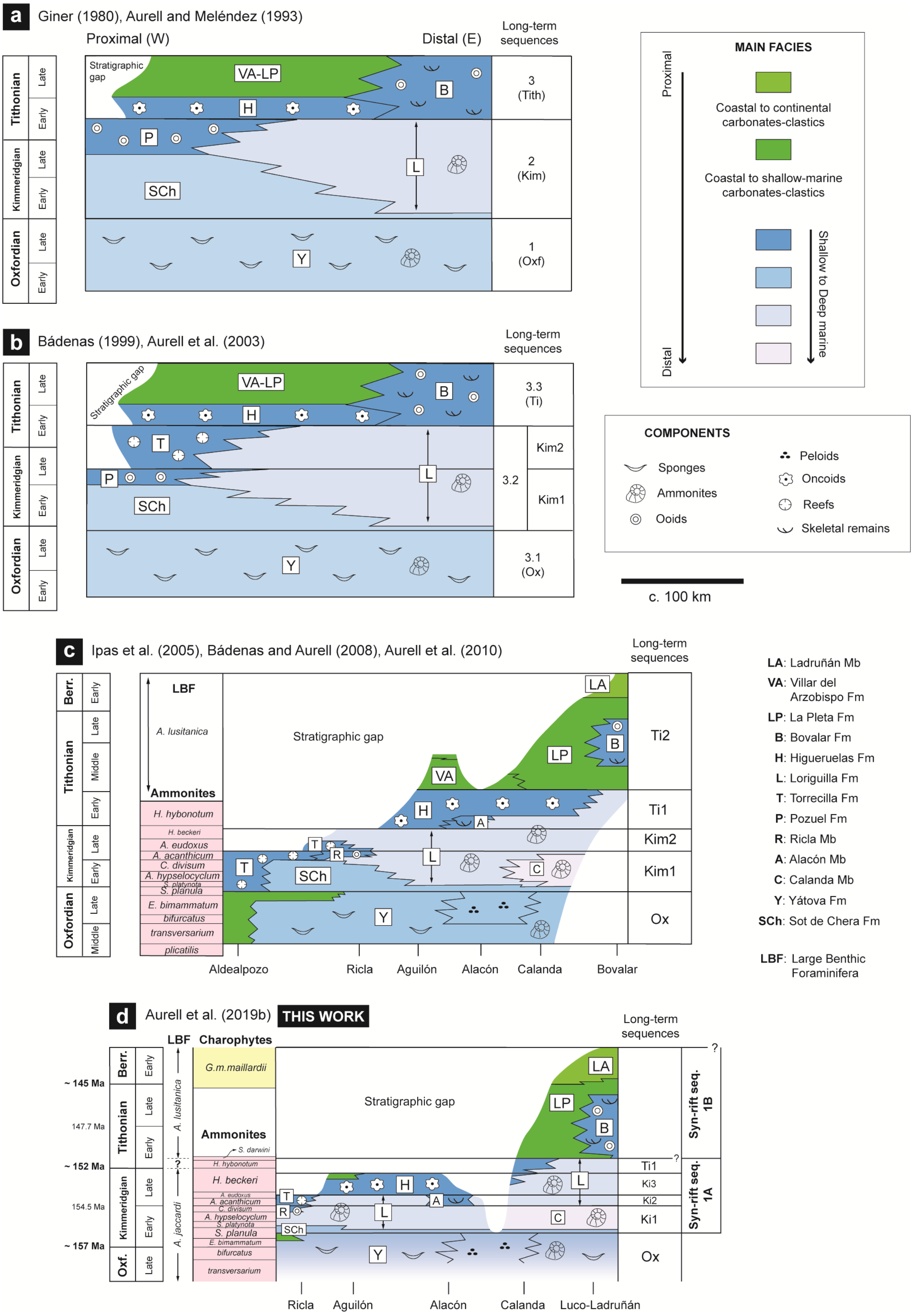
a
Giner (1980), Aurell and Meléndez (1993)
Proximal (W)
Distal (E)
Long-term sequences
Tithonian
Kimmeridgian
Oxfordian
Late
Early
Stratigraphic gap
VA-LP
B
H
P
L
SCh
Y
3 (Tith)
2 (Kim)
1 (Oxf)
b
Bádenas (1999), Aurell et al. (2003)
Stratigraphic gap
T
3.3 (Ti)
Kim2
3.2
Kim1
3.1 (Ox)
MAIN FACIES
Proximal
Distal
Coastal to continental carbonates-clastics
Coastal to shallow-marine carbonates-clastics
Shallow to Deep marine
COMPONENTS
Sponges
Ammonites
Ooids
Peloids
Oncoids
Reefs
Skeletal remains
c. 100 km
c
Ipas et al. (2005), Bádenas and Aurell (2008), Aurell et al. (2010)
Berr.
Middle
LBF
A. lusitanica
Ammonites
H. hybonotum
H. beckeri
A. eudoxus
A. acanthicum
C. divisum
A. hypselocyclum
S. platynota
S. planula
E. bimammatum
bifurcatus
transversarium
plicatilis
Stratigraphic gap
LA
LP
VA
A
R
C
Ti2
Ti1
Kim2
Kim1
Ox
Aldealpozo
Ricla
Aguilón
Alacón
Calanda
Bovalar
LA: Ladruñán Mb
VA: Villar del Arzobispo Fm
LP: La Pleta Fm
B: Bovalar Fm
H: Higueruelas Fm
L: Loriguilla Fm
T: Torrecilla Fm
P: Pozuel Fm
R: Ricla Mb
A: Alacón Mb
C: Calanda Mb
Y: Yátova Fm
SCh: Sot de Chera Fm
LBF: Large Benthic Foraminifera
d
Aurell et al. (2019b)
THIS WORK
LBF
Charophytes
G.m.maillardii
~ 145 Ma
147.7 Ma
~ 152 Ma
154.5 Ma
~ 157 Ma
Oxf.
A. jaccardi
S. darwini
Ki3
Ki2
Ki1
Syn-rift seq. 1B
Syn-rift seq. 1A
Luco-Ladruñán

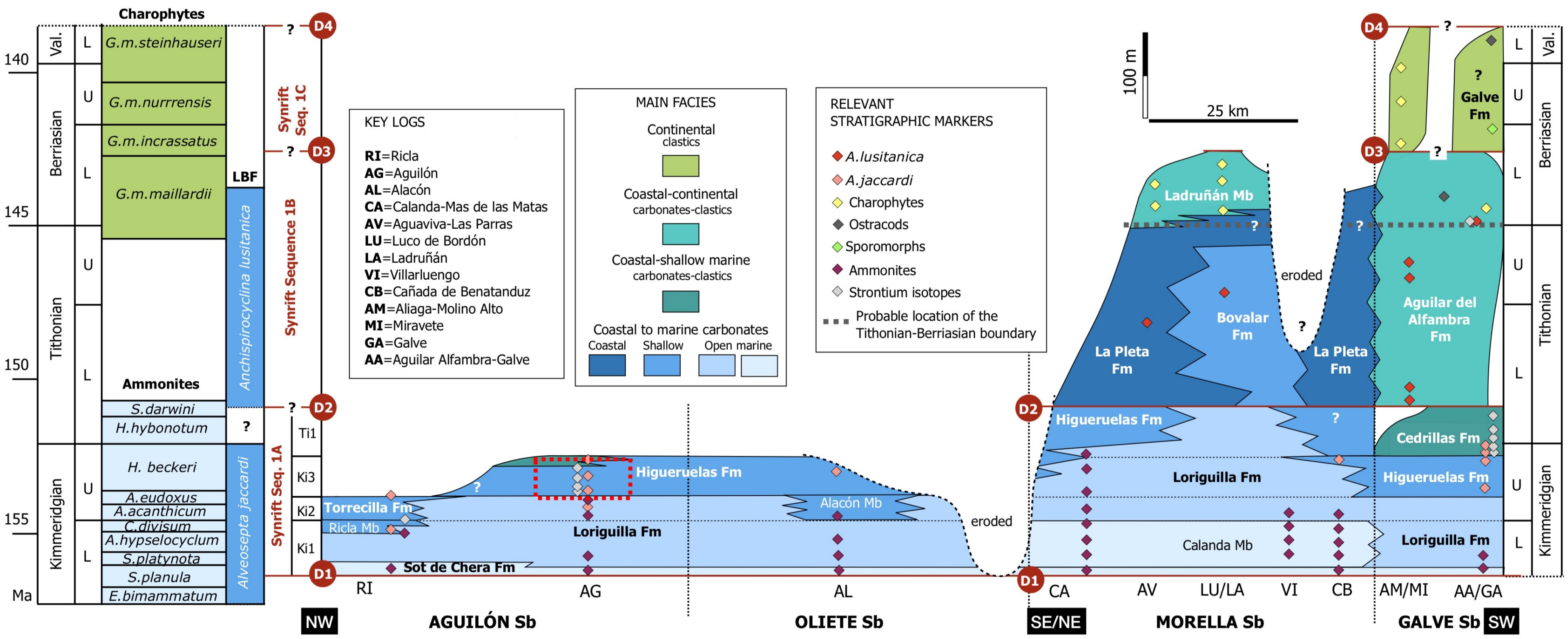

Fig. 4.4. *Chronostratigraphic scheme for the Kimmeridgian-Berriasian successions in the Aguilón, Oliete, Morella and Galve sub-basins (extracted from Aurell et al., 2019b). The red square indicates the shallow-marine deposits studied in the present Thesis. D1 to D4 refer to the major unconformities delimiting the three syn-rift sequences (1A, 1B and 1C). For location of the key logs, see Aurell et al. (2019b). Geological Time Scale according to Ogg et al. (2016).*

The Kimmeridgian-Berriasian successions are arranged in three syn-rift sequences (1A, 1B and 1C; Fig. 4.4) bounded by major unconformities (Liesa et al., 2019), which respond to significant changes in the sedimentary systems. The Kimmeridgian-early Tithonian syn-rift sequence 1A is characterized by the development of wide carbonate ramps in eastern Iberia (see Fig. 4.1b). The Kimmeridgian deposits are in turn divided into three depositional sequences, i.e. Ki1, Ki2 and Ki3, being the Higueruelas Fm represented in the sequence Ki3 (upper *eudoxus* and *beckeri* zones) in western areas of the basin (i.e. Aguilón, Oliete and Galve sectors; Fig. 4.4). This stratigraphic assignment is based on the record of the benthic foraminifera *Alveosepta jaccardi* (Schrodt) in the shallow-marine carbonate successions of the Ricla Mb, Torrecilla, Higueruelas and lowermost Cedrillas formations, combined with strontium isotope data from calcitic bivalve and brachiopod shells (part of these data compiled from Val et al., 2018, 2019), and the record of lower and mid-Kimmeridgian ammonites in the underlying Sot de Chera and Loriguilla formations and Calanda Mb (Geyer and Pelleduhn, 1979; Gautier, 1981; Atrops and Meléndez, 1984; Fezer and Geyer, 1988; Meléndez et al., 1990; Finkel, 1992; Pérez-Urresti et al., 1998; Bádenas et al., 2003; Moliner, 2009). In most of the Morella sub-basin (i.e. to the east, Calanda, Aguaviva-Las Parras and Cañada de Benatanduz sectors; Fig. 4.4), the Higueruelas Fm corresponds to the sequence Ti1 (*hybonotum* to lower *darwini* zones), based on the absence of *A. jaccardi* in this unit and on the record of earliest Tithonian ammonites in the uppermost part of the underlying Loriguilla Fm (Calanda area; Atrops and Meléndez, 1984).

The location of the Kimmeridgian-Tithonian boundary can be constrained by the last occurrence of *A. jaccardi* in the lowermost part of the coastal to shallow-marine siliciclastic deposits of the Cedrillas Fm in the Galve sector (which corresponds to the sequence Ti1), combined with strontium isotope data obtained from oyster shells (Val et al., 2019) (Fig. 4.4). This is also consistent with the presence of *A. jaccardi* and *Redmondellina powersi* (Redmond) in the uppermost part of the Higueruelas Fm in the Aguilón sector, and in the lower and middle part of the overlaying coastal-siliciclastic unit outcropping in this area (equivalent to the Cedrillas Fm), which corresponds to the upper part of the sequence Ki3. It is also worthy notice that the Cedrillas Fm is the new lithostratigraphic nomenclature described in the nearby Galve sub-basin by Aurell et al. (2019b) for the traditionally described Villar del Arzobispo Fm (e.g. Díaz-Molina and Yébenes, 1987; Aurell and Meléndez, 1993; Aurell et al., 1994; Ipas et al., 2007; Aurell et al., 2016), which was originally defined in the already independent Valencia Basin (e.g. Mas et al., 1984; Aurell et al., 2019a) (Fig. 4.1c).

During the Tithonian-early Berriasian syn-rift sequence 1B, there is a significant reduction of the sedimentation area (e.g. Liesa et al., 2019), which is restricted here to the Morella and Galve sub-basins (Fig. 4.4). The synsedimentary tectonics resulted in marked differences between the continental to shallow-marine successions recorded in these sub-basins, which mainly consisted on coastal mixed carbonate-siliciclastic deposits of the Aguilar del Alfambra Fm in the Galve sub-basin (e.g. Aurell et al., 2016; Bádenas et al., 2018), and continental, peritidal and shallow-marine carbonates of the Ladruñán Mb and La Pleta and Bovalar formations, respectively, in the Morella sub -basin. The age assignments of these units are well constrained by the record of the benthic foraminifera *Anchispirocyclina lusitanica* (Egger), strontium isotope data and the presence of key marker charophytes and ostracods. The onset of the laterally equivalent Aguilar del Alfambra, La Pleta and Bovalar formations occurs at the mid-early Tithonian, due to the first appearance of *A. lusitanica* in the lowermost levels of the Aguilar del Alfambra Fm in the Aliaga-Miravete sector (Galve sub-basin; Fig. 4.4). The record of this benthic foraminifera along the Aguilar del Alfambra Fm, together with strontium isotope data from oyster shells and the occurrence of key assemblages of ostracods and charophytes in the upper part of the unit (Aurell et al., 2016; see specimens in Aurell et al., 2019b), indicate that this formation spans from the mid-early Tithonian up to the early Berriasian (*Globator maillardii maillardii* zone). The position of the Tithonian-Berriasian boundary in the Morella sub-basin has been located around the transition from the peritidal carbonates of the La Pleta Fm and the marl-dominated succession of the Ladruñán Mb, which includes a rich charophyte assemblage of the latest Tithonian-early Berriasian *G.m.maillardii* zone (Canérot, 1974; Martín-Closas, 1989). In the Galve sub-basin, the Tithonian-Berriasian boundary is located in the upper part of the Aguilar del Alfambra Fm, being constrained by strontium isotopes from oyster shells combined with the first occurrence of key marker ostracods and charophytes (Aurell et al., 2016, 2019b; Bádenas et al., 2018).

Sedimentation became restricted to small isolated grabens and half-grabens in the Galve sub-basin during the syn-rift sequence 1C (Fig. 4.4), which is represented by the continental successions of the Galve Fm (Aurell et al., 2016), corresponding to red lutites with intercalated burrowed/cross-bedded sandstones, deposited in alluvial plains and related fluvial channels with overbank deposits. This unit has been tentatively assigned to the mid-Berriasian/mid-early Valanginian (*G.m. incrassatus* to most of *G.m. steinhauseri* zones), as indicated by the reported biostratigraphic association of key marker charophytes, ostracods (Aurell et al., 2016, 2019b) and sporomorphs (Santos et al., 2018).

In this Thesis, the biostratigraphic and chemostratigraphic analyses carried out in the shallow-marine carbonate succession of the Higueruelas Fm outcropping in the north-central part of the Iberian Chain (i.e. Aguilón sector; see Figs 4.2 and 4.4 for location), provided an accurate age calibration of the studied unit. As explained above, these deposits have been traditionally considered as early Tithonian in age (e.g. Aurell and Meléndez, 1993, Ipas et al., 2005; Aurell et al., 2010), or in more recent works as early-mid Kimmeridgian (Galve and Penyagolosa sectors; Campos-Soto et al., 2019). New data reported here used in the updated chronostratigraphic synthesis of Aurell et al. (2019b) included: (1) the distribution of relevant benthic foraminifera within the studied Higueruelas Fm, (2) new strontium isotope values obtained from well-preserved calcitic shells of bivalves and brachiopods, combined with (3) previous information based on the ammonite biostratigraphy of the underlying Loriguilla Fm. This set of data allowed to re-assign the age of the Higueruelas Fm in the studied sections (i.e. Mezalocha, Jaulín, Villanueva de Huerva, Tosos, Aguilón, Fuendetodos and Puebla de Albortón logs; Fig. 4.5) into latest Kimmeridgian. Specifically, the results of this chronostratigraphic approach have been supported by:

- The presence of mid-Kimmeridgian ammonites (i.e. *acanthicum/eudoxus* zones) in the mid-outer ramp facies of the underlying Loriguilla Fm (i.e. sequence Ki2) outcropping in the Aguilón sector. The key species correspond to *Progeronia breviceps* (Quenstedt) and *Aspidoceras longispinum apeninicum* (Sowerby) (Bádenas et al., 2003).

- The record of the benthic foraminifera *Alveosepta jaccardi* (Schrodt) all across the studied interval, which coexists with the benthic foraminifera *Redmondellina powersi* (Redmond) in the uppermost levels (Figs 4.5 and 4.6).

- The strontium isotope ($^{87}Sr/^{86}Sr$) data obtained from bivalves and brachiopods shells collected in some intervals of selected sedimentary logs (Puebla de Albortón, Fuendetodos and Tosos logs; Fig. 4.5). From the 12 samples collected for this analysis, only 4 samples were considered for age calibration (samples H1 to H4 in Fig. 4.5), since the rest of the samples showed anomaly values due to diagenetic processes (see Annexe 4 for the table gathering all the values). The isotopic values of the 4 selected samples show a slightly increasing trend across the studied unit from average 0.7069 up to 0.7070, which fits well with those recorded from the upper part of the *eudoxus* ammonite zone to most of the *beckeri* ammonite zone (i.e. latest Kimmeridgian), compared with the global strontium isotope curve described by Wierzbowski et al. (2017) after Gradstein et al. (2012) (Fig. 4.7). This age estimation also allows to determine the time span of the Higueruelas Fm in the studied area in 1.2 My (from 153.6 to 152.4 Ma).

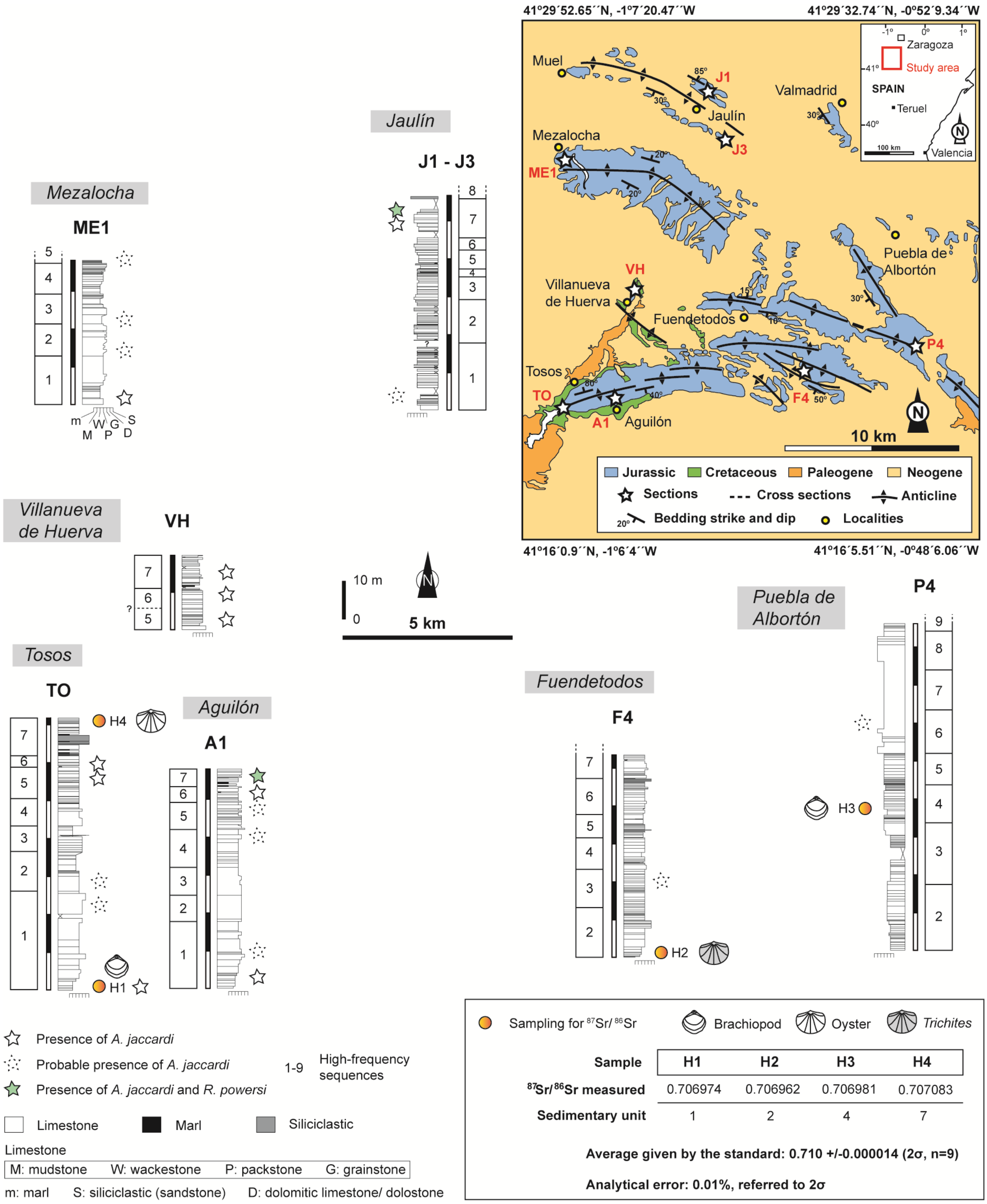

Fig. 4.5. *Location of the samples collected in studied sections of the Higueruelas Fm for the strontium isotope analyses performed in this Thesis (H1 to H4; isotopic values and the fossil type analysed are indicated), and distribution of the benthic foraminifera* Alveosepta jaccardi *(Schrodt) and* Redmondellina powersi *(Redmond) (modified from Aurell et al., 2019b). The position of the logs in the study area is indicated.*

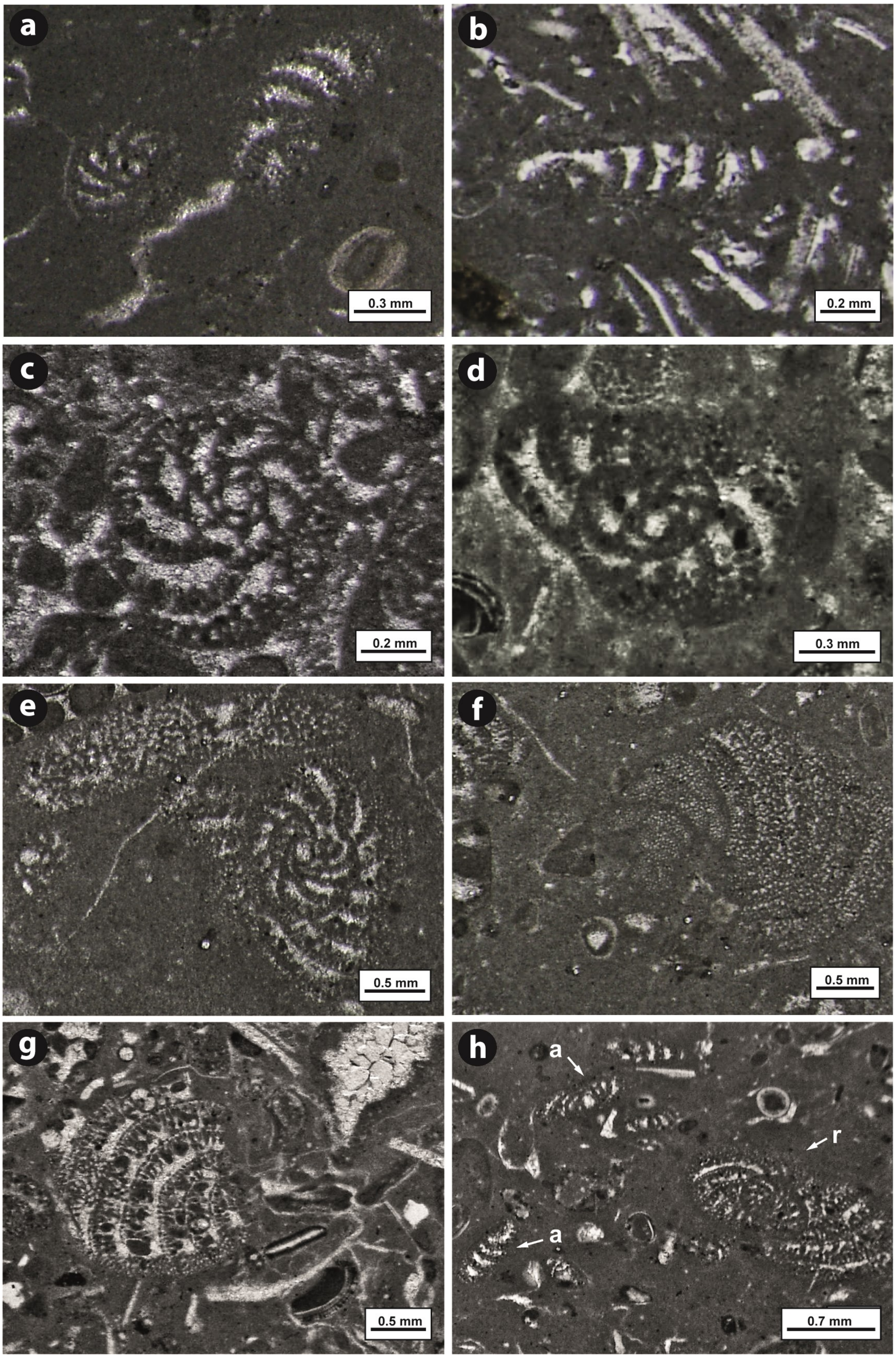

Fig. 4.6. Alveosepta jaccardi *(Schrodt) (a-d, h) and* Redmondellina powersi *(Redmond) (e-h) in the uppermost levels of the Higueruelas Fm in the studied sections. Notice the coexistence of* A. jaccardi *and* R. powersi *in (h) ("a" and "r", respectively). (a, e, f, h: sample J1-15; b: J1-7; c: VH-5; d, g: A1-80; see Annexe 1 for location).*

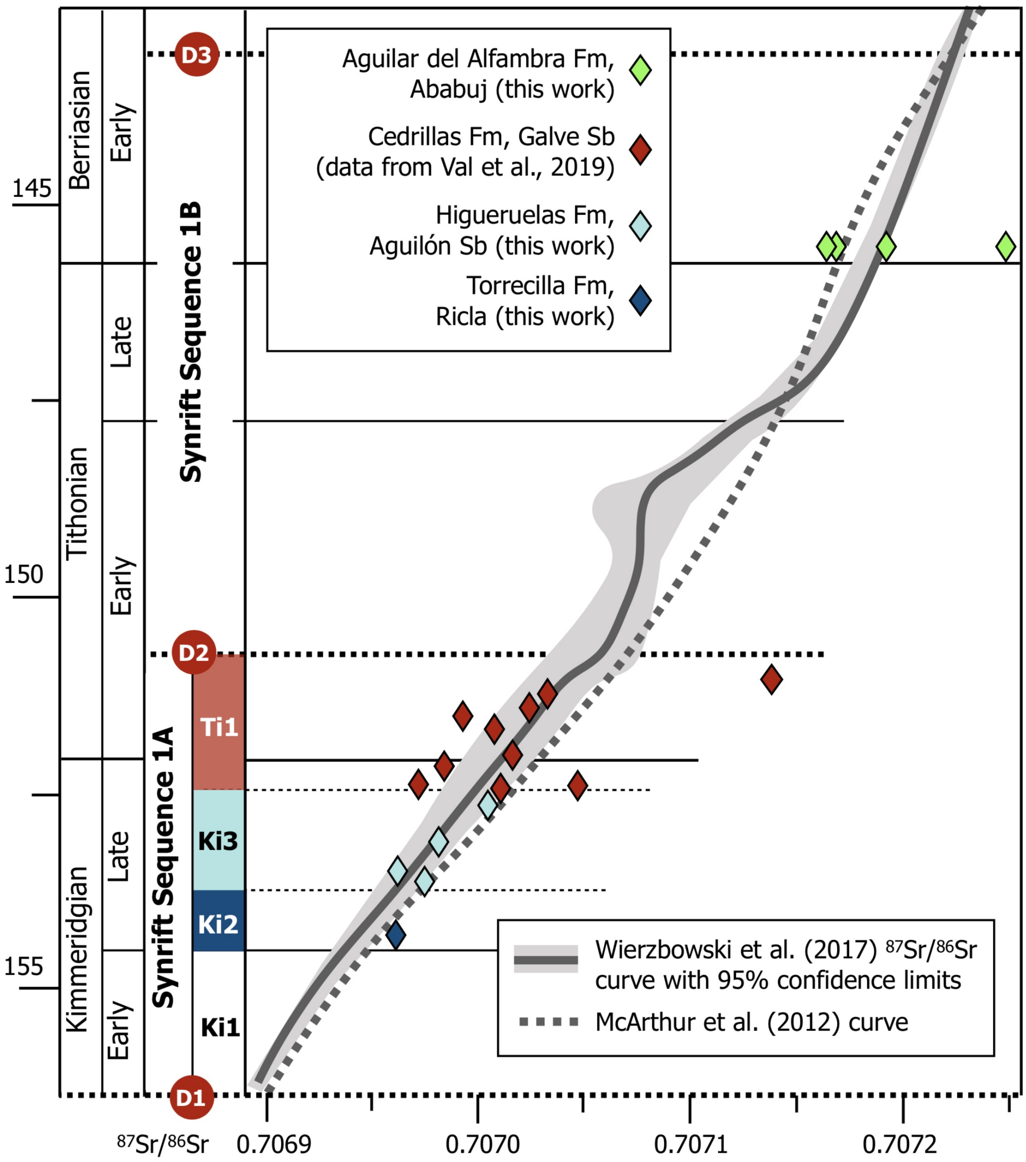

Fig. 4.7. Strontium isotope values obtained for the Kimmeridgian-early Berriasian units of the north-central Iberian Chain in Aurell et al. (2019b) (data obtained from bivalves and brachiopods shells), and comparison with the global strontium-isotopic curves of McArthur et al. (2012) and Wierzbowski et al. (2017) after Gradstein et al. (2012). The isotopic values obtained for the Higueruelas Fm (light-blue colour) fit well with the global isotopic trend of Wierzbowski et al. (2017) for the latest Kimmeridgian (i.e. sequence Ki3) (extracted from Aurell et al., 2019b).

Cretaceous Research 103 (2019) 104153

Contents lists available at ScienceDirect

Cretaceous Research

journal homepage: www.elsevier.com/locate/CretRes

Kimmeridgian–Berriasian stratigraphy and sedimentary evolution of the central Iberian Rift System (NE Spain)

M. Aurell [a, *], B. Bádenas [a], J.I. Canudo [a], D. Castanera [b], A. García-Penas [a], J.M. Gasca [a], C. Martín-Closas [c], L. Moliner [d], M. Moreno-Azanza [e, f], I. Rosales [g], L. Santas [a], C. Sequero [a], J. Val [a]

[a] Departamento Ciencias de la Tierra-IUCA, Universidad de Zaragoza, 50009, Zaragoza, Spain
[b] Institut Català de Paleontologia Miquel Crusafont, Universitat Autònoma de Barcelona, c/Escola Industrial 23, 08201, Sabadell, Barcelona, Spain
[c] Departament de Dinàmica de la Terra i de l'Oceà, Facultat de Ciències de la Terra, 08028, Barcelona, Spain
[d] Laboratorio ENSAYA, 50410, Cuarte de Huerva, Zaragoza, Spain
[e] Geobiotec, Departamento de Ciências da Terra, Universidade Nova de Lisboa, 2829-526 Caparica, Portugal
[f] GEAL Museu de Lourinhã, Lourinhã, Portugal
[g] Instituto Geológico y Minero de España (IGME), La Calera, 28760, Tres Cantos, Madrid, Spain

ARTICLE INFO

Article history:
Received 12 March 2019
Received in revised form
13 May 2019
Accepted in revised form 30 May 2019
Available online 5 June 2019

Keywords:
Tithonian
Berriasian
Iberia
Stratigraphy
Tectono-sedimentary evolution

ABSTRACT

Sequence-stratigraphic, biostratigraphic and strontium-isotopic data have made it possible to update what is known of the stratigraphy and sedimentary evolution of the Kimmeridgian–Berriasian synrift successions recorded in four subbasins (Aguilón, Oliete, Morella, Galve) of the central Iberian Rift System (NE Spain). The studied successions are arranged in three unconformity-bounded synrift sequences. Synrift sequence 1A (Kimmeridgian–mid-early Tithonian) includes four transgressive-regressive sequences deposited on low-angle carbonate ramps, characterized by shallow-water grain-supported facies and coeval open-marine rhythmic successions of marls and lime mudstones (overall thickness ranging from 120 to 250 m). Ammonite biostratigraphy, combined with the last occurrence of *Alveosepta jaccardi* (Schrodt) and strontium-isotopic data constrains the Kimmeridgian-Tithonian boundary towards the uppermost part of synrift sequence 1A. Synrift sequence 1B (mid-early Tithonian to mid-Berriasian) consists of coastal to shallow-marine carbonate to mixed carbonate-siliciclastic successions, with a continuous record in the depocentral areas of the Morella and Galve subbasins (up to 365 m in thickness). *Anchispirocyclina lusitanica* (Egger) is common in the lower and middle part of the sequence, whereas charophytes of the lower Berriasian *Globator maillardii maillardii* Zone are recorded in its upper part. Strontium-isotopic data and ostracods whose first occurrence is Berriasian, indicate that the Tithonian-Berriasian boundary is located towards the mid-upper part of the synrift sequence 1B. Synrift sequence 1C (mid-Berriasian–mid-early Valanginian) is locally recorded in the Galve subbasin and consists of siliciclastic continental successions (up to 100 m in thickness). The available biostratigraphic data (charophytes, ostracods, sporomorphs) indicate that this sequence was deposited upwards from early Berriasian *Globator maillardii incrassatus* Zone. The presence of the lower Valanginian successions at the upper part of synrift sequence 1C in certain subsiding areas of the Galve subbasin cannot be ruled out. The sequence-stratigraphic and biostratigraphic data reported here indicate that the Galve and Morella subbasins started to develop during the Kimmeridgian. Successive stages of tectonic activity affected these subbasins during the mid-early Tithonian, the mid-Berriasian, and around the Berriasian-Valanginian transition. The stratigraphy and tectono-sedimentary evolution of the central Iberian Rift System indicate that the Berriasian successions are linked to the “Jurassic cycle”.

1. Introduction

The problems associated with the definition of the Jurassic-Cretaceous system boundary are largely the result of a lack of significant biostratigraphic markers at the Tithonian-Berriasian and at the Berriasian-Valanginian boundaries, and of faunal provincialism

* Corresponding author.
E-mail address: maurell@unizar.es (M. Aurell).

https://doi.org/10.1016/j.cretres.2019.05.011
0195-6671/

caused by widespread regression (Remane, 1991). Due to this regression, the Tithonian-Berriasian saw major expansion of marginal-marine to continental environments, represented by *Purbeck* and *Weald* facies in many western European basins (e.g., Tennant et al., 2017). In the coeval Tethysian shallow-marine realms, sedimentation on "Jurassic-type" carbonate platforms (predominantly photozoan facies with occasional heterozoan carbonates) ended with the Berriasian, not with the Tithonian (Granier, 2019). Additional difficulties in unravelling the Tithonian–Berriasian sedimentary successions derive from the fact that many of them were deposited coeval to a rifting stage. The analysis and correlation of the continental to shallow-marine successions recorded in active rift basins is generally challenging due to the rapid facies and thickness changes associated with to discontinuous synsedimentary fault activity and subsidence.

The fragmentation of Pangea during the Late Jurassic–Early Cretaceous resulted in intense tectonic activity, on both regional and global scales, with accompanying palaeoceanographic changes including the continued of the opening of the Central Atlantic and Western Tethys (see Tennant et al., 2017 and references therein). The intracratonic Iberian Rift System was part of the network of rifted basins that evolved in the northwestern peri-Tethysian domain (Fig. 1A). Investigations into the southeast Iberian Rift System (i.e., the Maestrazgo Basin) in recent decades have contributed to a progressively increasing understanding of the stratigraphic framework of the Upper Jurassic–Lower Cretaceous synrift successions present in specific key areas at certain time intervals. In particular, the uppermost Jurassic–lowermost Cretaceous marginal-marine to shallow-marine successions of the Maestrazgo Basin have been studied in successive regional works (e.g. Canérot, 1974; Canérot et al., 1982; Salas, 1987; Martín-Closas, 1989; Aurell, 1990; Aurell et al., 1994, 2010, 2016; Salas et al., 2001; Bádenas et al., 2004, 2018; Cobos et al., 2010; Canudo et al., 2012; Campos-Soto et al., 2017, 2019; Liesa et al., 2019). In the western areas of the Maestrazgo Basin, the Tithonian-Berriasian boundary generally occurs within a carbonate to mixed-siliciclastic coastal succession referred to as *Purbeck facies* in pioneer studies (e.g., Canérot, 1974; Meléndez et al., 1979; Gautier, 1980, 1981), or as a *Tithonian–Berriasian Sequence* in later stratigraphic works (e.g., Salas, 1987; Aurell et al., 1994, 2010; Salas et al., 2001; Mas et al., 2004). In these regional studies, the Berriasian successions are traditionally included in the "Jurassic cycle", but the exact location of the Tithonian-Berriasian boundary cannot be established. However, recent reinterpretations based on larger benthic foraminifera biostratigraphy propose an older age for the sedimentation of this succession (mid-Kimmeridgian–Tithonian), questioning the presence of the Berriasian across the western Maestrazgo Basin (Campos-Soto et al., 2019).

The objective of the present work is to integrate the existing information with new sequence-stratigraphic, biostratigraphic (ammonites, benthic foraminifera, charophytes, ostracods) and strontium-isotopic data, providing a more precise account of the chronostratigraphic distribution of the sedimentary successions deposited during the Kimmeridgian–Berriasian in the central part of the Iberian Rift System. The facies distribution and sedimentary evolution documented here reflect the extensional tectonic activity affecting eastern Iberia during this time interval. In particular, the influence on the sedimentation and the nature of the unconformities that developed during successive stages of tectonic activity during the mid-early Tithonian, the mid-Berriasian and around the Berriasian-Valanginian transition have been further documented. Moreover, the reported data provide information about the location of the boundaries of both Tithonian and Berriasian stages within the shallow-marine, coastal to continental Iberian successions.

2. Geological setting

The Late Jurassic–Early Cretaceous rifting event affecting Iberia coincided with the rift propagation from the Central Atlantic northwards and with the opening of the Western Tethys (Salas et al., 2001). The Maestrazgo Basin of eastern Iberia was developed during this rifting event (Fig. 1A). This basin was divided into a set of well-differentiated depocentres (or subbasins) controlled by the synsedimentary activity of local normal faults, which were reactivated or formed during the Late Jurassic–Early Cretaceous rifting (Fig. 1B). The present stratigraphic work concerns the Kimmeridgian–Berriasian synrift successions recorded in four subbasins located in the western part of the Maestrazgo Basin: Aguilón, Oliete, Galve and Morella (Fig. 2A). The northern Aguilón and Oliete subbasins only recorded the Kimmeridgian succession, whereas the Morella and Galve subbasins include a more complete Tithonian–Berriasian succession (Fig. 2B).

The Upper Jurassic-Lower Cretaceous (Kimmeridgian–lower Albian) synrift successions recorded in the studied subbasins have been divided into two synrift sequences, separated by a major synrift unconformity associated with a wide erosional/non-depositional stratigraphic gap of variable amplitude around the Berriasian-Valanginian transition. The interpretation of Liesa et al. (2019) used here (Fig. 2B), updates previous interpretations in which this major synrift unconformity was considered older (i.e. mid-Berriasian: Liesa et al., 1996; Aurell et al., 2016). The lower synrift sequence 1 includes three tectono-sedimentary stages bounded by major unconformities (1A, 1B and 1C in Fig. 2B), with significant changes in the sedimentary systems that developed: (1A) open to shallow-marine Kimmeridgian–lowermost Tithonian carbonate-dominated ramps (e.g. Bádenas and Aurell, 2001; Aurell et al., 2010), (1B) Tithonian–mid-Berriasian coastal to shallow-marine carbonates-siliciclastics (e.g. Aurell et al., 1994), and (1C) locally recorded mid-Berriasian to lowermost Valanginian terrestrial siliciclastics (e.g. Aurell et al., 2016). According to Liesa et al. (2019), synrift sequence 2 also consists of three tectono-sedimentary stages (A, B and C in Fig. 2B) and includes the Valanginian–Barremian continental series or *Weald facies* (Soria et al., 1995; Salas et al., 2001), the uppermost Barremian–Aptian transitional to shallow carbonate platform successions or *Urgonian facies* (e.g. Bover-Arnal et al., 2010), and the lower Albian coal-rich succession of the Escucha Formation (e.g. Querol et al., 1992; Bover-Arnal et al., 2016).

3. Methods

The stratigraphic synthesis presented here is based on published and new data acquired from 36 key reference sections (Fig. 2A and Supplementary data S1), complemented with an extensive review of the available data on the Kimmeridgian–Berriasian successions in other areas of the central Iberian Rift System. In particular, the method of sequence stratigraphy (e.g. Catuneanu et al., 2011) was used in the study area to correlate facies and unconformity-bounded units at different scales, from high-frequency sequences to long-term transgressive-regressive sequences (e.g. Bádenas et al., 2003, 2004; Aurell et al., 2003, 2010; Bádenas and Aurell, 2018; Val et al., 2019). The results reported in these previous works are reviewed and summarized here.

Key intervals of some stratigraphic sections were sampled for strontium-isotopic analysis. Oyster, brachiopod and belemnite shells were collected. The $^{87}Sr/^{86}Sr$ isotopes were determined with a TIMS-Phoenix thermal ionization mass spectrometer at the *CAI Geocronología y Geoquímica Isotópica* of the Universidad Complutense de Madrid (Spain). All $^{87}Sr/^{86}Sr$ data were corrected for possible ^{87}Rb interferences and were normalised to a value of

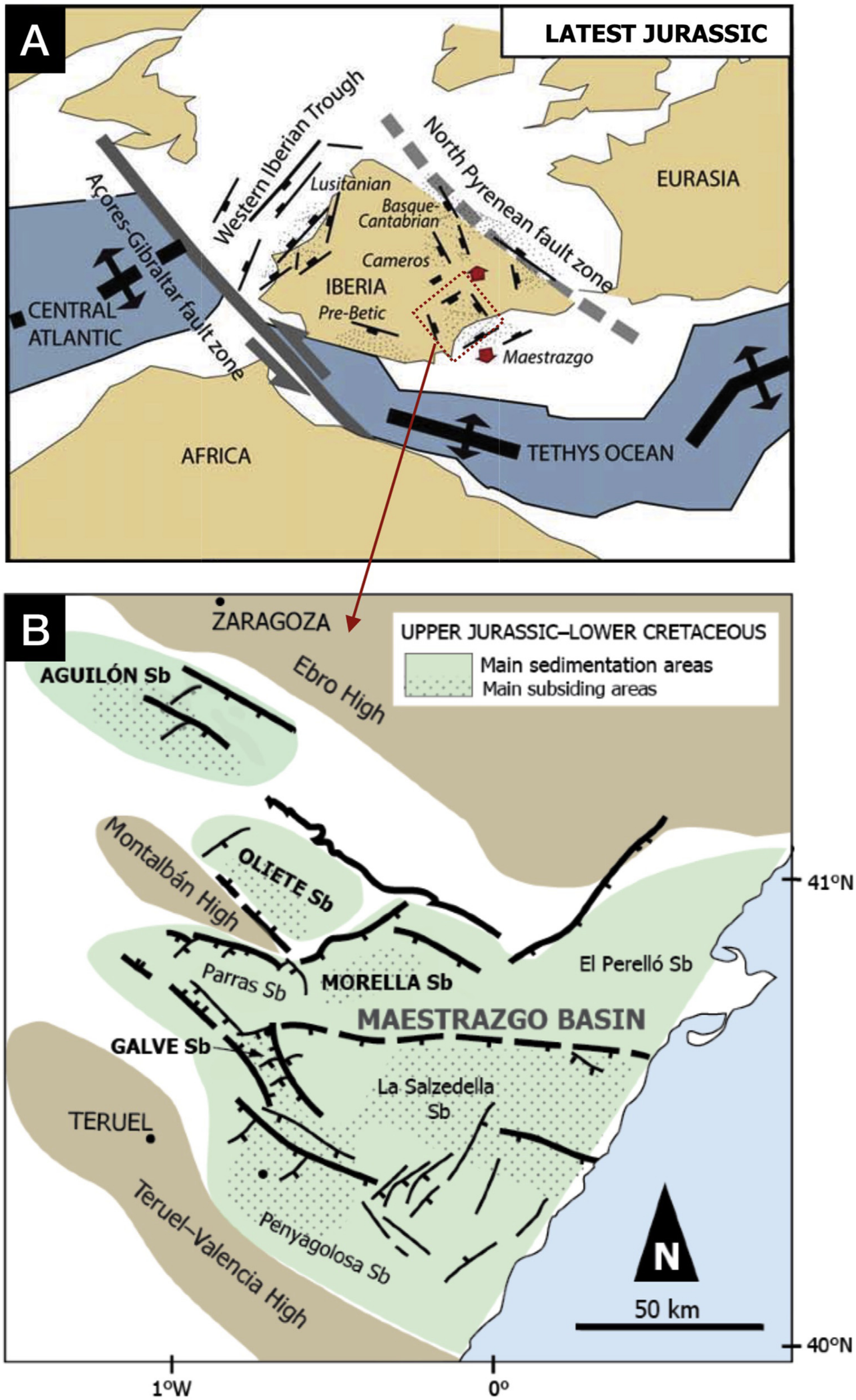

Fig. 1. Geological setting: (A) Location of Iberia in the Western Tethys in the latest Jurassic (modified from Liesa et al., 2019); (B) Location of the four studied subbasins, the Aguilón, Oliete, Morella and Galve, within the Maestrazgo Basin.

0.1194 for $^{87}Sr/^{86}Sr$ in order to correct possible mass-fractionation. During the period of analysis, the NBS-987 standard gave an average $^{87}Sr/^{86}Sr$ value of 0.710246 ± 0.000014 (2σ, $n = 9$), which was used to correct the measured values from a possible deviation referred to the standard. The analytical error of the $^{87}Sr/^{86}Sr$ ratio referred to 2σ was 0.01%. The comparison between the obtained

$^{87}Sr/^{86}Sr$ curve and the global marine $^{87}Sr/^{86}Sr$ curve defined for the Kimmeridgian–Berriasian (McArthur et al., 2012; Wierzbowski et al., 2017), together with biostratigraphical data have allowed a more precise age calibration of the studied units.

For micropaleontological analysis (i.e. ostracods, charophytes), surface bulk samples (1–3 kg) from promising lithologies (marly to mudstone levels) were taken from several sections of the ostracod/charophyte bearing units (i.e. Ladruñán Mb, Aguilar del Alfambra Fm, Galve Fm) in the Morella and Galve subbasins. Processing followed standard methods, treating the samples with water and 2% hydrogen peroxide. The samples were then washed through sieves (1000, 500 and eventually 125 μm mesh) and picked out under a binocular microscope. Selected specimens were scanned with a scanning electron microscope at the University of Zaragoza (JEOL 6400 SEM) and the University of Barcelona. Fossil specimens are housed in the Natural Science Museum of the University of Zaragoza, Spain (Museo de Ciencias Naturales de la Universidad de Zaragoza, MPZ).

4. Stratigraphy

The synthesis of the chronostratigraphic distribution and the correlation of the Kimmeridgian–lowermost Valanginian lithostratigraphic units across the four subbasins under study are shown in Fig. 3. The proposed correlation is the best-fit of the available biostratigraphic, isotopic and sequence-stratigraphic data and in many aspects updates previous stratigraphic interpretations.

The lower datum is the widespread discontinuity (D1) separating the prerift and synrift sequences (Fig. 2B). The age of this discontinuity is well constrained by ammonites in the middle part of the earliest Kimmeridgian *Subnebrodites planula* Zone, at the boundary between the *planula* and *galar* subzones (e.g. Salas et al., 2001; Aurell et al., 2003). In most of the central and eastern Iberian basins, the prerift sequence ends with a middle-upper Oxfordian 10–30 m thick succession of open-platform limestones and marls rich in siliceous sponges and ammonites, which laterally grades into shallow-marine carbonate-siliciclastic successions (e.g. Strasser et al., 2005; Ramajo and Aurell, 2008). The upper datum is the regional intra-rift unconformity (D4) located around the Berriasian-Valanginian transition on the basis of charophytes and foraminifers (e.g. Salas and Casas, 1993, 2001; Martín-Closas and Salas, 1994; Liesa et al., 2019), which corresponds to the boundary between the synrift sequences 1 and 2 (Figs. 2B and 3).

4.1. Aguilón subbasin

The Kimmeridgian successions recorded in the Aguilón subbasin show marked differences between the Ricla and Aguilón sectors (RI and AG: Fig. 3). The Upper Jurassic outcrops located north of the village of Ricla display a continuous exposure of the Kimmeridgian Ki1 and Ki2 sequences (Fig. 4A; Bádenas et al., 2005). These two sequences have a long-term transgressive-regressive facies evolution and are bounded by sedimentary discontinuities that can be traced at basin scale (e.g. Bádenas and Aurell, 2001; Aurell et al., 2010). In Ricla, the lower and middle part of the Ki1 sequence is represented by outer-ramp, marl-dominated successions (upper Sot de Chera Fm, c. 55 m thick) grading upwards to the middle-ramp, burrowed sandy limestones of the lower Loriguilla Fm (c. 60 m thick). The lower and middle part of the upper Sot de Chera Fm includes the ammonites *Sutneria galar* (Oppel) and *Orthosphinctes gigantoplex* (Quenstedt), and the boundary between the *planula* and *platynota* zones is assumed to be located towards the upper part of the Sot de Chera Fm (e.g. Colombié et al., 2014). The upper regressive stage of the Ki1 sequence corresponds to prograding shallow-platform deposits represented by the up to 30 m thick wedge-shaped oolitic-siliciclastic Ricla Mb (Bádenas et al., 2005; Kleipool et al., 2015). The Ricla Mb is bounded on top by a sharp sedimentary discontinuity that represents the Ki1-Ki2 sequence boundary. *Crussoliceras* sp. (early Kimmeridgian, *divisum* Zone) occurs c. 10 m below the Ricla Mb, and the boundary between the Ki1 and Ki2 sequences is assumed to be located near the early-late Kimmeridgian boundary (Val et al., 2017).

The thickness of the Ki2 sequence in Ricla ranges from 50 to 60 m. The sequence starts with a condensed limestone level rich in oncoids and skeletal grains, which has been related to a basinwide deepening event (Bádenas and Aurell, 2001). A new strontium-isotopic datum ($^{87}Sr/^{86}Sr = 0.706964$) from an oyster shell found in this condensed level is coherent with the occurrence of this flooding event at the onset of the late Kimmeridgian (Fig. 5). This condensed level is overlain by middle-ramp reefal limestones that grade distally into a lime mudstone succession (Torrecilla and upper Loriguilla formations, respectively; Bádenas et al., 2005). The skeletal levels found at the top of the Torrecilla Fm contain the benthic foraminifer *Alveosepta jaccardi* (Schrodt). This marine Kimmeridgian succession is overlain by upper Valanginian–Hauterivian continental clastics and carbonates (Soria et al., 1995; Fig. 2B).

The Kimmeridgian rocks form wide outcrops around the AG sector. There, the Ki1 and Ki2 sequences consist of outer ramp marls (Sot de Chera Fm) and lime mudstones (Loriguilla Fm), whereas the Ki3 sequence corresponds to the shallow-ramp carbonates of the Higueruelas Fm (Fig. 4B; Bádenas et al., 2003, 2005; Aurell et al., 2010; Sequero et al., 2018). The age of these sequences is constrained by ammonites, foraminifera and newly acquired strontium-isotopic data (Fig. 3, AG log).

The Ki1 sequence is formed by the marls of the Sot de Chera Fm (c. 50 m thick), including ammonites of the *galar* Subzone (Pérez-Urresti et al., 1998), and by the rhythmic alternation of silty lime mudstones and marls of the lower Loriguilla Fm (40–50 m thick) with scarce early Kimmeridgian ammonites (*Ataxioceratinae*). The Ki2 sequence is formed by up to 60 m of well-bedded lime mudstones of the upper Loriguilla Fm. Significant late Kimmeridgian ammonites found in this unit are *Progeronia breviceps* (Quenstedt) and *Aspidoceras longispinum apeninicum* (Sowerby). *Alveosepta jaccardi* is common in the uppermost part of the Loriguilla Fm (Bádenas et al., 2003).

The Ki3 sequence corresponds to the 50–80 m thick shallow-marine grain-supported peloidal, oncolitic and skeletal limestones of the Higueruelas Fm (see Supplementary data S2). The Higueruelas Fm was assigned in previous work to the lower Tithonian (Aurell, 1990; Ipas et al., 2007; Aurell et al., 2010). However, the record of *Alveosepta jaccardi* and *Redmondelllina powersi* (Redmond) in the uppermost levels of this unit (Fig. 6A and Supplementary data S2), combined with the ammonites found in the underlying Ki2 sequence, indicate that the Ki3 sequence (Higueruelas Fm) in the Aguilón sector was deposited during the late Kimmeridgian, most probably within the late *eudoxus* and *beckeri* zones. The strontium-isotopic ($^{87}Sr/^{86}Sr$) data obtained from some intervals of the logs of Puebla de Albortón, Fuendetodos and Tosos (logs 4, 6 and 7 in Fig. 2B; see Supplementary data S2) fit well with the global curve of Wierzbowski et al. (2017) during this late Kimmeridgian time interval (Fig. 5). In the area around Aguilón, the upper part of the Ki3 sequence locally consists of an up to 40–70 m thick siliciclastic succession with scarce intercalations of skeletal-rich carbonate beds (Ipas et al., 2007). The skeletal-rich beds found in the lower and middle parts of this siliciclastic-dominated succession still include the Kimmeridgian benthic foraminifera *A. jaccardi* and *R. powersi*. The upper boundary of the Ki3 sequence is an angular unconformity overlain by upper Valanginian–Hauterivian continental facies (Soria et al., 1995; Fig. 2B).

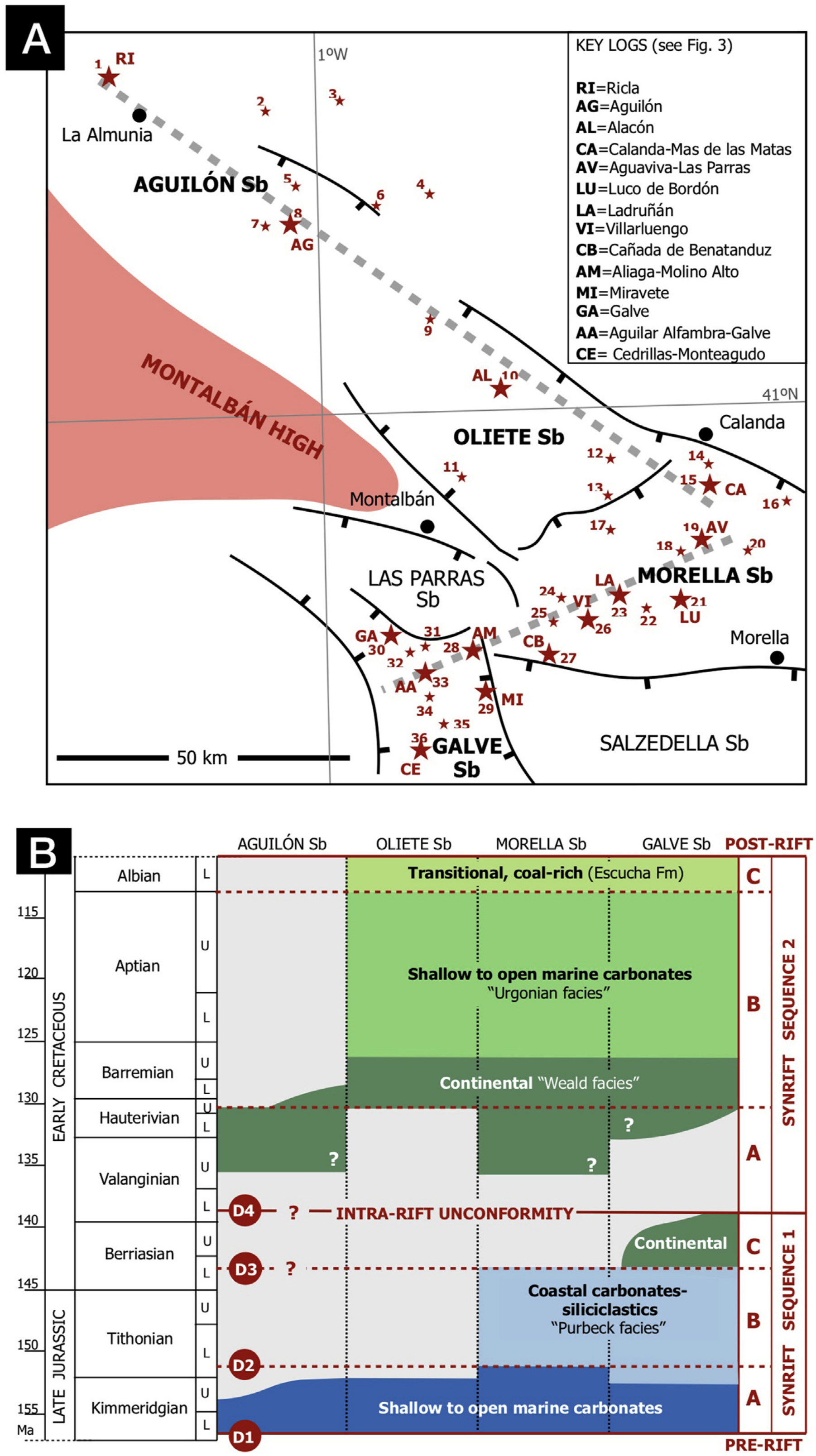

Fig. 2. (A) Distribution of the reference logs (see Supplementary data S1 for names of the logs and key references). The grey dashed line indicates the location of the correlation transect shown in Fig. 3; (B) Synthetic chronostratigraphic distribution of main facies and tectono-sedimentary sequences of the Kimmeridgian–Aptian in the Aguilón, Oliete, Morella and Galve subbasins (adapted from Liesa et al., 2019).

4.2. Oliete subbasin

The Oliete subbasin has an incomplete record of synrift sequence 1A (Fig. 3). During most of the Kimmeridgian, the southwestern area of this subbasin located near the Montalbán High was the deposition site of shallow-marine oolitic and reefal facies (Obón-Torre de las Arcas sector, number 11 in Fig. 2A; Aurell et al., 1999a). Towards the end of the Kimmeridgian, the southern area of the subbasin was eventually exposed and shallow-marine sedimentation became restricted to the north, around the locality of Alacón (AL) (Aurell et al., 2018).

In the more complete Kimmeridgian succession exposed around Alacón (AL log in Fig. 3), synrift sequence 1A includes the Ki1, Ki2 and Ki3 sequences that correspond to the Sot de Chera, Loriguilla, and Higueruelas formations. The Ki1 sequence is formed by the lower Kimmeridgian (*galar* Subzone) marls of the Sot de Chera Fm (up to 20 m thick) and the well-bedded lime mudstones and marls of the lower part of the Loriguilla Fm (c. 40 m). The latter is particularly rich in ammonites, allowing the *platynota* and *hypselocyclum/lothari* early Kimmeridgian ammonite zones to be identified (Moliner, 2009). The Ki2 sequence is represented by the shallow-ramp, grain-supported (peloidal, skeletal) limestones of the Alacón Mb (20–30 m thick). The lower part of this unit includes scarce ammonites from the early part of the late Kimmeridgian (Meléndez et al., 1990). The development of the shallow facies of the Alacón Mb was related to the influence of the Montalbán High (Cepriá et al., 2002). On top of this unit there is a level of pedogenic carbonate breccias developed during the subaerial exposure of the platform after the regional relative seal-level fall associated to the boundary between the Ki2 and Ki3 sequences (Fig. 4C; Aurell et al., 2010). The Ki3 sequence corresponds to the uppermost Kimmeridgian shallow-marine limestones of the Higueruelas Fm (up to 70 m thick). A major erosive unconformity and the associated stratigraphic gap are located above these shallow-marine Kimmeridgian rocks, which are directly overlain by the lower Barremian continental facies that characterizes the onset of the synrift sequence 2 sedimentation in the Oliete subbasin (Aurell et al., 2018; Fig. 2B).

4.3. Morella subbasin

The Kimmeridgian–Berriasian stratigraphy of the Morella subbasin shows marked differences with respect to the coeval sedimentary record in the northwestern Aguilón and the Oliete subbasins. In particular, the lower synrift sequence 1A has a complete record (up to the mid-early Tithonian) in the Morella subbasin, and the synrift sequence 1B is well developed in its depocentral areas (Fig. 3). In most of the northern and central area of the Morella subbasin studied here, the Berriasian successions are unconformably overlain by continental upper Valanginian–Hauterivian lacustrine limestones (Herbers Fm) or equivalent terrigenous continental units (e.g. Canérot, 1974; Gasca et al., 2017; Figs. 2D and 4D).

Synrift sequence 1A starts with the Ki1 sequence, which includes the marls of the Sot de Chera Fm (*galar* Subzone, up to 5 m thick across the whole subbasin) and a 10–30 m thick succession of limestones and marls (Calanda Mb), with a rich-ammonite record of the early Kimmeridgian *platynota*, *hypselocyclum/lothari,* and *divisum* zones (Geyer and Pelleduhn, 1979; Atrops and Meléndez, 1984; Fezer and Geyer, 1988; Meléndez et al., 1990; Finkel, 1992; Moliner, 2009). A prominent discontinuity (hardground) surface located on top of the condensed upper *divisum* Zone marks the boundary between the Ki1 and Ki2 sequences. The upper Kimmeridgian Ki2 and Ki3 sequences are generally represented by a continuous, 60–120 m thick succession of well-bedded, open-marine lime mudstones (Loriguilla Fm). In the outcrops located south of Calanda (CA log in Fig. 3), the upper Loriguilla Fm includes abundant siliceous sponges and ammonites of the *acanthicum*, *eudoxus* and *beckeri* zones (e.g. Geyer and Pelleduhn, 1979). In the Calanda-Val de la Piedra log (log 14 in Fig. 2A), the presence of earliest Tithonian (early *hybonotum* Zone) ammonites in the uppermost part of the Loriguilla Fm has been suggested (Atrops and Meléndez, 1984).

In the upper part of synrift sequence 1A, in the Calanda (CA) sector, most of the Ti1 sequence is formed by the shallow-marine limestones of the Higueruelas Fm (Fig. 3). In the Calanda-Mas de la Matas section (log 15 in Fig. 2A), the Higueruelas Fm consists of a 65 m thick succession of skeletal-peloidal-oncolitic grain-supported limestones, which are locally dolomitized (Aurell et al., 1999b).

In the Villarluengo and Cañada de Benatanduz sectors (see VI and CB in Fig. 3), the upper part of the Ki3 sequence and the Ti1 sequence are represented by thick-bedded limestones with grain-supported oncolitic-peloidal-skeletal facies typical of the Higueruelas Fm. The Kimmeridgian age of the lowermost part of the Higueruelas Fm is indicated by the presence of *Alveosepta jaccardi* in the CB log (log 27 in Fig. 2A).

Synrift sequence 1B is made up of shallow-marine to peritidal carbonate-dominated successions (partly dolomitic) in the Morella subbasin. These thick successions (200–300 m thick) were reported in previous regional stratigraphic analyses (Canérot, 1974; Salas, 1987; Martín-Closas, 1989; Aurell, 1990; Aurell et al., 2010) but were not logged in detail. The results of the logging performed here in three key localities of Aguaviva-Las Parras (AV), Luco de Bordón (LU) and Ladruñán (LA) are summarized in Fig. 7. Around the AV sector, synrift sequence 1B is represented by a 150–250 m thick succession dominated by peritidal, thin-bedded laminated cryptalgal limestones and lime mudstones typical of the La Pleta Fm. Around the LU/LA sector, these peritidal carbonates are located in the lower and upper parts of the sequence, whereas the middle part consists of thick-bedded, mud-to grain-supported shallow-marine carbonates typical of the Bovalar Fm (Fig. 4E). Synrift sequence 1B thus has a long-term transgressive/regressive trend, from the peritidal carbonates of the lower Pleta Fm, to the shallow-marine carbonates of the Bovalar Fm, including levels rich in the benthic foraminifer *Anchispirocyclina lusitanica* (Egger), to the peritidal carbonates of the upper Pleta Fm, and up to the continental to marine-marginal marl-dominated Ladruñán Mb (Fig. 3). In these depocentral areas of the Morella subbasin, the synrift sequence 1B consists of five correlatable units (see units 1–5 in Fig. 4E And 7), equivalent to the third-order sequences Ti2-1 to Ti2-5 defined in Aurell et al. (2010). These sequences show a transgressive-regressive or regressive facies evolution and are bounded by widespread sedimentary discontinuities. They display a range and sedimentary evolution comparable to the five third-order sequences 1–5 defined in Bádenas et al. (2004), located further east in the Montanejos and Salzedella sections (i.e. the southern Penyagolosa and Salzedella subbasins, see Fig. 1B).

The Ladruñán Mb includes charophytes of biostratigraphic interest. In particular, analysis of this unit in the localities of Jaganta and Ladruñán (logs 18 and 23 in Fig. 2A) has yielded *Dictyoclavator fieri* (Donze), *Nodosoclavator bradleyi* (Harris), and *Atopochara trivolvis* var. *horrida* (Harris), which characterize the latest Tithonian/mid-early Berriasian *Globator maillardii maillardii* Zone (Canérot, 1974; Martín-Closas, 1989; Riveline et al., 1996). The transition between the La Pleta Fm and the Ladruñán Mb is gradual and is assumed to occur around or above the Tithonian-Berriasian boundary (Fig. 3).

The carbonate successions of synrift sequence 1B are represented around the Cañada de Benatanduz (CB) sector by a 60–90 m thick succession of shallow-marine to thin-bedded peritidal

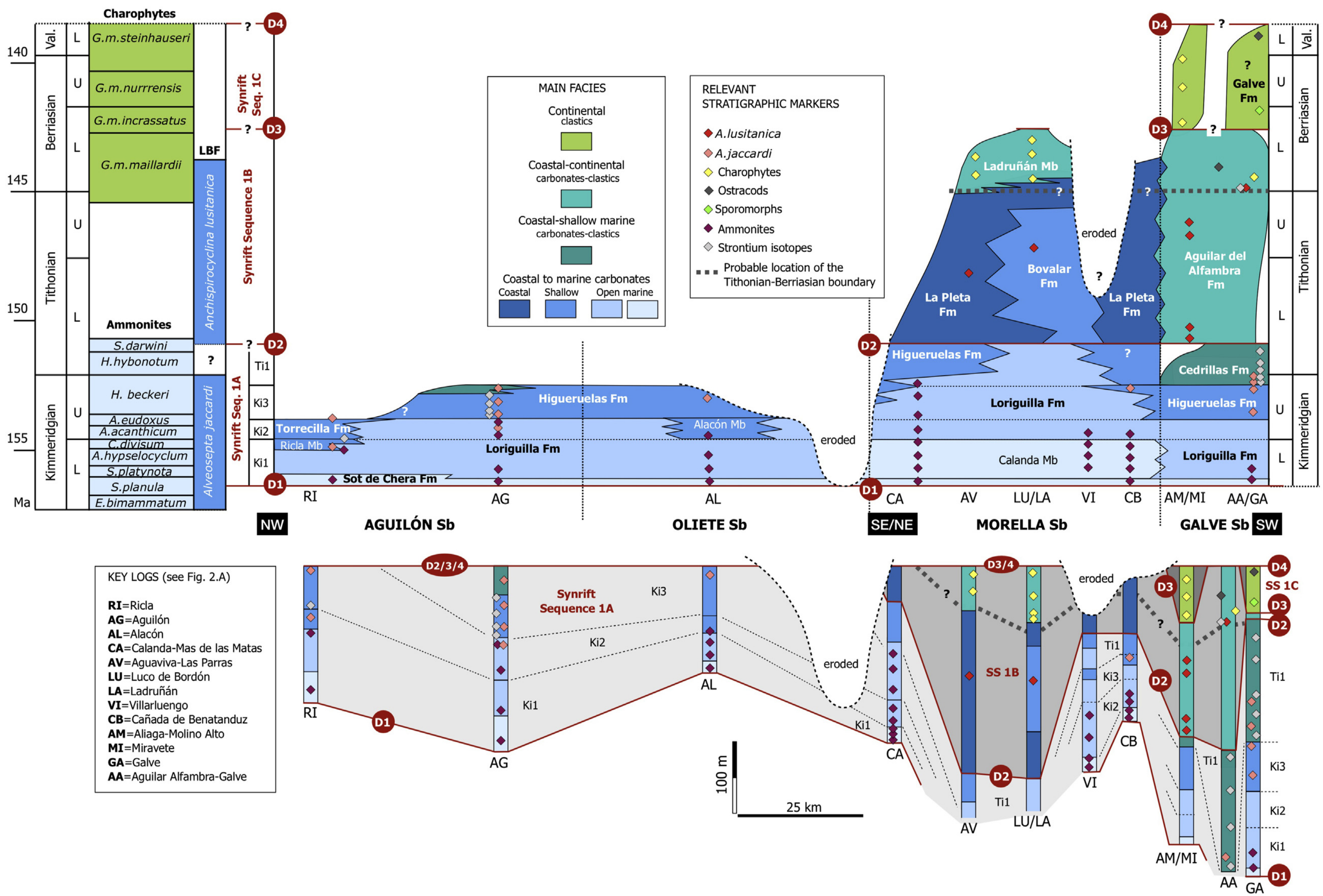

Fig. 3. Chronostratigraphic distribution of lithostratigraphic units of the Kimmeridgian–Berriasian of the Aguilón, Oliete, Morella and Galve subbasins. The lower part shows the thickness of lithostratigraphic units and the location of the relevant stratigraphic markers in the key logs (see Fig. 2A for location). In the upper part, the location of these stratigraphic markers within the unit is based in the assumption of constant average rates of sedimentation. The probable location of the Tithonian-Berriasian boundary in the mid-upper part of synrift sequence (SS) 1B is indicated with a grey dashed-line. The biostratigraphic ranges of the biozones used (ammonites, charophytes, larger benthic foraminifera (LBF)) are shown in the left part. Ammonites are found in the open-marine facies of synrift sequence 1A, foraminifera in the shallow-marine facies of synrift sequences 1A and 1B, and charophytes in the continental to marginal-marine facies of synrift sequences 1B and 1C. Geological Time Scale according to Ogg et al. (2016).

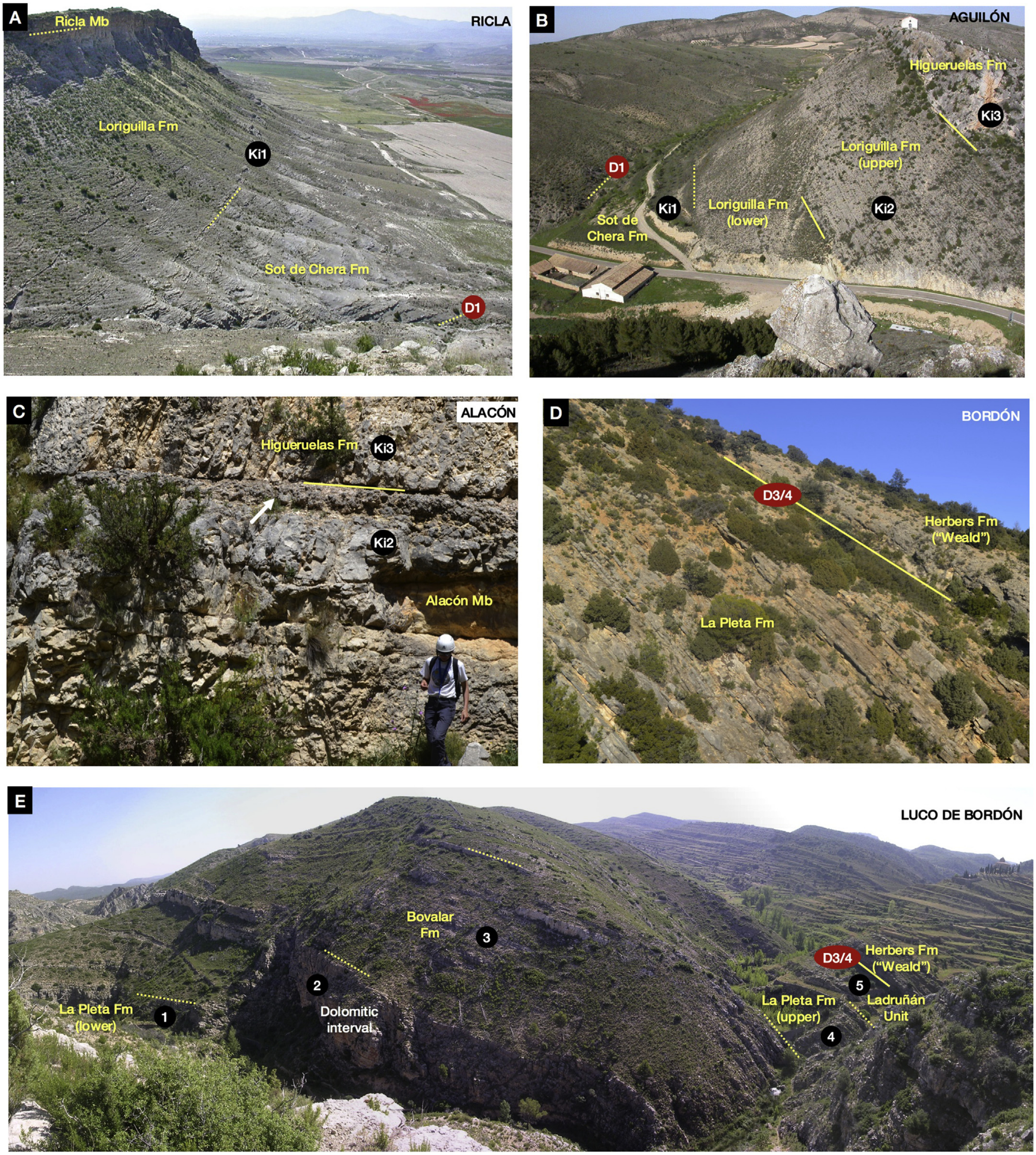

Fig. 4. (A) Distribution of lithostratigraphic units within the Ki1 sequence in Ricla (log 1 in Fig. 2A, Aguilón subbasin); (B) Distribution of lithostratigraphic units within the Ki1, Ki2, and Ki3 sequences in Aguilón (log 8 in Fig. 2A, Aguilón subbasin); (C) Soil development (see white arrow) indicating the subaerial exposure of the platform between the Ki2 and Ki3 sequences in Alacón (log 10 in Fig. 2A, Oliete subbasin); (D) Angular unconformity between the La Pleta Fm (synrift sequence 1B) and the upper Valanginian-Hauterivian lacustrine Herbers Fm in Bordón (log 22 in Fig. 2A, Morella subbasin); (E) Distribution of lithostratigraphic units in Luco de Bordón (log 22 in Fig. 2A). The boundaries of units 1–5 can be traced at regional scale (see Fig. 7).

carbonates attributed to the La Pleta Fm. Around the Villarluengo sector, synrift sequence 1B is poorly represented due to the erosion that occurred before the sedimentation of the continental Valanginian–Hauterivian successions (see VI in Fig. 3).

4.4. Galve subbasin

The Galve subbasin shows the most complete record of the studied synrift successions within the study area, because it also

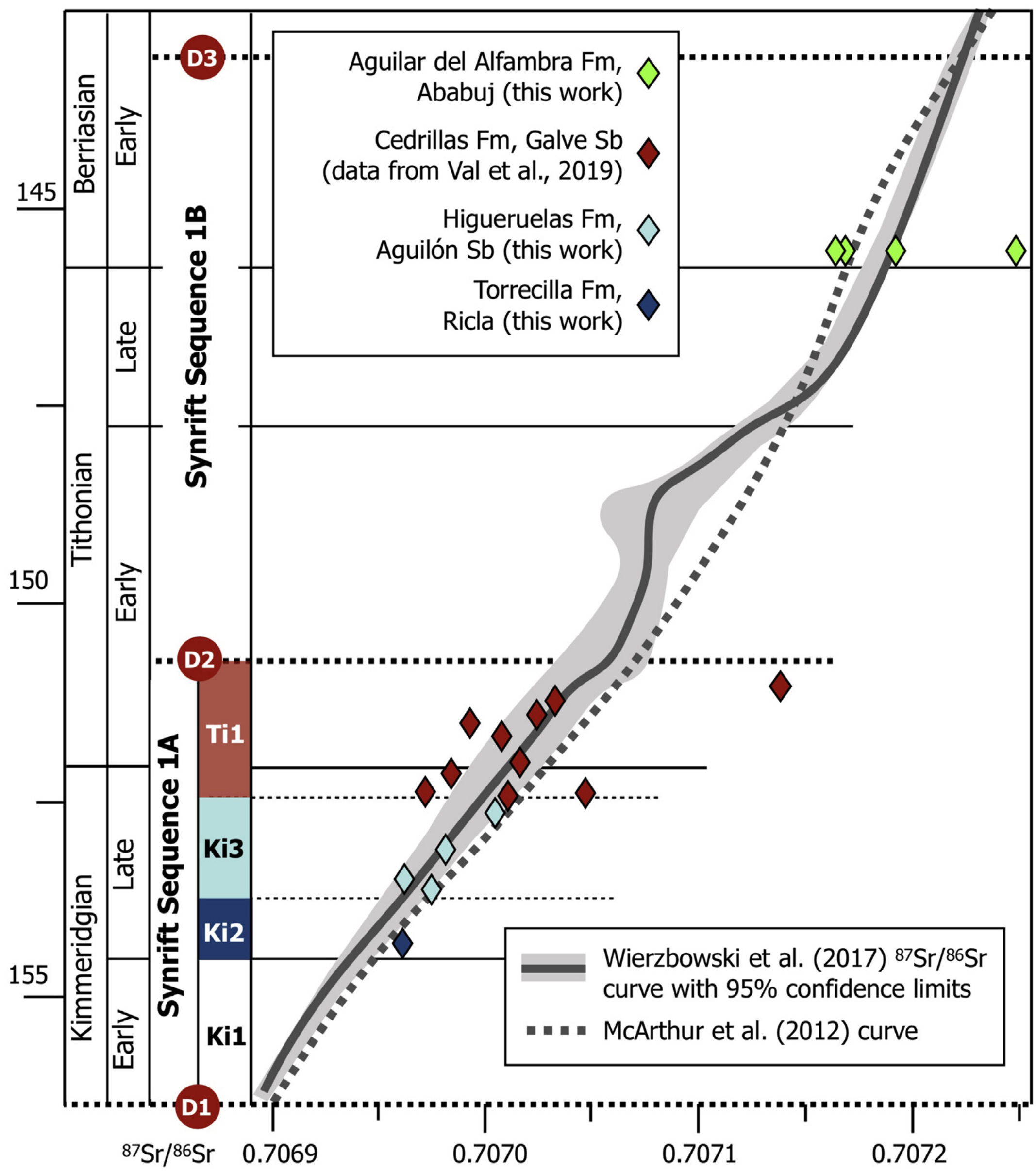

Fig. 5. Strontium-isotopic data ($^{87}Sr/^{86}Sr$) taken from belemnites, brachiopods and oyster shells, and comparison with the global curves of McArthur et al. (2012) and Wierzbowski et al. (2017). For location and data measured in Ricla (sequence Ki2) and Ababuj (synrift sequence 1B) see text. For location and data measured in the Aguilón subbasin (sequence Ki3) see Supplementary data S2. The data from the Galve subbasin (Ti1) were taken from Val et al. (2019). Samples in the Cedrillas and Aguilar del Alfambra formations with abnormally high values are considered as non-reliable and probably reflect a relatively more radiogenic isotopic signal linked to freshwater input (Bryant et al., 1995), in the context of the recorded coastal domains.

includes the local presence of the synrift sequence 1C. In this subbasin, the synrift sequence 1 is overlain by upper Hauterivian–lower Barremian lacustrine to palustrine marls and limestones, which represent the first unit of synrift sequence 2 (Aurell et al., 2016; Fig. 2B).

Synrift sequence 1A has a continuous record across the Galve subbasin, including the Ki1, Ki2, Ki3 a Ti1 sequences. The Ki1 and Ki2 sequences are formed by open-ramp marls and lime mudstones of the Sot de Chera (2–10 m thick) and Loriguilla (90–130 m thick). The lower part of the Loriguilla Fm includes early Kimmeridgian ammonites (Gautier, 1981, Ababuj area), which indicates that the sedimentation of the Loriguilla Fm occurred onwards from the *platynota* Zone. *Alveosepta jaccardi* is present in the Loriguilla Fm and is abundant in the lagoonal skeletal limestones found in the upper part of the overlying Higueruelas Fm. According to the available biostratigraphic and strontium-isotopic data (see Fig. 3), the shallow-marine limestones of the Higueruelas Fm (50–70 m thick) are interpreted to correspond to the uppermost Kimmeridgian Ki3 sequence. However, Campos-Soto et al. (2019) propose a mid-early Kimmeridgian age for the lower boundary of the Higueruelas Fm (Fig. 8). This interpretation is not consistent with the ammonites found in the underlying open-marine units (i.e. Sot de Chera and Loriguilla formations and Calanda Mb). These open-marine units are younger than the D1 mid-*planula* Zone major discontinuity separating the prerift (Yátova Fm) and synrift sequences (Fig. 2B), and in several localities of the Aguilón, Oliete and Morella subbasins late Kimmeridigan ammonites have been found (Fig. 3).

In the Galve subbasin, the onset of the Ti1 sequence is marked by a sharp increase in siliciclastic input. The Ti1 sequence

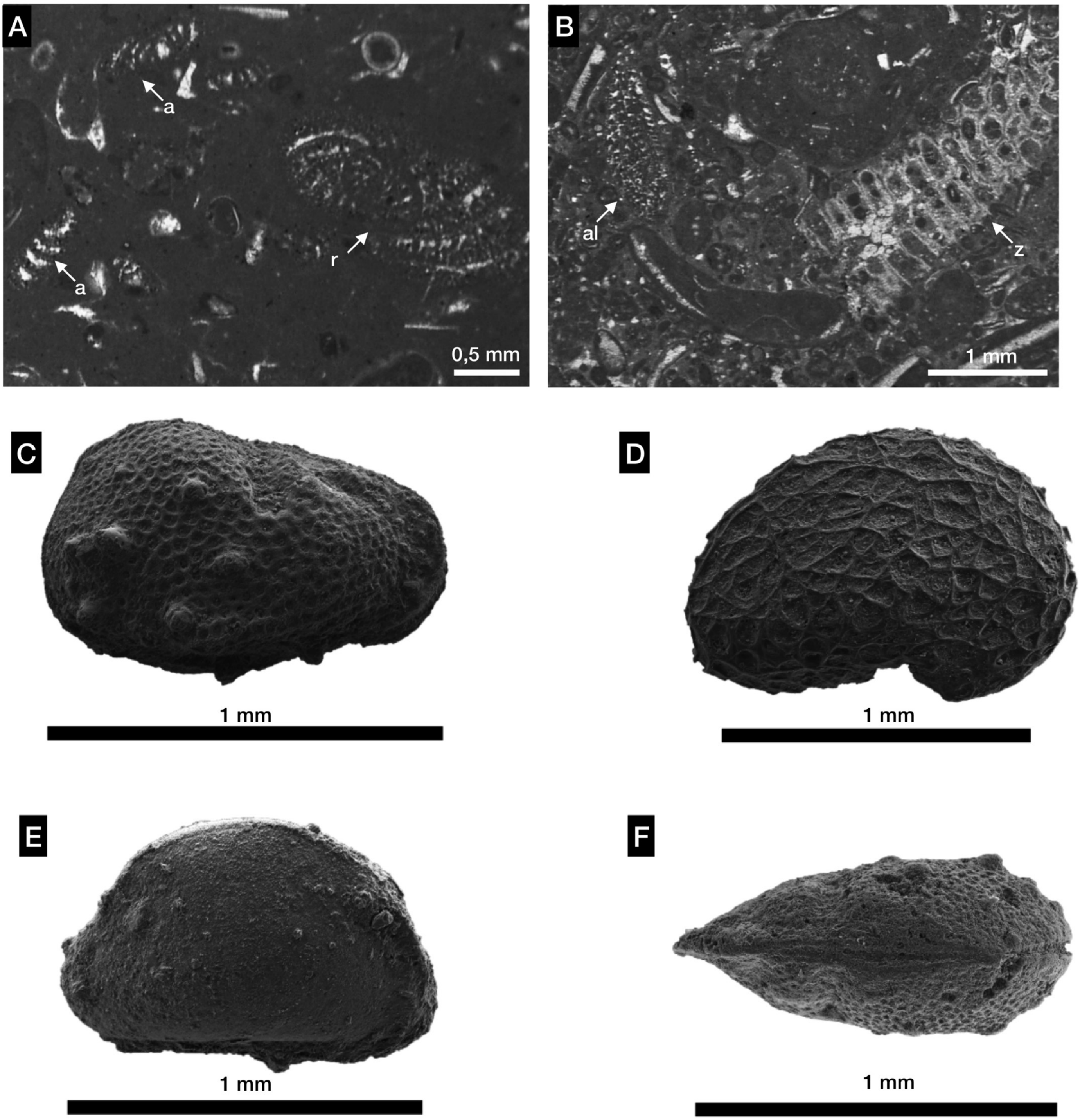

Fig. 6. (A) *Alveosepta jaccardi* (Schrodt) (a) and *Redmondelllina powersi* (Redmond) (r) in skeletal wackestones in the uppermost levels of the Higueruelas Fm (Jaulín log n.3, unit 7, see Supplementary data S2). (B) *Anchispirocyclina lusitanica* (al) and dasycladalean algae *Zergabriella embergeri* (Bouroullec & Deloffre) (z) in peloidal-skeletal packstones of the lowermost levels of the Aguilar del Alfambra Fm (Miravete log n.29, see AM in Fig. 3). (C) MPZ 2019/253, *Theriosynoecum fittoni* (Mantell) from the Aguilar del Alfambra Formation, Cerezos section (log 35; metre 330, Fig. 4 in Aurell et al., 2016); (D) MPZ 2019/254, cf. *Macrodentina* sp. from the Aguilar del Alfambra Formation, Cerezos section (log 35; metre 330, Fig. 4 in Aurell et al., 2016); (E) MPZ 2019/255, cf. *Asciocythere* sp. from the Aguilar del Alfambra Formation, Cerezos section (log 35; metre 330, Fig. 4 in Aurell et al., 2016), (F) MPZ 2019/256, cf. *Theriosynoecum fittoni* from the uppermost part of the Galve Fm in the Galve-Zabacheras log (site 2, Fig. 5 in Aurell et al., 2016).

corresponds to the Cedrillas Fm, a new unit formally defined in this work (see Supplementary material S3 for justification and details). The Cedrillas Fm consists of a mixed coastal carbonate-siliciclastic unit well developed in the central and western areas of the subbasin (i.e. Galve, Aguilar del Alfambra, and Cedrillas-Monteagudo; logs 30, 33 and 36 in Fig. 2A). In these areas, this unit ranges from 150 to 220 m in thickness (Fig. 9A). Lower subsidence rates in the eastern marginal areas of the subbasin between Aliaga and Miravete (see AM/MI in Fig. 3) caused a significant reduction in thickness to 10–20 m (Fig. 9B). In the central areas of the Galve subbasin, the Cedrillas Fm consists of four successive sedimentary sequences 30–80 m thick, with a lower interval of well-bedded

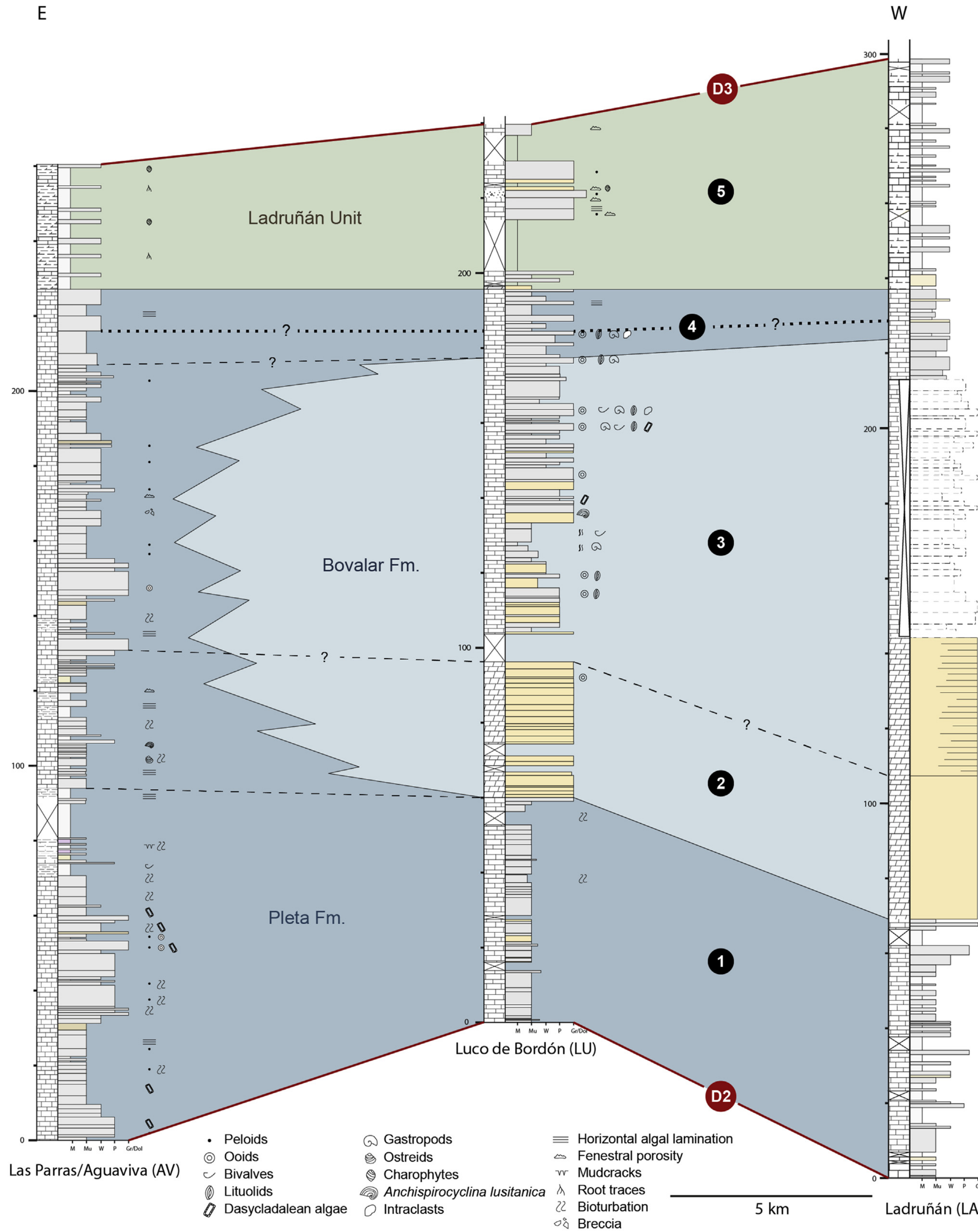

Fig. 7. Correlation of the synrift sequence 1B successions (Tithonian–lower Berriasian) exposed in Las Parras-Aguaviva (AG), Luco de Bordón (LU) and Ladruñán (LA), bounded by major discontinuities D2 and D3. Units 1–5 correspond to the sequences Ti2-1 to Ti2-5 defined in Aurell et al. (2010), which can be traced at regional scale (see Fig. 4E). The Tithonian-Berriasian boundary is probably located in the middle part of unit 4.

carbonates (bioclastic, peloidal, ooidal, micritic) and marls, and an upper interval of mudstones including lenticular to tabular cross-bedded sandstones (sequences S1–S4 in Val et al., 2019). The presence of *Alveosepta jaccardi* in the carbonate intervals of the S1 sequence and in the lower part of the S2 sequence (Gautier, 1980; Campos-Soto et al., 2017, 2019; Val et al., 2019), in conjunction with the overall trend of the strontium-isotopic data, indicates a latest Kimmeridgian–mid-early Tithonian age, most probably from the upper part of the *beckeri* Zone up to the transition between the *hybonotum*/*darwini* zones (Fig. 5; Val et al., 2019). The location of the lower boundary of this unit around the *acanthicum* and *eudoxus* zones proposed by Campos-Soto et al. (2019) is highly speculative and not supported by data (Fig. 8, see boundary between U1 and CLP).

The upper boundary of the Ti1 sequence is a widespread unconformity, which can be traced across the Morella and Galve subbasins (D2 in Fig. 3). Based in the strontium-isotopic data, Val et al. (2019) reassigned the age of this unconformity to the mid-early Tithonian (instead of mid-late Tithonian, in Aurell et al., 2016). In the Galve subbasin, the local presence of a low-angular unconformity associated to this widespread discontinuity indicates block tilting and erosion due to synsedimentary extensional tectonic reactivation at the boundary between synrift sequences 1A and 1B. This erosive surface has been mapped and documented in detail in the outcrops of Abeja (Aurell et al., 2016), in Galve (García-Penas and Aurell, 2017) and in Aguilar del Alfambra (Aurell et al., 2019).

Synrift sequence 1B corresponds to the Aguilar del Alfambra Fm. This unit varies in thickness across the Galve subbasin (0–365 m) due to strong control by synsedimentary extensional tectonics (Aurell et al., 2016). The Aguilar del Alfambra Fm includes a wide variety of siliciclastic and carbonate facies, which were deposited in a wave-dominated open-coast tidal flat (Bádenas et al., 2018). Similar to what is observed in the Morella subbasin, the synrift sequence 1B has a long-term transgressive/regressive trend, with a transgressive peak indicated by the presence of a bioclastic level (including *Anchispirocyclina lusitanica)* found at the mid-upper part of the unit. This level reached the relatively proximal localities of Aguilar del Alfambra and Ababuj (levels Ag5-2 and Ab5-1 in Bádenas et al., 2018). The biostratigraphic and strontium-isotopic data updated in this work, indicate that the Aguilar del Alfambra Fm spans from the mid-early Tithonian up to the early Berriasian (Fig. 3).

In the Miravete section (log 29 in Fig. 2A), the lowermost part and the middle part of the Aguilar del Alfambra Fm includes *Anchispirocyclina lusitanica* and the dasycladalean algae *Zergabriella embergeri* (Bouroullec & Deloffre) (Fig. 6B). In the Ababuj section (log 34 in Fig. 2A), the bioclastic level Ab5-1 found in the mid-upper part of the unit (metre 245 within the 345 m thick section; see Bádenas et al., 2018) contains the same microfossil association. This level also includes abundant oyster shells that have yielded four stable strontium-isotopic data ($^{87}Sr/^{86}Sr$) of 0.707164, 0.707167, 0.707190 and 0.707249, which, compared with the global curve of Wierzbowski et al. (2017), indicates a latest Tithonian-earliest Berriasian age (Fig. 5).

The presence of scarce ostracods is also relevant in confirming the Berriasian age for the upper part of the Aguilar del Alfambra Fm. *Theriosynoecum fittoni* (Mantell) (Berriasian–Barremian age range; Sames, 2011; Schudack and Schudack, 2012) was found in a fossiliferous level located in the upper part of the unit in the Cerezos section (log 35 in Fig. 2A; level in metre 330 within the 365 m thick section, see Aurell et al., 2016; sequence Ce7 in Bádenas et al., 2018). This level has yielded an additional ostracod assemblage dominated by *T. fittoni* (Fig. 6C) along with scarce specimens of cf. *Macrodentina* sp. (Fig. 6D) and cf. *Asciocythere* sp. (Fig. 6E). The latter taxon, tentatively related to *Asciocythere,* includes species previously described in the La Pleta and El Mangraner formations (*Asciocythere* cf. *circumdata* (Donze)) by Schudack and Schudack (2012). According to these authors (op. cit.), the stratigraphical range of *Asciocythere* cf. *circumdata* is Berriasian whereas other species of *Asciocythere* have also been reported by these authors but not before the Aptian (see Fig. 3 in Schudack and Schudack, 2012). As the geological context allows us to rule out the assignament of the Cerezos section to the Aptian, the presence of *Asciocythere* provides additional evidence of a Berriasian age for the upper part of the Aguilar del Alfambra Formation.

On the other hand, the charophyte specimens found by Canudo et al. (2012) at top of the Aguilar del Alfambra Fm in the Galve-Zabacheras section have been restudied. However, insufficient abundance and poor preservation precluded detailed taxonomic and biostratigraphic attributions. Instead, a new fossil-site located also in the upper part of the Aguilar del Alfambra Fm at La Peñuela outcrop (see location 31 in Fig. 2A) yielded a charophyte assemblage with *Clavator grovesii* var. *grovesii* (Harris) and *Clavator grovesii* var. *discordis* (Shaïkin), which is attributed to the Berriasian, with more probability for the early Berriasian (Martín-Closas, 2000). The location of this new fossil-site is tentatively considered time equivalent to the sequence Ag6 of Bádenas et al. (2018). Campos-Soto et al. (2019) assume that the Aguilar del Alfambra Fm does not reach the Berriasian (see SUP* in Fig. 8). However, the early Berriasian age of the upper part of the unit previously proposed in Aurell et al. (2016) is further confirmed by the new biostratigraphic (carophytes and ostracods) and strontium-isotopic data reported here.

Synrift sequence 1C is represented by the Galve Fm (Fig. 9C). Galve Fm has a discontinuous record and is variable in thicknesses (from 0 to 100 m) across the eastern and western margins of the subbasin. The eastern margin has been studied in detail in the Aliaga-Molino Alto section (log 28-AM, Fig. 2A). There, the Galve Fm consists of red clays with intercalated sandstones and conglomerates representing alluvial fan deposits confined to half-grabens. The recorded charophyte association, with *Atopochara trivolvis horrida* (Harris) and the occasional presence of *Clavator grovesii grovesii* (Harris) and *Atopochara trivolvis micranda* (Grambast), indicates that the sedimentation took place around the early to late Berriasian transition, in the *Globator maillardii incrassatus* and *G.m. nurrensis* zones. The location of the Berrriasian-Valanginian boundary towards the upper part of this succession cannot be ruled out (Aurell et al., 2016; see Fig. 10 therein).

Westwards, around the locality of Galve (log 30-GA, Fig. 2A), the Galve Fm consists of red clays with intercalated cross-bedded and tabular-burrowed sandstones representing channel and overbank deposits in an alluvial floodplain. Santos et al. (2018) report on the sporomorph assemblage in the lower part of the Galve Fm (Las Zabacheras fossil site, Galve-Zabacheras section), indicating the presence of some taxa whose first occurrence is Berriasian (in particular, *Cicatricosisporites imbricatus* (Markova)) and other taxa whose last occurrence has been reported in the lower Valanginian (*Impardecispora canadensis* (Pocock)). Furthermore, in the Galve-Zabacheras section, a marly level located in the upper part of the Galve Fm (see site number 2 in Fig. 5 of Aurell et al., 2016) has yielded numerous specimens of the Berriasian–Barremian ostracod *Theriosynoecum fittoni* (Fig. 6F), as well as an isolated charophyte specimen that was attributed by Canudo et al. (2012) to the latest Berriasian–Hauterivian *Globator maillardii steinhauserii* (Mojon). However, this assignment could not be confirmed in the present review.

In summary, the set of biostratigraphic data summarized above indicates that, in the Galve subbasin, the onset of the sedimentation of the Galve Fm occurred in the mid-Berriasian, around the boundary between the *G. m. maillardii and G. m. incrassatus* zones.

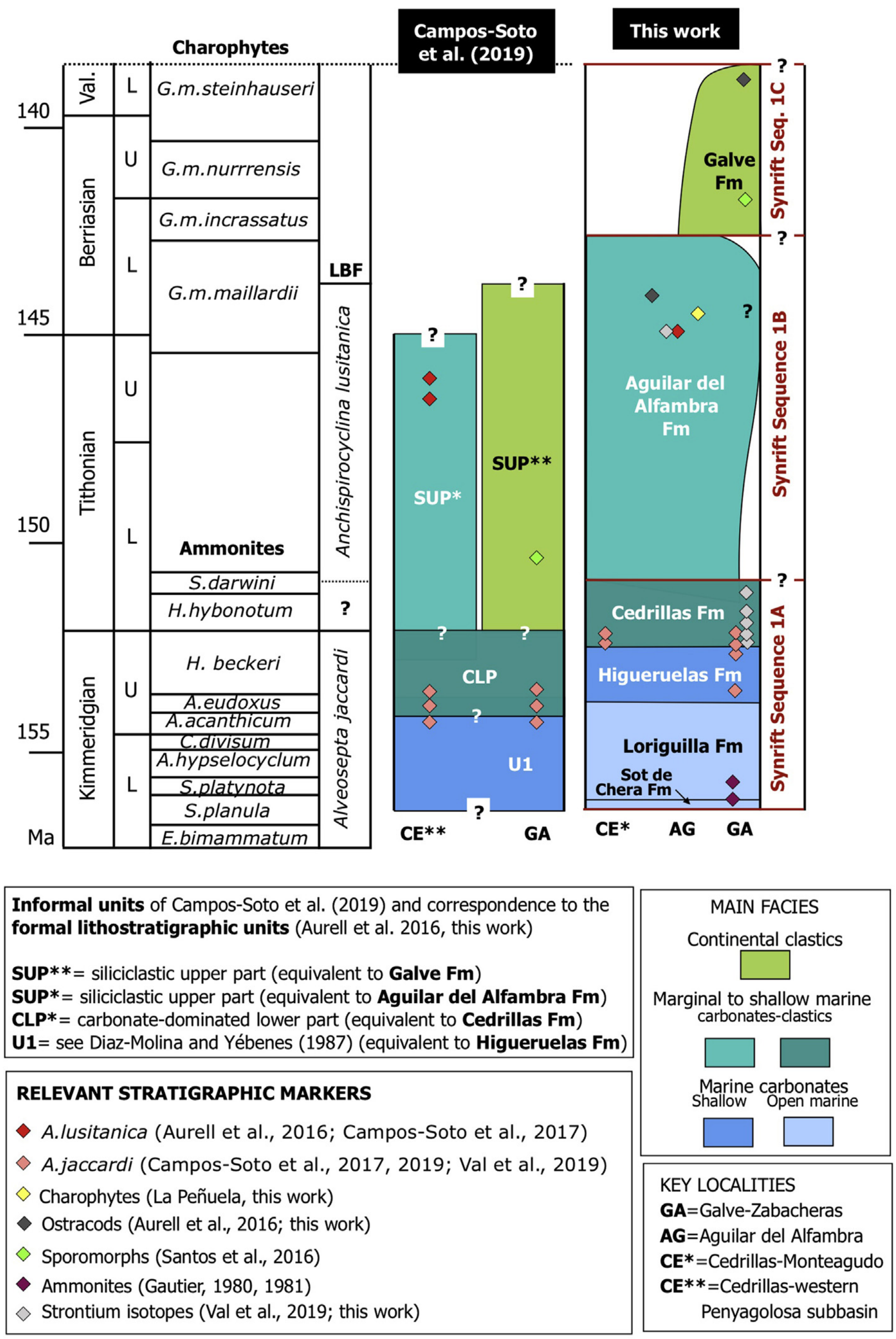

Fig. 8. Comparison between the Kimmeridgian–Berriasian stratigraphy of the Galve and western Penyagolosa subbasins proposed by Campos-Soto et al. (2019) and in this work. The correspondence between the names of the informal units used in Fig. 3 of Campos-Soto et al. (2019) and the formal lithostratigraphic units used here is indicated in the lower part of the figure. See text for explanation and discussion on the observed discrepancies. The location of the key stratigraphic markers within each unit is based in the assumption of constant average rates of sedimentation (distribution of the benthic foraminifera in the Cedrillas log taken from Campos-Soto et al., 2019) (Diaz-Molina and Yébenes, 1987).

In addition, the possible location of the Berriasian-Valanginian boundary towards the upper part of the Galve Fm remains uncertain (Aurell et al., 2016). In contrast, Campos-Soto et al. (2019) propose a Tithonian–mid-early Berriasian age for the Galve Fm in the Galve-Zabacheras outcrop (Fig. 8, see SUP** in GA). However, this age assignment is not consistent with the available biostratigraphic data, in particular by the Berriasian-lower Valanginian sporomorph assemblage found in the lower part of the Galve Fm in the Zabacheras fossil site (Santos et al., 2018). Moreover, these authors regard the mixed carbonate-siliciclastic marginal-marine deposits of the Aguilar del Alfambra Fm time equivalent to the continental siliciclastics of the Galve Fm (see SUP* and SUP** in Fig. 8). However, this interpretation is not consistent with the regional tectono-stratigraphic data, with the presence of an intermediate angular unconformity between these two units, which has been mapped in separated areas of the Galve subbasin (see Aurell et al., 2016 for details, in particular Figs. 6 and 9 therein, and García-Penas and Aurell, 2017).

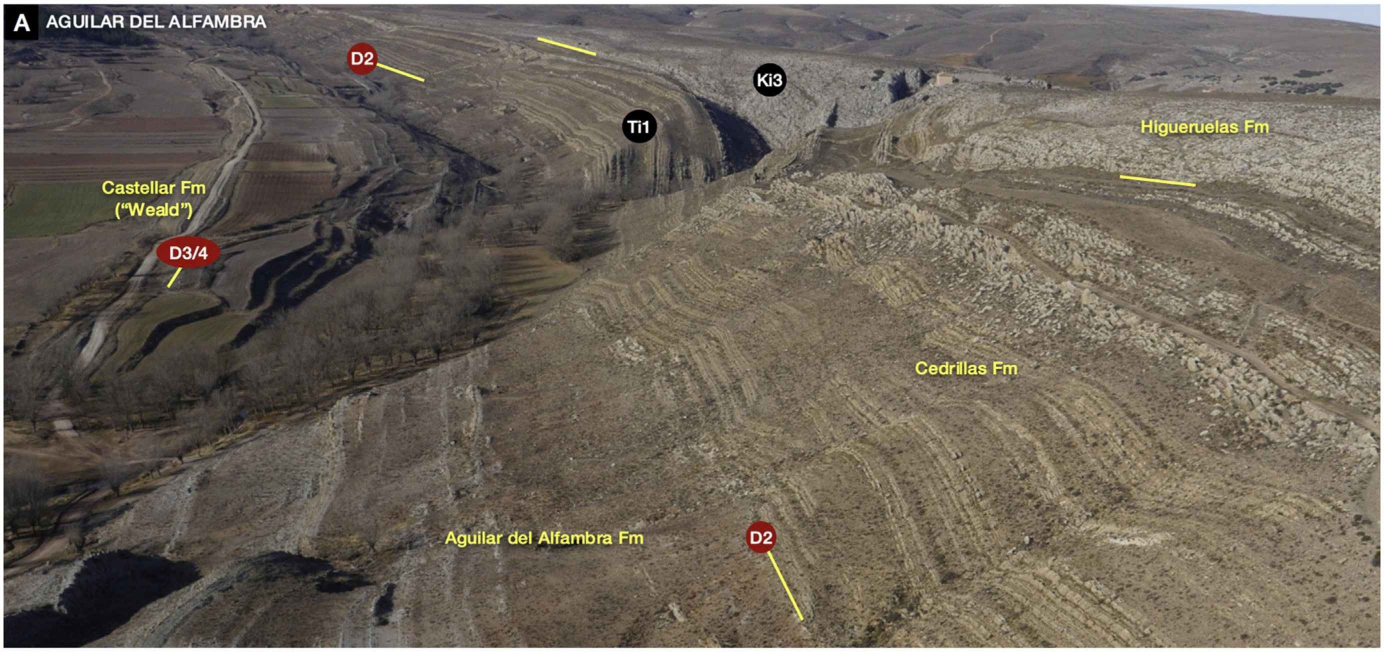
A AGUILAR DEL ALFAMBRA
D2
Ki3
Ti1
Higueruelas Fm
Castellar Fm
("Weald")
D3/4
Cedrillas Fm
Aguilar del Alfambra Fm
D2


B MIRAVETE
D2
Cedrillas Fm
Higueruelas Fm
Aguilar del Alfambra Fm
Ki3
Ti1

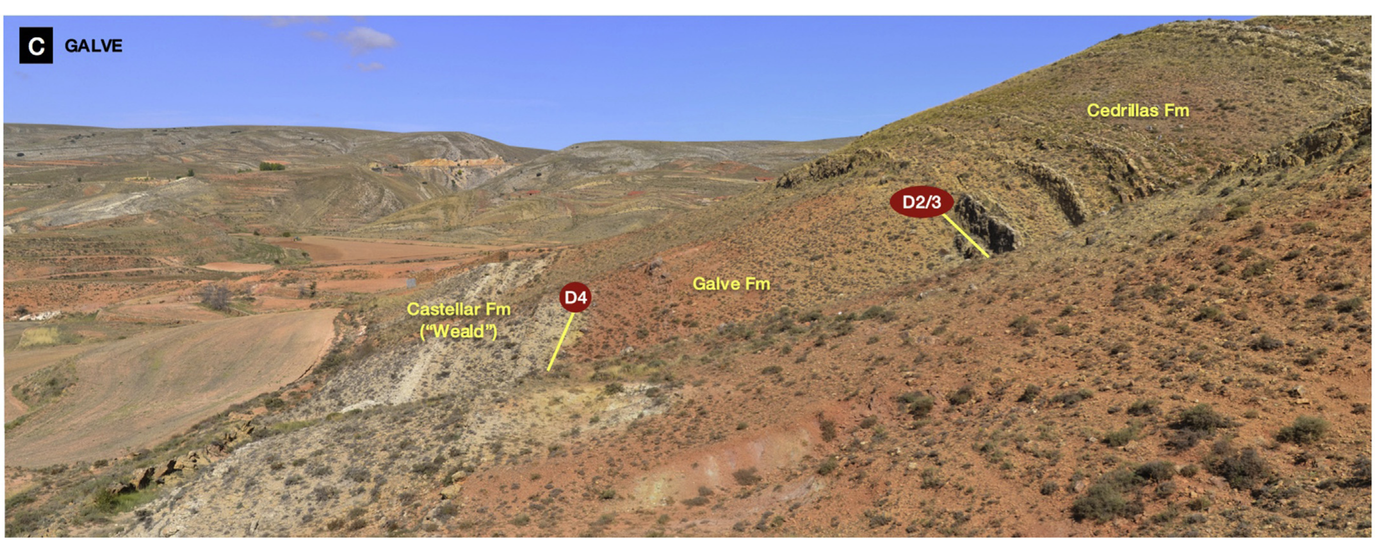
C GALVE
Cedrillas Fm
D2/3
Galve Fm
D4
Castellar Fm
("Weald")

5. Facies distribution and tectono-sedimentary evolution

The Upper Jurassic carbonate ramps that developed in eastern Iberia had a well-defined distribution of facies belts ranging from proximal (western) to distal (eastern) locations (e.g., Bádenas and Aurell, 2001). Differential tectonics involving the uplift of the marginal (western) areas of the Iberian Rift System from the latest Jurassic on, combined with a long-term regional fall in sea level, resulted in the progressive eastwards coastal offlap of these carbonate ramps (Aurell et al., 1994, 2003). In the subbasins under study, the observed facies evolution from the Kimmeridgian carbonate ramp successions to the Tithonian–Berriasian marginal-marine to continental carbonate to siliciclastic-dominated units allows the progressive eastward shoreline migration to be reconstructed in detail (Fig. 10).

At the onset of the synrift sequence 1A, during the deposition of sequences Ki1 and Ki2, wide carbonate ramps were developed in eastern Iberia. In the studied area, there are no significant lateral changes in thickness in the recorded Kimmeridgian successions (Sot de Chera, Loriguilla, Torrecilla formations and Ricla Mb; Fig. 3), indicating that there was not individualization of different subbasins at the time (Fig. 10A). However, the Montalbán High was already uplifted and influenced the distribution of the shallow (Alacón Mb) to open-marine facies (Loriguilla Fm; Cepriá et al., 2002; Aurell et al., 2018). Southwards of the study area, differential tectonic activity controlled the formation of the Salzedella subbasin (Salas, 1987; Bádenas and Aurell, 2001).

At the end of synrift sequence 1A, during the sedimentation of the Ki3 and Ti1 sequences (Loriguilla, Higueruelas, and Cedrillas formations), significant offlap resulted from the eventual restriction of sedimentation in the easternmost part of the study area (Fig. 10B). The Galve subbasin started to develop during the latest Kimmeridgian. The accommodation created in the central and eastern depocentral areas was filled by the thick coastal siliciclastic-carbonate successions of the Ti1 sequence (Cedrillas Fm; Val et al., 2019).

The Tithonian–early Berriasian synsedimentary tectonics resulted in marked differences between the continental, coastal and shallow-marine successions of synrift sequence 1B recorded in the Galve and Morella subbasins (Fig. 3). The sedimentation consisted mainly of coastal mixed carbonate-siliciclastic-dominated successions in the Galve subbasin (Aguilar del Alfambra Fm; Bádenas et al., 2018), whereas peritidal to shallow-marine carbonates occurred in the newly formed Morella subbasin (La Pleta and Bovalar formations and Ladruñán Mb; Fig. 10C).

During the late Berriasian–mid-early Valanginian, the continental sedimentation of synrift sequence 1C in the study area became restricted to small isolated grabens or half-grabens that developed in the Galve subbasin (Galve Fm; Fig. 10D). The synsedimentary tectonic activity during the sedimentation of this sequence was irregular and discontinuous. Continental to marine-marginal carbonate-dominated sedimentation around the Berriasian-Valanginian transition occurred southeastwards of the study area, in the Salzedella subbasin (Canérot et al., 1982; Martín-Closas and Salas, 1994; Salas et al., 2001; Bádenas et al., 2004).

The tectono-sedimentary evolution of the central Iberian Rift System reconstructed here deepens our understanding of the gradual propagation of synsedimentary tectonics associated with the initial stages of the Late Jurassic–Early Cretaceous rifting (Aurell et al., 1994; Salas et al., 2001). Differential subsidence giving rise to the individualization of the southeastern Salzedella subbasin started during the earliest Kimmeridgian (Salas, 1987; Bádenas and Aurell, 2001). The Galve and Morella subbasins characterized here started to develop later, in the latest Kimmeridigan and the early Tithonian, respectively. Finally, the northwestern Aguilón and Oliete subbasins were developed later still, during the mid-Valanginian and early Barremian stages, respectively (Soria et al., 1995; Aurell et al., 2018).

6. Discussion

The combination of biostratigraphic (ammonite and microfossil assemblages), sequence-stratigraphic and strontium-isotopic data compiled in this study allows us to constrain the chronostratigraphic framework of the Kimmeridgian–lowermost Valanginian (?) sedimentary record in the central part of the Iberian Rift System. In particular, the present work makes it possible to discuss the position of the lower and upper boundaries of the Tithonian and Berriasian stages.

The Kimmeridgian-Tithonian boundary occurs in the uppermost part of the synrift sequence 1A (Fig. 3). The location of this boundary is based on the presence of late Kimmeridgian ammonites in the K2 and Ki3 sequences, the last occurrence of *Alveosepta jaccardi* in the lower part of the Ti1 sequence, and strontium-isotopic data obtained from the Higueruelas Fm (Aguilón subbasin) and Cedrillas Fm (Galve subbasin). Neither *A. jaccardi*, nor *Anchispirocyclina lusitanica* has been found in the middle and upper part of the Ti1 sequence in the Galve and Morella subbasins, despite the existence of shallow-marine to lagoonal carbonate intervals rich in lituolids. However, in some localities in the Galve subbasin (Miravete-MI log, Aguilar del Alfambra Fm; Fig. 3), *A. lusitanica* has been found in the lowermost levels of the overlying synrift sequence 1B. Bádenas et al. (2004) also report on the occurrence of *A. lusitanica* starting from the onset of the time-equivalent Bovalar Fm (Montanejos and Salzedella sections). The available data in eastern Iberia thus lend support to the proposals put forward by Ramalho (1981) for the Lusitanian Basin and Peybernès (1998) for the European basins, according to which the first occurrence of *A. lusitanica* was not at the onset of the Tithonian but rather in the middle part of the early Tithonian, after the *hybonotum/darwini* ammonite zones (Fig. 11). The last occurrence of *A. lusitanica* has been reported to reach the mid-early Berriasian (e.g., Ramalho, 1981; Peybernès, 1988; Granier, 2019).

As regards the position of the Tithonian-Berriasian boundary in the studied area, this can be approached with the data available for the mid-upper part of the synrift sequence 1B (see dark grey dashed line in Fig. 3). In the Morella subbasin, this boundary is most probably located close to the boundary between the peritidal carbonates of the La Pleta Fm and the charophyte-rich marly-dominated succession of the Ladruñán Mb. In the Galve subbasin, the strontium-isotopic data and the presence of ostracods and charophytes whose first occurrence is in the Berriasian indicate that the Tithonian-Berriasian boundary is probably found towards the middle-upper part of the coastal mixed carbonate-siliciclastic succession of the Aguilar del Alfambra Fm.

The Berriasian-Valanginian boundary has been tentatively located at the upper part of synrift sequence 1C (Galve Fm, Fig. 3; see also Aurell et al., 2016). In the Galve subbasin, the largest stratigraphic gap occurs in association with the D4 synrift unconformity (Fig. 2B). For this reason, the D4 unconformity (most probably located at the earliest Valanginian) is here considered to be the boundary between the "Jurassic" and the "Lower Cretaceous" cycles (or synrift sequences 1 and 2; see also Liesa et al., 2019). Eastwards,

Fig. 9. Representative field views showing the distribution of lithostratigraphic units in the Galve subbasin. (A) Aguilar del Alfambra section (log 33 in Fig. 2A); notice that the Galve Fm is absent; (B) Miravete section (log 29 in Fig. 2A); notice that the Cedrillas Fm is very reduced in thickness; (C) Eastern flank of the Galve syncline (log 30 in Fig. 2A); notice that the Aguilar del Alfambra Fm is absent.

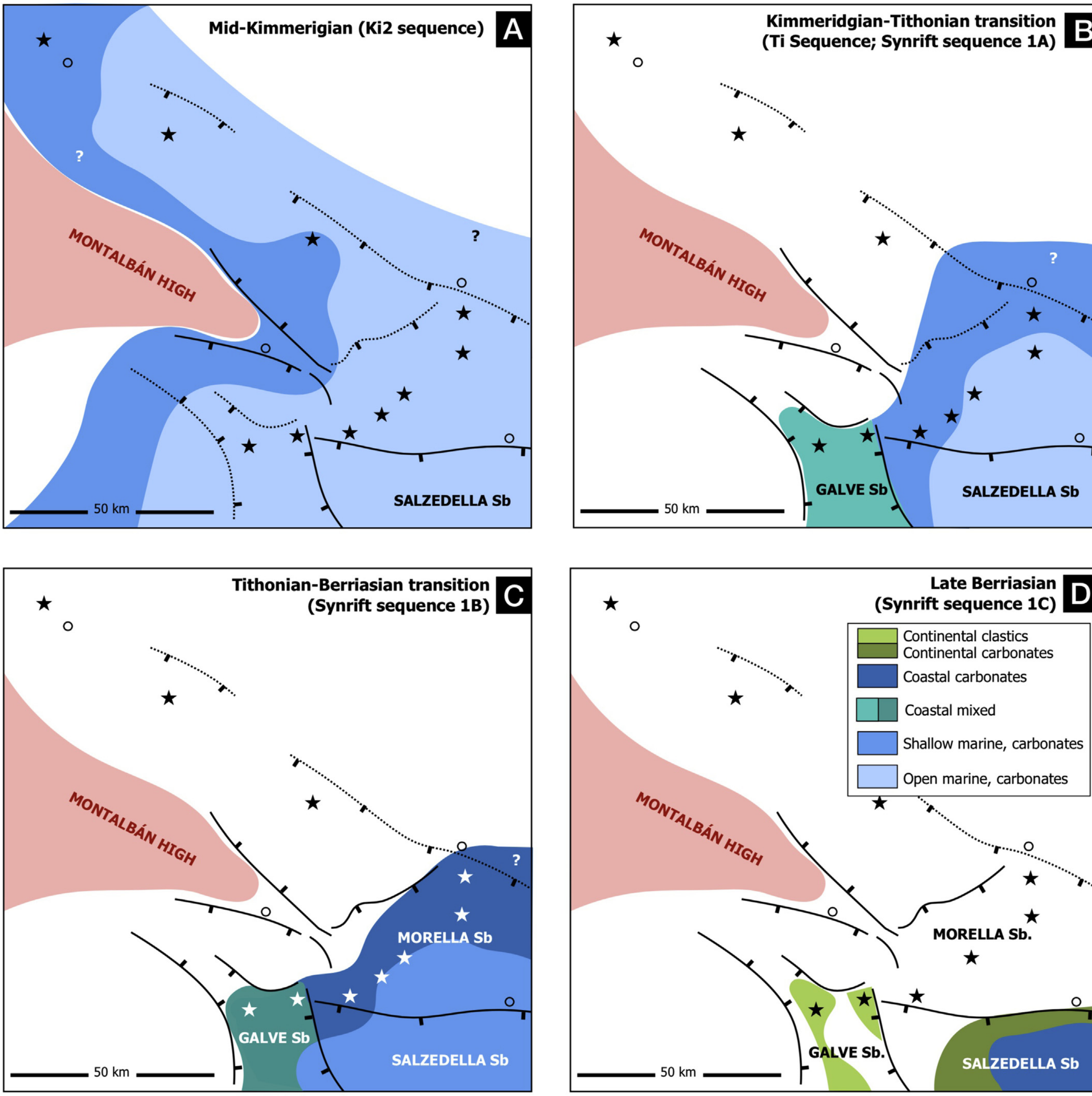

Fig. 10. Paleogeographic evolution of the central Iberian Rift System from mid-Kimmeridgian to late Berriasian. The information in D for the Salzedella subbasin is compiled from Canérot et al. (1982), Salas (1987), and Martín-Closas and Salas (1994).

in the Salzedella subbasin, there is evidence of a continuous sedimentation across the Berriasian–Valanginian boundary. Of particular interest are the continental carbonates of the El Mangraner Fm. In its type locality, the boundary between the *Globator maillardii nurrensis* and *G. m. steinhauseri* charophyte zone is located in the lower part of the El Mangraner Fm, and the age of this unit ranges from late Berriasian to early Valanginian (Salas et al., 1995; Martín-Closas and Salas, 1994, 1998). Northeastwards, in the Garraf Basin, the El Mangraner Fm includes charophytes of the late Berriasian *G. m. nurrensis* Zone (Albrich et al., 2006). In any case, the stratigraphic and tectono-sedimentary evolution of the different subbasins of the Maestrazgo Basin indicates that the Berriasian succession is related to the “Jurassic cycle”, not to the “Lower Cretaceous cycle”.

Despite the imprint of synsedimentary tectonics, the sequential architecture observed in the Kimmeridgian–early Berriasian Iberian marine successions has been related in previous work to eustatic and/or climatic changes driven by orbital cycles. In particular, the influence of the short and long eccentricity cycles has been found not only in the shallow-to open-marine domains of the Ki2 and Ki3 sequences (e.g., Bádenas et al., 2005; Bádenas and Aurell, 2018), but also in the mixed carbonate-siliciclastic shallow-marine to coastal succession of the Ti1 sequence deposited in the Galve subbasin around the Kimmeridgian-Tithonian transition (Val et al., 2019), and

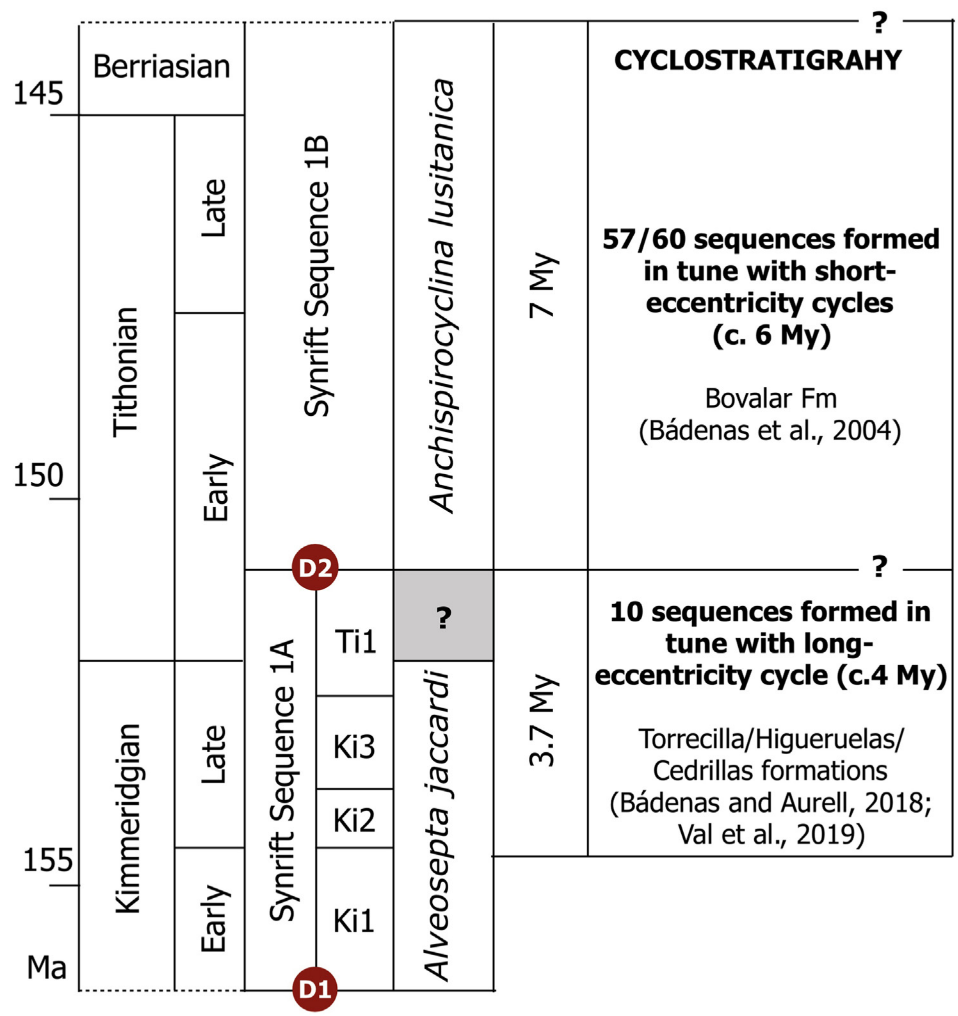

Fig. 11. Comparison between the stratigraphic calibration proposed in the present study and the cyclostratigraphic results obtained in previous works. Geological Time Scale from Ogg et al. (2016). For explanation see text.

in the mid-Tithonian to earliest Berriasian shallow-marine carbonate-dominated successions that include *Anchispirocyclina lusitanica*, well recorded in the depocentral areas of the eastern part of the Maestrazgo Basin (Salzedella and Montanejos sections, Bovalar Fm: Bádenas et al., 2004). This cyclostratigraphic analysis gives further support to the stratigraphic framework proposed here. The time calibration of the studied Kimmeridgian–Berriasian synrift successions (Fig. 3), is coherent with the overall duration based on the number of high-frequency sequences that previous work have proposed were formed in tune with the short (100 ky) and long (400 ky) eccentricity orbital cycles (Fig. 11). In particular, the upper part of synrift sequence 1A (Ki2, Ki3 and Ti1 sequences) includes 10 sequences formed in tune with the long eccentricity cycle (total duration of c.4 Myr), which fits the 3.7 Myr duration of this time interval proposed here. Moreover, the lower and middle part of the synrift sequence 1B including *Anchispirocyclina lusitanica* of c.7 Myr of duration, fits well with the 57–60 sequences formed in tune with the short-eccentricity cycle in the Bovalar Fm (Fig. 11). It is interesting to note that the influence of the long and short eccentricity cycles during the Kimmeridgian–Berriasian has also been reported from other, distant sedimentary domains (i.e. the Swiss Jura carbonate platform: Strasser, 1988, 2007; Colombié and Strasser, 2005), reinforcing the idea of a global eustatic/climatic signal influencing the sedimentation.

7. Conclusions

The Kimmeridgian–Berriasian synrift successions recorded in the central Iberian Rift System (NE Spain) consist of three synrift sequences (1A, 1B and 1C) bounded by major unconformities. These sequences have an irregular and variable record across the four studied subbasins, the Aguilón, Oliete, Morella, and Galve.

The Kimmeridgian–lowermost Tithonian synrift sequence 1A (150–400 m thick) consists of four transgressive-regressive sequences (Ki1, Ki2, Ki3 and Ti1 sequences). These sequences formed on successive low-angle carbonate ramps, characterized by grain-supported facies in shallow areas (including abundant levels with *Alveosepta jaccardi*), which graded offshore to monotonous successions of marls and lime mudstones, including ammonites that allow the precise biostratigraphic calibration of these successions. The progressive eastern offlap of these carbonate ramps resulted in the reduced extension of the uppermost Kimmeridgian–lower Tithonian Ti1 sequence, which is only recorded in the eastern Morella and the Galve subbasins. Grain-supported carbonates are predominant in the marginal areas of the Morella subbasin, whereas mixed carbonate-siliciclastic coastal sediments developed coevally around the Kimmeridgian-Tithonian transition in the Galve subbasin.

A major sedimentary change associated with normal fault reactivation occurred at the onset of synrift sequence 1B, during the mid-early Tithonian. Differential subsidence resulted in the local accumulation of a thick (up to 365 m) coastal to shallow-marine carbonate and siliciclastic successions in the depocentral areas of the Morella and Galve subbasins. The age of synrift sequence 1B (mid-early Tithonian to mid-Berriasian) is constrained by the presence of the benthic foraminifera *Anchispirocyclina lusitanica*, strontium-isotopic data, and the occurrence of charophytes of the *Globator maillardii maillardii* Zone in the upper part of the sequence. According to the available data, the Tithonian-Berriasian boundary is located towards the mid-upper part of synrift sequence 1B. In the Morella subbasin, this boundary is likely to be located around the boundary between the La Pleta Fm and the Ladruñan Mb. In the Galve subbasin, the strontium-isotopic and biostratigrapic (ostracods, charophytes) data suggest that this boundary is found in the mid-upper part of the Aguilar del Alfambra Fm.

Sedimentation of the mid-Berriasian—lowermost Valanginian synrift sequence 1C was irregular and is only represented in certain areas of the Galve subbasin, which records the up to 100 m thick continental succession of the Galve Fm. Biostratigraphic data constraining the age of the Galve Fm are provided by charophytes, ostracods, and sporomorphs. Sedimentation of this unit occurred during a phase of intense tectonic activity that involved the formation of isolated grabens and half-grabens in discrete parts of the Galve subbasin. The upper boundary of synrift sequence 1C is a major unconformity related to synsedimentary tectonic reactivation around the Berriasian-Valanginian boundary, and there is an associated stratigraphic gap of variable amplitude that comprises the Valanginian and the Hauterivian.

In conclusion, the stratigraphic and tectono-sedimentary evolution of the central Iberian Rift System summarized here reinforces the observation that the sedimentation during the Berriasian was linked to the "Jurassic cycle", providing arguments that support the placement of the Jurassic-Cretaceous system boundary at the end of the Berriasian stage rather than at the Tithonian-Berriasian boundary.

Acknowledgements

Parts of the results of this work were presented on the occasion of the JK2018 conference in Geneva (see Granier B. (ed., 2019), *International Meeting around the Jurassic-Cretaceous Boundary*, Carnets de Géologie, Madrid, ISBN13: 978-2-916733-18-0, Book 2019/01 (CG2019_B01), 100 p). This research was subsidized by the Spanish Ministry of Science and Innovation (project CGL2017-85038-P) and by the Government of Aragón-FEDER 2014—2020 *Construyendo Europa desde Aragón* (Group E18: *Aragosaurus: Recursos Geológicos y Paleoambientales*). Authors would like to acknowledge the use of Servicio General de Apoyo a la Investigación-SAI, Universidad de Zaragoza. DC is supported by AGAUR (Beatriu de Pinós Programme, BP2017). MMA is supported by a postdoctoral grant by FCT (grant number SFRH/BPD/113130/2015). Rupert Glasgow helped to improve the English of the manuscript. The authors are grateful for the reviews of Bruno Granier and André Strasser, and for the editorial work of Eduardo Koutsoukos whose useful suggestions have improved the quality of this paper.

References

Albrich, S., Bernaus, J.M., Boix, C., Caus, E., Martín-Closas, C., Salas, R., Vicedo, V., Villalonga, R., 2006. Caracterización bioestratigráfica y paleoambiental del Cretácico Inferior (Berriasiense-Barremiense) del macizo de Garraf (Cadena Costera Catalana). Revista Española de Micropaleontología 38 (2—3), 429—452.

Atrops, F., Meléndez, G., 1984. Kimmeridgian and Lower Tithonian from the Calanda-Berge area (Iberian Chain, Spain): Some biostratigraphic remarks. In: Proceedings 1st International Symposium on Jurassic Stratigraphy 2, pp. 377—392. Erlangen.

Aurell, M., 1990. El Jurásico Superior en la Cordillera Ibérica Central (provincias de Zaragoza y Teruel). Análisis de cuenca. PhD Thesis. Zaragoza University.

Aurell, M., Mas, R., Meléndez, A., Salas, R., 1994. El tránsito Jurásico—Cretácico en la Cordillera Ibérica: relación tectónica-sedimentación y evolución paleogeográfica. Cuadernos de Geología Ibérica 18, 369—396.

Aurell, M., Bádenas, B., Bello, J., Delvene, G., Meléndez, G., Pérez-Urresti, I., Ramajo, J., 1999a. El Calloviense y el Jurásico superior en la Cordillera Ibérica nororiental y la Zona de Enlace con la Cordillera Costero-Catalana, en los sectores de Sierra de Arcos, Calanda y Xerta-Paüls. Cuadernos de Geología Ibérica 25, 111—137.

Aurell, M., Bádenas, B., Bordonaba, A.P., 1999b. El Bathoniense— Kimmeridgiense (Jurásico Medio-Superior) en la región de Obón- Torre de las Arcas (Teruel). Geogaceta 25, 19—22.

Aurell, M., Robles, S., Bádenas, B., Quesada, S., Rosales, I., Meléndez, G., García-Ramos, J.C., 2003. Transgressive/regressive cycles and Jurassic palaeogeography of NE Iberia. Sedimentary Geology 162, 239—327.

Aurell, M., Bádenas, B., Ipas, J., Ramajo, J., 2010. Sedimentary evolution of an Upper Jurassic carbonate ramp (Iberian Basin, NE Spain). In: Buchem, F. van, Gerdes, K., Esteban, M. (Eds.), Reference Models of Mesozoic and Cenozoic Carbonate Systems in Europe and The Middle East, Stratigraphy and Diagenesis. Geological Society of London, pp. 87—109. Special Publication329.

Aurell, M., Bádenas, B., Gasca, J.M., Canudo, J.I., Liesa, C., Soria, A.R., Moreno-Azanza, M., Najes, L., 2016. Stratigraphy and evolution of the Galve sub-basin (Spain) in the middle Tithonian-early Barremian: implications for the setting and age of some dinosaur fossil sites. Cretaceous Research 65, 138—162.

Aurell, M., Soria, A.R., Bádenas, B., Liesa, C.L., Canudo, J.I., Gasca, J.M., Moreno-Azanza, M., Medrano-Aguado, E., Meléndez, A., 2018. Barremian synrift sedimentation in the Oliete sub-basin (Iberian Basin, Spain): palaeogeographical evolution and distribution of vertebrate remains. Journal of Iberian Geology 44, 285—308.

Aurell, M., Val, J., Bádenas, B., Liesa, C., 2019. Discordancias asociadas a una etapa de rift del final del Jurásico en el sector central de la Subcuenca de Galve (Aguilar del Alfambra, Teruel). Geogaceta 65, 15—18.

Bádenas, B., Aurell, M., 2001. Kimmeridgian palaeogeography and basin evolution of northeastern Iberia. Palaeogeography, Palaeoclimatology, Palaeoecology 168, 291—310.

Bádenas, B., Aurell, M., 2018. The down-dip preferential sequence record of orbital cycles in greenhouse carbonate ramps: examples from the Jurassic of the Iberian Basin (NE Spain). In: Montenari, M. (Ed.), Stratigraphy & Timescales volume 3: Astrochronology and Cyclostratigraphy. Elsevier, pp. 285—325.

Bádenas, B., Aurell, M., Rodríguez Tovar, F.J., Pardo-Izuzquiza, E., 2003. Sequence stratigraphy and bedding rhythms in an outer ramp limestone succession (Late Kimmeridgian, northeast Spain). Sedimentary Geology 161, 153—174.

Bádenas, B., Salas, R., Aurell, M., 2004. Three orders of regional sea-level changes control facies and stacking patterns of shallow carbonates in the Maestrat Basin (Tithonian-Berriasian, NE Spain). International Journal of Earth Sciences 93, 144—162.

Bádenas, B., Aurell, M., Gröcke, D.R., 2005. Facies analysis and correlation of high-order sequences in middle-outer ramp successions: variations in exported carbonate in basin-wide δ13Ccarb (Kimmeridgian, NE Spain). Sedimentology 52, 1253—1276.

Bádenas, B., Aurell, M., Gasca, J.M., 2018. Facies model of a mixed clastic-carbonate, wave-dominated open-coast tidal flat (Tithonian-Berriasian, north-east Spain). Sedimentology 65, 1631—1666.

Bover-Arnal, T., Moreno-Bedmar, J.A., Salas, R., Skelton, P.W., Bitzer, K., Gili, E., 2010. Sedimentary evolution of an Aptian syn-rift carbonate system (Maestrat Basin, E Spain): effects of accommodation and environmental change. Geologica Acta 8, 249—280.

Bover-Arnal, T., Moreno-Bedmar, J.A., Frijia, G., Pascual-Cebrian, E., Salas, R., 2016. Chronostratigraphy of the Barremian-Early Albian of the Maestrat Basin (E Iberian Peninsula): Integrating strontium-isotope stratigraphy and ammonoid biostratigraphy. Newsletters on Stratigraphy 49, 41—68.

Bryant, J.D., Jones, D.S., Mueller, P.A., 1995. Influence of fresh-water flux on $^{87}Sr/^{86}Sr$ chronostratigraphy in marginal marine environments and dating of vertebrate and invertebrate faunas. Journal of Paleontology 69, 1—6.

Campos-Soto, S., Cobos, A., Caus, E., Benito, M.I., Fernández-Labrador, L., Suarez-González, P., Quijada, E.I., Mas, R., Royo-Torres, R., Alcalá, L., 2017. Jurassic Coastal Park: a great diversity of palaeoenvironments for the dinosaurs of the Villar del Arzobispo Formation (Teruel, eastern Spain). Palaeogeography, Palaeoclimatology, Palaeoecology 485, 154—177.

Campos-Soto, S., Benito, M.I., Cobos, A., Caus, E., Quijada, E.I., Suarez- González, P., Mas, R., Royo-Torres, R., Alcalá, L., 2019. Revisiting the age and palaeoenvironments of the Upper Jurassic—Lower Cretaceous? dinosaur-bearing sedimentary record of eastern Spain: implications for Iberian palaeogeography. Journal of Iberian Geology. https://doi.org/10.1007/s41513-019-00106-y.

Canérot, J., 1974. Thèse Doctorat Sciences naturelles Toulouse. In: Recherches géologiques aux confins des chaines Ibériques et Catalanes (Espagne). Enadimsa.

Canérot, J., Cugny, P., Pardo, G., Salas, R., Villena, J., 1982. Ibérica Central y Maestrazgo. In: El Cretácico de España. Univ. Comp, Madrid, pp. 273—344.

Canudo, J.I., Gasca, J.M., Moreno-Azanza, M., Aurell, M., 2012. New information about the stratigraphic position and age of the sauropod *Aragosaurus ischiaticus* from the Early Cretaceous of the Iberian Peninsula. Geological Magazine 149 (2), 252—263.

Catuneanu, O., Galloway, W.E., Kendall, C.G.St.C., Miall, A.D., Posamentier, H.W., Strasser, A., Tucker, M.E., 2011. Sequence Stratigraphy: Methodology and Nomenclature. Newsletters on Stratigraphy 44 (3), 173—245.

Cepriá, J.J., Bádenas, B., Aurell, M., 2002. Evolución sedimentaria y paleogeografía del Jurásico superior (Kimmeridgiense superior- Titónico) en la Sierra de Arcos (Cordillera Ibérica). Cuadernos de Geología Ibérica 28, 93—106.

Cobos, A., Royo-Torres, R., Luque, L., Alcalá, L., Mampel, L., 2010. An Iberian stegosaurs paradise: the Villar del Arzobispo Formation (Tithonian-Berriasian) in Teruel (Spain). Palaeogeography, Palaeoclimatology, Palaeoecology 293, 223–236.
Colombié, C., Strasser, A., 2005. Facies, cycles and controls on the evolution of a keep-up carbonate platform (Kimmeridgian, Swiss Jura). Sedimentology 52, 1207–1228.
Colombié, C., Girauld, I.F., Schnyder, J., Götz, A., Boussaha, M., Aurell, M., Bádenas, B., 2014. Timing of sea level, tectonics and climate events during the uppermost Oxfordian (Planula Zone) on the Iberian ramp (northeast Spain). Palaeogeography, Palaeoclimatology, Palaeoecology 412, 17–31.
Díaz-Molina, M., Yébenes, A., 1987. La sedimentación litoral y continental durante el Cretácico Inferior. Sinclinal de Galve, Teruel. Estudios Geológicos (volumen extraordinario) 43, 3–21.
Fezer, R., Geyer, O.F., 1988. Der Oberjura von Calanda im nordöslichen Keltibericum (Provinz Teruel, Spanien). I Stratigrphie. Arbeiten aus dem Institut für Geologie und Paläontologie der Universität. Sttutgart 84, 207–237.
Finkel, R., 1992. Eine Ammoniten-Fauna aus dem Kimmeridgium des nord-östlichen Keltibericums (Spanien). Profil 3, 227–297.
García-Penas, A., Aurell, M., 2017. Tectonosedimentary evolution around the Jurassic–Cretaceous transition in Galve (Aguilar del Alfambra Formation, Teruel, Iberian Chain). Revista de la Sociedad Geológica de España 30, 79–90.
Gasca, J.M., Moreno-Azanza, M., Bádenas, B., Díaz-Martínez, I., Castanera, D., Canudo, J.I., Aurell, M., 2017. Integrated overview of the vertebrate fossil record of the Ladruñán anticline (Spain): evidence of a Barremian alluvial-lacustrine system in NE Iberia frequented by dinosaurs. Palaeogeography, Palaeoclimatology, Palaeoecology 472, 192–202.
Gautier, P.W., 1980. Memoria explicativa de la Hoja núm. 543 (Villarluengo). In: Mapa geológico de España 1:50.000, segunda serie. Instituto Geológico de España (IGME), Madrid.
Gautier, P.W., 1981. Memoria explicativa de la Hoja núm. 568 (Alcala de la Selva). In: Mapa geológico de España 1:50.000, segunda serie. Instituto Geológico de España (IGME), Madrid.
Geyer, O., Pelleduhn, R., 1979. Sobre la Estratigrafía y la facies espongiolítica del Kimmeridgiense de Calanda (provincia de Teruel). Cuadernos de Geología Ibérica 10, 67–72.
Granier, B., 2019. Dual biozonation scheme (benthic foraminifera and "calcareous" green algae) over the Jurassic-Cretaceous transition. Another plea to revert the system boundary to its historical Orbigny's and Oppel's definition. Cretaceous Research 93, 245–274.
Ipas, J., Aurell, M., Bádenas, B., Canudo, J.I., Liesa, C., Mas, J.R., Soria, A.R., 2007. Caracterización de la Formación Villar del Arzobispo al sur de Zaragoza (Titónico, Cordillera Ibérica). Geogaceta 41, 111–114.
Kleipool, L.,M., Reijmer, J.J.G., Bádenas, B., Aurell, M., 2015. Variations in petrophysical properties along a mixed siliciclastic carbonate ramp (Upper Jurassic, Ricla, NE Spain). Marine and Petroleum Geology 76, 329–343.
Liesa, C.L., Soria, A.R., Meléndez, A., 1996. Estudio preliminar sobre la tectónica sinsedimentaria del Cretácico inferior en el borde septentrional de la Cubeta de Aliaga (Cordillera Ibérica). Geogaceta 20 (7), 1707–1710.
Liesa, C.L., Soria, A.R., Casas, A., Aurell, M., Meléndez, N., Bádenas, B., Fregenal-Martínez, M., Navarrete, R., Peropadre, C., Rodríguez-López, J.P., 2019. The Late Jurassic–Early Cretaceous rifting stage at the central and eastern Iberian Basin. In: Quesada, C., Oliveira, J.T. (Eds.), The geology of Iberia: A Geodynamic Approach. Volume 5: The Alpine Cycle. Springer, Heidelberg.
Martín-Closas, C., 1989. Els caròfits del Cretaci Inferior de les conques periferiques del Bloc de l'Ebre. PhD thesis. University of Barcelona.
Martín-Closas, C., Salas, R., 1994. Lower Cretaceous Charophytes. Biostratigraphy and evolution in the Maestrat Basin (Eastern Iberian Ranges). In: Excursion Guidebook, VIII Meeting of the European Group of Charophyte Specialists, Barcelona, p. 89. Diagonal, Barcelona (ISBN 84-605-0645-2).
Martín-Closas, C., Salas, R., 1998. Lower Cretaceous Charophyte biozonation in the Maestrat Basin (Iberian Ranges, Spain). A reply to P.O. Mojon. Géologie Alpine 74, 97–110.
Martín-Closas, C., 2000. Els caròfits del Juràssic superior i el Cretaci inferior de la Península Ibèrica. Arxius de les Seccions de Ciències de l'Institut d'Estudis Catalans , Secció de Ciències i Tecnologia 125, 1–304 in Catalan with an abridged English version).
Mas, R., García, A., Salas, R., Meléndez, A., Alonso, A., Aurell, M., Bádenas, B., Benito, M.I., Carenas, J.F., García-Hidalgo, J., Gil, J., Segura, M., 2004. Segunda fase de rifting: Jurásico Superior-Cretácico Inferior. In: Vera, J.A. (Ed.), Geología de España. SGE- IGME, Madrid, pp. 503–510.
McArthur, J.M., Howarth, R.J., Shields, G.A., 2012. Strontium isotope stratigraphy. In: Gradstein, F.M., Ogg, J.G., Schmitz, M.D., Ogg, G.M. (Eds.), A Geologic Time Scale 2012. Elsevier, Oxford, pp. 127–144.
Meléndez, G., Aurell, M., Atrops, F., 1990. Las unidades del Jurásico superior en el sector noroccidental de la Cordillera Ibérica: nuevas subdivisiones litoestratigráficas. Cuadernos de Geología Ibérica 14, 225–246.
Meléndez, A., Pardo, G., Pendón, J.G., Villena, J., 1979. Las facies terminales del Jurásico en el sector central de la Cordillera Ibérica. Cuadernos de Geología 10, 137–148.
Moliner, L., 2009. Ataxioceratinae (ammonitina) del Kimmeridgiense inferior en el NE de la provincia de Teruel (cordillera Ibérica oriental y Maestrazgo). PhD thesis. University of Granada.
Ogg, J.G., Ogg, G., Gradstein, F.M., 2016. A Concise Geologic Time Scale. Elsevier B.V.
Pérez-Urresti, I., Delvene, G., Meléndez, G., Ramajo, J., 1998. El Oxfordiense Superior y la posición del límite Oxfordiense-Kimmeridgiense en el sector de Tosos-Aguilón (Rama Aragonesa de la Cordillera Ibérica, España). Geogaceta 24, 251–254.
Peybernès, B., 1998. Larger benthic foraminifera. Columns for Jurassic chart of Mesozoic and Cenozoic sequence chronostratigraphic framework of European basins, by Hardenbol J, Thierry J, Farley MB, Jacquin T, De Gracianski PC, Vail PR (coordinators) Mesozoic and Cenozoic sequence chronostrati- graphic framework of European basins. In: Gracianski, P.C. de, Hardenbol, J., Jacquin, T., Vail, P.R. (Eds.), Mesozoic and Cenozoic Sequence Stratigraphy of European Basins. SEPM (Society for Sedimentary Geology). Special Publication 60, charts 7.
Querol, X., Salas, R., Pardo, G., Ardevol, L., 1992. Albian coal-bearing deposits of the Iberian Range in northeastern Spain. In: McCabe, J.P., Panish, J.T. (Eds.), Controls and distribution and quality of Cretaceous coals. Geological Society of America, pp. 193–208. Special Paper 267.
Ramajo, J., Aurell, M., 2008. Long-term Callovian–Oxfordian sea-level changes and sedimentation in the Iberian carbonate platform (Jurassic, Spain): possible eustatic implications. Basin Research 20, 163–184.
Ramalho, M.M., 1981. Note préliminaire sur le microfacies du Jurassique supérieur portugais. Communicações Serviços Geológicos de Portugal 67, 41–45.
Remane, J., 1991. The Jurassic-Cretaceous boundary: problems of definition and procedure. Cretaceous Research 12, 447–453.
Riveline, J., Berger, J.P., Feist, M., Martín-Closas, C., Schudack, M., Soulie-Märsche, I., 1996. European Mesozoic-Cenozoic charophyte biozonation. Bulletin de la Société géologique de France 167 (3), 453–468.
Salas, R., 1987. El Malm y el Cretaci inferior entre el Massis de Garraf i la Serra d'Espadà. Ph.D. Thesis. University of Barcelona.
Salas, R., Casas, A., 1993. Mesozoic extensional tectonics, stratigraphy and crustal evolution during the Alpine cycle of the eastern Iberian Basin. Tectonophysics 228, 33–55.
Salas, R., Martín-Closas, C., Querol, X., Guimerá, J., Roca, E., 1995. Evolución tectonosedimentaria de las cuencas del Maestrazgo y Aliaga-Penyagolosa durante el Cretácico inferior. In: Salas, R., Martín-Closas, C. (Eds.), El Cretácico inferior del Nordeste de Iberia. University of Barcelona, pp. 13–94.
Salas, R., Guimerà, J., Mas, R., Martín-Closas, C., Meléndez, A., Alonso, A., 2001. Evolution of the Mesozoic central Iberian rift system and its Cainozoic inversion (Iberian chain). Mémoires du Muséum national d'Histoire naturelle 186, 145–185.
Sames, B., 2011. Early Cretaceous *Theriosynoecum* Branson 1936 in North America and Europe. Micropaleontology 57 (4–5), 291–344.
Santos, A.A., Villanueva-Amadoz, U., Royo-Torres, R., Sender, L.M., Cobos, A., Alcala, L., Diez, J.B., 2018. Palaeobotanical records associated with the first dinosaur defined in Spain: Palynostratigraphy, taxonomy and palaeoenvironmental remarks. Cretaceous Research 90, 318–334.
Schudack, U., Schudack, M., 2012. Non-Cypridean Ostracoda from the Lower Cretaceous of the Iberian Chain (Spain). Neues Jahrbuch für Geologie und Paläontologie-Abhandlungen 266 (3), 251–271.
Sequero, C., Bádenas, B., Aurell, M., 2018. Facies mosaic in the inner areas of a shallow carbonate ramp (Upper Jurassic, Higueruelas Fm, NE Spain). Facies 64 (2), 9. https://doi.org/10.1007/s10347-018-0521-8.
Soria, A.R., Martín-Closas, C., Meléndez, A., Meléndez, N., Aurell, M., 1995. Estratigrafía del Cretácico inferior del sector central de la Cordillera Ibérica. Estudios Geol 51, 141–152.
Strasser, A., 1988. Shallowing-upward sequences in Purbeckian peritidal carbonates (lowermost Cretaceous, Swiss and French Jura Mountains). Sedimentology 35, 369–383.
Strasser, A., 2007. Astronomical time scale for the Middle Oxfordian to Late Kimmeridgian in the Swiss and French Jura Mountains. Swiss Journal of Geosciences 100, 407–429.
Strasser, A., Aurell, M., Bádenas, B., Meléndez, G., Tomás, S., 2005. From platform to basin to swell: orbital control on sedimentary sequences in the Oxfordian, Spain. Terra Nova 17, 407–413.
Tennant, P.J., Mannion, P.D., Upchurch, P., Sutton, M.D., Price, G.D., 2017. Biotic and environmental dynamics through the Late Jurassic–Early Cretaceous transition: evidence for protracted faunal and ecological turnover. Biological Reviews 92, 776–814.
Val, V., Bádenas, B., Aurell, M., Rosales, I., 2017. Cyclostratigraphy and chemostratigraphy of a bioclastic storm-dominated carbonate ramp (late Pliensbachian, Iberian Basin). Sedimentary Geology 355, 93–113.
Val, J., Aurell, M., Bádenas, B., Castanera, D., Subias, S., 2019. Cyclic carbonate–siliciclastic sedimentation in a shallow marine to coastal environment (latest Kimmeridgian–early Tithonian, Galve sub-basin, Spain). Journal of Iberian Geology 45, 195–222.
Wierzbowski, H., Anczkiewicz, R., Pawlak, J., Rogov, M.A., Kuznetsov, A.B., 2017. Revised Middle-Upper Jurassic strontium isotope stratigraphy. Chemical Geology 466, 239–255.

Appendix A. Supplementary data

Supplementary data to this article can be found online at https://doi.org/10.1016/j.cretres.2019.05.011.

5. FACIES ARCHITECTURE AND SEDIMENTARY MODELS OF THE LATEST KIMMERIDGIAN SHALLOW CARBONATE RAMP

CHAPTER

5

FACIES ARCHITECTURE AND SEDIMENTARY MODELS OF THE LATEST KIMMERIDGIAN SHALLOW CARBONATE RAMP

INTRODUCTION AND GOALS

The internal facies architecture in ancient shallow carbonate ramp successions is generally complex, because of the multiple palaeoenvironmental factors controlling the spatial facies distribution and sedimentary evolution of the platform (e.g. Burchette and Wright, 1992; Bádenas and Aurell, 2010; Pomar, 2018). Similar to modern shallow carbonate platforms (e.g. the Bahamas), complex patterns of depositional subenvironments can occur in specific areas of the carbonate ramp, showing a patchy distribution (i.e. facies mosaics) (e.g. Strasser and Védrine, 2009; Bádenas et al., 2010; Rankey, 2016). Therefore, the sedimentological characterization of these types of carbonate systems requires the analysis of continuous outcrops with data acquisition from closely-spaced logs, allowing to control the lateral and vertical facies relationships as detailed as possible, in both strike and down-dip directions (e.g. Bádenas and Aurell, 2010; Bádenas et al., 2010).

Understanding the facies architecture in carbonate ramps is relevant for exploration of carbonate reservoirs. In contrast to rimmed shelves, the low-angle depositional slope of carbonate ramps enables a greater progradation of the sedimentary bodies, being those represented by grain-supported facies of particular relevance as carbonate reservoirs. Therefore, the knowledge of the extent and heterogeneities of these sedimentary bodies is crucial in developing strategies for reservoir exploration, as it is the case of the shallow carbonate ramp deposits of the most important hydrocarbon carbonate reservoirs worldwide (e.g. the Arab-D Formation in Persian Gulf, Al-Awwad and Collins, 2013; or the Smackover Formation in the USA East Gulf, Benson, 1988). In this regard, because of the limited knowledge provided by subsurface data, outcrop analogue studies become essential for predictability of internal facies heterogeneities in shallow carbonate ramp systems.

The uppermost Kimmeridgian Higueruelas Fm represents the shallow areas of a carbonate ramp that developed in the northern Iberian Basin (NE Spain) (e.g. Aurell and Meléndez, 1986; Aurell et al., 2003, 2010, 2012; Ipas et al., 2004). It is composed of a wide variety of non-skeletal grains (mainly oncoids, ooids and peloids) and skeletal components (e.g. bivalves, dasyclads, gastropods, echinoderms, foraminifera, corals, stromatoporoids), as well as discrete chaetetid-stromatoporoid-coral buildups in mid-ramp settings. Previous sedimentological analyses on the Higueruelas Fm were based on the analysis of widely-spaced logs (e.g. Aurell and Meléndez, 1986, 1987; Aurell, 1990; Ipas, 2003; Ipas et al., 2004), and provided a first classification of main facies and depositional subenvironments.

In this Chapter, the along-strike and down-dip reconstruction of the facies heterogeneities for this latest Kimmeridgian shallow carbonate ramp in the outcrops of the Higueruelas Fm situated south of the city of Zaragoza, was accomplished by the bed-by-bed field description of 35 closely-spaced sedimentary logs and facies mapping in selected outcrops, in an area of 20 x 30 km in extent, complemented with petrographic characterization under binocular microscope on 1200 polished slabs and 300 thin sections. The results recorded in this Chapter are presented in two peer-reviewed scientific papers, corresponding to the along-strike and down-dip reconstruction of facies heterogeneities of this shallow carbonate ramp at different outcropping scales. Detailed information concerning the description of the sedimentary logs, field pictures of the Higueruelas Fm in each study sector, the mapping of facies, units and key surfaces in continuous outcrops, and the location of the collected samples for petrographic descriptions is presented as supplementary data in Annexe 1. A compilation of macro-scale polished slabs and microphotographs in thin sections for all the facies defined in this work is also recorded in Annexe 2.

From the 35 stratigraphic sections analysed in this Chapter, 21 logs are distributed throughout the study area from the localities of Muel to Aguilón, with an average separation distance of 5 km. Recognition and correlation of 9 sedimentary units or high-frequency sequences bounded by continuous, km-scale sharp bedding surfaces, allowed deciphering the lateral and vertical facies relationships in several western-eastern (i.e. down dip) orientated cross-sections. In addition, the excellent outcrop conditions of the Higueruelas Fm around the locality of Mezalocha, recording sedimentation in the inner areas of the carbonate ramp, were suitable for a detailed analysis of facies distribution and their lateral extent in these domains of the platform, by physical tracing of master bedding surfaces and facies mapping along continuous outcrops in an area of 1 x 2 km in extent.

The characterization of the internal facies heterogeneities of the latest Kimmeridgian shallow carbonate ramp succession in both strike and down-dip directions, provides key guidelines concerning the interpretation of facies distributions and factors controlling the stratigraphic facies architecture in shallow carbonate ramp systems constituted by similar components. Concerning the reservoir characterization, the sedimentary models proposed here have important implications for obtaining more realistic reconstructions of the facies heterogeneities at interwell scale, being of great interest for facies stacking pattern predictability in carbonate reservoirs of similar age and composition.

Facies (2018) 64:9
https://doi.org/10.1007/s10347-018-0521-8

ORIGINAL ARTICLE

Facies mosaic in the inner areas of a shallow carbonate ramp (Upper Jurassic, Higueruelas Fm, NE Spain)

C. Sequero[1] · B. Bádenas[1] · M. Aurell[1]

Received: 21 September 2017 / Accepted: 9 January 2018

Abstract
The internal facies and sedimentary architecture of an Upper Jurassic inner carbonate ramp were reconstructed after the analysis and correlation of 14 logs in a 1 × 2 km outcrop area around the Mezalocha locality (south of Zaragoza, NE Spain). The studied interval is 10–16 m thick and belongs to the upper part of the uppermost Kimmeridgian–lower Tithonian Higueruelas Fm. On the basis of texture and relative proportion of the main skeletal and non-skeletal components, 6 facies and 12 subfacies were differentiated, which record subtidal (backshoal/washover, sheltered lagoon and pond/restricted lagoon) to intertidal subenvironments. The backshoal/washover subenvironment is characterized by peloidal wackestone–packstone and grainstone. The lagoon subenvironment includes oncolitic, stromatoporoid, and oncolitic-stromatoporoid (wackestone and packstone) facies. The intertidal subenvironment is represented by peloidal mudstone and packstone–grainstone with fenestral porosity. Gastropod-oncolitic (wackestone–packstone and grainstone) facies with intercalated marl may reflect local ponds in the intertidal or restricted lagoon subenvironments. Detailed facies mapping allowed us to document 7 sedimentary units within a general shallowing-upward trend, which reflect a mosaic distribution, especially for stromatoporoid and fenestral facies, with facies patches locally more than 500 m in lateral extent. External and internal factors controlled this heterogeneity, including resedimentation, topographic relief and substrate stability, combined with variations in sea-level. This mosaic facies distribution provides useful tools for more precise reconstructions of depositional heterogeneities, and this variability must be taken into account in order to obtain a solid sedimentary framework at the kilometer scale.

Keywords Carbonate ramp · Facies mosaic · Intertidal · Sheltered lagoon · Higueruelas Fm · Upper Jurassic

Introduction

Facies reconstructions of shallow-water areas of ancient epeiric, tropical–subtropical carbonate ramps are difficult to decipher due to the lack of good outcrop control of these complex internal ramp areas, and as a consequence, knowledge of the internal and external factors that controlled the sedimentary and facies evolution is limited (e.g., Burchette and Wright 1992; Bádenas and Aurell 2010). It is well known that in modern shallow-water carbonate platforms (e.g., the Bahamas), the depositional environments show a high variability in lateral extent and distribution (e.g., Rankey and Reeder 2010; Rankey 2016), and commonly display a complex pattern of depositional subenvironments with a patchy distribution (i.e., facies mosaics; Strasser and Védrine 2009).

The concept of a facies mosaic has been the subject of re-analysis by several authors (e.g., Schlager 2000, 2003; Burgess and Wright 2003; Burgess and Emery 2004; Wright and Burgess 2005; Védrine et al. 2007; Strasser and Védrine 2009; Bádenas et al. 2010; Rankey 2016). The carbonate facies models of Wilson (1975), Jones and Desrochers (1992) and Flügel (2004) described facies zones that give a general picture of the potential distribution of sedimentary environments and biota. On the other hand, Read (1985), Burchette and Wright (1992) and Pomar (2001) have emphasized the differences between the geometries of carbonate ramps and other kinds of carbonate platform, and discussed their implications for the facies distribution of marine carbonate systems. Wright and Burgess (2005) pointed out the high temporal and spatial variability of depositional environments that leads to facies mosaics, which correspond to reality better than the linear arrangement of facies belts shown

✉ C. Sequero
csequero@unizar.es

[1] Departamento Ciencias de la Tierra-IUCA, Universidad de Zaragoza, 50009 Zaragoza, Spain

Published online: 02 February 2018

in many models. This is the case with the complex spatial variation and associated vertical stacking of peritidal carbonate facies at the sub-meter scale, which reflect the interplay between intrinsic factors specific to the environments of deposition (Verwer et al. 2009; Bádenas et al. 2010), such as the existence of preferential carbonate-producing areas, sediment redistribution caused by hydrodynamic conditions, or local depositional relief (Ginsburg 1971; Pratt and James 1986), and external eustatic and tectonic controls, such as sea-level changes controlled by Milankovitch orbital forcing (Goldhammer et al. 1990; Lehrmann and Goldhammer 1999; Strasser et al. 1999). Accordingly, some authors attribute vertical facies stacking to random migration of depositional environments and stress the importance of stochastic processes during sediment accumulation in modern carbonate settings, questioning the existence of meter-scale shallowing-upward cyclicity (Drummond and Wilkinson 1993; Wilkinson et al. 1996; Wilkinson and Drummond 2004).

A number of studies have tested the complex distribution of facies on carbonate platforms: Gischler and Lomando (1999) documented the high complexity of facies distribution of isolated carbonate platforms in Belize; Riegl and Piller (1999) mapped the great lateral variability of coral carpets, reefs and carbonate sand in Safaga Bay (Egypt), and Rankey (2002) discussed the fractal nature of facies patches on the tidal flats of Andros Island (Bahamas). Strasser and Védrine (2009) showed the facies heterogeneities on a shallow-water carbonate ramp of the Oxfordian (Late Jurassic) of the Swiss Jura Mountains and the facies evolution along selected time-lines, underlining that ancient, shallow-water carbonate systems are as complex as modern ones. Verwer et al. (2009) also noted a patchy distribution for a shoal-barrier complex in a Lower Jurassic platform in Djebel Bou Dahar (High Atlas, Morocco), and observed the higher lateral continuity of facies when the relative water depth increased during flooding of the platform top.

The studied examples have shown that the complex relationship of internal and external factors controlling facies distribution varies greatly with the nature of the carbonate systems (i.e., carbonate-producing biota). To increase our knowledge and understanding of the concept of a facies mosaic, therefore, further detailed case studies are required. The main purpose of this work is to investigate the lateral continuity and facies variability of the inner areas of a shallow carbonate ramp that developed around the Kimmeridgian–Tithonian transition (Higueruelas Fm, Iberian Basin), which reflect a mosaic facies distribution, and to decipher the depositional controls. The lateral and vertical distribution of facies are revealed through an extensive sedimentological analysis of the outcrops located near the Mezalocha locality (northeast Spain). Previous works on the Upper Jurassic Higueruelas Fm in northeastern Iberia have documented a spatial distribution of facies based on the correlation of separate stratigraphic logs (Aurell and Meléndez 1986, 1987; Cepriá et al. 2002; Ipas et al. 2004). Here, a more detailed scheme of the spatial relationships of the facies is presented by means of the exhaustive facies mapping and physical tracing of a number of sharp, reference bedding planes for correlation of the stratigraphic logs. The mosaic facies distribution can provide useful tools for achieving precise reconstructions of depositional heterogeneities in similar settings, and an understanding of the factors controlling these facies mosaics may be relevant to the interpretation of the vertical stacking of facies in high-frequency cycles and the correlation of cycles at larger scales.

Fig. 1 **a** Paleogeography of western Europe during the late Kimmeridgian (modified from Dercourt et al. 1993). **b** Facies distribution around the Kimmeridgian–Tithonian transition in the northern Iberian Basin with the location of Mezalocha and the other logged outcrops (from Ipas et al. 2004). **c** Vertical facies evolution for the Higueruelas Formation in Mezalocha (from Ipas et al. 2004). The upper part corresponds to the succession studied in this work. **d** Field view of the Higueruelas Fm and the underlying Loriguilla Fm. The lower boundary of the Higueruelas Fm corresponds to a basin-wide discontinuity surface. The dashed red line overlaps the stratigraphic section studied here

Geological setting

During the Late Jurassic, shallow epeiric seas covered wide areas of western Europe, and carbonate sedimentation was dominant in the platforms facing the Tethys Ocean to the east (Dercourt et al. 1993). This was the case with the wide carbonate ramp that developed in the Iberian Basin, east of the Iberian Massif (Fig. 1a, b; Aurell et al. 1994, 2002; Bádenas and Aurell 2001). The sedimentary evolution of this carbonate ramp during the Kimmeridgian–Tithonian transition in this carbonate ramp was characterized by a major regression controlled by the tectonic uplift of the Iberian Massif combined with a long-term regional fall in sea-level (Bádenas and Aurell 2001; Aurell et al. 2003).

In the central Iberian Basin, three third-order depositional sequences have been recognized for the Kimmeridgian–lower Tithonian sedimentary succession (Kim1, Kim2 and Ti1 sequences; Bádenas and Aurell 2001; Aurell et al. 2010). The stratigraphic succession studied in the present work belongs to the upper Kimmeridgian–lower Tithonian Ti1 sequence and is located in the north-central part of the Iberian Basin (Fig. 1b). Here, the Ti1 sequence is represented by the shallow-water carbonate deposits of the Higueruelas Fm, which records a wide range of grain-supported textures with variable proportions of skeletal remains (e.g., corals, stromatoporoids, foraminifera, molluscs, serpulids, echinoderms) and non-skeletal components (oncoids,

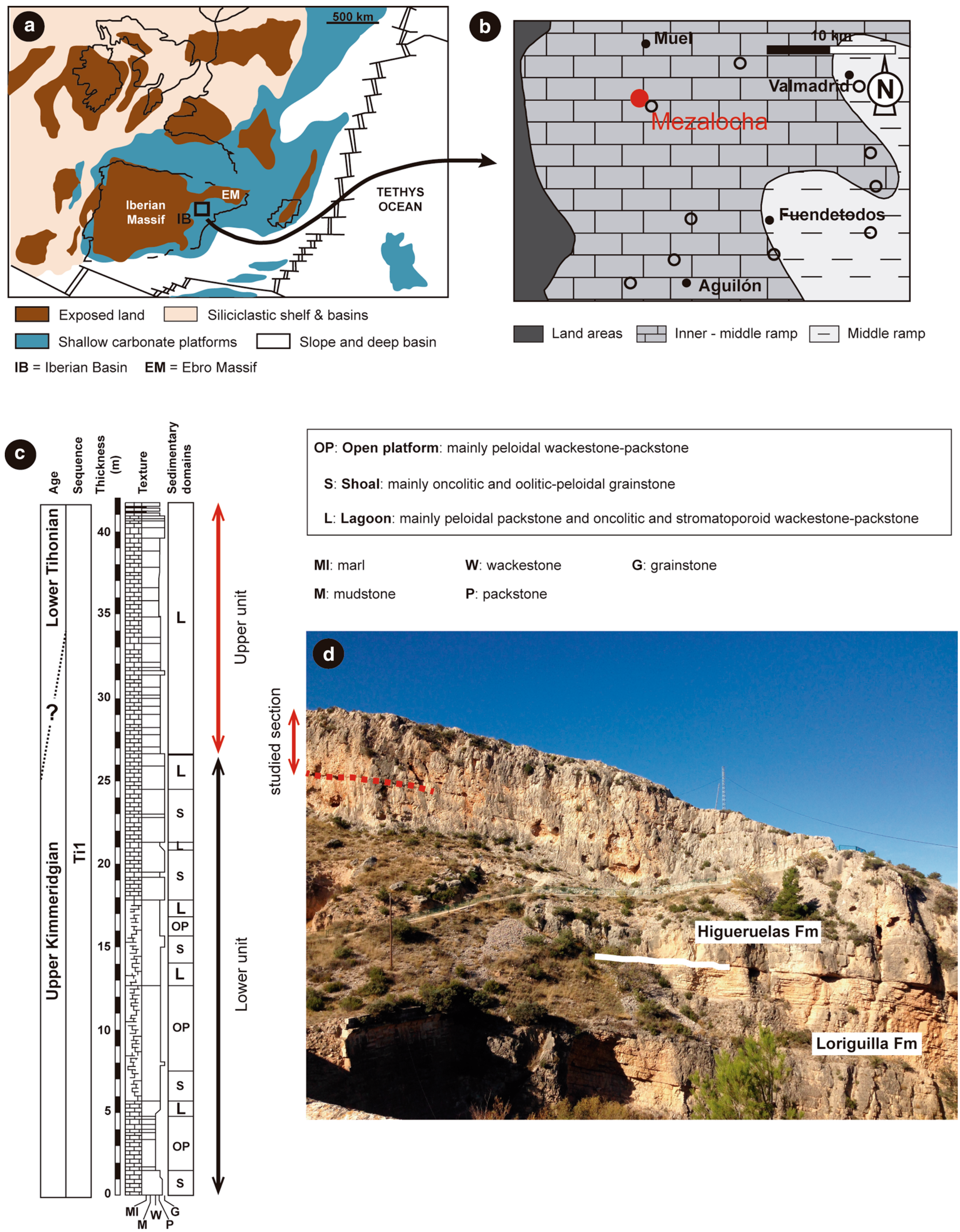
a
500 km
Iberian Massif
IB
EM
TETHYS OCEAN
Exposed land
Siliciclastic shelf & basins
Shallow carbonate platforms
Slope and deep basin
IB = Iberian Basin EM = Ebro Massif
b
Muel
10 km
Valmadrid
N
Mezalocha
Fuendetodos
Aguilón
Land areas
Inner - middle ramp
Middle ramp
c
Age
Sequence
Thickness (m)
Texture
Sedimentary domains
Lower Tithonian
?
Upper Kimmeridgian
Ti1
40
35
30
25
20
15
10
5
0
L
S
OP
Upper unit
Lower unit
Ml M W P G
OP: Open platform: mainly peloidal wackestone-packstone
S: Shoal: mainly oncolitic and oolitic-peloidal grainstone
L: Lagoon: mainly peloidal packstone and oncolitic and stromatoporoid wackestone-packstone
Ml: marl
M: mudstone
W: wackestone
P: packstone
G: grainstone
d
studied section
Higueruelas Fm
Loriguilla Fm

ooids, peloids, aggregate grains) (e.g., Aurell and Meléndez 1986; Ipas et al. 2004).

In the studied outcrops located around Mezalocha, the Higueruelas Fm is 40–50 m thick and displays two main lithological units (Fig. 1c): (1) a lower unit (~ 26 m thick), characterized by very thick beds (1 m to several meters thick) of limestone which represent an alternation of oolitic-peloidal and oncolitic shoal facies, shallow peloidal open-platform and local peloidal lagoon facies; and (2) an upper unit (~ 15 m thick), characterized by dm- to m-thick tabular limestones, mostly comprising lagoon facies (Ipas et al. 2004), which constitutes the subject of the present study. The lower boundary of the Higueruelas Fm corresponds to the regional discontinuity surface that developed on top of the well-bedded dm-thick lime mudstones of the Loriguilla Fm (Aurell et al. 2010; Fig. 1d). The upper boundary of the Higueruelas Fm in the study area is a sharp erosive contact with the Neogene continental units of the Ebro Basin (lower Miocene tectonosedimentary unit T5; Muñoz et al. 2002).

In the Mezalocha area, the Kimmeridgian–Tithonian boundary is assumed to be located in the upper part of the Higueruelas Fm (Fig. 1c). Scarce mid-late Kimmeridgian ammonites are found in the open-platform facies of the underlying Kim2 sequence (i.e., upper Loriguilla Fm) in Aguilón and Fuendetodos outcrops (see Fig. 1b for location). Significant recorded ammonites are *Progeronia breviceps* (Quenstedt) and *Aspidoceras longispinum apeninicum* (Sowerby) in the middle and upper part of the Loriguilla Fm, respectively (Bádenas et al. 2003). In addition, the presence of *Anchispirocyclina lusitanica* (Egger) indicates a Tithonian age for the overlying terrigenous unit outcropping in nearby areas (i.e., Villar del Arzobispo Fm, Aguilón area, see Fig. 1b: Ipas et al. 2007; Hernández-Samaniego and Ramírez-Merino 2005).

Methodology

The present study focuses on the upper (~ 15 m thick) unit of the Higueruelas Fm in the outcrops located around the locality of Mezalocha, which represent an area of 1 × 2 km in extent (Fig. 2). Here, a low tectonic dip (˂ 20°) and good outcrop conditions in small active and inactive quarries allow an accurate analysis of the uppermost Kimmeridgian–lower Tithonian inner ramp lagoonal facies. Regarding the general paleogeographic reconstruction of the Iberian Basin during this time interval (Fig. 1b), the distal facies for the studied Mezalocha outcrops are thought to be located to the southeast.

Facies analysis was based on a bed-by-bed field description of 14 closely spaced sedimentological logs (M1 to M14 in Fig. 2), and this was complemented with the petrographic description of rock samples in 111 thin-sections and 438 polished slabs (two samples/m on average). Petrographic analysis allowed us to determine the semi-quantitative proportion of skeletal and non-skeletal components, as well as the texture following the Dunham (1962) classification. For the description of non-skeletal grains, the proposed nomenclature for oncoids (Dahanayake 1977), ooids (Strasser 1986) and peloids (Flügel 2004) was adopted.

The physical tracing of bedding planes was carried out in order to decipher their geometry and lateral continuity. Facies and subfacies were differentiated in the studied logs mainly on the basis of the texture and the relative proportion of the main skeletal and non-skeletal components. Identifying the lateral facies changes between logs was helped by the recognition of a number of continuous sharp bedding planes physically traced along the outcrops, which were considered to be isochrones at outcrop-scale. In areas without lateral continuity of outcrop, lateral facies correlation was accomplished using the best fit of facies between logs based on vertical facies distribution. The sedimentary features of facies and subfacies and their lateral and vertical stacking patterns were the key criteria for their paleoenvironmental interpretation.

Bedding pattern

The limestones of the upper part of the Higueruelas Fm are arranged in tabular beds (0.1–2 m in thickness), with sharp to diffuse bedding planes (Figs. 3 and 4). In particular, the physical tracing of bedding planes allowed the identification of 6 sharp bedding planes that are continuous at outcrop scale, some of which correspond to Fe-enriched surfaces (see 1–6 in Figs. 3a and 4). Locally, cm-thick marly beds overlie these sharp surfaces. These sharp bedding planes allowed us to document 7 sedimentary units (A–G in Fig. 3a, b), with an average thickness of between 0.6 and 4 m. Lateral variations in thickness are found within the sedimentary units, especially for B (0.6–3 m), C (1.2–3.4 m) and D (0.7–4 m).

Varying numbers of diffuse bedding planes were identified in the individual logs within the 7 sedimentary units. These surfaces cannot be physically traced at outcrop scale, reflecting the fact that they correspond to discontinuous bedding planes. As no evidence of lenticular bedding geometries has been observed in the outcrops, the proposed correlation of the diffuse bedding surfaces (Fig. 3a) suggests an aggradational pattern of these beds similar to that of the sedimentary units A–G, instead of a lateral pinching out of beds.

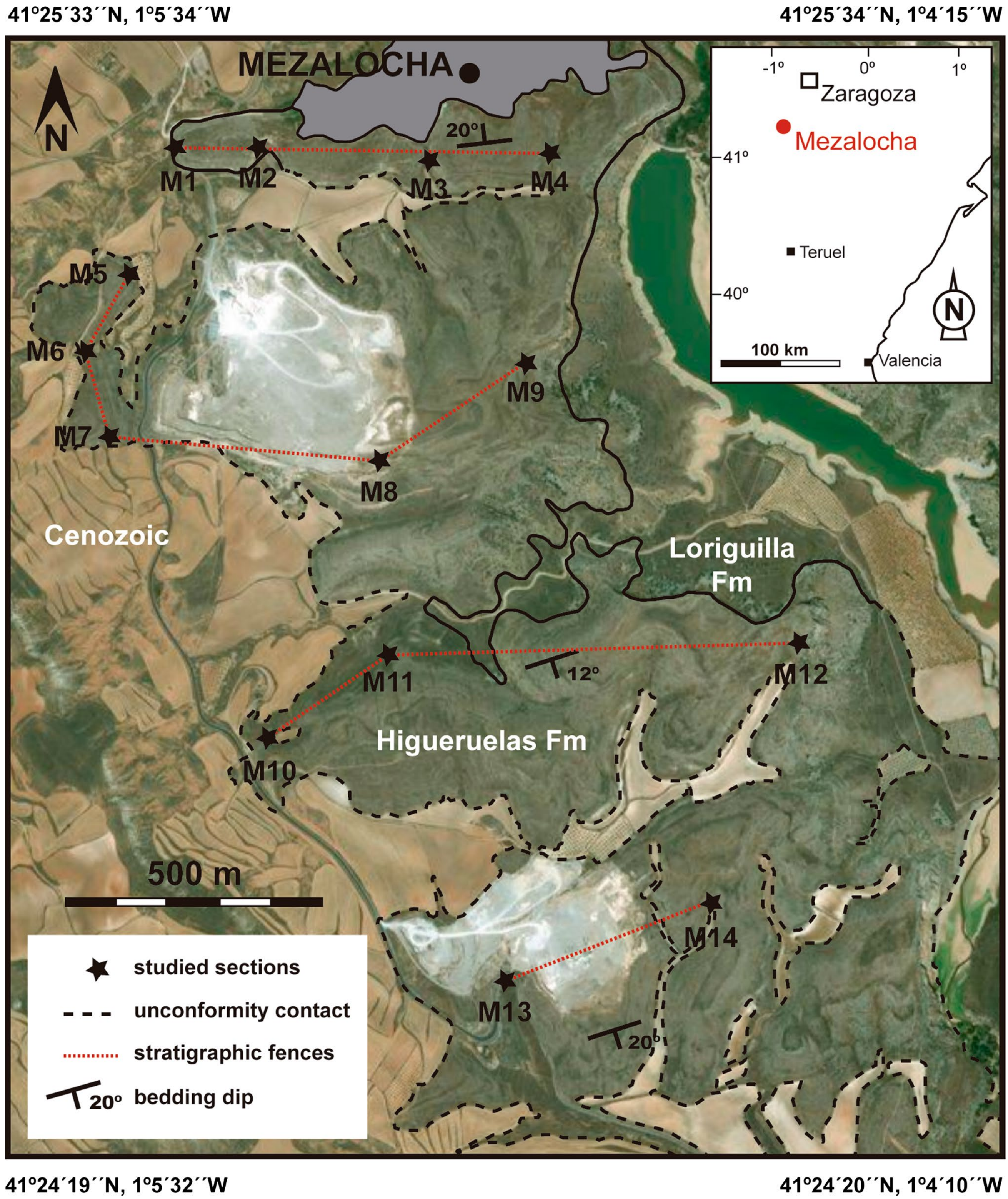

Fig. 2 Location of the studied sections (M1 to M14) across the Mezalocha outcrops, located south of Zaragoza (northeast Spain)

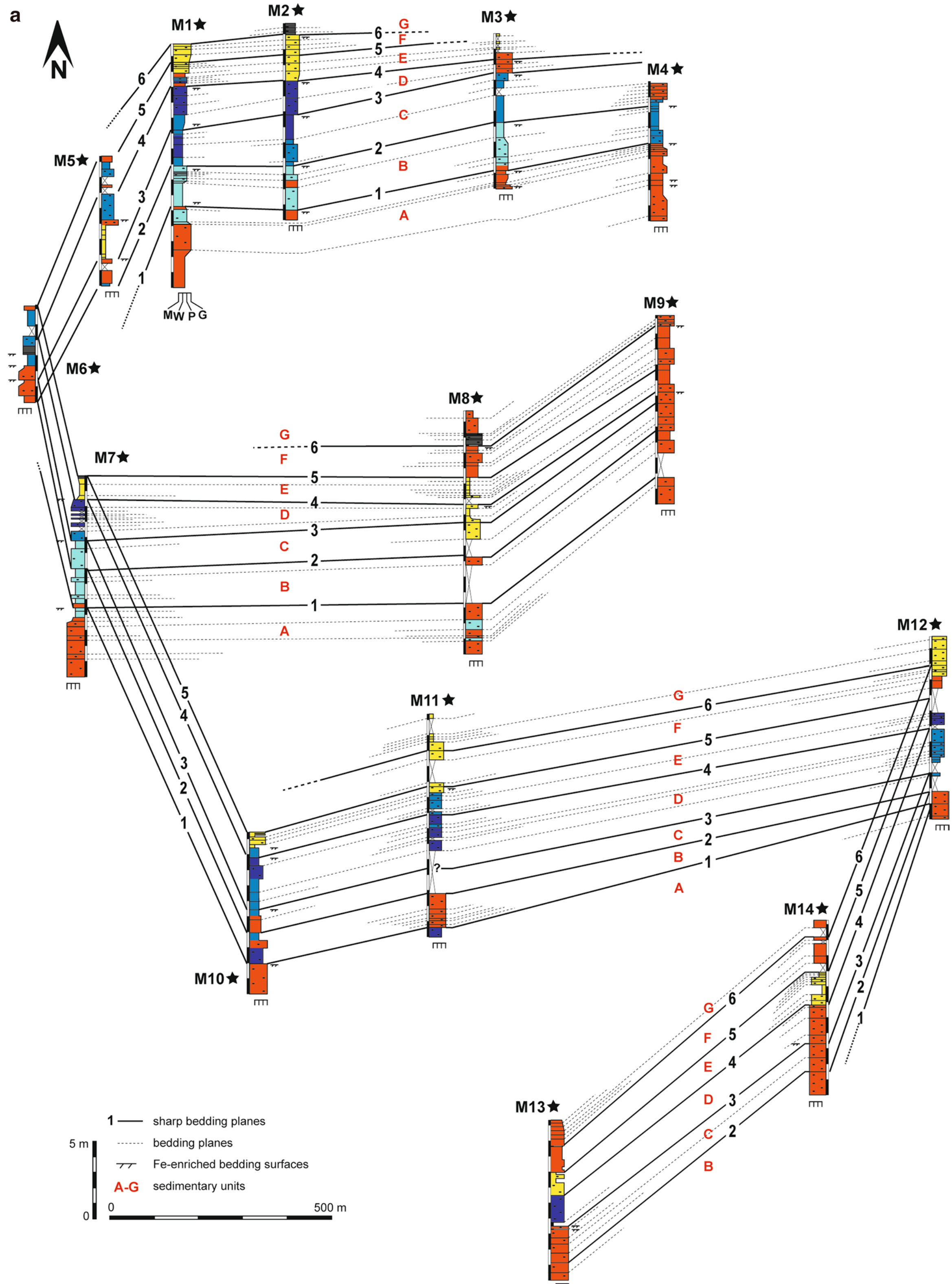

Fig. 3 **a** Vertical distribution of facies and bedding surfaces in the 14 stratigraphic logs (M1 to M14) in the Mezalocha outcrops. The correlation between logs is based on the physical tracing of 6 sharp bedding planes (black lines), which have made it possible to document 7 sedimentary units (A–G). The proposed correlation of bedding surfaces within the sedimentary units is also indicated (dashed lines). **b** Correlation panels showing the lateral and vertical facies changes between the 14 stratigraphic logs. **c** Facies and subfacies relationships

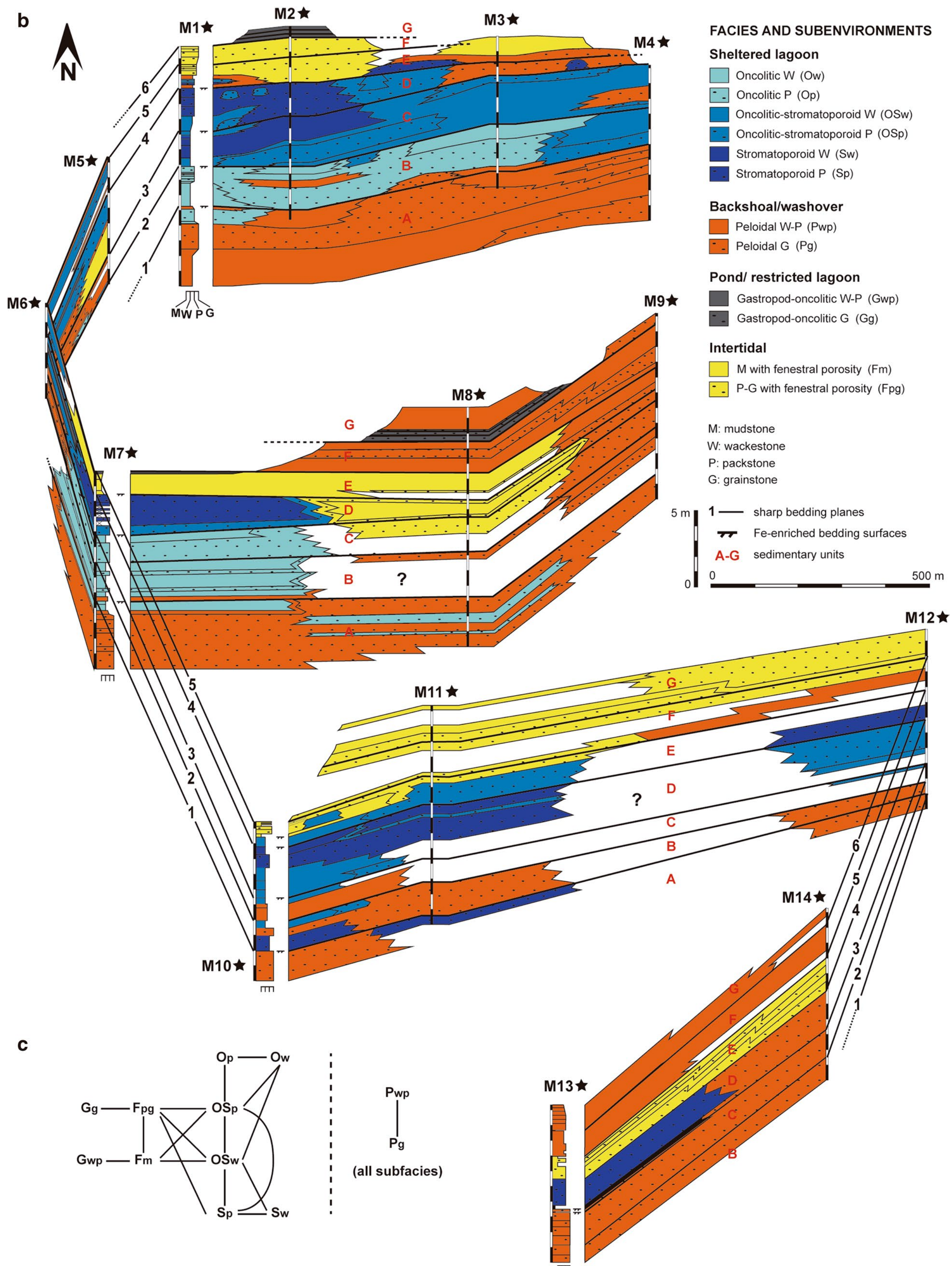

Fig. 3 (continued)

Facies analysis

On the basis of their components, textures and sedimentary structures, 6 facies and 12 subfacies were distinguished across the entire study area (Table 1, Figs. 5, 6, 7). Their vertical and lateral distribution within the 7 sedimentary units A–G, is shown in Fig. 3b. Each facies is characterized by a suite of dominant carbonate grains, and their corresponding subfacies are mainly differentiated according to the texture and proportion of dominant grains: (1) peloidal (P) facies encompasses grainstone (Pg) and wackestone–packstone (Pwp) subfacies; (2) oncolitic (O) facies includes packstone (Op) and wackestone (Ow) subfacies; (3) stromatoporoid (S) facies comprises packstone (Sp) and wackestone (Sw) subfacies; (4) oncolitic-stromatoporoid (OS) facies encompasses packstone (OSp) and wackestone (OSw) subfacies; (5) fenestral (F) facies includes packstone–grainstone (Fpg) and mudstone (Fm) subfacies; and (6) gastropod-oncolitic (G) facies comprises grainstone (Gg) and wackestone–packstone (Gwp) subfacies.

On the basis of their sedimentary features and the lateral and vertical facies relationships, each facies and subfacies was assigned to a particular subenvironment within the inner domains of the studied carbonate ramp: i.e., backshoal/washover, sheltered lagoon, intertidal and local subtidal pond/restricted lagoon subenvironments.

Backshoal/washover facies

The backshoal/washover deposits are represented by the peloidal (P) facies (Fig. 5a–d). This facies is generally arranged in dm- to m-thick tabular to irregular beds, with parallel and local cm-thick sets of planar cross-lamination, local mm- to cm-thick oncolitic, skeletal and oolitic laminae with normal gradation, and common bioturbation. It is characterized by an abundance of irregular and poorly sorted lithic peloids, and variable proportions of oncoids, ooids and skeletal grains (Table 1). The peloidal Pg subfacies (Fig. 5b–d) contains a higher proportion of ooids (type 1 and 1/3 ooids) compared with the peloidal Pwp subfacies (Fig. 5a), which has more abundant type I and II oncoids (Fig. 7a). The main skeletal components are bivalves, echinoderms, brachiopods, *Tubiphytes*, dasycladacean algae, gastropods and foraminifera (lituolids, textulariids and miliolids).

This facies changes laterally and vertically into almost all facies and subfacies (see Fig. 3b, c). The lateral and vertical relationships of the P facies, the grain-supported texture, the mixture of different types of high-energy non-skeletal grain (lithic peloids, type 1 and 1/3 ooids and type I and II oncoids; e.g., Flügel 2004; Strasser 1986; Dahanayake 1977), and the presence of parallel- and planar cross-lamination, and cm-thick accumulations of ooids, oncoids and bioclasts, indicate that the P facies corresponds to resedimented sediments (washover) as well as backshoal sediments of distal oolitic-peloidal and oncolitic banks or shoals. These shoal facies are not registered in the studied upper unit of the Higueruelas Fm, but they have been documented by Aurell and Meléndez (1986) and Ipas et al. (2004) in the lower part of the underlying unit in the Mezalocha outcrops (see Fig. 1c). The variation in texture and proportion of dominant carbonate grains between the Pg and Pwp subfacies is thought to be due to different high-energy conditions and the influence of the distal banks or shoals. The grainstone texture and the predominance of lithic peloids and type 1 and 1/3 ooids in the Pg subfacies reflect high-energy conditions (e.g., Flügel 2004; Strasser 1986), i.e., backshoal areas close to the distal oolitic-peloidal shoals or washover deposits. By contrast, the presence of carbonate mud and the predominance of oncoids in the Pwp subfacies indicate deposition in lower-energy conditions, probably in backshoal areas of oncolitic-dominated shoals closer to the lagoon. Common bioturbation, the presence of aggregate grains and the micritization of skeletal and non-skeletal components reflect stabilization in the backshoal environment (Table 1; e.g., Bádenas and Aurell 2010).

Sheltered lagoon facies

The sheltered lagoon subenvironment includes the oncolitic (O), stromatoporoid (S) and oncolitic-stromatoporoid (OS) facies that are complexly laterally and vertically related (Fig. 3b, c), although the lateral relationships of the grain-supported subfacies (Op–OSp–Sp) and muddy subfacies (Ow–OSw–Sw) dominate. These facies are generally arranged in dm- to m-thick beds and usually show bioturbation (Table 1).

Oncolitic (O) facies

This is characterized by an abundance of type III oncoids (Figs. 5e, f and 7b), which display bioclastic cores and thick crusts mainly composed of an alternation of organism-bearing encrustations (e.g., *Bacinella irregularis*, *Lithocodium aggregatum*, *Cayeuxia-Ortonella*, *Girvanella*, *Thaumatoporella parvovesiculifera*) and micritic laminae. The oncoids are surrounded by a fine-grain-sized fraction composed mainly of lithic peloids. The Op and Ow subfacies are differentiated on the basis of the texture and on the presence of type 1 and 1/3 ooids in the oncolitic packstone (Op) subfacies (Fig. 5e, f). The skeletal content is low but includes a high diversity of bioclasts, mainly foraminifera, bivalves, echinoderms and brachiopods, which are commonly micritized (Table 1).

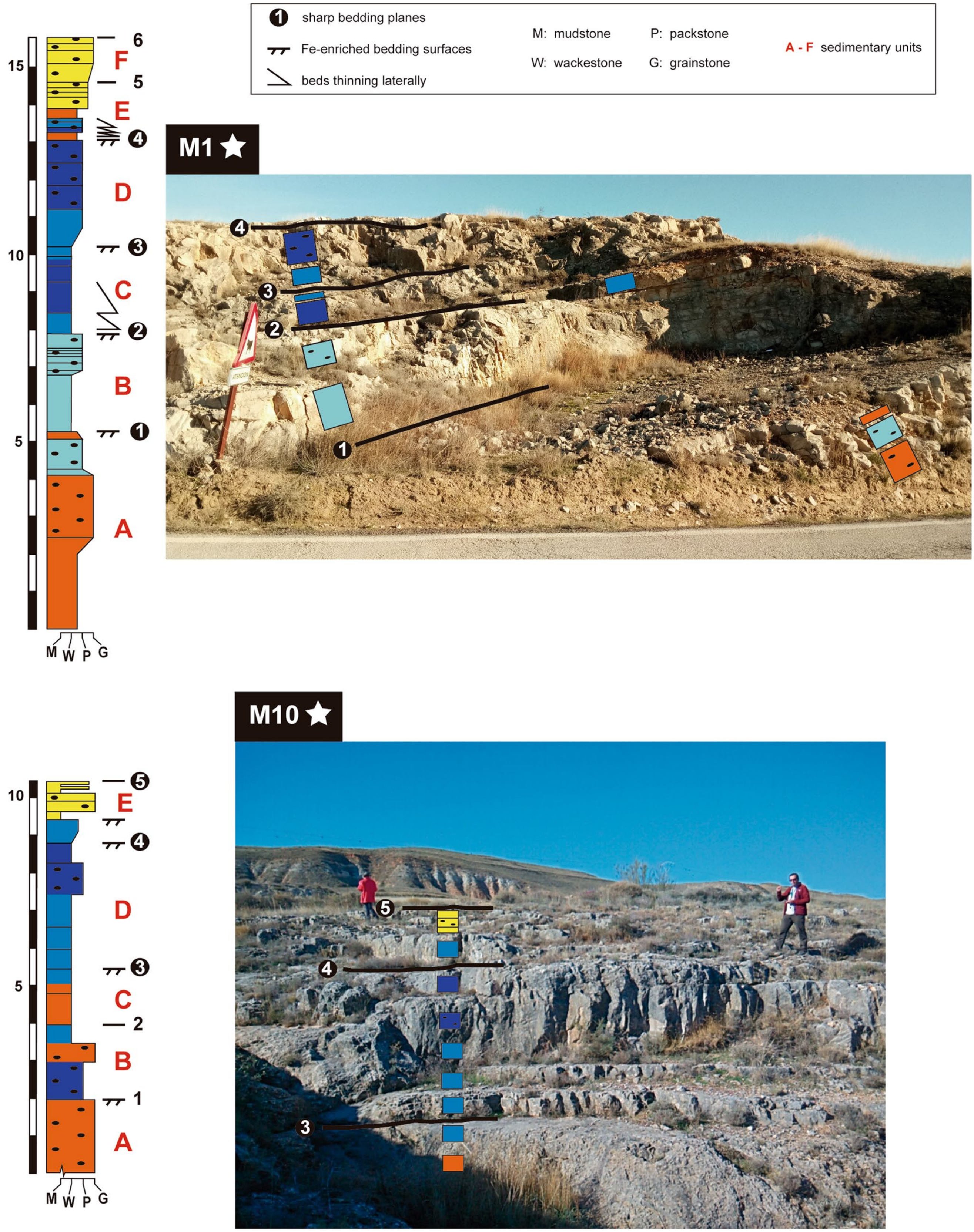

Fig. 4 Field view of sharp bedding planes (numbers in circles) recognized in the stratigraphic sections M1 and M10. These bedding planes can be traced across the entire study area. Notice the irregular aspect of stromatoporoid and oncolitic-stromatoporoid facies, versus the tabular aspect of oncolitic facies

Table 1 Facies and subfacies description

Facies and environments	Subfacies and components	Non-skeletal grains	Skeletal grains	Stratification and sedimentary structures
Peloidal facies (P) Backshoal/washover	Grainstone (Pg) Peloids (< 50%) Ooids (< 40%) Oncoids (< 30%) Skeletal grains (< 15%) Wackestone–packstone (Pwp) Peloids (< 50%) Oncoids (< 30%) Ooids (< 20%) Skeletal grains (< 10%)	Irregular and poorly sorted lithic peloids (∅ < 0.3 mm) Well-sorted, ovoid to spherical type 1 and 1/3 ooids (∅ < 0.3 mm), with bioclastic and intraclastic nuclei. Scarce compound and aggregate ooids Well-rounded to irregular, commonly ferruginized, type I and II oncoids (∅ < 2 cm), with bioclasts, intraclasts and aggregate grains in the nuclei and scarce organism-bearing encrustations (*Lithocodium aggregatum*, *Bacinella irregularis*, *Troglotella*, *Girvanella*, *Thaumatoporella parvovesiculifera*, *Cayeuxia-Ortonella*). Local type IVS oncoids Scattered intraclasts (micritic, bioclastic-oolitic-peloidal W-G), and sand-size quartz grains	Commonly micritized: mainly miliolids (*Quinqueloculina* sp., *Nautiloculina oolithica*), textulariids (*Redmondoides lugeoni*), echinoderms, bivalves, lituolids (*Kurnubia palastinensis, Kurnubia jurassica*, *Alveosepta* sp.), dasycladacean algae (*Clypeina jurassica*, *Salpingoporella annulata, Salpingoporella pygmaea*), gastropods, *Tubiphytes-Crescentiella* and brachiopods Scattered *Thaumatoporella parvovesiculifera*, *Cayeuxia-Ortonella*, serpulids, ostracods, stromatoporoids, rotaliids (*Mohlerina basiliensis*), involutina (*Andesenolina*) and sponge spicules	Tabular to irregular dm- to m-thick beds, locally thinning laterally Local parallel- and cross-lamination Local mm- to cm-thick oncolitic, skeletal and oolitic laminae with normal gradation Common bioturbation
Oncolitic facies (O) Sheltered lagoon	Packstone (Op) Oncoids (< 40%) Peloids (< 30%) Ooids (< 5%) Skeletal grains (< 15%) Wackestone (Ow) Oncoids (< 40%) Peloids (< 30%) Skeletal grains (< 5%)	Irregular type III oncoids (∅ < 5 cm), with bioclastic cores and thick crusts of organism-bearing encrustations (*Bacinella, Lithocodium, Cayeuxia-Ortonella, Girvanella, Thaumatoporella*) and micritic laminae. Scarce mm-size type I and II oncoids Well-sorted lithic peloids Type 1 and 1/3 ooids (mean ∅ < 0.1 mm), micritic intraclasts and microbial peloids	Commonly micritized: mainly lituolids (*Alveosepta*, *Labyrinthina mirabilis*), miliolids (*Quinqueloculina*), textulariids (*Remondoides lugeoni*, *K. jurassica*), bivalves, echinoderms and brachiopods Scattered gastropods, dasycladacean algae (*Salpingoporella*, *Clypeina*, *Pseudocyclammina*), rotaliids (*M. basiliensis*), involutina (*Trocholina*), *Cayeuxia-Ortonella*, *Tubiphytes-Crescentiella*, serpulids, ostracods, sponge spicules, stromatoporoids and corals (locally in situ)	Tabular dm- to m-thick beds Local cm-thick oncolitic laminae Bioturbation
Stromatoporoid facies (S) Sheltered lagoon	Packstone (Sp) Stromatoporoid cm-size fragments (< 40%) Fine grained, peloidal and skeletal, fraction (< 25%) Wackestone (Sw) Stromatoporoids (cm-size fragments and in situ) (< 40%) Fine grained, peloidal and skeletal, fraction (< 25%)	Microbial peloids (mean ∅ = 100 µm) and lithic peloids Type I and II oncoids (∅ < 1 cm), with bioclastic cores (stromatoporoids and corals) and thin crusts with organism-bearing encrustations (*Lithocodium*, *Bacinella*, *Thaumatoporella*, *Girvanella*) Type 1 and 1/3 ooids, compound ooids and oncoids, aggregate grains, micritic intraclasts	Stromatoporoids (*Cladocoropsis mirabilis*, *C. lindstroemi, Actinostromina grossa*), corals (*Stylophyllum polycanthum*) and chaetetids (*Spongiomorpha ramosa*). Common *Tubiphytes-Crescentiella* encrustations and bivalve borings (with peloidal infilling sediment) Small skeletal grains: mainly bivalves, brachiopods, echinoderms, lituolids (*Labyrinthina mirabilis*), miliolids (*Quinqueloculina*, *N. oolithica*), textulariids (*R. lugeoni*, *K. palastinensis*) and dasycladacean algae (*S. annulata, S. pygmaea, Pseudoclypeina distomensis*). Scattered gastropods, *Cayeuxia-Ortonella*, *Thaumatoporella*, ostracods, serpulids, sponge spicules, rotaliids (*Mohlerina basiliensis*) and involutina (*Trocholina*)	Tabular to irregular dm- to m-thick beds, locally thinning laterally Bioclastic mm- to cm-thick laminae Bioturbation
Oncolitic-stromatoporoid facies (OS) Sheltered lagoon	Packstone (OSp) Oncoids (< 30%) Stromatoporoids and coral fragments (< 30%) Fine grained, peloidal and skeletal, fraction (< 25%) Wackestone (OSw) Oncoids (< 40%) Stromatoporoid and coral fragments (< 40%) Fine grained, peloidal and skeletal, fraction (< 20%)	Well-rounded to irregular type I, II and III oncoids (∅ < 3 cm-size), commonly ferruginized, with bioclastic (stromatoporoids, bivalves) and intraclastic cores, and mm- to cm-thick crusts with organism-bearing encrustations (*Lithocodium, Bacinella, Girvanella, Troglotella*). Local bivalve borings (with peloidal infilling sediment) and compound oncoids Irregular to well-rounded lithic and microbial peloids Type 1 and 1/3 ooids, with foraminifera and peloids in the nuclei Scattered intraclasts, aggregate grains and sand-size quartz grains	Stromatoporoids and corals as in the stromatoporoid facies Small skeletal grains: mainly *Tubiphytes-Crescentiella*, lituolids (*L. mirabilis, Alveosepta*), miliolids (*Quinqueloculina, N. oolithica*), textulariids (*K. palastinensis, R. lugeoni*), bivalves, gastropods, echinoderms and brachiopods. Scattered *Cayeuxia-Ortonella*, dasycladacean algae (*C. jurassica, S. annulata*), ostracods, serpulids, *Thaumatoporella*, sponge spicules, rotaliids (*M. basiliensis*) and involutina (*Andesenolina*)	Tabular to irregular dm- to m-thick beds Components accumulated in mm- to cm-thick laminae Bioturbation

Table 1 (continued)

Facies and environments	Subfacies and components	Non-skeletal grains	Skeletal grains	Stratification and sedimentary structures
Fenestral facies (F) Intertidal	Packstone–grainstone with fenestral porosity (Fpg) Peloids (< 30%) Ooids (< 15%) Oncoids (< 10%) Skeletal grains (< 7%) Mudstone with fenestral porosity (Fm)	Poorly sorted and irregular to well-rounded lithic peloids Type 1 and 1/3 ooids, mm-size type II oncoids with intraclastic nuclei and thin crusts with *Bacinella* Scattered sand-size quartz grains	Lituolids, miliolids (*Quinqueloculina*), textularids (*K. jurassica*, *Ammobaculites* sp.), bivalves and *Tubiphytes-Crescentiella* as main skeletal grains Scattered dasycladacean algae (*Salpingoporella*, *C. jurassica*), gastropods, brachiopods, echinoderms, ostracods, *Cayeuxia-Ortonella*, serpulids, involutina and stromatoporoids	Tabular to irregular dm-thick beds 10–25% of isolated fenestral pores (Ø < 2 mm-size), parallel fenestral laminites (< 3 mm thick) and dome-like stromatolitic crusts. Common *Girvanella* and *Bacinella* growths, forming mm to cm-sized encrusting laminae Local bioturbation
Gastropod-oncolitic facies (G) Ponds in the intertidal area or restricted lagoon	Grainstone (Gg) Gastropods (< 20%) Oncoids (< 25%) Peloids (< 15%) Ooids (< 30%) Skeletal grains (< 20%) Wackestone–packstone (Gwp) Gastropods (< 20%) Oncoids (< 30%) Peloids (< 20%) Ooids (< 5%) Skeletal grains (< 10%)	Irregular to well-rounded type I, II and IVS oncoids (Ø < 1 cm-size), with bioclastic cores (gastropods, bivalves, dasycladacean algae, corals, stromatoporoids, lituolids) and thin crusts with *Bacinella* Irregular to well-rounded lithic peloids Well-rounded to ovoid type 1 and 1/3 ooids (Ø < 0.3 mm), with bioclastic nuclei (mainly gastropods and foraminifera) Scattered intraclasts, aggregate grains and sand-size quartz grains	Broken and whole gastropods Small skeletal grains, commonly micritized: mainly bivalves, lituolids, miliolids (*N. oolithica*) and textularids (*R. lugeoni*). Dasycladacean algae (*Pseudocyclammina*, *S. dinarica*) and echinoderms are locally abundant. Scattered brachiopods, *Thaumatoporella*, sponge spicules, *Cayeuxia-Ortonella*, *Tubiphytes-Crescentiella* and involutina (*Andesenolina*)	Tabular cm- to dm-thick beds, locally intercalated with cm-thick marly beds Components accumulated in cm-thick laminae Local bioturbation

The predominance of large and irregular type III oncoids, bioturbation and the variety of skeletal components reflect deposition in non-restricted shallow waters in generally calm conditions with intermittent high-energy conditions. During long periods under calm conditions, oncolitic bacterial growth (i.e., *Bacinella*, *Lithocodium*, *Cayeuxia-Ortonella*, *Girvanella*, *Thaumatoporella*) and micritization of skeletal grains is favored. Short high-energy periods favor the generation of micritic laminae in the oncoids (Dahanayake 1977). The presence of type 1 and 1/3 ooids in the Op subfacies and type I and II oncoids is due to the variable input of resedimented grains from the laterally related facies, mainly from the backshoal/washover peloidal (P) facies (Fig. 3b, c).

Stromatoporoid (S) facies

The stromatoporoid (S) facies is generally arranged in dm- to m-thick, irregular and tabular beds, and is characterized by an abundance of broken and in situ stromatoporoids (commonly *Cladocoropsis*), along with cm-size fragments of corals and chaetetids. *Tubiphytes-Crescentiella* encrustations are common on stromatoporoids (Figs. 5g, h and 7d). The fine-grain-sized fraction is composed of peloids (microbial and lithic peloids) and small skeletal grains, mainly of bivalves, brachiopods, echinoderms, foraminifera and dasycladacean algae (Table 1). Type I and II oncoids and type 1 and 1/3 ooids are also recognized in low proportions. The stromatoporoid packstone (Sp) and wackestone (Sw) subfacies are differentiated on the basis of the texture and the presence of in situ stromatoporoids in Sw (Fig. 5g). Bioturbation and mm-thick bioclastic accumulations are more common in Sp.

The stromatoporoid facies forms patches, locally more than 500 m in lateral extent and commonly related to oncolitic-stromatoporoid (OS) facies (Fig. 3b). The usual presence of *Cladocoropsis* in lagoonal facies has been highlighted by previous authors (e.g., Flügel 1974; Turnsek et al. 1981; Leinfelder et al. 2005; Aurell et al. 2012). Microbial peloids suggest high microbial activity, especially in Sw subfacies, related to lower-energy areas within the lagoon. The relatively low abundance of corals compared to stromatoporoids in the S facies seems to be related to the hydrodynamic conditions within the depositional environment; *Cladocoropsis* meadows and other stromatoporoids can be widespread in lagoonal areas as they are adapted to overheated waters, strong abrasion and probably oligotrophic conditions (Leinfelder et al. 2005). The presence of algae (dasycladacean, *Cayeuxia-Ortonella*, *Thaumatoporella*) indicates well-oxygenated, normal marine waters. Variable proportions of lithic peloids, gastropods, type I and II oncoids and type 1 and 1/3 ooids show the influence of the laterally related oncolitic-stromatoporoid (OS) and peloidal (P) facies (Fig. 3b, c).

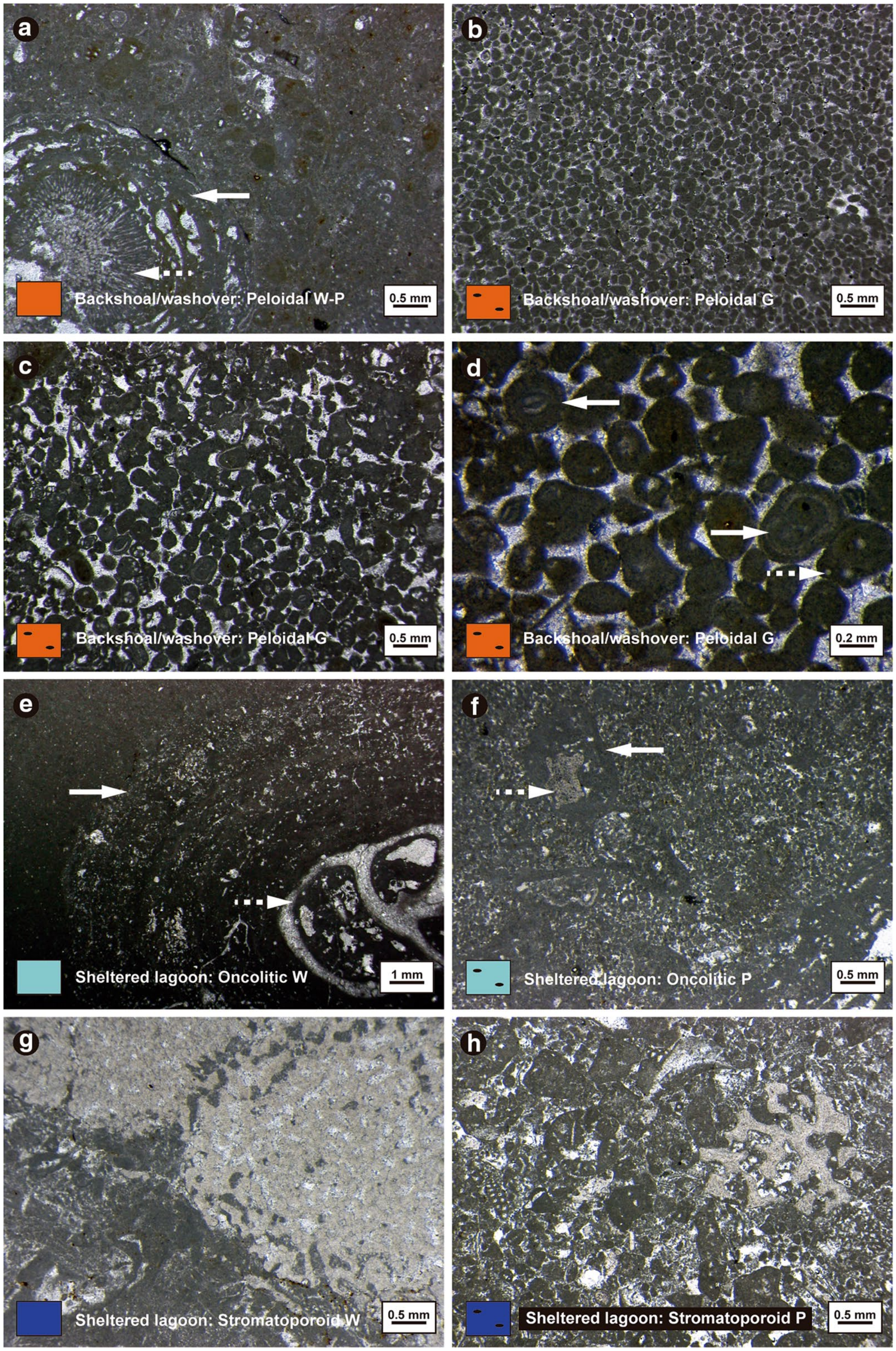

Oncolitic-stromatoporoid (OS) facies

The oncolitic-stromatoporoid (OS) facies is an intermediate facies of O and S facies, characterized as it is by a similar proportion of oncoids (types I, II and III) and stromatoporoid and coral fragments (Fig. 6a, b). The fine-grain-sized fraction is mainly composed of peloids (lithic and microbial peloids) and small skeletal grains, mainly comprising debris

◂**Fig. 5** **a**–**d** Peloidal facies (backshoal subenvironment). **a** Peloidal wackestone-packstone subfacies showing poorly sorted lithic peloids, some bioclasts and type II oncoids, with bioclastic core (*Cayeuxia-Ortonella*, dashed arrow) and micritic and grumose laminae (white arrow) displaying sparitic patches of *Bacinella–Lithocodium*. **b**–**d** Proximal backshoal subfacies composed of well-sorted (**b**) to poorly sorted (**c**) lithic peloids, type 1 and 1/3 ooids (white arrows in **d**) and compound and aggregate grains (dashed arrow in **d**). **e**, **f** Oncolitic wackestone (**e**) and packstone (**f**) subfacies (lagoon subenvironment), with type III oncoids showing thick crusts with micritic and sparitic laminae of *Bacinella* and *Girvanella* (white arrow in **e**), lithic peloids and type II oncoids (white arrow in **f**). Oncoids display bioclastic cores (gastropod for the type III oncoid in **e**, dashed arrow; echinoderm for the type II oncoids in **f**, dashed arrow). **g**, **h** Stromatoporoid wackestone (**g**) and packstone (**h**) subfacies (lagoon subenvironment), showing fragments of *Cladocoropsis*, poorly sorted peloids, microbial peloids and micritized bioclasts

from *Tubiphytes-Crescentiella*, foraminifera, bivalves, gastropods, echinoderms and brachiopods (Table 1). The OSw and OSp subfacies are differentiated on the basis of texture and a higher proportion of type 1 and 1/3 ooids in OSp (Fig. 6b). Bioturbation and mm- to cm-thick accumulations of coarse grains are also more common in this subfacies. By contrast, oncoids and stromatoporoid and coral fragments are more abundant in OSw subfacies.

The OS facies represents a transition between the oncolitic (O) and stromatoporoid (S) facies, with which it is complexly related (e.g., unit D in Fig. 3b; see the complex O–OS–S facies relationship in Fig. 3c). These facies relationships reflect the fact that the OS facies are lagoonal sediments surrounding the stromatoporoid patches (S facies; e.g., unit D in Fig. 3b). The higher proportion of type 1 and 1/3 ooids and mm- to cm-thick laminae in the OSp subfacies reflects the greater influence of resedimented grains from backshoal areas (P facies) compared to OSw. The higher proportion of oncoids and stromatoporoid and coral fragments in the OSw subfacies indicates lower energy-conditions and the greater influence of the other muddy lagoonal subfacies (Ow and Sw).

Intertidal facies

The intertidal facies is represented by the fenestral (F) facies (Fig. 6c–e). This facies is generally arranged in dm-thick tabular to irregular beds, and is characterized by the presence of fenestral pores and lithic peloids, and in lower proportions ooids, oncoids and skeletal grains, mainly of foraminifera, bivalves and *Tubiphytes-Crescentiella* (Table 1). The packstone–grainstone (Fpg) subfacies contains a higher proportion of peloids, type 1 and 1/3 ooids, type II oncoids and bioclasts compared with the mudstone (Fm) subfacies (Fig. 6c, d). *Girvanella* and *Bacinella* growths (Fig. 6e) forming mm- to cm-sized lamina packages, parallel fenestral laminites and dome-like stromatolitic crusts are also common.

This facies represents both the subaerial exposure of mud-supported and grain-supported lagoonal and washover sediments (Op, OSp, OSw and Sp subfacies), as indicated by the presence of fenestral porosity and its patchy distribution (200 m to more than 600 m in lateral extent), and a wider intertidal belt laterally related with muddy and grainy lagoonal sediments (Fig. 3b, c). The fenestral pores may be caused by the entrapment of air bubbles in the sediment by turbulent flows related to waves, algal activity or the drying and rapid precipitation of cements (e.g., Shinn 1968; Flügel 2004). The presence of *Girvanella* and *Bacinella* growths and dome-like stromatolitic crusts indicates microbial activity. Textural differences between the Fpg and Fm subfacies are due to the different facies being subjected to subaerial exposure (i.e., F patches) and the variable water energy and to the influence of sediment which is resedimented from surrounding areas (i.e., F intertidal belt).

Ponds in the intertidal area or restricted lagoon facies

This subenvironment is represented by the gastropod-oncolitic (G) facies (Fig. 6f–h). This facies is generally arranged in cm- to dm-thick tabular beds, and has locally intercalated marl. It is characterized by a predominance of broken and whole gastropods and type I, II and IVS oncoids (Fig. 7c), with variable proportions of lithic peloids, type 1 and 1/3 ooids and small, commonly micritized skeletal grains, mainly of bivalves and foraminifera (Table 1). The gastropod-oncolitic Gwp subfacies has a higher proportion of lituolids (Fig. 6f), whereas ooids and skeletal grains in cm-thick laminae are more abundant in the gastropod-oncolitic Gg subfacies. The gastropod-oncolitic G facies is related laterally with the peloidal (P) facies and with the fenestral (F) facies (G–F relationship in Fig. 3c). In particular, Gg–Fpg and Gwp–Fm lateral relationships are observed.

The remarkable predominance of gastropods, intercalations of marl and lateral associations with the fenestral facies indicate that the G facies probably corresponds to restricted ponds within the intertidal belt or to a restricted lagoon facies. Although there is not a good control of the lateral extent of this facies (see unit G in Fig. 3b), its relationship with the backshoal/washover P facies and with the intertidal F facies supports both interpretations. Textural differences and varying proportions of skeletal and non-skeletal grains between the Gg and Gwp subfacies are due to the influence of the surrounding sediment from the grain-supported and mud-supported fenestral facies and peloidal facies with which it is laterally related. Components accumulated in cm-thick laminae reflect grains resedimented during high-energy events, probably storms. Locally intercalated marl indicates periods of higher detrital input, when carbonate production is reduced or diluted.

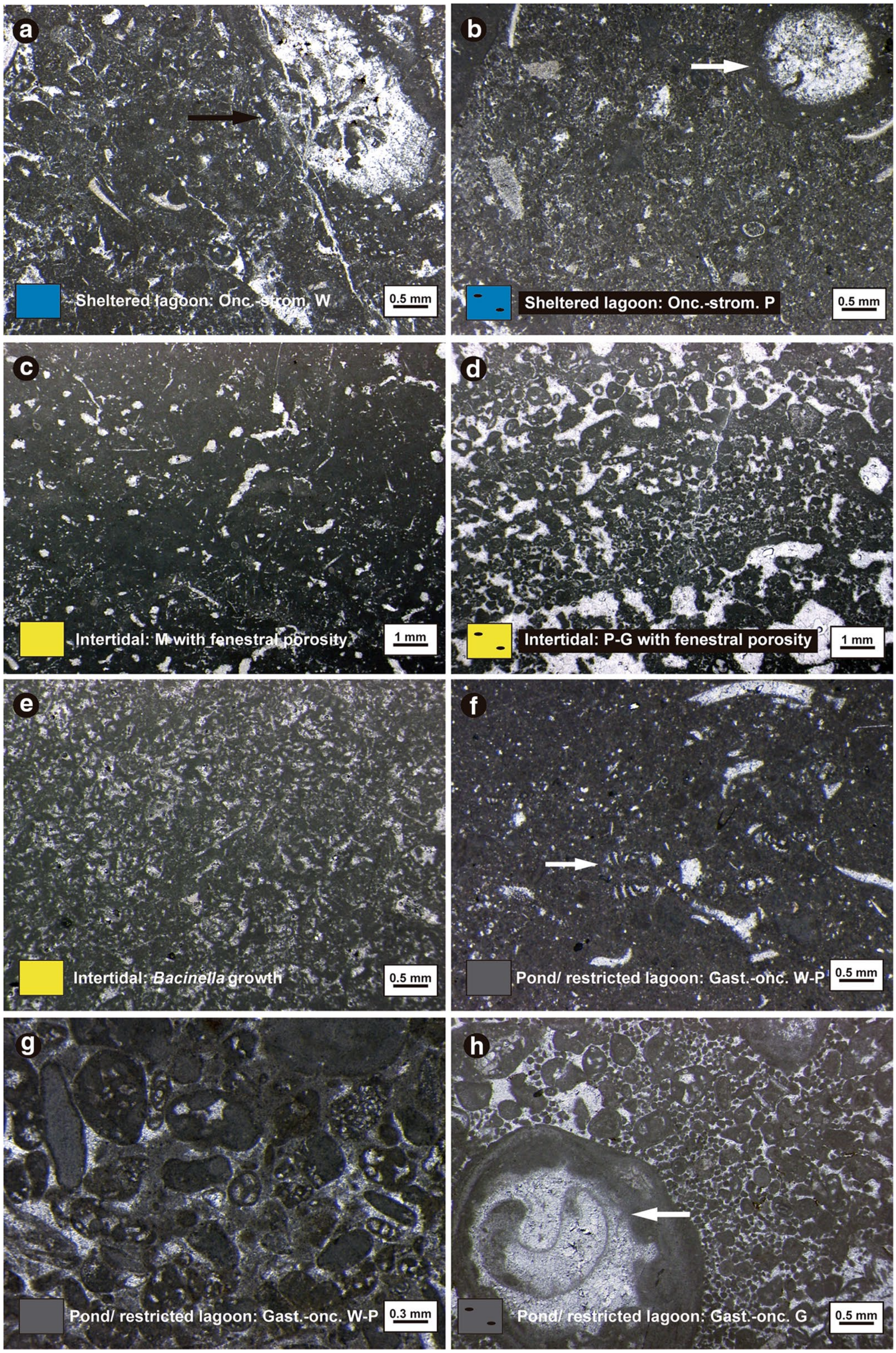

Fig. 6 **a**, **b** Oncolitic-stromatoporoid wackestone (**a**) and packstone (**b**) subfacies (sheltered lagoon subenvironment); the arrows indicate type II oncoids with bioclastic cores (corals) and thin crusts with grumose laminae. **c**, **d** Fenestral pores (intertidal subenvironment) in peloidal mudstone (**c**) and packstone-grainstone (**d**) layers. Note the dome-like stromatolitic structure formed by the fenestral porosity in **d**. **e** *Bacinella* growth in fenestral facies. **f–h** Gastropod-oncolitic facies (pond/restricted lagoon subenvironment). Lituolids are common in gastropod-oncolitic wackestone–packstone subfacies (white arrow in **f**), and components are usually micritized (**g**); **h** Well-sorted peloids, micritized bioclasts and ooids and type II oncoids in gastropod-oncolitic grainstone subfacies, with mainly gastropods as bioclastic cores (white arrow)

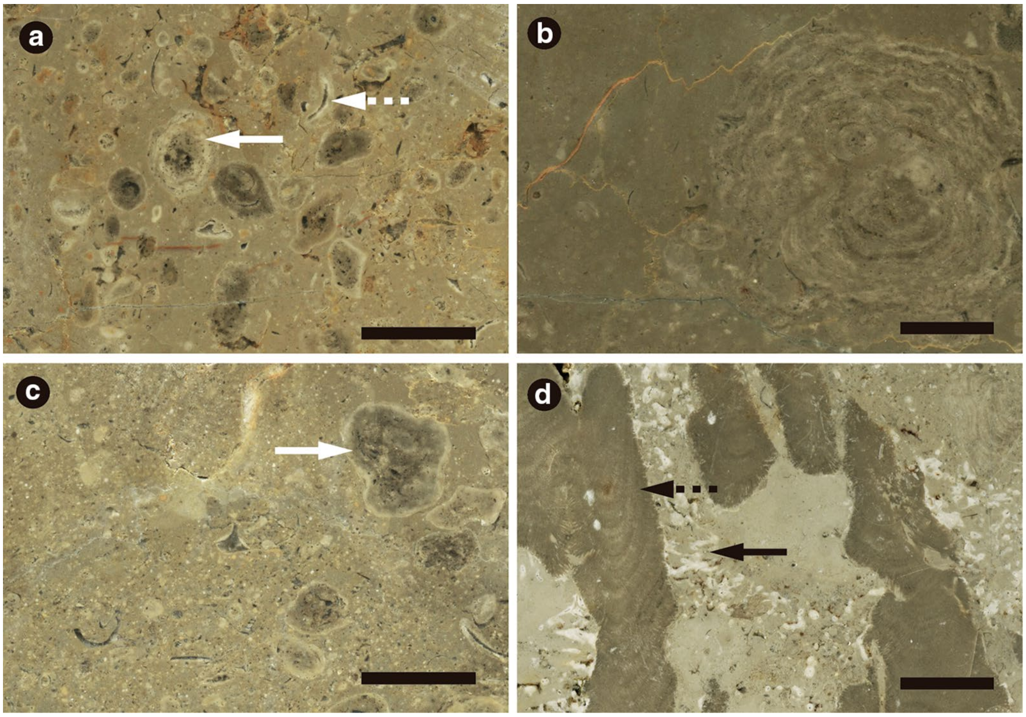

Fig. 7 **a**–**c** Polished slabs showing the different types of oncoids which characterize these facies. Type I and II oncoids (dashed and white arrows in **a**, respectively) are common in peloidal, oncolitic-stromatoporoid and gastropod-oncolitic facies. Type III oncoids are characteristic of oncolitic facies, and also appear in oncolitic-stromatoporoid facies (**b**). Type IVS oncoids (white arrow in **c**) appear especially in gastropod-oncolitic W–P subfacies, and also in peloidal W–P subfacies. **d** *Cladocoropsis*-type stromatoporoid in stromatoporoid facies (dashed arrow). *Tubiphytes-Crescentiella* encrustations (black arrow) usually grow around stromatoporoids. Scale bar is 1 cm

Facies mosaic and sedimentary evolution

The sedimentary model for the uppermost Kimmeridgian–lower Tithonian platform in the Mezalocha outcrops reflects a facies mosaic instead of continuous parallel–subparallel facies belts (Fig. 8a), as revealed by the detailed facies mapping following the 7 sedimentary units (A–G in Figs. 3 and 8b). The detailed facies maps in Fig. 8b also include the isopach lines for the successive sedimentary units (without decompaction, as W–P textures mostly dominate) to unravel the possible relationships of facies and variations in thickness.

At a long-term scale, the studied upper succession of the Higueruelas Fm reflects a shallowing-upward trend, from backshoal/washover and sheltered lagoon to intertidal and pond/restricted lagoon subenvironments. Units A and B show that the sheltered lagoon developed to the northwest, with a predominance of oncolitic O facies, with Ow subfacies located in the more internal and protected areas of the lagoon. The backshoal/washover P facies is located to the southeast and locally includes small patches of stromatoporoid S (around 300 m in extent) and oncolitic-stromatoporoid OS facies. This facies distribution is consistent with the general paleogeographic reconstruction indicating the distal facies located to the southeast (see Fig. 1b). In units C to E, the oncolitic O facies is considerably reduced, and stromatoporoid S facies patches dominate. These patches are more than 500 m in lateral extent and grade laterally mainly to oncolitic-stromatoporoid OS facies. In addition, the backshoal/washover facies is minor in extent compared with the initial units, and patches of the fenestral F facies developed mainly related to backshoal/washover peloidal (P) deposits and the OS facies (200 m to more than 500 m in lateral extent). In units F and G, there is a widespread development of the intertidal subenvironment represented by the fenestral facies, laterally associated with the backshoal/washover facies and local patches of pond/restricted lagoon gastropod-oncolitic G facies, thus representing the final shallowing episode in the studied area. As regards variations in thickness, there is a progressive increase in thickness from the backshoal/washover environment to the sheltered lagoon facies (e.g., 1–3 m, respectively, in units C to D). The average thickness is reduced and more homogeneous in the latest units dominated by the intertidal F facies (around 2 m in units E and F).

In summary, the backshoal/washover facies is present in all the sedimentary episodes, and changes laterally to almost all facies, since it is the result of the resedimentation

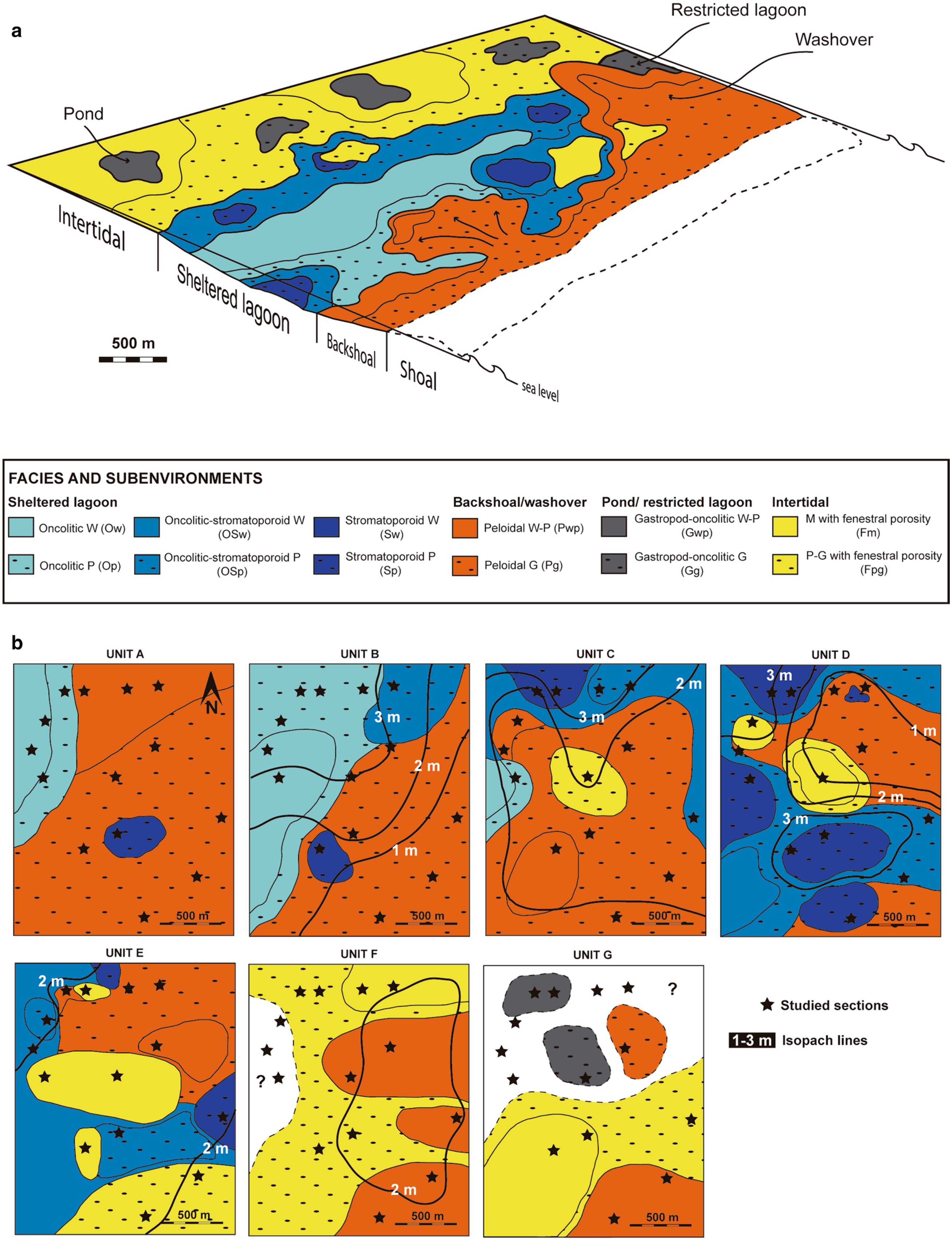

a
Restricted lagoon
Washover
Pond
Intertidal
Sheltered lagoon
Backshoal
Shoal
sea level
500 m
FACIES AND SUBENVIRONMENTS
Sheltered lagoon
Oncolitic W (Ow)
Oncolitic P (Op)
Oncolitic-stromatoporoid W (OSw)
Oncolitic-stromatoporoid P (OSp)
Stromatoporoid W (Sw)
Stromatoporoid P (Sp)
Backshoal/washover
Peloidal W-P (Pwp)
Peloidal G (Pg)
Pond/ restricted lagoon
Gastropod-oncolitic W-P (Gwp)
Gastropod-oncolitic G (Gg)
Intertidal
M with fenestral porosity (Fm)
P-G with fenestral porosity (Fpg)
b
UNIT A
N
500 m
UNIT B
3 m
2 m
1 m
500 m
UNIT C
2 m
3 m
500 m
UNIT D
3 m
1 m
2 m
3 m
500 m
UNIT E
2 m
2 m
500 m
UNIT F
?
2 m
500 m
UNIT G
?
500 m
Studied sections
1-3 m Isopach lines

◀**Fig. 8** **a** Sedimentary model showing the facies distribution of the carbonate ramp in the Mezalocha outcrops around the Kimmeridgian–Tithonian transition. **b** Successive facies maps reconstructed for the 7 sedimentary units identified within the studied succession. Isopach lines (1–3) for each sedimentary unit are also included except for sedimentary units A and G (no control of thickness)

of oolitic, peloidal and oncolitic shoals. Within the lagoon area, which records the highest sedimentary thickness, there is a predominance of oncolitic (type III oncoids) facies in the units A and B, but of stromatoporoid and oncolitic-stromatoporoid facies in units C to E. Fenestral facies evolve from local patches in units C to E, to a wide intertidal belt in units F and G, with local development of ponds in the intertidal area or restricted lagoon. The spatial relationships of the facies across successive evolutionary units reflect a facies mosaic. In particular, stromatoporoid (S) and fenestral (F) facies clearly show a patchy distribution, with facies patches locally more than 500 m in lateral extent.

Discussion

Factors controlling the mosaic distribution

A combination of several internal and external factors controlled the facies heterogeneity in the studied inner ramp facies, including the long-term regional fall in sea-level, along with the irregular bottom topography, substrate stability and variable water energy. As regards the internal dynamics of the platform, one of the key factors increasing the variability and extent of facies is the presence of an irregular topography (Kerans and Tinker 1997; Della Porta et al. 2002; Hillgärtner 2006). Oolitic, peloidal and oncolitic shoals seaward of the lagoon acted as barriers for water energy, and controlled the occurrence of more protected areas, where low-energy conditions favored the development of oncolitic, stromatoporoid and oncolitic-stromatoporoid facies. The irregular topography is also determined by the input of resedimented material from the outer banks or shoals: storm-induced flows lead to abrupt changes in facies distribution by redistributing sediment in large quantities (i.e., washover deposits, see Fig. 8a) and by creating barriers between depositional subenvironments (Strasser and Védrine 2009), thus controlling the spatial and lateral extent of the lagoon facies. Within the sheltered lagoon, the patchy distribution of stromatoporoid facies reflects areas of preferential growth for stromatoporoids that were probably related with local hard substrates and areas with higher-energy hydrodynamic conditions that occurred in corridors created between the peloidal washovers (e.g., unit D in Fig. 8b). The greater thickness of the lagoon facies compared to the backshoal/washover peloidal facies (e.g., sedimentary units B to D in Fig. 8b) can be interpreted as a combination of the variable depositional depth or topography (i.e., relatively deeper lagoon areas) and differences in carbonate accumulation, which was potentially higher in the lagoon than in the backshoal area subjected to erosion by high-energy events. Small changes in depositional depth after the deposition of washover deposits would control the generation of fenestral facies patches in sedimentary units C to E (see Fig. 8).

External factors also contribute to facies evolution and their heterogeneity. Fluctuations in climate and regional sea-level become important factors that lead to changes in the composition and distribution of the depositional subenvironments, generated by variations in water energy, water temperature, transparency, nutrient availability and sediment input, which control the ecology of carbonate-producing organisms (e.g., Védrine et al. 2007; Strasser and Védrine 2009). Most of the skeletal content that characterizes the studied facies (e.g., dasycladacean algae, bivalves, brachiopods, echinoderms), as well as the types of oncoids and ooids, indicate normal salinity, oligotrophic conditions and good water transparency (e.g., Strasser 1984; Flügel 2004). In this respect, the low siliciclastic input (and reduced nutrient input) contributed to the extensive generation of type III oncoids, characterized by light-dependence and oligotrophic micro-encrusters (e.g., Leinfelder et al. 1993; Dupraz and Strasser 1999). Stromatoporoid facies, arranged in patches in the lagoon, also indicates good water transparency and oligotrophic conditions (Bádenas et al. 2010), but also a higher tolerance to water energy, salinity and water temperature (Leinfelder et al. 2005). However, in the case under study it is unlikely that variations in salinity and/or water temperature determined the widespread development of the stromatoporoid and oncolitic-stromatoporoid facies within the lagoon, since most of the defined facies include a similar bioclastic (normal marine) association (Table 1). Thus, the change from predominantly oncoid generation (units A and B) to a widespread development of stromatoporoid and oncolitic-stromatoporoid facies in units C to E (Fig. 8b) was related to higher-energy conditions driven by the long-term regional fall in sea-level, combined with the presence of encrusted surfaces and high-energy narrow corridors, rather than to changes in the paleoenvironmental conditions due to the climate.

Implications of a facies mosaic in cyclostratigraphic analysis

The stacking pattern of facies and their related depositional subenvironments are usually taken into account in cyclostratigraphy in order to define meter-scale high-frequency cycles. However, for shallow-marine carbonates, the intrinsic processes (depositional topography, hydrodynamic conditions, carbonate production and accumulation)

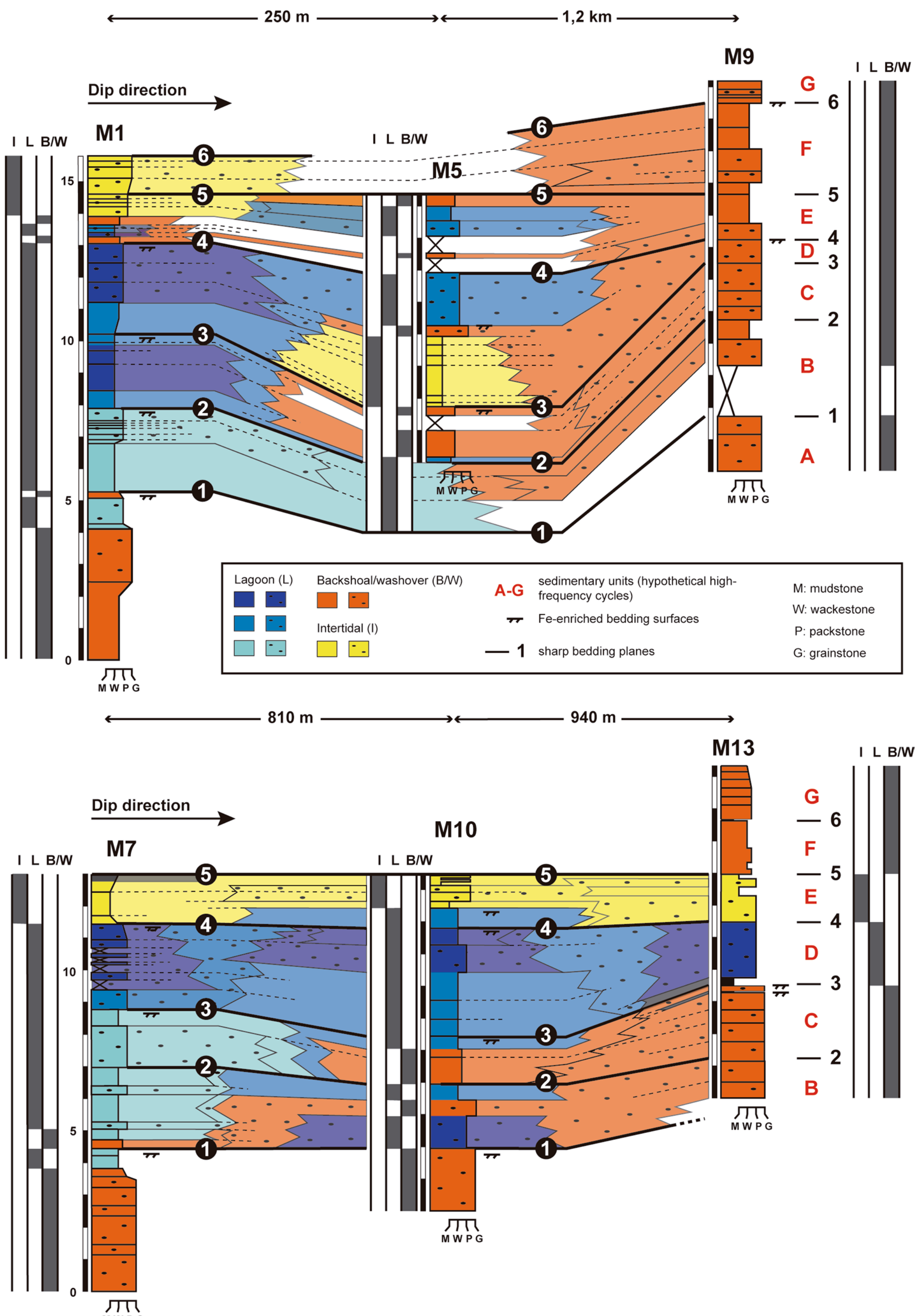

250 m
1,2 km
Dip direction
M1
M5
M9
I L B/W
A B C D E F G
1 2 3 4 5 6
M W P G
Lagoon (L)
Backshoal/washover (B/W)
Intertidal (I)
A-G sedimentary units (hypothetical high-frequency cycles)
Fe-enriched bedding surfaces
1 sharp bedding planes
M: mudstone
W: wackestone
P: packstone
G: grainstone
810 m
940 m
M7
M10
M13

◀**Fig. 9** Correlation of the hypothetical high-frequency cycles (A–G) recognized in M1–M5–M9 and M7–M10–M13 transects, defined by the presence of sharp bedding planes, and the vertical evolution of the subenvironments. Notice that the vertical facies evolution in a single high-frequency cycle may show significant variation from one log to another

variably interfere with the signal produced by external driving mechanisms (e.g., relative sea-level variations controlling accommodation, climate), thus reducing the potential for facies pattern predictability. Hence, vertical facies trend analysis may sometimes not be a reliable method of delimiting and correlating high-frequency cycles in shallow-marine stratigraphic successions, since different facies stacking patterns may be present within a cycle depending on the area of deposition (e.g., Verwer et al. 2009; Bádenas et al. 2010).

The identification and physical tracing of sharp bedding planes may serve as a useful tool for delimiting high-frequency cycles, since such bedding planes may represent sedimentary surfaces with no sedimentation or erosion linked to external driving mechanisms (i.e., potential cycle boundaries). For the studied sections in the Mezalocha outcrops, sharp bedding (isochronous) surfaces 1–6 would represent the cycle boundaries of the hypothetical elementary cycles A to G that developed within the long-term regional-scale shallowing-upward sequence defined for the Higueruelas Fm (Ipas et al. 2004). The usual Fe-enrichment on these surfaces and the presence of local overlying cm-thick marly beds support an interpretation of them as representing sedimentary surfaces with no sedimentation or erosion (Christ et al. 2012). Examples of the hypothetical cycles A to G in selected stratigraphic logs are shown in Fig. 9. It is noteworthy that the same high-frequency cycle can show variable thickness and vertical facies trends in areas very close to one another, i.e., cycles B and C are aggradational or shallowing-upward depending on the log, and cycle D is aggradational in all the selected logs, except deepening-upward in log M5.

This lateral variability can be regarded as a consequence of the spatial complexity of the inner ramp environment, where internal factors interfere greatly with the more ordered signal of possible high-frequency sea-level cycles. Considering that there was no significant lateral variation in subsidence during deposition, the generally greater thickness of the sheltered lagoon facies within the hypothetical high-frequency cycles compared to the backshoal/washover peloidal facies (Fig. 8) can be interpreted as a combination of the variable depositional depth or topography (i.e., relatively deeper lagoon areas) with differences in carbonate accumulation, which is potentially higher in the lagoon compared to the backshoal area subjected to erosion by high-energy events. Another example of an internal factor is provided by event beds (peloidal washovers sharply intercalated within lagoon facies: e.g., sedimentary units C and D in Fig. 8b), which could create small elevated areas in the lagoon where discrete intertidal patches were generated, leaving corridors where relatively higher hydrodynamic conditions allowed the stromatoporoid patches to proliferate. Erosion due to a fall in base level linked to the high-frequency fall in sea-level, combined with sedimentary condensation at the initial stages of the rise in sea-level of the following cycle, would generate the sharp bedding surfaces bounding the high-frequency cycles.

Therefore, for larger-scale correlations of separated logs, recognition of these sharp bedding planes may serve as a useful tool for differentiating and correlating cycle boundaries. In this regard, correlation becomes easier for lower-frequency cycles, when additional tools for the identification of the same cycle can be used, such as a general vertical facies trend and the recognition of stratal patterns (e.g., strata-thickening upward, strata-thinning or any particular stratal trend). At the level of the high-frequency sequences, correlation is sometimes difficult because their vertical facies stacking does not always display unequivocal deepening-shallowing or opening-closing trends, as seen for the sections studied in the Mezalocha outcrops, since autocyclic processes partly control facies evolution (Strasser 1991). Thus, if high-frequency cycles are to be used as a tool for cyclostratigraphic correlation, this should be preceded by a detailed analysis of the facies architecture of the cycles in selected continuous outcrops (e.g., Bádenas et al. 2010; Amour et al. 2011).

Comparisons with other similar environments

The spatial complexity of inner ramp facies has been deciphered for the uppermost Kimmeridgian–lower Tithonian Higueruelas Fm. The general paleogeographic distribution of facies, with the open-marine areas to the southeast, is coherent with the basin-wide paleogeographic reconstructions for Kimmeridgian–Tithonian times in northeastern Iberia (Aurell et al. 1994; Bádenas and Aurell 2001; see Fig. 1b). Some of these shallow carbonate facies have also been documented in other Upper Jurassic ramps of the Iberian Basin, showing similar spatial complexity of facies, especially for stromatoporoid facies. San Miguel et al. (2017) recognized levels with stromatoporoid boulders in the more proximal domain of the upper Kimmeridgian carbonate ramp in the Jabaloyas area of northeastern Spain, where higher-energy events (i.e., episodic storms) resulted in the accumulation of stromatoporoid boulder carpets along a paleoshoreline (lateral extent in the dip direction of the stromatoporoid-bearing layers of 2 km). Pomar et al. (2015) documented the facies architecture and bedding patterns of the lower Kimmeridgian Pozuel Formation in the Moscardón and Frías de Albarracín outcrops, where landward of a high-energy cross-bedded oolitic facies belt, corals and stromatoporoids formed small patches, with microbial-dominated mounds with abundant *Tubiphytes-Crescentiella* in the innermost parts. These mounds are a few meters thick and are amalgamated, forming dip-oriented ribbons of mounds surrounded by bioclastic and intraclastic sediment controlled by up- and down-currents. Patches of stromatoporoids, with a lateral extent of more than 500 m, have been recognized in the studied Mezalocha outcrops, in corridors within the lagoon, where the currents would have probably been constrained (e.g., sedimentary unit D in Fig. 8b).

For subtidal carbonate environments in other Jurassic outcrops outside the Iberian Basin, remarkable similarities can also be found between some facies observed in the upper part of the Higueruelas Fm and some defined for the upper Kimmeridgian carbonate ramp deposits of the Arab-D Formation (Persian Gulf, Saudi Arabia; Ayoub and En Nadi 2000; Al-Saad and Ibrahim 2005), which represents the largest oil reservoir in the world (Al-Awwad and Collins 2013). The Arab-D carbonates consist mainly of well-sorted oolitic packstone–grainstone, deposited in active shoals and stromatoporoid-dominated patch reefs in the foreshoal environment (Grötsch et al. 2003). However, a significant difference from the studied strata around Mezalocha is the presence of large-scale stromatoporoid reefs, arranged as belts instead of patches. Lehmann et al. (2010) recognized meter-thick stromatoporoid buildups from middle to outer ramp areas of the Upper Jurassic carbonate platform in offshore Abu Dhabi (eastern Saudi Arabia), more than 3 km in lateral extent. For the inner to outer carbonate ramp of onshore Abu Dhabi, sedimentological analysis indicates that stromatoporoid fragments are a key component in the lagoon, but no bioconstructions are recognized (Marchionda et al. 2018). The quality of this reservoir is due to the interparticle porosity in peloidal and oolitic grainstone and the great porosity resulting from the dissolution of stromatoporoid bioclasts. Consequently, for hydrocarbon prospecting campaigns, it is important to take into account the variable lateral extent of stromatoporoid facies in accordance with the characteristics of subtidal environments.

Other examples where the complexity and spatial limitations of stromatoporoid-dominated deposits are also revealed occur in Paleozoic carbonate platforms. Sandström and Kershaw (2002) documented decimeter- to meter-scale stromatoporoid-dominated biostromes in the inner areas of a rimmed carbonate platform of the Ludlow-age Hemse Group (Silurian) in the eastern Gotland (Sweden), which represent one of the world's richest Paleozoic stromatoporoid deposits. The lateral extent of these biostromes varies from a few tens of meters to more than 1 km. Smaller bioconstructions are found in the lagoonal deposits of a mixed carbonate–siliciclastic ramp in the upper Devonian Alexandra Reef System (Canada; MacNeil and Jones 2016), where clearly defined meter-scale stromatoporoid bioherms measuring 10 to 30 m in lateral extent are recognized.

Conclusions

In order to establish correlations of facies and sedimentary cycles at the kilometer scale, detailed facies analysis is required to decipher whether shallow-water carbonate deposits correspond to facies belts or facies mosaics. In this work, the spatial relationship and lateral continuity of the facies ascertained for the uppermost Kimmeridgian–lower Tithonian inner carbonate ramp deposits of the Mezalocha outcrops (NE Spain) reflect a facies mosaic, instead of continuous parallel–subparallel facies belts.

Sedimentological analysis and detailed facies mapping of these inner carbonate ramp deposits resulted in the definition of 6 facies and 12 subfacies, which record the transition from backshoal/washover and sheltered lagoon to intertidal and pond/restricted lagoon subenvironments. The backshoal/washover deposits are characterized by peloidal (wackestone–packstone and grainstone) facies, with lithic peloids and variable proportions of ooids and oncoids resedimented from oolitic-peloidal and oncolitic shoals. The sheltered lagoon deposits include oncolitic, stromatoporoid and oncolitic-stromatoporoid (wackestone and packstone) facies. The oncolitic facies is dominated by type III oncoids, formed predominantly during low-energy periods (microbial laminae) alternating with short high-energy episodes (micritic laminae). The stromatoporoid facies presents variable proportions of both in situ and reworked stromatoporoids, with the common presence of corals and chaetetids. This facies occurs in different positions within the lagoon, and grades laterally to oncolitic-stromatoporoid facies, characterized by type I, II and III oncoids and fragments of stromatoporoids. The intertidal subenvironment is represented by mudstone and packstone–grainstone with fenestral facies. The gastropod-oncolitic wackestone–packstone and grainstone facies, intercalated with marl, may represent local ponds in the intertidal area or a restricted lagoon.

The studied succession reflects a general shallowing-upward trend. Seven sedimentary units, reflecting significant changes in facies, were recognized: from dominant oncolitic facies in the initial units A and B; stromatoporoid and oncolitic-stromatoporoid facies in units C to E; and intertidal and pond/restricted lagoon subenvironments in units F and G. The backshoal/washover facies is present in all the sedimentary units. The spatial distribution of facies indicates a facies mosaic instead of continuous parallel–subparallel facies belts. In particular, stromatoporoid and fenestral facies show a patchy distribution, facies patches being locally more than 500 m in lateral extent. This patchy distribution was controlled by internal and external factors. Sheltered lagoon facies developed in the protected area of external oolitic-peloidal and oncolitic shoals or banks, where the extensive generation of type III oncoids, characterized by light-dependence and oligotrophic micro-encrusters, was favored by the low siliciclastic input. The development of stromatoporoid-bearing patchy facies was controlled by higher-energy conditions related to the long-term regional fall in sea-level, combined with the presence of high-energy narrow corridors and local hard substrates. Storm action led to the deposition of backshoal and washover sediments that were locally exposed to form patches of fenestral facies.

The mosaic facies distribution ascertained in this work can provide useful tools for achieving reconstructions of depositional heterogeneities in similar settings, and an understanding of the factors controlling these facies mosaics may be relevant for the interpretation of the vertical stacking of facies in high-frequency cycles and for correlations of cycles at larger scales.

Acknowledgements This paper was funded by projects CGL2014-53548-P and CGL2017-85038-P of the Spanish Ministry of Science and Innovation and the H54 Research Group-IUCA Aragosaurus: recursos geológicos y paleoambientes, supported by the Gobierno de Aragón and the European Social Fund. The research of Cristina Sequero is funded by a FPU Grant (Spanish Ministry of Science and Innovation). We are grateful for the revision that has been done by Michele Morsilli, an anonymous reviewer and the Editor-in-Chief, Maurice Tucker. We also thank Rupert Glasgow for accepting to review the English quality.

References

Al-Awwad SF, Collins LB (2013) Arabian carbonate reservoirs: a depositional model of the Arab-D reservoir in Khurais field, Saudi Arabia. Am Assoc Pet Geol 97:1099–1119

Al-Saad H, Ibrahim M (2005) Facies and palynofacies characteristics of the Upper Jurassic Arab D reservoir in Qatar. Rev Paléobiol 24(1):225–241

Amour F, Mutti M, Christ N, Immenhauser A, Agar SM, Benson GS, Tomás S, Always R, Kabiri L (2011) Capturing and modelling metre-scale spatial facies heterogeneity in a Jurassic ramp setting (Central High Atlas, Morocco). Sedimentology 59:1158–1189

Aurell M, Meléndez A (1986) Sedimentología de la Formación Calizas con oncolitos de Higueruelas (Malm) en la región de Muel-Belchite (Provincia de Zaragoza). Acta Geol Hisp 21–22:307–312

Aurell M, Meléndez A (1987) Las bioconstrucciones de corales y sus facies asociadas durante el Mal en la Cordillera Ibérica Central (prov. De Zaragoza). Estud Geol 43:261–269

Aurell M, Mas R, Meléndez A, Salas R (1994) El tránsito Jurásico-Cretácico en la Cordillera Ibérica: relación tectónica-sedimentación y evolución paleogeográfica. Cuad Geol Ibérica 18:369–396

Aurell M, Meléndez G, Olóriz F, Bádenas B, Caracuel J, García-Ramos JC, Goy A, Linares A, Quesada S, Robles S, Rodríguez-Tovar FJ, Rosales I, Sandoval J, Suárez de Centi C, Tavera JM, Valenzuela M (2002) The geology of Spain. Geological Society, London, pp 213–254

Aurell M, Robles S, Bádenas B, Rosales I, Quesada S, Meléndez G, García-Ramos JC (2003) Transgressive-regressive cycles and Jurassic palaeogeography of northeast Iberia. Sediment Geol 162:239–271

Aurell M, Bádenas B, Ipas J, Ramajo J (2010) Sedimentary evolution of an Upper Jurassic epeiric carbonate ramp Iberian Basin NE Spain. In: Buchem FSP, Gerdes KD, Esteban M (eds) Mesozoic and Cenozoic carbonate systems of the Mediterranean and the Middle East: stratigraphic and diagenetic reference models, vol 329. Geological Society, Special Publications, London, pp 89–111

Aurell M, Ipas J, Bádenas B, Muñoz A (2012) Distribución de facies con corales y estromatopóridos en el dominio interno de una plataforma carbonatada (Titónico, Cordillera Ibérica). Geogaceta 51:67–70

Ayoub R, En Nadi IM (2000) Stratigraphic framework and reservoir development of the Upper Jurassic in Abu Dhabi area, UAE. In: Alsharhan AS, Scott RW (eds) Middle East Models of Jurassic/Cretaceous carbonate system, vol 69. SEPM Society for Sedimentary, Tulsa, pp 229–248

Bádenas B, Aurell M (2001) Kimmeridgian palaeogeography and basin evolution of northeastern Iberia. Palaeogeogr Palaeoclimatol Palaeoecol 168:291–310

Bádenas B, Aurell M (2010) Facies models of a shallow-water carbonate ramp based on distribution of non-skeletal grains (Kimmeridgian, Spain). Facies 56:89–110

Bádenas B, Aurell M, Rodríguez-Tovar FJ, Pardo-Igúzquiza E (2003) Sequence stratigraphy and bedding rhythms of an outer ramp limestone succession (Late Kimmeridgian, Northeast Spain). Sediment Geol 161:153–174

Bádenas B, Aurell M, Bosence D (2010) Continuity and facies heterogeneities of shallow carbonate ramp cycles (Sinemurian, Lower Jurassic, North-east Spain). Sedimentology 57:1021–1048

Burchette TP, Wright VP (1992) Carbonate ramp depositional systems. Sediment Geol 79:3–57

Burgess PM, Emery DJ (2004) Sensitive dependence, divergence and unpredictable behaviour in a stratigraphic forward model of a carbonate system. In: Curtis A, Wood R (eds) Geological prior information: informing science and engineering, vol 239. Geological Society, Special Publications, London, pp 77–94

Burgess PM, Wright VP (2003) Numerical forward modeling of carbonate platform dynamics: an evaluation of complexity and completeness in carbonate strata. J Sediment Res 73(5):637–652

Cepriá JJ, Bádenas B, Aurell M (2002) Evolución sedimentaria y paleogeografía del Jurásico Superior (Kimmeridgiense superior-Titónico) en la Sierra de Arcos (Cordillera Ibérica). J Iber Geol 28:93–106

Christ N, Immenhauser A, Amour F, Mutti M, Tomás S, Agar SM, Always R, Kabiri L (2012) Characterization and interpretation of discontinuity surfaces in a Jurassic ramp setting (High Atlas, Morocco). Sedimentology 59:249–290

Dahanayake K (1977) Classification of oncoids from the Upper Jurassic carbonates of the French Jura. Sediment Geol 18:337–353

Della Porta G, Kenter JAM, Immenhauser A, Bahamonde J (2002) Lithofacies character and architecture across a Pennsylvanian inner-platform transect (Sierra de Cuera, Asturias, Spain). J Sediment Res 72:898–916

Dercourt J, Ricou L, Vrielynck B (1993) Atlas Tethys palaeoenvironmental maps. CCGM, Paris

Drummond CN, Wilkinson BH (1993) Aperiodic accumulation of cyclic peritidal carbonate. Geology 21:1023–1026

Dunham RJ (1962) Classification of carbonate rocks according to depositional texture. Am Assoc Pet Geol Mem 1:108–121

Dupraz C, Strasser A (1999) Microbialites and micro-encrusters in shallow coral bioherms (Middle to Late Oxfordian, Swiss Jura mountains). Facies 40:101–129

Flügel E (1974) Fazies-Interpretation der *Cladocoropsis*-Kalke (Malm) auf Karaburun, W-Anatolien. Arch Lagerstätt-Forsch Ostalpen Sd-Bd 2:79–94

Flügel E (2004) Microfacies of carbonate rocks: analysis, interpretation and application. Springer, Berlin, p 976
Ginsburg RN (1971) Landward movement of carbonate mud: new model for progressive cycles in carbonates. AAPG Bull 55:340
Gischler E, Lomando AJ (1999) Recent sedimentary facies of isolated carbonate platforms, Belize-Yucatan system, Central America. J Sediment Res 69(3):747–763
Goldhammer RK, Dunn PA, Hardie LA (1990) Depositional cycles, composite sea-level changes, cycle stacking patterns, and the hierarchy of stratigraphic forcing: examples from Alpine Triassic platform carbonates. Geol Soc Am Bull 102:535–562
Grötsch J, Suwaina O, Ajlani G, Taher A, El-Khassawneh R, Lokier S, Coy G, van der Weerd E, Masalmeh S, van Dorp J (2003) The Arab Formation in central Abu Dhabi: 3-D reservoir architecture and static and dynamic modelling. GeoArabia Gulf PetroLink Bahrain 8(1):47–86
Hernández-Samaniego A, Ramírez-Merino JI (2005) Mapa Geológico y Memoria explicativa, Hoja Escala 1:50.000 de Longares (411). In: IGME (ed), pp 97
Hillgärtner H (2006) High-resolution correlation in Cretaceous platform carbonates of the Middle East: rules to solve the puzzle? In: AAPG European Region conference: Architecture of carbonate systems through time, Mallorca 2006, Program Book 26
Ipas J, Aurell M, Bádenas B (2004) Ambientes sedimentarios y secuencias en la Fm. Higueruelas (Jurásico Superior) en la Cordillera Ibérica Septentrional. Geogaceta 35:7–10
Ipas J, Aurell M, Bádenas B, Canudo JI, Liesa C, Mas JR, Soria AR (2007) Caracterización de la Formación Villar del Arzobispo al sur de Zaragoza (Titónico, Cordillera Ibérica). Geogaceta 41:111–114
Jones B, Desrochers A (1992) Shallow platform carbonates. In: Walker RG, James NP (eds) Facies models: response to sea level change. Geol Assocs Can, St. John's, pp 277–301
Kerans C, Tinker SW (1997) Sequence stratigraphy and characterization of carbonate reservoirs: SEMP Short Courses Notes 40. SEMP, Tulsa, p 130
Lehmann CT, Al Hosany KI, Matarid T, Sayed MI (2010) Addressing reservoir heterogeneities in the Development of Upper Jurassic Carbonate Reservoirs, offshore Abu Dhabi. Society of Petroleum Engineers, SPE 137888, Abu Dhabi
Lehrmann DJ, Goldhammer RK (1999) Secular variations in parasequence and facies stacking patterns of platform carbonates: a guide to application of stacking-patterns analysis in strata of diverse ages and settings. In: Harris PM, Saller AH, Simo JA (eds) Advances in carbonate sequence stratigraphy: application to reservoirs, outcrops, and models, vol 63. SEPM Special Publication, Tulsa, pp 187–226
Leinfelder RR, Nose M, Schmid D, Werner M (1993) Microbial crusts of the Late Jurassic: composition, palaeoecological significance and importance in reef construction. Facies 29:195–230
Leinfelder RR, Schlagintweit F, Werner W, Ebli O, Nose M, Schmid D, Hughes G (2005) Significance of stromatoporoids in Jurassic reefs and carbonate platforms—concepts and implications. Facies 51:287–325
MacNeil AJ, Jones B (2016) Stromatoporoid growth forms and Devonian reef fabrics in the Upper Devonian Alexandra Reef System, Canada—insight on the challenges of applying Devonian reef facies models. Sedimentology 63:1425–1457
Marchionda E, Deschamps R, Gobianchi M, Nader FH, Di Giulio A, Morad DJ, Al Darmaki F, Ceriani A (2018) Field-scale depositional evolution of the Upper Jurassic Arab Formation (onshore Abu Dhabi, UAE). Mar Pet Geol 89:350–369
Muñoz A, Arenas C, González A, Luzón A, Pardo G, Pérez A, Villena J (2002) Ebro Basin (northeastern Spain). In: Gibbons W, Moreno MT (eds) The geology of Spain. Geological Society, London, pp 301–309
Pomar L (2001) Types of carbonate platforms: a genetic approach. Basin Res 13:313–334
Pomar L, Aurell M, Bádenas B, Morsilli M, Al-Awwad SF (2015) Depositional model for a prograding oolitic wedge, Upper Jurassic, Iberian basin. Mar Pet Geol 67:556–582
Pratt BR, James NP (1986) The St. George Group (Lower Ordovician) of western Newfoundland: tidal flat island model for carbonate sedimentation in shallow epeiric seas. Sedimentology 33:313–343
Rankey EC (2002) Spatial patterns of sediment accumulation on a Holocene carbonate tidal flat Northwest Andros Island, Bahamas. J Sediment Res 72:591–601
Rankey EC (2016) On facies belts and facies mosaics: Holocene isolated platforms, South China Sea. Sedimentology 63:2190–2216
Rankey EC, Reeder SL (2010) Controls on platform-scale patterns of surface sediments, shallow Holocene platforms, Bahamas. Sedimentology 57:1545–1565
Read JF (1985) Carbonate platform facies models. AAPG Bull 69:1–21
Riegl B, Piller WE (1999) Coral frameworks revisited-reefs and corals carpets in the northern Red Sea. Coral Reefs 18:241–253
San Miguel G, Aurell M, Beatriz B (2017) Occurrence of high-diversity metazoan- to microbial-dominated bioconstructions in a shallow Kimmeridgian carbonate ramp (Jabaloyas, Spain). Facies 63:13
Sandström O, Kershaw S (2002) Ludlow (Silurian) stromatoporoid biostromes from Gotland, Sweden: facies, depositional models and modern analogues. Sedimentology 49:379–395
Schlager W (2000) Sedimentation rates and growth potential of tropical, cool water and mud mound carbonate factories. In: Insalaco E, Skelton PW, Palmer TJ (eds) Carbonate platform systems: components and interactions, vol 178. Geology Society Special Publications, London, pp 217–227
Schlager W (2003) Benthic carbonate factories of the Phanerozoic. Int J Earth Sci 92:445–464
Shinn EA (1968) Practical significance of birdseye structures in carbonate rocks. J Sediment Petrol 38:215–223
Strasser A (1984) Black-pebble occurrence and genesis in Holocene carbonate sediments (Florida Keys, Bahamas, and Tunisia). J Sediment Petrol 54(4):1097–1109
Strasser A (1986) Ooids in Purbeck limestones (lowermost Cretaceous) of the Swiss and French Jura. Sedimentology 33:711–727
Strasser A (1991) Lagoonal-peritidal sequences in carbonate environments: autocyclic and allocyclic processes. In: Einsele G, Ricken W, Seilacher A (eds) Cycles and events in stratigraphy. Springer, Berlin, pp 709–721
Strasser A, Védrine S (2009) Controls on facies mosaics of carbonate platforms: a case study from the Oxfordian of the Swiss Jura. In: Special publication of the International Association of Sedimentologists, vol 41, pp 199–213
Strasser A, Pittet B, Hillgärtner H, Pasquier JB (1999) Depositional sequences in shallow carbonate-dominated sedimentary systems: concepts for a high-resolution analysis. Sediment Geol 128:201–221
Turnsek D, Buser S, Ogorelec B (1981) An Upper Jurassic reef complex from Slovenia, Yugoslavia. In: Toomey DF (ed) European fossil reef models, vol 30. SEPM Special Publications, Tulsa, pp 361–369
Védrine S, Strasser A, Hug W (2007) Oncoid growth and distribution controlled by sea-level fluctuations and climate (Late Oxfordian, Swiss Jura Mountains). Facies 53(4):535–552
Verwer K, Della Porta G, Merino-Tomé O, Kenter JAM (2009) Control and predictability of carbonate facies architecture in a Lower Jurassic three-dimensional barrier-shoal complex (Djebel Bou Dahar, High Atlas, Morocco). Sedimentology 56:1801–1831
Wilkinson BH, Drummond CN (2004) Facies mosaic across the Persian Gulf and around Antigua—stochastic and deterministic products of shallow-water sediment accumulation. J Sediment Res 74:513–526

Wilkinson BH, Diedrich NW, Drummond CN (1996) Facies succession in peritidal carbonate sequences. J Sediment Res 66:1065–1078
Wilson JL (1975) Carbonate facies in geologic history. Springer, New York, p 471
Wright VP, Burgess PM (2005) The carbonate factory continuum, facies mosaic and microfacies: an appraisal of some of the key concepts underpinning carbonate sedimentology. Facies 51:17–23

Marine and Petroleum Geology 109 (2019) 145–174

Contents lists available at ScienceDirect

Marine and Petroleum Geology

journal homepage: www.elsevier.com/locate/marpetgeo

Research paper

Sedimentary evolution of a shallow carbonate ramp (Kimmeridgian, NE Spain): Unravelling controlling factors for facies heterogeneities at reservoir scale

Cristina Sequero*, Marcos Aurell, Beatriz Bádenas

Departamento de Ciencias de la Tierra-IUCA, Universidad de Zaragoza, 50009 Zaragoza, Spain

ARTICLE INFO

Keywords:
Shallow carbonate ramp
Kimmeridgian
Iberian Basin
Facies heterogeneities
Hydrocarbon reservoir analogue

ABSTRACT

The facies evolution of a Late Jurassic (latest Kimmeridgian) shallow carbonate ramp was reconstructed after the analysis and correlation of 21 logs in a 20 × 30 km outcrop area located south of Zaragoza (northeast Spain). The studied succession belongs to the Higueruelas Formation, which is of potential use as an analogue for understanding facies heterogeneities in certain hydrocarbon carbonate reservoirs (e.g. the Arab Formation, Persian Gulf). The studied succession is arranged in nine sedimentary units bounded by discontinuity surfaces that can be traced over kilometres. Facies analysis permitted the reconstruction of two sedimentary models showing the transition from inner ramp subenvironments (i.e. intertidal, lagoon, backshoal/washover, shoal-sand blanket) to the mid-ramp foreshoal and offshore domains: an oncolitic-peloidal-oolitic and an oolitic-peloidal-dominated ramp. The oncolitic-peloidal-oolitic-dominated ramp is characterized by peloidal-oolitic and oncolitic-dominated shoal-sand blankets that developed in higher-energy inner areas, protecting peloidal-oolitic backshoal and oncolitic lagoon domains including a mosaic of stromatoporoid carpets. Peloidal facies with fenestral porosity accumulated in an intertidal belt or as patches on top of the shoal-sand blankets and washover deposits. Offshore from the shoal-sand blankets, chaetetid/stromatoporoid/coral-rich buildups grew on the more proximal mid-ramp, surrounded by peloidal and peloidal-bioclastic grain- to mud-supported facies. An oolitic-peloidal-dominated ramp developed in a second stage of the evolution of the platform, characterized by the presence of a wide restricted peloidal-bioclastic-oolitic lagoon on the inner ramp grading into a backshoal area dominated by storm-related intraclastic-peloidal deposits. Stromatoporoid carpets disappeared and oncolitic-dominated deposits were constrained to the foreshoal and backshoal domains, and locally to local ponds that developed in the intertidal belt or the restricted lagoon. Internal and external factors controlling facies heterogeneity and the sedimentary evolution of the carbonate ramp include resedimentation, topographic relief, and long- to short-term sea-level fluctuations.

1. Introduction

Reconstruction of facies heterogeneities on epeiric shallow carbonate ramps is difficult due to the absence of recent analogues as well as to the complexity of the interacting factors that controlled the facies distribution and sedimentary evolution (e.g. Burchette and Wright, 1992; Bádenas and Aurell, 2010; Pomar, 2018). A particular point of interest in studying ancient epeiric shallow carbonate ramps is the definition of the lateral and vertical extent of carbonate bodies. A significant difference between epeiric ramps and rimmed platforms is the wide lateral extension of the facies belts, and in particular of carbonate sand bodies, in the former (Burchette and Wright, 1992). Rimmed platforms are limited in their progradation by the bordering deep ocean, whereas in ramps the potential for progradation of the carbonate sand shoals over the low-angle depositional slope results in much greater extension and potential for preservation of grain-supported facies (Droste, 2006; Bádenas and Aurell, 2010). A knowledge of the geometry and lateral continuity of porous and permeable grain-supported facies and their relationship with mud-supported facies is a key aspect of reservoir exploration and development strategies in ancient carbonate platforms (e.g. Borkhataria et al., 2005).

Outcrop analogue studies play an essential role in unravelling the internal heterogeneities of subsurface shallow carbonate systems, and the construction of depositional models is a condition for evaluating carbonate reservoirs (Pomar et al., 2015). In carbonate rocks, the study of outcrop analogues is of additional interest due to the dependence of

* Corresponding author.
E-mail address: cristinasq92@gmail.com (C. Sequero).

https://doi.org/10.1016/j.marpetgeo.2019.06.018
Received 22 March 2019; Received in revised form 6 June 2019; Accepted 9 June 2019
Available online 11 June 2019
0264-8172/

sediment production upon carbonate-producing organisms and, consequently, the reliance of carbonate production on environmental conditions. Numerous modern analogue studies of shallow marine environments (Wilkinson et al., 1999; Rankey and Reeder, 2011; Harris et al., 2014; Purkis et al., 2015) have revealed important heterogeneities in facies distribution controlled by a range of factors such as sea-level fluctuations and hydrodynamic conditions, as well as by changes in carbonate-producing biota, which are controlled in turn by their ecological requirements, such as temperature, ocean chemistry and nutrient availability (Pomar and Kendall, 2007; Strasser and Védrine, 2009; Harris et al., 2014; Hönig and John, 2015). In the case of carbonate ramps, several works have demonstrated that despite their usually well-defined facies belts, these facies belts can vary laterally (along strike and along dip), and facies mosaics in some ramp subenvironments can also develop in relation with biological and hydrodynamic factors (e.g. Bádenas et al., 2010; Tomás et al., 2010; Amour et al., 2013; San Miguel et al., 2017a; Tomassetti et al., 2018), thus complicating the heterogeneity and predictability of the facies. More studies on carbonate ramp systems are thus required to unravel the distribution of rock bodies for further 3D modelling of volume and/or fluid-flow assessment.

The shallow facies of the late Kimmeridgian carbonate ramp that developed in the north-central part of the Iberian Basin are of particular interest due to the wide record of skeletal and non-skeletal grains similar to those found in the most important hydrocarbon carbonate reservoirs worldwide (i.e. the Arab-D Fm, Persian Gulf; Al-Awwad and Collins, 2013). The main purpose of the present work is to characterize the facies distribution and sedimentary evolution of this shallow carbonate ramp exposed in the outcrops south of Zaragoza (Iberian Basin, NE Spain). Bed-by-bed facies analysis and the correlation of closely-spaced logs provide a precise scheme showing the vertical and lateral (along strike and along dip) facies distribution. This allows the dimensions of the facies belts to be ascertained, as well as the lateral distribution (from inner- to mid-ramp) of the more common non-skeletal components (peloids, ooids, oncoids, intraclasts) and the preferential growth of stromatoporoid carpets and chaetetid-stromatoporoid-coral buildups. On the basis of the relative proportions of the more common non-skeletal grains, two sedimentary models are proposed. These models are of potential interest for improving subsurface interpretations of carbonate ramps, in particular with respect to dimensions and internal heterogeneities of reservoir-rock bodies.

2. Geological setting and stratigraphy

During the Kimmeridgian (Late Jurassic), shallow epeiric seas covered wide areas of western Europe (Fig. 1A). Terrigenous sedimentation occurred to the north and west, whereas carbonate sedimentation was dominant on eastern and northeastern platforms facing the Tethys Ocean (Dercourt et al., 1993). A large part of the Iberian Plate was uplifted, forming the Iberian Massif. To the east of this massif, wide carbonate ramps developed during the Kimmeridgian in the so-called Iberian Basin, an intra-cratonic basin that originated during the Mesozoic extensional phase (Fig. 1B; Salas and Casas, 1993; Aurell et al., 2003, 2010). These carbonate ramps were affected by NW-directed hurricanes and winter winds (Bádenas and Aurell, 2001), in accordance with the palaeoclimate models proposed by Marsaglia and Klein (1983) and Price et al. (1995) (Fig. 1B).

During the Kimmeridgian, the Iberian Basin displays a sedimentary evolution characterized by low-angle carbonate ramps recorded increasingly towards the eastern areas of the basin, due to a long-term fall in relative sea level that was partly controlled by the tectonic uplift of the Iberian Massif (Bádenas and Aurell, 2001; Aurell et al., 2003). These carbonate ramp successions are arranged in three third-order depositional sequences (sequences Ki1, Ki2 and Ki3; Fig. 1C; Aurell et al., 2010, in press). Sequences Ki1 and Ki2 correspond to shallow oolitic and reefal facies (Ricla Mb and Torrecilla Fm), passing down dip into the mid- and outer-ramp marls and lime mudstones of the Sot the Chera and Loriguilla formations (Bádenas and Aurell, 2001; Aurell et al., 2010). The stratigraphic succession studied here belongs to the latest Kimmeridgian sequence Ki3, represented in the north-central part of the Iberian Basin by the shallow-water carbonate deposits of the Higueruelas Fm (Aurell and Meléndez, 1986, 1987; Ipas et al., 2004; Aurell et al., 2010). This unit has a wide range of grain-supported facies characterized by a predominance of non-skeletal grains (mainly oncoids, but also ooids, peloids, intraclasts and aggregate grains) and also includes small carpets and buildups of corals, chaetetids and stromatoporoids (e.g. Bádenas and Aurell, 2003; Aurell et al., 2012; Sequero et al., 2018). The latest Kimmeridgian age attributed to the Higueruelas Fm is based on the widespread record of the benthic foraminifera *Alveosepta jaccardi* combined with the presence of mid-Kimmeridgian ammonites (i.e. *acanthicum/eudoxus* zones) in the underlying Loriguilla Fm (Bádenas et al., 2003). New strontium-isotope data from belemnites, brachiopods and oyster shells reported by Aurell et al. (in press) are coherent with the sedimentation of the Higueruelas Fm during the upper *A. eudoxus* zone and the *H. beckeri* zone (Fig. 1C).

The Higueruelas Fm is widely exposed south of Zaragoza (northeastern Spain, north Iberian Chain), in the outcrops located from the localities of Muel to Aguilón studied here (Fig. 2). The thickness of the unit ranges from 40 to 80 m in the east (i.e. basinward), reflecting a relatively homogeneous subsidence (e.g. Aurell et al., 2003). The boundaries of the Higueruelas Fm generally correspond to regional discontinuity surfaces (Fig. 1D): the lower boundary is the contact with the underlying well-bedded (dm-scale) open-marine lime mudstone succession of the Loriguilla Fm (i.e. the boundary between the sequences Ki2 and Ki3); the upper boundary corresponds either to a basin-wide discontinuity (i.e. the upper boundary of the sequence Ki3) or to a boundary marked by the onset of coastal siliciclastic-dominated deposits in the more proximal, western logs studied in this work (e.g. Aguilón sector; Fig. 1D).

3. Studied successions and methodology

The 40 to 80 m-thick shallow-marine carbonate successions of the Higueruelas Fm were studied in 21 logs along the outcrops located south of Zaragoza (Fig. 2). The studied area is 20 × 30 km in extent, and the mean distance between logs is around 5 km. The studied sections are situated mainly on the flanks of E-W to NW-SE anticlines that developed during the Alpine compression (Cortés Gracia and Casas Sainz, 1996). The dip angle of the flank beds is generally low (10–30°, locally 80° in the localities of Tosos and Jaulín).

Facies analysis was based on both the bed-by-bed field descriptions of the 21 logs and the petrographic analysis of 1200 polished slabs and 300 thin sections. The description of texture was based on the Dunham (1962) classification. For the characterization of non-skeletal grains, the proposed nomenclatures for oncoids (Dahanayake, 1977, 1978), ooids (Strasser, 1986), and peloids (Flügel, 2004) were followed. The main characteristics of these non-skeletal grains are summarized in Table 1. The semi-quantitative proportion of skeletal and non-skeletal components in polished slabs and thin sections was ascertained by visual estimates using the comparison chart of percentages of constituents developed for limestones by Baccelle and Bosellini (1965).

Log correlation was carried out along three E-W-orientated (i.e. down-dip) cross-sections (Fig. 3). The lower datum for correlation is the sharp discontinuity surface between the thick-bedded (dm- to m-thick) limestones of the Higueruelas Fm (sequence Ki3) and the thin-bedded (dm-thick) lime mudstones of the underlying Loriguilla Fm (sequence Ki2; Fig. 1C) in the more proximal areas (i.e. studied sections in the localities of Muel, Jaulín, Mezalocha, Tosos and Aguilón). This discontinuity surface passes down dip (e.g. F1, F3 logs; Fig. 3) into a well-marked bedding surface within the uppermost Loriguilla Fm, which is coherent with the lateral relationship at basin-scale of the Higueruelas and Loriguilla formations (Bádenas and Aurell, 2001; Aurell et al.,

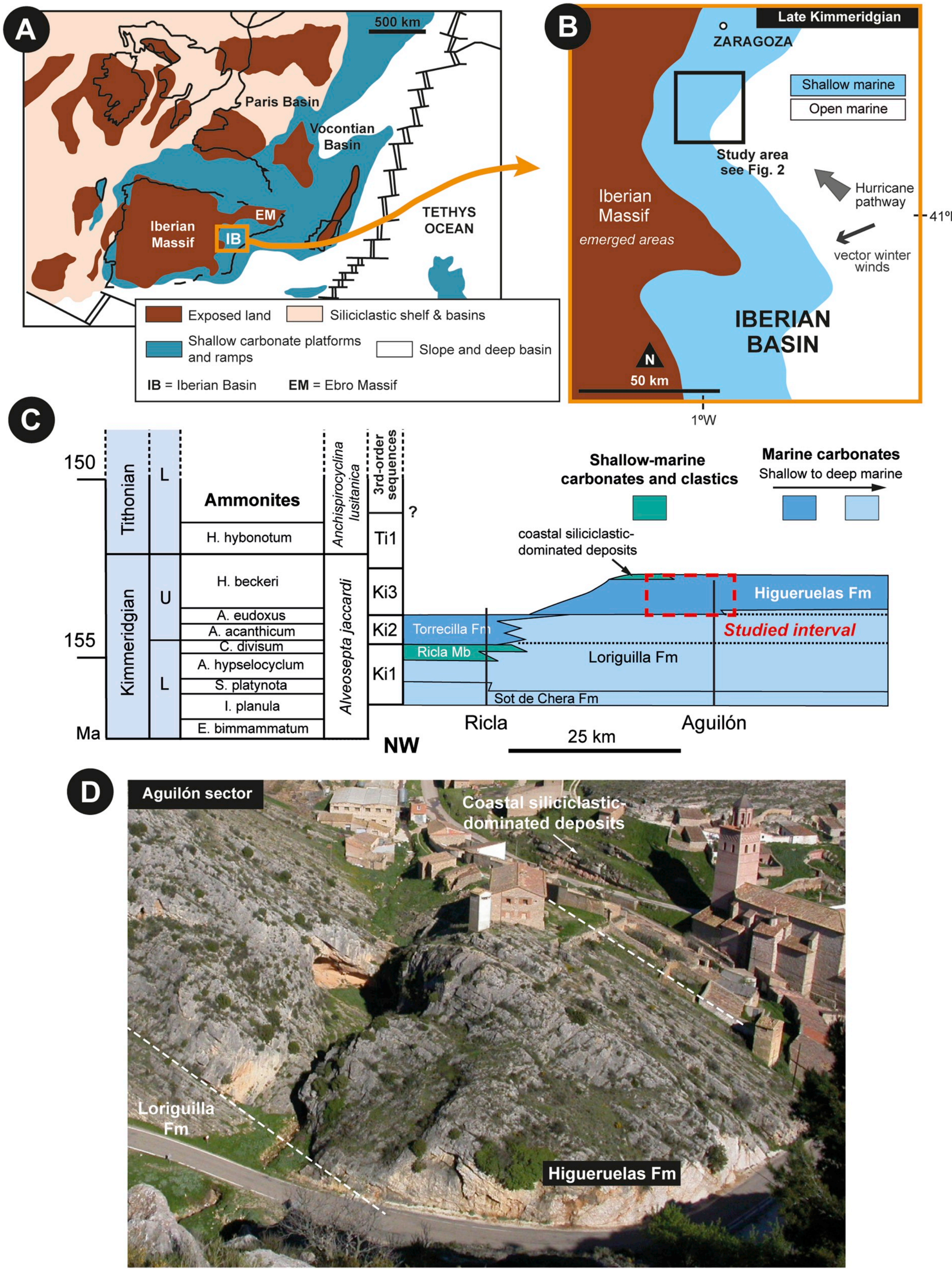

Fig. 1. (A) Palaeogeography of western Europe during the late Kimmeridgian (modified from Dercourt et al., 1993). (B) Main facies belts in the northeastern Iberian Basin during the late Kimmeridgian (compiled from Aurell et al., 2003 and Ipas et al., 2004). (C) Synthetic stratigraphy of the Kimmeridgian in the northern Iberian Basin including the main facies belts (modified from Aurell et al., 2010, in press). The Higueruelas Fm corresponds to the sequence Ki3. (D) Field view of the Higueruelas Fm, the underlying Loriguilla Fm and the overlying coastal siliciclastic-dominated deposits. The lower and upper boundaries of the Higueruelas Fm correspond to basin-wide discontinuity surfaces.

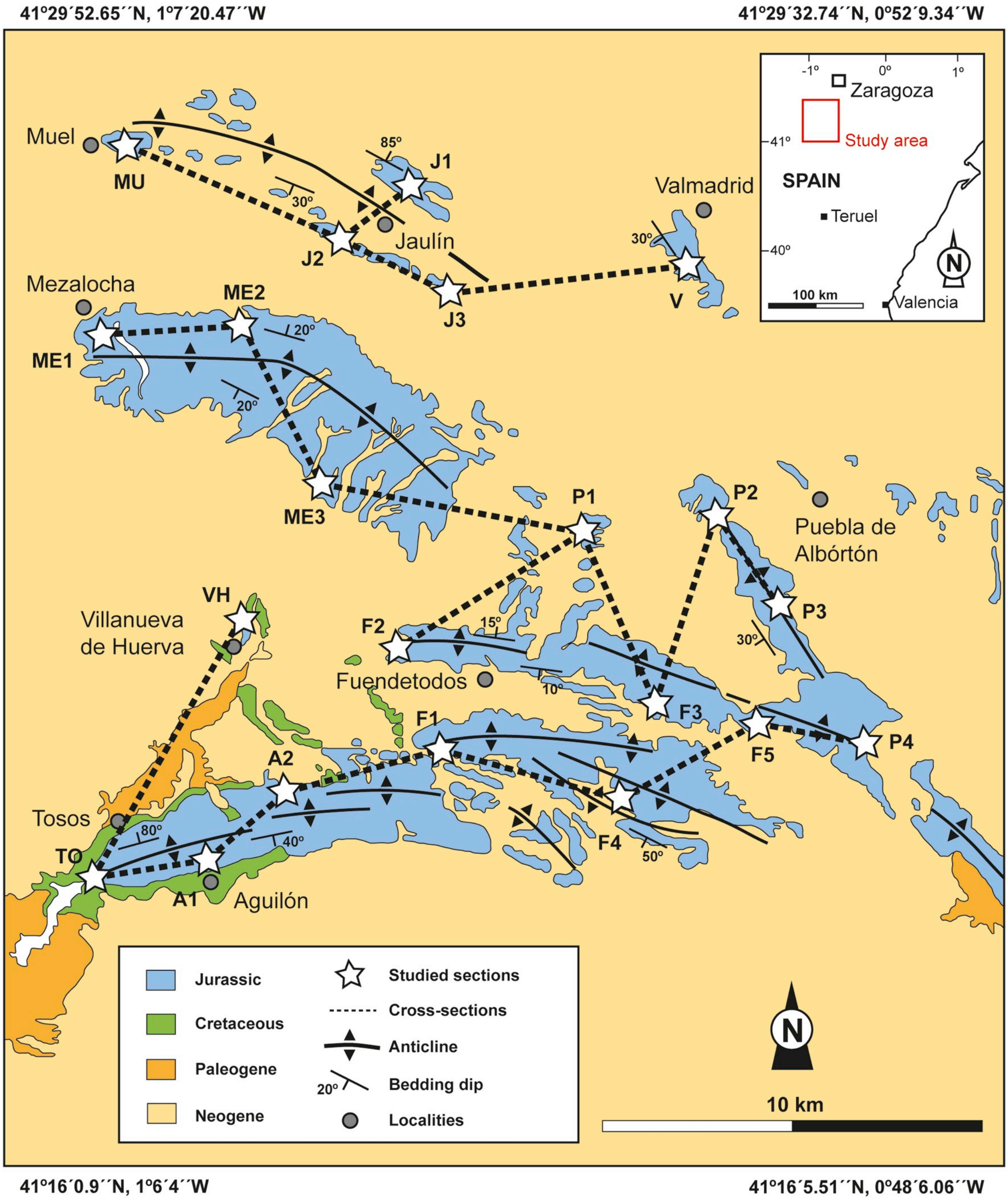

Fig. 2. Extent of the Jurassic outcrops and location of the studied logs south of Zaragoza (northeast Spain) (modified from Cortés Gracia and Casas Sainz, 1996). Dashed lines indicate the cross-sections shown in Figs. 5–7.

Table 1
Characteristics of the main non-skeletal grains.

Non-skeletal grain	Type	Size and shape	Internal structure
Oncoid (Dahanayake, 1977, 1978)	I	Few millimetres; spherical to elliptical	Concentric and continuous micritic laminae
	II	Few millimetres to 1 cm; elliptical to sub-spherical	Micritic laminae with organism-bearing encrustations
	III	Few cms (up to 2 cm); spherical to irregular with wavy contours	Alternating micritic and organism-bearing laminae
	IV	Few mms to 7 cm; very irregular, lobate contours	Microbial meshwork, no lamination
Ooid (Strasser, 1986)	1	Up to 2 mm; spherical	Concentric thinly micritic laminae
	3		Fine-radial laminae
	1/3		Alternating fine-radial and micritic laminae
	4		Few thick-radial laminae
Peloid (Flügel, 2004)	Lithic	Variable in size; well-rounded to irregular	Micrite
	Microbial	Up to 600 µm; well-rounded	

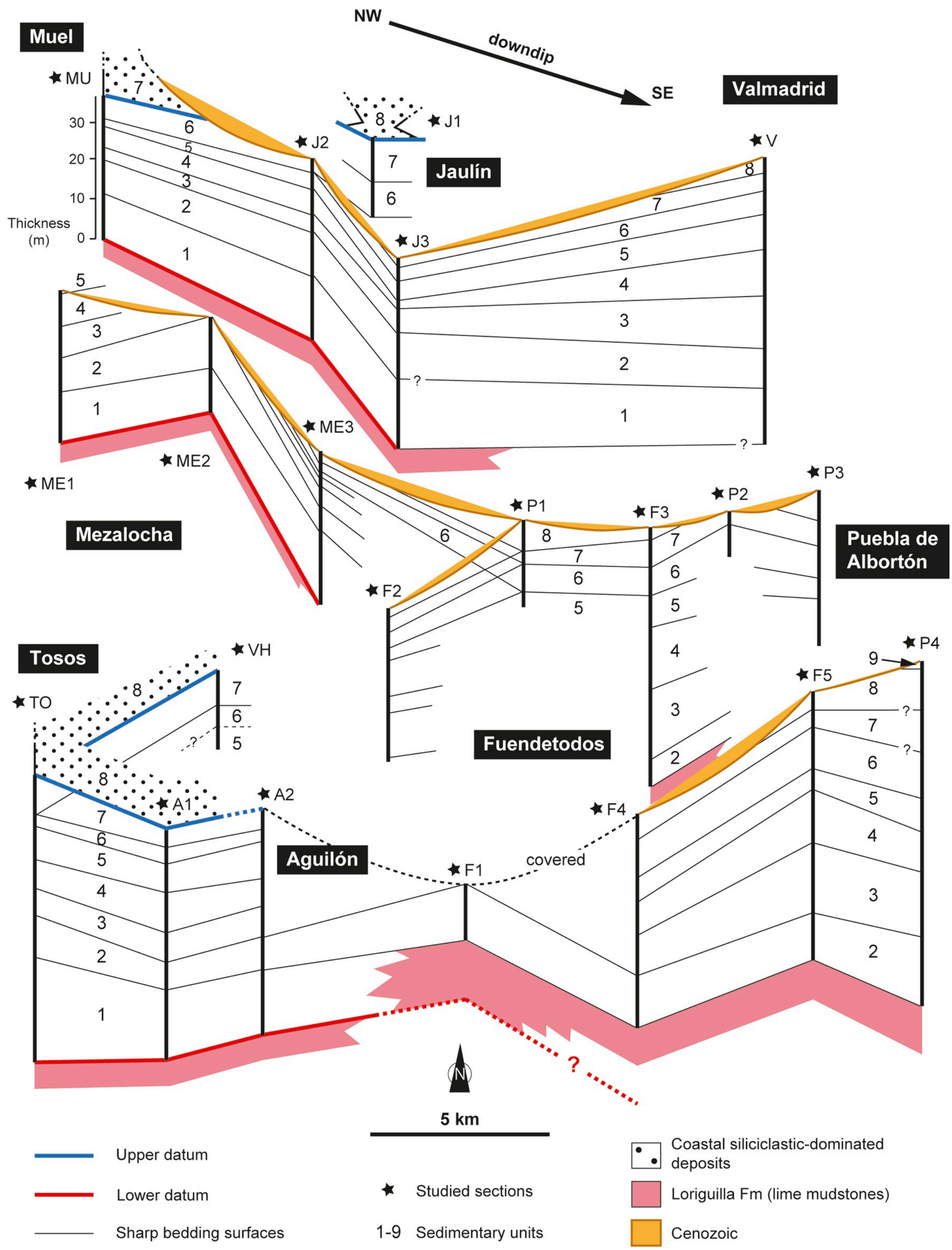

Fig. 3. Correlation between the studied logs in the three cross-sections, based on the identification of time-equivalent sharp bedding surfaces (black lines), which allowed nine sedimentary units (1–9) to be documented. This best-fit solution is coherent with the vertical facies trends observed within the sedimentary units. The lower and upper datum for correlation is also indicated (red and blue lines, respectively), as well as the eroded areas in the upper part, prior to the deposition of Cenozoic sediments. (For interpretation of the references to colour in this figure legend, the reader is referred to the Web version of this article.)

2003). This implies that the boundary between the Higueruelas and Loriguilla formations is diachronous to the SE of the studied area. The analysis of the upper part of the Higueruelas Fm is locally prevented due to the erosive gap of variable amplitude and duration prior to the sedimentation of the overlying Cenozoic units (Fig. 3). In the more proximal areas (sections TO, A1, VH, MU and J1; Fig. 3), the uppermost part of the studied sequence Ki3 consists of the transition from carbonates to coastal siliciclastic-dominated facies (Ipas et al., 2007). In these proximal areas, therefore, the upper datum of the present study is the boundary between the Higueruelas Fm and these coastal facies, which is diachronous in the northwestern area (i.e. section MU) due to the earlier transition to siliciclastic deposits.

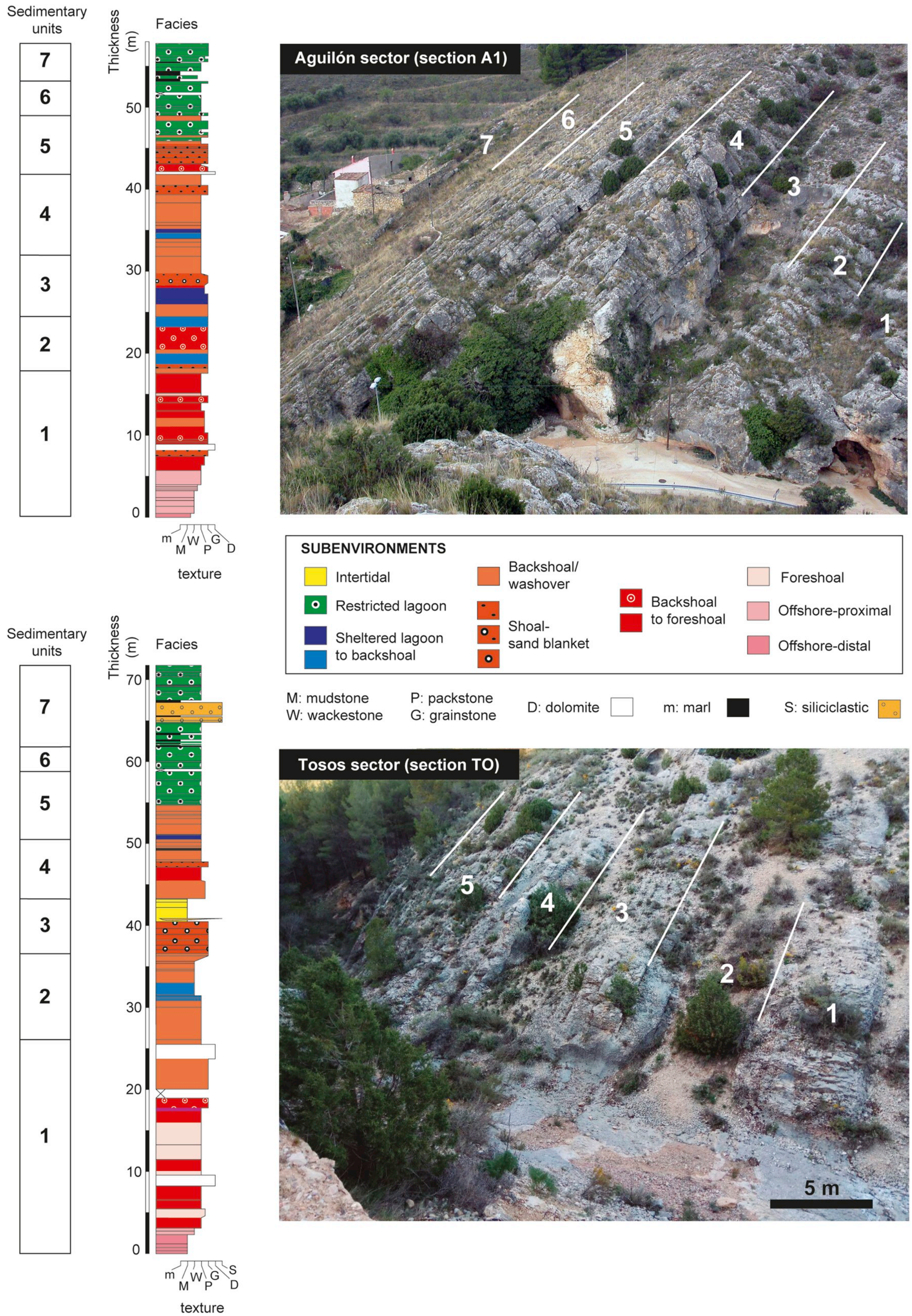

Fig. 4. Vertical facies evolution within the sedimentary units (1–7) identified for the Higueruelas Fm in the stratigraphic sections A1 and TO (see Fig. 2 for location). White lines indicate the position of the sharp bedding planes.

Well-marked bedding surfaces bounding nine sedimentary units were identified and correlated within the Higueruelas Fm in all the outcrops (1–9 in Figs. 3 and 4). These are planar surfaces, some of which are bioturbated or Fe-encrusted, and they occasionally correspond to hardgrounds. Locally cm-thick marly beds are associated with these surfaces. As no physical tracing between isolated outcrops of the

Higueruelas Fm was possible (Fig. 2), log correlation was based on the best-fit correlation between these sharp bedding surfaces, also constrained by the vertical facies distribution observed in the successive sedimentary units defined in the individual logs. These sharp bedding surfaces are assumed to represent sedimentary discontinuities that can be traced across the entire studied area, and their correlation is supported by physical tracing along continuous outcrops (e.g. Mezalocha sector; Sequero et al., 2018). The km-scale lateral continuity of similar well-defined bedding surfaces has been demonstrated in other Kimmeridgian shallow carbonate ramp successions of the Iberian Basin (e.g. Bádenas and Aurell, 2010; Bádenas et al., 2010).

The sedimentary features of the facies, combined with their lateral and vertical relationships within the sedimentary units, were the key criteria for their palaeoenvironmental interpretation. Palaeogeographic maps were reconstructed for each sedimentary stage without palinspastic restoration, bearing in mind the low angle of the beds in the anticline flanks and the near absence of thrusts within the studied outcrops (Fig. 2).

4. Facies architecture

On the basis of texture, components and sedimentary structures, 19 facies were differentiated in the studied interval, representing deposition from inner- to mid-ramp areas. An example of their vertical distribution within the distinct sedimentary units is illustrated in Fig. 4, and their lateral distribution is indicated in cross-sections in Figs. 5–7. On the basis of their dominant components, the facies are grouped into three facies associations: peloidal and oolitic-dominated facies, oncolitic-dominated facies, and stromatoporoid/chaetetid/coral-rich facies. Their lateral relationships are identified by their detailed correlation within the sedimentary units between logs (see section 5). Facies descriptions are summarized below and illustrations of the different facies can be seen in Figs. 8–12. Detailed information is included in Tables 1–3.

4.1. Peloidal and oolitic-dominated facies association

This association comprises 11 facies characterized by the predominance of peloids and ooids, and variable proportions of oncoids, intraclasts and bioclastic remains (Tables 2 and 3). These facies represent intertidal areas (i.e. peloidal mudstone to packstone-grainstone with fenestral porosity), restricted lagoon areas (peloidal-bioclastic-type 3 and 4 ooid wackestone to grainstone), backshoal areas (peloidal-type 1 and 1/3 ooid wackestone to grainstone, and bioturbated peloidal packstone to grainstone) and shoal-sand blankets (peloidal to oolitic grainstone facies) on the inner ramp, to foreshoal (peloidal wackestone-packstone to grainstone), offshore-proximal (peloidal-bioclastic wackestone to packstone) and offshore-distal areas (bioclastic-peloidal mudstone) on the middle ramp. The lateral relationship of intertidal, lagoon and backshoal facies can be seen in sedimentary units 5 to 7 (Figs. 5–7). The lateral relationship of backshoal, shoal-sand blanket, foreshoal and offshore facies is evident in most of the units (e.g. units 1 and 2 in Fig. 7; units 2 and 3 in Fig. 5).

Peloidal mudstone (M) to packstone-grainstone (P-G) with fenestral

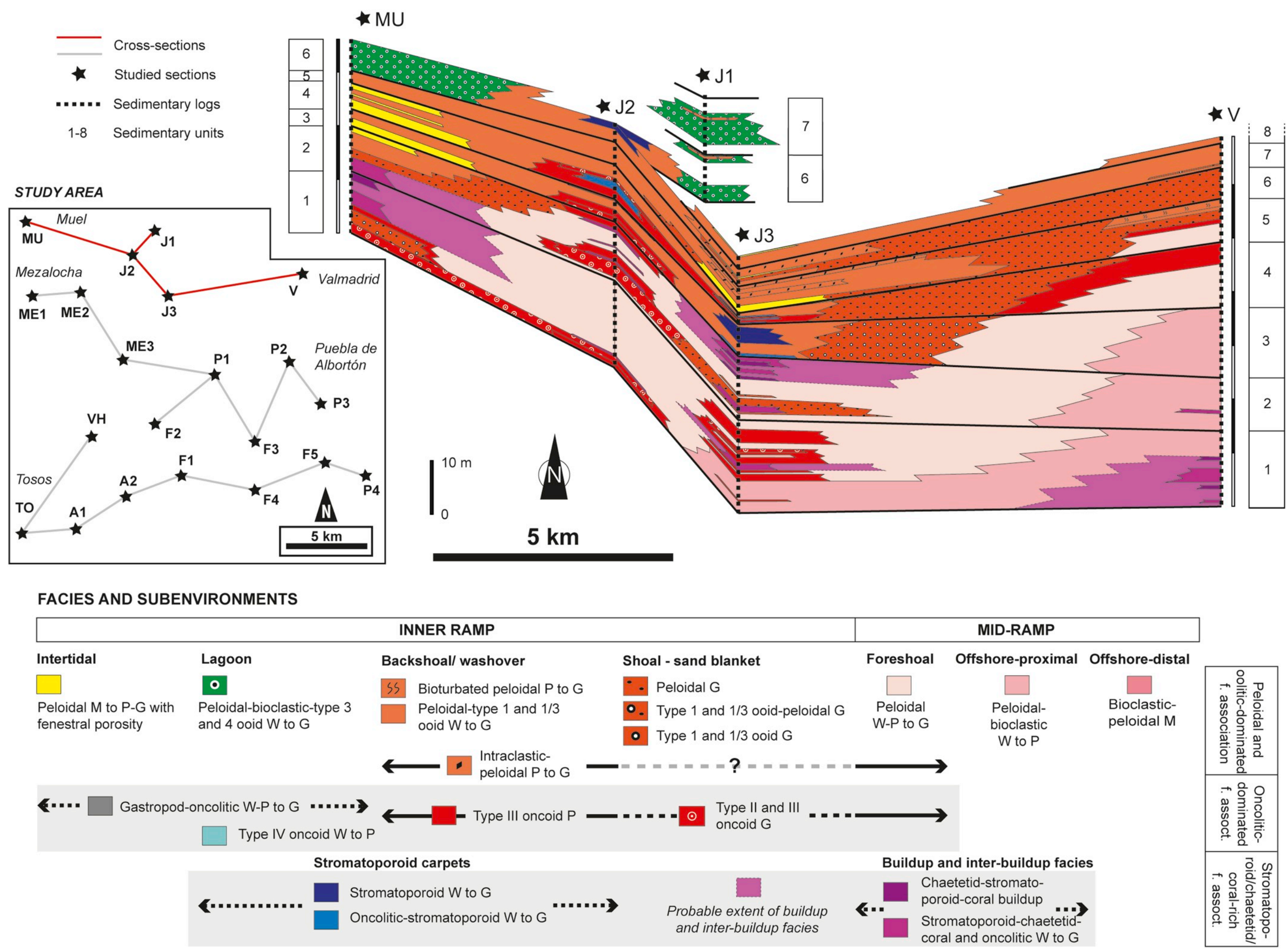

Fig. 5. Facies distribution in the northern cross-section.

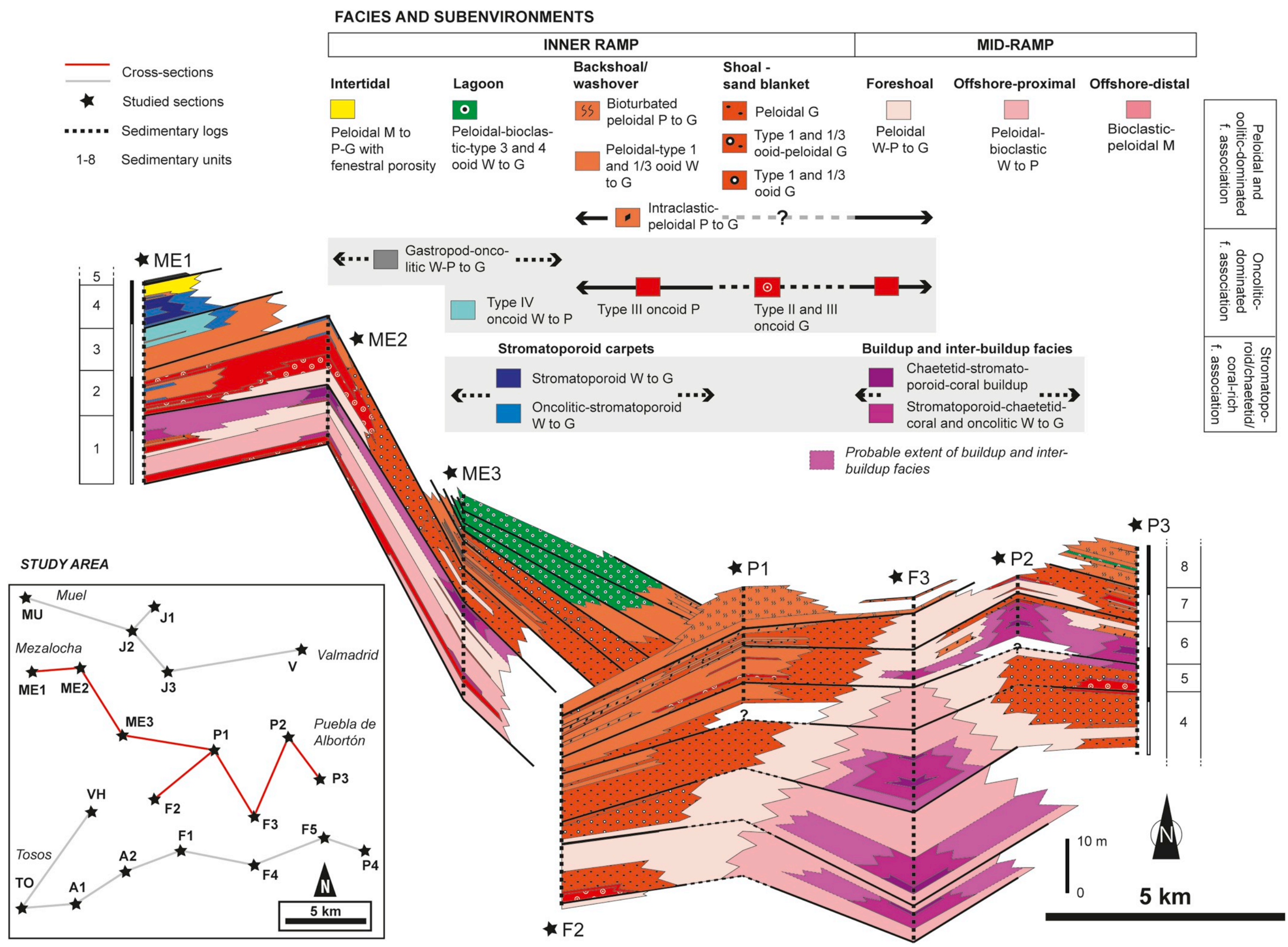

Fig. 6. Facies distribution in the central cross-section.

porosity is characterized by the predominance of lithic peloids, and a lower proportion of type 1 and 1/3 ooids (Strasser, 1986), type II oncoids (Dahanayake, 1977) (Table 1), and skeletal grains (mainly of lituolids, miliolids, texturaliids, bivalves and *Tubiphytes-Crescentiella*; Fig. 8a). Fenestral porosity indicates the trapping of air bubbles in the sediment by turbulent flows related to waves, algal growth and decay, or desiccation and the rapid precipitation of cements (e.g. Shinn, 1968; Flügel, 2004). The presence of *Girvanella* and *Bacinella* growths and dome-like stromatolitic structures indicates sediment trapping by microbial mats in intertidal areas. Facies correlation indicates that these mud-supported and grain-supported sediments represent a continuous intertidal belt located to the northwest (Figs. 5 and 6) and local tidal caps on grain-supported deposits (e.g. peloidal-oolitic shoal-sand blankets and washover deposits in sections TO and J3, respectively, Figs. 5 and 7; see also Sequero et al., 2018).

Peloidal-bioclastic-type 3 and 4 ooid wackestone (W) to grainstone (G) occurs in the upper part of the succession (Figs. 5–7). It is composed of well-sorted and rounded lithic peloids, radial type 3 and 4 ooids (Strasser, 1986) and highly micritized or ferruginous bioclasts (mainly bivalves, lituolids, gastropods, ostracods and echinoderms; Fig. 8b, c). The facies shows frequent bioturbation (*Thalassinoides* traces) and cm-thick bioclastic laminae with normal gradation and parallel lamination. The observed features indicate alternating low-energy conditions (burrowing and micritization of skeletal grains) and moderate-energy conditions (lithic peloids, radial type 3 and 4 ooids, cm-thick bioclastic laminae). Deposition probably took place in a restricted lagoon, as indicated by the low diversity of the skeletal remains. Some intercalated marls indicate periods of higher detrital input.

Peloidal-type 1 and 1/3 ooid W to G and bioturbated peloidal P to G facies represent the backshoal/washover peloidal-oolitic facies. The peloidal-oolitic W to G has abundant lithic peloids, and variable proportions of ooids, oncoids and skeletal grains (Fig. 8d-f). Compound and aggregate grains are common, and the main skeletal grains are foraminifera (lituolids, miliolids, textulariids), brachiopods, bivalves, echinoderms, gastropods and dasycladacean algae. The facies shows a mixture of components derived from the laterally related facies, e.g. protected-marine fauna (i.e. dasycladacean algae; Fig. 8e) similar to the lagoon facies, and type 1 and 1/3 ooids and oncoids similar to those of the shoal-sand blanket facies. This mixture of components, and the presence of aggregate grains, bioturbation, parallel and cross-lamination, and mm- to cm-thick oncolitic, skeletal and oolitic laminae with normal gradation, indicate that this facies corresponds to washover deposits as well as backshoal sediments (e.g. Bádenas and Aurell, 2010). Bioturbated peloidal P to G occurs at the top of the succession, also laterally related to restricted lagoon and peloidal shoal-sand blanket facies (e.g. unit 5 in Fig. 5; and unit 8 in Fig. 6). The predominance of well-sorted lithic peloids (Fig. 8g), micritized skeletal grains (mainly lituolids, miliolids, gastropods, echinoderms and bivalves), and intense burrowing (*Thalassinoides* traces) reflect accumulation in a backshoal subenvironment close to the peloidal shoal-sand blankets.

The peloidal to oolitic grainstone facies include three types of facies, each one characterized by the predominance of specific non-skeletal grains (Fig. 9a-c): peloidal G with well-sorted and rounded lithic

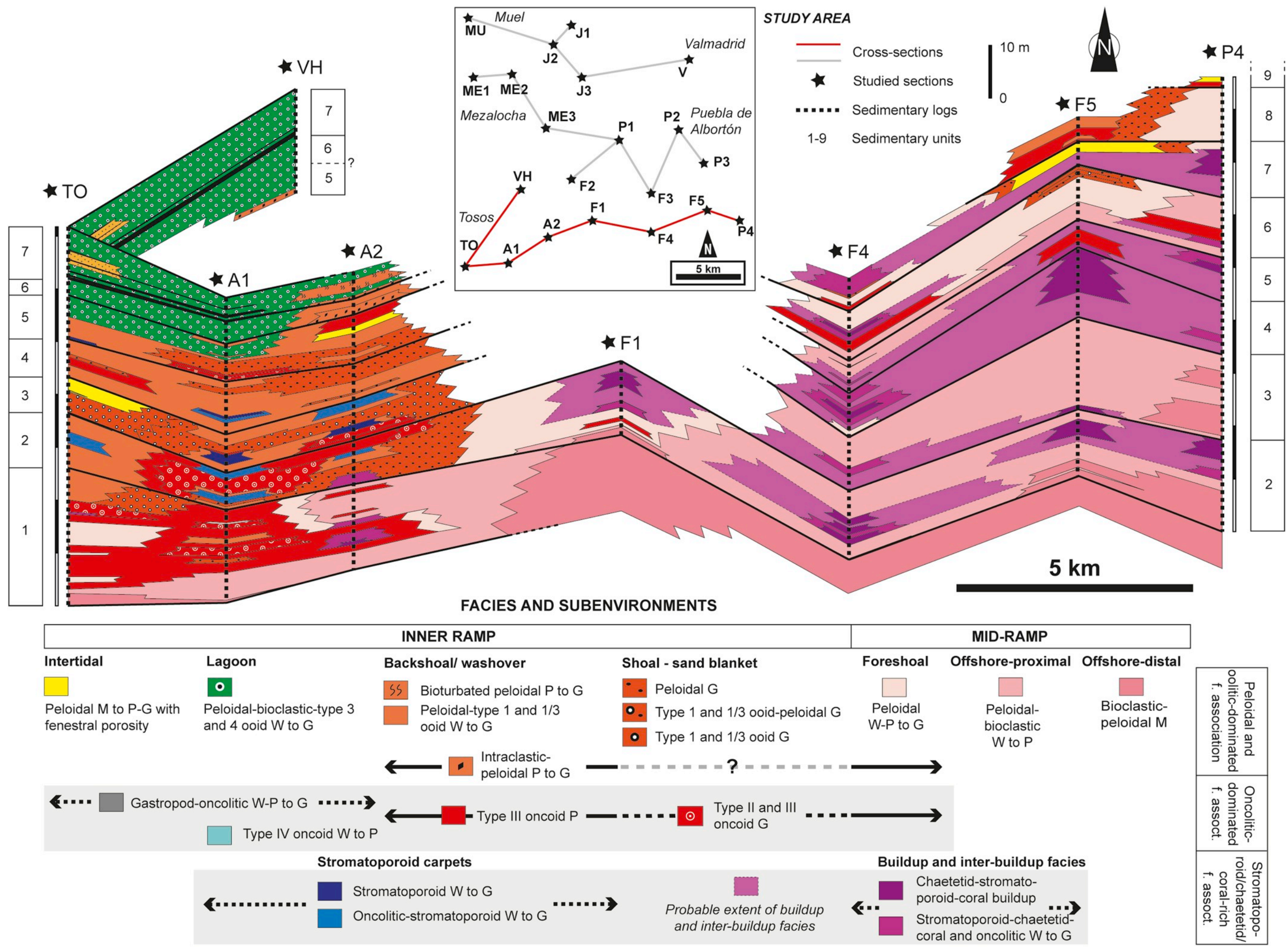

Fig. 7. Facies distribution in the southern cross-section.

peloids (Fig. 9a) and a lesser proportion of type 1 and 1/3 ooids and type IV oncoids; type 1 and 1/3 ooid-peloidal G, with a similar percentage of lithic peloids and type 1 and 1/3 ooids (Fig. 9b); and type 1 and 1/3 ooid G, dominated by smaller (up to 0.5 mm-sized) and well-sorted type 1 and 1/3 ooids (Fig. 9c). The grainstone texture, the predominance of high-energy ooids (type 1 and 1/3 ooids) and lithic peloids, and the scarce skeletal content reflect the continuous agitation of shoal-sand blankets above the fair-weather wave base (i.e. inner ramp). Despite the absence of cross-bedding, frequent local tidal caps on these facies (e.g. sections TO and F5 in Fig. 7) reflect a certain relief above the sea bottom.

Peloidal W-P to G has similar components and structures (common bioturbation, local parallel lamination) to those described in peloidal to oolitic shoal-sand blankets. It includes mainly lithic peloids and type 1 and 1/3 ooids (Fig. 9d), although this facies has a higher matrix and skeletal content (mainly lituolids, miliolids, echinoderms, brachiopods and bivalves). These characteristics and its lateral relationship with shoal-sand blanket and offshore facies (Figs. 5–7) indicate deposition in the foreshoal subenvironment, below the fair-weather wave base.

The peloidal-bioclastic W to P and bioclastic-peloidal M facies developed down-dip of the foreshoal facies (Figs. 5–7) and reflect a progressive loss of non-skeletal grains from shallow areas. The peloidal-bioclastic W to P is mainly formed by lithic and local microbial peloids (Fig. 9e; Table 1), with a lower proportion of oncoids (type II and IV oncoids with thick crusts of *Bacinella* and *Girvanella*) and a skeletal content characteristic of open-marine areas, including some belemnites (Tables 2 and 3). The intercalation with foreshoal and mud-dominated offshore facies, frequent bioturbation (*Chondrites* and *Planolites* traces) and an open-marine faunal association indicate deposition in an offshore-proximal subenvironment with generally low energy. The bioclastic-peloidal M has scarce lithic peloids and type I and II oncoids, as well as open-marine skeletal grains (Fig. 9f). These characteristics, the frequent bioturbation and its lateral relationship with offshore-proximal facies indicate deposition in a low-energy offshore-distal subenvironment. The scarce type I and II oncoids were probably resedimented from proximal areas during storms.

One particular facies, intraclastic-peloidal P to G, appears in the upper part of the succession, laterally related to various facies, mainly backshoal/washover to foreshoal facies (e.g. unit 6; Figs. 5 and 6). The intraclastic-peloidal facies occurs as isolated dm-thick beds, with components accumulated in mm- to cm-thick laminae. The limited lateral extent of this facies obtained from the correlation, combined with the predominance of lithic peloids and mm- to cm-sized intraclasts of mud- and grain-supported facies (Fig. 8h; Table 2), indicates that this facies would correspond to storm lobes in both backshoal and foreshoal subenvironments, with resedimented intraclasts derived from lateral mud- and grain-supported facies.

4.2. Oncolitic-dominated facies association

This association comprises four facies characterized by an abundance of oncoids, formed in pond/restricted lagoon, sheltered lagoon, backshoal, shoal-sand blanket to foreshoal subenvironments (Figs. 5–7; Tables 2 and 3). Sheltered lagoon facies (type IV oncoid W to P) and

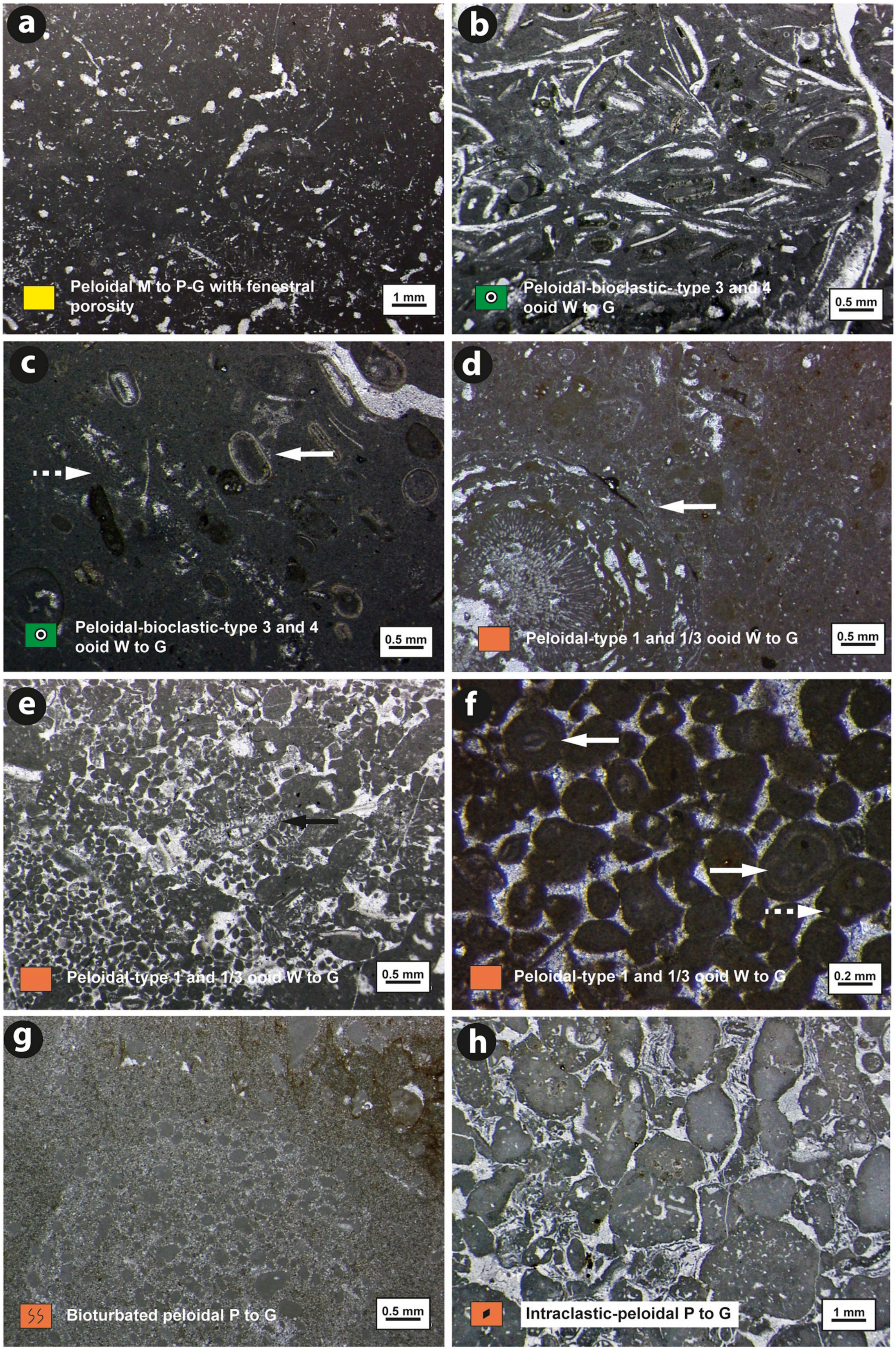

Fig. 8. (a) Fenestral porosity (intertidal subenvironment) in peloidal mudstone facies. (b, c) Restricted lagoon facies with well-sorted lithic peloids, bioclasts (bivalves, lituolids: b and dashed arrow in c, respectively) and type 3 ooids (white arrow in c), showing thinly laminated fine-radial cortices. (d–f) Backshoal facies with poorly sorted peloids, type II oncoids (white arrow in d), protected-marine bioclasts (dasycladacean algae: black arrow in e), type 1/3 ooids and aggregate grains (white and dashed arrows in f, respectively). (g) Backshoal peloidal facies with intense burrowing. (h) Storm-related deposit with mm- to cm-sized intraclasts and poorly sorted peloids. Facies symbols are included in the pictures (see facies legend in Figs. 5–7).

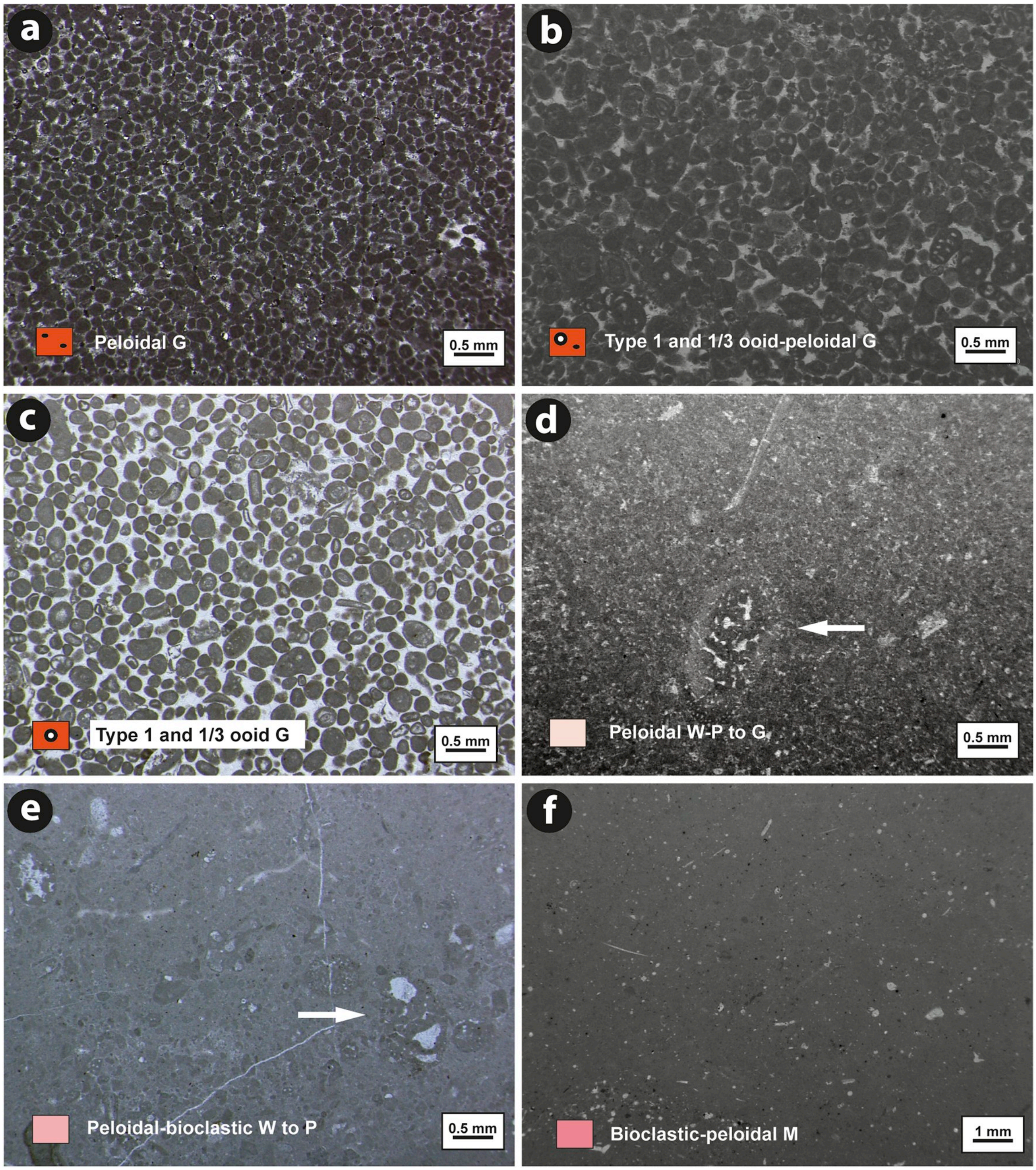

Fig. 9. (a–c) Peloidal to oolitic shoal-sand blanket facies composed of well-sorted lithic peloids, type 1 and 1/3 ooids and scarce bioclasts. (d) Well-sorted lithic peloids in foreshoal facies with some bioclasts (e.g. lituolids: white arrow). (e) Offshore-proximal facies with lituolids (white arrow) and poorly sorted peloids. (f) Sponge spicules in bioclastic-peloidal mudstone facies (offshore-distal subenvironment).

pond/restricted lagoon facies (gastropod-oncolitic W-P to G) are only present in the northwestern area in sedimentary units 3 and 5, respectively (section ME1; Fig. 6). The pond/restricted lagoon gastropod-oncolitic facies is laterally related to restricted peloidal-bioclastic-oolitic-dominated lagoon and peloidal-dominated fenestral facies (see also the facies correlation in this area by Sequero et al., 2018). The sheltered lagoon oncolitic facies is laterally associated with the peloidal-oolitic backshoal facies, and grades laterally into the backshoal to foreshoal oncolitic-dominated facies (type III oncoid P, and type II and III oncoid G; e.g. sedimentary units 1–4 and 8; Figs. 5–7).

Gastropod-oncolitic W-P to G is characterized by an abundance of broken and whole gastropods, and type I, II and IV oncoids (Fig. 10a), and has variable proportions of lithic peloids, type 1 and 1/3 ooids and small, commonly micritized skeletal grains (mainly of bivalves, lituolids, miliolids and textulariids). The predominance of gastropods, the presence of non-skeletal components similar to the laterally related fenestral facies, and the intercalation of marls indicate deposition in a restricted lagoon or in ponds within the intertidal area. Components that accumulated in cm-thick laminae reflect high-energy events, probably storms.

Type IV oncoid W to P has abundant irregular type IV oncoids (up to 7 cm in size), with bioclastic cores and thick crusts composed of a meshwork of cyanobacteria (mainly *Bacinella-Lithocodium*) (Fig. 10b, c). Type III oncoids are also common. The oncoids are surrounded by a fine-grain-sized fraction composed of lithic peloids and skeletal grains (mainly micritized lituolids, miliolids, textulariids, bivalves, echinoderms and brachiopods). The predominance of type IV oncoids, bioturbation and micritized skeletal grains reflect deposition in a sheltered, low-energy lagoon. Type III oncoids suggest short, higher-energy periods favouring the generation of micritic laminae (e.g. Dahanayake,

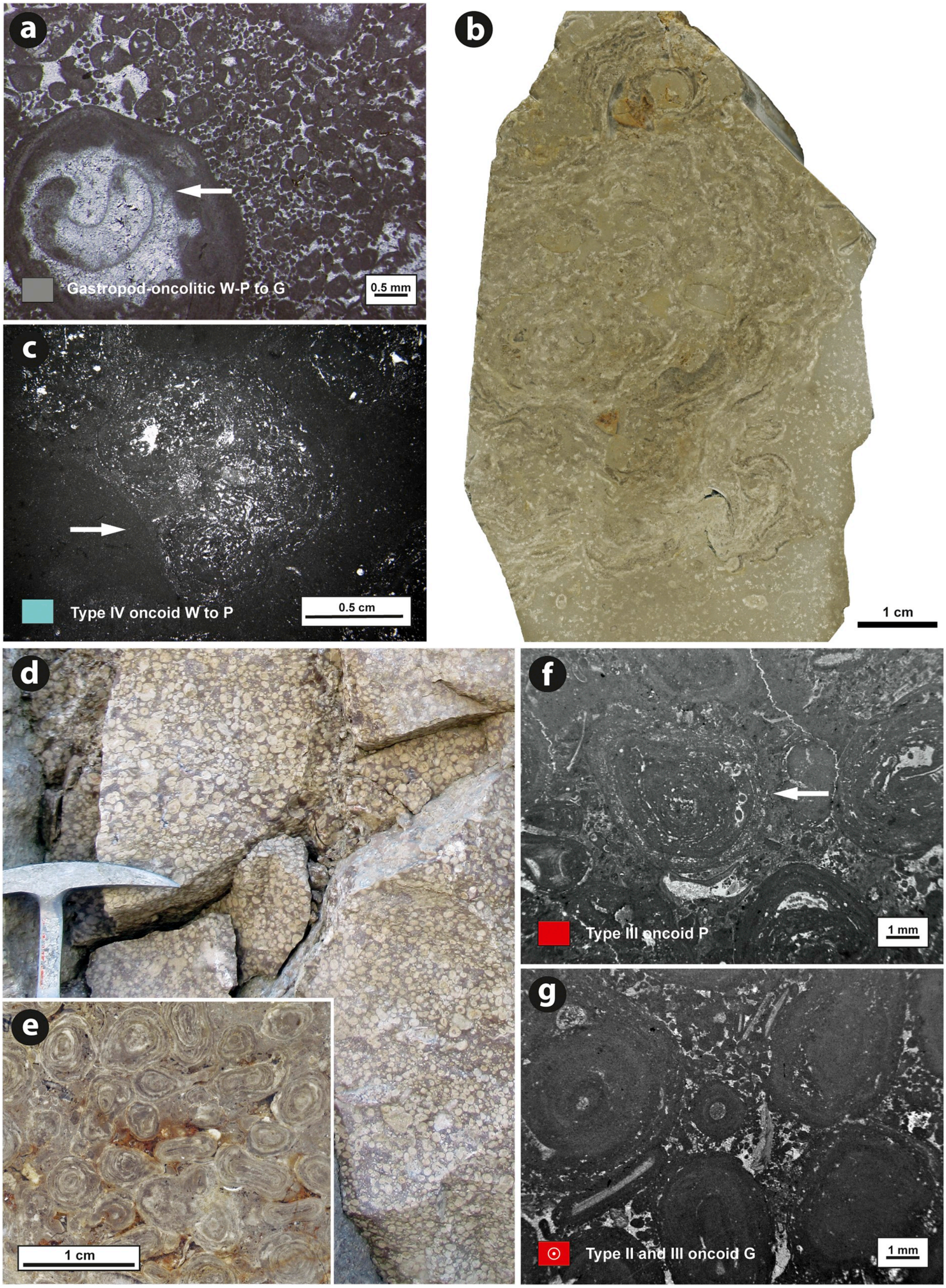

Fig. 10. (a) Well-sorted peloids, micritized bioclasts, ooids and type I oncoids in gastropod-oncolitic facies, with mainly gastropods as bioclastic cores (white arrow). (b, c) Oncolitic facies in sheltered lagoon subenvironment in macro-scale example (b) and thin section (c), with type IV oncoids composed of a microbial meshwork (white arrow in c). (d, e) Macro-scale examples of type III oncoid-dominated facies with oncolitic-supported texture. (f) Type III oncoid (white arrow) in foreshoal oncolitic-dominated facies, composed of alternating micritic and organism-bearing laminae of similar thickness. (g) Type II oncoids in shoal-sand blanket oncolitic-dominated facies, composed of thick micritic laminae with organism-bearing encrustations.

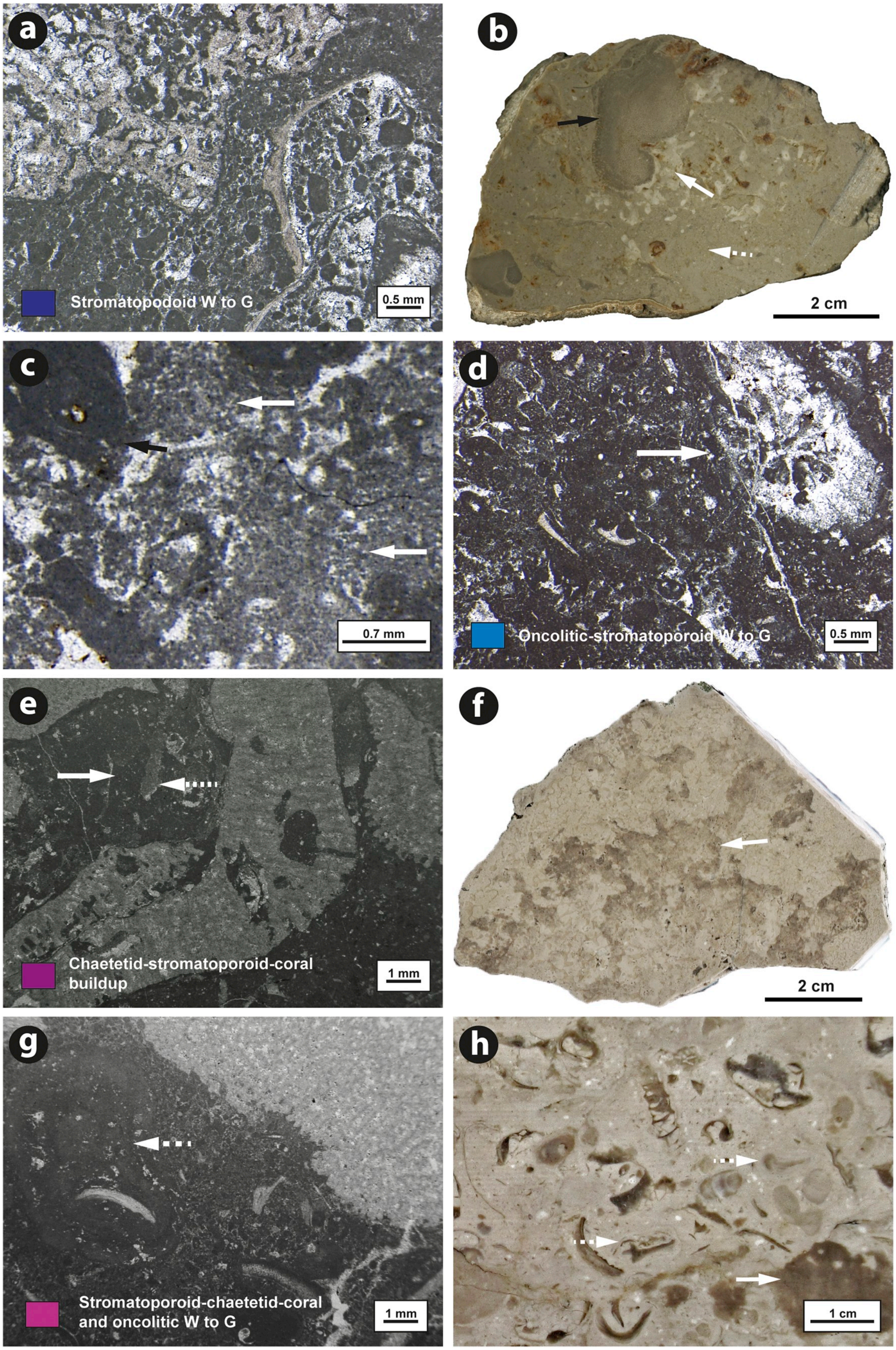

(caption on next page)

Fig. 11. (a–d) Stromatoporoid-rich facies in sheltered lagoon subenvironment. (a, b) Fragments of *Cladocoropsis*, poorly sorted peloids, microbial peloids and micritized bioclasts in stromatoporoid W to G facies. Stromatoporoids appear as isolated cm-sized fragments (black arrow in b) surrounding by a matrix composed of peloids, ooids and bioclasts (dashed arrow in b). *Tubiphytes* encrustations are common on stromatoporoids (white arrow in b). (c) Microbial peloids (white arrows) and *Tubiphytes* (black arrow) in stromatoporoid-rich facies. (d) Type II oncoid with bioclastic core (coral; white arrow) and thin crust with micritic laminae and organism-bearing encrustations in oncolitic-stromatoporoid W to G facies. (e–h) Chaetetid-stromatoporoid-coral buildup (e, f) and inter-buildup stromatoporoid-chaetetid-coral and oncolitic W to G (g, h) facies, showing fragments of chaetetids, microbial crusts with internal cavities (white and dashed arrows in e, respectively), and type II oncoids in inter-buildup facies (dashed arrow in g). (f) Macro-scale example of microbial crusts (white arrow) in chaetetid-stromatoporoid-coral buildup facies. (h) Macro-scale example of inter-buildup stromatoporoid-chaetetid-coral and oncolitic W to G facies, showing fragments of chaetetids (white arrow), bioclasts and oncoids (dashed arrows).

1977). Small micritic oncoids, ooids and intraclasts were resedimented from the laterally related facies, mainly from the peloidal-oolitic backshoal/washover facies.

Type III oncoid P comprises 20–60% oncoids, in some cases forming oncolitic-supported textures (Fig. 10d-f). This facies has abundant type III oncoids (up to 2 cm in size), with bioclastic and intraclastic cores, and alternating micritic laminae and organism-bearing encrustations, mostly of *Bacinella-Lithocodium* (Fig. 10f). Type II, IV and compound oncoids are common, and the fine-grain-sized fraction is composed of peloids (lithic and microbial peloids), type 1 and 1/3 ooids and skeletal grains (lituolids, miliolids, textulariids, echinoderms, gastropods, bivalves, brachiopods, stromatoporoids and chaetetids). The abundance of type III oncoids suggests alternating higher- and lower-energy conditions, the latter favourable for microbial growth. The lateral facies relationships indicate that this facies occurs in the backshoal and foreshoal subenvironments (e.g. units 1–2 in Figs. 6 and 7).

Type II and III oncoid G, which has similar proportions of oncoids to type III oncoid P, is characterized by an abundance of type II and III oncoids (up to 2 cm in size), with bioclastic and intraclastic cores, thick micritic laminae and a minor development of organism-bearing encrustations (mainly *Bacinella*) (Fig. 10g). Type I and compound oncoids are also common, and the fine-grain-sized fraction is composed of lithic peloids, type 1 and 1/3 ooids and skeletal grains (lituolids, echinoderms, bivalves and brachiopods). The grainstone texture, the abundance of type II and III oncoids and the lateral facies associations indicate that this facies occurs in the shoal-sand blanket subenvironment (e.g. units 1–2 in Figs. 5 and 7).

4.3. Stromatoporoid/chaetetid/coral-rich facies association

This association is characterized by an abundance of stromatoporoids, chaetetids and corals, and includes four facies: stromatoporoid W to G and oncolitic-stromatoporoid W to G in lagoon to backshoal areas; and chaetetid-stromatoporoid-coral buildups and laterally associated stromatoporoid-chaetetid-coral and oncolitic W to G, which developed in mid-ramp foreshoal to offshore-proximal areas (Figs. 5–7; Tables 2 and 3). The lateral relationship of these facies has been characterized in most of the units (e.g. units 2–5 in Fig. 7). The stromatoporoid W to G and oncolitic-stromatoporoid W to G facies are laterally associated with oncolitic-dominated and peloidal and oolitic-dominated lagoon and backshoal facies, respectively. The chaetetid-stromatoporoid-coral buildups and stromatoporoid-chaetetid-coral and oncolitic W to G facies are laterally associated with peloidal and peloidal and bioclastic-dominated foreshoal and offshore-proximal facies, respectively, and locally with oncolitic-dominated foreshoal facies.

The stromatoporoid W to G has abundant broken and in-situ stromatoporoids (mainly *Cladocoropsis*), and cm-sized fragments of chaetetids and corals, both with *Tubiphytes-Crescentiella* encrustations and bivalve borings (Fig. 11a, b). Local cm-sized domal growth forms of stromatoporoids are recognized. The fine-grain-sized fraction is mainly composed of peloids (lithic and microbial peloids; Fig. 11c) and small skeletal grains (mainly bivalves, brachiopods, echinoderms, lituolids, miliolids, texturaliids and dasycladacean algae). The oncolitic-stromatoporoid W to G has abundant oncoids (mainly type II and IV) and stromatoporoid, chaetetid and coral fragments (Fig. 11d). The fine-grain-sized fraction is mainly composed of peloids (lithic and microbial peloids) and small skeletal grains (mainly debris of *Tubiphytes-Crescentiella*, lituolids, miliolids, textulariids, bivalves, gastropods, echinoderms and brachiopods). Bioturbation and mm- to cm-thick accumulations of coarse grains are also common.

The stromatoporoid W to G and lateral oncolitic-stromatoporoid W to G represent stromatoporoid carpets in lagoon to backshoal areas. The term "carpet" refers to densely spaced stromatoporoid colonies that do not create a distinctly three-dimensional structure, but form relatively thin veneers of colonial organisms following the existing sea-floor morphology (e.g. Riegl and Piller, 2000). The facies mapping in the Mezalocha outcrops (Fig. 6) reflects the fact that these carpets did not develop in the entire lagoon but formed patches, locally more than 500 m in lateral extent (Sequero et al., 2018). The oncolitic-stromatoporoid W to G corresponds to sediment surrounding the stromatoporoid carpets (Figs. 5–7; see also Sequero et al., 2018), as indicated by their lateral relationship and the similarity of the components in these two facies (Tables 2 and 3). The common presence of stromatoporoids in lagoonal settings has been highlighted by previous authors (e.g. Flügel, 1974; Turnsek et al., 1981; Leinfelder et al., 2005; Aurell et al., 2012; San Miguel et al., 2017a). The predominance of stromatoporoids over corals was probably due to moderate water-energy, oligotrophic conditions in the lagoon and backshoal subenvironments (e.g. Leinfelder et al., 2005). The presence in the fine-grain-sized fraction of peloids, bivalves, echinoderms, foraminifera, dasycladacean algae, *Thaumatoporella* and *Cayeuxia-Ortonella* (Tables 2 and 3) indicates well-oxygenated, normal-marine waters.

The chaetetid-stromatoporoid-coral buildups have a lenticular geometry up to 8 m high and around 250 m wide (i.e. section F5; Fig. 12; Bádenas and Aurell, 2003). The reef fabric consists of chaetetids (e.g. *Ptychochaetetes*, *Blastochaetetes*; Tables 2 and 3) and less abundant stromatoporoids and corals (Fig. 11e, f), surrounded by micritic to peloidal microbial crusts with encrusting organisms (serpulids, foraminifera, sponges, *Cayeuxia-Ortonella*, *Thaumatoporella*, *Lithocodium*, *Bacinella*, *Girvanella*, *Troglotella*; Bádenas and Aurell, 2003). The internal structure is similar to those observed in the so-called disrupted frame reefs defined by Riding (2002), where broken and weakly eroded colonial organisms constitute the three-dimensional structure. The fine-grain-sized fraction recognized in internal cavities (a few mm to cm in size) is mainly composed of microbial peloids, small skeletal grains (mainly brachiopods, bivalves, echinoderms, serpulids, *Cayeuxia-Ortonella* and sponges), microbial crust fragments and oncoids (mainly type I and II). Bivalve and sponge borings are also found. The stromatoporoid-chaetetid-coral and oncolitic W to G, which is laterally related to these buildups, is characterized by cm-sized fragments of stromatoporoids, chaetetids and corals with variable proportions of oncoids (type II, III and IV) (Fig. 11g, h). The fine-grain-sized fraction is composed of microbial and lithic peloids, and mm- to cm-sized echinoderms, bivalves, brachiopods and gastropods. Bivalve and serpulid borings on stromatoporoids and chaetetids are also common.

The buildups developed in the foreshoal and offshore-proximal subenvironments, below the fair-weather wave base within the photic zone, as indicated by the presence of light-dependent organisms (e.g. *Cayeuxia-Ortonella*, *Girvanella*, *Bacinella*, *Thaumatoporella*) and their intercalation within foreshoal to offshore-proximal peloidal and peloidal-bioclastic facies (Figs. 5–7; Tables 2 and 3). The stromatoporoid-chaetetid-coral and oncolitic W to G represents inter-buildup sediment,

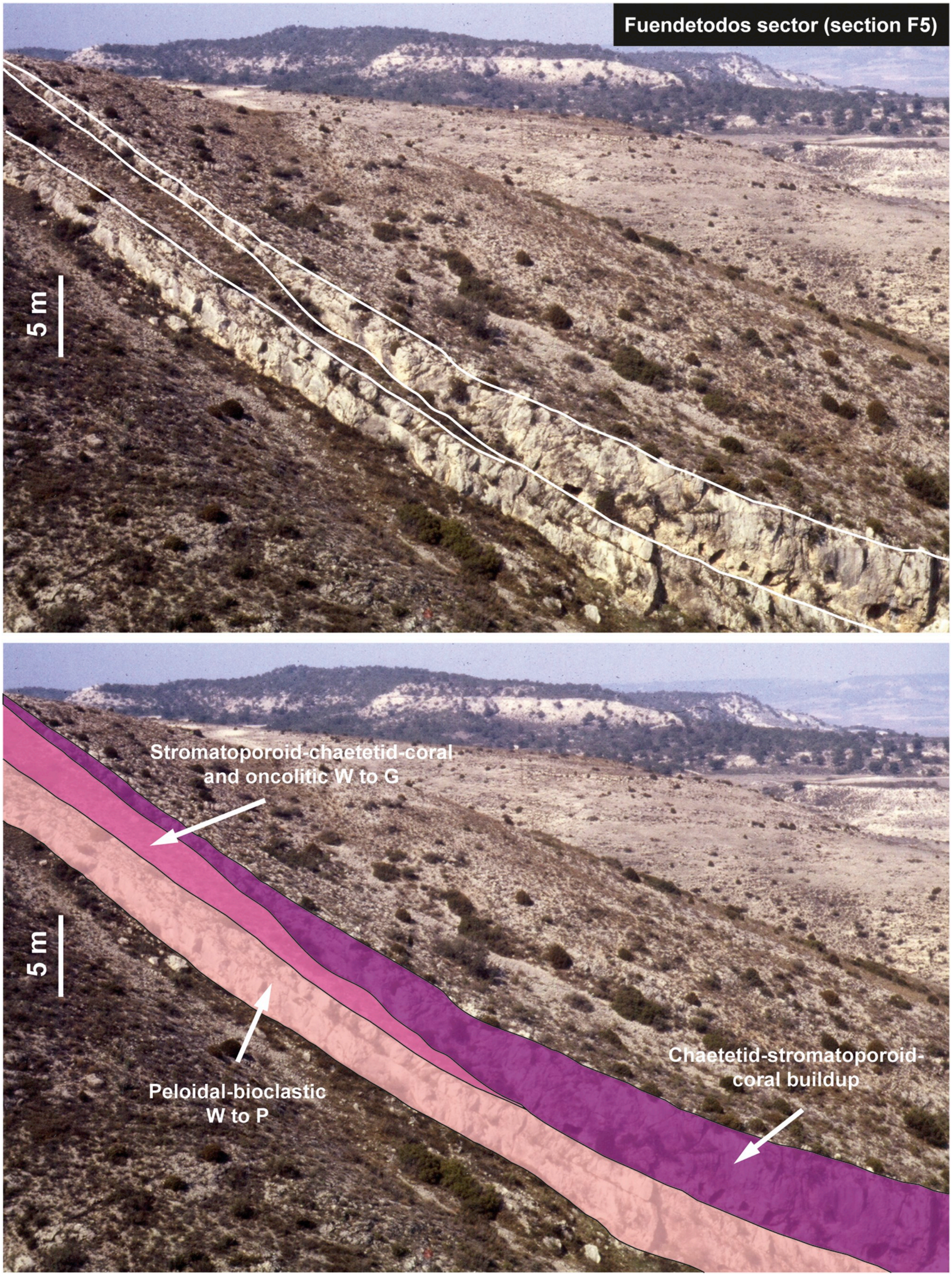

Fig. 12. Field view and facies distribution of chaetetid-stromatoporoid-coral buildup, inter-buildup stromatoporoid-chaetetid-coral and oncolitic W to G, and offshore-proximal peloidal-bioclastic W to P facies in unit 4 of the stratigraphic section F5 (see Fig. 2 for location) (modified from Bádenas and Aurell, 2003).

Table 2
Facies description.

Facies/*Subenvironments*		Non-skeletal grains	Skeletal grains	Stratification and sedimentary structures
Peloidal and oolitic-dominated facies association				
Intertidal	**Peloidal M to P-G with fenestral porosity**	< 30% lithic peloids: poorly sorted (ø < 0.3 mm), irregular to well-rounded < 15% type 1 and 1/3 ooids (ø < 0.5 mm) < 10% type II oncoids: mm-sized, intraclastic nuclei, cortices with *Bacinella irregularis* Scarce intraclasts and sand-size quartz grains	< 7%: lituolids (2), miliolids (4), texturaliids (3, 5), bivalves and *Tubiphytes-Crescentiella*; scarce dasycladacean algae (4, 6, 8), gastropods, brachiopods, echinoderms, ostracods, *Cayeuxia-Ortonella*, involutiniids (3) and stromatoporoids	Tabular to irregular cm- to m-thick beds Fenestral porosity (10–25% of isolated fenestral pores ø < 2 mm), parallel fenestral laminites (< 3 mm thick); dome-like stromatolitic crusts with occasional mm- to cm-thick *Girvanella* and *Bacinella* encrusting laminae; local bioturbation
Restricted lagoon	**Peloidal-bioclastic-type 3 and 4 ooid W to G**	< 45% lithic peloids: well-sorted (ø < 0.2 mm), well-rounded < 45% type 3 and 4 ooids: poorly sorted (ø < 2 mm) and partly micritized, bioclastic and intraclastic (micritic) nuclei; common type 1/3 and 1/4 ooids, compound and aggregate ooids. Scarce intraclasts and sand-size quartz grains, and occasional glauconite	< 40%: highly micritized or ferruginous bivalves, lituolids (1, 3, 6, 8), gastropods, ostracods and echinoderms; scarce miliolids (1, 3), textulariids (5), dasycladacean algae (1, 3, 5), brachiopods and bony fish scales	Tabular dm- to m-thick beds, intercalated with marls; frequent ferruginization Frequent bioturbation (*Thalassinoides* traces, filled by pellets); cm-thick bioclastic laminae with normal gradation and parallel lamination
Backshoal/ washover	**Peloidal-type 1 and 1/3 ooid W to G**	< 75% lithic peloids: poorly to well-sorted (ø < 0.3 mm), irregular to well-rounded < 50% type 1 and 1/3 ooids: ø < 2 mm, bioclastic and intraclastic (micrite) nuclei, common compound and aggregate ooids < 20% type II and IV oncoids: ø < 2 cm, bioclasts, intraclasts and aggregate grains in the nuclei; type IV oncoids with *Lithocodium aggregatum*, *Bacinella*, *Girvanella*, *Cayeuxia-Ortonella*, *Troglotella*; common compound and aggregate oncoids; scarce type I and III oncoids	< 20%: commonly micritized: lituolids (1, 5, 6), textulariids (2, 3, 4, 5), miliolids (3, 4), brachiopods, bivalves, echinoderms, gastropods and dasycladacean algae (4, 6, 8); scarce *Tubiphytes*, rotaliids, serpulids, *Cayeuxia-Ortonella*, involutiniids (1, 3), ostracods, corals (1, 2), chaetetids (1, 3), stromatoporoids (3), *Thaumatoporella parvovesiculifera* and bryozoans	Tabular to irregular dm- to m-thick beds Local parallel- and cross-lamination; mm- to cm-thick oncolitic, skeletal and oolitic laminae with normal gradation; common bioturbation
	Bioturbated peloidal P to G	< 65% lithic peloids: well-sorted (ø < 0.3 mm), rounded to irregular < 25% type 1/3 ooids: ø < 2 mm, sometimes ferruginized; scarce type 1, 4 and 1/4 ooids < 12% type IV oncoids: mm-sized Local ferruginized intraclasts (micritic facies with bioclasts).	< 15%: micritized lituolids (1, 6), gastropods, echinoderms, bivalves and miliolids (3); scarce brachiopods, ostracods, textulariids (5), dasycladacean algae (6), corals (locally in-situ), bryozoans and serpulids	Tabular dm-thick beds; frequent ferruginization Intense burrowing (*Thalassinoides* traces); local parallel lamination
Shoal-sand blanket	**Peloidal G**	< 75% lithic peloids: well-sorted (ø < 0.2 mm) and rounded < 15% type 1 and 1/3 ooids: poorly to well-sorted (ø < 2 mm), bioclastic and intraclastic (micritic) nuclei < 15% type I, II, III and IV oncoids: ø < 1 cm, spherical to irregular, bioclasts, intraclasts (micrite) and aggregate grains in the nuclei; occasional compound oncoids Scarce intraclasts (micritic and grain-supported facies with peloids, ooids and bioclasts) and aggregate grains	< 10%: textulariids (3, 4, 5), miliolids (3, 4), lituolids (5, 6), echinoderms, bivalves, brachiopods and gastropods; scarce stromatoporoid and coral fragments, *Tubiphytes*, *Cayeuxia-Ortonella*, involutiniids, dasycladacean algae and *Thaumatoporella*	Tabular to irregular dm- to m-thick beds Common parallel lamination; local bioturbation and cm-thick oncolitic laminae with normal gradation
	Type 1 and 1/3 ooid-peloidal G	< 40% lithic peloids: well-sorted (ø < 0.2 mm), rounded < 40% type 1 and 1/3 ooids: poorly sorted (ø < 2 mm), ovoid to spherical, bioclastic and intraclastic (micrite) nuclei; common aggregate ooids < 10% type I, II and IV oncoids: ø < 1 cm, spherical to irregular, bioclasts and aggregate grains in the nuclei; type IV oncoids with *Bacinella*, *Girvanella*, *Troglotella*; common compound oncoids	< 5%: lituolids (5), miliolids (3), textulariids (5), brachiopods, gastropods and bivalves; scarce corals, stromatoporoids, serpulids, *Tubiphytes*, *Cayeuxia-Ortonella* and dasycladacean algae	Tabular to irregular dm- to m-thick beds Local bioturbation and parallel- and cross-lamination
	Type 1 and 1/3 ooid G	< 60% type 1 and 1/3 ooids: well-sorted (ø < 0.5 mm), ovoid to spherical, bioclastic and intraclastic (micrite) nuclei; occasional type 1/4 ooids < 20% lithic peloids: well-sorted (ø < 0.2 mm) and rounded < 8% type I, II and IV oncoids: well-sorted (ø < 0.5 cm) and spherical, bioclastic nuclei Scarce intraclasts (micritic facies with peloids, ooids, bioclasts and fine quartz sand)	< 5%: brachiopods, lituolids, miliolids (3) and gastropods; scarce echinoderms, dasycladacean algae, texturaliids and *Troglotella*	Tabular to irregular cm- to m-thick beds Local bioturbation
Foreshoal	**Peloidal W-P to G**	< 70% lithic peloids: poorly to well-sorted (ø < 0.2 mm) < 35% type 1 and 1/3 ooids: well-sorted (ø < 2 mm), bioclastic	< 20%: lituolids (6), echinoderms, brachiopods, bivalves (1, 2) and miliolids (3); scarce gastropods, textulariids (3,	Tabular to irregular dm- to m-thick beds Common bioturbation; local parallel lamination

(*continued on next page*)

Table 2 (*continued*)

Facies/*Subenvironments*		Non-skeletal grains	Skeletal grains	Stratification and sedimentary structures
		and intraclastic (micrite) nuclei; scarce compound and aggregate ooids < 20% type I, II, III and IV oncoids: ø < 2 cm, spherical to irregular, bioclastic and intraclastic (grain-supported facies with peloids, ooids and bioclasts) nuclei, cortices with *Lithocodium*, *Bacinella*, *Cayeuxia-Ortonella* and *Troglotella*, and serpulids; occasional compound oncoids Scarce intraclasts (micrite and grain-supported facies with peloids, ooids and bioclasts)	4, 5), rotaliids, involutiniids, *Tubiphytes*, stromatoporoids (3), corals (locally in-situ), chaetetids and dasycladacean algae (2, 6, 8)	
Storm lobes in backshoal and foreshoal	**Intraclastic-peloidal P to G**	< 45% intraclasts and < 40% lithic peloids: poorly sorted (mm to cm in size) and poorly rounded fragments of micritic facies (with bioclasts and fine quartz sand) and grain-supported facies (ooids, peloids and bioclasts), grading into rounded poorly to well-sorted lithic peloids (ø < 0.3 mm) < 14% type IV oncoids: small irregular	< 15%: mm to cm in size, commonly micritized, gastropods, bivalves, *Cayeuxia-Ortonella*, brachiopods, miliolids (2, 3), lituolids (2, 6) and texturaliids (3, 4, 5); scarce dasycladacean algae (6, 8), echinoderms, corals, involutiniids (3), ostracods and bryozoans	Tabular to irregular dm-thick beds Common mm- to cm-thick bioclastic and intraclastic laminae, and local intraclastic mm-thick graded laminae; local bioturbation
Offshore-proximal	**Peloidal-bioclastic W to P**	< 70% lithic peloids: poorly to well-sorted (ø < 0.3 mm) and rounded; local microbial peloids (ø = 100 µm in mean diameter) < 10% type I, II and IV oncoids: ø < 1 cm, spherical to irregular, bioclastic and intraclastic (grain-supported facies with peloids, ooids and bioclasts) nuclei; type II and IV oncoids with cortices including *Bacinella* and *Girvanella*, serpulids, foraminifers and *Tubiphytes*; local type III oncoids, compound and aggregate oncoids Scarce type 1 and 1/3 ooids, well-sorted (ø < 2 mm), ovoid to spherical, bioclastic nuclei; and intraclasts (micritic facies)	< 20%: mm- to cm-sized, lituolids (4, 6, 7), corals (locally in-situ), echinoderms, serpulids (1, 2), chaetetids, bivalves, gastropods and brachiopods; scarce stromatoporoids (3), sponges, miliolids (2), textulariids (5, 6), involutiniids (2), lageniids (1, 2, 3), *Tubiphytes*, *Lithocodium*, dasycladacean algae (8) and belemnites	Tabular to irregular dm- to m-thick beds Frequent bioturbation (*Chondrites* and *Planolites* traces); local cm-thick oncolitic laminae
Offshore-distal	**Bioclastic-peloidal M**	< 8% lithic peloids: poorly sorted (ø < 0.1 mm), irregular to well-rounded Scarce type I and II oncoids: mm-sized, bioclastic nuclei; cortices with occasional serpulids; local compound oncoids Occasional intraclasts and fine quartz sand	< 8%: lituolids (4, 6), echinoderms, bivalves, gastropods and sponges; scarce serpulids (1, 2), brachiopods, miliolids, texturaliids (1, 3, 6), lageniids (2, 3), rotaliids, involutina (2), *Tubiphytes*, *Troglotella*, *Lithocodium*, dasycladacean algae (8) and reefal debris (stromatoporoids, chaetetids and corals)	Tabular dm- to m-thick beds Frequent bioturbation (*Chondrites* and *Planolites* traces)
Oncolitic-dominated facies association				
Pond/restricted lagoon	**Gastropod-oncolitic W-P to G**	< 30% type I, II and IV oncoids: ø < 1 cm, spherical to irregular, bioclastic nuclei; type IV oncoids with *Bacinella* < 30% type 1 and 1/3 ooids: ø < 2 mm, ovoid to spherical, bioclastic and intraclastic (micrite) nuclei < 20% lithic peloids: ø < 0.2 mm, irregular to well-rounded	< 20%: broken and whole gastropods; small skeletal grains, commonly micritized, of bivalves, lituolids (1, 6), miliolids (3) and texturaliids (5); scarce dasycladacean algae (7), echinoderms, brachiopods, *Thaumatoporella*, sponges, *Cayeuxia-Ortonella*, *Tubiphytes* and involutiniids (1)	Tabular cm- to dm-thick beds, locally intercalated with cm-thick marly beds Components accumulated in cm-thick laminae; local bioturbation
Sheltered lagoon	**Type IV oncoid W to P**	< 40% type IV oncoids: ø < 7 cm, irregular, bioclastic nuclei, thick crusts with *Bacinella*, *Lithocodium*, *Cayeuxia-Ortonella*, *Girvanella*, *Thaumatoporella* and sponges, sometimes forming the entire cortex; common type III oncoids; local mm-sized type I and II oncoids < 30% lithic peloids: well-sorted (ø < 0.2 mm), local microbial peloids Scarce type 1 and 1/3 ooids (ø < 1 mm) and intraclasts (micritic and grain-supported facies with peloids)	< 15%: commonly micritized, lituolids (1, 5, 6), miliolids (4), texturaliids (3, 5), bivalves, echinoderms and brachiopods; scarce gastropods, dasycladacean algae (3, 6, 8), rotaliids, involutiniids (3), *Cayeuxia-Ortonella*, *Tubiphytes*, ostracods, sponges, stromatoporoids and corals (locally in-situ)	Tabular dm- to m-thick beds Local cm-thick oncolitic laminae; bioturbation
Backshoal and foreshoal	**Type III oncoid P**	20–60% type III oncoids: ø < 2 cm, occasionally < 4 cm, spherical to irregular, with bioclastic and intraclastic (mud- and grain-supported facies with peloids, ooids and bioclasts) nuclei, cortices with *Bacinella*, *Lithocodium*, *Troglotella*, *Girvanella* and *Cayeuxia-Ortonella*, and sponges, foraminifera, serpulids and *Tubiphytes*; common type II, IV and compound oncoids. < 45% microbial and poorly to well-sorted lithic peloids (ø < 0.3 mm) < 30% type 1 and 1/3 ooids: poorly sorted (ø < 2 mm)	< 20% lituolids (1, 4, 5, 6), miliolids (3, 4), textulariids (2, 3, 5, 6), echinoderms, gastropods, mm- to cm-sized fragments of bivalves (2) and brachiopods, and stromatoporoids (3, 6) and chaetetids (4) in mm- to cm-sized fragments and in-situ; scarce serpulids (1, 2), dasycladacean algae (4), *Tubiphytes*, sponges, bryozoan, *Cayeuxia-Ortonella*, involutiniids (2, 3), rotaliids and coral fragments	Tabular to irregular dm- to m-thick beds Local mm- to cm-thick oncolitic laminae; local bioturbation and borings in oncoids and stromatoporoids

(*continued on next page*)

Table 2 (*continued*)

Facies/*Subenvironments*		Non-skeletal grains	Skeletal grains	Stratification and sedimentary structures
Shoal-sand blanket	**Type II and III oncoid G**	20–60% type II and III oncoids: ø < 2 cm, spherical to irregular, with bioclastic and intraclastic (grain-supported facies with peloids, ooids and bioclasts) nuclei, cortices with *Bacinella*, *Lithocodium*, *Troglotella*, *Thaumatoporella*, *Girvanella* and *Cayeuxia-Ortonella*, and serpulids; common type I and compound oncoids < 30% poorly sorted lithic peloids (ø < 0.3 mm) < 20% type 1 and 1/3 ooids: poorly sorted (ø < 2 mm)	< 10% lituolids (5), echinoderms, bivalves and mm- to cm-sized fragments of brachiopods; scarce miliolids (3), texturaliids (5), gastropods, serpulids (1, 2), *Tubiphytes*, dasycladacean algae (6), stromatoporoids (1, 3, 6), chaetetids (1, 4), corals, involutiniids (3) and *Cayeuxia-Ortonella*	Tabular to irregular dm- to m-thick beds
Stromatoporoid/chaetetid/coral-rich facies association				
Stromatoporoid carpets				
Sheltered lagoon to backshoal	**Stromatoporoid W to G**	< 20% microbial and lithic peloids < 10% type I and II oncoids: ø < 1 cm, bioclastic nuclei; type II oncoids with *Lithocodium*, *Bacinella*, *Thaumatoporella* and *Girvanella* Scarce type 1 and 1/3 ooids (ø < 1 mm)	< 40% cm-sized and in-situ stromatoporoids (1, 2, 3, 6), and lower proportion of chaetetids (1, 6) and corals (2); common *Tubiphytes* encrustations < 15% fine-grained skeletal fraction: mainly bivalves, brachiopods, echinoderms, lituolids (5), miliolids (3, 4), textulariids (4, 5) and dasycladacean algae (5, 6, 8)	Tabular to irregular dm- to m-thick beds Bioclastic mm- to cm-thick laminae; bivalve borings on stromatoporoids and bioturbation
	Oncolitic-stromatoporoid W to G	< 20% type I, II, III and IV oncoids: ø < 3 cm, well-rounded to irregular, bioclastic and intraclastic (micrite) nuclei; type III and IV oncoids with *Lithocodium*, *Bacinella*, *Girvanella*, *Cayeuxia-Ortonella* and *Troglotella* < 10% lithic and microbial peloids: ø < 0.2 mm, irregular to well-rounded Scarce type 1 and 1/3 ooids (ø < 2 mm)	< 40% cm-sized stromatoporoids and corals as in stromatoporoid W to G < 15% fine-grained skeletal fraction: mainly *Tubiphytes*, lituolids (1, 5), miliolids (3, 4), textulariids (3, 4, 5), bivalves, gastropods, echinoderms and brachiopods	Tabular to irregular dm- to m-thick beds Components accumulated in mm- to cm-thick laminae; common bioturbation and local bivalve borings on stromatoporoids
Buildup and inter-buildup facies				
Foreshoal to offshore-proximal	**Chaetetid-stromatoporoid-coral buildup**	< 40% microbial and poorly sorted and rounded lithic peloids, (ø < 0.2 mm) < 10% type I and II oncoids: ø < 1 cm, bioclastic nuclei; type II oncoids with *Bacinella*, *Lithocodium* and *Troglotella*, and other encrusters (serpulids) Scarce type III and IV oncoids	< 40% primary reef builders: cm-sized and in-situ chaetetids (1, 2, 4, 5, 6) and stromatoporoids (1, 3, 4, 6); corals (1, 2) are locally abundant < 10% secondary reef builders: dense micritic to local peloidal microbial crust, with encrusters around the primary reef builders: serpulids, foraminifera, sponges, *Cayeuxia-Ortonella*, *Girvanella*, *Thaumatoporella*, *Bacinella*, *Tubiphytes*, *Troglotella* and *Lithocodium* < 10% fine-grained skeletal fraction: mm- to cm-sized brachiopods, bivalves, echinoderms, serpulids (1), *Cayeuxia-Ortonella* and sponges	Up to 8 m high with low step margins Bivalve and sponge borings on chaetetids, corals and stromatoporoids, filled by mud-supported sediment with microbial peloids; inter-growth cavities filled by mud-supported sediment with microbial peloids, bioclasts, microbial crust fragments and oncoids; bioturbation (grain-supported facies)
	Stromatoporoid-chaetetid-coral and oncolitic W to G	< 30% type II, III and IV oncoids: ø < 2 cm, spherical to irregular; cortices with *Bacinella*, *Girvanella*, *Lithocodium*, *Thaumatoporella*, *Troglotella* and *Cayeuxia-Ortonella*, and serpulids and gastropods; common compound and aggregate oncoids < 40% microbial and poorly sorted and rounded lithic peloids (ø < 0.2 mm) Scarce type 1 and 1/3 ooids (ø < 2 mm)	< 25% mm- to cm-sized stromatoporoids (1, 3, 5, 6) and chaetetids (1, 5); corals (2) are locally abundant < 20% fine-grained skeletal fraction: mm- to cm-sized echinoderms, bivalves, brachiopods and gastropods; scarce sponges, serpulids (1, 2), lituolids (4), miliolids (2), textulariids (3, 5, 6), *Tubiphytes*, *Thaumatoporella*, *Cayeuxia-Ortonella* and dasycladacean algae	Tabular to irregular dm- to m-thick beds Bivalve and serpulid borings on stromatoporoids and chaetetids; local serpulid borings in oncoids and cm-thick oncolitic laminae; bioturbation

Table 3
Skeletal components in Table 2.

Skeletal components				
Foraminifera				**Chlorophyta**
Lituolidae	**Miliolidae**			**Dasycladacean algae**
[1] *Alveosepta jaccardi*	[1] *Charentia evoluta*	[4] *Kurnubia palastinensis*	[3] *Nodosaria* sp.	[1] *Acicularia*
[2] *Ammobaculites* sp.	[2] *Nautiloculina circularis*	[5] *Redmondoides lugeoni*		[2] *Campbeliella striata*
[3] *Choffatella*	[3] *Nautiloculina oolithica*	[6] *Siphovalvulina*	**Involutina**	[3] *Clypeina* sp.
[4] *Everticyclammina*	[4] *Quinqueloculina* sp.		[1] *Andesenolina*	[4] *Clypeina jurassica*
[5] *Labyrinthina mirabilis*		**Rotalidae** (*Mohlerina basiliensis*)	[2] *Protopeneroplis striata*	[5] *Pseudoclypeina distomensis*
[6] *Pseudocyclammina* sp.	**Textulariidae**		[3] *Trocholina alpina*	[6] *Salpingoporella annulata*
[7] *Rectocyclammina*	[1] *Bositra buchi*	**Lagenidae**		[7] *Salpingoporella dinarica*
[8] *Redmondellina powersi*	[2] *Conicokurnubia*	[1] *Dentalina*		[8] *Salpingoporella pygmaea*
	[3] *Kurnubia jurassica*	[2] *Lenticulina sublenticularis*		
Reefal components			**Bivalves**	**Serpulids**
Chaetetids	**Stromatoporoids**	**Corals**	[1] Ostreids	[1] *Serpula socialis*
[1] *Blastochaetetes* sp.	[1] *Actinostromina grossa*	[1] *Latistraea foulassensis*	[2] *Trichites* sp.	[2] *Terebella lapilloides*
[2] *Bouenia* sp.	[2] *Cladocoropsis lindstroemi*	[2] *Stylophyllum polycanthum*		
[3] *Parachaetetes*	[3] *Cladocoropsis mirabilis*			
[4] *Ptychochaetetes globosus*	[4] *Cylicopsis verticalis*			
[5] *Solenopora*	[5] *Ellipsactinia*			
[6] *Spongiomorpha ramosa*	[6] *Parallelopora*			

as indicated by its lateral relationship with the chaetetid-stromatoporoid-coral buildups (Figs. 5–7) and the similarity of the components in these two facies (Tables 2 and 3). The cm-sized fragments of stromatoporoids, chaetetids and corals resulted from the destruction and reworking of the buildups, whereas oncoids are formed in-situ.

5. Facies evolution and sedimentary models

The facies distribution observed throughout the nine sedimentary units allowed the spatial distribution of the facies to be determined, showing their variable extent and the complexity in their lateral (along strike and down dip) relationships (Figs. 13 and 14). On the basis of the relative abundance of specific facies and their spatial distribution, two facies models are proposed: an oncolitic-peloidal-oolitic-dominated ramp, encompassing sedimentary units 1 to 4, and an oolitic-peloidal-dominated ramp, in sedimentary units 5 to 9 (Fig. 15). The down-dip gradation of the main non-skeletal grains in these two models is indicated in the simplified sedimentary models of Fig. 16.

5.1. Oncolitic-peloidal-oolitic-dominated ramp

This sedimentary model corresponds to sedimentary units 1 to 4 (Figs. 13 and 15A) and is mainly characterized by: (1) the relative abundance of oncolitic-dominated facies from backshoal to foreshoal subenvironments, (2) the development of a low-energy oncolitic sheltered lagoon, and (3) the growth of stromatoporoid carpets in backshoal/washover areas.

Peloidal-oolitic shoal-sand blankets dominate, with a general north-to-south orientation of the facies belt. Laterally (along strike), oncolitic shoal-sand blankets (type II and III oncoid G) are also present. In particular, the widest record of oncolitic-dominated shoal-sand blankets is found in sedimentary unit 1 (Fig. 13A), passing laterally (along strike) to peloidal-oolitic shoals (type 1 and 1/3 ooid-peloidal G) and laterally (down dip) to oncolitic backshoal and foreshoal (type III oncoid P) facies. The foreshoal domain is peloidal-dominated (peloidal W-P to G) and passes down dip (to the SE) to peloidal-bioclastic offshore-proximal and offshore-distal facies. Chaetetid-stromatoporoid-coral buildup and inter-buildup facies occur in the foreshoal and offshore-proximal subenvironments, with a patchy distribution (from 2 km to up to 10 km in width).

The onset of sedimentary unit 2 is marked by the progradation of the shoal-sand blanket eastward (Fig. 13B), and the first appearance of intertidal domains and stromatoporoid carpets in the backshoal area dominated by peloidal-oolitic sediments (peloidal-type 1 and 1/3 ooid W to G facies). Peloidal and lateral (along strike) oncolitic shoal-sand blankets developed with a down-dip extension of around 5 km and with local intertidal patches on top. Facies in the foreshoal and offshore subenvironments are similar to unit 1, but the offshore-proximal area is twice as wide in unit 2 (around 10 km) as in unit 1.

A low-energy oncolitic sheltered lagoon develops in sedimentary unit 3 (Fig. 13C), laterally (down dip) in relation to the peloidal-oolitic backshoal/washover facies (peloidal-type 1 and 1/3 ooid W to G). An intertidal belt is recognized in the northwestern sector, laterally to the peloidal-oolitic backshoal of units 2–4. Stromatoporoid-rich carpets grew in the backshoal area within peloidal-oolitic backshoal sediments and oncolitic backshoal sediments (type III oncoid P), also in the lagoon (unit 4; Fig. 13D), with a patchy distribution (500 m in lateral extent). Peloidal-oolitic shoal-sand blankets (type 1 and 1/3 ooid-peloidal G) with local intertidal patches predominate, although locally (along strike) type II and III oncoid shoals are recognized (around section J1; Fig. 13C). The shoal-sand blankets in sedimentary unit 3 are of a similar down-dip extension to those in unit 2 but they prograde eastward in unit 3. In unit 4, this high-energy facies belt has a wider down-dip extension (up to 12 km; Fig. 13D). Chaetetid-stromatoporoid-coral buildups grew in the offshore-proximal subenvironment, with a similar patchy distribution and extension (up to 10 km) to those in units 1–2.

In summary, the resulting oncolitic-peloidal-oolitic-dominated ramp shows a down-dip (NW-SE) succession of facies belts, but also some mosaic facies of variable extension (Fig. 15A): intertidal belt (at least 3 km in down-dip extension); local sheltered lagoon; backshoal/washover (3–8 km in down-dip extension) with a mosaic of stromatoporoid carpets and related oncolitic sediments (patches of 500 m in width); shoal-sand blanket (3–12 km in down-dip extension) with local intertidal caps (less than 3 km in diameter) on top; and foreshoal (2–7 km) and offshore domains (3–10 km in the offshore-proximal subenvironment), with patches of chaetetid-stromatoporoid-coral buildup and inter-buildup facies (from 2 km to up to 10 km in diameter). Lithic peloids, type 1 and 1/3 ooids, and type II, III and IV oncoids are the main non-skeletal grains, especially in the inner ramp (Fig. 16A): peloids characterize the intertidal domain; low-energy conditions in the sheltered lagoon determined the abundance of type IV oncoids; the backshoal/washover, shoal-sand blanket and foreshoal subenvironments are mainly composed of peloids and type 1 and 1/3 ooids, with

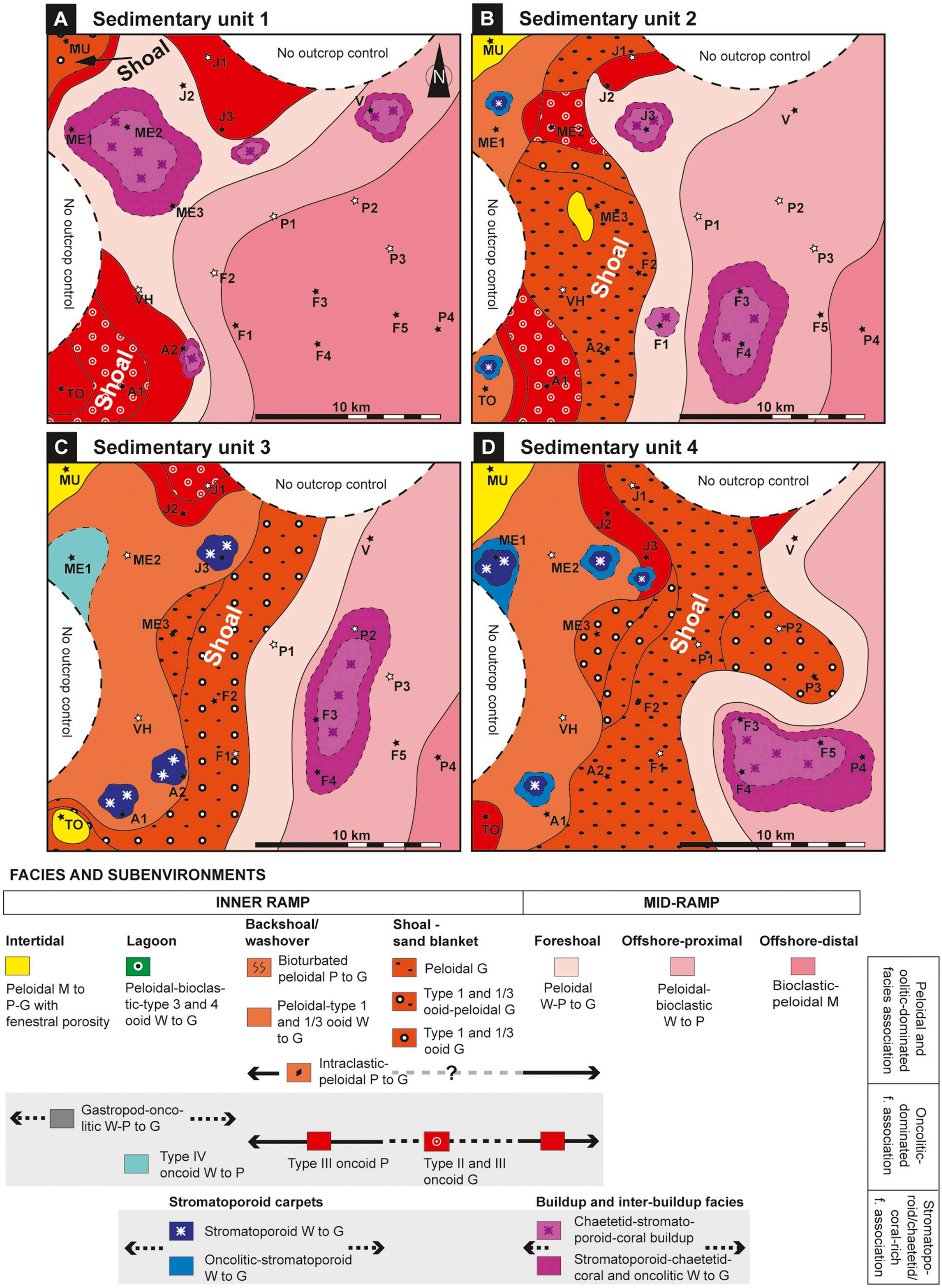

Fig. 13. Facies maps reconstructed for sedimentary units 1 to 4.

lateral (along strike) areas where type II and/or III oncoids predominate. These components decrease in abundance down dip, especially in the offshore-distal subenvironment, where only scarce peloids and type I and II oncoids are found. As regards metazoans, stromatoporoids predominate in backshoal and sheltered lagoon areas, whereas chaetetid-stromatoporoid-coral associations predominate in buildup

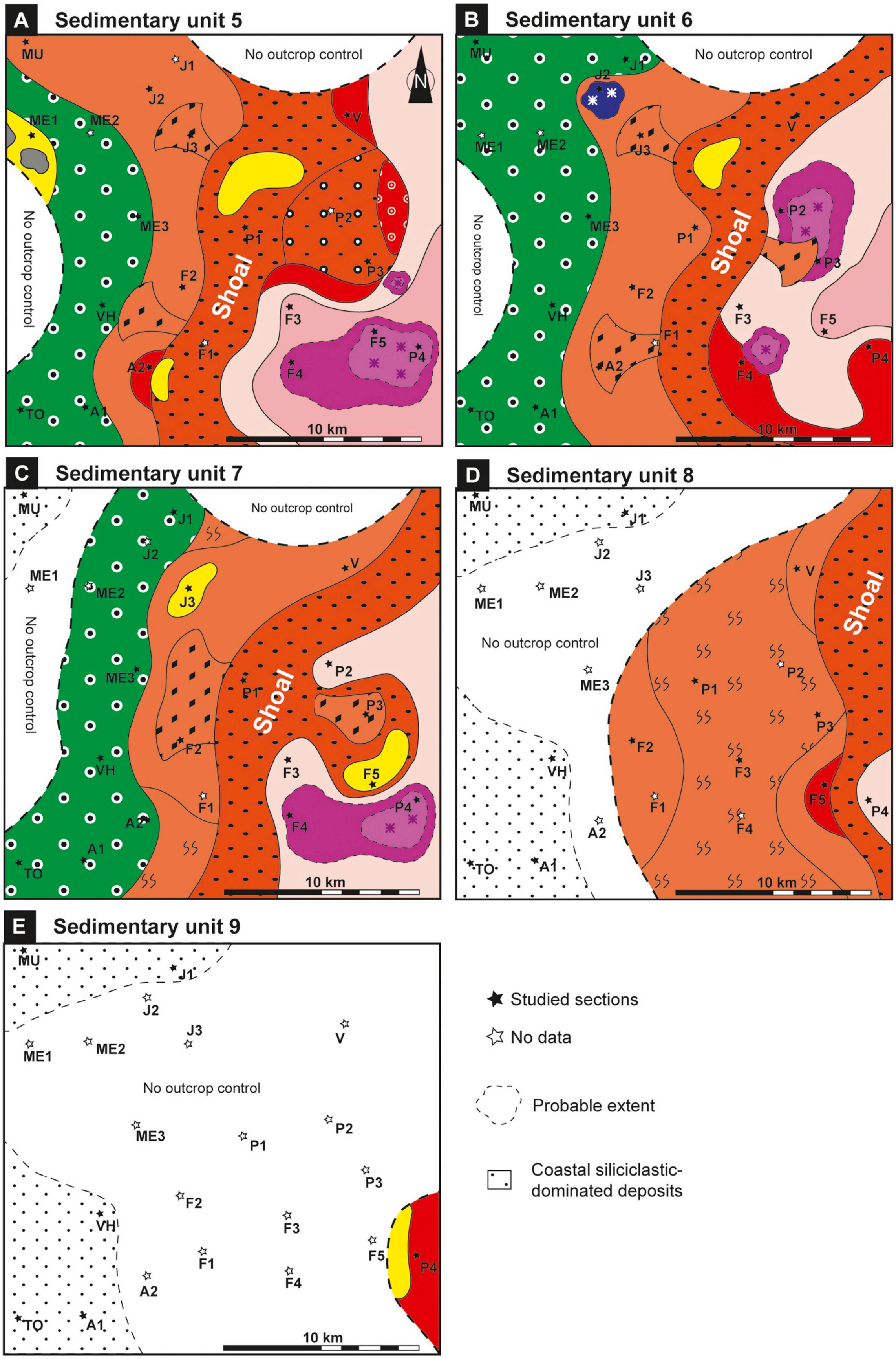

Fig. 14. Facies maps reconstructed for sedimentary units 5 to 9.

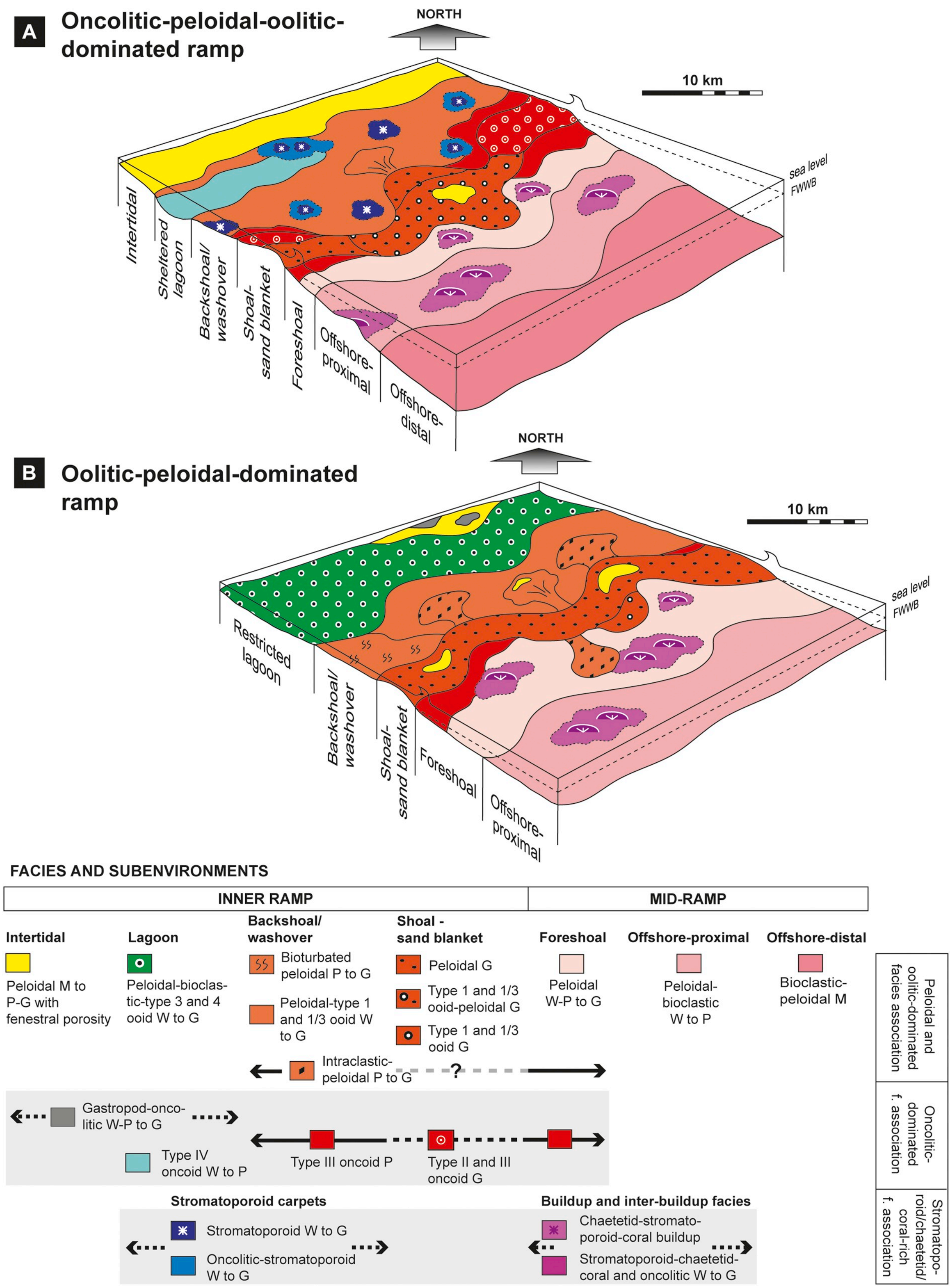

Fig. 15. Sedimentary models showing the facies distribution of the latest Kimmeridgian carbonate ramp during the deposition of sedimentary units 1–4 (A) and 5–9 (B).

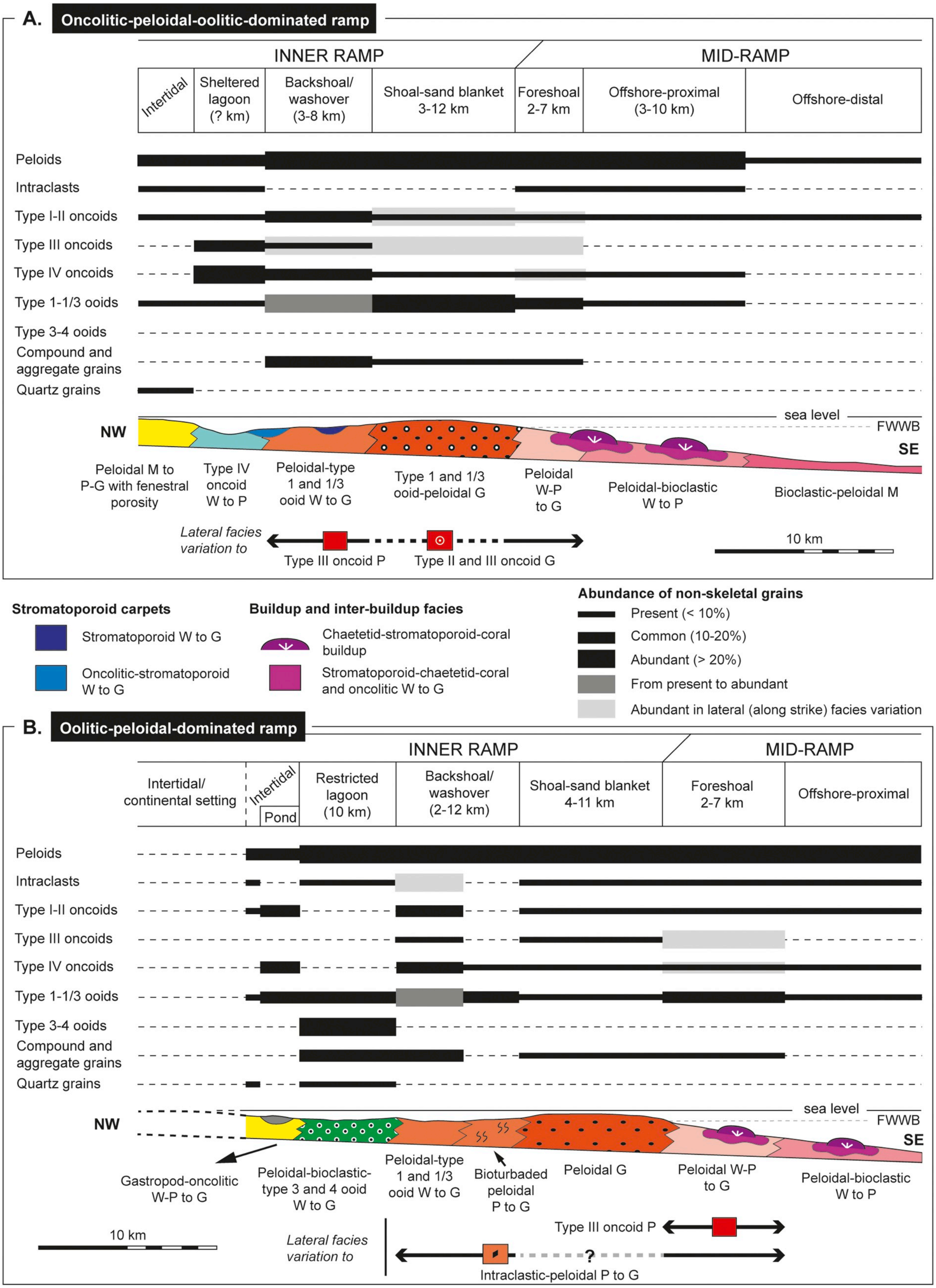

Fig. 16. Summary of the facies and non-skeletal component distribution for the two proposed sedimentary models. Black and grey horizontal bars indicate the abundance of non-skeletal grains (type I-II oncoid distribution in the oncolitic-peloidal-oolitic-dominated ramp refers mainly to type II oncoids, as type I oncoids generally appear in low abundance). The distribution of stromatoporoid/chaetetid/coral-rich facies is also included.

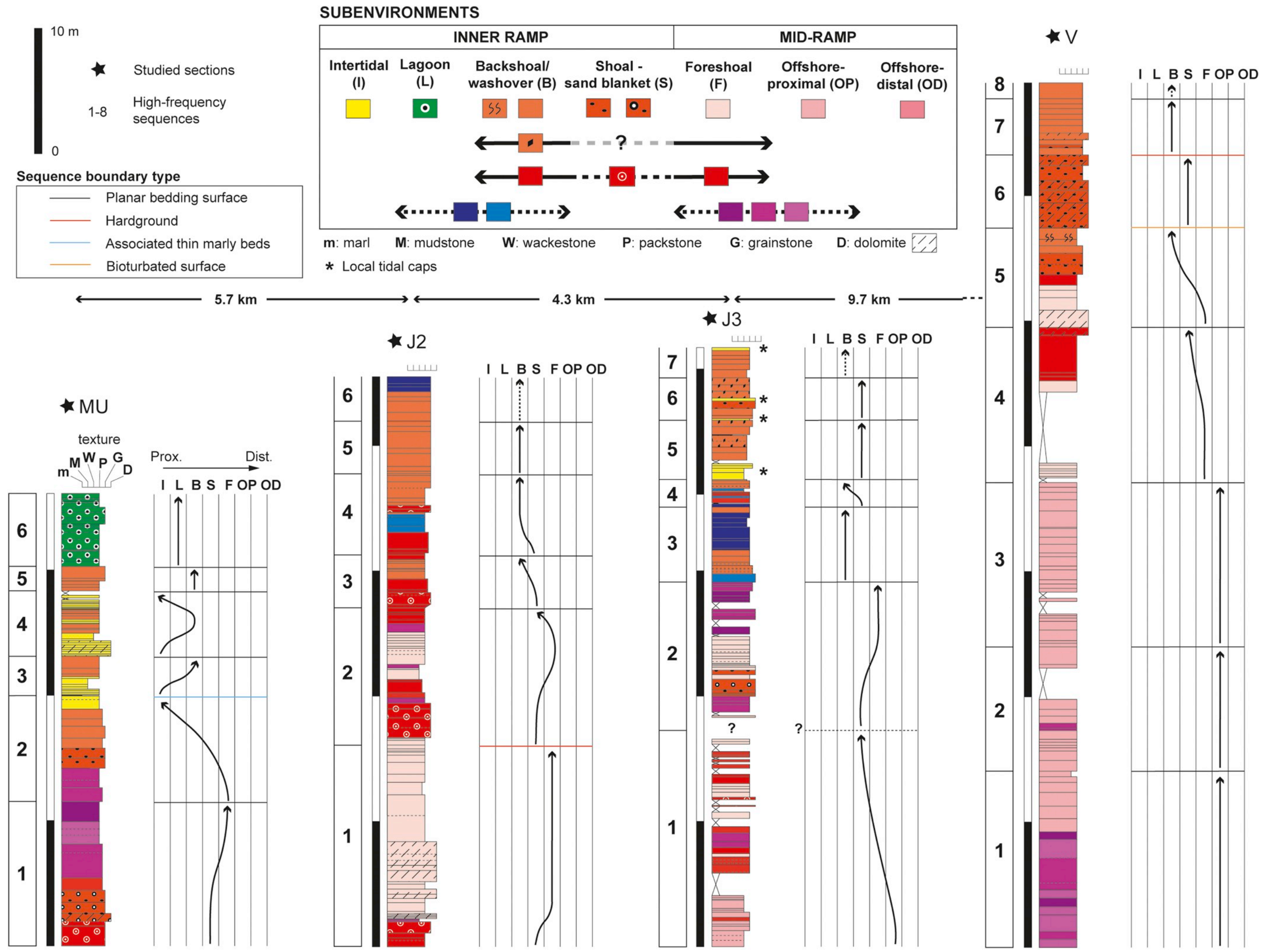

Fig. 17. Sedimentary trends within the high-frequency sequences (1–8) recognized in the MU-J2-J3-V transect, based on lateral facies relationships observed in the reconstructed palaeogeographic maps (see Figs. 13 and 14). Characteristics of the sequence boundaries are also included. Notice the variability of the vertical sedimentary trend of a single correlated high-frequency sequence between closely-spaced sections.

and inter-buildup facies in the foreshoal and offshore-proximal subenvironments, below the fair-weather wave base.

5.2. Oolitic-peloidal-dominated ramp

The oolitic-peloidal-dominated ramp corresponds to sedimentary units 5 to 9 (Figs. 14 and 15B), and is mainly characterized by: (1) the widespread development of a restricted lagoon, (2) the predominance of peloidal shoal-sand blankets, and (3) the occurrence of intraclastic-peloidal storm lobes in backshoal and foreshoal areas.

Sedimentary unit 5 reflects the development of a wide peloidal-bioclastic-oolitic restricted lagoon (peloidal-bioclastic-type 3 and 4 ooid W to G), with a down-dip extension of around 10 km, locally grading onshore into the intertidal domain with local ponds (gastropod-oncolitic W-P to G; Fig. 14A). The backshoal area is peloidal-oolitic and intraclastic-dominated (peloidal-type 1 and 1/3 ooid W to G and intraclastic-peloidal P to G), the latter related to storm lobes (2–7 km in width). The sheltered lagoon and stromatoporoid carpets present in the previous stage have disappeared; only very local stromatoporoid carpets are found in the backshoal area in sedimentary unit 6 (i.e. section J2; Fig. 14B). The shoal-sand blankets are mainly composed of peloids, with significant variations in lateral extent (from 4 to 11 km), as observed in the previous stage. Local intertidal caps (1–5 km in width) are observed on top of the backshoal/washover and shoal-sand blanket deposits. Also local intraclastic-peloidal storm lobes occur in the foreshoal subenvironment. Chaetetid-stromatoporoid-coral buildup and inter-buildup facies developed in the foreshoal and offshore-proximal subenvironments, with a similar patchy distribution and extension to the previous stage (2–7 km). Oncolitic-dominated backshoal, shoal-sand blanket and foreshoal facies are considerably reduced, occurring only locally in sedimentary units 5, 6 and 8. Bioturbated peloidal P to G backshoal facies occurs in sedimentary units 7 and 8 (Fig. 14C and D), being widely developed in sedimentary unit 8 (10 km in lateral extent) and grading down dip into peloidal shoal-sand blanket and peloidal-oolitic backshoal facies. As a whole, there is a progressive progradation of shallow facies to the east and an increase in siliciclastic input in shallower areas (i.e. coastal siliciclastic-dominated deposits; Figs. 3 and 14C-E).

There is no stratigraphic record of carbonate shallow-marine facies belts in most of the sections for sedimentary unit 9, except local intertidal and oncolitic-dominated facies (Fig. 14E).

In summary, the facies distribution observed in this oolitic-peloidal-dominated ramp shows the down-dip gradation of peloidal-dominated intertidal belt, restricted lagoon (around 10 km wide), backshoal/washover (2–12 km in lateral extent), shoal-sand blanket (4–11 km in width), foreshoal (2–7 km wide) and offshore-proximal subenvironments, with local oncolitic-dominated facies in intertidal/restricted lagoon (i.e. local ponds in the intertidal belt or restricted lagoon;

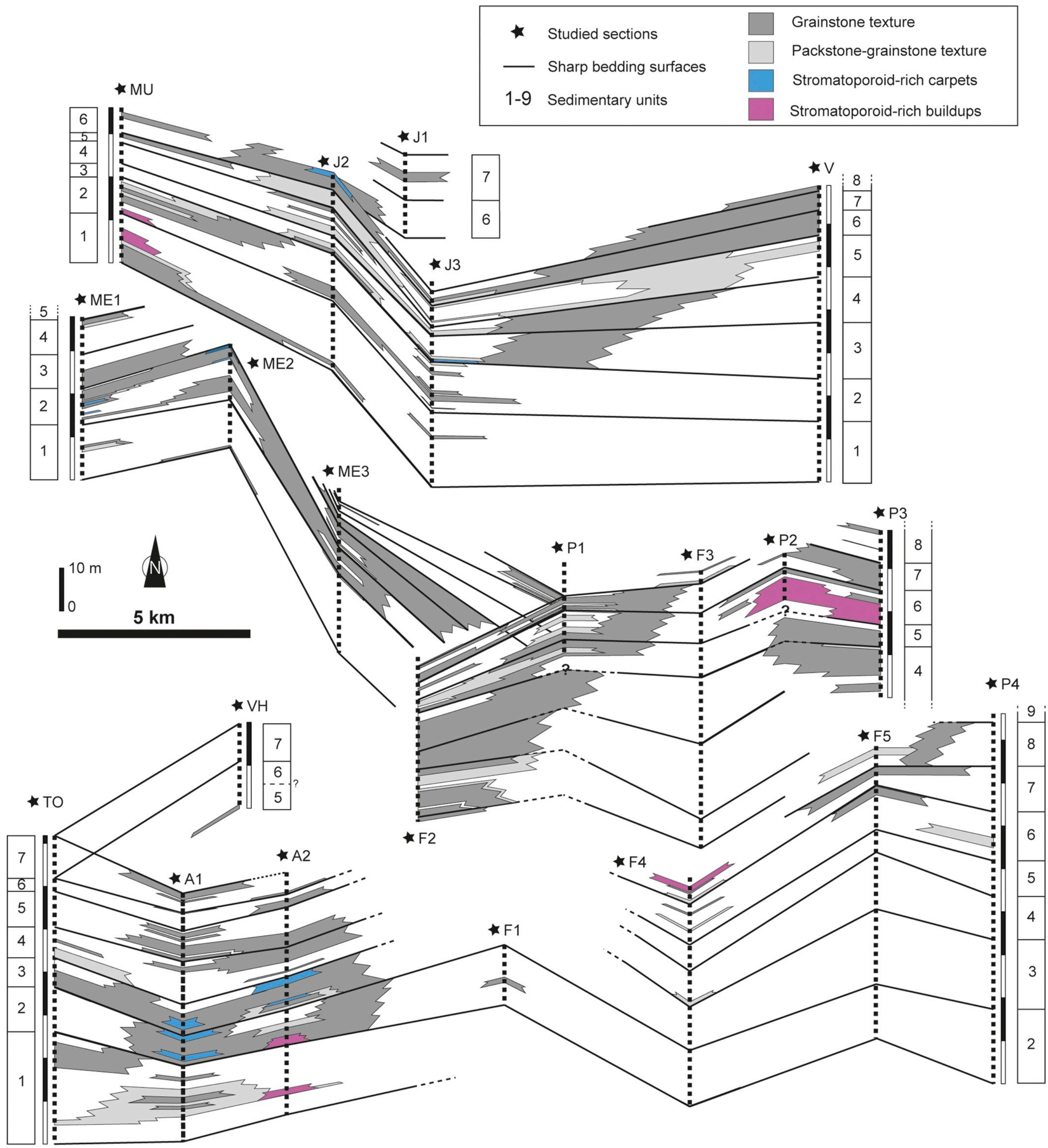

Fig. 18. Lateral and vertical distribution of the grain-supported facies (packstone-grainstone and grainstone textures) in the studied cross-sections. The distribution of stromatoporoid-rich carpets and buildups is also included.

around 2 km wide), backshoal and foreshoal areas (2–3 km in down-dip extent), storm lobes (2–7 km in width) in backshoal and foreshoal domains, and local intertidal caps (1–5 km in diameter) on top of backshoal and shoal-sand blanket deposits (Fig. 15B). Peloids constitute the main non-skeletal component from inner- to mid-ramp domains, as well as type 3 and 4 ooids in the restricted lagoon and a minor proportion of type 1 and 1/3 ooids from intertidal to backshoal and foreshoal subenvironments (Fig. 16B). Intraclasts are also abundant in storm-related lobes, mostly occurring in the backshoal area, as well as type III oncoids especially in the foreshoal area. Intense local burrowing takes place in peloidal-dominated backshoal deposits, laterally related to the peloidal shoal-sand blankets. As regards the stromatoporoid/chaetetid/coral-rich facies, only chaetetid-stromatoporoid-coral buildup and inter-buildup facies are maintained from the foreshoal to offshore-proximal subenvironments. The stromatoporoid carpets in the lagoon and backshoal have disappeared.

At a long-term scale, the sedimentary evolution of the carbonate ramp throughout the nine sedimentary units reflects a shallowing-upward trend, with the progradation of the inner ramp facies towards the east-southeast.

6. Discussion

6.1. Factors controlling facies distribution

The facies heterogeneity and sedimentary evolution observed throughout the nine sedimentary units reflect the combined role of internal processes and external factors. Long- to short-term variations in accommodation space related to sea-level fluctuations, along with irregular bottom topography, water transparency and water energy conditioned the spatial distribution and lateral continuity of the facies (e.g. Kerans and Tinker, 1997; Della Porta et al., 2002; Hillgärtner, 2006).

The spatial distribution of the shoal-sand blankets determined the nature of the laterally related inner ramp and mid-ramp facies. The shoal-sand blankets show a general N-S orientation, with significant differences in their lateral extent (i.e. from 3 to 12 km; Figs. 13 and 14). They are mainly composed of peloidal and oolitic G (type 1 ooid with micritic laminae or type 1/3 with alternating micritic and sparitic laminae), which grades laterally (along strike) into oncolitic G (type II and III oncoids), with peloids and ooids in similar measure in the fine-grain-sized fraction. Lithic peloids and ooids found in the peloidal to oolitic G facies represent continued high-energy conditions (Strasser, 1986) compared to the type II and III oncoid G facies, which reflects lower water agitation since these oncoids are partially composed of organism-bearing encrustations (Dahanayake, 1977). Certain sectors of the shoal-sand blankets are partially or completely represented by the oncolitic-dominated facies. These along-strike variations in non-skeletal grains were probably controlled by the irregular topography of the shoal-sand blanket belt, with possible depressions/protected areas where lower water energy favoured the generation of type II and III oncoids. Differences in depositional topography are also highlighted by the presence of intertidal caps on top of peloidal-oolitic shoal-sand blankets, but not on the oncolitic shoal facies. The shoal-sand blankets show a similar N-S orientation throughout the nine sedimentary units, but vary in their lateral extent (from 3 to 12 km). This belt could have been controlled by wave energy, which redistributed the sediment especially during storms (e.g. Reijmer et al., 2009). The prevailing NE-SW direction of winter winds and the SE-NW direction of the hurricane pathways affecting the Iberian Basin (Marsaglia and Klein, 1983; Golonka et al., 1994; Price et al., 1995, Fig. 1B) suggest that longshore currents possibly controlled the N-S orientation of this facies belt, and that storm resedimentation determined the variations in down-dip lateral extension. The influence of storms on this carbonate ramp is highlighted by the recurrence of storm-related intraclastic-peloidal lobes in both backshoal and foreshoal subenvironments, especially in the oolitic-peloidal-dominated ramp (see sedimentary units 5 to 7 in Fig. 14).

Offshore from the shoal-sand blanket, a gradation of sediments composed of peloids, ooids, oncoids and bioclasts is observed, from foreshoal peloidal W-P to G, to offshore-distal bioclastic-peloidal M. This is related to the down-dip decrease in water energy. The open-marine areas are favourable for the growth of chaetetid-stromatoporoid-coral buildups, below the fair-weather wave base. The presence of these suspension-feeding metazoans and light-dependent micro-encrusters reflects low- to moderate water energy, water transparency and oligotrophic conditions (Leinfelder et al., 1993). Local heterogeneities in the distribution of some non-skeletal grains are found in the inter-buildup facies, some of which is dominated by in-situ-generated oncoids with organism-bearing encrustations (i.e. type II, III and IV oncoids). The preferential growth of these buildups and inter-buildup oncolitic sediments in some areas of the foreshoal and offshore-proximal subenvironments is open to interpretation. It could be related to areas where storms remobilized unconsolidated sediment and left the underlying hard substrate exposed and available for colonization by metazoans.

In the earlier stage of evolution (sedimentary units 1 to 4), an oncolitic-peloidal-oolitic-dominated ramp developed, with a local sheltered lagoon characterized by an abundance of large and irregular type IV oncoids (Figs. 13 and 15A). The shoal-sand blankets acted as a barrier to water energy and favoured the generation of low-energy conditions for bacterial growth. Low-energy conditions, negligible siliciclastic input and possible low sedimentation rates contributed to the extensive growth of oncoids with light-dependent and oligotrophic micro-encrusters (e.g. Leinfelder et al., 1993; Dupraz and Strasser, 1999). The reduced lateral extent of this lagoon was conditioned by the sediment reworked in the backshoal area and by storm-induced flows (i.e. washover deposits), which led to abrupt changes in facies distribution by redistributing sediment in large quantities (Strasser and Védrine, 2009). Stromatoporoid-rich carpets occurred within the sheltered lagoon and backshoal subenvironments, where the bioclastic association also indicates good water transparency and oligotrophic conditions. On the basis of a detailed sedimentological study in the northwestern area (i.e. around the locality of Mezalocha; see Fig. 2) by Sequero et al. (2018), it was suggested that the preferential growth of these stromatoporoid-rich carpets within the lagoon and backshoal/washover subenvironments was probably related with the presence of local hard substrates and areas with higher-energy conditions that occurred in corridors created between washover deposits.

The oolitic-peloidal-dominated ramp in units 5–9 (Figs. 14 and 15B) reflects the predominance of peloids and ooids to the detriment of oncoids. Restricted conditions characterize the inner ramp lagoon (peloidal-bioclastic-type 3 and 4 ooid W to G) with a minor development of oncolitic facies (gastropod-oncolitic W-P to G and type III oncoid P) compared with the previous stage. Peloidal-dominated facies are widely developed from the lagoon to offshore-proximal subenvironments. The relative abundance of peloidal facies at this stage in the evolution of the platform, together with the near disappearance of stromatoporoid-rich carpets in the lagoon and backshoal, point to an increase in water energy and/or fluctuations in salinity conditions that would not have been favourable for microbial activity and the growth of stromatoporoids, chaetetids and corals. A lateral siliciclastic-dominated unit is recorded in unit 7 in the northwestern area (Fig. 14C), suggesting an increased terrigenous input to the lagoon carbonates. General lower-energy conditions were established in the backshoal subenvironment during the deposition of sedimentary unit 8 (Fig. 14D), as indicated by the intense burrowing and the absence of storm-related deposits.

As a whole, the observed facies distribution can be related to long- to short-term sea-level fluctuations. The progressive progradation of the shallow facies belts (Figs. 13 and 14) is likely to be associated with the long-term fall in relative sea level occurring at the end of the Jurassic in the Iberian Basin (Salas et al., 2001; Aurell et al., 2003, 2010). The decrease in accommodation space would have controlled aspects such as the generation of more restricted conditions in the inner ramp, as the connection with the open-marine areas was reduced, and the local subaerial exposure of both backshoal and shoal-sand blanket deposits.

The internal processes occurring in this carbonate ramp, which in great measure determine the distribution and lateral migration of the facies, may also overprint possible environmental changes induced by insolation variations in the Milankovitch frequency band (e.g. Strasser, 2018). The influence of orbitally-induced cycles on the sedimentation of Jurassic Iberian platforms has previously been documented in Kimmeridgian-Tithonian shallow to deeper marine carbonate successions (e.g. Bádenas et al., 2004, 2005). In particular in the shallow areas of the carbonate ramp, the influence of sea-level fluctuations related to short-term eccentricity cycles resulted in the formation of high-frequency sequences bounded by discontinuity surfaces that can be physically traced at km-scale (Bádenas and Aurell, 2010, 2018). According to the lateral continuity assumed here for the well-marked bedding surfaces, the nine sedimentary units differentiated within the Higueruelas Fm (Fig. 3) could represent high-frequency sequences linked to high-order sea-level fluctuations. Examples of sedimentary trends in the high-frequency sequences and their bounding surfaces are shown in Fig. 17. Most of the sequence boundaries are planar bedding surfaces, locally bioturbated surfaces (e.g. between sequences 5 and 6 in section V), hardgrounds (e.g. between sequences 1 and 2 in section J2) or are associated with cm-thick marly beds (e.g. between sequences 2 and 3 in section MU). The vertical facies trend within the sequences is variable (aggradational, shallowing, deepening and locally deepening-shallowing), and in a single correlated high-frequency sequence can vary from log to log. For instance, sequence 2 displays a shallowing trend in more proximal areas (i.e. section MU), but a deepening or aggradational trend in distal areas (i.e. sections J3 and V). The presence of well-marked high-frequency sequence boundaries, but not of maximum flooding surfaces, fits well with their development in a long-term regressive stage, whereas marked maximum flooding surfaces in high-frequency sequences would tend to be recorded during the maximum flooding intervals of long-term sequences (Strasser et al., 1999). Judging by the number of sequences (i.e. nine sedimentary units) and by the time span of the sequence Ki3 in the central part of the Iberian Basin as obtained by biostratigraphic data (ammonites, larger benthic foraminifera) and strontium-isotope data (around 1.2 Myr; Aurell et al., in press), the estimated duration for each sequence is around 133 ky, thus falling within the range of short-term eccentricity orbital cycles (ca. 100 ky).

6.2. Lateral continuity of grain-supported facies: implications for reservoir exploration

A knowledge of the lateral continuity of facies belts and their stacking patterns in outcrop analogues of carbonate reservoirs is important in assessing the dimensions of potential reservoir-rock bodies on the basis of subsurface data. Most of the facies that characterize the Higueruelas Fm are similar to those found in the Arab-D Formation, the major hydrocarbon carbonate reservoir in the Middle East (Al-Awwad and Collins, 2013). As in the analogue Higueruelas Fm, the deposits of the Arab-D Fm occurred in the shallow domains of an upper Kimmeridgian carbonate ramp (Ayoub and En Nadi, 2000; Al-Saad and Ibrahim, 2005), and the more productive facies generally consist of well-sorted oolitic packstone-grainstones forming active shoals and patch buildups mainly composed of stromatoporoids in the foreshoal subenvironment (Grötsch et al., 2003). The quality of many of these reservoirs is due to the interparticle porosity in the peloidal and oolitic grainstones, and the vuggy porosity resulting from the dissolution of stromatoporoid bioclasts (Wender et al., 1998; Grötsch et al., 2003; Hughes, 2004; Lindsay et al., 2006).

A gradation of grain-supported facies from intertidal to foreshoal subenvironments has been characterized in the Higueruelas Fm. Grain-supported peloidal-oolitic and oncolitic-dominated facies characterize the backshoal, shoal-sand blanket and foreshoal domains, which also include stromatoporoid-rich carpets and chaetetid-stromatoporoid-coral buildup and inter-buildup facies in inner- and mid-ramp areas, respectively. Packstone-grainstone and grainstone textures from these facies are highlighted in Fig. 18, in order to reveal the dimension and lateral continuity of potential analogue carbonate reservoir-rock bodies in the Higueruelas Fm.

Grainstone textures are mostly recorded in the shoal-sand blankets, laterally related to backshoal and foreshoal grainstone facies (Figs. 5–7) grading locally into packstone-grainstone textures. Lateral continuity is observed for these grainstone bodies, as is their great down-dip extent, especially in sedimentary units 2, 4 and 5 (Figs. 13 and 14). Stromatoporoid carpets developed in packstone-grainstone and grainstone backshoal deposits in sedimentary units 2, 3 and 6, whereas stromatoporoid buildups and inter-buildup facies occurred in packstone-grainstone foreshoal sediments in units 1, 2, 6 and 7 (Fig. 18). This spotlights an additional interest in these backshoal and foreshoal deposits, since vuggy porosity resulting from the dissolution of stromatoporoid bioclasts is another major reservoir-improving factor.

Characterization of the dimension and lateral continuity of potential carbonate reservoir-rock bodies in outcrop analogues is essential for hydrocarbon exploration, but so are the barriers (i.e. continuous low-permeability layers) that compartmentalize the reservoir field, which usually correspond to mud-supported sedimentary facies or highly cemented deposits caused by diagenesis (e.g. San Miguel et al., 2017b). Previous studies on upper Kimmeridgian mid-ramp successions in NE Spain (San Miguel et al., 2017c) have documented diagenetic processes prior to compaction affecting grainstone and reefal sedimentary bodies. Such processes include cementation, pore-enhancing processes such as the micritization of carbonate grains, and reflux dolomitization. Dolomitization is also observed in the Higueruelas Fm, particularly in northern areas (i.e. the localities of Muel and Jaulín; see Fig. 2), and has been tentatively related to hydrothermal fluids circulating through normal faults reactivated during the Alpine compression (Aurell, 1990). Hydrothermal dolomitization has also been proposed for age-equivalent carbonate rocks of the neighbouring Maestrat Basin (e.g. Rodríguez-Morillas et al., 2013; Travé et al., 2019). The sedimentological heterogeneities (i.e. dimension and lateral extent) revealed for the potential reservoir facies in the studied successions of the Higueruelas Fm make these shallow-marine deposits the target of future studies focusing on their diagenetic heterogeneities.

6.3. Comparison with other similar environments

The distribution of the Kimmeridgian carbonate facies from shallow to relatively deep offshore settings has previously been documented in the successions deposited in southern marginal areas of the Iberian Basin. In the shallow-platform facies of the sequence Ki2 (Torrecilla Fm; Fig. 1C), Bádenas and Aurell (2010) described sand-shoal deposits dominated by variable proportions of peloids and type 3 and 1/3 ooids, with variations in their lateral extent comparable to those observed in the Higueruelas Fm (i.e. 3–12 km, see Figs. 13 and 14). Oncolitic-dominated facies are also recorded in this environment: type I and II oncoid G facies replaced the oolitic shoals in specific areas of the ramp; *Bacinella*-oncoids were widespread in a low-energy lagoon; and type III oncoids were generally deposited offshore, laterally related to coral reefs. In contrast, for the latest Kimmeridgian carbonate ramp studied in this work, specific hydrodynamic conditions partly controlled by the irregular bottom topography led to a wider distribution of oncoids partly or completely dominated by organism-bearing encrustations (i.e. type II, III and IV oncoids), being abundant in the sheltered lagoon and areas of the backshoal, shoal-sand blanket and foreshoal subenvironments.

As regards shallow carbonate environments in Kimmeridgian successions outside the Iberian Basin, of particular interest for hydrocarbon exploration are the upper Kimmeridgian carbonate ramp deposits of the Arab-D Fm (Ayoub and En Nadi, 2000; Al-Saad and Ibrahim, 2005). Significant facies in the Arab-D reservoirs are the well-sorted oolitic packstone-grainstone facies forming active shoals, and stromatoporoid-dominated buildups in the foreshoal environment. This set of facies shows a significant difference regarding the dimension of the stromatoporoid-rich facies, as large-scale stromatoporoid reefs arranged as belts occur in the Arab-D deposits, instead of the patchy distribution of the stromatoporoid buildups in the studied Higueruelas Fm. Lagoonal stromatoporoid carpets have been recorded in the Higueruelas Fm, but also in sequence Ki2 (Jabaloyas outcrop; San Miguel et al., 2017a), a stromatoporoid facies not recorded in the Arab-D Fm. Lehmann et al. (2010) recognized m-thick stromatoporoid buildups from middle to outer-ramp areas of the Upper Jurassic carbonate platform in offshore Abu Dhabi (eastern Saudi Arabia), more than 3 km in lateral extent. In contrast, the chaetetid-stromatoporoid-coral buildups characterized in the Higueruelas Fm are recognized in relatively proximal areas of the middle ramp, and are no more than 250 m in lateral extent.

The overall lateral extent of the sand-shoal complex in the Upper Jurassic Arab Fm reaches 17–20 km in width, whereas in the carbonate ramp under study the lateral extent of the shoal-sand blankets ranges from 3 to 12 km. Previous studies of similar carbonate shoals in the Upper Muschelkalk (Middle Triassic) have documented a high degree of lateral continuity of high-energy shoal lithofacies at scales from a few km to > 10 km in dip- and strike directions (e.g. Ruf and Aigner, 2004; Petrovic and Aigner, 2017). In relation to the particular lateral migration of the shoal-sand blanket described in this work, Marchionda et al. (2018) also document different directions of progradation of oolitic shoals in the Kimmeridgian-Tithonian shallow carbonate ramp of the Arab Fm (onshore Abu Dhabi), suggesting a local topographic control related to halokinetic activity in the substratum (i.e. substratum diapiric motions leading to local changes in accommodation). This situation diverges from the sedimentary control on the lateral migration of the shoal-sand blanket sediment described in the present paper, which has been related primarily to the redistribution of the sediment by hydrodynamic factors.

7. Conclusions

The complexity of the spatial facies distribution and sedimentary evolution of the inner- to mid-ramp areas of a latest Kimmeridgian shallow carbonate ramp (Higueruelas Fm, north-central Iberian Basin) has been deciphered, highlighting the combined role of the external and internal factors operating on these shallow marine environments. The overall facies evolution reflects a long-term shallowing-upward trend, related to the long-term fall in relative sea level that occurred during the late Kimmeridgian in the Iberian Basin.

Analysis of the vertical and lateral facies distribution in nine sedimentary units has allowed us to propose two sedimentary models of ramp evolution, with significant variations in facies belts and the presence of facies mosaics in specific areas of the ramps. The oncolitic-peloidal-oolitic-dominated carbonate ramp (sedimentary units 1–4) included an intertidal belt characterized by peloidal mudstones to packstone-grainstones with fenestral porosity, a low-energy sheltered lagoon characterized by an abundance of large type IV oncoids, and oolitic-peloidal backshoal, shoal-sand blanket and foreshoal subenvironments, which grade offshore to bioclastic-peloidal mudstones. Oncolitic-dominated packstones to grainstones developed along strike in high-energy areas, and a mosaic of stromatoporoid carpets and chaetetid-stromatoporoid-coral buildups also accumulated in inner- to mid-ramp domains, respectively.

A significant shift in the palaeoenvironmental conditions, probably related to higher-energy conditions and increased terrigenous supply, took place during the deposition of sedimentary units 5 to 9, giving rise to an oolitic-peloidal-dominated carbonate ramp, with very local records of oncolitic facies. This ramp included a wide restricted lagoon, without stromatoporoid-rich carpets, and peloidal-dominated backshoal, shoal-sand blanket and foreshoal subenvironments, with frequent intraclastic-peloidal storm-related deposits, as well as the near disappearance of stromatoporoid-rich carpets in the backshoal. Chaetetid-stromatoporoid-coral buildups developed offshore, in the mid-ramp setting.

Variations in hydrodynamic factors (waves and storms) and sea-bottom topography controlled the observed along-strike and down-dip variations in lateral extent and in the predominant non-skeletal content that developed especially in inner-ramp areas. Backshoal, shoal-sand blanket and foreshoal grain-supported facies, with lithic peloids and ooids, developed in higher-energy areas, whereas oncoids were concentrated in depressed areas of the shoal body. Inshore in the lagoon, low-energy conditions favoured bacterial growth in oncoids and the development of stromatoporoid-rich carpets, whereas fluctuations in salinity, energy and siliciclastic input resulted in a peloidal-bioclastic-oolitic lagoon without oncoids or stromatoporoids. The influence of probable short eccentricity cycles is inferred from the time span of the studied sequence Ki3 and the lateral continuity of the bounding surfaces of the nine identified sedimentary units (i.e. high-frequency sequences) within Ki3. Eccentricity-related sea-level fluctuations, internal processes of sediment production and redistribution, and long-term regression controlled the variable sedimentary trends observed within these high-frequency sequences.

The facies distribution and down-dip heterogeneities summarized in the two proposed carbonate-ramp models can be applied to the interpretation of shallow carbonate platforms that include similar non-skeletal components. In particular, the reported data lead to a detailed description of the distribution and lateral extent of oolitic, peloidal, oncolitic and stromatoporoid-rich grain-supported facies, which can be useful in reservoir characterization.

Acknowledgments

This paper was funded by projects CGL 2017-85038-P and Group E18 (Aragosaurus: Recursos Geológicos y Paleoambientales) subsidized by the Spanish Ministry of Science and Innovation, the European Regional Development Fund and the Government of Aragón. The research of Cristina Sequero is funded by a FPU Grant (Spanish Ministry of Science and Innovation). The authors would like to acknowledge the financial support from the International Association of Sedimentologists (IAS Postgraduate Grant Scheme) and the use of the Servicio General de Apoyo a la Investigación-SAI, Universidad de Zaragoza. We also thank Laura Tomassetti and André Strasser for the revision, and Rupert Glasgow for accepting to review the English quality.

Appendix A. Supplementary data

Supplementary data to this article can be found online at https://doi.org/10.1016/j.marpetgeo.2019.06.018.

References

Al-Awwad, S.F., Collins, L.B., 2013. Arabian carbonate reservoirs: a depositional model of the Arab-D reservoir in Khurais field, Saudi Arabia. AAPG 97, 1099–1119.

Al-Saad, H., Ibrahim, M., 2005. Facies and palynofacies characteristics of the upper Jurassic Arab D reservoir in Qatar. Rev. Paléobiol. 24 (1), 225–241.

Amour, F., Mutti, M., Christ, N., Inmenhauser, A., Benson, G.S., Agar, S.M., Tomás, S., Kabiri, L., 2013. Outcrop analog for an oolitic carbonate reservoir: a scale-dependent geologic modeling approach based on stratigraphic hierarchy. AAPG 97 (5), 845–871.

Aurell, M., 1990. El Jurásico Superior en la Cordillera Ibérica Central (provincias de Zaragoza y Teruel). Análisis de cuenca. PhD Thesis. Zaragoza University.

Aurell, M., Meléndez, A., 1986. Sedimentología de la Formación Calizas con oncolitos de Higueruelas (Malm) en la región de Muel-Belchite (Provincia de Zaragoza). Acta Geol. Hispánica 21–22, 307–312.

Aurell, M., Meléndez, A., 1987. Las bioconstrucciones de corales y sus facies asociadas durante el Malm en la Cordillera Ibérica Central (prov. de Zaragoza). Estud. Geol. 43, 261–269.

Aurell, M., Robles, S., Bádenas, B., Rosales, I., Quesada, S., Meléndez, G., García-Ramos, J.C., 2003. Transgressive-regressive cycles and Jurassic palaeogeography of northeast Iberia. Sediment. Geol. 162, 239–271.

Aurell, M., Bádenas, B., Ipas, J., Ramajo, J., 2010. Sedimentary evolution of an upper Jurassic epeiric carbonate ramp, Iberian Basin, NE Spain. In: In: Van Buchem, F.S.P., Gerdes, K.D., Esteban, M. (Eds.), Mesozoic and Cenozoic Carbonate Systems of the Mediterranean and the Middle East: Stratigraphic and Diagenetic Reference Models, vol. 329. Geol. Soc. London Spec. Public, pp. 89–111.

Aurell, M., Ipas, J., Bádenas, B., Muñoz, A., 2012. Distribución de facies con corales y estromatopóridos en el dominio interno de una plataforma carbonatada (Titónico, Cordillera Ibérica). Geogaceta 51, 67–70.

Aurell, M., Bádenas, B., Canudo, J.I., Castanera, D., García-Penas, A., Gasca, J.M., Martín-Closas, C., Moliner, L., Moreno-Azanza, M., Rosales, I., Santás, L., Sequero, C., Val, J., 2019. Kimmeridgian-Berriasian stratigraphy and sedimentary evolution of the central Iberian Rift System (NE Spain). Cretac. Res (in press).

Ayoub, R., En Nadi, I.M., 2000. Stratigraphic framework and reservoir development of the upper Jurassic in Abu Dhabi area, U.A.E. In: In: Alsharhan, A.S., Scott, R.W. (Eds.), Middle East Models of Jurassic/Cretaceous Carbonate System, vol. 69. pp. 229–248.

Baccelle, L., Bosellini, A., 1965. Diagrammi per la stima visiva della composizione

percentuale nelle rocce sedimentarie. Ann. Uni. Ferrara, N.S., Sez. IX: Sci. Geol. Paleontol 1, 59–62.
Bádenas, B., Aurell, M., 2001. Kimmeridgian palaeogeography and basin evolution of northeastern Iberia. Palaeogeogr. Palaeoclimatol. Palaeoecol. 168, 291–310.
Bádenas, B., Aurell, M., 2003. Análisis comparado y controles en la sedimentación de dos arrecifes de la zona media de una rampa carbonatada del Jurásico Superior de la Cordillera Ibérica. Rev. Soc. Geol. Espana 16 (3–4), 151–166.
Bádenas, B., Aurell, M., 2010. Facies models of a shallow-water carbonate ramp based on distribution of non-skeletal grains (Kimmeridgian, Spain). Facies 56, 89–110.
Bádenas, B., Aurell, M., 2018. The down-dip preferential sequence record of orbital cycles in greenhouse carbonate ramps: examples from the Jurassic of the Iberian Basin (NE Spain). In: In: Montenari, M. (Ed.), Stratigraphy and Timescales, vol. 3. pp. 285–325.
Bádenas, B., Aurell, M., Rodríguez-Tovar, F.J., Pardo-Igúzquiza, E., 2003. Sequence stratigraphy and bedding rhythms of an outer ramp limestone succession (Late Kimmeridgian, Northeast Spain). Sediment. Geol. 161, 153–174.
Bádenas, B., Salas, R., Aurell, M., 2004. Three orders of regional sealevel changes control facies and stacking patterns of shallow platform carbonates in the Maestrat Basin (Tithonian-Berriasian, NE Spain). Int. J. Earth Sci. (Geol Rundsch) 93, 144–162.
Bádenas, B., Aurell, M., Gröcke, D.R., 2005. Facies analysis and correlation of high-order sequences in middle-outer ramp successions: variations in exported carbonate in basinwide d13C (Kimmeridgian, NE Spain). Sedimentology 52, 1253–1276.
Bádenas, B., Aurell, M., Bosence, D., 2010. Continuity and facies heterogeneities of shallow carbonate ramp cycles (Sinemurian, Lower Jurassic, North-east Spain). Sedimentology 57, 1021–1048.
Borkhataria, R., Aigner, T., Pöppelreiter, M.C., Pipping, J.C.P., 2005. Characterization of epeiric "layer-cake" carbonate reservoirs: upper Muschelkalk (middle Triassic), The Netherlands. J. Pet. Geol. 28, 119–146.
Burchette, T.P., Wright, V.P., 1992. Carbonate ramp depositional systems. Sediment. Geol. 79, 3–57.
Cortés Gracia, A.L., Casas Sainz, A.M., 1996. Deformación alpina de zócalo y cobertera en el borde norte de la Cordillera Ibérica (Cubeta de Azuara-Sierra de Herrera). Rev. Soc. Geol. Espana 9 (1–2), 51–66.
Dahanayake, K., 1977. Classification of oncoids from the upper Jurassic carbonates of the French Jura. Sediment. Geol. 18, 337–353.
Dahanayake, K., 1978. Sequential position and environmental significance of different types of oncoids. Sediment. Geol. 20, 301–316.
Della Porta, G., Kenter, J.A.M., Immenhauser, A., Bahamonde, J., 2002. Lithofacies character and architecture across a Pennsylvanian inner-platform transect (Sierra de Cuera, Asturias, Spain). J. Sediment. Res. 72, 898–916.
Dercourt, J., Ricou, L., Vrielynck, B., 1993. Atlas: Tethys Palaeoenvironmental Maps. CCGM, Paris.
Droste, H., 2006. A New Model for Epeiric Carbonate Platforms. GEO 2006 Middle East Conference and Exhibition 27-29 March 2006. Manama, Bahrain.
Dunham, R.J., 1962. Classification of carbonate rocks according to depositional texture. AAPG Memoir. 1, 108–121.
Dupraz, C., Strasser, A., 1999. Microbialites and micro-encrusters in shallow coral bioherms (Middle to Late Oxfordian, Swiss Jura mountains). Facies 40, 101–129.
Flügel, E., 1974. Fazies-Interpretation der *Cladocoropsis*-Kalke (Malm) auf Karaburun, W-Anatolien. Arch Lagerstätt-Forsch Ostalpen Sd-Bd 2, 79–94.
Flügel, E., 2004. Microfacies of Carbonate Rocks. Analysis, Interpretation and Application. Springer-Verlag, Germany.
Golonka, J., Ross, M.J., Scotese, C.R., 1994. Phanerozoic paleogeographic and paleoclimatic modeling maps. In: Pangea: Global Environments and Resources, vol. 17. Canadian Society of Petroleum Geologists, Memoir, pp. 1–47.
Grötsch, J., Suwaina, O., Ajlani, G., Taher, A., El-Khassawneh, R., Lokier, S., Coy, G., van der Weerd, E., Masalmeh, S., van Dorp, J., 2003. The Arab Formation in central Abu Dhabi: 3-D reservoir architecture and static and dynamic modelling. GeoArabia, Gulf PetroLink, Bahrain. 8 (1), 47–86.
Harris, P.M., Purkis, S.J., Ellis, J., Swart, P.K., Reijmer, J.J.G., 2014. Mapping bathymetry and depositional facies on great Bahama bank. Sedimentology 62, 566–589.
Hillgärtner, H., 2006. High-resolution correlation in Cretaceous platform carbonates of the Middle East: rules to solve the puzzle? In: AAPG European Region Conference: Architecture of Carbonate Systems through Time, Mallorca 2006, Program Book 26.
Hönig, M.R., John, C.M., 2015. Sedimentological and isotopic heterogeneities within a Jurassic carbonate ramp (UAE) and implications for reservoirs in the Middle East. Mar. Pet. Geol. 68, 240–257.
Hughes, G.W., 2004. Middle to Upper Jurassic Saudi Arabian carbonate petroleum reservoirs: biostratigraphy, micropaleontology, and paleoenvironments. GeoArabia 9, 79–114.
Ipas, J., Aurell, M., Bádenas, B., 2004. Ambientes sedimentarios y secuencias en la Fm. Higueruelas (Jurásico Superior) en la Cordillera Ibérica Septentrional. Geogaceta 35, 7–10.
Ipas, J., Aurell, M., Bádenas, B., Canudo, J.I., Liesa, C., Mas, J.R., Soria, A.R., 2007. Caracterización de la Formación Villar del Arzobispo al sur de Zaragoza (Titónico, Cordillera Ibérica). Geogaceta 41, 111–114.
Kerans, C., Tinker, S.W., 1997. Sequence stratigraphy and characterization of carbonate reservoirs. In: SEMP Short Courses Notes, vol. 40 SEMP, Tulsa, OK.
Lehmann, C.T., Al Hosany, K.I., Matarid, T., Sayed, M.I., 2010. Addressing Reservoir Heterogeneities in the Development of Upper Jurassic Carbonate Reservoirs, Offshore Abu Dhabi. Society of Petroleum Engineers SPE 137888.
Leinfelder, R.R., Nose, M., Schmid, D., Werner, M., 1993. Microbial crusts of the late Jurassic: composition, Palaeoecological significance and importance in reef construction. Facies 29, 195–230.
Leinfelder, R.R., Schlagintweit, F., Werner, W., Ebli, O., Nose, M., Schmid, D., Hughes, G., 2005. Significance of stromatoporoids in Jurassic reefs and carbonate platforms-concepts and implications. Facies 51, 287–325.
Lindsay, R.F., Cantrell, D.L., Hughes, G.W., Keith, T.H., Mueller III, H.W., Russel, D., 2006. Ghawar Arab-D reservoir: widespread porosity in shoaling-upward carbonate cycles. Saudi Arabia AAPG Mem. 88, 97–138.
Marchionda, E., Deschamps, R., Gobianchi, M., Nader, F.H., Di Giulio, A., Morad, D.J., Al Darmaki, F., Ceriani, A., 2018. Field-scale depositional evolution of the upper Jurassic Arab Formation (onshore Abu Dhabi, UAE). Mar. Pet. Geol. 89, 350–369.
Marsaglia, K.M., Klein, G.deV., 1983. The palaeogeography of Paleozoic and Mesozoic storm depositional systems. J. Geol. 91, 117–142.
Petrovic, A., Aigner, T., 2017. Are shoal reservoirs discrete bodies? A coquina shoal outcrop analogue from the Mid-Triassic Upper Muschelkalk, SW Germany. J. Pet. Geol. 40 (3), 249–275.
Pomar, L., 2018. Carbonate factories through the earth history. EGU General Assembly Conf. Abstr. 20, 3861.
Pomar, L., Kendall, C.S.C., 2007. Architecture of carbonate platforms: a response to hydrodynamics and evolving ecology. In: In: Lukasik, J., Simo, J.A. (Eds.), Controls on Carbonate Platform and Reef Development, vol. 89. SEPM Spec. Publ., Tulsa, OK, pp. 187–216.
Pomar, L., Aurell, M., Bádenas, B., Morsilli, M., Al-Awwad, S.F., 2015. Depositional model for a prograding oolitic wedge, upper Jurassic, Iberian Basin. Mar. Pet. Geol. 67, 556–582.
Price, G.D., Sellwood, B.W., Valdes, P.J., 1995. Sedimentological evaluation of general circulation model simulations for the "greenhouse" Earth: Cretaceous and Jurassic case studies. Sediment. Geol. 100, 159–180.
Purkis, S., Casini, G., Hunt, D., Colpaert, A., 2015. Morphometric patterns in modern carbonate platforms can be applied to the ancient rock record: similarities between modern Alacranes Reef and Upper Palaeozoic platforms of the Barents Sea. Sediment. Geol. 321, 49–69.
Rankey, E.C., Reeder, S.L., 2011. Holocene oolitic Marine sand complexes of the Bahamas. J. Sediment. Res. 81, 97–117.
Reijmer, J.J.G., Swart, P.K., Bauch, T., Otto, R., Reuning, L., Roth, S., Zechel, S., 2009. A re evaluation of facies on Great Bahama Bank I: new facies maps of western Great Bahamas Bank. In: In: Swart, P.K., Eberli, G.P., McKenzie, J.A. (Eds.), Perspectives in Carbonate Geology, vol. 41. IAS Spec. Publ., pp. 29–46.
Riding, R., 2002. Structure and composition of organic reefs and carbonate mud mounds: concepts and categories. Earth Sci. Rev. 58, 163–231.
Riegl, B., Piller, W.E., 2000. Reefs and coral carpets in the Miocene paratethys (Badenian, Leitha limestone, Austria). In: Mar. Env. Sci. Faculty Proceedings, Presentations, Spechees, Lectures, pp. 111.
Rodríguez-Morillas, N., Playà, E., Travé, A., Martín-Martín, J.D., 2013. Diagenetic processes in a partially dolomitized carbonate reservoir: Casablanca oil field, Mediterranean Sea, offshore Spain. Geol. Acta 11 (2), 195–214.
Ruf, M., Aigner, T., 2004. Facies and poroperm characteristics of a carbonate shoal (Muschelkalk, South German Basin): a reservoir analogue investigation. J. Pet. Geol. 27, 215–239.
Salas, R., Casas, A., 1993. Mesozoic extensional tectonics, stratigraphy and crustal evolution during the Alpine cycle of the eastern Iberian basin. Tectonophysics 228, 33–55.
Salas, R., Guimerà, J., Mas, R., Martín-Closas, C., Meléndez, A., Alonso, A., 2001. Evolution of the Mesozoic central Iberian rift system and its Cainozoic inversion (Iberian chain). In: In: Ziegler, P.A., Cavazza, W., Robertson, A.H.F., Crasquin-Soleau, S. (Eds.), Peri-Tethys Memoir 6: Peri-Tethyan Rift/Wrench and Passive Margins, vol. 186. Mém. Mus. Natn. Hist. nat., pp. 145–185.
San Miguel, G., Aurell, M., Bádenas, B., 2017a. Occurrence of high-diversity metazoan- to microbial-dominated bioconstructions in a shallow Kimmeridgian carbonate ramp (Jabaloyas, Spain). Facies 63, 13.
San Miguel, G., Aurell, M., Bádenas, B., 2017b. Diagenetic evolution of a shallow marine Kimmeridgian carbonate ramp (Jabaloyas, NE Spain): implications for hydrocarbon reservoir quality. Arab. J. Geosci. 10, 376.
San Miguel, G., Duaso, M., Prados, G., Aurell, M., Kenter, J., 2017c. Early diagenetic events in Late Kimmeridgian carbonate ramps (Iberian Basin, NE Spain): implications for outcrop characterization and deciphering and prediction of carbonate reservoir heterogeneitiy. In: 33rd International Meeting of Sedimentology, pp. 803.
Sequero, C., Bádenas, B., Aurell, M., 2018. Facies mosaic in the inner areas of a shallow carbonate ramp (Upper Jurassic, Higueruelas Fm, NE Spain). Facies 64, 9.
Shinn, E.A., 1968. Practical significance of birdseye structures in carbonate rocks. J. Sediment. Pet. 38, 215–223.
Strasser, A., 1986. Ooids in Purbeck limestones (lowermost Cretaceous) of the Swiss and French Jura. Sedimentology 33, 711–727.
Strasser, A., 2018. Cyclostratigraphy of shallow-marine carbonates-limitations and opportunities. In: In: Montenari, M. (Ed.), Stratigraphy and Timescales, vol. 3. pp. 151–187.
Strasser, A., Védrine, S., 2009. Controls on facies mosaics of carbonate platforms: a case study from the Oxfordian of the Swiss Jura. In: In: Swart, P., Eberli, G., McKenzie, J. (Eds.), Perspectives in Carbonate Geology: a Tribute to the Career of Robert Nathan Ginsburg, vol. 41. IAS Spec. Publ., pp. 199–213.
Strasser, A., Pittet, B., Hillgärtner, H., Pasquier, J.B., 1999. Depositional sequences in shallow carbonate-dominated sedimentary systems: concepts for a high-resolution analysis. Sediment. Geol. 128, 201–221.
Tomás, S., Zitzmann, M., Homman, M., Rumpf, M., Amour, F., Benisek, M., Marcano, G., Mutti, M., Betzler, C., 2010. From ramp to platform: building a 3D model of

depositional geometries and facies architectures in transitional carbonates in the Miocene, northern Sardinia. Facies 56, 195–210.
Tomassetti, L., Petracchini, L., Brandano, M., Trippetta, F., Tomassi, A., 2018. Modeling lateral facies heterogeneity of an upper Oligocene carbonate ramp (Salento, southern Italy). Mar. Pet. Geol. 96, 254–270.
Travé, A., Nadal, J., Playà, E., Salas, R., Martín-Martín, J.D., Gomez-Rivas, E., 2019. Fracture-related dolomitization affecting late Jurassic-lowermost Cretaceous syn-rift deposits (Maestrat Basin, southern Iberian chain, eastern Spain). In: Doronzo, D.M. (Ed.), Petrogenesis and Exploration of the Earth's Interior, pp. 163–165.
Turnsek, D., Buser, S., Ogorelec, B., 1981. An upper Jurassic reef complex from Slovenia, Yugoslavia. In: In: Toomey, D.F. (Ed.), European Fossil Reef Models, vol. 30. SEPM Spec. Publ., pp. 361–369.
Wender, L.E., Bryant, J.W., Dickens, M.F., Neville, A.S., Al-Moqbel, A.M., 1998. Paleozoic (pre-Khuff) hydrocarbon geology of the Ghawar area, eastern Saudi Arabia. GeoArabia 3, 273–301.
Wilkinson, B.H., Drummond, C.N., Diedrich, N.W., Rothman, E.D., 1999. Poisson processes of carbonate accumulation on Paleozoic and Holocene platforms. J. Sediment. Res. 69, 338–350.

6. FACTORS CONTROLLING ONCOID DISTRIBUTION ON THE LATEST KIMMERIDGIAN SHALLOW CARBONATE RAMP

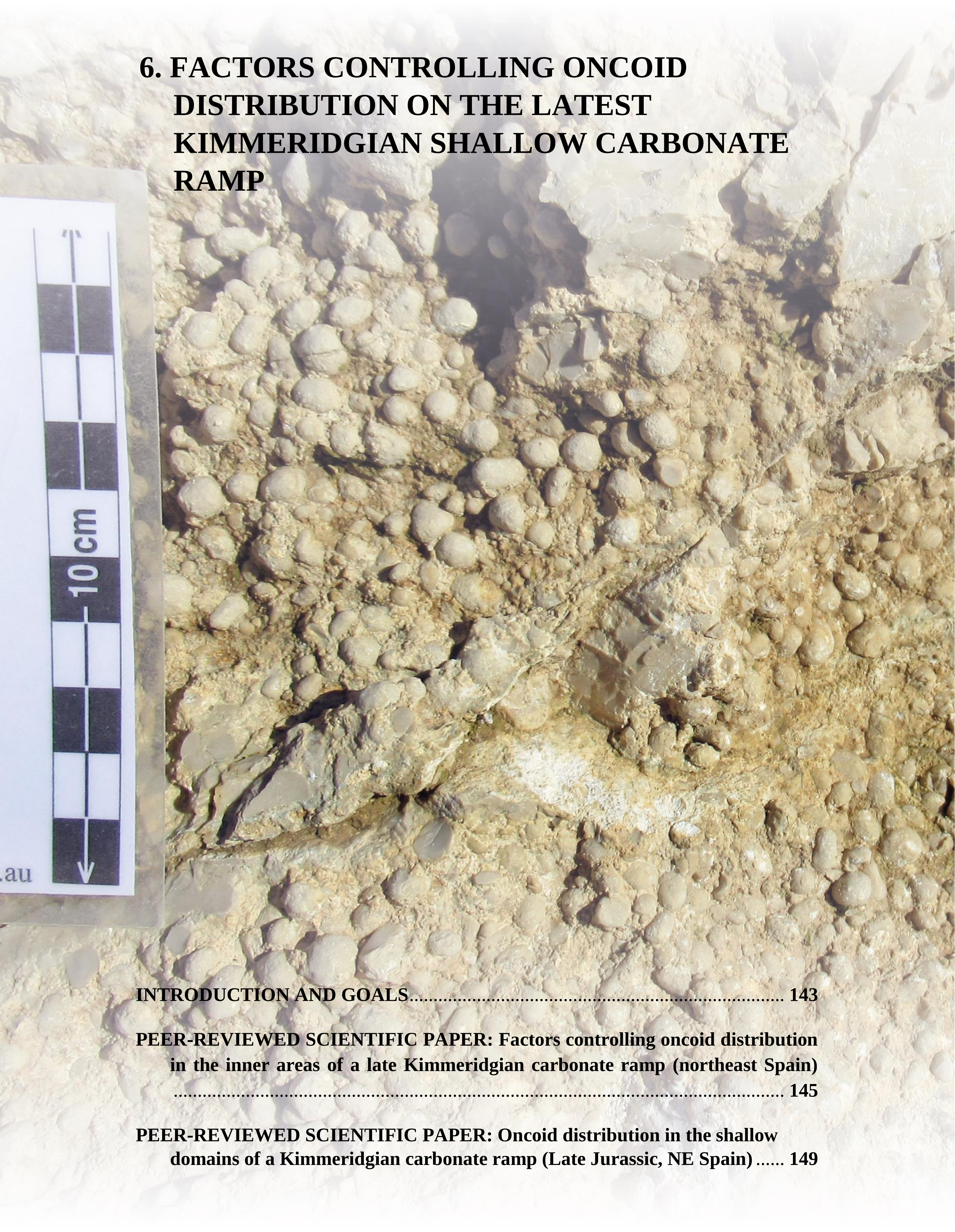

CHAPTER

6

FACTORS CONTROLLING ONCOID DISTRIBUTION ON THE LATEST KIMMERIDGIAN SHALLOW CARBONATE RAMP

INTRODUCTION AND GOALS

The uppermost Kimmeridgian shallow carbonate ramp deposits of the Higueruelas Fm are characterized by a great variety of oncoids, being recognized as the most characteristic component giving the name to this formation (i.e. the Oncolitic limestones of the Higueruelas Fm; Gómez and Goy, 1979).

Oncoids are referred in the literature as coated grains larger than 2 mm in diameter, which exhibit coatings composed of concentric or irregular laminae, surrounding a nucleus of variable nature (e.g. detrital, skeletal or other coating grains such as ooids) (e.g. Tucker and Wright, 1990; Flügel, 2004; Zhang et al., 2015). The oncoids recognized in the Higueruelas Fm show a wide range of sizes and shapes, but also distinctive characteristics within the cortex, encompassing variable proportions of different types of laminae (i.e. continuous or discontinuous micritic and organism-bearing laminae of mainly cyanobacteria, such as *Bacinella irregularis* or *Lithocodium aggregatum*). In some cases, the microbial activity dominates the entire structure of the oncoid, resulting in non-laminated microbial meshworks (even regarded in the literature as a type of microbialite) (e.g. Peryt, 1981; Jones and Renaut, 1997; Riding, 2000; Shapiro et al., 2009).

As reported in previous works (e.g. Dahanayake et al., 1985; Tucker and Wright, 1990; Lanés and Palma, 1998; Flügel, 2004; Hägele et al., 2006; Shi and Chen, 2006; Védrine et al., 2007; Bádenas and Aurell, 2010), the size, shape and internal structure of oncoids can provide valuable information on the palaeoenvironmental conditions of the depositional environment in which they formed, since these parameters are controlled by many different biological and physical factors, such as the water energy (i.e. the degree of grain overturning), microbial activity and chemical composition of the seawater (i.e. salinity, trophic levels) (e.g. Dahanayake, 1978; Flügel, 2004; Védrine et al., 2007; Olivier et al., 2011).

The along-strike and down-dip facies heterogeneities throughout the successive sedimentary stages (see Chapter 5), allowed to characterize the distribution and lateral extent of the oncolitic facies, which are represented in variable abundance from inner- (sheltered lagoon, backshoal, shoal-sand blanket) to mid-ramp domains (foreshoal, offshore-proximal), in some cases with a patchy distribution. Accordingly, the main objective for the work presented in this Chapter is to characterize the different types of oncoids and their distribution across the studied shallow carbonate ramp during deposition of the sedimentary stages 1 to 4 defined in Chapter 5 (i.e. those showing more abundance and variety of oncoids), in order to evaluate the palaeoenvironmental factors controlling the formation of the different oncoid types and their distribution. The results obtained in this Chapter are presented in two peer-reviewed scientific papers, one of them corresponding to a preliminary analysis of this oncoid distribution in the inner areas of the carbonate ramp. Detailed information concerning the distribution of the different oncoid types in the studied sedimentary logs, and location of the collected samples for petrographic descriptions in the laboratory, is included in Annexe 1.

The criteria used for classification of oncoids are those previously defined in the Dahanayake (1977) nomenclature, by evaluating their petrographic characteristics. In this regard, a revised version of the Dahanayake (1977) nomenclature for marine oncoids is also proposed in this work, which reports on further details about the internal characteristics of the oncoids, so it could provide additional tools for assessing palaeoenvironmental interpretations of oncoid distributions in similar environments.

Check for updates

Factors Controlling Oncoid Distribution in the Inner Areas of a Late Kimmeridgian Carbonate Ramp (Northeast Spain)

Cristina Sequero, Beatriz Bádenas, and Marcos Aurell

Abstract

The factors controlling the oncoid distribution in the interior areas of a latest Kimmeridgian shallow carbonate ramp were examined based on a detailed sedimentological and petrographic analysis of the upper sequence of the Higueruelas Formation (Iberian Basin, Northeast Spain). Four types of oncoids are defined: small micrite-dominated type I and II oncoids are generally found in low proportion in all sub-environments (from backshoal/washover, lagoon to intertidal). Large *Bacinella*-dominated type III and IV oncoids predominate in low-energy lagoonal areas. Variable energy water, oligotrophic conditions and probably low sedimentation rates controlled oncoid growth and distribution, thus highlighting their potential as palaeo-environmental proxies.

Keywords

Oncoids • Lagoon • Carbonate ramp • Latest kimmeridgian • Iberian basin

1 Introduction

Different types of marine oncoids and their palaeoenvironmental significance have been described in the Late Jurassic [1, 2, 5, 8]. In this work, the different oncoid types occurring abundantly in the interior areas of a latest Kimmeridgian carbonate ramp (Higueruelas Formation, Iberian Basin, Northeast Spain) are studied in detail in order to decipher the main environmental factors involved in the formation of the different oncoid types and their distribution.

2 Sedimentological Setting and Methodology

The shallow-water domains of the latest Kimmeridgian of the Iberian Basin (Fig. 1a) are represented by the oncolitic limestones of the Higueruelas Formation. This work concerns the upper (10–16 m thickness) shallowing-upward sequence of the unit (Fig. 1b), exposed in an outcrop area of 1 × 2 km in extent. Facies analysis was based on a detailed sedimentological field description of 14 closely logs and petrographic description of rock samples in 438 polished slabs and 111 thin sections.

The palaeoenvironmental interpretation by Sequero et al. [7] provides the sedimentological framework for the detailed analysis of oncoids presented here (Figs. 1b and 2a). Five facies encompassing from intertidal to shallow subtidal lagoon and backshoal areas were distinguished (Fig. 2a). Oncolitic and oncolitic-stromatoporoid wackestone to packstones with local patches of stromatoporoids, predominate in the sheltered lagoon. Backshoal/washover peloidal wackestone to grainstones represent resedimented sediment from distal oolitic-peloidal and oncolitic-dominated shoals. Peloidal mudstone to grainstones with fenestral porosity and gastropod-oncolitic wackestone to grainstones are accumulated in intertidal areas with small ponds.

C. Sequero (✉) · B. Bádenas · M. Aurell
University of Zaragoza, Zaragoza, Spain
e-mail: csequero@unizar.es

M. Boughdiri et al. (eds.), *Paleobiodiversity and Tectono-Sedimentary Records in the Mediterranean Tethys and Related Eastern Areas*, Advances in Science, Technology & Innovation, https://doi.org/10.1007/978-3-030-01452-0_41

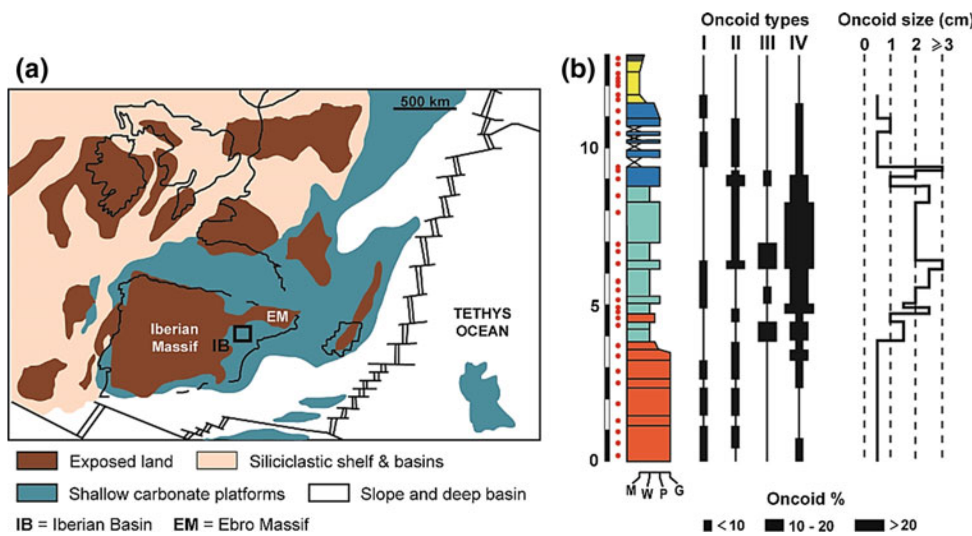

Fig. 1 **a** Paleogeographic distribution in western Europe during the late Kimmeridgian (adapted from Dercourt et al. [3]) indicating the location of the studied area. **b** Vertical facies distribution in the uppermost sequence of the Higueruelas Formation (log M7 from Sequero et al. [7]), showing the vertical distribution of oncoid types and size (legend for facies in Fig. 2a)

3 Oncoid Distribution and Controlling Factors

Four types of oncoids (type I, II, III and IV; [2]) show a preferential distribution and relative abundance within the intertidal to shallow subtidal areas have been recognized (Figs. 1b and 2). Type I and II oncoids are present in all facies in very low proportion. They are spherical to elliptical and few millimeters to 1 cm in size. The cortex is formed by micritic laminae (type I, Fig. 2b, A) and micritic laminae with organism-bearing laminae of *Bacinella irregularis* (type II, Fig. 2b, B). Type III oncoids are common in oncolitic facies. They are up to 3 cm in size and from sub-elliptical to spherical with undulated surfaces (Fig. 2b, C). The cortex is formed by an alternation of micritic and organism-bearing (mostly *Bacinella-Lithocodium* association) laminae. Type IV oncoids are abundant in oncolitic facies, and also common in oncolitic-stromatoporoid and pond facies. They display irregular shapes with lobate contours ranging from a few millimeters to 7 cm in size (Fig. 2b, D). They are exclusively formed of mostly *Bacinella-Lithocodium* meshwork. Large type IV oncoids are found in oncolitic facies.

The interaction of the different palaeo-environmental factors controlled the oncoid growth and distribution in the studied inner ramp. Shoals protecting the lagoon controlled the occurrence of low-energy conditions which are favorable for the development and abundance of large type IV oncoids in the lagoon; whereas, micrite-dominated type I and II oncoids were probably resedimented by storms and distributed throughout the inner ramp domain. Low siliciclastic input and probable low sedimentation rates contributed to the generation of the *Bacinella-Lithocodium* association that characterize type III and IV oncoids [6], since these cyanobacteria indicate oligotrophic levels, medium-level salinity and high-transparent waters [4].

4 Conclusion

The spatial distribution obtained for the oncoids in the inner areas of a latest Kimmeridgian carbonate ramp highlights that oncoids constitute a useful tool for the high-resolution palaeo-environmental studies. Large *Bacinella*-dominated type III and IV oncoids predominate in the inner areas of a sheltered lagoon, where low-energy conditions, low siliciclastic input and probably low sedimentation rates

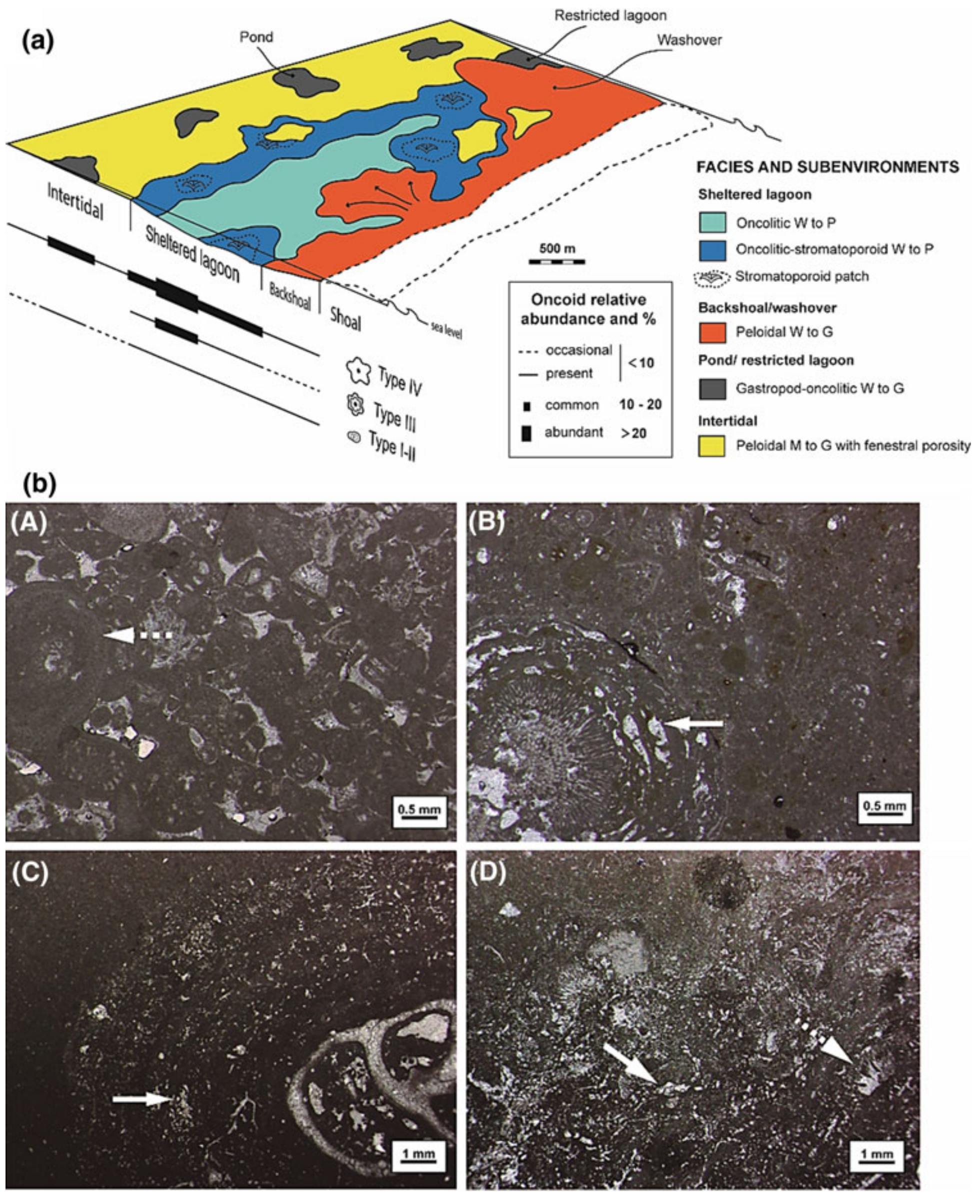

Fig. 2 **a** Facies distribution in the sedimentary model proposed for the studied carbonate inner ramp [7], and abundance of different oncoid types. **b A–D** Thin section images in plane polarized light of oncoids: type I (**A**, dashed arrow), type II (**B**), type III (**C**) and type IV (**D**) oncoids. Note the *Bacinella* (white arrows in **B–D**) and *Lithocodium* (dashed arrow in **D**)

contributed to the extensive growth of cyanobacteria. Type I and II oncoids, which are present in all sub-environments in very low proportion, are probably resedimented by storms.

Similar palaeo-environmental interpretations are found for oncoids studied in the Late Jurassic [1, 2, 8], where the lateral and vertical distribution of oncoids through small-scale depositional sequences is also congruent with relative sea-level changes or variations in the platform morphology [8].

References

1. Bádenas, B., Aurell, M.: Facies model of shallow-water carbonate ramp based on distribution of non-skeletal grains (Kimmeridgian, Spain). Facies **56**, 89–110 (2010)
2. Dahanayake, K.: Sequential position and environmental significance of different types of oncoids. Sediment. Geol. **20**, 301–316 (1978)
3. Dercourt, J., Ricou, L., Vrielynck, B.: Atlas Tethys palaeoenvironmental Maps. CCGM, Paris (1993)
4. Flügel, E.: Microfacies of Carbonate Rocks: Analysis, Interpretation and Application. Springer, Berlin (2004)

5. Gygi, R.A.: Structure pattern of distribution and paleobathymetry of late Jurassic microbialites (stromatolites and oncoids) in northern Switzerland. Eclogae Geol. Helv. **85**, 799–824 (1992)
6. Leinfelder, R.R., Nose, M., Schmid, D., Werner, M.: Microbial crusts of the Late Jurassic: composition, palaeoecological significance and importance in reef construction. Facies **29**, 195–230 (1993)
7. Sequero, C., Bádenas, B., Aurell, M.: Facies mosaic in the inner areas of a shallow carbonate ramp (Upper Jurassic, Higueruelas Fm, NE Spain). Facies **64**, 9 (2018)
8. Védrine, S., Strasser, A., Hug, W.: Oncoid growth and distribution by sea-level fluctuations and climate (Late Oxfordian, Swiss Jura Mountains). Facies **53**(4), 535–552 (2007)

Sedimentary Geology 398 (2020) 105585

Contents lists available at ScienceDirect

Sedimentary Geology

journal homepage: www.elsevier.com/locate/sedgeo

Oncoid distribution in the shallow domains of a Kimmeridgian carbonate ramp (Late Jurassic, NE Spain)

Cristina Sequero *, Marcos Aurell, Beatriz Bádenas

Department of Earth Sciences-IUCA, University of Zaragoza, 50009, Spain

ARTICLE INFO

Article history:
Received 18 October 2019
Received in revised form 19 December 2019
Accepted 20 December 2019
Available online 26 December 2019

Editor: Dr. Brian Jones

Keywords:
Oncoids
Kimmeridgian
Iberian Basin
Shallow carbonate ramp
Palaeoenvironmental proxies

ABSTRACT

The distribution and abundance of oncoids in the shallow domains of a latest Kimmeridgian carbonate ramp was accomplished on the basis of a detailed sedimentological and petrographic analysis of the lower part of the Higueruelas Formation (Iberian Basin, northeastern Spain). Six types of oncoids are recognized based on the internal structure of the cortex, and show a preferential distribution on the carbonate ramp, which record from intertidal, lagoon, backshoal, shoal-sand blanket, foreshoal to offshore domains. Spherical type I oncoids, composed of continuous micritic laminae, occur in all the subenvironments in low proportions. Sub-spherical type II oncoids, constituted by micritic laminae and discontinuous organism-bearing laminae of mostly *Bacinella irregularis*, dominate in the higher-energy shoal-sand blanket domain. Type III oncoids, with alternating micritic and organism-bearing laminae of mostly *Bacinella irregularis-Lithocodium aggregatum* association, include two varieties: type IIIa oncoids, with micritic and organism-bearing laminae of similar thickness, preferentially formed in the foreshoal domain; and type IIIb oncoids, with thinner micritic laminae, formed in a low-energy sheltered lagoon. Irregular type IV oncoids characterize the low-energy settings, and include two varieties: type IVa oncoids, mainly consisting of a *Bacinella-Lithocodium* meshwork, which occur abundantly in the lagoon; and less abundant type IVb oncoids, composed of a continuous organism-bearing laminae of *Lithocodium*, which are found in the offshore domain. Water energy and platform morphology played an important role in formation and distribution of the oncoids in these shallow domains, where normal-marine water and oligotrophic conditions are highlighted by the high-diversity of light-dependant micro-encrusters in type III and IV oncoids. Comparable oncoid distribution patterns of diverse Late Jurassic shallow carbonate platforms enhance their potential use as reliable palaeoenvironmental proxies.

1. Introduction

Analysis of distribution of non-skeletal grains in shallow marine carbonate deposits is of great interest due its applicability in deciphering key factors controlling the sedimentation in these environments (e.g. variations in hydrodynamic conditions, trophic level fluctuations), partially controlled by the sea-floor topography (e.g. Bádenas and Aurell, 2010). In particular, oncoids are a kind of carbonate grains usually present in shallow-water facies which have been used by several authors to obtain palaeoenvironmental information about the depositional environment in which they are formed, as their morphology, size and internal structure are controlled by many different biological and physical factors (e.g. Dahanayake, 1978; Flügel, 2004; Védrine et al., 2007; Olivier et al., 2011). Oncoids have been described in the literature as nodules or coated grains that exhibit >2 mm in diameter, and include cortex formed by irregular or concentric laminae surrounding skeletal or non-skeletal grains as nuclei (Tucker and Wright, 1990; Flügel, 2004; Zhang et al., 2015).

In shallow-marine deposits of the Phanerozoic, carbonate oncoids have been recorded in a wide range of environments, from intertidal, lagoon, shoal to open-marine settings, locally associated to reefal structures (e.g. Li et al., 2000; Shi and Chen, 2006; Védrine et al., 2007; Bádenas and Aurell, 2010; Reolid and Nieto, 2010; Olivier et al., 2011; Lazar et al., 2013; Sequero et al., 2019). Despite oncoids have been traditionally used as indicators of moderately agitated environments, as their rounded morphology and lamination are frequently associated to grain overturning (e.g. Tucker and Wright, 1990; Lanés and Palma, 1998; Flügel, 2004; Shi and Chen, 2006), several authors have described oncoids entirely formed by in-situ microbial growth in low-energy settings (e.g. Dahanayake et al., 1985; Hägele et al., 2006; Védrine et al., 2007; Bádenas and Aurell, 2010; Zaton et al., 2012; Sequero et al., 2019), also considered as a type of microbialites (e.g. Peryt, 1981; Jones and Renaut, 1997; Riding, 2000; Shapiro et al., 2009). In addition, analysis of oncoids on shallow domains has been previously used in order to characterize high-frequency cycles (e.g. Védrine et al., 2007;

* Corresponding author.
E-mail address: csequero@unizar.es (C. Sequero).

https://doi.org/10.1016/j.sedgeo.2019.105585

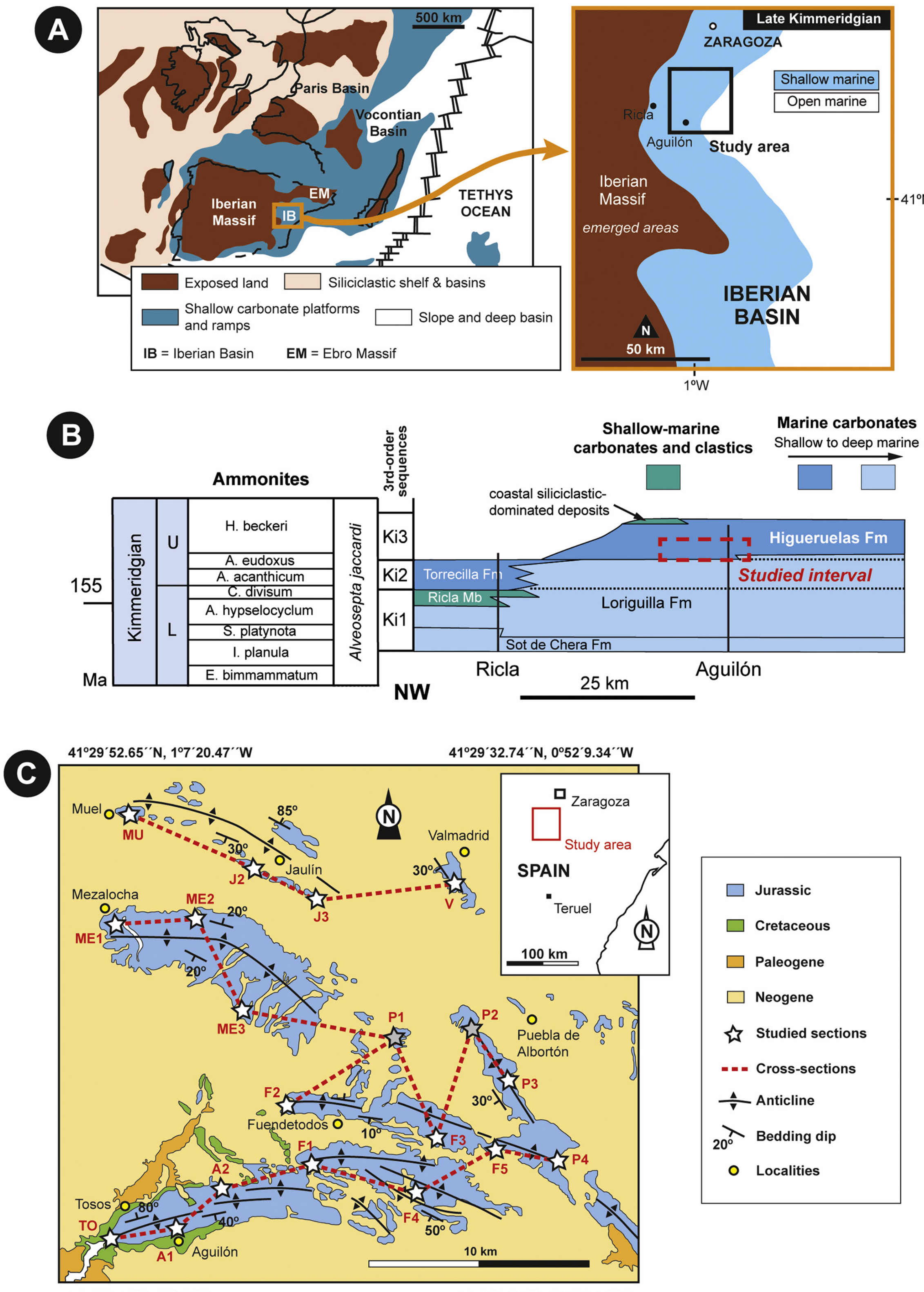

Fig. 1. (A) Palaeogeographical reconstruction of western Tethys during the late Kimmeridgian (adapted from Dercourt et al., 1993), and distribution of the main sedimentary domains in the northeastern Iberian Basin (compiled from Aurell et al., 2003 and Ipas et al., 2004). (B) Summary of the stratigraphy for the Kimmeridgian in the northern Iberian Basin including the main sedimentary domains (modified from Aurell et al., 2019). The studied interval encompasses the lower part of the Higueruelas Formation, which is included in sequence Ki3. (C) The Jurassic outcrops in the study area (modified from Cortés Gracia and Casas Sainz, 1996) and the location of the studied sections (stars). Dashed lines refer to the interpreted cross-sections shown in Fig. 4 (see also clarification for sections P1 and P2, in grey colour).

Brandano et al., 2015), as their relative abundance and distribution show a correlation with sea-level fluctuations.

In the present study, oncoids occur abundantly from inner- to mid-ramp areas of the latest Kimmeridgian carbonate ramp that developed in the Iberian Basin (northeastern Spain), showing a wide variability in size, shape and internal structure. The main aim of this work is to examine the petrographic characteristics of these oncoids as well as their abundance and distribution along the shallow domains of this carbonate ramp, in order to decipher the environmental factors controlling the formation of the different oncoid types and their distribution. We also propose a revised version of Dahanayake (1977) classification of marine oncoids, which can be applied in palaeoenvironmental interpretations of similar depositional environments.

2. Geological context

Shallow marine carbonate-dominated platforms and ramps occupied extensive areas of Western Europe during the Late Jurassic (Fig. 1A; Dercourt et al., 1993). Oncoids studied in this work were deposited in the shallow areas of the low angle carbonate ramp developed in the intra-cratonic Iberian Basin (NE Spain) during the Kimmeridgian (Salas and Casas, 1993; Aurell et al., 2003).

The stratigraphy of the Iberian Kimmeridgian carbonate ramps across a transect located in the northern Iberian Basin is summarized in Fig. 1B. The Kimmeridgian consists of three third-order depositional sequences (i.e. Ki1, Ki2 and Ki3). The shallow carbonate deposits studied here correspond to sequence Ki3, which are represented in the thick-bedded (dm- to m-thick) shallow marine limestones of the Higueruelas Formation. The widespread occurrence of the benthic foraminifera *Alveosepta jaccardi* combined to strontium-isotopic data, indicates that this unit was deposited at the latest Kimmeridgian, most probably during the upper *eudoxus* and *beckeri* Zones (Fig. 1B; Aurell et al., 2019). At basin scale, the shallow carbonate ramp facies of the Higueruelas Formation pass gradually into outer-ramp lime mudstones and marls of the Loriguilla Formation, recorded to the east of the basin (Fig. 1A and B; Aurell et al., 2003, 2019). The progressive shallowing and eventual emersion of the carbonate ramp at the end of the Kimmeridgian has been related to the long-term fall in regional sea level, which was in part controlled by the tectonic uplift of the western emerged areas of the Iberian Massif (Bádenas and Aurell, 2001; Aurell et al., 2003).

The outcrops studied in this work are located south of Zaragoza (Spain), where the Higueruelas Formation is widely-exposed across large anticline structures (Fig. 1C). The thickness of the studied formation in this area ranges from 40 m in the western proximal localities to 80 m basinward (to the southeast). The overall facies distribution and sequence stratigraphy of this unit was previously characterized in Aurell and Meléndez (1986) and Ipas et al. (2004). Further characterization of facies and sedimentary evolution of the unit has been performed by Sequero et al. (2019). These authors identified 9 high-frequency sequences (i.e. sedimentary units 1–9) of variable thickness (2 to 26 m-thick) that were tentatively regarded as formed in tune with the short eccentricity cycles. The detailed analysis of the different oncoid types and distribution presented here is focused in the lower part of the Higueruelas Formation (30 to 50 m-thick), which includes the largest abundance and variety of oncoids (Fig. 2).

3. Studied successions and methodology

The selected interval for analysing abundance and distribution of the different oncoid types in the shallow domains of the latest Kimmeridgian carbonate ramp encompasses the sedimentary units 1 to 4 recognized in the lower part of the Higueruelas Formation (Fig. 2). These units represent high-frequency sequences bounded by discontinuity surfaces that can be physically traced along continuous outcrops (i.e. Mezalocha sector; Sequero et al., 2018), and are recognized across the entire study area (Sequero et al., 2019).

Characterization of size, morphology and internal structure of oncoids was performed on 896 rock samples collected from 17 closely-spaced logs throughout several outcrops situated south of Zaragoza (Fig. 1C), covering an area of 20 × 30 km in extent, and complemented by detailed (at bed-scale) field descriptions of the sections. Characteristics of the internal structure of the oncoids were analysed under microscopic observations on 83 thin sections selected from the collected rock samples. The comparison diagrams of volume percentages of constituents suggested by Baccelle and Bosellini (1965) were used in order to determine the semi-quantitative proportion of oncoids on polished slabs and thin sections. Following the proposed nomenclature of Dahanayake (1977), the internal structure of the cortex, in particular the differentiation of micritic laminae and organism-bearing laminae, was the criteria used here for oncoid description and classification.

The sedimentological framework for the present work is provided by Sequero et al. (2019), so that only a brief description of facies will be included in the next section. Correlation of logs was done along three cross-sections which are orientated from proximal to distal areas (i.e. western–eastern cross-sections), and was carried out by the identification of continuous (km-scale) well-marked bounding surfaces of the studied sedimentary units 1–4 (Sequero et al., 2019). The lateral (along strike and down dip) distribution and abundance of the different oncoid types will be evaluated all across the shallow carbonate ramp in successive palaeoenvironmental maps reconstructed for each sedimentary unit. Analysis of the spatial distribution and internal characteristics of the different oncoids will allow us to decipher main factors controlling oncoid growth and distribution.

4. Facies architecture and sedimentary model

High-resolution facies analysis performed by Sequero et al. (2019) indicates that the latest Kimmeridgian shallow carbonate ramp deposits include three main facies associations (peloidal and oolitic-dominated, oncolitic-dominated and stromatoporoid/chaetetid/coral-rich facies associations), which represent deposition in intertidal, lagoon, backshoal/washover, shoal-sand blanket, foreshoal, offshore-proximal and offshore-distal subenvironments (Fig. 3).

The peloidal and oolitic-dominated facies association comprises 6 facies deposited in intertidal areas (peloidal mudstone (M) to packstone-grainstones (P-G) with fenestral porosity), in backshoal, shoal-sand blanket and foreshoal subenvironments (peloidal to oolitic wackestones (W) to grainstones) and offshore domains (peloidal-bioclastic packstones to mudstones) (Fig. 3). These facies have low proportions of oncoids and are mainly composed of lithic peloids (Flügel, 2004), type 1 and 1/3 ooids (i.e. ooids with micritic laminae and alternating fine-radial sparitic and micritic laminae, respectively, according to Strasser, 1986), and scarce bioclasts (e.g. bivalves, brachiopods, echinoderms, foraminifera).

The oncolitic-dominated facies association is characterized by the abundance of oncoids and encompasses 3 facies formed in the sheltered lagoon (oncolitic W to P, with large and irregular oncoids), backshoal-foreshoal (oncolitic P) and shoal-sand blanket subenvironments (oncolitic G). The fine-grain-sized fraction in these oncolitic-dominated facies is mainly composed of lithic peloids, type 1 and 1/3 ooids and minor proportion of bioclasts.

The stromatoporoid/chaetetid/coral-rich facies association includes four facies that can be grouped in two groups of facies, and show a patchy distribution (Fig. 3): 1) lagoon to backshoal stromatoporoid W to G, composed by abundant broken and in-situ stromatoporoids that represent stromatoporoid carpets, surrounded by oncolitic-stromatoporoid W to G with variable proportions of oncoids and cm-sized fragments of stromatoporoids, chaetetids and corals; 2) chaetetid-stromatoporoid-coral buildups, with

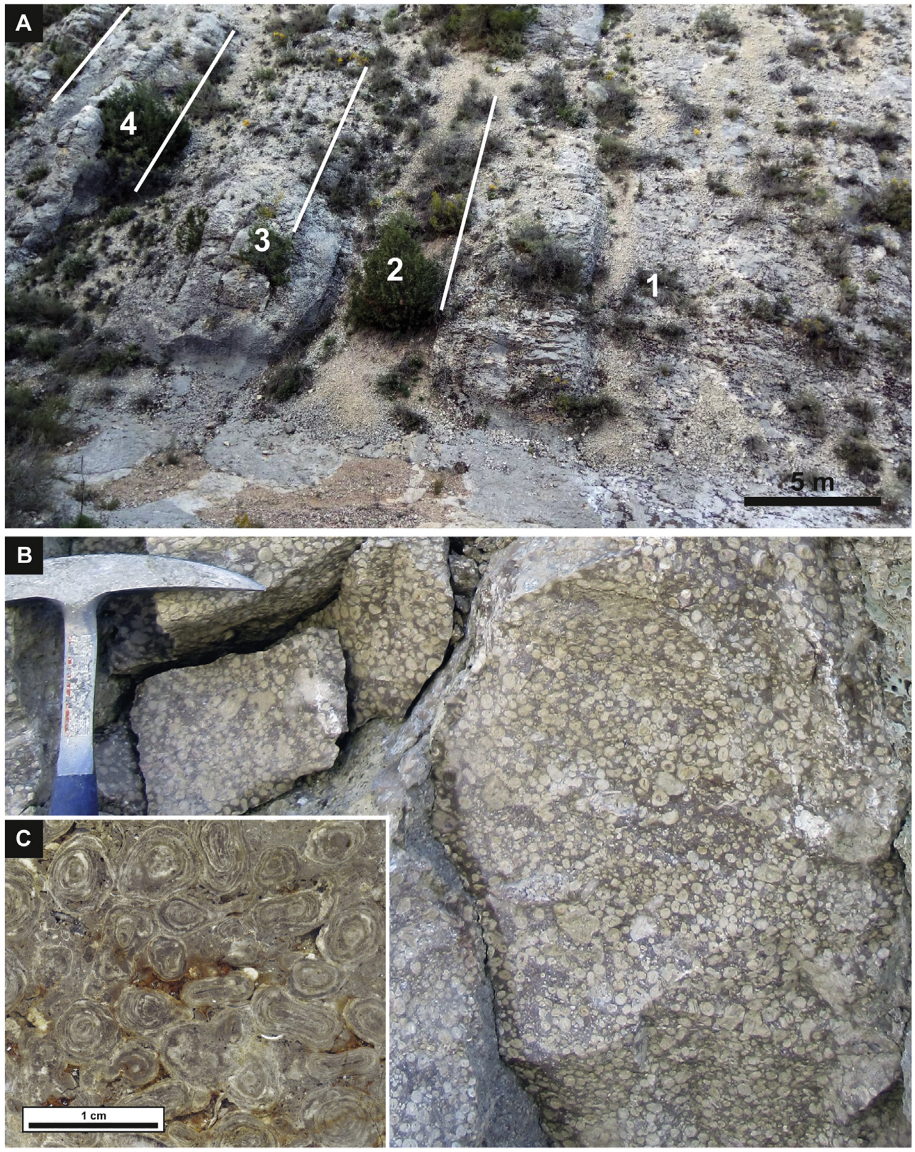

Fig. 2. (A) Field view of the lower part of the Higueruelas Formation in Tosos sector (section TO in Fig. 1C; units 1 to 4). (B, C) Macro-scale examples of oncolitic-dominated facies with oncolitic-supported texture in Valmadrid sector (B; section V, unit 4) and Mezalocha sector (C; section ME1, unit 1).

lenticular geometries (up to 8 m high), and inter-buildup stromatoporoid-chaetetid-coral and oncolitic W to G facies, with cm-sized fragments of stromatoporoids, chaetetids and corals and variable proportions of oncoids, developed in foreshoal to offshore-proximal areas.

The selected facies for the analysis of oncoid types performed here correspond to facies belonging to the oncolitic-dominated and stromatoporoid/chaetetid/coral-rich facies associations, with significant volume percentages of oncoids (Figs. 3 and 4). In particular, these facies correspond to: 1) Oncolitic W to P facies, developed in the lagoon, including from 20 to 40% of oncoids; 2) Oncolitic-stromatoporoid W to G facies surrounding stromatoporoid carpets, developed in the lagoon and backshoal areas, showing between 10 and 30% of oncoids; 3) Oncolitic P and G facies, with higher proportions of oncoids (from 20 to 60%), even recording oncolitic-supported textures (>40%; Fig. 2B, C), formed in backshoal, shoal-sand blanket and foreshoal subenvironments, which grade laterally (along strike) into peloidal and oolitic-dominated facies; and 4) inter-buildup stromatoporoid-chaetetid-coral and oncolitic W to G facies, including from 10 to 30% of oncoids, laterally associated to chaetetid-stromatoporoid-coral buildups of foreshoal and offshore-proximal areas.

The down-dip (W-E) facies distribution in sedimentary units 1–4 analysed by Sequero et al. (2019) (i.e. peloidal and oolitic-dominated, oncolitic-dominated and stromatoporoid/chaetetid/coral-rich facies associations; Fig. 4) indicates that the widest record of oncoids is observed in units 1 and 2, with the development of extensive oncolitic-dominated backshoal-shoal-foreshoal subenvironments (oncolitic P and G facies; e.g. sections ME2 and A1), and of oncolitic inter-buildup facies (stromatoporoid-chaetetid-coral and oncolitic W to G) in foreshoal and offshore-proximal areas (e.g. sections J3 and F3). Oncolitic W to P lagoon facies is only recorded in unit 3 in the northwestern area (i.e. section ME1). Oncolitic-stromatoporoid W to G facies is distributed as small patches from the lagoon to backshoal areas in sedimentary units 2 to 4 (e.g. sections ME1 and TO). In units 3 and 4, the lateral extent of the backshoal-shoal-foreshoal oncolitic-dominated facies is reduced, and the oncolitic inter-buildup facies is constrained to the southwest (e.g. sections F3 and F5).

5. Oncoid types

The oncoids recorded in the Higueruelas Formation display a wide variability in size, shape and internal structure. They show well-

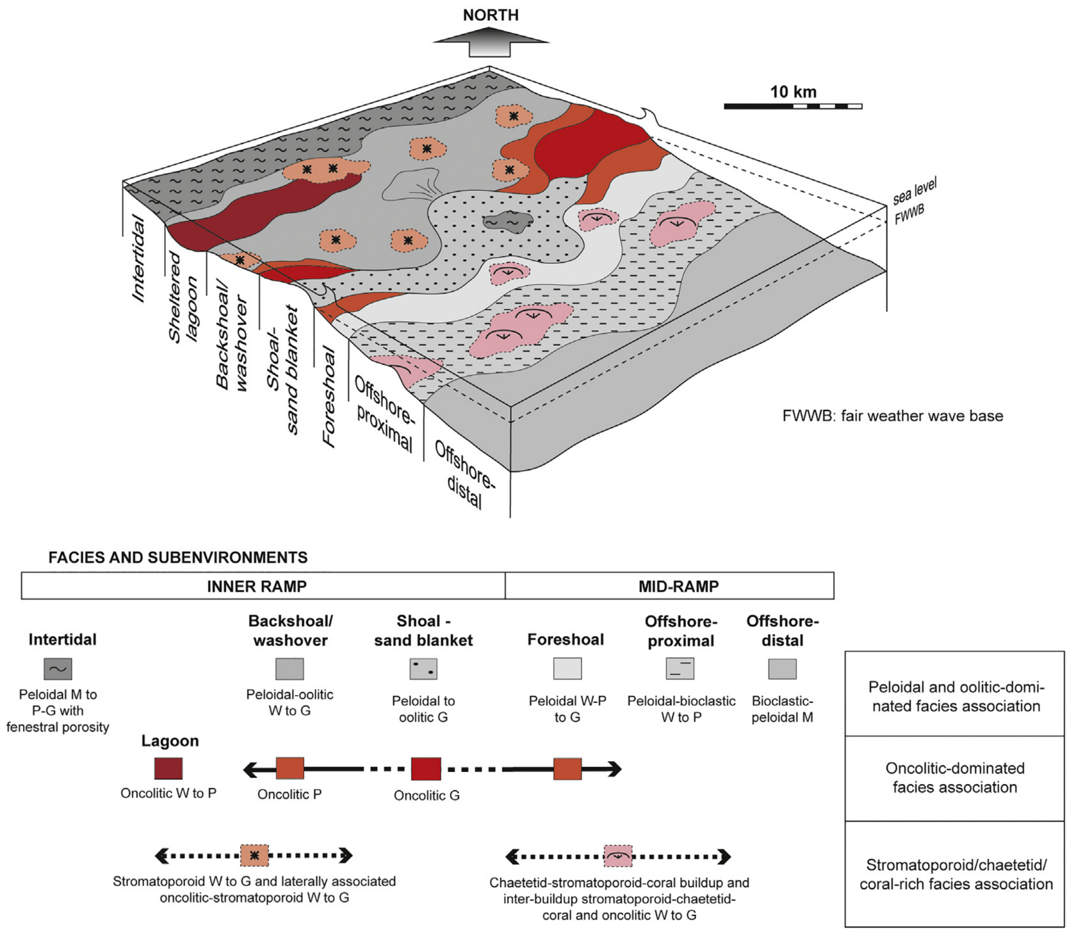

Fig. 3. Sedimentary model showing the three facies associations distribution on the latest Kimmeridgian shallow carbonate ramp (modified from Sequero et al., 2019).

rounded to irregular shapes, few millimetres to several centimetres in diameter, bioclastic and intraclastic nuclei when present, and cortex of variable thickness. On the basis of the internal structure of the cortex, six types of oncoids are defined: types I, II, IIIa, IIIb, IVa and IVb oncoids. Types I, II, III and IV follow the nomenclature of Dahanayake (1977), and subtypes a and b for oncoids of types III and IV are proposed here. Main characteristics of oncoids are illustrated in Figs. 5–8 and summarized in Fig. 9.

Type I oncoids are spherical to elliptical in shape, and have diameters of a few millimetres. The cortex is composed of continuous micritic laminae, without micro-encrusters (Fig. 5a–d).

Type II oncoids have up to 1 cm in size, are sub-spherical to irregular in shape with smooth contours, and are composed of micritic laminae with discontinuous organism-bearing laminae of mostly *Bacinella irregularis* (Radoicic, 1959; Fig. 5e–h), which represents a cyanobacterial structure (e.g. Schmid, 1996; Dupraz, 1999; Shiraishi and Kano, 2004). *Lithocodium aggregatum* (Elliott, 1956) is also present in these oncoids, which is attributed to colonies of calcified cyanobacteria (Cherchi and Schroeder, 2006). Other organisms (e.g. serpulids, sponges) are eventually included in the cortex (Fig. 9).

Type III oncoids have diameters up to 3 cm, and are spherical to irregular in shape with wavy contours. They are composed by alternating continuous and concentric micritic and organism-bearing laminae of mostly *Bacinella-Lithocodium* association (Figs. 6 and 8a), with the common presence of other micro-encrusters (e.g. *Troglotella incrustans*: Wernli and Fookes, 1992; Fig. 8d). Serpulids, sponges and foraminifera are also included in the cortex. Two varieties, i.e. types IIIa and IIIb oncoids, are differentiated based on the thickness of micritic and organism-bearing laminae: type IIIa oncoids, smaller in size (up to 2 cm), show alternating micritic and organism-bearing laminae with similar thickness (0.25 to 1 mm-thick; Fig. 6a–d), whereas type IIIb oncoids are more irregular in shape and are formed by alternating thinner micritic laminae and thick organism-bearing laminae (micritic laminae up to 0.2 mm-thick; Fig. 6e–h).

Type IV oncoids have a wide range of sizes and display irregular to very irregular shapes with lobate contours. Two varieties are differentiated, i.e. types IVa and IVb oncoids, regarding the characteristics of the cortex. Type IVa oncoids are few millimetres to 7 cm in diameter, and are exclusively formed by a microbial meshwork with a high diversity of micro-encrusters (mostly *Bacinella-Lithocodium* association, and common *Thaumatoporella parvovesiculifera*, *Cayeuxia-Ortonella* and *Girvanella*; Figs. 7a–d and 8b, c), and also sponges and foraminifera. Type IVb oncoids are up to 1 cm in diameter, display irregular shapes with wavy contours and have thick cortex entirely formed by several superimposed layers of *Lithocodium aggregatum* (Fig. 7e–h).

6. Oncoid distribution

Analysis of the abundance of the described oncoid types across the logged sections (see selected logs in Figs. 10–13) indicates that these types of oncoids have a preferential distribution and abundance in the oncolitic-dominated and stromatoporoid/chaetetid/coral-rich facies associations, thus allowing recognizing their spatial distribution from lagoon to offshore-proximal domains of the carbonate ramp. Figs. 14 and 15 illustrate the volume percentage of oncoids compared with the facies maps of stratigraphic units 1–4 in Sequero et al. (2019).

Sedimentary unit 1 (Fig. 14A) records deposition from backshoal to offshore-distal subenvironments. During this stage, greater abundance of oncoids (>40%) is recorded in backshoal-shoal-foreshoal oncolitic P and G facies. In particular, these facies include dominant types II and

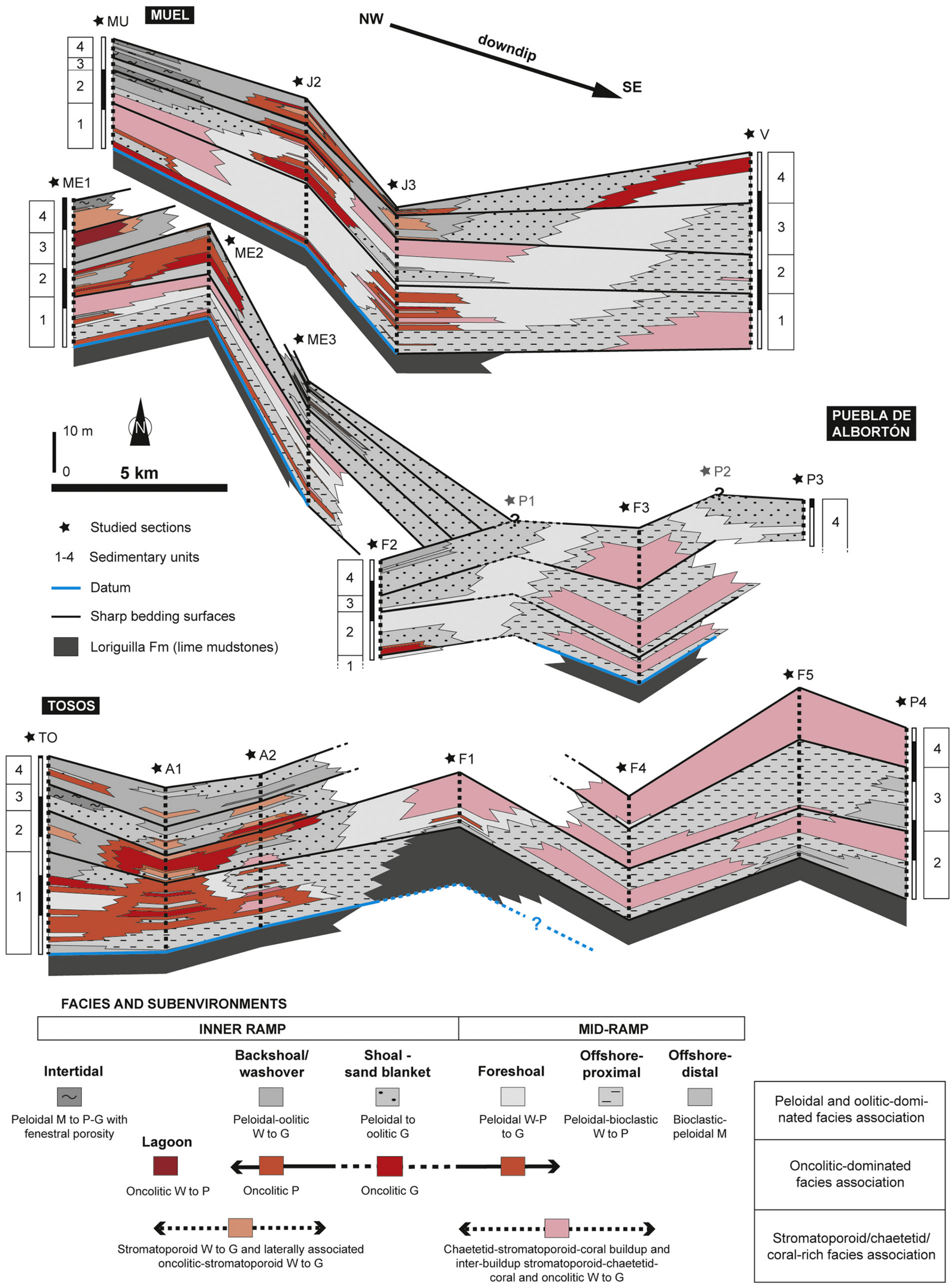

Fig. 4. Facies distribution in the three cross-sections (modified from Sequero et al., 2019). Log correlation was based on the identification of time-equivalent sharp bedding surfaces (black lines) bounding four sedimentary units (1–4). The lower datum for correlation (indicated in blue line) corresponds to the boundary between the Higueruelas Formation and the underlying Loriguilla Formation (sequence Ki2; see Fig. 1B). Sections P1 and P2 (in grey colour) do not record the deposition of sedimentary units 1–4, but the inferred lateral facies correlation is included in this work. (For interpretation of the references to colour in this figure legend, the reader is referred to the web version of this article.)

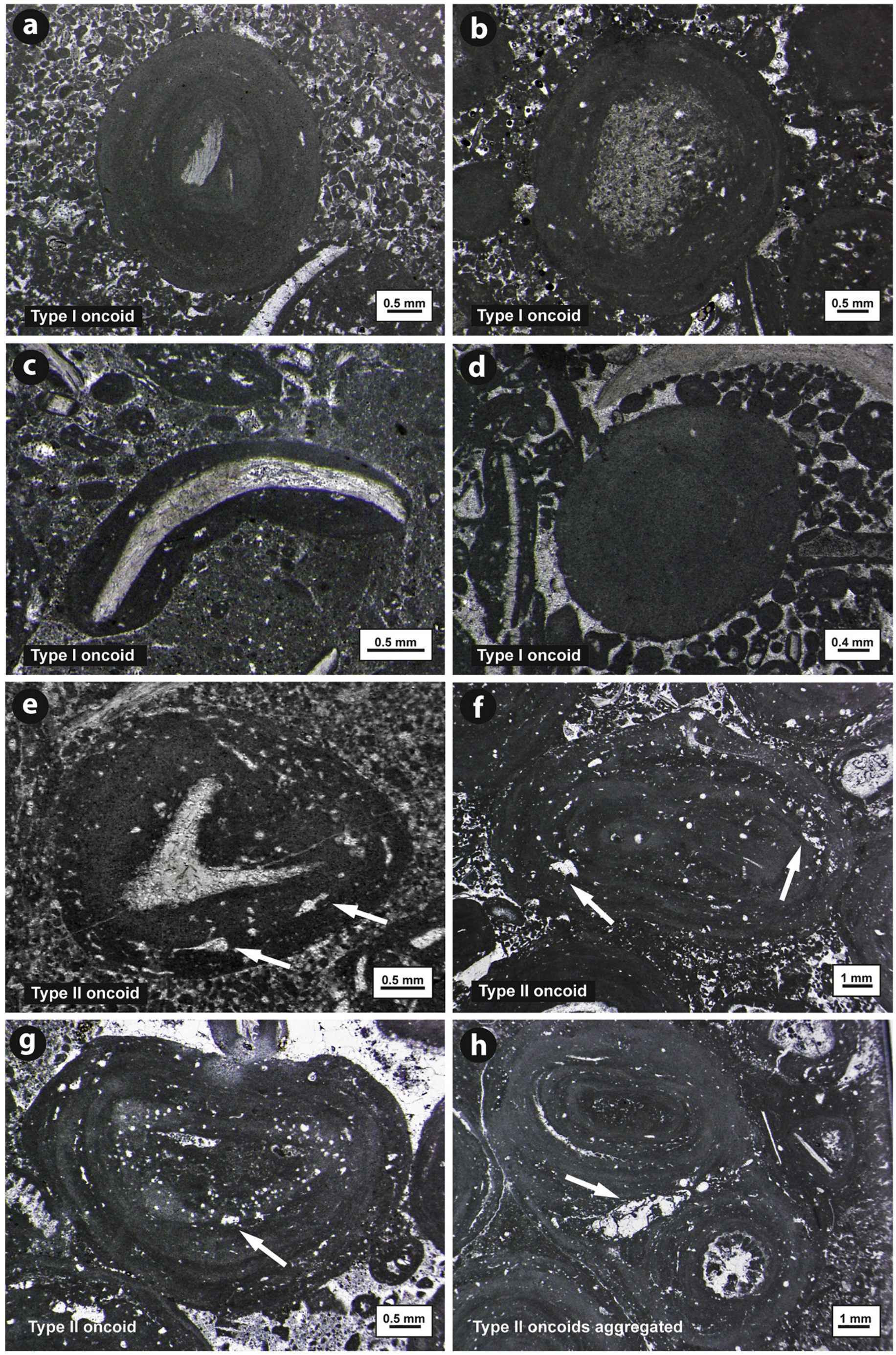

Fig. 5. (a–d) Type I oncoids. (a, b) Spherical and well-rounded type I oncoids showing thick (a) and thin (b) micritic laminae, with fragments of brachiopod and stromatoporoid as nucleus, respectively. Type I oncoid in (a) belongs to oncolitic inter-buildup facies in Puebla de Albortón sector, section P2 (see Fig. 1C). Type I oncoid in (b) belongs to section J2 (Jaulín sector), thin section 45 (see Fig. 11). (c) Elongate type I oncoid with a large fragment of brachiopod as nucleus. Section J3. (d) Spherical and well-rounded type I oncoid with no visible nucleus and diffuse micritic laminae. Section J2, thin section 24. (e, h) Type II oncoids, showing thick micritic crusts with sparitic patches of *Bacinella irregularis* (white arrows). (e) Millimetre-sized type II oncoid with a fragment of bivalve as nucleus. Section A2 (Aguilón sector), thin section 8 (see Fig. 12). (f, g) Elliptical type II oncoids with no visible nucleus and smooth contours. Section J2, thin sections 26 and 29, respectively. (h) Type II oncoids aggregated by *Bacinella irregularis* (arrow), showing bioclastic nuclei (lituolid, top left; coral, bottom right). Section J2, thin section 28.

IIIa oncoids. By contrast, in foreshoal to offshore-proximal inter-buildup stromatoporoid-chaetetid-coral and oncolitic W to G facies, oncoids are less abundant (up to 30%), and mainly correspond to types IIIa and IVa oncoids.

Sedimentary unit 2 allows characterizing the oncoid distribution from backshoal to offshore-proximal subenvironments (Fig. 14B). Oncolitic-stromatoporoid W to G facies laterally associated to stromatoporoid W to G recorded in backshoal areas, is dominated by type IVa oncoids in relative high abundance (up to 25%). Oncoids are abundant in the oncolitic-dominated backshoal to foreshoal facies (percentages >40%), being type II oncoids dominant and occasionally type IIIa oncoids in the backshoal domain. Types II, IIIa and IVa oncoids (percentages up to 30%) characterize the oncolitic inter-buildup facies of foreshoal and offshore-proximal areas. Type IVb oncoids are only

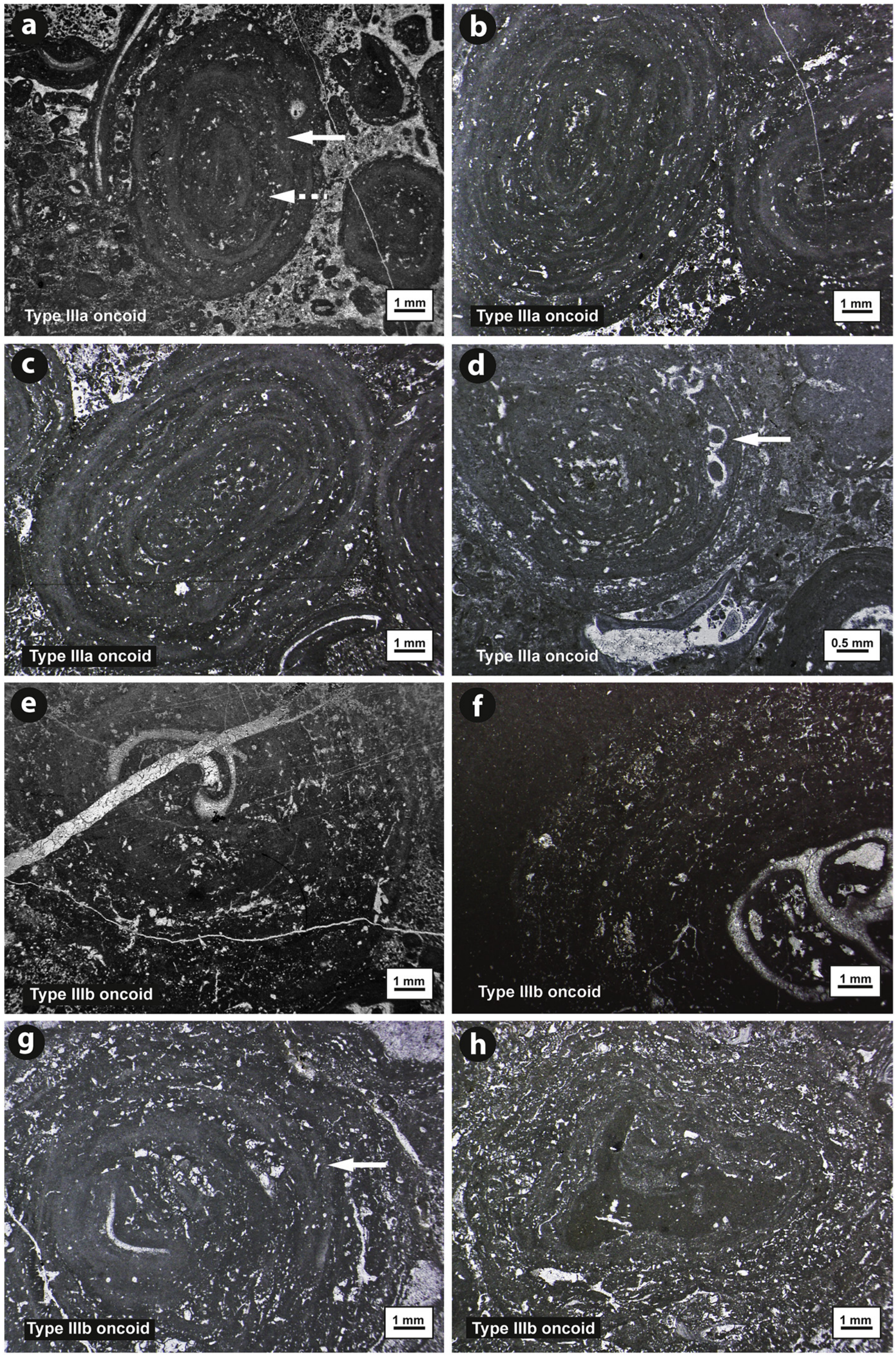

Fig. 6. (a–d) Type IIIa oncoids showing thick crusts with alternating continuous and concentric micritic and organism-bearing laminae of similar thickness (white and dashed arrows in a, respectively), elliptical shapes and smooth contours. Occasionally serpulid worms colonized the oncoid surface, and then were integrated into the cortex (white arrow in d). Sections A1 (a, thin section 9), ME2 (b, thin section 12), TO (c), and ME1 (d, thin section 1) (see Figs. 10–12). (e–h) Type IIIb oncoids showing irregular shapes with wavy contours, with cortex constituted by irregular organism-bearing laminae of mainly *Bacinella-Lithocodium* and thinner micritic laminae. Bioclastic nuclei (e.g. gastropods in e, f) are common. Micritic laminae can also appear as discontinuous (white arrow in g). Sections A1 (e, thin section 17), ME1 (f, thin section 46), J2 (g, thin section 39) and ME3 (h).

recorded in the peloidal-dominated offshore-proximal domain, together with millimetre-sized types I, II and IVa oncoids (<10% total percentage).

In sedimentary units 3 and 4 (Fig. 15), oncolitic-dominated facies that characterized the backshoal to foreshoal domains are reduced in extension, compared with previous stages. In sedimentary unit 3 (Fig. 15A), lagoon oncolitic W to P facies is recorded, being characterized by large and irregular types IVa and IIIb oncoids (up to 40% total percentage). The oncolitic-dominated backshoal and shoal-sand blanket subenvironments are dominated by type IIIb oncoids (>40% total percentage). Oncolitic-stromatoporoid W to G facies is not recorded here laterally associated to stromatoporoid W to G facies, and total percentage of oncoids in these stromatoporoid carpets is not significant (<5%). The oncolitic inter-buildup facies is well-developed in the offshore-proximal domain, and is characterized by type IVa oncoids among other oncoid types (up to 30%).

Type IVa oncoids also predominate in the lagoon and backshoal oncolitic-stromatoporoid W to G facies in sedimentary unit 4 (up to

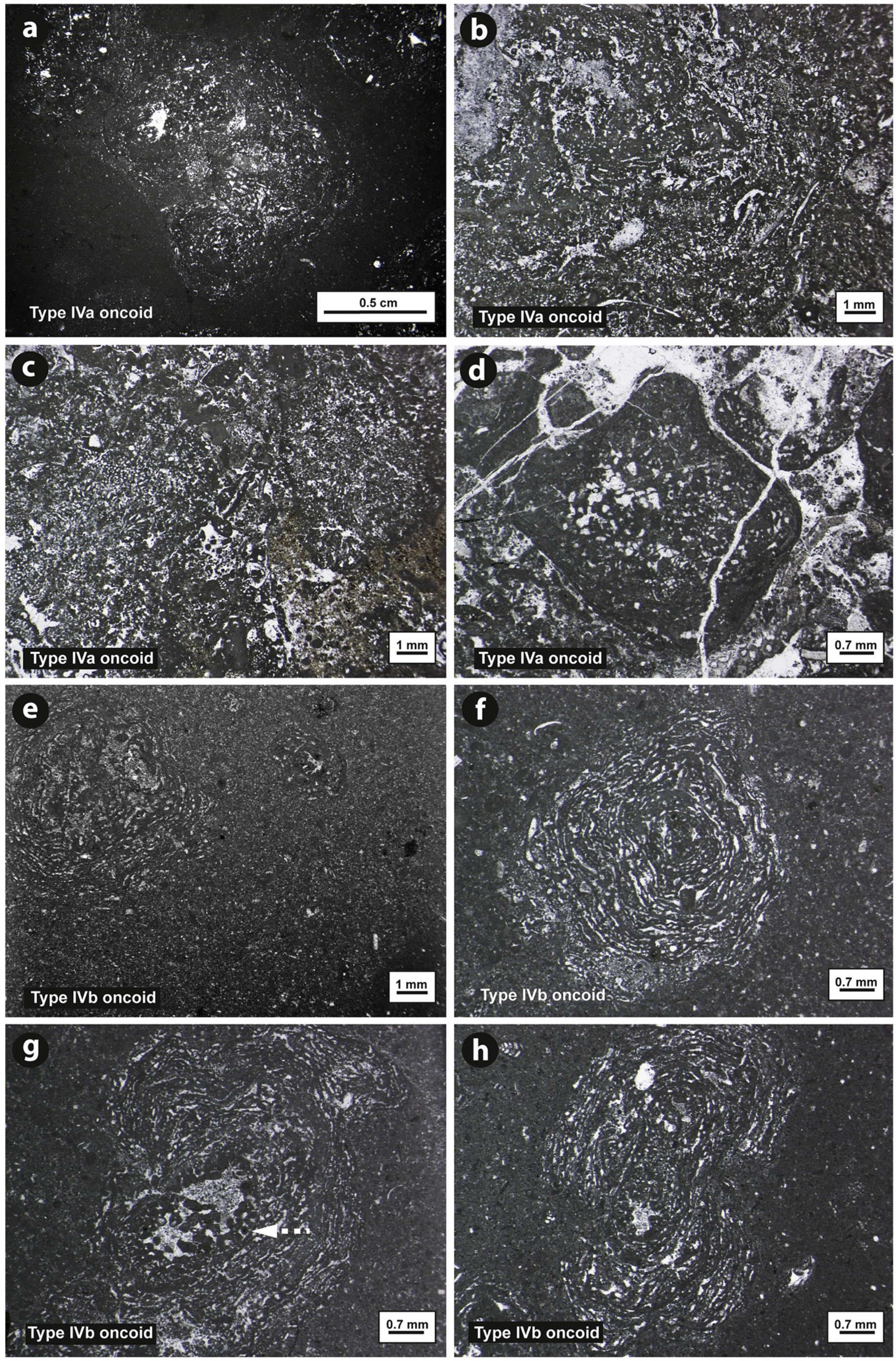

Fig. 7. (a–d) Type IVa oncoids with irregular and lobate contours, entirely composed of a microbial meshwork with a high-diversity of micro-encrusters, mainly *Bacinella irregularis*. Sections ME1 (a, thin section 43), J3 (b), ME3 (c, thin section 34) and A1 (d, thin section 33) (see Figs. 10–12). (e–h) Irregular type IVb oncoids, entirely composed of thick crusts with continuous organism-bearing laminae of *Lithocodium aggregatum*. Bioclastic nuclei are common, mainly lituolids (dashed arrow in g). Sections F4 (e), F3 (f, g, proximal to sample 26; see Fig. 13) and V (h).

30%; Fig. 15B), and in the backshoal oncolitic P facies together with type II oncoids (>40%). In the mid-ramp, types II and IIIa oncoids dominate in the foreshoal oncolitic P facies (>40%), and also in the inter-buildup stromatoporoid-chaetetid-coral and oncolitic W to G facies together with type IVa oncoids (up to 30%). Scarce type IVb oncoids also appear in this facies (<10%).

Based on the described volume proportion of oncoids in sedimentary units 1–4, the down-dip distribution of the different oncoid types and their abundance in the studied carbonate ramp is proposed (Fig. 16). Spherical type I oncoids, characterized by continuous micritic laminae, are present (<10%) in all the defined subenvironments. Type II oncoids (sub-spherical, composed by micritic laminae with discontinuous organism-bearing laminae of mostly *Bacinella irregularis*) and type IIIa oncoids (irregular to spherical, with alternating continuous and concentric micritic and organism-bearing laminae of *Bacinella irregularis-Lithocodium aggregatum*) are common to abundant in the oncolitic backshoal-shoal-foreshoal environment, laterally related to peloidal-oolitic shoals (see Figs. 14 and 15), being type II oncoids the most abundant (>20%) in the oncolitic shoal and type IIIa oncoids generally in the foreshoal domain. Type IIIb oncoids (with thicker

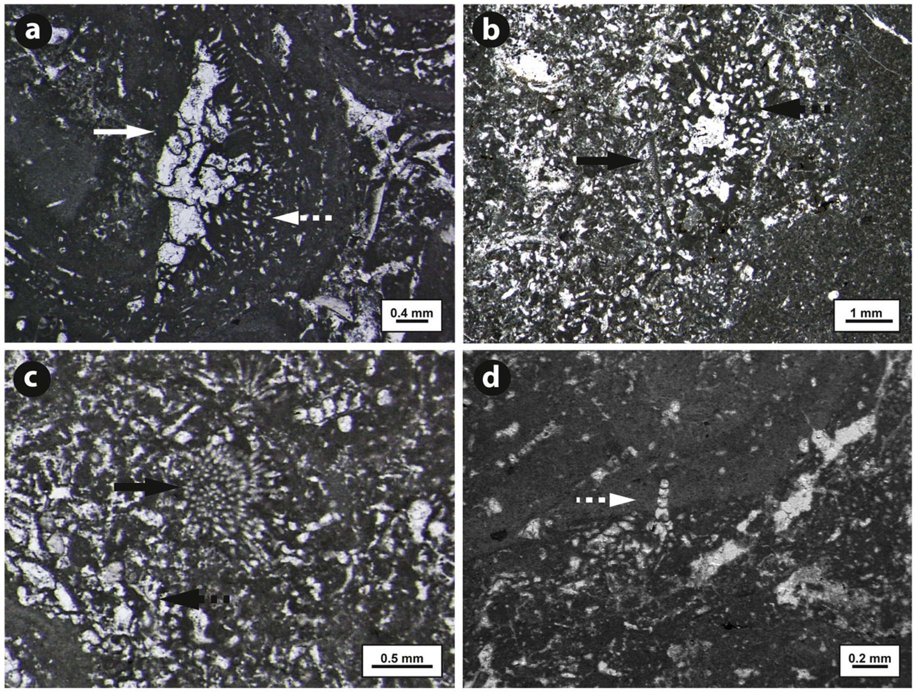

Fig. 8. Detailed view of micro-encrusters in oncoids. (a) Vesicular structure of *Bacinella irregularis* (white arrow) associated with *Lithocodium aggregatum* (dashed arrow) in type IIIa oncoid. Section J2, thin section 38 (see Fig. 11). (b) *Thaumatoporella parvovesiculifera* (black arrow) and *Bacinella-Lithocodium* association (dashed arrow) in type IVa oncoid. Section ME1, thin section 46 (see Fig. 10). (c) *Cayeuxia-Ortonella* (black arrow) surrounded by *Bacinella irregularis* (dashed arrow) in type IVa oncoid. Section J3. (d) *Troglotella incrustans* (dashed arrow) in type IIIa oncoid. Section A1, thin section 10 (see Fig. 12).

organism-bearing laminae) and irregular type IVa oncoids (exclusively formed by a microbial meshwork mostly of *Bacinella-Lithocodium*) characterize the lagoon, being mainly dominated by type IVa oncoids. Type IVa oncoids are also common in the lagoon to backshoal oncolitic-stromatoporoid W to G and foreshoal to offshore-proximal inter-buildup stromatoporoid-chaetetid-coral and oncolitic W to G facies, the latter also characterized by types II and IIIa oncoids. Millimetre-sized and irregular type IVb oncoids (with thick cortex entirely formed by *Lithocodium aggregatum*) are present in the offshore-proximal peloidal and oncolitic inter-buildup facies.

		Type I	Type II	Type IIIa	Type IIIb	Type IVa	Type IVb
Morphological characteristics	Size	few millimetres	few millimetres to 1 cm	few cms (up to 2 cm)	few cms (up to 3 cm)	few mms to 7 cm	few mms to 1 cm
	Shape	elliptical to spherical	sub-spherical to irregular with smooth contours	spherical to irregular with wavy contours	irregular, wavy contours	very irregular, lobate contours	irregular, wavy contours
Internal structure of the cortex	Lamination type	concentric and continuous micritic laminae	micritic laminae with discontinuous organism-bearing laminae	alternating continuous and concentric micritic and organism-bearing laminae	alternating organism-bearing with thin micritic laminae, usually continuous	microbial meshwork, no lamination	organism-bearing continuous laminae
	Micro-encrusters	absence of micro-encrusters	mostly *Bacinella irregularis*, also *Lithocodium aggregatum*	mostly *Bacinella irregularis* and *Lithocodium aggregatum; common Girvanella, Thaumatoporella parvovesiculifera, Cayeuxia-Ortonella, Troglotella incrustans*			*Lithocodium aggregatum*
	Bioclasts		serpulids, sponges, echinoderms, bivalves, brachiopods, corals, stromatoporoids, foraminifera (lituolids), gastropods, dasycladacean algae				
	Others			peloids, ooids			
Subenvironment		backshoal to offshore-distal	lagoon to offshore-distal	backshoal to offshore-proximal	lagoon to offshore-proximal	lagoon to offshore-proximal	foreshoal to offshore-proximal
Frequent oncoid association		II, IVa	I, IIIa, IVa	II, IVa	II, IIIa, IVa	II, IIIa, IIIb	I, II, IVa

Fig. 9. Oncoid types identified in the Higueruelas Formation. Descriptions of morphology and internal structure of the oncoids, depositional subenvironment conditions and frequent oncoid associations are indicated.

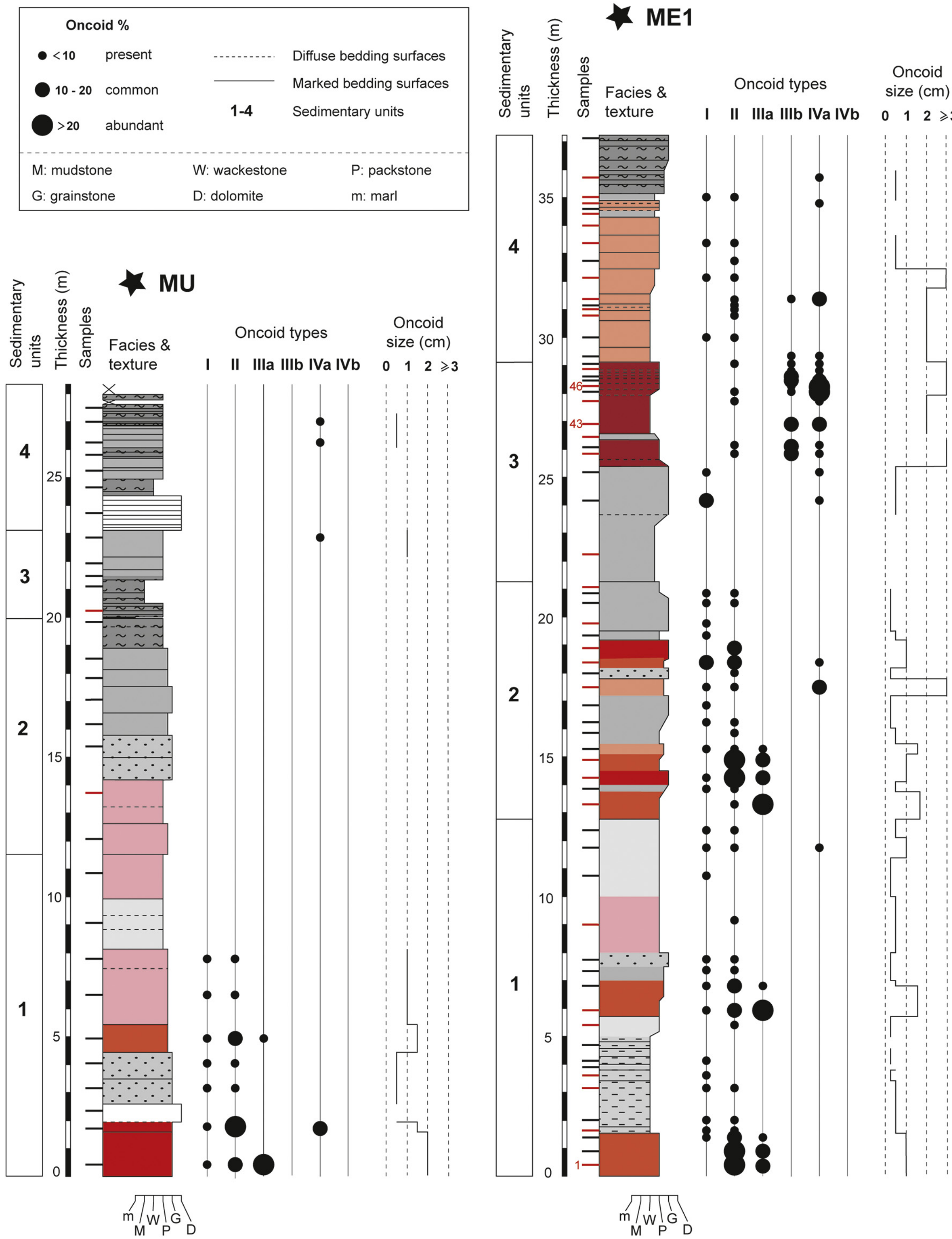

Fig. 10. Distribution, abundance and size of the different oncoid types in sections MU and ME1 (Muel and Mezalocha sectors, respectively; see Fig. 1C). Samples in red colour include petrographic description on thin section. Oncoid % refers to proportion of this non-skeletal component in relation to the total volume of the sample. Facies legend is included in Fig. 13. (For interpretation of the references to colour in this figure legend, the reader is referred to the web version of this article.)

7. Discussion

7.1. Factors controlling oncoid growth and distribution

Oncoid morphology and internal structure, which mainly reveal the degree of agitation and the palaeoecological conditions, can help in deciphering characteristics of the depositional subenvironments (e.g. Peryt, 1983; Wright, 1983; Ratcliffe, 1988). Fig. 17A summarizes the deduced conditions of water energy and diversity of micro-encrusters (related to palaeoecological conditions) for the described oncoids.

As a general rule, rounded morphology and well-defined micritic laminae in oncoids (i.e. types I and II) is consequence of turbulent waters, whereas lower-energy conditions result in irregular shapes, occasional discontinuous laminae and microbial encrustations (i.e. types III and IV oncoids) (Dahanayake, 1978; Peryt, 1983; Wright, 1983). In the case studied here, the percentage of high-energy type I oncoids

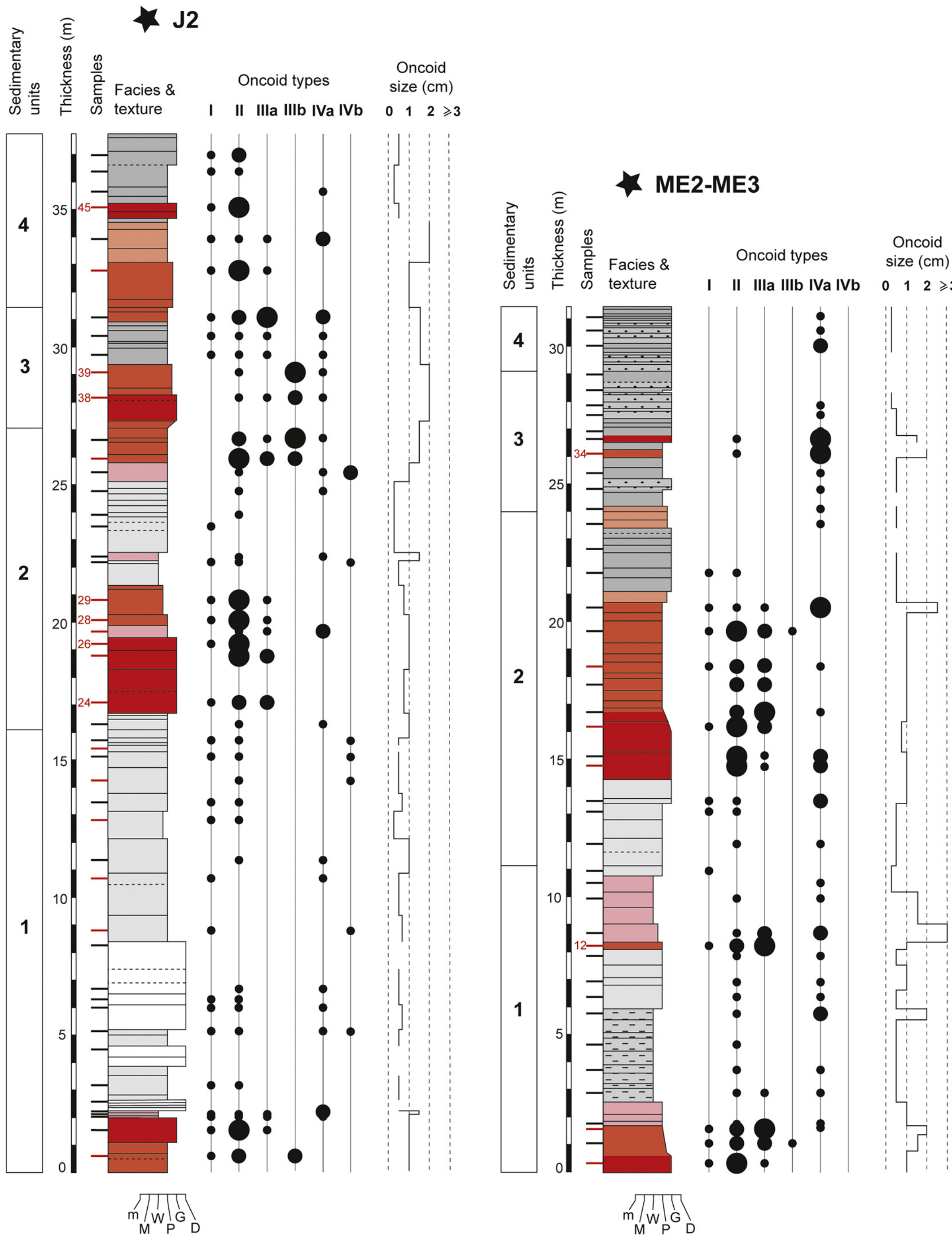

Fig. 11. Distribution, abundance and size of the oncoid types in section J2 and compiled section ME2-ME3 (Jaulín and Mezalocha sectors, respectively). Samples in red colour include petrographic description on thin section. (For interpretation of the references to colour in this figure legend, the reader is referred to the web version of this article.)

(e.g. Dahanayake, 1977) is not significant (<10%; see Fig. 16), so they are not included in Fig. 17A. The sub-spherical type II (composed by micritic laminae with discontinuous organism-bearing laminae) and irregular to spherical type IIIa oncoids (with alternating micritic and organism-bearing laminae with similar thickness) are preferentially formed in high- to moderate-energy inner- to mid-ramp domains (i.e. backshoal to foreshoal subenvironments; Fig. 17A), with a preferential distribution of type II oncoids in higher-energy inner areas (i.e. shoal-sand blankets) and type IIIa oncoids in moderate-energy mid-ramp areas (i.e. foreshoal). Type IIIb oncoids (with thicker organism-bearing laminae) formed preferentially in lower-energy inner areas, i.e. in the sheltered lagoon (see Fig. 16). This distribution of types II, IIIa and IIIb oncoids is coherent with previous interpretations relating alternation of micritic laminae with more agitated episodes, and organism-bearing laminae with calm periods during which bacterial growth occurs (Dahanayake, 1978; Védrine et al., 2007). Large type IVa oncoids, which are entirely composed of a microbial meshwork, occur abundantly in the more protected low-energy inner areas (i.e. sheltered lagoon), and are also common in moderate-energy inner areas (i.e. backshoal oncolitic-stromatoporoid W to G facies) and generally in low-energy mid-ramp domains (i.e. offshore-proximal inter-buildup facies). The predominance of large microbial oncoids in inner areas of the carbonate ramp was determined by the presence of shoal-sand blankets seaward, that acted as a barrier for water energy and favoured the occurrence of

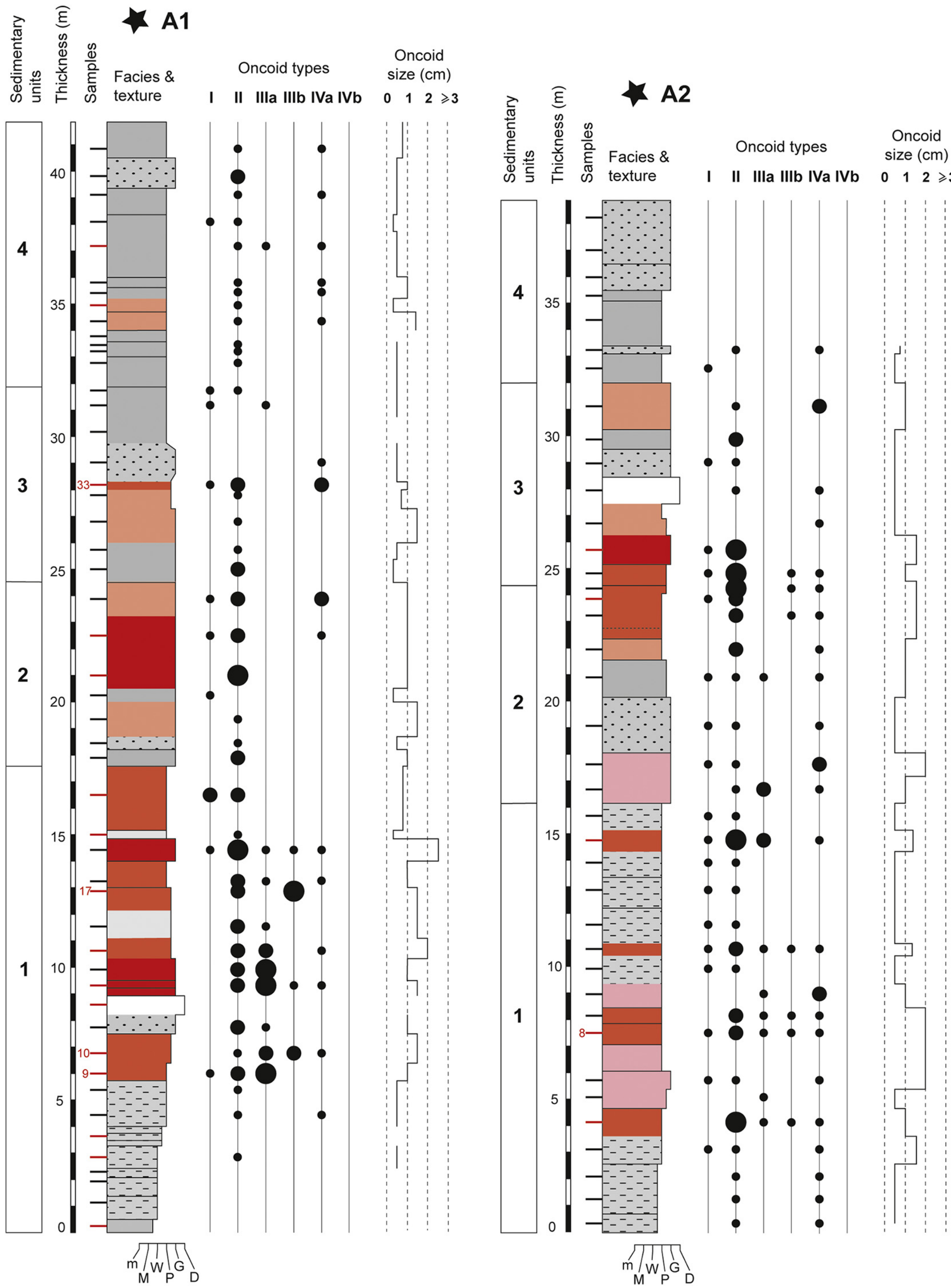

Fig. 12. Distribution, abundance and size of the oncoid types in sections A1 and A2 (Aguilón sector). Samples in red colour include petrographic description on thin section. (For interpretation of the references to colour in this figure legend, the reader is referred to the web version of this article.)

long periods under calm conditions when microbial activity dominate. Short higher-energy episodes in this area are highlighted by the common presence of irregular type IIIb oncoids. However, type IVb oncoids (exclusively formed by *Lithocodium aggregatum*) preferentially grew in distal areas of the mid-ramp (offshore-proximal subenvironment; Fig. 16), in low-energy conditions.

Analysis of micro-encrusters in organism-bearing laminae recorded in types III and IVa oncoids (Fig. 17A) reflects high-diversity micro-encrusters associations (Flügel, 2004), mostly consisting of *Bacinella* and *Lithocodium* as main micro-encrusters but also *Thaumatoporella parvovesiculifera*, *Girvanella*, *Cayeuxia-Ortonella* and/or *Troglotella* (Fig. 9). The presence of these light-dependant micro-encrusters implies clear and normal-marine waters and oligotrophic conditions (e.g. Leinfelder et al., 1993; Dupraz and Strasser, 1999; Wetzel and Strasser, 2001). Since the micro-encrusters association is similar in oncoids characterized from inner- to mid-ramp domains, no differentiation in trophic conditions is assumed for these subenvironments. However, the presence in offshore-proximal areas of type IVb oncoids exclusively formed by *Lithocodium aggregatum* meshwork is open to interpretation, as no other evidences such as variations in the bioclastic content have

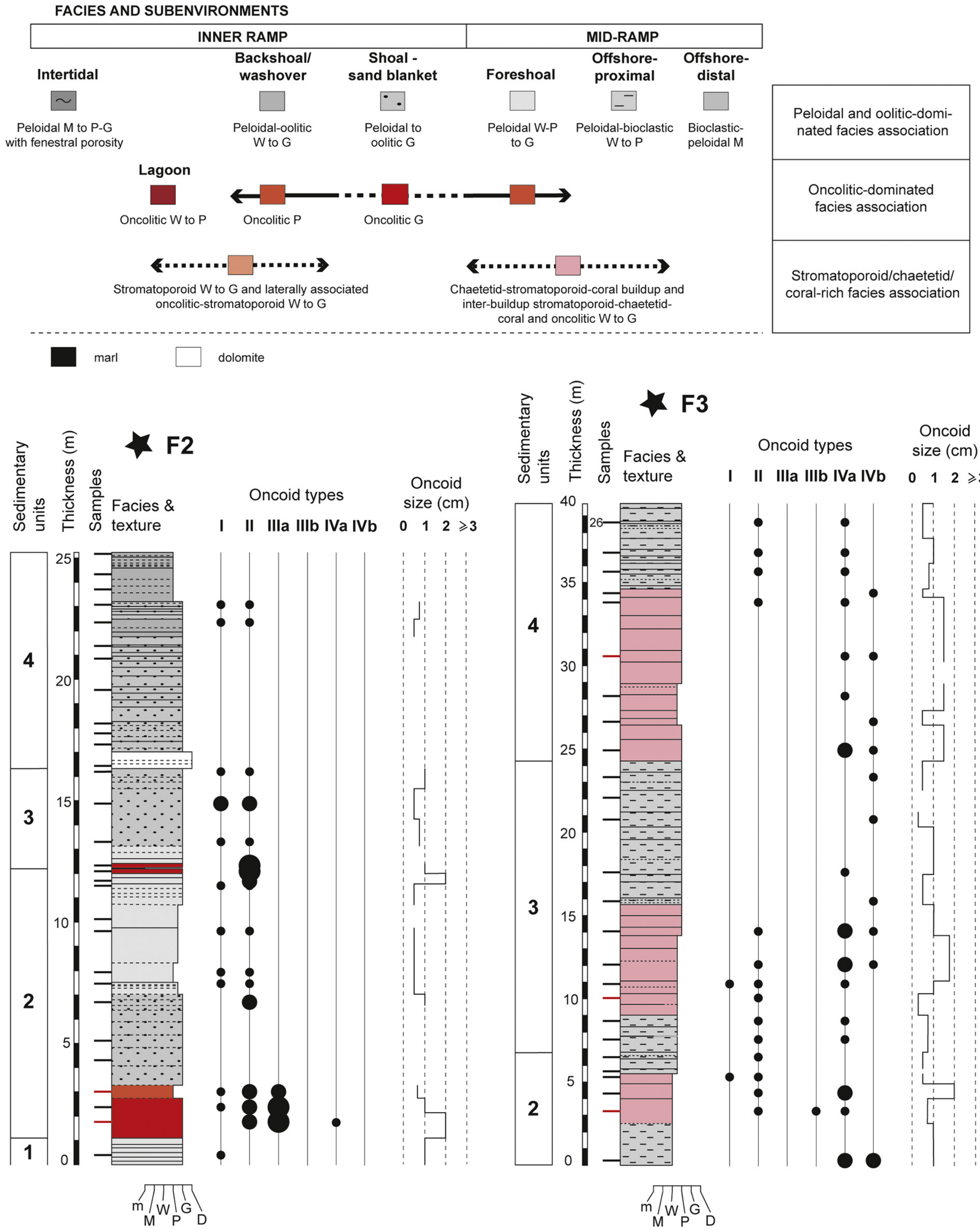

Fig. 13. Distribution, abundance and size of the oncoid types in sections F2 and F3 (Fuendetodos sector). Samples in red colour include petrographic description on thin section. (For interpretation of the references to colour in this figure legend, the reader is referred to the web version of this article.)

been recognized. These "*Lithocodium*-oncoids" are occasionally found in the inter-buildup facies together with types III and IVa oncoids, which include a high-diversity of micro-encrusters (Fig. 15B).

In summary, the distribution obtained for the different oncoids described in the shallow areas of the latest Kimmeridgian carbonate ramp highlights that specific oncoid types characterize certain depositional settings. Types II and III oncoids characterize moderate to high-energy inner- to mid-ramp areas (i.e. backshoal to foreshoal areas), whereas type IV oncoids are more abundant in low-energy subenvironments (i.e. sheltered lagoon). High-diversity of light-dependant micro-encrusters in types III and IV oncoids reflects clear and normal-marine waters, and oligotrophic conditions, being open to interpretation the presence of *Lithocodium* (type IVb) oncoids in offshore-proximal areas.

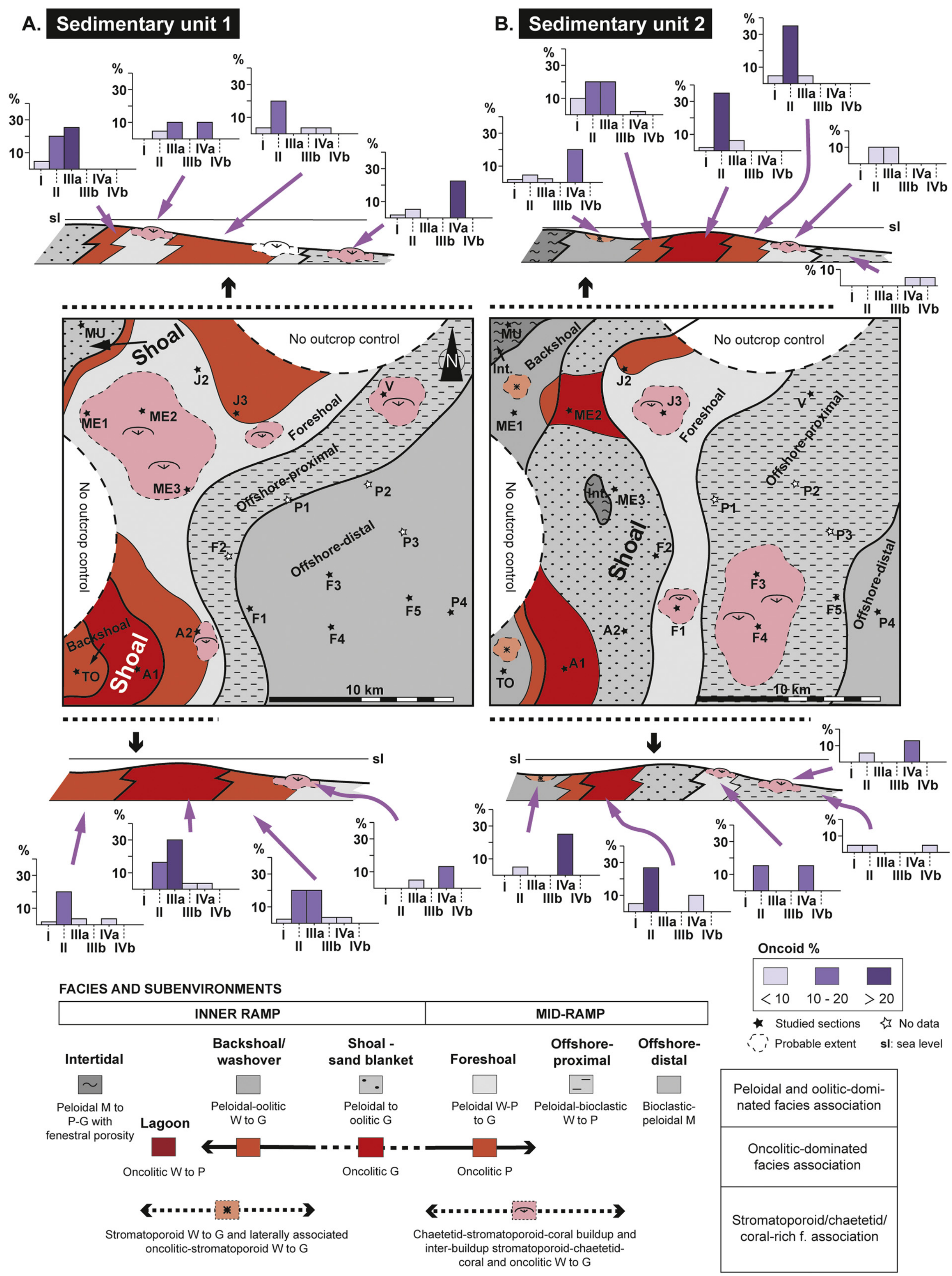

Fig. 14. Volume percentage of the oncoid types compared with the facies maps reconstructed for sedimentary units 1 (A) and 2 (B) (facies maps modified from Sequero et al., 2019), along selected transects indicated in dashed lines. White colour for stromatoporoid/chaetetid/coral-rich facies in the selected transects refers to volume percentage of oncoids <10%.

Similar to Dahanayake (1977) scheme, the oncoid classification for shallow-marine environments proposed here is based in the configuration of the different types of laminae identified in the cortex, i.e. micritic and organism-bearing laminae (types I, II and III oncoids), as well as the absence of micritic laminae (type IV oncoids). However, the revised nomenclature described here also considers thickness of organism-bearing laminae as a relevant feature that should be taken into account for palaeoenvironmental interpretations. In this regards, subdivision of

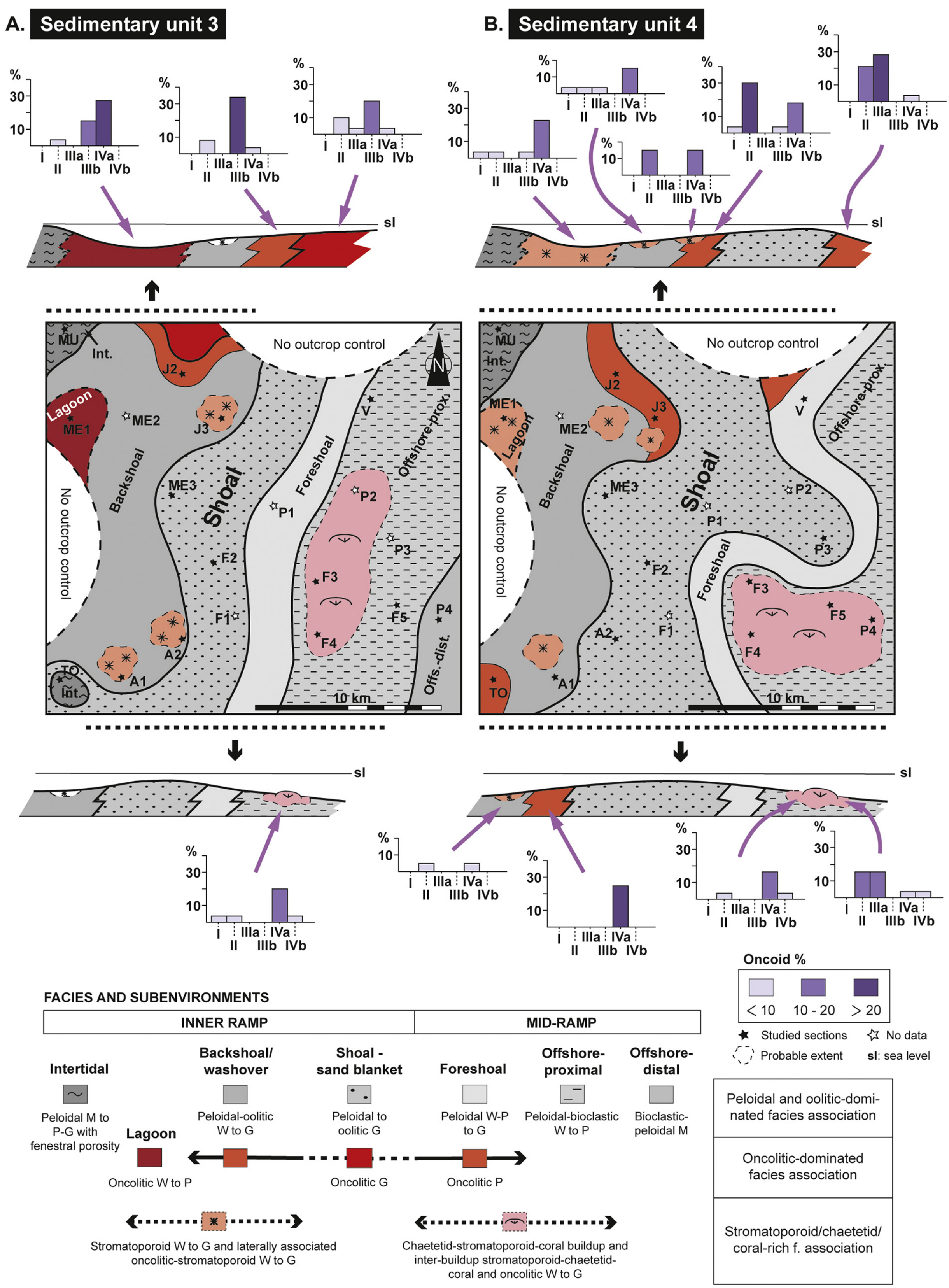

Fig. 15. Volume percentage of the oncoid types compared with the facies maps reconstructed for sedimentary units 3 (A) and 4 (B) (facies maps modified from Sequero et al., 2019), along selected transects indicated in dashed lines. White colour for stromatoporoid/chaetetid/coral-rich facies in the selected transects refers to volume percentage of oncoids <10%.

type III oncoids of Dahanayake (1977) into types IIIa and IIIb affords more information about the characteristics of the depositional subenvironments, as indicates their preferential distribution described above (Figs. 16 and 17A). Regarding type IV oncoids, the presence or absence of laminae of calcified microorganisms is the criteria used here to distinguish between types IVa (microbial meshwork) and

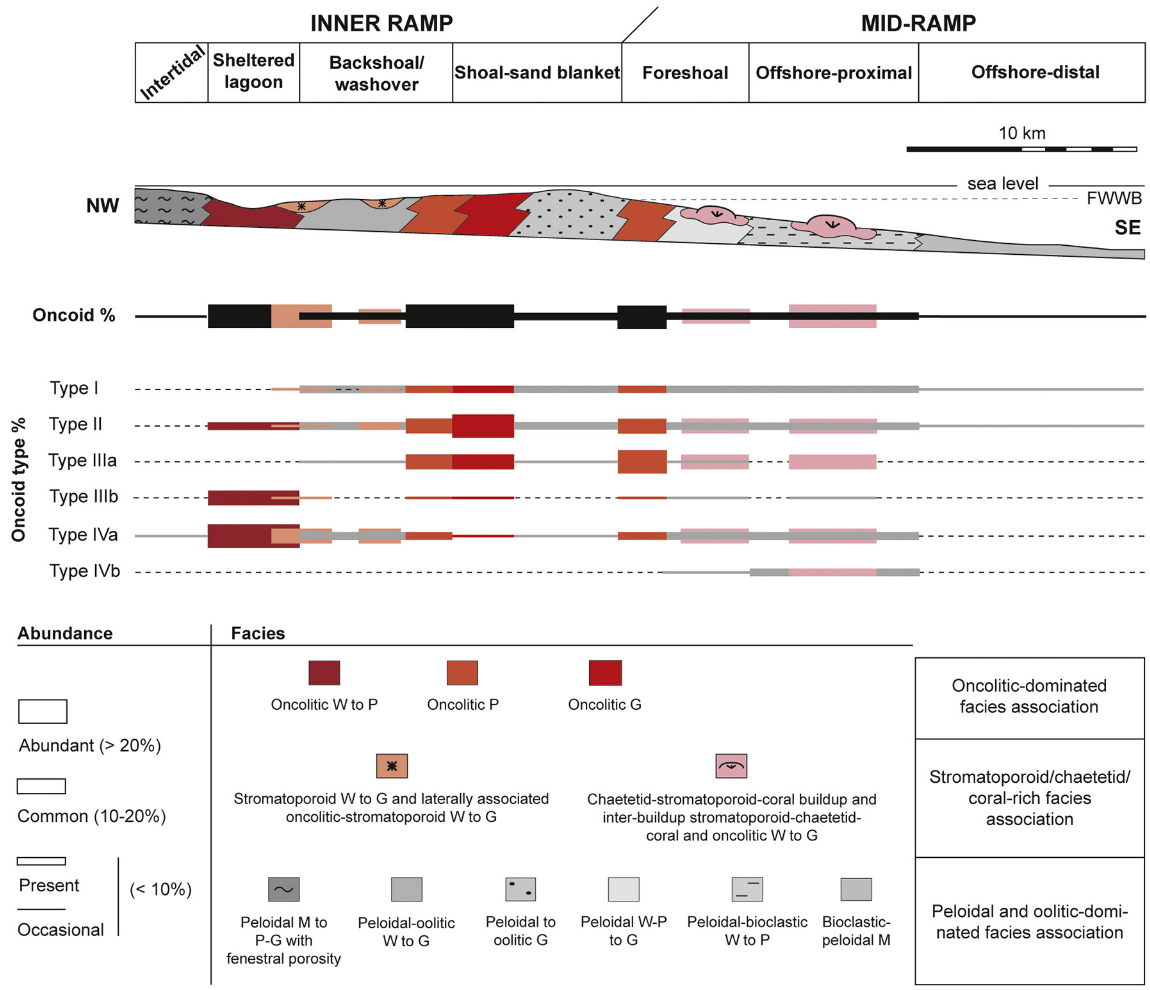

Fig. 16. Distribution and volume percentage of total oncoids (oncoid %) and of oncoid types (oncoid type %) in the schematic facies model proposed in Sequero et al. (2019). The distribution and volume percentage of the oncoid types for the peloidal and oolitic-dominated facies are also included (grey horizontal bars).

IVb oncoids (superimposed layers of calcified microorganisms), whereas Dahanayake (1977) classification only considers a group of type IV oncoids defined by a microbial meshwork (i.e. equivalent to type IVa oncoids).

The proposed classification for marine carbonate oncoids highlights the role of microbial activity in their generation combined with the variable influence of water energy, resulting in a wide spectrum of shapes, sizes and internal structures. Therefore, high-energy conditions result in smaller, well-rounded and laminated micrite-dominated oncoids (types I and II), whereas low- to very low-energy conditions are suitable for bacterial growth, with the generation of irregular microbial oncoids (types III and IV). Accordingly, the environmental factors described here as controlling oncoid formation agree with two of the main factors suggested in the literature for marine carbonate oncoids, i.e. activity of cyanobacteria and energy conditions (e.g. Dahanayake, 1978; Flügel, 2004; Riding, 2006; Pederson et al., 2015; Pingzhou et al., 2019).

It is important to remark that because other carbonate grains can show similar characteristics to those described for oncoids, their recognition can be sometimes challenging. In the literature, definitions given for oncoid generally refer to coated grains, larger than 2 mm in diameter, formed by a cortex of biogenic origin and variable thickness and shape surrounding a nucleus or nuclei (e.g. Tucker and Wright, 1990; Flügel, 2004). Nevertheless, the presence of nuclei is not diagnostic criteria for recognizing oncoids, as it is known that in-situ microbial accretion generates a particular type of oncoid, without a visible nucleus (i.e. type IV oncoids of Dahanayake, 1977). Biogenic origin of the cortex (both micritic laminae and organism-bearing laminae in Dahanayake, 1977) is the main criteria for identification oncoids. However, differentiation of type I oncoids from micritic ooids can also be complicated, as both can show concentric micritic laminae. In this work, a diameter larger than 2 mm is used as diagnostic for type I oncoids. Hence, distinction and classification of oncoids can be considered as a sum of characteristics (size, shape and internal structure) which reflect the balance between hydrodynamic conditions and microbial activity, either representing continuous grain overturning (micritic-dominated types I and II oncoids) and/or microbial accretion under calm conditions (types III and IV oncoids).

7.2. Comparison with similar studies

Distribution and palaeoenvironmental significance of different oncoid types have been previously analysed in an older Kimmeridgian carbonate ramp of the Iberian Basin, showing similar characteristics in the oncoids recognized (Fig. 17B). Bádenas and Aurell (2010) described shoal facies dominated by type I and II oncoids for a mid-Kimmeridgian carbonate ramp in the central part of the basin (sequence Ki2; Fig. 1B). *Bacinella*-oncoid floatstone facies characterized a low-energy lagoon in the inner ramp, whereas type III oncoid rudstone-floatstone facies formed in proximal mid-ramp settings, laterally related to coral reefs. In the present work, similar distribution is observed for the *Bacinella-Lithocodium*-dominated oncoids (i.e. types III and IV oncoids), although type III oncoids have a wider distribution from inner- to mid-ramp

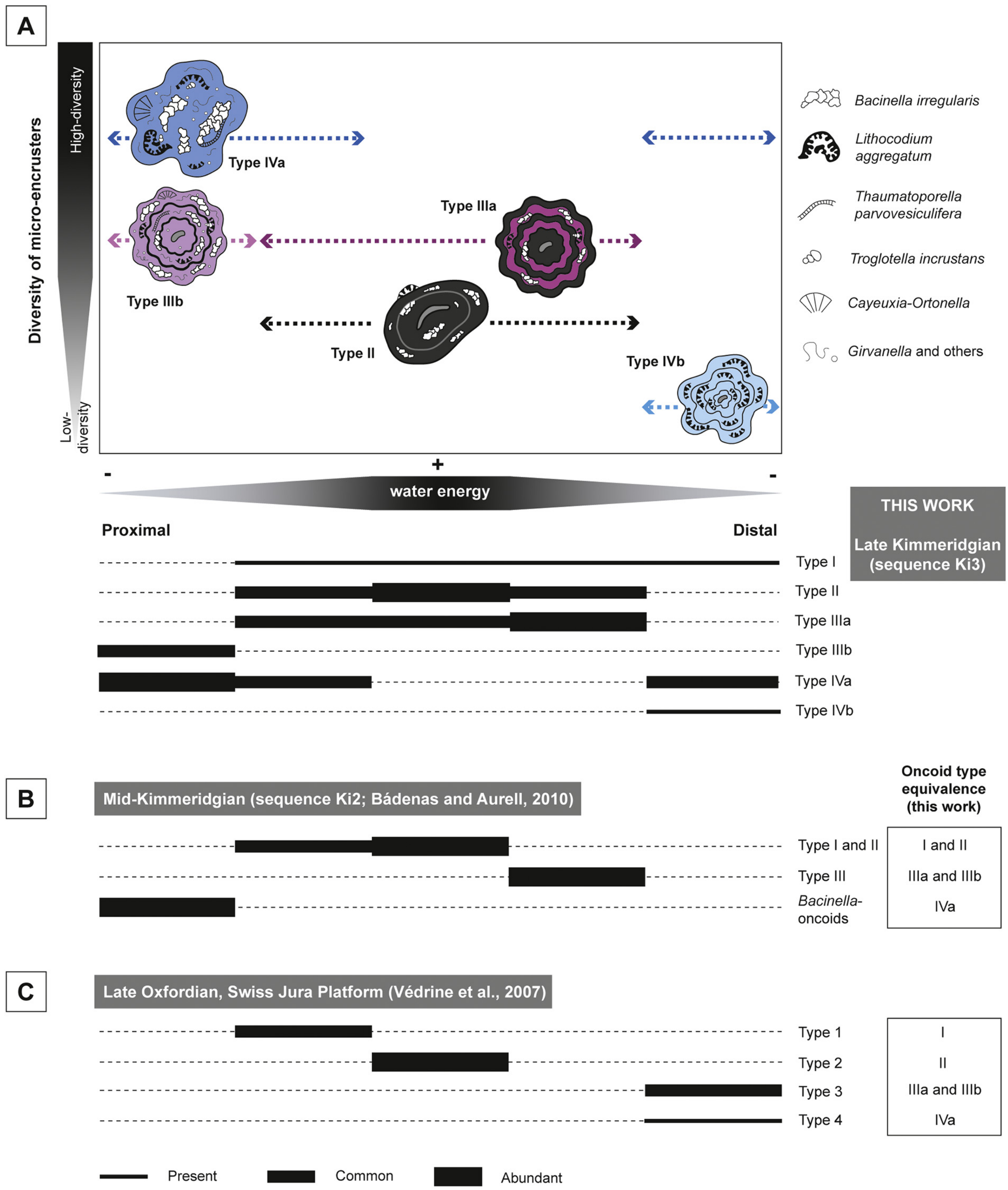

Fig. 17. (A) Preferential distribution pattern and diversity of micro-encrusters for the oncoid types identified in the Higueruelas Formation. (B, C) Oncoid distributions in the shallow domains of a mid-Kimmeridgian carbonate ramp in the central part of the Iberian Basin (B; compiled from Bádenas and Aurell, 2010) and in the Late Oxfordian Swiss Jura Platform (C; compiled from Védrine et al., 2007; Védrine, 2008). Black horizontal bars indicate the abundance of the oncoid types.

areas. In addition, type II oncoids dominate in the shoal-sand blankets but not type I oncoids, which appear in low proportions. Scarcer proportion of high-energy type I oncoids in the late Kimmeridgian carbonate ramp studied here compared with the mid-Kimmeridgian carbonate ramp, probably relates with the different general hydrodynamic conditions of the relative higher-energy areas (backshoal-shoal-foreshoal) and depositional profile of the two ramps: the late Kimmeridgian ramp studied here had a more flat morphology of the shallow areas with wider backshoal-shoal-foreshoal areas (up to 31 km in maximum lateral extension: Sequero et al., 2019); by contrast, in the mid-Kimmeridgian storm-dominated ramp, these environments had <23 km in maximum lateral extension, with ubiquitous cross-bedding in shoal facies, reflecting higher-energy conditions compared with the late Kimmeridgian ramp studied here.

Similar interpretations for oncoid distribution have been reported in Late Jurassic carbonate platforms outside the Iberian Basin. In the late Oxfordian Jura Platform (Fig. 17C), Védrine et al. (2007) identified micrite-dominated types 1 and 2 oncoids (equivalent to types I and II oncoids of Dahanayake, 1977) as representing moderate- to high-energy conditions in protected and semi-open lagoons, respectively, and *Bacinella* and *Lithocodium*-dominated types 3 and 4 oncoids (equivalent to types III and IV, respectively) in low-energy settings within open lagoons. Similar to the late Kimmeridgian carbonate ramp, an intense microbial activity is present in the Jura Platform, and plays an important role in the formation of oncoids. However, in the Jura Platform, type 3 (i.e. type III) oncoids are concentrated in the low-energy open-marine settings, laterally related to reefal facies (Olivier et al., 2011), with only scarce type 4 (i.e. type IV) oncoids, whereas in the studied latest Kimmeridgian carbonate ramp these oncoids also predominate in low- to moderate-energy inner- and mid-ramp domains. Regarding the micrite-dominated oncoids, only type 2 (i.e. type II) oncoids predominate in the moderate- to higher-energy settings of the studied latest Kimmeridgian carbonate ramp, but scarce type 1 (i.e. type I) oncoids are found from proximal to distal domains.

As a whole, the analyses of oncoid types in Late Jurassic shallow carbonate deposits reflect their preferential distributions from proximal to distal areas, with particular differences regarding the characteristics of the platform (Fig. 17). Types II and III oncoids predominate in high- to moderate-energy settings on shallow carbonate ramps in the Iberian Basin, whereas in the Swiss Jura carbonate platform types I and II oncoids are commonly found in moderate- to high-energy inner areas, respectively, and type III oncoids are preferentially formed in low-energy open-marine settings. Type IV oncoids predominate in the protected inner areas of the Iberian carbonate ramps but are found in low proportions in distal low-energy areas of the Swiss Jura Platform. These differences in the distribution of the oncoid types are probably due to the specific hydrodynamic conditions affecting these shallow marine environments, which are related to variations in the topographic relief and consequently the distribution of the facies. Remarkable heterogeneities are observed in the facies distribution of the late Oxfordian Jura Platform, showing significant lateral facies changes (Pillet, 1996; Gsponer, 1999; Jordan, 1999; Hug, 2003; Samankassou et al., 2003). Morphological highs in the inner areas of the platform and along the platform margin created suitable conditions for the generation of several oolitic bars, as well as reefs along the platform margin, both acting as barriers for water energy and favouring the generation of isolated or protected lagoons, some of them with a patchy distribution (Hug, 2003; Strasser and Védrine, 2009). In the Iberian Basin, the ramp geometry during the Late Jurassic led to more gradual facies changes mainly controlled by hydrodynamic factors (e.g. Bádenas and Aurell, 2010; Sequero et al., 2019). Oncoids grew from lagoon to proximal mid-ramp areas, also showing heterogeneities in their distribution (i.e. mosaic distributions) related to the growth of stromatoporoid carpets and chaetetid-stromatoporoid-coral buildups in the inner- and mid-ramp settings, respectively.

8. Conclusions

Characteristics of the oncoids recognized in the shallow domains of a latest Kimmeridgian carbonate ramp (Higueruelas Formation, north-central Iberian Basin) are the result of the interplay of water energy and microbial activity in oligotrophic conditions. Grain overturning in turbulent waters and/or microbial accretion under calm conditions gives rise to a wide variety of morphologies, sizes and internal structures of oncoids. Following Dahanayake (1977) nomenclature, the proposed oncoid classification reports on further details about the internal characteristics of the cortex, differentiating six types of oncoids which show from non-laminated microbial meshworks (more irregular in shape) to well-rounded and laminated micritic coatings without micro-encrusters. The preferential distribution of these oncoids from inner- (lagoon, backshoal, shoal-sand blanket) to mid-ramp settings (foreshoal, offshore-proximal) affords additional information about the internal processes and sea-bottom topography.

Water agitation in the shoal-sand blankets controlled the predominance of the micritic-dominated type II oncoids, including discontinuous organism-bearing laminae of mostly *Bacinella irregularis*. High-energy type I oncoids (continuous micritic laminae) instead do not characterize this domain. This feature is probably related to the lower hydrodynamic conditions of the shoal-sand blankets recorded, if compared with other oncoid-bearing shoal facies in the Jurassic of the Iberian Basin and French Jura, derived from the low-angle depositional profile of the studied carbonate ramp. Fluctuating higher- and lower-energy conditions result in the generation of type III oncoids, showing alternating micritic and organism-bearing laminae of mostly *Bacinella irregularis-Lithocodium aggregatum*. Variations in thickness of these laminae in this type of oncoids allowed to subdivide them in type IIIa oncoids (micritic and organism-bearing laminae with similar thickness), preferentially formed in foreshoal domain and type IIIb oncoids (with thinner micritic laminae) generated in low-energy sheltered lagoon with longer periods of calm conditions. Microbial growth controlled the generation of irregular type IV oncoids, encompassing type IVa oncoids (*Bacinella-Lithocodium* meshworks) that occurred abundantly in the lagoon, being also common in backshoal oncolitic-stromatoporoid and mid-ramp inter-buildup facies; and type IVb oncoids (*Lithocodium* meshworks) that preferentially formed in offshore-proximal subenvironment.

The analysis of oncoids in different Late Jurassic shallow carbonate platforms reflects a preferential distribution of type II oncoids in moderate- to high-energy environments, and in low-energy settings for type IV oncoids, whereas differences in abundance and distribution of types I and III oncoids are related to variations in general hydrodynamic conditions or platform morphology. Comparable oncoid distribution patterns on diverse shallow-marine carbonate settings enhance their potential use as reliable palaeoenvironmental proxies.

Acknowledgments

The authors gratefully acknowledge the financial support of projects CGL 2017-85038-P and Group E18 (Aragosaurus: Recursos Geológicos y Paleoambientales), sponsored by the Spanish Ministry of Science and Innovation, the European Regional Development Fund and the Government of Aragón, and of a FPU Grant subsidised by the Spanish Ministry of Science and Innovation, which finances the research of Cristina Sequero. We also appreciate the financial support provided by the International Association of Sedimentologists (IAS Postgraduate Grant Scheme) and the use of the Servicio General de Apoyo a la Investigación-SAI, Universidad de Zaragoza. Authors are grateful to A. Pérez-López and an anonymous reviewer for their constructive comments.

References

Aurell, M., Meléndez, A., 1986. Sedimentología de la Formación Calizas con oncolitos de Higueruelas (Malm) en la región de Muel-Belchite (Provincia de Zaragoza). Acta Geol. Hisp. 21–22, 307–312.

Aurell, M., Robles, S., Bádenas, B., Rosales, I., Quesada, S., Meléndez, G., García-Ramos, J.C., 2003. Transgressive-regressive cycles and Jurassic palaeogeography of Northeast Iberia. Sediment. Geol. 162, 239–271.

Aurell, M., Bádenas, B., Canudo, J.I., Castanera, D., García-Penas, A., Gasca, J.M., Martín-Closas, C., Moliner, L., Moreno-Azanza, M., Rosales, I., Santas, L., Sequero, C., Val, J., 2019. Kimmeridgian-Berriasian stratigraphy and sedimentary evolution of the central Iberian Rift System (NE Spain). Cretac. Res. 103.

Baccelle, L., Bosellini, A., 1965. Diagrammi per la stima visiva della composizione percentuale nelle rocce sedimentarie. Ann. Uni. Ferrara, N.S., Sez. IX. Sci. Geol. Paleontol. 1, 59–62.

Bádenas, B., Aurell, M., 2001. Kimmeridgian palaeogeography and basin evolution of northeastern Iberia. Palaeogr. Palaeoclimatol. Palaeoeco. 168, 291–310.

Bádenas, B., Aurell, M., 2010. Facies models of a shallow-water carbonate ramp based on distribution of non-skeletal grains (Kimmeridgian, Spain). Facies 56, 89–110.

Brandano, M., Corda, L., Tomassetti, L., Testa, D.V., 2015. On the peritidal cycles and their diagenetic evolution in the Lower Jurassic carbonates of the Calcare Massiccio Formation (Central Apennines). Geol. Carpath. 66 (5), 393–407.

Cherchi, A., Schroeder, R., 2006. Remarks on the systematic position of *Lithocodium* Elliott, a problematic microorganism from the Mesozoic carbonate platforms of the Tethyan realm. Facies 52, 435–440.
Cortés Gracia, A.L., Casas Sainz, A.M., 1996. Deformación alpina de zócalo y cobertera en el borde norte de la Cordillera Ibérica (Cubeta de Azuara-Sierra de Herrera). Rev. Soc. Geol. Esp. 9 (1–2), 51–66.
Dahanayake, K., 1977. Classification of oncoids from the Upper Jurassic carbonates of the French Jura. Sediment. Geol. 18, 337–353.
Dahanayake, K., 1978. Sequential position and environmental significance of different types of oncoids. Sediment. Geol. 20, 301–316.
Dahanayake, K., Gerdes, G., Krumbein, W.E., 1985. Stromatolites, oncolites and oolites biogenically formed in situ. Naturwissenschaften 7, 513–518.
Dercourt, J., Ricou, L., Vrielynck, B., 1993. Atlas: Tethys Palaeoenvironmental Maps. CCGM, Paris.
Dupraz, C., 1999. Paléontologie, paléoécologie et évolution des facies récifaux de l'Oxfordien moyen-supérieur (Jura suisse et français). GeoFocus 2. Univ. Fribourg, p. 200.
Dupraz, C., Strasser, A., 1999. Microbialites and micro-encrusters in shallow coral bioherms (Middle to Late Oxfordian, Swiss Jura Mountains). Facies 40, 101–130.
Elliott, G.F., 1956. Further records of fossil calcareous algae from the Middle East. Micropaleontology 2, 327–334.
Flügel, E., 2004. Microfacies of Carbonate Rocks. Analysis, Interpretation and Application. Springer-Verlag, Germany.
Gsponer, P., 1999. Étude géologique et sédimentologique de l'anticlinal du Chasseral dans la région de la Heutte (Ph.D. Thesis). Fribourg University, Germany.
Hägele, D., Leinfelder, R., Grau, J., Burmeister, E.G., Struck, U., 2006. Oncoids from the river Alz (southern Germany): tiny ecosystems in a phosphorus-limited environment. Palaeogr. Palaeoclimatol. Palaeoeco. 237, 378–395.
Hug, W., 2003. Sequenzielle Faziesentwicklung der Karbonatplattform des Schweizer Jura im Späten Oxford und frühesten Kimmeridge. GeoFocus 7. Univ. Fribourg, p. 155.
Ipas, J., Aurell, M., Bádenas, B., 2004. Ambientes sedimentarios y secuencias en la Fm. Higueruelas (Jurásico Superior) en la Cordillera Ibérica Septentrional. Geogaceta 35, 7–10.
Jones, B., Renaut, R.W., 1997. Formation of silica oncoids around geysers and hot springs at El Tatio, Chile. Sedimentology 44, 287–304.
Jordan, P., 1999. Géologie de la région de Montoz (Jura Bernois) avec analyse séquentielle de deux proWls de l'Oxfordien moyen et supérieur (Ph.D. Thesis). Fribourg University, Germany.
Lanés, S., Palma, R.M., 1998. Environmental implications of oncoids and associated sediments from the Remoredo Formation (Lower Jurassic) Mendoza, Argentina. Palaeogr. Palaeoclimatol. Palaeoeco. 140, 357–366.
Lazar, I., Gradinaru, M., Petrescu, L., 2013. Ferruginous microstromatolites related to Middle Jurassic condensed sequences and hardgrounds (Bucegi Mountains, Southern Carpathians, Romania). Facies 59, 359–390.
Leinfelder, R.R., Nose, M., Schmid, D., Werner, M., 1993. Microbial crusts of the late Jurassic: composition, palaeoecological significance and importance in reef construction. Facies 29, 195–230.
Li, X.Z., Guan, S.R., Xie, Q.B., Wang, Z.C., 2000. The oncoids genesis in the middle member of the Guanzhuang Formation of Eocene in Pingyi Basin. Acta Petrol. Sin. 16, 261–268.
Olivier, N., Colombié, C., Pittet, B., Lathuilière, B., 2011. Microbial carbonates and corals on the marginal French Jura platform (Late Oxfordian, Molinges section). Facies 57, 469–492.
Pederson, C.L., Donald, F.M., Klaus, J.S., Swart, P.K., 2015. Deposition and diagenesis of marine oncoids: implications for development of carbonate porosity. J. Sediment. Res. 85, 1323–1333.
Peryt, T.M., 1981. Phanerozoic oncoids—an overview. Facies 4, 197–213.
Peryt, T.M., 1983. Oncoids: a comment to recent developments. In: Peryt, T.M. (Ed.), Coated Grains. Springer Verlag, Berlin, pp. 273–275.
Pillet, B., 1996. Contrôles climatiques, eustatiques et tectoniques sur des systèmes mixtes carbonates–siliciclastiques de plate-forme: exemples de l'Oxfordien (Jura suisse, Normandie, Espagne) (Ph.D. Thesis). Fribourg University, Germany.
Pingzhou, S., Hongming, T., Zhengyu, W., Xuguang, S., 2019. Katian oncoids of the lower Ordovician Lianglitage Formation in the Tarim Basin, Northwest China. Carbonates Evaporites 34, 1525–1535.
Radoicic, R., 1959. Some problematic microfossils from the Dinarian Cretaceous. Bull. Serv. Geol. Geophys. RP Serbie 17, 87–92.
Ratcliffe, K.T., 1988. Oncoids as environmental indicators in the Much Wenlock Limestone Formation of the English Midlands. J. Geol. Soc. Lond. 145, 117–124.
Reolid, M., Nieto, L.M., 2010. Jurassic Fe–Mn macro-oncoids from pelagic swells of the External Subbetic (Spain): evidences of microbial origin. Geol. Acta 8, 151–168.
Riding, R., 2000. Microbial carbonates: the geological record of calcified bacterial–algal mats and biofilms. Sedimentology 47, 179–214.
Riding, R., 2006. Microbial carbonate abundance compared with fluctuations in metazoan diversity over geological time. Sediment. Geol. 185 (3), 229–238.
Salas, R., Casas, A., 1993. Mesozoic extensional tectonics, stratigraphy and crustal evolution during the Alpine cycle of the eastern Iberian basin. Tectonophysics 228, 33–55.
Samankassou, E., Strasser, A., Di Gioia, E., Rauber, G., Dupraz, C., 2003. High-resolution record of lateral variations on a shallow carbonate platform (Upper Oxfordian, Swiss Jura Mountains). Eclogae Geol. Helv. 96, 425–440.
Schmid, D.U., 1996. Marine mikrobolithe und mikroinkrustierer aus dem Oberjura. Profil 9, 101–251.
Sequero, C., Bádenas, B., Aurell, M., 2018. Facies mosaic in the inner areas of a shallow carbonate ramp (Upper Jurassic, Higueruelas Fm, NE Spain). Facies 64 (9).
Sequero, C., Aurell, M., Bádenas, B., 2019. Sedimentary evolution of a shallow carbonate ramp (Kimmeridgian, NE Spain): unravelling controlling factors for facies heterogeneities at reservoir scale. Mar. Pet. Geol. 109, 145–174.
Shapiro, R.S., Fricke, H.C., Fox, K., 2009. Dinosaur-bearing oncoids fromephemeral lakes of the Lower Cretaceous Cedar Mountain Formation, Utah. Palaios 24, 51–58.
Shi, G.R., Chen, Z.Q., 2006. Lower Permian oncolites from South China: implications for equatorial sea-level responses to Late Palaeozoic Gondwanan glaciation. J. Asian Earth Sci. 26, 424–436.
Shiraishi, F., Kano, A., 2004. Composition and spatial distribution of microencrusters and microbial crusts in upper Jurassic-lowermost Cretaceous reef limestone (Torinosu Limestone, southwest Japan). Facies 50, 217–227.
Strasser, A., 1986. Ooids in Purbeck limestones (lowermost Cretaceous) of the Swiss and French Jura. Sedimentology 33, 711–727.
Strasser, A., Védrine, S., 2009. Controls on facies mosaics of carbonate platforms: a case study from the Oxfordian of the Swiss Jura. Intern. Assoc. Sediment. Spec. Publ. 41, 199–213.
Tucker, M.E., Wright, V.P., 1990. Carbonate Sedimentology. Wiley-Blackwell, Oxford, pp. 1–482.
Védrine, S., 2008. Co-occurrence of the foraminifer *Mohlerina basiliensis* with *Bacinella-Lithocodium* oncoids: palaeoenvironmental and palaeoecological implications (Late Oxfordian, Swiss Jura). J. Micropalaeontol. 27, 35–44.
Védrine, S., Strasser, A., Hug, W., 2007. Oncoid growth and distribution controlled by sea-level fluctuations and climate (Late Oxfordian, Swiss Jura Mountains). Facies 53, 535–552.
Wernli, R., Fookes, E., 1992. *Troglotella incrustans* n. gen., n. sp., un étrange et noveau foraminifère calcicavicole du complexe récifal Kimméridgien de Saint-Germains-de-Joux (Ain, France). Boll. Soc. Paleontol. Ital. 31, 95–103.
Wetzel, A., Strasser, A., 2001. Sedimentology, palaeoecology, and high-resolution sequence stratigraphy of a carbonate-siliciclastic shelf (Oxfordian, Swiss Jura Mountains). Field trip of International Association of Sedimentologists 2001 Davos.
Wright, V.P., 1983. Morphogenesis of oncoids in the Lower Carboniferous Llanelly Formation of South Wales. In: Peryt, T.M. (Ed.), Coated Grains. Springer Verlag, Berlin.
Zaton, M., Kremer, B., Marynowski, L., Wilson, M.A., Krawczynski, W., 2012. Middle Jurassic (Bathonian) encrusted oncoids from the Polish Jura, southern Poland. Facies 58, 57–77.
Zhang, W., Shi, X., Jiang, G., Tang, G., Wang, X., 2015. Mass-occurrence of oncoids at the Cambrian Series 2-Series 3 transition: implications for microbial resurgence following an Early Cambrian extinction. Gondwana Res. 28, 432–450.

7. CARBON AND OXYGEN STABLE ISOTOPE RECORD OF THE HIGUERUELAS FORMATION

C H A P T E R

7

CARBON AND OXYGEN STABLE ISOTOPE RECORD OF THE HIGUERUELAS FORMATION

INTRODUCTION AND GOALS

Carbon and oxygen stable isotope analyses are regarded as a potential tool for addressing key aspects concerning the palaeoenvironmental factors governing sedimentation on ancient shallow-marine carbonate systems (e.g. Veizer et al., 1986; Magaritz and Holser, 1990; Immenhauser et al., 2003; Swart and Eberli, 2005; Madhavaraju et al., 2013). However, since multiple factors control the chemical variability of shallow seawaters (e.g. evaporation, carbon transfer, changes in salinity or water-masses restrictions; Patterson and Walter, 1994; Immenhauser et al., 2003; Colombié et al., 2011; Zuo et al., 2018), the evaluation of the carbon and oxygen stable isotope record becomes more challenging than those performed in deep-marine successions (e.g. van de Schootbrugge et al., 2000; Wierzbowski, 2004), also considering that singular isotopic compositions can be recorded by the variable components which constitute the shallow-marine carbonates (e.g. skeletal remains, coated grains, micrite matrix) (Hudson, 1977; Anderson and Arthur, 1983; Jenkyns and Clayton, 1986; McConnaughey, 1989a, b; Nelson and Smith, 1996; Schobben et al., 2015). In addition, diverse diagenetic processes usually alter the primary isotopic signature in variable magnitude (e.g. Brand and Veizer, 1981; Moore, 1989; Marshall, 1992; Glumac and Walker, 1998; Immenhauser et al., 2002; Coimbra et al., 2014; Huck et al. 2017). However, some authors propose that even in the presence of diagenetic alteration, carbon and oxygen stable isotope compositions can provide some valuable information about the palaeoenvironmental setting (e.g. Bartolini et al., 2003; Colombié et al., 2011; Al-Mojel et al., 2018; Zuo et al., 2018), even enabling the use of the carbon stable isotope curve as a correlation tool between long-distance separated logs (e.g. Glumac and Walker, 1998; Grötsch et al., 1998; Colombié et al., 2011; Eltom et al., 2018; Zuo et al., 2018).

In this Chapter, carbon and oxygen stable isotope analyses have been performed on the Higueruelas Fm in two selected sections representing the proximal and relatively distal areas of this ramp, situated around the localities of Tosos (proximal) and Fuendetodos (relatively distal). The data exposed are the bases for the elaboration of a scientific paper which will be published on a SCI international journal, in cooperation with Dr. Giovanna Della Porta from the Earth Sciences Department *Ardito Desio* of the University of Milan (Italy), who had a major contribution in the isotopic analyses that form the basis of this study.

The initial aim of this study was to obtain further information regarding the palaeoenvironmental factors controlling sedimentation on the studied latest Kimmeridgian shallow carbonate ramp. However, the preliminary results indicate that the post-depositional diagenetic evolution of the Higueruelas Fm in the two selected localities exerted a strong influence on the isotopic composition, so the purpose of this work turned into evaluating the diagenetic imprint on the carbon and oxygen stable isotope record of these shallow-marine carbonates in each sector.

The results obtained in this work can provide key aspects concerning the variable impact of the diagenetic alteration on the carbon and oxygen stable isotope record in ancient shallow-marine carbonates, according to a particular post-depositional diagenetic history. Taking into account that diagenesis usually implies concomitant chemical and textural changes on the analysed sediment (e.g. Brand and Veizer, 1980, 1981; Lavoie and Bourque, 1993; Colombié et al., 2011; Coimbra et al., 2014; Huck et al., 2017), further investigations on the diagenetic alteration of these shallow-marine carbonate deposits will encompass deeper petrographic analyses of the analysed samples in terms of diagenetic features.

CARBON AND OXYGEN STABLE ISOTOPE RECORD OF UPPER KIMMERIDGIAN SHALLOW-MARINE CARBONATES (IBERIAN BASIN, NE SPAIN): THE IMPACT OF BURIAL AND METEORIC DIAGENESIS

C. Sequero[1], G. Della Porta[2], B. Bádenas[1], M. Aurell[1]

[1]Departamento de Ciencias de la Tierra-IUCA, Universidad de Zaragoza, 50009, Zaragoza, Spain

[2]Dipartimento di Scienze della Terra "Ardito Desio", Università degli Studi di Milano, 20133, Milano, Italy

Abstract

Bulk carbon and oxygen stable isotopes of ancient shallow-marine carbonates can record the effect of multiple palaeoenvironmental factors, but also the imprint of several post-depositional processes which alter the original isotopic composition. In this work, carbon and oxygen stable isotope analyses were performed on bulk-carbonate and bivalve calcitic-shell samples from two stratigraphic sections (Tosos and Fuendetodos) of the uppermost Kimmeridgian inner- to mid-ramp deposits developed in the north-central part of the Iberian Basin (NE Spain). These successions underwent different diagenetic histories which differently altered the primary isotopic composition in each section. Particular post-depositional burial conditions and a variable exposure to meteoric weathering from the end of the Kimmeridgian to the Cenozoic, is reflected in the different alteration pattern of the isotopic signal, showing a significant deviation to lower values in both $\delta^{13}C$ and $\delta^{18}O$ for those carbonates mostly exposed to meteoric weathering (Fuendetodos section), but only in the $\delta^{18}O$ record those deposits mainly affected by burial diagenesis (Tosos section). The diagenetic resetting reported on these shallow-marine carbonates unables the use of these $\delta^{13}C$ and $\delta^{18}O$ records for addressing palaeoenvironmental interpretations, but instead arises interesting points regarding the variable diagenetic imprint on the studied shallow-marine carbonate successions concerning their particular burial and tectonic history.

1. Introduction

Unravelling the carbon and oxygen stable isotope composition of paleo-seawater in ancient shallow-marine carbonates is sometimes challenging, due to: 1) the multiple factors that control the chemical variability of shallow seawaters (e.g. evaporation, carbon transfer, changes in salinity or water-masses restrictions; Patterson and Walter, 1994; Immenhauser et al., 2003; Colombié et al., 2011; Zuo et al., 2018); 2) the potential singular isotopic compositions recorded by their different components (e.g. skeletal remains, coated grains, micrite matrix; Hudson, 1977; Anderson and Arthur, 1983; Jenkyns and Clayton, 1986; McConnaughey, 1989a, b; Nelson and Smith, 1996; Schobben et al., 2015); and 3) the diagenetic processes that can alter the primary isotopic signature, thus complicating the use of these isotopic records as palaeoenvironmental proxies (e.g. Brand and Veizer, 1981; Moore, 1989; Marshall, 1992; Glumac and Walker, 1998; Immenhauser et al., 2002; Coimbra et al., 2014; Huck et al. 2017).

The magnitude of the diagenetic alteration can be variable for distinct carbonate grains, also depending on the degree of the porosity and permeability of the sediments, being the coarser fabrics more favourable for infiltration of diagenetic waters (e.g. Marshall, 1992; Immenhauser et al., 2002;

Vincent et al., 2004; Coimbra et al., 2014; Huck et al., 2017; Al-Mojel et al., 2018). Diagenetic fluids (e.g. meteoric waters, high-temperature burial or hydrothermal fluids) lead to the dissolution and re-precipitation of variable mineralogies, or the formation of more stable mineralogical phases (e.g. O'Neil, 1977; Allan and Mathews, 1982; Given and Lohmann, 1985; Jenkyns and Clayton, 1986; Moore, 1989; Carpenter and Lohmann, 1989, 1997; Tucker, 1993; Joachimski, 1994; Sharp, 2007; van der Kooij et al., 2009; Brand et al., 2012; Coimbra et al., 2014; Al-Mojel et al., 2018). Therefore, diagenesis usually implies concomitant chemical and textural changes on carbonates, which must be taken into account for interpretation of the isotopic signature (e.g. Brand and Veizer, 1980, 1981; Lavoie and Bourque, 1993; Colombié et al., 2011; Coimbra et al., 2014; Huck et al., 2017).

Diagenesis in marine carbonates commonly implies a decrease in $\delta^{18}O$ values by the influence of ^{18}O-depleted meteoric waters and/or relatively high-temperature burial fluids, being the magnitude of such alteration depending on the degree of the fluid-rock interaction (e.g. Hudson, 1977; Brand and Veizer, 1980; Allan and Matthews, 1982; Given and Lohmann, 1985; Plunkett, 1997; van der Kooij et al., 2009; Grotzinger et al., 2011; Madden and Wilson, 2013; Coimbra et al., 2014; Al-Mojel et al., 2018). Post-depositional alteration also generally leads to a decrease in $\delta^{13}C$ values, which is normally attributed to the interaction with meteoric solutions enriched in organic ^{12}C by soil weathering (e.g. Hudson, 1977; Allan and Matthews, 1982; O'Neil, 1987; Lohmann, 1988; Patterson and Walter, 1994; Moore, 2001; Immenhauser et al., 2002; Lavastre et al. 2011; Bahamonde et al., 2017). In ancient shallow-marine carbonate successions, the effect of meteoric and/or burial diagenesis on the carbon and oxygen stable isotope record has been highlighted by several authors, reporting local negative $\delta^{13}C$ and $\delta^{18}O$ excursions in bulk carbonates related to major infiltrations of meteoric waters in coarser fabrics, or decreasing $\delta^{18}O$ values from burial cements (e.g. Immenhauser et al., 2003; Coimbra et al., 2014; Huck et al., 2017; Al-Mojel et al., 2018). However, some authors propose that even in the presence of diagenetic alteration, carbon and oxygen stable isotope composition can provide some valuable information about the palaeoenvironmental setting (e.g. Bartolini et al., 2003; Colombié et al., 2011; Al-Mojel et al., 2018; Zuo et al., 2018), even using the carbon stable isotope stratigraphy as a correlation tool between long-distance separated logs (e.g. Glumac and Walker, 1998; Grötsch et al., 1998; Colombié et al., 2011; Eltom et al., 2018; Zuo et al., 2018).

In this work, bulk carbon and oxygen stable isotope analyses were performed in two stratigraphic sections of the Higueruelas Fm (NE Spain), representing the proximal and relatively distal areas of the latest Kimmeridgian carbonate ramp that developed in the north-central part of the Iberian Basin. These sections were selected for isotopic sampling in order to consider the possible influence of facies and palaeoenvironmental differences on the recorded primary isotopic signature. However, the obtained results showed that post-depositional processes had a strong impact on the recorded isotopic composition in each sector linked to their particular burial evolution, mostly related to the Early Cretaceous and Cenozoic tectono-sedimentary evolution in this part of the Iberian Basin. Accordingly, the major objectives proposed here are: (1) to evaluate the variable diagenetic response of the carbon and oxygen stable isotope signature from these shallow-marine carbonate deposits in two selected sections affected by different post-depositional histories, and (2) to discuss about the preservation of a possible palaeoenvironmental signal from the stable isotope data with a local and/or regional significance.

2. Geological setting

The studied uppermost Kimmeridgian carbonate rocks represent inner- to mid-ramp deposits of a carbonate ramp that developed in the north-central part of the Iberian Basin in the northeastern Iberian Plate (e.g. Aurell et al., 2003, 2010) (Fig. 1a, b). At basin scale, these shallow-marine deposits grade eastwards into outer-ramp marls and lime mudstones of the Loriguilla Fm (e.g. Aurell et al., 2003, 2010) (Fig. 1c). The long-term regional fall in relative sea level documented at the end of the Kimmeridgian, which was in part controlled by the tectonic uplift of the Iberian Massif (Fig. 1a), resulted in the progressively shallowing and subaerial exposure of the carbonate ramp in these domains (e.g. Bádenas and Aurell, 2001; Aurell et al., 2003).

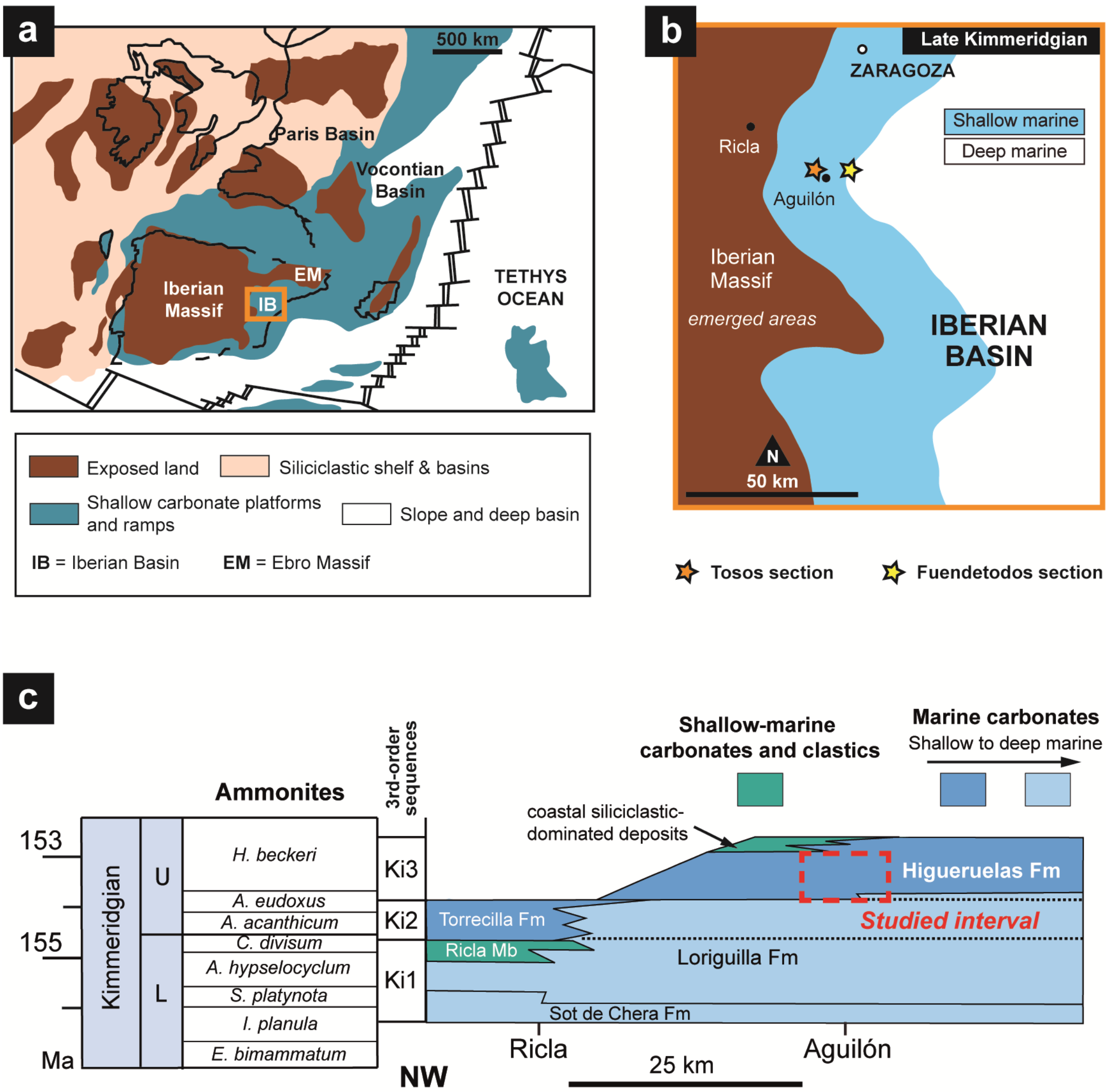

Fig. 1. a) Palaeogeography of western Europe during the Late Jurassic, with the location of the Iberian Basin (modified from Dercourt et al., 1993). b) Main facies belts in the Iberian Basin during the late Kimmeridgian (square in a) and location of the studied sections (south of the city of Zaragoza, NE Spain; compiled from Aurell et al., 2003 and Ipas et al., 2004). c) Kimmeridgian stratigraphy in the northern Iberian Basin (modified from Aurell et al., 2019). The Higueruelas Fm, which is represented in the third-order sequence Ki3, overlies the open-marine marls and lime mudstones of the Loriguilla Fm, which is in turn laterally equivalent to the shallow-marine carbonates of the Higueruelas Fm in eastern areas of the northern Iberian Basin (i.e. deep-marine areas in b).

The Higueruelas Fm is exposed in a system of W-E and NW-SE orientated anticlines located south of the city of Zaragoza (NE Spain) (Fig. 2a), which represent Cenozoic Alpine structures within the north-central Iberian Chain (e.g. Guimerà and Álvaro, 1990). In this area, the Higueruelas Fm is 40 to 80 m in thickness, and is characterized by packstones and grainstones with a wide variety of skeletal and non-skeletal grains (mainly peloids, ooids and oncoids), and local chaetetid-stromatoporoid-coral buildups (e.g. Aurell and Meléndez, 1986; Bádenas and Aurell, 2003; Ipas et al., 2004; Aurell et al., 2012; Sequero et al., 2019). Detailed stratigraphic and sedimentological studies revealed the existence of 9 correlatable m-thick high-frequency sequences (Sequero et al., 2019). In this work, high-frequency sequences 1 to 7 of two sedimentary logs, representing proximal (Tosos section) and relatively distal (Fuendetodos section) areas of the carbonate ramp, have been selected for carbon and oxygen stable isotope analyses (Figs 1b and 2a).

The post-depositional evolution of the Higueruelas Fm in the two selected sections shows remarkable differences. After emersion of the carbonate ramp at the end of the Kimmeridgian, the Late Jurassic-Early Cretaceous rifting stage resulted in a major structuration of the Iberian Basin in different sub-basins controlled by extensional faults, which later on were inverted during the Cenozoic Alpine compression (e.g. Guimerà and Álvaro, 1990; Salas and Guimerà, 1996; Aurell et al., 2019; Liesa et al., 2019). In particular, the two studied sections belong to the so-called Aguilón sub-basin, controlled by NW-SE orientated extensional faults (Aurell et al., 2019) (Fig. 2b). Here, after a long-lasting episode of no sedimentation (Tithonian-middle Valanginian), sedimentation resumed with the deposition of up to 300 m of Lower Cretaceous (mid-Valanginian-lower Barremian) continental successions (Villanueva the Huerva and Aguilón formations; e.g. Soria et al., 1995). Subsiding areas were located SW of the Aguilón fault system and Villanueva de Huerva monocline (e.g. Cortés et al., 1999) (Fig. 2c). Tosos sector belonged to the subsiding area southwest of the Aguilón fault system, and consequently a thick (180 m) succession of mid-Valanginian-lower Barremian deposits accumulated over the Higueruelas Fm. By contrast, Fuendetodos sector was placed on the non-subsiding area NE of the Villanueva de Huerva monocline, therefore lacking the mid-Valanginian-lower Barremian sedimentary record. After deposition of the Lower Cretaceous units, there was a major erosive and non-depositional gap until the deposition of syn-tectonic (Alpine) continental Cenozoic units (Paleocene to middle Miocene). Around Tosos, this set of Cenozoic units has up to 600 m in thickness (Pérez et al., 1985; Pérez, 1989). However, Fuendetodos sector was close to an Alpine structure (Mezalocha anticline) that represented a paleo-high that remained exposed until the onset of the Miocene (Fig. 2c). In particular, around Fuendetodos, the Higueruelas Fm is only covered by a c. 200 m-thick succession of middle Miocene lacustrine carbonates (Pérez et al., 1985; Pérez, 1989). Therefore, the studied Higueruelas Fm underwent a different burial history in the studied sectors: in Tosos, these deposits were affected by two stages of subaerial exposure (latest Kimmeridgian-middle Valanginian, and middle Barremian-Paleocene), whereas Fuendetodos remained mostly exposed from the latest Kimmeridgian to the middle Miocene.

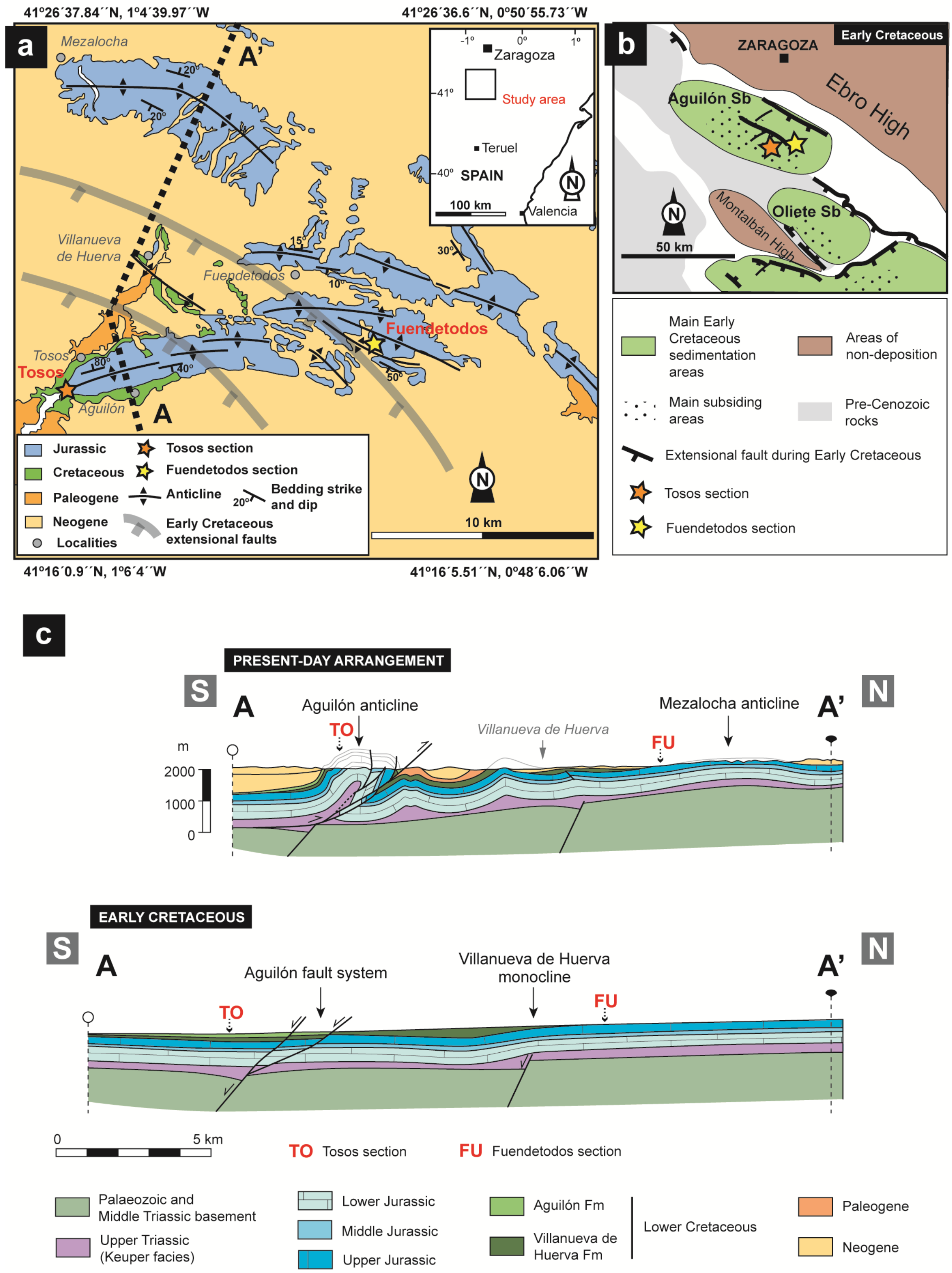

***Fig. 2**. a) Extent of the Jurassic outcrops in the study area with the position of the studied logs (stars) and the cross-section A-A' shown in (c). The position of the Early Cretaceous extensional faults are included (grey colour) (modified from Cortés Gracia and Casas Sainz, 1996). b) Main sedimentation areas and active faults during the Late Jurassic-Early Cretaceous rifting episode in the northern Iberian Basin. The studied sections (stars) are situated in the newly formed Aguilón sub-basin (Aguilón Sb) (modified from Liesa et al., 2019). c) Balanced cross-section (present-day arrangement) and suggested section restored to the top of the syn-rift sequence (Early Cretaceous) for the transect A-A' indicated in (a). The position of Tosos (TO) and Fuendetodos (FU) sections are included (modified from Cortés et al., 1999).*

3. Studied successions and sedimentological framework

The uppermost Kimmeridgian Higueruelas Fm studied in Tosos and Fuendetodos sections are 71 m and 52 m in thickness, respectively. Distance between the two sections, without restoring tectonic shortening, is around 15 km (Fig. 3). The studied successions encompass high-frequency sequences 1 to 7 (Tosos) and 2 to 7 (Fuendetodos), and include a total of 14 facies representing deposition from inner-ramp domains (intertidal, lagoon, backshoal and shoal-sand blanket) to mid-ramp foreshoal and offshore areas (Sequero et al., 2019). Some dm- to m-thick beds of total or partially dolomitized facies are also recorded.

In the proximal Tosos section, the long-term shallowing-upward trend at the end of the Kimmeridgian is reflected by the evolution from mid-ramp facies (peloidal, peloidal-bioclastic and oncolitic wackestone-packstone) in sequence 1, to inner-ramp deposits (oolitic, peloidal-oolitic and oncolitic packstone-grainstone and stromatoporoid-rich facies) from the upper part of sequence 1 to sequence 5; and to restricted lagoon facies (peloidal, bioclastic and oolitic packstone with local sandstones and marls) in sequences 5 to 7 (Fig. 3). In the relatively distal Fuendetodos section, the long-term shallowing-upward trend is recorded by the evolution from mid-ramp (offshore) peloidal and bioclastic wackestone-packstone alternating with chaetetid-stromatoporoid-coral-rich buildup and inter-buildup facies in sequences 2 to 5, to mid-ramp (foreshoal) peloidal, inter-buildup and oncolitic packstone-grainstone in sequences 6 and 7.

4. Methodology

4.1. Petrographic characterization

A total of 72 samples in thin sections, already used for differentiating depositional facies by Sequero et al. (2019), were analysed for the petrographic descriptions of facies under binocular microscope, in particular differentiating between primary carbonate components (i.e. micrite matrix and carbonate grains) from diagenetic calcite cements. Dolomitized facies (Fig. 3) have not been studied in this work. Nomenclature for calcite cements follows Flügel (2004) classification.

Petrographic analysis was complemented by cathodoluminescence (CL) microscopy on 21 thin sections (7 in Tosos and 14 in Fuendetodos), with a Technosyn Cold Cathodo Luminiscope, operating under 10-14 kV beam potential, 0.5 μA beam current and a 0.05-0.1 Torr pressure. CL analyses were used to characterize the primary carbonate components and diagenetic calcite cements, on the basis of the absence or type of luminescence, as traditionally followed in the literature (e.g. Machel, 1985; Savard et al., 1995; Richter et al., 2003; Hiatt and Pufahl, 2014).

Fig. 3 (Next page)*. Sedimentary logs and carbon and oxygen stable isotope stratigraphy of Tosos and Fuendetodos sections, including the sequence-stratigraphic correlation. Samples in red colour include cathodoluminescence observations. Facies descriptions and interpretations are based on Sequero et al. (2019).*

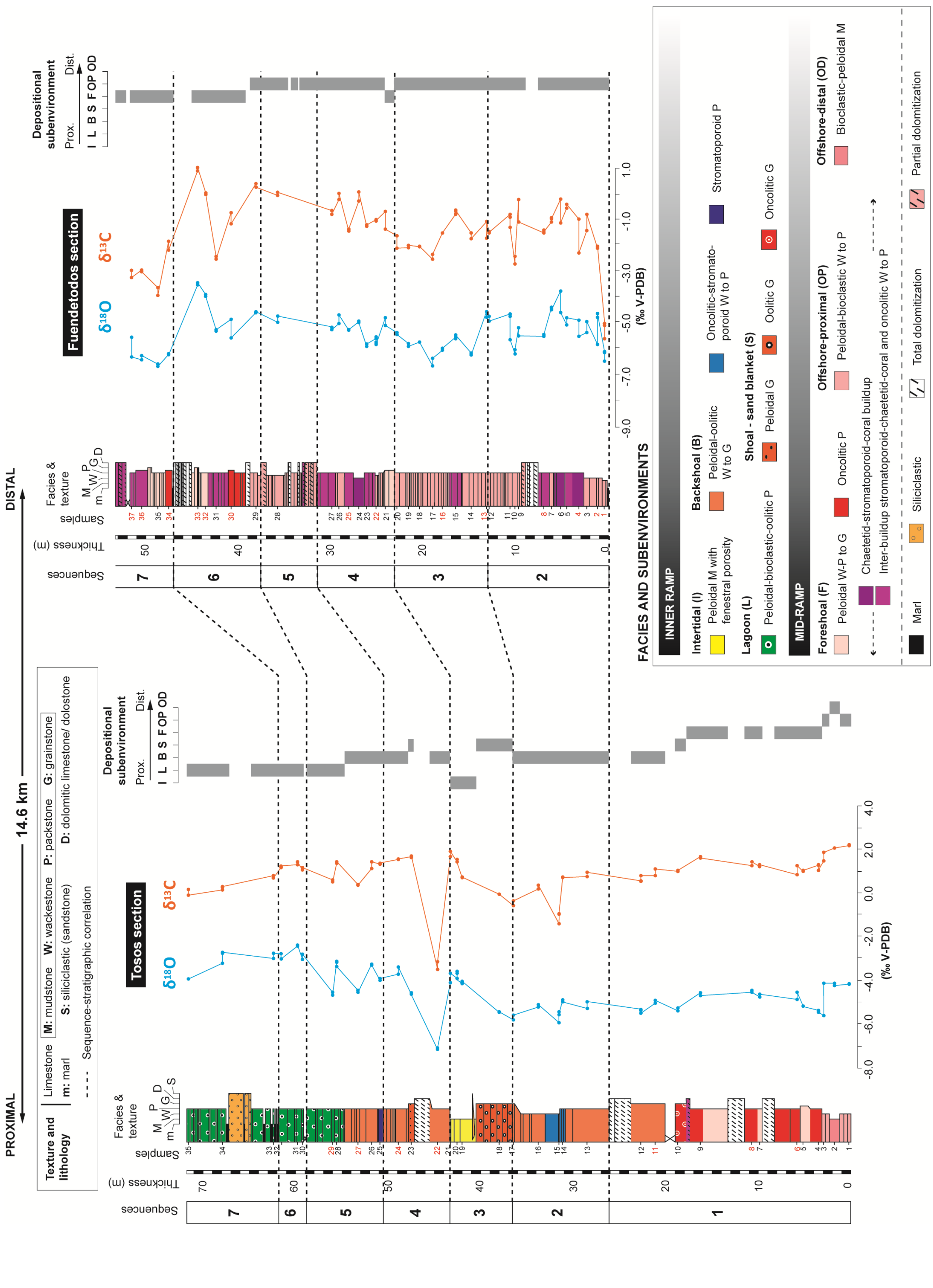
PROXIMAL
14.6 km
DISTAL
Texture and lithology
Limestone
M: mudstone
W: wackestone
P: packstone
G: grainstone
m: marl
S: siliciclastic (sandstone)
D: dolomitic limestone/ dolostone
Sequence-stratigraphic correlation
Tosos section
Fuendetodos section
δ18O
δ13C
(‰ V-PDB)
Sequences
Thickness (m)
Samples
Facies & texture
Depositional subenvironment
Prox.
Dist.
I L B S F OP OD
FACIES AND SUBENVIRONMENTS
INNER RAMP
Intertidal (I)
Peloidal M with fenestral porosity
Lagoon (L)
Peloidal-bioclastic-oolitic P
Backshoal (B)
Peloidal-oolitic W to G
Oncolitic-stromatoporoid W to P
Stromatoporoid P
Shoal - sand blanket (S)
Peloidal G
Oolitic G
Oncolitic G
MID-RAMP
Foreshoal (F)
Peloidal W-P to G
Oncolitic P
Offshore-proximal (OP)
Peloidal-bioclastic W to P
Offshore-distal (OD)
Bioclastic-peloidal M
Chaetetid-stromatoporoid-coral buildup
Inter-buildup stromatoporoid-chaetetid-coral and oncolitic W to P
Marl
Siliciclastic
Total dolomitization
Partial dolomitization

4.2. Carbon and oxygen stable isotope analyses

The carbon and oxygen stable isotope analyses were performed on the 72 bulk-rock samples collected in Tosos (n = 35) and Fuendetodos (n = 37) sections, and on calcitic shells from three specimens of *Trichites* (large-sized bivalve with very thick outer shell wall) found in the offshore-proximal peloidal-bioclastic wackestone facies within sequence 2 of the Fuendetodos section. In order to ensure the reliability of the carbon and oxygen stable isotope composition in each sample, a double measure per sample was carried out, obtaining a total of 169 stable isotope analyses (n = 77 in Tosos section, and n = 92 in Fuendetodos section) (see Annexe 4 for the table gathering the values).

For the carbon and oxygen stable isotope analyses, carbonate powders were extracted using a handheld micro-drill, avoiding diagenetic calcite cements and large bioclastic fragments of corals or stromatoporoids, due to the disequilibrium-isotopic precipitation by organisms (e.g. McConnaughey, 1989a, b). However, the incorporation of a certain amount of diagenetic calcite cements filling the mouldic space of skeletal debris, interparticle spaces, and sometimes fenestral pores, was in some cases inevitable.

The carbon and oxygen stable isotope analyses were performed using an automated carbonate preparation device (GasBench II) connected to a Delta V Advantage (Thermo Fisher Scientific Inc.) isotope ratio mass spectrometer at the Earth Sciences Department *Ardito Desio*, University of Milan (Italy). Carbonate powders were reacted with > 99% orthophosphoric acid at 70ºC. The carbon and oxygen stable isotope compositions are expressed in the conventional delta notation calibrated to the Vienna Pee-Dee Belemnite (V-PDB) scale by the international standards IAEA-603 and NBS-18 and an internal laboratory standard. Analytical reproductibility for these analyses, being checked by repeated analyses of the certified carbonate standards and after ten consecutively isotopic measurements, was better than ± 0.1‰ for both $\delta^{13}C$ and $\delta^{18}O$ values.

5. Results

5.1. Petrographic and cathodoluminescence characteristics

The bulk-carbonate samples analysed in both Tosos and Fuendetodos sections include a wide variety of primary carbonate components in variable proportions, mainly micrite matrix, peloids, ooids, oncoids and skeletal debris, as well as diagenetic calcite cements filling mouldic vugs (generated by dissolution of skeletal debris), interparticle pores, fenestral pores and fissures (Figs 4 and 5; see also Annexe 3 for additional pictures).

Three types of diagenetic calcite cements have been recognized: granular, drusy and blocky. Granular to drusy calcite cements tend to fill both mouldic and interparticle porosity. They generally constitute less than 10% of the thin section surface, and are formed by anhedral to subhedral equigranular (granular) and non-equigranular (drusy) crystals ranging from < 10 to 30 µm in size (Figs 4a-c and 5a-d). In the drusy calcite cements, crystal size increases towards the centre of the void (Fig. 4b). Blocky calcite cements precipitate in fenestral pores, rectilinear fissures (i.e. calcite veins; Fig. 4d) and occasionally mouldic vugs (Fig. 5c). They constitute < 10% of the thin section surface, and are formed by anhedral to subhedral crystals from hundreds of µm to several mm in size.

The proportion of primary carbonate components and diagenetic calcite cements is variable regarding the facies type. In offshore mudstone to packstone and intertidal mudstone facies, peloids and micrite matrix constitute the main analysed components, representing the diagenetic calcite cements < 10% of the total volume of the sample filling interparticle spaces, fenestral pores, mouldic vugs and/or rectilinear fissures (Fig. 4a, d). For lagoon, backshoal and foreshoal wackestone to packstone facies, samples are mainly composed of variable proportions of micrite matrix, peloids, ooids and oncoids, as well as diagenetic calcite cements mainly filling interparticle and mouldic pores (Figs 4c and 5a-d). These calcite cements constitute < 10% of the total volume of the samples, occasionally 15% in backshoal oncolitic-stromatoporoid wackestone to packstone facies. However, for the backshoal, shoal-sand blanket and foreshoal grainstone facies (with peloids, ooids and/or oncoids), the proportion of diagenetic calcite cements is higher (around 15% of the total volume) (Fig. 4b).

Primary carbonate components in most of the samples show no luminescence under CL (Figs 4a'-d' and 5a'), occasionally dull (red) luminescence. Granular to drusy calcite cements filling mouldic and interparticle pores commonly show non- to dull (red) luminescence (Figs 4a'-c' and 5a'). Blocky calcite cements display zoned (dark-yellow nuclei evolving to bright-yellow rims), dull (yellow) or no luminescence (Figs 4d' and 5c'). Particularly in the Tosos section, primary carbonate components and diagenetic calcite cements can both show orange- to yellow-coloured luminescence in specific samples (i.e. samples 22, 24 and 29; Fig. 3), appearing these samples as uniformly bright-luminescent (Fig. 5b'-d').

5.2. Carbon and oxygen stable isotope records

Carbon and oxygen stable isotope records in Tosos and Fuendetodos sections are represented in Figure 3 (see also Annexe 4 for the values listed in table). The double measure per sample (labelled A and B attached to the name of the sample in the table) confirms the consistency of the carbon and oxygen stable isotope composition obtained for each analytical point, with a mean reproductibility of ± 0.2‰ for both $\delta^{13}C$ and $\delta^{18}O$ values.

The bulk $\delta^{13}C$ and $\delta^{18}O$ records of the shallow Tosos succession range between -3.5 to 2.3‰ for $\delta^{13}C$ and -7.1 to -2.4‰ for $\delta^{18}O$ (Fig. 6), with a mean value of 0.8‰ and -4.4‰, respectively. In general, this section shows low-amplitude fluctuations for both $\delta^{13}C$ and $\delta^{18}O$ records, in the order of ≤ 1‰ respect to the mean values (Fig. 3). Occasionally, there are negative shifts in the order of 2‰ for the $\delta^{13}C$ record in the backshoal oncolitic-stromatoporoid wackestone-packstone facies within the sequence 2 (at 31.5 m), and in the order of 3-4‰ in both $\delta^{13}C$ and $\delta^{18}O$ values for backshoal peloidal-oolitic packstone facies at the onset of sequence 4 (at 44.5 m).

The bulk $\delta^{13}C$ and $\delta^{18}O$ values along the relatively deep Fuendetodos succession vary between -5.6 to 1‰ and -6.6 to -3.5‰, respectively (Fig. 6), with a mean value of -1.4‰ for $\delta^{13}C$ and -5.3‰ for $\delta^{18}O$, thus reflecting a general ^{13}C and ^{18}O depletion compared to Tosos section. In addition, both $\delta^{13}C$ and $\delta^{18}O$ values show slightly higher-amplitude oscillations than in Tosos, in the order of 1-2‰ (Fig. 3). Two pronounced excursions respect to the mean values are reported for the $\delta^{13}C$ record, accompanied by a coupled and less pronounced shift in the $\delta^{18}O$ values: a negative excursion at the onset of sequence 2 (at 0.5 m) within offshore-proximal peloidal-bioclastic wackestone facies, with a deviation in the order of 3‰ for $\delta^{13}C$ and 1‰ for $\delta^{18}O$; and a positive shift in sequence 6 (at 44.5 m), coinciding with deposition of foreshoal peloidal grainstone facies, being the $\delta^{13}C$ and $\delta^{18}O$ records

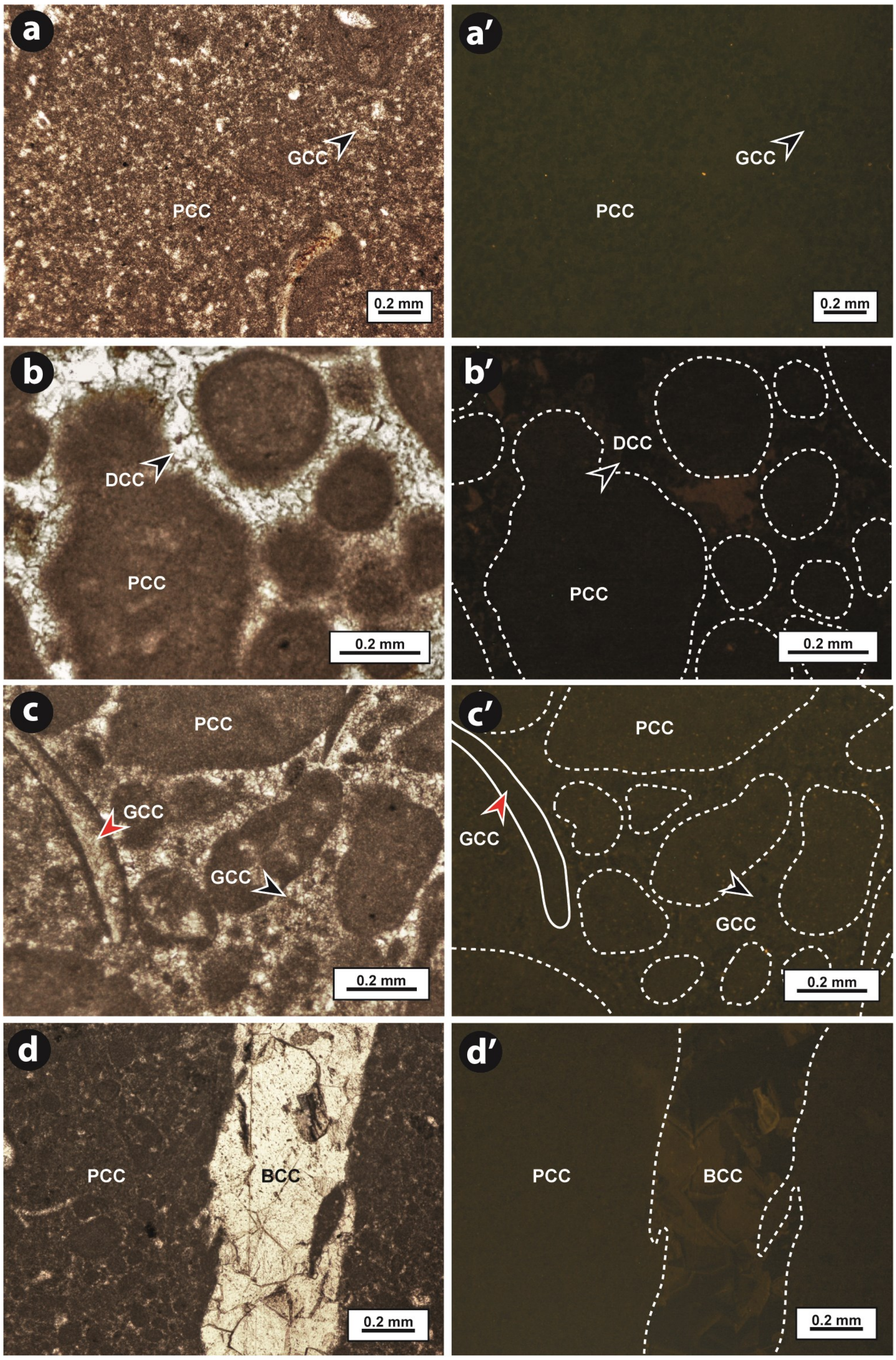

***Fig. 4**. Plain-light (a-d) and cathodoluminescence (a'-d') microphotographs of primary carbonate components (PCC) and diagenetic calcite cements (GCC: granular calcite cement; DCC: drusy calcite cement; BCC: blocky calcite cement) from the Fuendetodos section. The micrite matrix, peloids, ooids and some skeletal grains show no luminescence (a'-d'; the main primary carbonate components are indicated with dashed lines in b' and c'), whereas the diagenetic calcite cements display from non- to dull (red or yellow) luminescence: (a-a') GCC filling interparticle pores (arrows) with no luminescence; (b-b') DCC in interparticle pores (arrows) with non- to dull (red) luminescence; (c-c') GCC in bioclastic vugs (red arrows) and interparticle pores (black arrows) with non- to dull (red) luminescence; (d-d') BCC filling a rectilinear fissure, showing dull (yellow) luminescence. (a-a') Sample 1, offshore-proximal peloidal-bioclastic wackestone; (b-b') sample 33, foreshoal peloidal grainstone; (c-c') sample 36, foreshoal inter-buildup stromatoporoid-chaetetid-coral and oncolitic packstone; (d-d') sample 25, offshore-proximal inter-buildup stromatoporoid-chaetetid-coral and oncolitic packstone.*

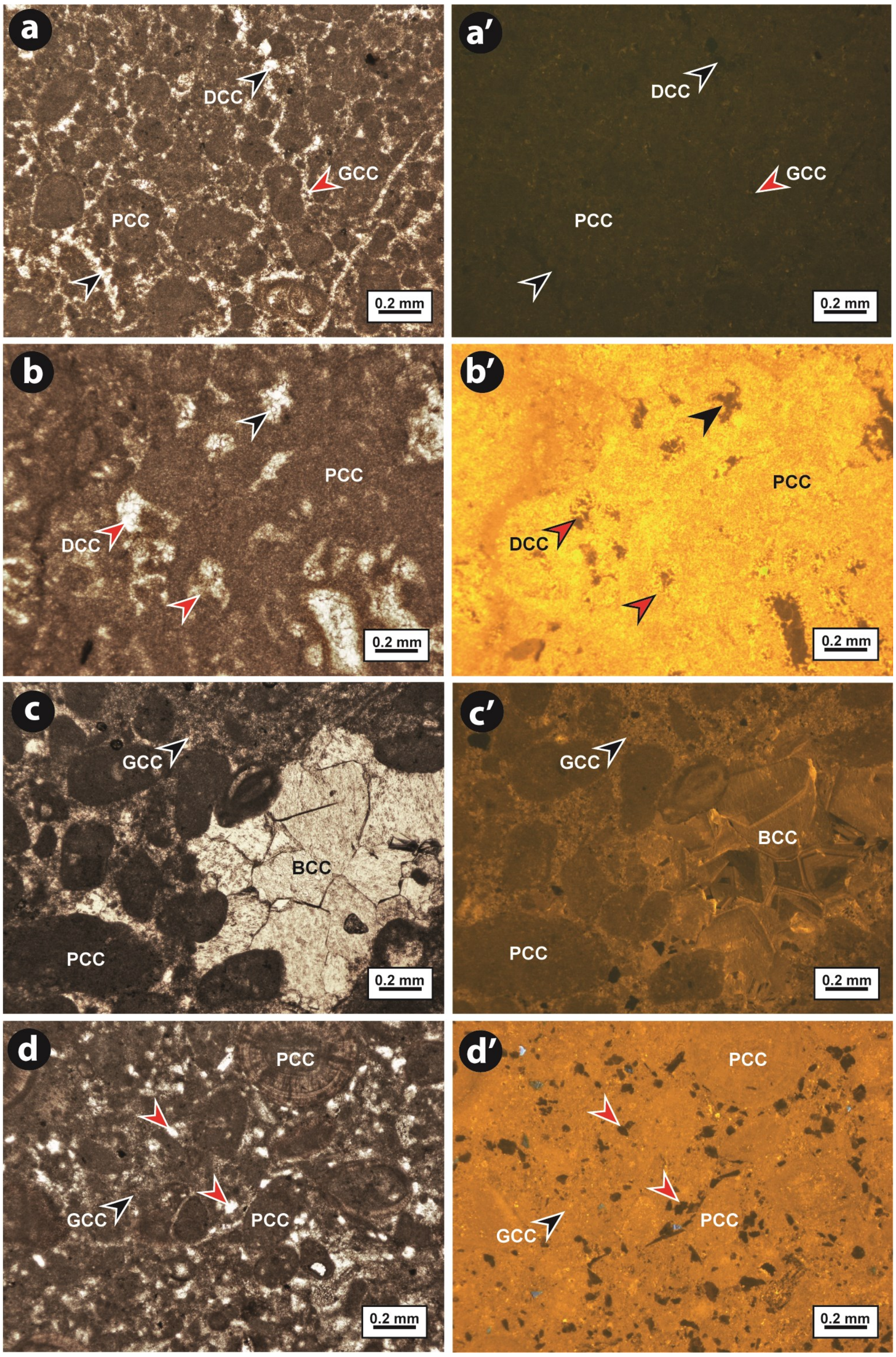

***Fig. 5**. Plain-light (a-d) and cathodoluminescence (a'-d') microphotographs of primary carbonate components (PCC) and diagenetic calcite cements (GCC: granular calcite cement; DCC: drusy calcite cement; BCC: blocky calcite cement) from the Tosos section. The micrite matrix and other carbonate components (peloids, ooids, skeletal grains; a-d) show from no luminescence (a') to bright yellow- or orange-coloured luminescence (b'-d'), and also for the diagenetic calcite cements: (a-a') DCC and GCC (black and red arrows, respectively) in interparticle pores with no luminescence; (b-b') PCC with yellow-coloured luminescence, and DCC in interparticle pores and mouldic vugs (black and red arrows, respectively) showing from non- to yellow-coloured luminescence; (c-c') PCC and GCC (arrows) in interparticle pores with yellow-coloured luminescence, and BCC in a probable mouldic vug displaying zoned (dark-yellow nuclei evolving to bright-yellow rims) luminescence; (d-d') PCC and GCC (black arrows) showing orange-coloured luminescence. Note the non-luminescent appearance for the quartz grains (red arrows). (a-a') Sample 6, foreshoal oncolitic packstone; (b-b') sample 22, backshoal peloidal-oolitic packstone; (c-c') sample 24, backshoal peloidal-oolitic packstone; (d-d') sample 29, restricted lagoon peloidal-bioclastic-oolitic packstone.*

deviated in the order of 3 and 2‰, respectively. The isotopic signal on the three specimens of *Trichites* collected in the lower part of this section shows the higher $\delta^{13}C$ values but a wider range for the $\delta^{18}O$ signature (Fig. 6), ranging between 1.3 to 2.5‰ for $\delta^{13}C$ and -4.8 to -2.2‰ for $\delta^{18}O$.

The bulk carbon and oxygen stable isotope stratigraphy in both sections reveals no distinctive long-term $\delta^{13}C$ and $\delta^{18}O$ patterns, and the $\delta^{13}C$ and $\delta^{18}O$ trends observed within time-equivalent high-frequency sequences highly vary from one section to another (Fig. 3). Moreover, the bulk isotopic stratigraphy shows that the $\delta^{13}C$ and $\delta^{18}O$ values fluctuate in covariance, being the degree of such $\delta^{18}O/\delta^{13}C$ covariance relatively lower in Tosos (r^2 = 0.29) but moderate in Fuendetodos (r^2 = 0.52) (Fig. 7). In addition, the cross-plots of the bulk $\delta^{13}C$ and $\delta^{18}O$ values per facies types in each section do not show differentiated isotopic composition patterns regarding the facies type (Fig. 7), with the exception of the restricted lagoon peloidal-bioclastic-oolitic packstone facies in the Tosos section, which shows higher $\delta^{18}O$ values compared to the rest of the facies (Fig. 7a).

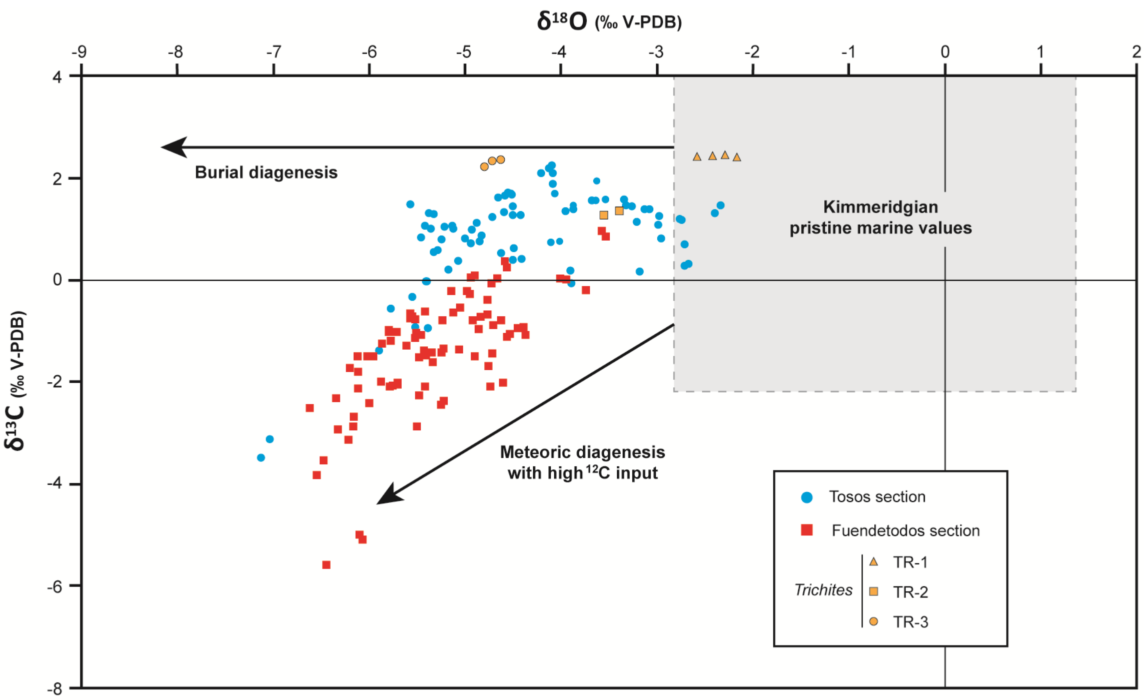

Fig. 6. *Scatter ($\delta^{18}O$, $\delta^{13}C$) diagram comparing the analysed bulk carbonates in Tosos and Fuendetodos sections, including the isotopic composition of the calcitic bivalve shells from the three specimens of Trichites collected in the lower part of the Fuendetodos section (samples TR-1 to TR-3). The field of Kimmeridgian pristine marine values is based on the compilation of the stable isotope compositions obtained from well-preserved fossils (mainly belemnites) in Riboulleau et al. (1998), Jenkyns et al. (2002), Wierzbowski (2004) and Nunn and Price (2010). Trajectories indicating isotopic fields of carbonates influenced by burial and meteoric diagenesis are indicated, the latter incorporating high organic ^{12}C content (based on Lavastre et al., 2011).*

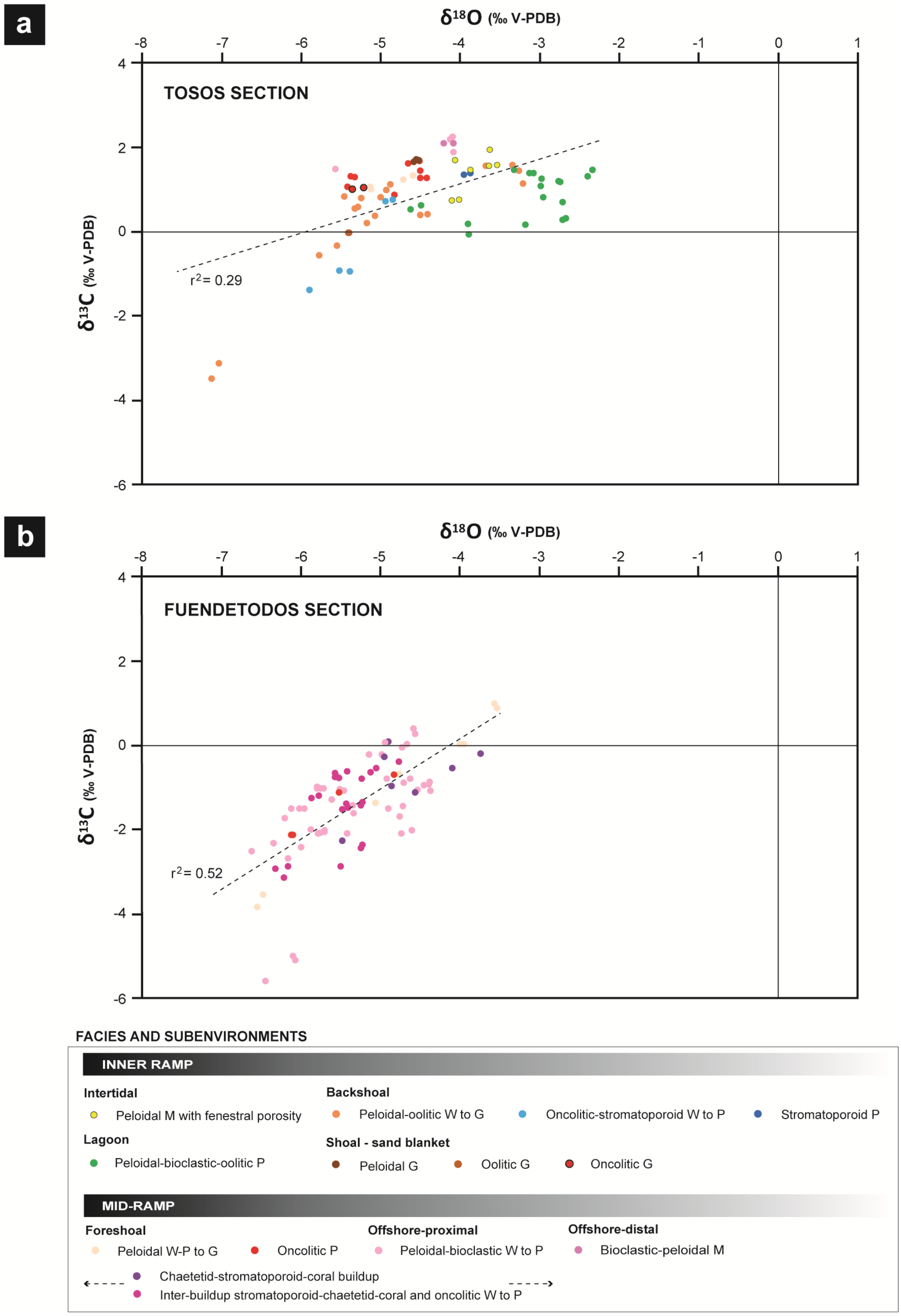

***Fig.** 7. Cross-plots of $\delta^{13}C$ and $\delta^{18}O$ values of the analysed bulk carbonates in Tosos (a) and Fuendetodos (b) sections according to the facies type. The $\delta^{18}O/\delta^{13}C$ covariance is relatively low in the Tosos section ($r^2 = 0.29$), but moderate in the Fuendetodos section ($r^2 = 0.52$). The scatter of the $\delta^{13}C$ and $\delta^{18}O$ data for both sections does not show distinct patterns regarding the facies type, with the exception of the restricted lagoon peloidal-bioclastic-oolitic packstone facies in the Tosos section (a).*

6. Interpretation and discussion

6.1. Diagenetic alteration on carbon and oxygen stable isotope record

The primary carbon and oxygen stable isotope data can be altered by several diagenetic processes, in some cases obliterating the imprint of local and/or regional isotopic records with palaeoenvironmental significance (e.g. Given and Lohmann, 1985; Marshall, 1992; Immenhauser et al., 2002; Huck et al., 2017). This is the case of the uppermost Kimmeridgian shallow-marine carbonate successions studied in this work, where the scatter diagram for the measured bulk $\delta^{13}C$ and $\delta^{18}O$ values of Tosos and Fuendetodos sections shows that diagenesis significantly altered the original isotopic signature of these carbonate deposits in both localities, although with distinctive differences in each section (Fig. 6).

Oxygen isotope values for bulk carbonates in Tosos (-7.1 to -2.4‰) and Fuendetodos (-6.6 to -3.5‰) are lower than those described in the literature for the Kimmeridgian pristine marine carbonates (between -2.8 to 1.4‰; e.g. Riboulleau et al., 1998; Jenkyns et al., 2002; Wierzbowski, 2004; Nunn and Price, 2010). If we consider that these Kimmeridgian pristine marine values are valid for the Kimmeridgian shallow-water domains in the Iberian Basin, the different magnitude of such deviation in Fuendetodos and Tosos can be used to discuss the imprint of the diagenetic alteration. In particular, the deviation of the $\delta^{18}O$ values respect to the Kimmeridgian pristine marine carbonates is higher in Fuendetodos than in Tosos, in the order of 1 to 3‰ for Tosos and of 2 to 3‰ for Fuendetodos. The variation for carbon isotope values also shows remarkable differences between both sections. In Tosos section, the $\delta^{13}C$ values (-3.5 to 2.3‰, with most of the values ranging between -1.4 to 2.3‰) are similar to those described in the Kimmeridgian pristine marine carbonates (between -2.3 to 4.7‰; e.g. Riboulleau et al., 1998; Jenkyns et al., 2002; Wierzbowski, 2004; Nunn and Price, 2010), but in Fuendetodos, these values are lower than those described in the literature (-5.6 to 1‰, with most of the values ranging between -3.8 to 0.25‰), in the order of 3 to 4‰.

The three specimens of *Trichites* collected in Fuendetodos section have potential to record the original latest Kimmeridgian seawater stable isotope composition, as reported by previous authors (e.g. Zuo et al., 2018). However, the diagenetic overprint reported on the bulk carbonates in the studied sections can be also reflected on the $\delta^{13}C$ and $\delta^{18}O$ values of the *Trichites* calcitic shells (Fig. 6): sample TR-1 shows the closer $\delta^{13}C$ and $\delta^{18}O$ values respect to the Kimmeridgian pristine marine carbonates (a mean value of 2.4‰ for $\delta^{13}C$ and of -2.4‰ for $\delta^{18}O$; see Annexe 4 for the values listed in table), but also fall within the range of those reported for the diagenetically altered bulk carbonates in the Tosos section. In addition, the two other specimens (samples TR-2 and TR-3) display a higher deviation in the $\delta^{18}O$ signature, in the order of 1-2‰ respect to the Kimmeridgian pristine marine values. Therefore, these $\delta^{13}C$ and $\delta^{18}O$ values of these specimens of *Trichites* seem to have been also diagenetically altered.

The diagenetic alteration affecting the studied carbonate deposits overprinted a possible palaeoenvironmental signal from the isotopic record. The covarying trend of the $\delta^{13}C$ and $\delta^{18}O$ stratigraphy in Tosos and Fuendetodos sections can be interpreted as an indicator of this diagenetic resetting, as traditionally reported in the literature (e.g. Allan and Mathews, 1982; Fike et al., 2006; Grotzinger et al., 2011; Metzger and Fike, 2013), although recently it has been suggested that such covariance is not a definitive marker of diagenetic alteration (Swart and Oehlert, 2018). However, in this case, this assumption can be considered since no other evidences in both Tosos and Fuendetodos sections support the preservation of a palaeoenvironmental signal from the isotopic record, such as:

1) the absence of a facies-dependent pattern on the isotopic record which could be associated with changes in the depositional conditions (e.g. Patterson and Walter, 1994; Immenhauser et al., 2002, 2003; Colombié et al., 2011; Zuo et al., 2018) (Fig. 7); 2) the non-recognition of distinctive long-term variation patterns from the $\delta^{13}C$ and $\delta^{18}O$ stratigraphy (Fig. 3), showing these values low-amplitude oscillations in both sections with local excursions; and 3) the highly varying vertical $\delta^{13}C$ and $\delta^{18}O$ trends observed within the time-equivalent high-frequency sequences from one section to another (Fig. 3), being not possible to stablish a significance for these isotopic variations.

6.2. Comparison between Tosos-Fuendetodos: burial vs meteoric diagenetic alteration

The $\delta^{18}O$ record in Tosos section, with most of the data points deviated towards very low $\delta^{18}O$ values (Fig. 6), is characteristic of closed high-temperature burial diagenetic systems with low rock-water interaction (e.g. Banner and Hanson, 1990; Marshall, 1992; Plunkett, 1997; van der Kooij et al., 2009; Madden and Wilson, 2013; Swart, 2015). Hot burial fluids in contact with carbonate rocks originate a depletion in the $\delta^{18}O$ values, but a low interaction between circulating fluids and rocks barely alters the carbon stable isotope composition, because of its different temperature-related fractionation and comparatively low content in most of the diagenetic fluids (Brand and Veizer, 1981; Magaritz, 1983; Lohmann, 1988; Morse and MacKenzie, 1990; Marshall, 1992; Immenhauser et al., 2002). This fits with the $\delta^{13}C$ values in Tosos section, being these values close to those of the Kimmeridgian pristine marine carbonates (Fig. 6). In contrast, the dispersion observed for the data in the Fuendetodos section, with a significant depletion in both $\delta^{13}C$ and $\delta^{18}O$ values, suggests a higher water-rock interaction under circulating ^{18}O-depleted meteoric fluids incorporating organic ^{12}C probably derived from soil weathering (e.g. Hudson, 1977; Allan and Matthews, 1982; O'Neil, 1987; Lohmann, 1988; Vogel, 1993; Patterson and Walter, 1994; Moore, 2001; Immenhauser et al., 2002; Lavastre et al. 2011; Bahamonde et al., 2017). In addition, the $\delta^{18}O/\delta^{13}C$ covariance in Fuendetodos is higher and relatively significant ($r^2 = 0.52$) compared to Tosos ($r^2 = 0.29$), highlighting a major disturbance of the primary isotopic composition in Fuendetodos (e.g. Marshall, 1992; Veizer et al., 1997; Rosales et al., 2001).

The variable diagenetic overprint recorded on the isotopic composition in Tosos and Fuendetodos sections is consistent with the different post-depositional processes occurring in this part of the Iberian Basin from the end of the Kimmeridgian. In Tosos, the uppermost Kimmeridgian carbonates of the Higueruelas Fm studied here are overlain by a thick (up to 800 m) continental succession deposited during the middle Valanginian-middle Miocene (e.g. Pérez et al., 1985; Pérez, 1989; Soria et al., 1995), with two long-lasting periods of subaerial exposure during the latest Kimmeridgian-middle Valanginian, and the middle Barremian-Paleocene. In contrast, the Fuendetodos sector remained mostly exposed until the Cenozoic, and the Higueruelas Fm is only overlain by a c. 200 m-thick succession of middle Miocene lacustrine carbonates (e.g. Pérez et al., 1985; Pérez, 1989). These particular post-depositional histories controlled different diagenetic processes affecting the uppermost Kimmeridgian deposits in both localities, as reflected on the isotopic record (Fig. 6): in Tosos sector, the Higueruelas Fm was affected by a long burial history (negative deviation of $\delta^{18}O$, but not of $\delta^{13}C$ values, due to hot burial diagenetic fluids), whereas these deposits in Fuendetodos sector were mainly subjected to meteoric alteration (negative deviation of both $\delta^{18}O$ and $\delta^{13}C$ values).

6.3. Is diagenetic alteration dependent on facies type?

As mentioned above, palaeoenvironmental factors controlling sedimentation in the latest Kimmeridgian shallow carbonate ramp are not reflected on the isotopic composition obtained for these carbonates in Tosos and Fuendetodos sections. Different diagenetic processes governing the post-depositional evolution of the Higueruelas Fm have instead determined the $\delta^{13}C$ and $\delta^{18}O$ signature in each section. In this regard, considering the variability in the textural characteristics observed for the analysed deposits, the effect of the diagenetic alteration on the carbon and oxygen stable isotope record can be variable in function of the fabric type, being the coarser fabrics more favourable for fluid circulation which may derive in a higher diagenetic overprint (e.g. Marshall, 1992; Immenhauser et al., 2002; Vincent et al., 2004; Coimbra et al., 2014; Huck et al., 2017; Al-Mojel et al., 2018). Therefore, for the Higueruelas Fm, a tentatively approximation of the possible link between textural characteristics and the degree of alteration of the primary isotopic signature has been approached with the available data in Figure 8.

In Tosos, a variable response to the diagenetic alteration regarding the fabric type can be appreciated (Fig. 8a). There is a particular difference in the isotopic composition scatter for the grainstone textures, showing the lowest $\delta^{13}C$ and $\delta^{18}O$ values compared to the rest of the fabrics. In the Fuendetodos section, however, the diagenetic alteration indistinctly affected the carbonate deposits, not reporting differentiated $\delta^{13}C$ and $\delta^{18}O$ values regarding the fabric type (Fig. 8b). This distinct pattern in the texture-diagenetic alteration relationship in Tosos and Fuendetodos sections could be related with the different post-depositional processes affecting the Higueruelas Fm in both localities. This distinction highlights that for the Tosos section, which underwent a long burial history, it is probable that the diagenetic alteration on these carbonates were predominantly controlled by this diagenetic process, and so as reflecting a variable fluid-rock interaction regarding the porosity and permeability of the sediment. In contrast, the Higueruelas Fm in the Fuendetodos section was mostly exposed to meteoric weathering, and therefore to a probably more complex succession of diagenetic events (meteoric waters of different nature), thus obliterating a texture-diagenetic alteration pattern. This is also supported by the higher diagenetic alteration reported for Fuendetodos (i.e. the lowest $\delta^{13}C$ and $\delta^{18}O$ values) compared to Tosos section.

The differences observed in the relationship between the fabric type and the diagenetic alteration in Tosos and Fuendetodos sections, arise an interesting question concerning the variable effect of different diagenetic processes affecting carbonate deposits constituted by similar components. In this regard, the information obtained by the petrographic and cathodoluminescence descriptions provides relevant data to take into account for evaluating the variable diagenetic imprint in both sections. Luminescence is a common indicator of diagenetic alteration (e.g. Popp et al., 1986; Middleton et al., 1991), being the orange- or yellow-coloured luminescence normally attributed to the incorporation of Mn^{2+} under non-oxidizing (generally burial) conditions during water-rock interaction. The absence of luminescence can be in turn attributed to both the absence of diagenetic alteration or the incorporation of iron-rich diagenetic fluids, since Fe^{2+} is a common inhibitor resulting in dull or no luminescence (e.g. Machel, 1985; Marshall, 1992; Savard et al., 1995; Richter et al., 2003; Flügel, 2004; Hiatt and Pufahl, 2014). Therefore, the absence or weakly luminescence generally observed for the diagenetically altered carbonates of the Higueruelas Fm (non-luminescent micrite and carbonate grains, and a general non- to dull (red) luminescence for the diagenetic calcite cements; Figs 4a'-d' and 5a'), points to the incorporation of Fe^{2+} in the crystal lattice. Accordingly, it is remarkable that both primary carbonate components and diagenetic calcite cements in both sections, despite of being governed by different diagenetic processes reflected on their variable isotopic compositions, show similar cathodoluminescence properties (Figs 4a'-d' and 5a'), excepting some of the samples in the Tosos section (i.e. samples 22, 24 and 29; Fig. 3), which appear with a uniformly yellow- to orange-coloured luminescence (Fig. 5b'-d'). However, since only a small group of the total of the analysed bulk carbonates (i.e. 21 samples from a total of 72) were selected in this work for the CL analysis, this discrepancy between isotopic signatures and cathodoluminescence characteristics must be better investigated with more CL observations, also including staining the samples with potassium ferricyanide (an acid solution which reacts in presence of ferrous iron) and/or performing trace elements geochemical analyses to assist the Fe^{2+} content of the carbonates, thus linking the observed non- to dull luminescence with the probable influence of iron-rich diagenetic fluids.

The remarkable differences concerning the isotopic signature between Tosos and Fuendetodos sections (Fig. 6), together with the variable response of the fabric types to the diagenetic alteration regarding the section (Fig. 8) and the cathodoluminescence observations (Figs 4 and 5), lay the background for further analyses in order to understand the variable imprint of the different diagenetic processes affecting these shallow-marine carbonates in each section. This diagenetic study must concern a detailed petrographic characterization of these deposits in terms of diagenetic features, including more cathodoluminescence observations and staining the samples with potassium ferricyanide and/or performing trace elements geochemical analyses (particularly Mn and Fe). In addition, in order to evaluate the imprint of such diagenetic processes, it is important to consider that the degree of porosity and permeability of these deposits, particularly for the grainstone fabrics, also depends on the type of the dominant components (e.g. peloids, ooids and/or oncoids), since the grain size is an important factor that determines the volume of interparticle spaces. On the other hand, special attention also concerns to evaluate the evolution of the porosity and permeability of the sediment during the post-depositional burial stage (i.e. early vs late cementation), by the identification of different diagenetic phases from the calcite cements (granular, drusy and blocky calcite cements) filling the interparticle and fenestral pores, mouldic vugs and/or calcite veins, according with their time of formation (i.e. the paragenetic sequence). This characterization would help to clarify the link between the variable isotopic response in relation to the fabric type obtained in each section, according to their different post-depositional history.

Fig. 8 (Next page). *Cross-plots of $\delta^{13}C$ and $\delta^{18}O$ values of the analysed bulk carbonates in Tosos (a) and Fuendetodos (b) sections according to fabric types. For simplification, four categories of textures are indicated: mudstone, wackestone (including mudstone-wackestone), packstone (including wackestone-packstone) and grainstone (including packstone-grainstone). A relationship between the degree of diagenetic alteration and the fabric type is observed in the Tosos section (a), but not in the Fuendetodos section (b).*

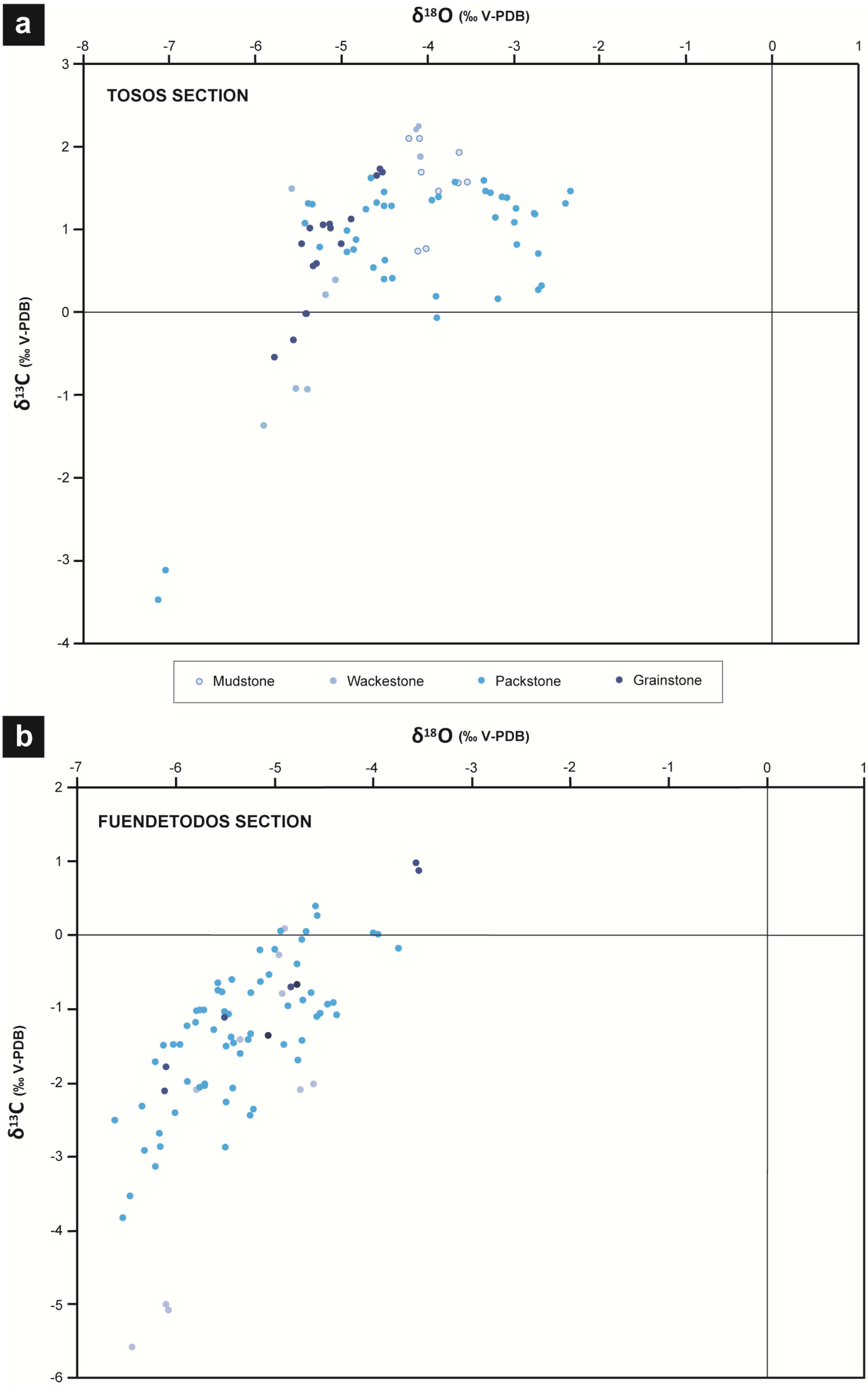
a
δ18O (‰ V-PDB)
δ13C (‰ V-PDB)
TOSOS SECTION
Mudstone
Wackestone
Packstone
Grainstone
b
δ18O (‰ V-PDB)
δ13C (‰ V-PDB)
FUENDETODOS SECTION

7. Conclusions

Bulk carbon and oxygen stable isotope compositions recorded in the uppermost Kimmeridgian shallow carbonate ramp deposits in the northern Iberian Basin (Higueruelas Fm, NE Spain), reveal the variable effect of the burial and meteoric diagenesis in two selected sections representing the proximal (Tosos section) and relatively distal (Fuendetodos section) areas of the carbonate ramp.

In Tosos section, the cross-plot of the bulk $\delta^{13}C$ and $\delta^{18}O$ values shows a significant decrease in the $\delta^{18}O$ signature compared with the Kimmeridgian pristine marine carbonates, but instead a similar carbon isotope composition. This type of diagenetic alteration results from a post-depositional evolution in a closed high-temperature burial system with a low interaction between the host carbonate rock and diagenetic fluids. In this area, the Higueruelas Fm was affected by a long burial history, as these deposits are overlain by a c. 800 m-thick continental succession deposited during the middle Valanginian-middle Miocene. On the contrary, the Higueruelas Fm around the Fuendetodos sector remained mostly exposed to meteoric weathering from the latest Kimmeridgian until the early Miocene, recording a significant depletion in both $\delta^{13}C$ and $\delta^{18}O$ values. In both sections, the strong influence exerted by the diagenetic alteration makes the $\delta^{13}C$ and $\delta^{18}O$ records unsuitable for addressing palaeoenvironmental reconstructions.

Differences in the magnitude of the diagenetic alteration could also be dependent on the facies types. In Tosos section, the grainstone textures are those showing the lowest $\delta^{13}C$ and $\delta^{18}O$ values compared to the rest of the fabrics; but for Fuendetodos section, no differentiated isotopic composition patterns regarding the fabric type are observed. In contrast to the isotopic record, the similarities reported for the petrographic and cathodoluminescence observations with the available data, point to further investigate the effect of different diagenetic processes affecting carbonate deposits constituted by similar components.

An interesting point that arises in this study is being able to correlate the post-depositional evolution of the Higueruelas Fm in each section with the resultant carbon and oxygen stable isotope record. In addition, differences in the texture-diagenetic alteration relationship revealed for Tosos and Fuendetodos sections, lead to posing a link between the variable isotopic response of these carbonates in relation to the fabric type and the complexity in the diagenetic processes according to particular post-depositional histories.

Acknowledgments

This work was funded by projects CGL 2017-85038-P and Group E18 (Aragosaurus: Recursos Geológicos y Paleoambientales) subsidized by the Spanish Ministry of Science and Innovation, the European Regional Development Fund and the Government of Aragón. The research of Cristina Sequero is funded by a FPU Grant subsidized by the Spanish Ministry of Science and Innovation. We also appreciate the financial support provided by the International Association of Sedimentologists (IAS Postgraduate Grant Scheme) and the use of the Servicio General de Apoyo a la Investigación-SAI, Universidad de Zaragoza. The authors also gratefully acknowledge Idoia Rosales (Instituto Geológico y Minero de España, IGME) for the laboratory assistance in cathodoluminescence microscopy, and Ana Moreno (Instituto Pirenaico de Ecología, IPE, Spain) for providing the laboratory instrumental for sampling.

References

Allan, J.R., Matthews, R.K., 1982. Isotope signatures associated with early meteoric diagenesis. Sedimentology 29, 797-817.

Al-Mojel, A., Dera, G., Razin, P., Le Nindre, Y-M., 2018. Carbon and oxygen isotope stratigraphy of Jurassic platform carbonates from Saudi Arabia: Implications for diagenesis, correlations and global paleoenvironmental changes. Palaeogeography, Palaeoclimatology, Palaeoecology 511, 388-402.

Anderson, T.F., Arthur, M.A., 1983. Stable isotopes of oxygen and carbon and their application to sedimentologic and paleoenvironmental problems. In: Arthur, M.A., Anderson, T.F., Kaplan, I.R., Veizer, J., Land, L.S. (Eds.), Stable Isotopes in Sedimentary Geology. SEPM Short Course 10, Tulsa, pp. 1-151.

Aurell, M., Meléndez, A., 1986. Sedimentología de la Formación Calizas con oncolitos de Higueruelas (Malm) en la región de Muel-Belchite (Provincia de Zaragoza). Acta Geológica Hispánica 21-22, 307-312.

Aurell, M., Robles, S., Bádenas, B., Rosales, I., Quesada, S., Meléndez, G., García-Ramos, J.C., 2003. Transgressive-regressive cycles and Jurassic palaeogeography of northeast Iberia. Sedimentary Geology 162, 239-271.

Aurell, M., Bádenas, B., Ipas, J., Ramajo, J., 2010. Sedimentary evolution of an Upper Jurassic epeiric carbonate ramp, Iberian Basin, NE Spain. In: Van Buchem, F.S.P., Gerdes, K.D., Esteban. M. (Eds.), Mesozoic and Cenozoic Carbonate Systems of the Mediterranean and the Middle East: Stratigraphic and Diagenetic Reference Models. Geological Society, London, Special Publications 329, pp. 89-111.

Aurell, M., Ipas, J., Bádenas, B., Muñoz, A., 2012. Distribución de facies con corales y estromatopóridos en el dominio interno de una plataforma carbonatada (Titónico, Cordillera Ibérica). Geogaceta 51, 67-70.

Aurell, M., Bádenas, B., Canudo, J.I., Castanera, D., García-Penas, A., Gasca, J.M., Martín-Closas, C., Moliner, L., Moreno-Azanza, M., Rosales, I., Santas, L., Sequero, C., Val, J., 2019. Kimmeridgian-Berriasian stratigraphy and sedimentary evolution of the central Iberian Rift System (NE Spain). Cretaceous Research 103, 104153.

Bádenas, B., Aurell, M., 2001. Kimmeridgian palaeogeography and basin evolution of northeastern Iberia. Palaeogeography, Palaeoclimatology, Palaeoecology 168, 291-310.

Bádenas, B., Aurell, M., 2003. Análisis comparado y controles en la sedimentación de dos arrecifes de la zona media de una rampa carbonatada del Jurásico Superior de la Cordillera Ibérica. Revista de la Sociedad Geológica de España 16 (3-4), 151-166.

Bahamonde, J.R., Della Porta, G., Merino-Tomé, O.A., 2017. Lateral variability of shallow-water facies and high-frequency cycles in foreland basin carbonate platforms (Pennsylvanian, NW Spain). Facies 63 (6).

Banner, J.L., Hanson, G.N., 1990. Calculation of simultaneous isotopic and trace element variations during water-rock interaction with applications to carbonate diagenesis. Geochimica et Cosmochimica Acta 54 (11), 3123-3137.

Bartolini, A., Pittet, B., Mattioli, E., Hunziker, J.C., 2003. Shallow-platform palaeoenvironmental conditions recorded in deep-shelf sediments: C and O stable isotopes in Upper Jurassic sections of southern Germany (Oxfordian–Kimmeridgian). Sedimentary Geology 160, 107-130.

Brand, U., Veizer, J., 1980. Chemical diagenesis of a multicomponent carbonate system -1: trace elements. Journal of Sedimentary Petrology 50, 1219-1236.

Brand, U., Veizer, J., 1981. Chemical diagenesis of a multicomponent carbonate system -2: Stable isotopes. Journal of Sedimentary Petrology 51, 987-997.

Brand, U., Posenato, R., Came, R., Affek, H., Angiolini, L., Azmy, K., Farabegoli, E., 2012. The end-Permian mass extinction: a rapid volcanic CO2 and CH4-climatic catastrophe. Chemical Geology 322, 121-144.

Carpenter, S.J., Lohmann, K.C., 1989. $\delta^{18}O$ and $\delta^{13}C$ variations in Late Devonian marine cements from the Golden Spike and Nevis reefs, Alberta, Canada. Journal of Sedimentary Petrology 59, 792-814.

Carpenter, S.J., Lohmann, K.C., 1997. Carbon isotope ratios of Phanerozoic marine cements: re-evaluating the global carbon and sulfur systems. Geochimica et Cosmochimica Acta 61, 4831-4846.

Coimbra, R., Immenhauser, A., Olóriz, F., 2014. Spatial geochemistry of Upper Jurassic marine carbonates (Iberian subplate). Earth-Science Reviews 139, 1-32.

Colombié C., Lécuyer C., Strasser A., 2011. Carbon- and oxygen-isotope records of palaeoenvironmental and carbonate production changes in shallow-marine carbonates (Kimmeridgian, Swiss Jura). Geological Magazine 148 (1), 133-153.

Cortés Gracia, A.L., Casas Sainz, A.M., 1996. Deformación alpina de zócalo y cobertera en el borde norte de la Cordillera Ibérica (Cubeta de Azuara-Sierra de Herrera). Revista de la Sociedad Geológica de España 9 (1-2), 51-66.

Cortés, A.L., Liesa, C.L., Soria, A.R., Meléndez, A., 1999. Role of extensional structures on the location of folds and thrusts during tectonic inversion (northern Iberian Chain, Spain). Geodinamica Acta 12 (2), 113-132.

Dercourt, J., Ricou, L., Vrielynck, B., 1993. Atlas: Tethys palaeoenvironmental Maps. Gauthier-Villars, Paris, pp. 14.

Eltom, H.A., Gonzalez, L.A., Hasiotis, S.T., Rankey, E.C., Cantrell, D.L., 2018. Paleogeographic and paleo-oceanographic influences on carbon isotope signatures: Implications for global and regional correlation, Middle-Upper Jurassic of Saudi Arabia. Sedimentary Geology 364, 89-102.

Fike, D.A., Grotzinger, J.P., Pratt, L.M., Summons, R.E., 2006. Oxidation of the Ediacaran Ocean. Nature 444, 744-747.

Flügel, E., 2004. Microfacies of Carbonate Rocks. Analysis, Interpretation and Application. Springer-Verlag, Germany, pp. 976.

Given, R.K., Lohmann, K.C., 1985. Derivation of the original isotopic composition of Permian marine carbonates. Journal of Sedimentary Petrology 55, 430-439.

Glumac, B., Walker, K., 1998. A Late Cambrian positive carbon-isotope excursion in the southern Appalachians: relation to biostratigraphy, sequence stratigraphy, environments of deposition, and diagenesis. Journal of Sedimentary Research 68 (6), 1212-1222.

Grötsch, H.J., Billing, I., Vahrenkamp, V., 1998. Carbon-isotope stratigraphy in shallow-water carbonates: implications for Cretaceous black-shale deposition. Sedimentology 45, 623-634.

Grotzinger, J.P., Fike, D.A. Fischer, W.W., 2011. Enigmatic origin of the largest-known carbon isotope excursion in Earth's history. Nature Geoscience 4, 285-292.

Guimerà, J., Álvaro, M., 1990. Structure et évolution de la compression alpine dans la Chaîne Ibérique et la Chaîne côtière catalane (Espagne). Bulletin de la Societé géologique de France 6 (2), 339-348.

Hiatt, E.E., Pufahl, P.K., 2014. Cathodoluminescence petrography of carbonate rocks: a review of applications for understanding diagenesis, reservoir quality, and pore system evolution. In: Coulson, I.M. (Ed.), Cathodoluminescence and its application to geoscience. Mineralogical Association of Canada Short Course 45, pp. 75-96.

Huck, S., Wohlwend, S., Coimbra, R., Christ, N., Weissert, H., 2017. Disentangling shallow-water bulk carbonate carbon isotope archives with evidence for multi-stage diagenesis: An in-depth component-specific petrographic and geochemical study from Oman (mid-Cretaceous). The Depositional Record 3, 233-257.

Hudson, J.D., 1977. Stable isotopes and limestone lithification. Journal of the Geological Society 133 (6), 637-660.

Immenhauser, A., Kenter, J.A.M., Ganssen, G., Bahamonde, J.R., Van Vliet, A., Saher, M.H., 2002. Origin and significance of isotope shifts in Pennsylvanian carbonates (Asturias, NW Spain). Journal of Sedimentary Research 72 (1), 82-94.

Immenhauser, A., Della Porta, G., Kenter, J.A., Bahamonde, J.R., 2003. An alternative model for positive shifts in shallow-marine carbonate $\delta^{13}C$ and $\delta^{18}O$. Sedimentology 50 (5), 953-959.

Ipas, J., Aurell, M., Bádenas, B., 2004. Ambientes sedimentarios y secuencias en la Fm. Higueruelas (Jurásico Superior) en la Cordillera Ibérica Septentrional. Geogaceta 35, 7-10.

Jenkyns, H.C., Clayton, C.J., 1986. Lower Jurassic epicontinental carbonates and mudstones from England and Wales: chemostratigraphic signals and the early Toarcian anoxic event. Sedimentology 44, 687-706.

Jenkyns, H.C., Jones, C.E., Gröcke, D.R., Hesselbo, S.P., Parkinson, D.N., 2002. Chemostratigraphy of the Jurassic System: applications, limitations and implications for palaeoceanography. Journal of the Geological Society, London, 159, 351-378.

Joachimski, M.M., 1994. Subaerial exposure and deposition of shallowing upward sequences: evidence from stable isotopes of Purbeckian peritidal carbonates (basal Cretaceous), Swiss and French Jura Mountains. Sedimentology 41, 805-824.

Lavastre, V., Ader, M., Buschaert, S., Petit, E., Javoy, M., 2011. Water circulation control on carbonate- δ^{18}O records in a low permeability clay formation and surrounding limestones: the Upper Dogger–Oxfordian sequence from the eastern Paris basin, France. Applied Geochemistry 26 (5), 818-827.

Lavoie, D., Bourque, P.A., 1993. Marine burial and meteoric diagenesis of early Silurian carbonate ramps, Quebec Appalachians, Canada. Journal of Sedimentary Petrology 63 (2), 233-247.

Liesa, C.L., Soria, A.R., Casas, A., Aurell, M., Meléndez, N., Bádenas, B., Fregenal-Martínez, M., Navarrete, R., Peropadre, C., Rodríguez-López, J.P., 2019. The South Iberian, Central-Iberian and Maestrazgo basins. In: Quesada, C., Oliveira, J.T. (Eds.), The Geology of Iberia: A Geodynamic Approach Vol. 3. Springer Nature Switzerland AG, Alpine Cycle, pp. 214-228.

Lohmann, K.C., 1988. Geochemical patterns of meteoric diagenetic systems and their application to studies of paleokarst. In: James, N.P., Choquette, P.W. (Eds.), Paleokarst. Springer-Verlag, Berlin, pp. 50-80.

Machel, H.G., 1985. Cathodoluminiscence in calcite and dolomite and its chemical interpretation. Geoscience Canada 12 (4), 139-147.

Madden, R., Wilson, M.E., 2013. Diagenesis of a SE Asian Cenozoic carbonate platform margin and its adjacent basinal deposits. Sedimentary Geology 286-287, 20-38.

Magaritz, M., 1983. Carbon and oxygen isotope composition of recent and ancient coated grains. In: Peryt, T.M. (Ed.), Coated Grains. Berlin, Springer-Verlag, pp. 27-37.

Marshall, J.D., 1992. Climatic and oceanographic isotopic signals from the carbonate rock record and their preservation. Geological Magazine 129, 143-160.

McConnaughey, T.A., 1989a. ^{13}C and ^{18}O isotopic disequilibrium in biological carbonates: I. Patterns. Geochimica et Cosmochimica Acta, 53, 151-162.

McConnaughey, T.A., 1989b. ^{13}C and ^{18}O isotopic disequilibrium in biological carbonates: II. *In vitro* simulation of kinetic isotope effects. Geochimica et Cosmochimica Acta 53, 163-171.

Metzger, J.G., Fike, D.A., 2013. Techniques for assessing spatial heterogeneity of carbonate δ^{13}C values: Implications for craton-wide isotope gradients. Sedimentology 60, 1405-1431.

Middleton, P.D., Marshall, J.D., Brenchley, P.J., 1991. Evidence for isotopic changes associated with the Late Ordovician glaciation from brachiopods and marine cements from central Sweden. In: Barnes, C.R., Williams, S.H. (Eds.), Advances in Ordovician Geology. Geological Survey of Canada, pp. 313-323.

Moore, C.H., 1989. Carbonate Diagenesis and Porosity. Developments in Sedimentology Vol. 46, Amsterdam, Elsevier, pp. 337.

Moore, C.H., 2001. Carbonate Reservoirs: Porosity evolution and diagenesis in a sequence stratigraphic framework. Elsevier, pp. 460.

Morse, J.W., Mackenzie, F.T., 1990. Geochemistry of sedimentary carbonates: Developments in Sedimentology vol. 48, pp.707.

Nelson, C.S., Smith, A.M., 1996. Stable oxygen and carbon isotope compositional fields for skeletal and diagenetic components in New Zealand Cenozoic nontropical carbonate sediments and limestones: a synthesis and review. New Zealand Journal of Geology and Geophysics 39, 93-107.

Nunn, E.V., Price, G.D., 2010. Late Jurassic (Kimmeridgian-Tithonian) stable isotopes ($\delta^{18}O$, $\delta^{13}C$) and Mg/Ca ratios: New paleoclimate data from Helmsdale, northeast Scotland. Palaeogeography, Palaeoclimatology, Palaeoecology 292, 325-335.

O'Neil, J.R., 1977. Stable isotopes in mineralogy. Physics and Chemistry of Minerals 2, 105-123.

O'Neil, J.R., 1987. Preservation of H, C, and O isotopic ratios in the low temperature environment. In: Kyser, T.K. (Ed.), Stable Isotope Geochemistry of Low Temperature Fluids. Mineralogical Association of Canada, Saskatoon, pp. 85-128.

Patterson, W.P. and Walter, L.M., 1994. Depletion of ^{13}C in seawater ΣCO2 on modern carbonate platforms: Significance for the carbon isotopic record of carbonates. Geology 22, 885-888.

Pérez, A., 1989. Estratigrafia y sedimentologia del Terciario del borde meridional de la Depresión del Ebro (sector riojano- aragonés) y cubetas de Muniesa y Montalban. PhD Thesis, Universidad de Zaragoza, Spain, pp. 525.

Pérez, A., Azanza, B., Cuenca, G., Pardo, G., Villena, J., 1985. Nuevos datos estratigráficos y paleontológicos sobre el Terciario del borde meridional de la depresión del Ebro (provincia de Zaragoza). Estudios Geológicos 41, 405-411.

Plunkett, J.M., 1997. Early Diagenesis of Shallow Platform Carbonates in the Oxfordian of the Swiss Jura Mountains. Unpublished PhD Thesis, Université de Fribourg, Switzerland, pp. 166.

Popp, B.N., Anderson, T.F., Sandberg, P.A., 1986. Brachiopods as indicators of original isotopic compositions in some Paleozoic limestones. Geological Society of American Bulletin 97, 1262-1269.

Riboulleau, A., Baudin, F., Daux, V., Hantzpergue, P., Renard, M., Zakharov, V., 1998. Evolution de la paléotempératures des eaux de la plateforme russe au cours du Jurassique supérieur. Comptes Rendus de l'Académie des Sciences de Paris, Sciences de la Terre et des Planètes 326, 239-246.

Richter D.K., Götte T., Götze J., Neuser R.D., 2003. Progress in application of cathodoluminescence (CL) in sedimentary geology. Mineral Petrology 79 (3-4), 127-166.

Rosales, I., Quesada., S., Robles, S., 2001. Primary and diagenetic isotopic signals in fossils and hemipelagic carbonates: the Lower Jurassic of northern Spain. Sedimentology 48, 1149-1169.

Salas, R., Guimerà, J., 1996. Rasgos estructurales principales de la cuenca cretácica inferior del Maestrazgo (Cordillera Ibérica oriental). Geogaceta 20 (7), 1704-1706.

Savard, M.M., Veizer, J., Hinton, R.H., 1995. Cathodoluminescence at low Fe and Mn concentrations: A SIMS study of zones in natural calcites. Journal of Sedimentary Research 65 (1a), 208-213.

Schobben, M., Ullmann, C.V., Leda, L., Korn, D., Struck, U., Reimold, W.U., Ghaderi, A., Algeo, T.J., Korte, C., 2015. Discerning primary versus diagenetic signals in carbonate carbon and oxygen isotope records: An example from the Permian–Triassic boundary of Iran. Chemical Geology 422, 94-107.

Sequero, C., Aurell, M., Bádenas, B., 2019. Sedimentary evolution of a shallow carbonate ramp (Kimmeridgian, NE Spain): Unravelling controlling factors for facies heterogeneities at reservoir scale. Marine and Petroleum Geology 109, 145-174.

Sharp, Z., 2007. Principles of stable isotope geochemistry. Pearson/Prentice Hall, University of Michigan, pp. 344.

Soria, A.R., Martín-Closas, C., Meléndez, A., Meléndez, N., Aurell, M., 1995. Estratigrafía del Cretácico inferior del sector central de la Cordillera Ibérica. Estudios Geológicos 51, 141-152.

Swart, P.K., 2015. The geochemistry of carbonate diagenesis: the past, present and future. Sedimentology 62 (5), 1233-1304.

Swart, P.K., Oehlert, A.M., 2018. Revised interpretations of stable C and O patterns in carbonate rocks resulting from meteoric diagenesis. Sedimentary Geology 364, 14-23.

Tucker, M.E., 1993. Carbonate diagenesis and sequence stratigraphy. Sedimentology Reviews 1, 51-72.

van der Kooij, B., Immenhauser, A., Csoma, A., Bahamonde, J., Steuber, T., 2009. Spatial geochemistry of a Carboniferous platform-margin-to-basin transect: balancing environmental and diagenetic factors. Sedimentary Geology 219, 136-150.

Veizer, J., Bruckschen, P., Pawellek, F., Diener, A., Podlaha, O.G., Carden, G.A.F., Jasper, T., Korte, C., Strauss, H., Azmy, K. and Ala, D., 1997. Oxygen isotope evolution of Phanerozoic seawater. Palaeogeography, Palaeoclimatology, Palaeoecology 132, 159-172.

Vincent, B., Emmanuel, L., Loreau, J.P., 2004. Significance of the isotopic signal ($\delta^{18}O$, $\delta^{13}C$) of neritic carbonates: diagenetic component and original component (Upper Jurassic of the East of the Paris Basin, France). Comptes Rendus Geoscience 336 (1), 29-39.

Vogel, J.C., 1993. Variability of carbon isotope fractionation during photosynthesis. In: Ehleringer, J.R., Hall, A.E., Farquhar, G.D. (Eds.), Stable Isotopes and Plant Carbon–Water Relations. Academic Press, San Diego, CA, pp. 29-38.

Wierzbowski, H., 2004. Carbon and oxygen isotope composition of Oxfordian–Early Kimmeridgian belemnite rostra: palaeoenvironmental implications for Late Jurassic seas. Palaeogeography, Palaeoclimatology, Palaeoecology 203, 153-168.

Zuo, F., Heimhofer, U., Huck, S. Bodin, S., Erbacher, J., Bai, H., 2018. Coupled $\delta^{13}C$ and $^{87}Sr/^{86}Sr$ chemostratigraphy of Kimmeridgian shoal-water deposits: A new composite record from the Lower Saxony Basin, Germany. Sedimentary Geology 376, 18-31.

8. SUMMARY, COMPARATIVE ANALYSIS AND WAY FORWARD

C H A P T E R

8

SUMMARY, COMPARATIVE ANALYSIS AND WAY FORWARD

8.1. FACIES MODELS

8.1.1. Key features of the sedimentary models

The precise reconstruction of the lateral and vertical facies distribution in the Higueruelas Fm acquired in this Thesis, allowed to construct facies models showing the along-strike and down-dip distribution of the different types of components and facies. These facies models are characterized by a wide variety of skeletal and non-skeletal grains (mainly peloids, ooids and oncoids), being the latter the most abundant components in this unit. Since oncoids are the most characteristic components of the Higueruelas Fm, a detailed analysis of the internal structure of different types of oncoids was also accomplished, proposing a new classification of oncoids based on Dahanayake (1977) nomenclature and their spatial distribution on these shallow domains. In addition, analysis of peloids and ooids, following Flügel (2004) and Strasser (1986) classifications, respectively, and other components (intraclasts, skeletal grains), allowed to precise the different ramp subenvironments and their sedimentary conditions.

The shallow domains of the latest Kimmeridgian carbonate ramp are characterized by intertidal, lagoon, backshoal and shoal-sand blanket domains in the inner ramp, to foreshoal and offshore settings in the middle ramp, showing complex facies belts and facies mosaics in specific areas. On the basis of the relative abundance of non-skeletal grains, two depositional models are distinguished, which correspond to different stages of evolution of the carbonate ramp (Figs 8.1 and 8.2).

The *oncolitic-peloidal-oolitic-dominated ramp Model 1* (Fig. 8.1a) includes an intertidal facies belt, a low-energy sheltered lagoon with abundant large and irregular microbial-dominated oncoids (types IIIb and IVa oncoids), and moderate- to high-energy peloidal-oolitic backshoal, shoal-sand blanket and foreshoal domains (mainly with lithic peloids and type 1 and 1/3 ooids), grading offshore into mid-ramp bioclastic-peloidal mudstones (Fig. 8.1b). The down-dip lateral extent of the backshoal to offshore-proximal subenvironments is variable, ranging between 2 km and 12 km. The down-dip dimension of the sheltered lagoon is supposed to reach several km. Local intertidal caps occur on top of the shoal-sand blanket deposits, reaching tens of m to few km in lateral extent. In addition, the peloidal-oolitic backshoal to foreshoal packstone to grainstone facies grade laterally (along strike) into oncolitic-dominated facies, with abundant micrite- and micrite-microbial-dominated oncoids (types II and IIIa oncoids, respectively). Stromatoporoids colonize specific areas of the sheltered lagoon and backshoal domains as local carpets, reaching up to 500 m in lateral extent. In the open-marine areas, chaetetid-stromatoporoid-coral buildups (lenses up to 8 m high and up to 250 m in width) grow in specific areas of proximal mid-ramp domains. Stromatoporoid-rich deposits, both inner-ramp carpets and mid-ramp buildups, are surrounded by oncolitic (mainly type IVa oncoids)-stromatoporoid facies, forming both these two facies areas of several km in lateral extent, reaching up to 10 km in mid-ramp settings.

The *oolitic-peloidal-dominated ramp Model 2* (Fig. 8.2a) characterizes sedimentation during a second stage of evolution of the platform, involving significant palaeoenvironmental changes affecting the inner-ramp settings, which are represented by a wide restricted lagoon, with peloids and ooids (type 3 and 4) and low diversity of bioclasts (mainly bivalves and lituolids) (Fig. 8.2b), grading into peloidal-dominated backshoal, shoal-sand blanket and foreshoal domains. Intraclastic-peloidal storm-beds also appear frequently in both backshoal and foreshoal areas, and the backshoal deposits occasionally show intense burrowing (i.e. *Thalassinoides* traces). The key differences with Model 1 are the disappearance of inner-ramp stromatoporoid carpets, and the minor development of the oncolitic facies, which are constrained to some areas (i.e. local ponds in the intertidal belt, backshoal and foreshoal domains, and around the mid-ramp chaetetid-stromatoporoid-coral buildups).

The transition from Model 1 to Model 2 is determined by the long-term regional fall in relative sea level occurring at the end of the Jurassic in the Iberian Basin (Bádenas and Aurell, 2001a; Aurell et al., 2003), which led to more restricted conditions and an increase of siliciclastic input in proximal domains, coeval to the progressive progradation of the facies belts to the southeast. In detail, the complex facies distribution in the two carbonate ramp models was mainly controlled by the combined effect of three factors:

1) *Variations in hydrodynamic conditions:* the development of the microbial-dominated oncoids (type IIIb and IVa oncoids) within the sheltered lagoon represented in Model 1, occurred under low- to very low-energy conditions, which were favoured by the barrier effect of shoal-sand blankets (Fig. 8.1). The higher tolerance of stromatoporoids to water energy enabled their colonization from lagoon to backshoal domains (i.e. stromatoporoid carpets), with a preferential distribution probably related to the presence of local hard substrates. In the middle ramp, low- to moderate-energy conditions below the fair-weather wave base allowed the growth of chaetetid-stromatoporoid-coral buildups (Figs 8.1 and 8.2), whose patchy distribution could also be related to the presence of local hard substrates. Alternating higher- and lower-energy conditions from the backshoal to foreshoal domains determined the along-strike lateral change from peloidal-oolitic to oncolitic-dominated facies, with the predominance of smaller and well-rounded micrite-dominated type II oncoids within the shoal body, and micrite-microbial-dominated type IIIa oncoids particularly in the foreshoal domain (Fig. 8.1b). In Model 2, the recurrence of storm-related beds in both backshoal and foreshoal domains reveals an increase in water energy (Fig. 8.2).

2) *The irregular sea-bottom topography*: the along-strike lateral variation from peloidal-oolitic to oncolitic-dominated facies within the shoal body in Model 1, reveals an irregular depositional topography for this facies belt (Fig. 8.1), with possible depressions/protected areas where lower-energy conditions favoured the generation of micrite-dominated oncoids (type II). This is also highlighted by the presence of intertidal patches on top of the peloidal-oolitic shoal-sand blanket deposits, but not on top of the oncolitic-dominated shoals. This contrasts with Model 2, where probable higher-energy conditions determined the minor presence of these relatively protected areas with generation of oncoids (Fig. 8.2).

3) *Fluctuations in salinity*: in the inner-ramp settings of Model 1, the predominant low-energy conditions, together with a low siliciclastic input, favoured the development of the sheltered lagoon with the generation of the large and irregular microbial oncoids with mainly *Bacinella irregularis-Lithocodium aggregatum* association (Fig. 8.1). In Model 2, fluctuations in salinity due to the reduced connection with the open-marine areas controlled by the long-term regional fall in relative sea level, combined with an increase in water energy and terrigenous input to the lagoon carbonates, conditioned that sedimentation in the inner ramp occurred within a peloidal-bioclastic-oolitic restricted lagoon, without oncoids or stromatoporoid carpets, grading into a backshoal area dominated by peloids and storm-related deposits (Fig. 8.2).

Fig. 8.1 (Next page)*. a) Depositional model of the latest Kimmeridgian shallow carbonate ramp during the first stage of evolution of the platform, dominated by peloids, ooids and oncoids (sedimentary units or high-frequency sequences 1 to 4). The high occurrence of stromatoporoids (i.e. stromatoporoid W to G facies) and chaetetid-stromatoporoid-coral buildups occurs in specific areas of the inner- and mid-ramp domains, respectively (see details on their dimensions in the text). b) Distribution of non-skeletal grains along the defined depositional subenvironments of this ramp model. The down-dip lateral extent of the depositional subenvironments is also indicated.*

(*): the name of these facies is modified from those originally defined in Chapter 5, due to deeper analyses concerning the oncoid types and their distribution presented in Chapter 6.

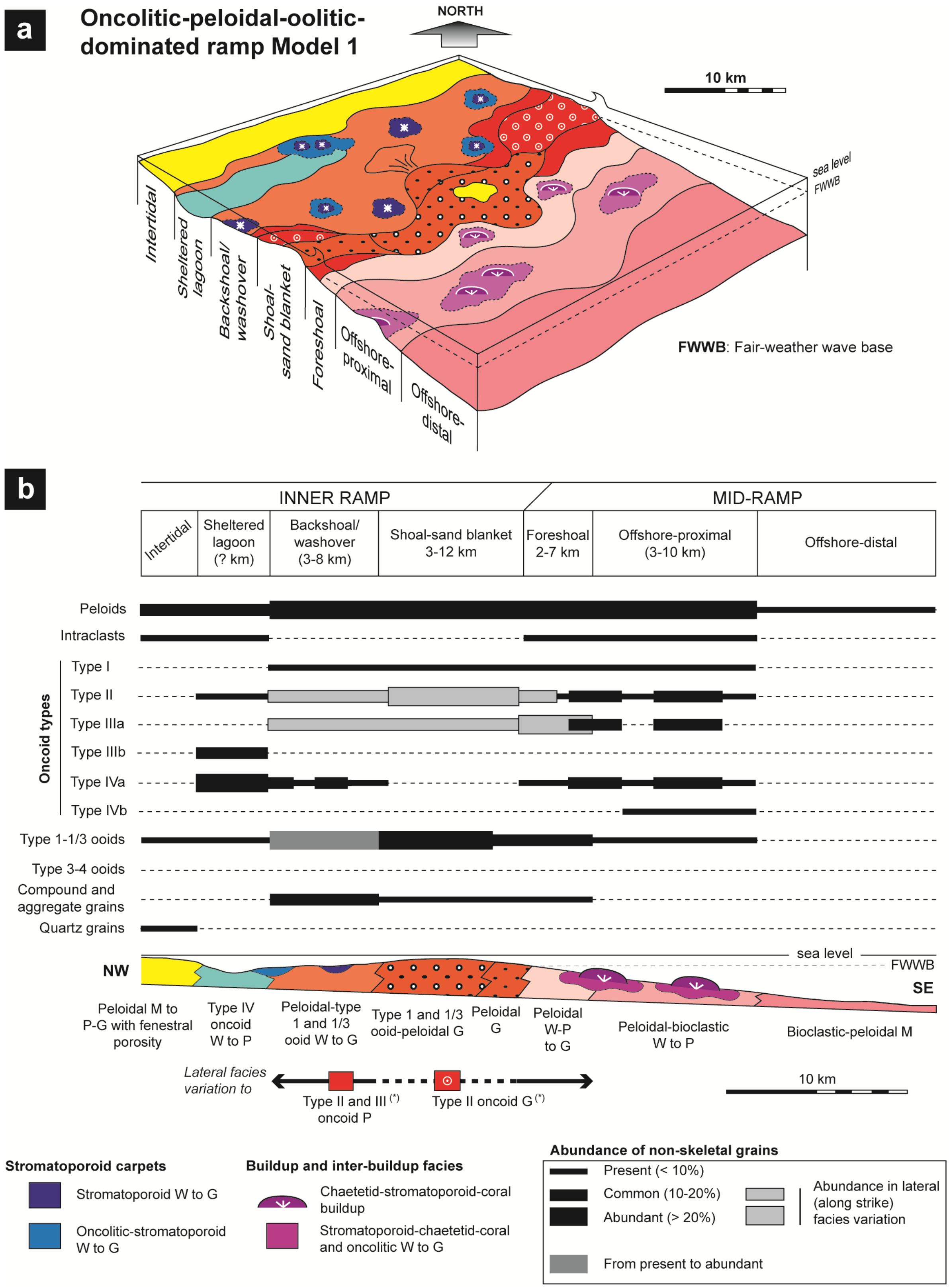
a
Oncolitic-peloidal-oolitic-dominated ramp Model 1
NORTH
10 km
sea level
FWWB
Intertidal
Sheltered lagoon
Backshoal/ washover
Shoal-sand blanket
Foreshoal
Offshore-proximal
Offshore-distal
FWWB: Fair-weather wave base
b
INNER RAMP
MID-RAMP
Intertidal
Sheltered lagoon (? km)
Backshoal/ washover (3-8 km)
Shoal-sand blanket 3-12 km
Foreshoal 2-7 km
Offshore-proximal (3-10 km)
Offshore-distal
Peloids
Intraclasts
Oncoid types
Type I
Type II
Type IIIa
Type IIIb
Type IVa
Type IVb
Type 1-1/3 ooids
Type 3-4 ooids
Compound and aggregate grains
Quartz grains
NW
sea level
FWWB
SE
Peloidal M to P-G with fenestral porosity
Type IV oncoid W to P
Peloidal-type 1 and 1/3 ooid W to G
Type 1 and 1/3 ooid-peloidal G
Peloidal G
Peloidal W-P to G
Peloidal-bioclastic W to P
Bioclastic-peloidal M
Lateral facies variation to
Type II and III (*) oncoid P
Type II oncoid G (*)
10 km
Stromatoporoid carpets
Stromatoporoid W to G
Oncolitic-stromatoporoid W to G
Buildup and inter-buildup facies
Chaetetid-stromatoporoid-coral buildup
Stromatoporoid-chaetetid-coral and oncolitic W to G
Abundance of non-skeletal grains
Present (< 10%)
Common (10-20%)
Abundant (> 20%)
Abundance in lateral (along strike) facies variation
From present to abundant

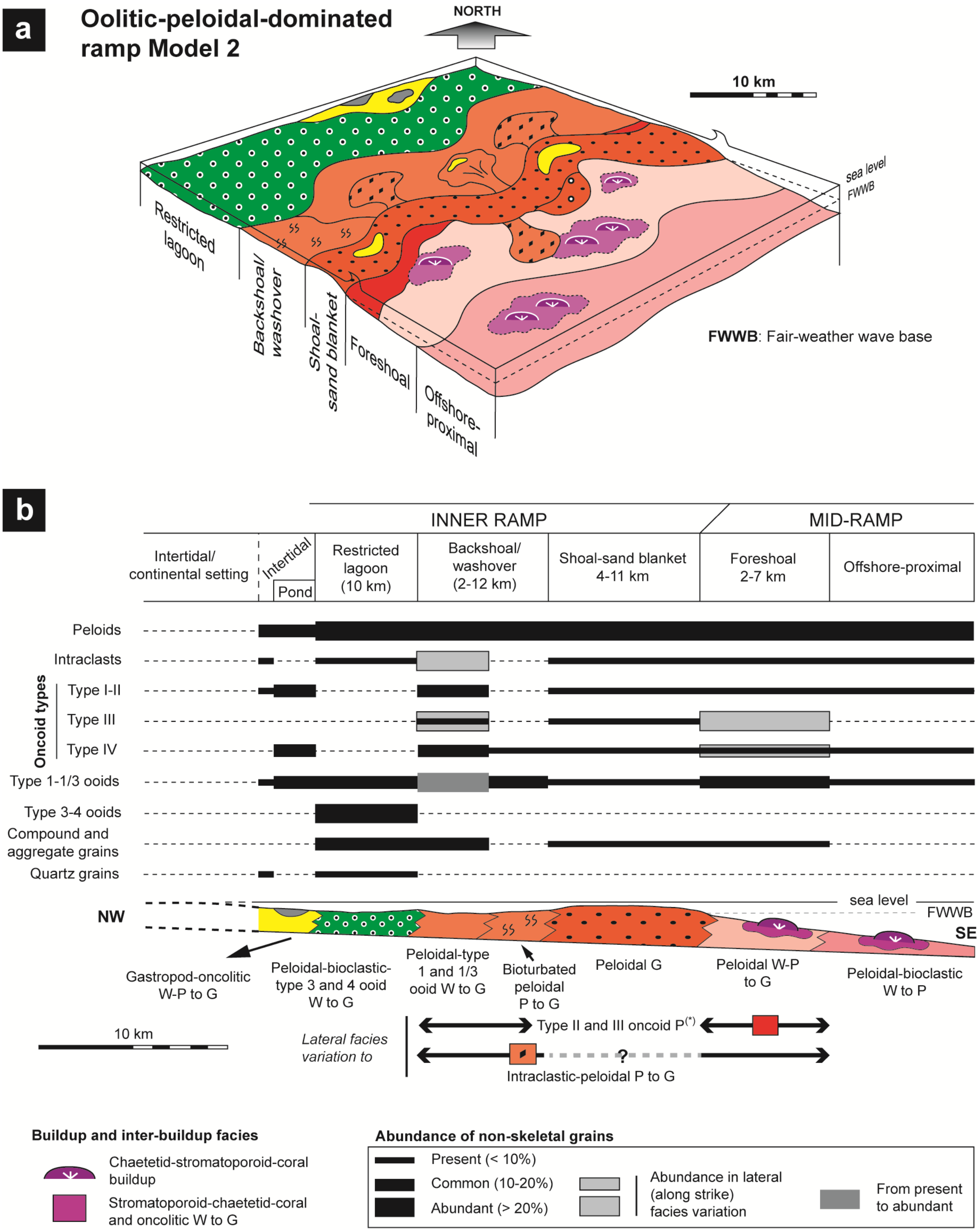

Fig. 8.2. a) Depositional model of the latest Kimmeridgian shallow carbonate ramp during the second stage of evolution of the platform, dominated by peloids and ooids (sedimentary units or high-frequency sequences 5 to 9). b) Distribution of non-skeletal grains along the defined depositional subenvironments of this ramp model. The down-dip lateral extent of the depositional subenvironments is also indicated.

(*): the name of this facies is modified from that originally defined in Chapter 5, due to deeper analyses concerning the oncoid types and their distribution presented in Chapter 6.

8.1.2. Comparative analysis: understanding facies heterogeneities at reservoir scale

The reconstruction of facies distributions on ancient shallow carbonate ramps in previous studies (e.g. Bádenas and Aurell, 2010; Lehmann et al., 2010; Alnazghah et al., 2013; Petrovic and Aigner, 2017; San Miguel et al., 2017a, b; Fallatah and Kerans, 2018; Marchionda et al., 2018) have demonstrated that ramp-type carbonate platforms are complex systems characterized by gradual facies changes, conditioned by the low-angle topography of the ramp. Moreover, the sedimentological characterization of this type of carbonate systems has an additional interest in reservoir exploration, as it is known that some of the most important subsurface hydrocarbon reservoirs worldwide are represented by carbonate ramp deposits (e.g. the Arab-D Formation in Persian Gulf, or the Smackover Formation in the USA East Gulf; Benson, 1988; Grötsch et al., 2003; Al-Awwad and Collins, 2013).

The along-strike and down-dip complex facies distribution obtained here, combined with the well understanding of the factors controlling facies heterogeneities, provide key aspects concerning the sedimentological analysis of carbonate ramp systems dominated by similar components, with particular potential to understand the interwell-scale facies heterogeneities by subsurface data. The comparative analysis between ancient shallow carbonate ramps regarding the preferential distribution of non-skeletal grains, spatial facies arrangements (facies belts vs facies mosaics) and the dimension of the grain-supported sedimentary bodies, highlights the relevance of such detailed sedimentological characterizations in both strike and down-dip directions, in particular for those facies of interest in reservoir characterization.

The comparative analysis of the facies distribution obtained for the latest Kimmeridgian shallow carbonate ramp analysed in this Thesis with several Mesozoic carbonate ramps of some peri-Tethyan basins, including also the Iberian Basin, is provided here in order to highlight the complexity of these carbonate systems (Figs 8.3 and 8.4; Table 8.1). Of particular interest are the similarities and differences concerning the type of components and dimension of shoal and stromatoporoid-bearing deposits (Table 8.1):

1) *Mid-Kimmeridgian shallow carbonate ramp deposits in the central Iberian Basin* (recently defined as Jabaloyas Fm by Aurell et al., 2019a) (Bádenas and Aurell, 2010; Alnazghah et al., 2013; San Miguel et al., 2017a). This ramp has a complex along-strike and down-dip facies distribution comparable to that found for the shallow carbonate ramp of the Higueruelas Fm studied in this Thesis, with a similar configuration from lagoon, backshoal and shoal deposits in the inner ramp, to mid-ramp foreshoal and offshore domains with reefal facies (Fig. 8.3). Variations in the down-dip lateral extent of the shoal deposits are comparable to those observed in the Higueruelas Fm (i.e. 3-12 km in the Higueruelas Fm, and 3-10 km in the Jabaloyas Fm; Fig. 8.3a, b), also regarded as continuous facies belts. In addition, a similar composition is reported for these shallow domains: *Bacinella*-oncoids (equivalent to type IVa oncoids) dominate within a low-energy sheltered lagoon, including the development of stromatoporoid-rich facies of hundreds of m in extent (San Miguel et al., 2017a; Fig. 8.3c), grading into a backshoal-shoal-foreshoal area dominated by peloids, type 3 and 1/3 ooids and bioclasts, with along-strike lateral variations to oncolitic-dominated facies within the shoal and foreshoal domains (Bádenas and Aurell, 2010; Alnazghah et al., 2013; Fig. 8.3b). Type III oncoids are generally deposited offshore, laterally equivalent to the reefal deposits, whereas type I and II oncoids are the dominant grains in the oncolitic shoals.

Compared with the mid-Kimmeridgian ramp, the Higueruelas Fm has a wider distribution of type II and III oncoids from the backshoal to foreshoal domains, but a scarcer proportion of type I oncoids in the shoal-sand blanket deposits (Fig. 8.3a, b). These differences, particularly the scarce proportion of high-energy type I oncoids, are related to the different general hydrodynamic conditions: the mid-Kimmeridgian ramp is a storm-dominated ramp with relatively higher-energy conditions and a higher-angle topography compared with the studied latest Kimmeridgian carbonate ramp, as reflects the ~30 km maximum lateral extent of the backshoal-shoal-foreshoal belt in the case studied here, compared with the ~20 km for the mid-Kimmeridgian ramp.

Another significant difference concerns the dimension and fabric of the buildups. The mid-Kimmeridgian Jabaloyas Fm includes a higher variety of buildups (coral-microbial buildups, coral-bearing thrombolites and microbial buildups: San Miguel et al., 2017a; Fig. 8.3c), compared with the latest Kimmeridgian Higueruelas Fm. The coral-microbial buildups in the Jabaloyas Fm show a similar association of metazoan builders and micro-encrusters as the mid-ramp buildups described in the Higueruelas Fm. However, microbial buildups have not been described here, whose development is favoured by particular ecological requirements, such as higher nutrient and sediment supply (e.g. Leinfelder et al., 2002; San Miguel et al., 2017a). Regarding the coral-microbial buildups, a significant difference with the Higueruelas Fm is found in their geometry: in the Jabaloyas Fm, the buildups are pinnacles of up to 8-19 m high and 5-7 m wide, instead of wide lenses of up to 8 m high and 250 m in width recognized in the Higueruelas Fm. The accommodation space created during the mid-Kimmeridgian controlled the preferential vertical growth of the buildups with pinnacle morphology on the mid-Kimmeridgian carbonate ramp (Aurell and Bádenas, 1994; Bádenas and Aurell, 2010; San Miguel et al., 2017a), whereas during the latest Kimmeridgian, the long-term regressive context reduced the accommodation space available for the growing of buildups on proximal mid-ramp domains.

2) *Upper Kimmeridgian shallow carbonate ramp deposits of the Arab-D Fm in Saudi Arabia* (Lehmann et al., 2010; Marchionda et al., 2018). The dimension and lateral extent of the shallow carbonate ramp facies in the Arab-D Fm have been discussed by several authors. Lehmann et al. (2010) proposed a depositional model for this ramp in offshore Abu Dhabi (Rub'Al Khali Basin, eastern Saudi Arabia), including sabkha, intertidal, restricted shallow subtidal, backshoal, shoal and mid-ramp foreshoal domains, with stromatoporoid-rich buildups (up to 8-11 m high) occurring from the backshoal to foreshoal domains (Fig. 8.4c). Therefore, the Arabian carbonate ramp mainly differs from the Higueruelas Fm in the development of a sabkha domain and the general more restricted conditions of the lagoon, due to the more arid conditions governing in this part of the Tethyan realm during the late Kimmeridgian, resulting in a mixed carbonate/evaporitic sedimentation (e.g. Grötsch et al., 2003; Al-Awwad and Collins, 2013). In another hand, the down-dip lateral extent of the sand-shoal deposits (peloidal, bioclastic and oolitic packstones-grainstones) in the Arab-D Fm is similar as those reported for the Higueruelas Fm (2 to < 10 km); however, their lateral continuity as a continuous belt is discussed, suggesting a system of shoal/inter-shoal deposits, instead of a continuous km-scale belt similar to the Higueruelas Fm. By contrast, other studies on the Arab-D Fm (onshore Abu Dhabi; Marchionda et al., 2018) infer the km-scale lateral continuity of these shoal bodies as continuous belts at reservoir scale (i.e. in an area of 30 x 40 km in extent), even reporting 17-20 km in down-dip lateral extent. On the other hand, oncolitic shoal facies similar to that of the Higueruelas Fm (Fig. 8.3a) are not reported in the Arab-D Fm.

Another significant difference concerns the location of those areas with high occurrence of the stromatoporoid-rich buildups, which correspond to the backshoal to foreshoal domains in the

Arab-D Fm, but only the mid-ramp settings in the Higueruelas Fm (Fig. 8.4a, c). In addition, the absence of stromatoporoid-rich carpets within the lagoonal domains, as shown for the Higueruelas Fm (Fig. 8.4a, b), is probably consequence of the restricted conditions which characterized the shallow domains of the Arabian carbonate ramp.

3) *Middle Triassic shallow carbonate ramp deposits of the Quaderkalk Fm in SW Germany* (Petrovic and Aigner, 2017; Petrovic et al., 2018). Sand-shoal deposits in this ramp have a high degree of lateral continuity, i.e. from few km to > 10 km in both strike and down-dip directions, similar to those of the Higueruelas Fm. However, in this case, the shoal bodies are not arranged as continuous belts as shown for the Higueruelas Fm, but instead appear as shoal complexes with a mosaic distribution, reaching each shoal body several tens of km^2 (Fig. 8.4d). Stromatoporoid-bearing deposits are not reported for this carbonate ramp.

4) *Oxfordian shallow carbonate ramp deposits of the Hanifa Fm in central Saudi Arabia* (Fallatah and Kerans, 2018). Isolated shoal bodies similar to those reported for the Middle Triassic Quaderkalk Fm are described in the Oxfordian of the central Saudi Arabia (Hanifa Fm), whose development is instead controlled by topographic highs, evolving to offshore islands. However, the lateral extent of these high-energy deposits is not well documented.

   Moreover, two types of stromatoporoid-rich deposits are described in the mid-ramp domains of this Oxfordian platform, with different geometry than those of the Higueruelas Fm (Table 8.1): 1) up to 11 m-thick stromatoporoid-coral bioherms forming disconnected bodies in proximal mid -ramp areas parallel to the shoreline; and 2) up to 1.5 m-thick stromatoporoid-coral biostromes occurring in the low-energy middle ramp, showing a higher lateral continuity (Fallatah and Kerans, 2018). The areas of high occurrence of these stromatoporoid-rich deposits can reach tens of km in lateral extent. Oncolitic rudstones (*Bacinella-Lithocodium*-type III oncoids) are also documented laterally associated with the stromatoporoid-coral bioherms.

Fig. 8.3 (Next page). *a, b) Comparison between the 2D depositional models for the latest Kimmeridgian shallow carbonate ramp studied in this Thesis (a) and the mid-Kimmeridgian shallow carbonate ramp in the central Iberian Basin (b, Jabaloyas Fm; modified from Bádenas and Aurell, 2010). c) Stratigraphic correlation showing the distribution and characteristics of inner-ramp stromatoporoid-rich levels and mid-ramp reefal facies on the mid-Kimmeridgian shallow carbonate ramp (extracted from San Miguel et al., 2017a).*

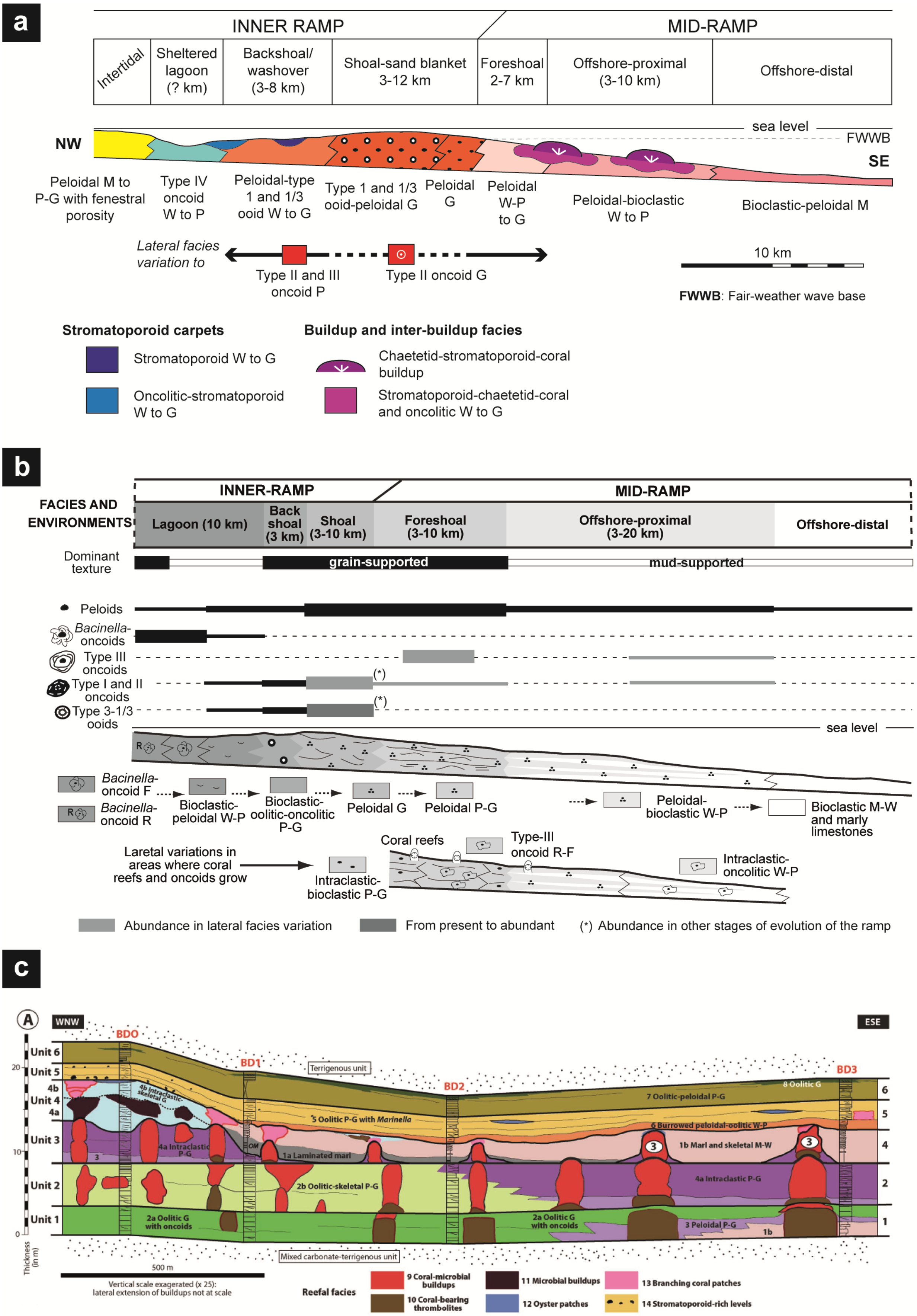
a
INNER RAMP
MID-RAMP
Intertidal
Sheltered lagoon (? km)
Backshoal/ washover (3-8 km)
Shoal-sand blanket 3-12 km
Foreshoal 2-7 km
Offshore-proximal (3-10 km)
Offshore-distal
sea level
FWWB
NW
SE
Peloidal M to P-G with fenestral porosity
Type IV oncoid W to P
Peloidal-type 1 and 1/3 ooid W to G
Type 1 and 1/3 ooid-peloidal G
Peloidal G
Peloidal W-P to G
Peloidal-bioclastic W to P
Bioclastic-peloidal M
Lateral facies variation to
Type II and III oncoid P
Type II oncoid G
10 km
FWWB: Fair-weather wave base
Stromatoporoid carpets
Stromatoporoid W to G
Oncolitic-stromatoporoid W to G
Buildup and inter-buildup facies
Chaetetid-stromatoporoid-coral buildup
Stromatoporoid-chaetetid-coral and oncolitic W to G
b
FACIES AND ENVIRONMENTS
INNER-RAMP
MID-RAMP
Lagoon (10 km)
Back shoal (3 km)
Shoal (3-10 km)
Foreshoal (3-10 km)
Offshore-proximal (3-20 km)
Offshore-distal
Dominant texture
grain-supported
mud-supported
Peloids
Bacinella-oncoids
Type III oncoids
Type I and II oncoids
Type 3-1/3 ooids
(*)
sea level
Bacinella-oncoid F
Bacinella-oncoid R
Bioclastic-peloidal W-P
Bioclastic-oolitic-oncolitic P-G
Peloidal G
Peloidal P-G
Peloidal-bioclastic W-P
Bioclastic M-W and marly limestones
Laretal variations in areas where coral reefs and oncoids grow
Coral reefs
Type-III oncoid R-F
Intraclastic-bioclastic P-G
Intraclastic-oncolitic W-P
Abundance in lateral facies variation
From present to abundant
(*) Abundance in other stages of evolution of the ramp
c
A
WNW
ESE
BDO
BD1
BD2
BD3
Terrigenous unit
Unit 6
Unit 5
Unit 4
Unit 3
Unit 2
Unit 1
4b
4a
20
10
0
Thickness (in m)
4b Intraclastic-skeletal G
4a Intraclastic P-G
5 Oolitic P-G with Marinella
7 Oolitic-peloidal P-G
8 Oolitic G
6 Burrowed peloidal-oolitic W-P
1b Marl and skeletal M-W
1a Laminated marl
2b Oolitic-skeletal P-G
4a Intraclastic P-G
2a Oolitic G with oncoids
3 Peloidal P-G
1b
Mixed carbonate-terrigenous unit
500 m
Vertical scale exagerated (x 25): lateral extension of buildups not at scale
Reefal facies
9 Coral-microbial buildups
10 Coral-bearing thrombolites
11 Microbial buildups
12 Oyster patches
13 Branching coral patches
14 Stromatoporoid-rich levels

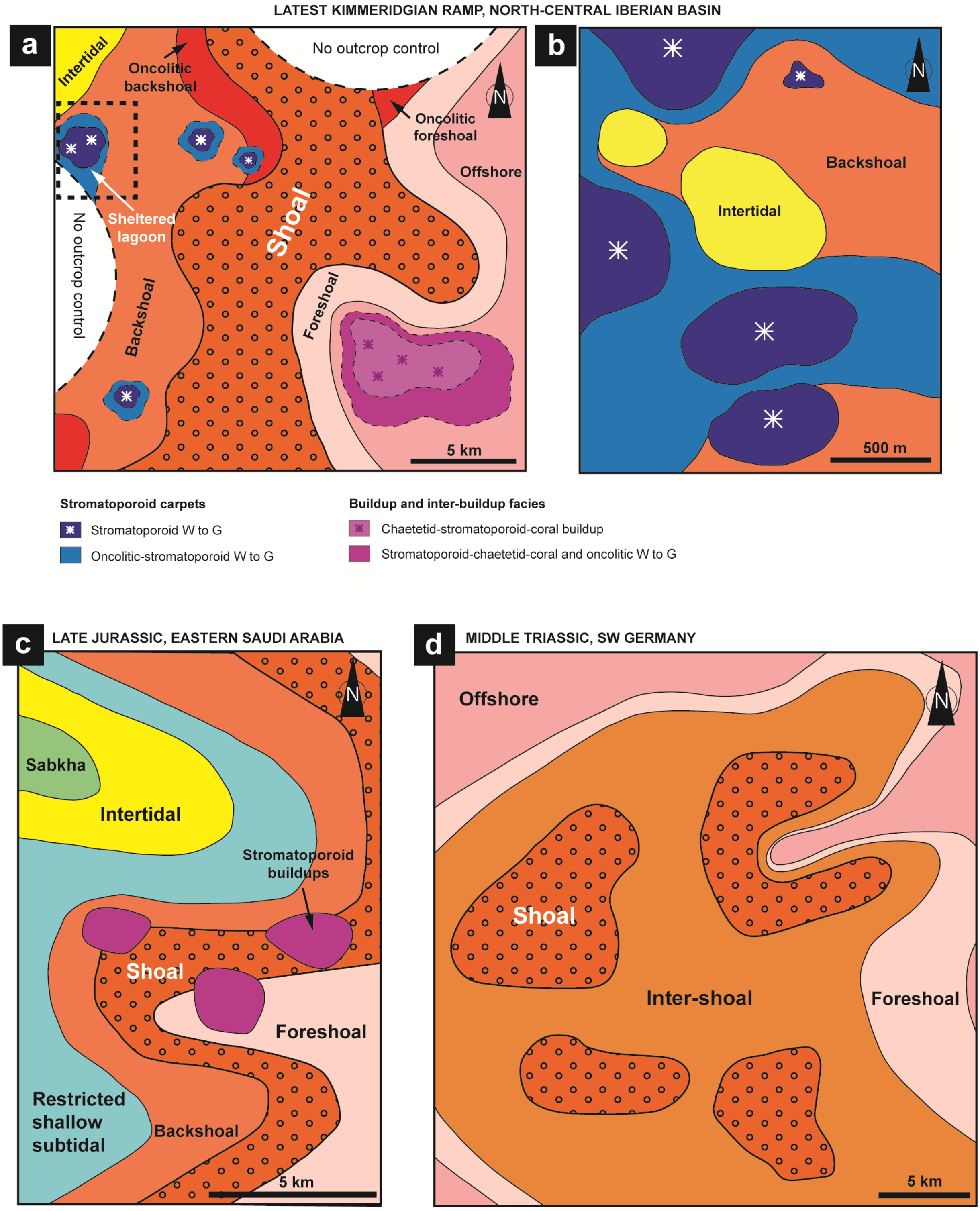

Fig. 8.4. *Comparison between the spatial facies distribution for the latest Kimmeridgian shallow carbonate ramp studied in this Thesis (a, b, simplified from the originals in Chapter 5; the area shown in b corresponds to that in the black dashed square in a), and shallow carbonate ramp systems in eastern Saudi Arabia (c, Upper Jurassic Arab-D Fm; modified from Lehmann et al., 2010) and SW Germany (d, Middle Triassic Quaderkalk Fm; modified from Petrovic and Aigner, 2017).*

	Region, lithological unit and age		Facies type: Shoal deposits	Facies type: Stromatoporoid-bearing deposits – Inner ramp	Facies type: Stromatoporoid-bearing deposits – Mid-ramp
IBERIAN BASIN	Higueruelas Fm Latest Kimmeridgian **THIS WORK**	North-central Iberian Basin (Zaragoza region)	▪ Continuous shoal-sand blanket belts ▪ 3-12 km in down-dip extent ▪ Along-strike lateral variation from peloidal-oolitic to oncolitic facies (dominant type II oncoids)	Lagoonal to backshoal stromatoporoid-rich facies, laterally related to oncolitic-stromatoporoid facies, forming these two facies areas from hundreds of m to several km in lateral extent	Areas of high occurrence of proximal mid-ramp up to 8 m-high and 250 m-wide chaetetid-stromatoporoid-coral buildups, surrounded by stromatoporoid -chaetetid-coral and oncolitic facies, constituting areas of several km in lateral extent
IBERIAN BASIN	Jabaloyas Fm Middle Kimmeridgian	Central Iberian Basin (Teruel region) (Bádenas and Aurell, 2010; Alnazghah et al., 2013; San Miguel et al., 2017a)	▪ Continuous shoal belts ▪ 3-10 km in down-dip extent ▪ Along-strike lateral variation from oolitic to oncolitic facies (dominant type I and II oncoids)	Lagoonal stromatoporoid-rich rubble beds of hundreds of m in lateral extent	Areas of high occurrence of 8 to 19 m-high and 5 to 7 m-wide reefal pinnacles in proximal to distal mid-ramp domains
OUTSIDE THE IBERIAN BASIN	Arab-D Fm Late Kimmeridgian	Eastern Saudi Arabia (offshore Abu Dhabi) (Lehmann et al., 2010)	▪ Lateral continuity discussed; probable system of shoal/inter-shoal deposits ▪ 2 to < 10 km in down-dip extent	Areas of high occurrence of up to 8-11 m-high buildups, up to 3 km in lateral extent, from backshoal to foreshoal ramp domains	
OUTSIDE THE IBERIAN BASIN	Arab-D Fm Late Kimmeridgian	Eastern Saudi Arabia (onshore Abu Dhabi) (Marchionda et al., 2018)	▪ Continuous shoal belts ▪ 17-20 km in down-dip lateral extent	No data	
OUTSIDE THE IBERIAN BASIN	Hanifa Fm Oxfordian	Central Saudi Arabia (Fallatah and Kerans, 2018)	System of isolated shoal bodies controlled by topographic highs (lateral extent not documented)	No stromatoporoid-bearing facies	Areas of high occurrence reaching tens of km in lateral extent: ▪ Proximal mid-ramp: up to 11 m-thick stromatoporoid-coral bioherms. Oncolitic rudstones (type III oncoids) laterally associated ▪ Distal mid-ramp: up to 1.5 m-thick stromatoporoid-coral biostromes
OUTSIDE THE IBERIAN BASIN	Quaderkalk Fm Middle Triassic	SW Germany (Petrovic and Aigner, 2017; Petrovic et al., 2018)	▪ Shoal complexes with a mosaic distribution ▪ Lateral extent of each shoal body from few km to > 10 km	No stromatoporoid-bearing facies	

***Table 8.1**. Comparison of the characteristics of shoal and stromatoporoid-bearing deposits between the latest Kimmeridgian shallow carbonate ramp in the Iberian Basin and several Mesozoic shallow carbonate ramp systems within the peri-Tethyan realm. Oncoid types refer to Dahanayake (1977) nomenclature.*

The particular differences for shoal and stromatoporoid-bearing deposits between the Higueruelas Fm and the mentioned examples, point out the importance of deciphering (when possible) the along-strike and down-dip distribution of shallow carbonate ramp facies in outcrop analogues, particularly if these facies have potential as reservoir-rock bodies. This is not always an easy task, depending on the quality of the outcrops and the scale of observation. As a summary, differences in the configuration of the shoal deposits are notorious: from shoal/inter-shoal complexes with a mosaic distribution (i.e. Middle Triassic Quaderkalk Fm in SW Germany: Fig. 8.4d; Oxfordian Hanifa Fm in central Saudi Arabia) to continuous facies belts (Upper Jurassic Jabaloyas and Higueruelas formations in the Iberian Basin, and the Upper Jurassic Arab-D Fm in eastern Saudi Arabia: Figs 8.3a-b and 8.4a, c). Regarding the stromatoporoid-rich facies, they usually form part of buildups in mid-ramp settings (the Oxfordian Hanifa Fm, and the Upper Jurassic Arab-D, Jabaloyas and Higueruelas formations), and less common in inner-ramp domains (Arab-D Fm), in both cases covering areas of several km in lateral extent (Figs 8.3c and 8.4a, c). The stromatoporoid-bearing facies can also occur as stromatoporoid carpets or rubble beds in inner-ramp domains (Higueruelas and Jabaloyas formations, respectively), where areas of high density of stromatoporoids extend hundreds of m (Figs 8.3c and 8.4b). In addition, these inner-ramp stromatoporoid-rich carpets can reach several km if including their laterally associated oncolitic-stromatoporoid facies defined in this work (i.e. oncolitic-stromatoporoid W to G facies in Fig 8.4a, b).

8.1.3. Way forward

In this Thesis, the sedimentological analysis of the latest Kimmeridgian shallow carbonate ramp can provide interesting insights for reconstructing or comparing with shallow carbonate ramp environments constituted by similar carbonate components (e.g. further comparative with the Arab-D Fm, with implications for carbonate reservoir characterization).

In addition, the key messages given for the characterization and interpretation of the facies heterogeneities of the Higueruelas Fm in the study area, can be applied in reconstructing depositional subenvironments in other shallow areas of this carbonate ramp along the western margin of the Iberian Basin (i.e. Teruel or Valencia regions; see Fig. 4.1 in Chapter 4 for location), and so as evaluating possible differences regarding the lateral continuity of facies belts and distribution of facies mosaics at basin scale.

It would be also interesting to investigate facies heterogeneities as the shallow facies belt progrades to eastern and southeastern areas of the Iberian Basin, where thick successions of the Higueruelas Fm have been recognized (e.g. the uppermost Kimmeridgian-lower Tithonian Higueruelas Fm in the Morella sub-basin, E Iberian Basin; see Fig. 4.4 in Chapter 4 for location).

8.2. STRATIGRAPHIC ARCHITECTURE

8.2.1. Key features of the stratigraphic architecture

Since multiple factors control the facies stacking patterns on shallow carbonate ramp successions, inferring valuable and more realistic internal facies architectures depends on the scale of observation (Figs 8.5 and 8.6). Accordingly, such complexity in the internal facies architecture increases when detailed analyses are performed in small outcrop windows. In this Thesis, the high-resolution sequential analysis of closely-spaced sedimentary logs (i.e. mean distance between logs from hundreds of m to around 5 km; Figs 8.5a and 8.6a), and facies mapping in continuous outcrops (i.e. Mezalocha sector; Fig. 8.5a), in both strike and down-dip directions, have been crucial for an accurate characterization of the lateral and vertical facies arrangements, and so as unravelling the factors controlling this stratigraphic facies architecture, particularly in those areas of the carbonate ramp showing higher facies heterogeneities due to facies mosaic distributions (mostly in the inner-ramp domains).

Results indicate that, in the Higueruelas Fm, the dimension of the sedimentary bodies is highly variable, showing m-scale lateral and vertical facies changes. In particular, the individual sedimentary bodies defined by the grain-supported backshoal to foreshoal facies (in particular packstone-grainstone and grainstone textures), with from hundreds of m to up to ~30 km (along strike) and ~15 km (down dip) of lateral extent, have only from few dm to up to 7 m in vertical extent. In addition, these potential reservoir-rock bodies record internal facies heterogeneities, grading from peloidal-oolitic into oncolitic and stromatoporoid-bearing grain-supported facies, which is also important in order to evaluate the interparticle porosity of these deposits: the oncolitic-dominated grain-supported facies are up to 8 km in both strike and down-dip directions, and from few dm to 3 m in vertical extent; whereas the peloidal-oolitic grain-supported facies display up to ~30 km (along strike) and ~15 km (down dip) in lateral extent, and from few dm to 7 m in thickness. Concerning the stromatoporoid-bearing grain-supported facies (i.e. in backshoal and foreshoal domains), their vertical extent is also very reduced compared with their lateral extent (backshoal stromatoporoid carpets: 0.5-2 m in thickness, and from hundreds of m to up to 2 km in lateral extent; foreshoal buildup and inter-buildup facies: 1-5 m thick, and up to 10 km in lateral extent). It is noteworthy that these stromatoporoid-bearing deposits have a particular interest for reservoir characterization, due to the additional porosity generated by dissolution of the stromatoporoid bioclasts (e.g. Hughes, 1996, 2004; Lehmann et al., 2010).

The stratigraphic facies architecture revealed for the Higueruelas Fm is the result of the interplay of internal and external factors controlling carbonate accumulation and changes in accommodation space. Understanding these factors is relevant for inferring more realistic models for facies pattern predictability when these types of carbonate systems are analysed by subsurface data. The facies architecture of the Higueruelas Fm, and in particular the reduced vertical extent of the different sedimentary (facies) bodies, was controlled by the combination of: 1) the own spatial distribution of the facies (facies heterogeneities in the two depositional models), and their complex controlling factors (see section 8.1), and 2) the reduced accommodation space created by both the long-term regional fall in relative sea level occurring at the end of the Jurassic under relatively homogeneous subsidence (Bádenas and Aurell, 2001a; Aurell et al., 2003), and the higher-order sea-level fluctuations induced by short-eccentricity climate variations, controlling facies architecture at detailed scale (i.e. high-frequency sequences).

8.2.2. Comparison with other similar case studies: the stratigraphic architecture revealed

Previous works to reach a deep understanding of the stratigraphic facies architecture of ancient carbonate ramp successions report the importance of considering the scale-dependent facies heterogeneity, particularly for the characterization of the lateral and vertical dimension of reservoir-rock bodies:

1) San Miguel et al. (2017a) described a similar complexity in the internal facies architecture compared to the Higueruelas Fm for the *mid-Kimmeridgian shallow carbonate ramp deposits of the Jabaloyas Fm in central areas of the Iberian Basin* (NE Spain), in an outcrop window of 2 km wide and 23 m thick (see Fig. 8.3c). In particular, these authors also reported a vertical extent of few dm to few m (up to 4 m) for the hundreds-of-m to km-long inner- to mid-ramp grain-supported sedimentary bodies (i.e. oolitic, skeletal, intraclastic and peloidal packstone-grainstone to grainstone facies). However, significant differences are recorded in the stromatoporoid-bearing facies. Inner-ramp stromatoporoid-rich levels are only up to 1 m in thickness, compared with the up to 2-3 m in the Higueruelas Fm. Mid-ramp buildups in the Jabaloyas Fm show pinnacle geometries of up to 8-19 m high and 5-7 m wide, compared with the low-angle lenticular geometry for the mid-ramp buildups in the Higueruelas Fm (i.e. up to 8 m high and 250 m wide), which form with their laterally associated inter-buildup stromatoporoid-bearing facies sedimentary bodies which can reach up to 10 m in thickness and up to 10 km in lateral extent.

2) Amour et al. (2013) illustrated the facies architecture for the *Middle Jurassic shallow carbonate ramp deposits of the Assoul Fm in the High Atlas mountain range of Morocco*. This characterization was performed on the basis of the physical tracing of beds between sections in a study window of 1 km wide and 100 m thick (Fig. 8.5b), with a mean separation distance between logs of hundreds of m. Similar to the Higueruelas Fm, these authors pointed out a complex internal facies architecture, with m-scale lateral and vertical facies changes. The main differences concern the dimension of the inner-ramp reefal facies of the Assoul Fm, which is significantly lower (reaching few m in both lateral and vertical extent) compared with that of the lagoon stromatoporoid-rich facies reported for the Higueruelas Fm (hundreds of m in lateral extent; Fig. 8.5a); and the dimension of the different facies types which constitute the shoal complex in the Assoul Fm (i.e. oolitic and peloidal grain-supported facies), with 150 to 300 m in lateral extent, compared with the hundreds-of-m to km-long continuity for those in the Higueruelas Fm.

3) The reservoir-scale characterization of the internal facies architecture of the *Middle Triassic shallow carbonate ramp deposits of the Quaderkalk Fm in SW Germany* by Petrovic and Aigner (2017), is based on the analysis of a 3-10 m-thick succession along 33 km (Fig. 8.6b), with an average separation distance between logs of 4 to 8 km, similar to the Higueruelas Fm (Fig. 8.6a). In this case, the shoal bodies within the complex shoal mosaic described in the Quaderkalk Fm (with up to 6-10 km in lateral extent) reach from 1 to 5 m in thickness (Fig. 8.6b), similar to the vertical extent of the shoal-sand blanket facies belt in the Higueruelas Fm (Fig. 8.6a). The main difference concerns the lateral extent of the different facies types which constitute the shoal bodies, which in the Quaderkalk Fm are significantly lower (reaching tens to hundreds of m in down-dip and strike directions) compared with that of the facies types forming the shoal-sand blanket belt in the Higueruelas Fm (up to ~15 to 30 km in down-dip and strike directions, respectively).

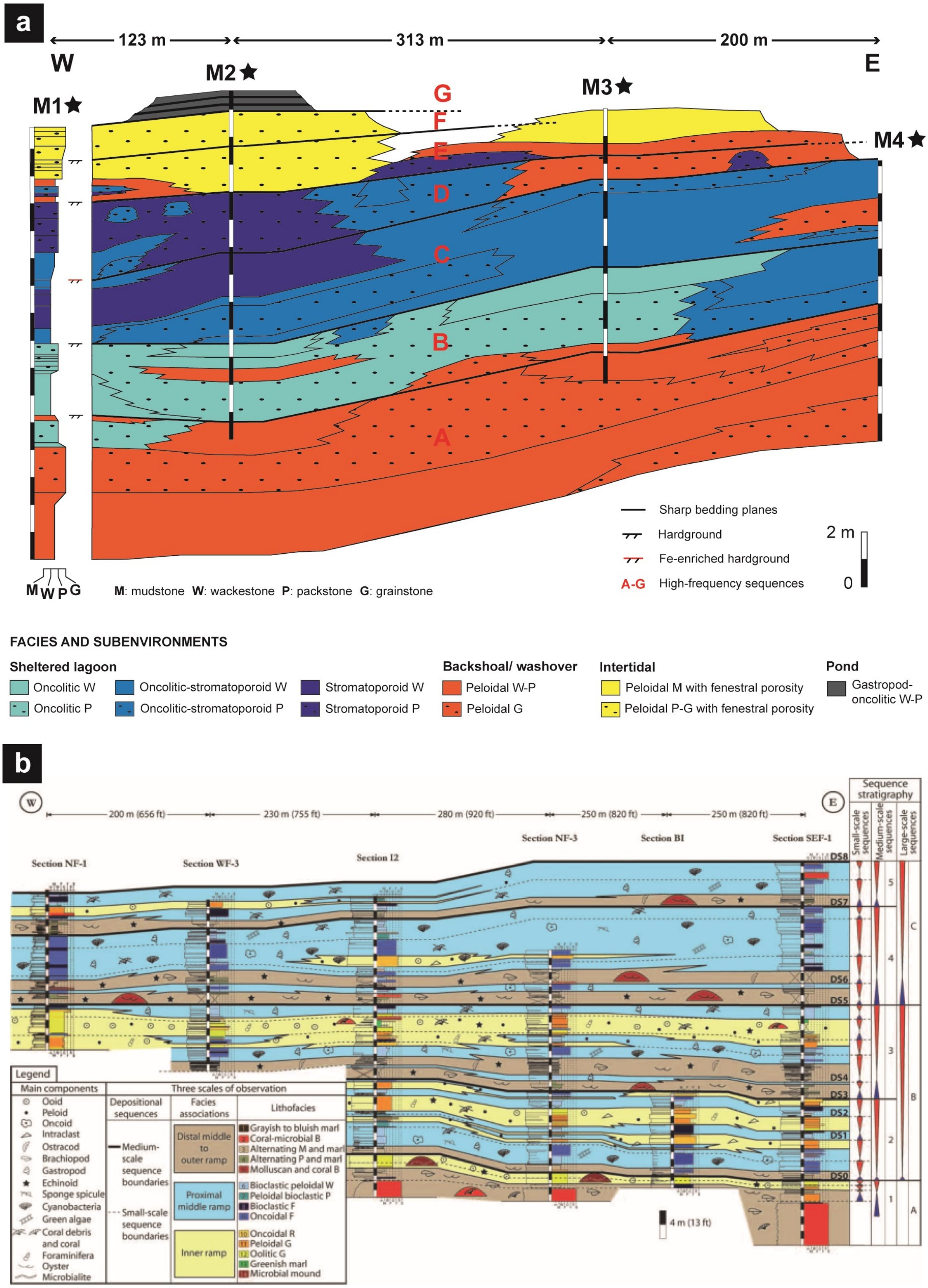

***Fig. 8.5**. Comparison between the internal facies architecture obtained for the Higueruelas Fm around the Mezalocha sector (a, derived from facies mapping in continuous outcrops; see Chapter 5) and for the Middle Jurassic shallow carbonate ramp succession of the Assoul Fm in the High Atlas mountain range of Morocco (b, extracted from Amour et al., 2013) at outcrop window scale (mean distance between logs of hundreds of m).*

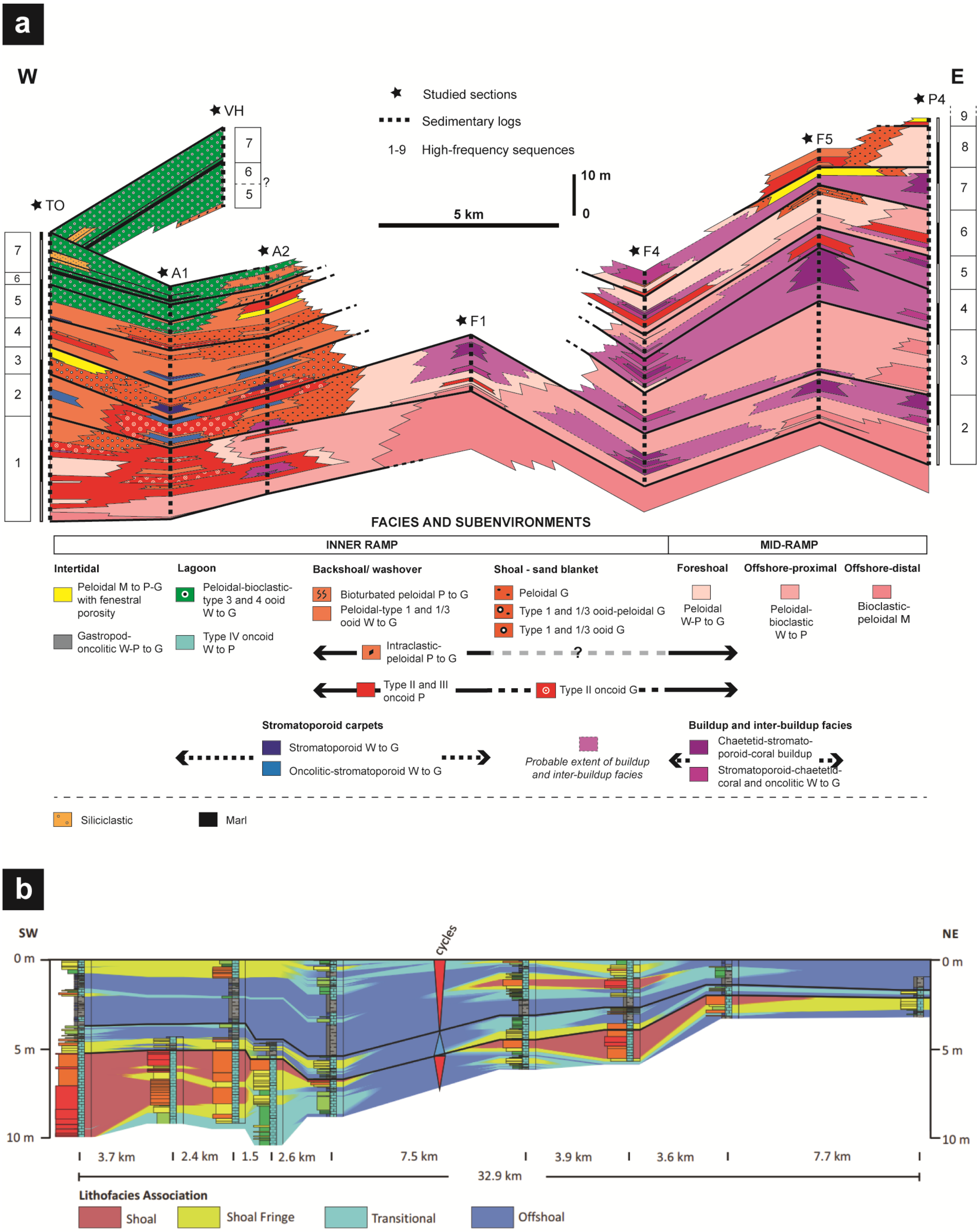

Fig. 8.6. *Comparison between the internal facies architecture obtained for the Higueruelas Fm in the southern cross-section (a; see Chapter 5) and the Middle Triassic shallow carbonate ramp succession of the Quaderkalk Fm in SW Germany (b, extracted from Petrovic and Aigner, 2017) at reservoir scale (mean distance between logs of several km).*

4) The reservoir-scale characterization of the internal facies architecture for the *upper Kimmeridgian shallow carbonate ramp deposits of the Arab-D Fm in Saudi Arabia*, is performed by well-log correlation of a ~200 m-thick succession along 25 km (Fig. 8.7), with an average separation distance between logs of > 10 km (Marchionda et al., 2018). Sand-shoal sedimentary bodies described in this unit by Marchionda et al. (2018) show from ~40 km (along strike) and 17 -20 km (down dip) in lateral extent, and between 15-20 m in vertical extent (Fig. 8.7), therefore have a significantly higher dimension compared to the shoal bodies of the Higueruelas Fm (Fig. 8.6a). Also inner- and mid-ramp stromatoporoid buildups in the Arab-D Fm are thicker (up to 11 m high) than the mid-ramp stromatoporoid-rich buildups in the Higueruelas Fm (up to 8 m high).

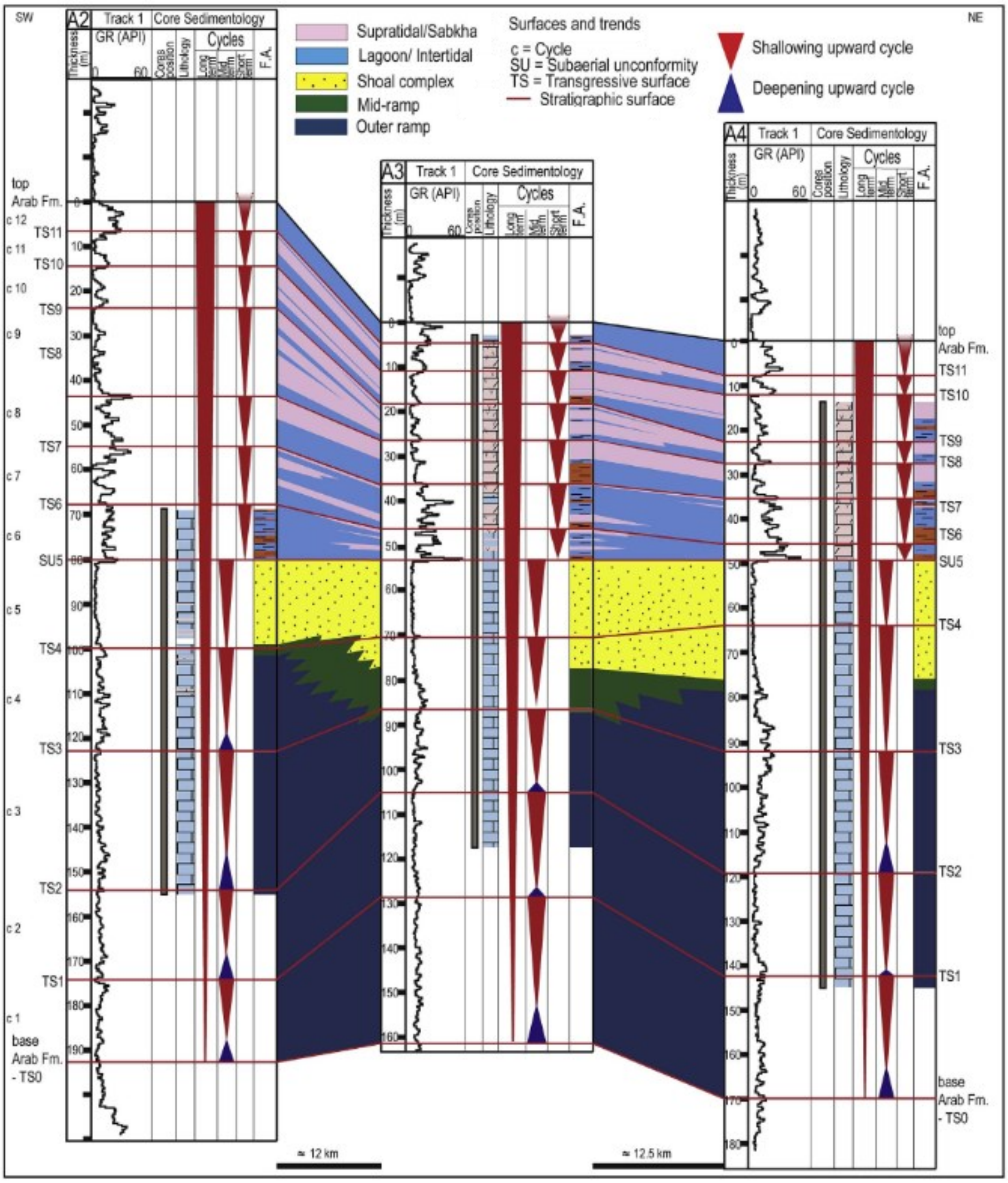

Fig. 8.7. Stratigraphic architecture of the upper Kimmeridgian shallow carbonate ramp succession of the Ara-D Fm in Saudi Arabia (extracted from Marchionda et al., 2018).

As a summary, vertical and lateral extent defined by different rock (facies)-bodies in shallow carbonate ramp deposits is highly variable, also depending on the scale of observation. Taking into account the complex internal facies architecture revealed for shallow carbonate ramp successions, unravelling such heterogeneities at reservoir scale becomes essential for carbonate reservoir characterization, in particular for those facies which are potential reservoir-rock bodies. The comparison above reflects that the accuracy of such internal facies architecture increases at small outcrop-window scale (i.e. the Jabaloyas and Assoul formations, and the Higueruelas Fm in the Mezalocha outcrops; Figs 8.3c and 8.5), whereas the km-long lateral extent of the sedimentary bodies is revealed at reservoir scale (the Quaderkalk and Arab-D formations, and the Higueruelas Fm along the cross-sections covering the entire study area; Figs 8.6 and 8.7).

8.2.3. Way forward

The complex stratigraphic facies architecture obtained in the Higueruelas Fm affords key information about the internal processes controlling facies distribution in shallow carbonate ramp successions, which can be useful for addressing facies pattern predictability in similar stratigraphic records on the basis of subsurface data.

Accordingly, further investigations of the internal facies architecture of the Higueruelas Fm should include the high-resolution sequential analysis of these carbonate successions at basin scale, covering areas of hundreds of km in lateral extent, for the characterization of the facies architecture at large-reservoir scale.

In addition, it would be also interesting to apply 3D modelling techniques to the Higueruelas Fm, in order to test the predictability of facies stacking patterns at different outcropping scales. In the literature, particularly in carbonate ramp systems showing shoal complexes, previous authors have performed reconstructions of internal facies architectures using geostatistical modelling techniques, which combine multiple data from lateral and vertical facies relationships (e.g. Petrovic et al., 2018). Some of the algorithms tested for modelling are the so-called stochastic truncated Gaussian simulation (TGS) or stochastic multiple-point simulation (MPS), used for building facies heterogeneities at regional and local scale, respectively (e.g. Caers and Zhang, 2004; Zakrevsky, 2011). Such statistic methods can be applied to the Higueruelas Fm in order to evaluate the degree of facies pattern predictability, by comparing the 3D facies modelling with the reconstructed facies heterogeneities from the field data.

8.3. POST-DEPOSITIONAL EVOLUTION

8.3.1. Key features of the preliminary data on the post-depositional evolution

The carbon and oxygen stable isotope analyses performed on the Higueruelas Fm in two selected sections (Tosos and Fuendetodos; see Chapter 7), have revealed two distinctive diagenetic imprints on the stable isotope signature related to the different post-depositional diagenetic evolution of the Higueruelas Fm in each sector (Fig. 8.8a). Around Tosos, the deposition of a thick (800 m) continental succession from the Early Cretaceous until the Miocene, conditioned that these carbonates were mainly affected by burial diagenesis. Around Fuendetodos, however, the Higueruelas Fm remained mostly exposed to meteoric weathering from the end of the Kimmeridgian to the Cenozoic, being overlain only by a c. 200 m-thick succession of middle Miocene lacustrine carbonates (see Fig. 2 in Chapter 7).

Despite of the distinctive stable isotope signature revealed for the Higueruelas Fm in each sector, no differences in the petrographic and cathodoluminescence (CL) characteristics were reported, with the exception of punctual intervals in Tosos section (see Figs 4 and 5 in Chapter 7; also additional pictures in Annexe 3). However, since only a small group of samples (21 from a total of 72 samples analysed) were observed under CL analysis, this preliminary observation requires to be confirmed after the analysis of more samples.

On the other hand, concerning the stable isotope data, besides the distinctive stable isotope signature revealed for Tosos and Fuendetodos sections, it is also remarkable that a certain relationship between the magnitude of the diagenetic alteration and the fabric type has been revealed in Tosos section, being the grainstone textures more diagenetically altered compared to the rest of the fabrics (Fig. 8.8b). By contrast, in Fuendetodos section, the probable complexity of the diagenetic events which occurred during the long-lasting meteoric alteration, obliterated any differentiated isotopic composition pattern regarding the fabric type.

Fig. 8.8 (Next page)*. Carbon and oxygen stable isotope records of the Higueruelas Fm in Tosos and Fuendetodos sections. These values show a significant deviation respect to the Kimmeridgian pristine marine carbonates reported in the literature (a, sensu Riboulleau et al., 1998; Jenkyns et al., 2002; Wierzbowski, 2004 and Nunn and Price, 2010), with a distinctive isotopic signature due to the different post-depositional diagenetic evolution of the Higueruelas Fm in each sector: burial diagenesis (Tosos) or meteoric diagenesis (Fuendetodos). In addition, a relationship between the fabric type and the magnitude of the diagenetic alteration is observed in the Tosos section, but not in Fuendetodos (b).*

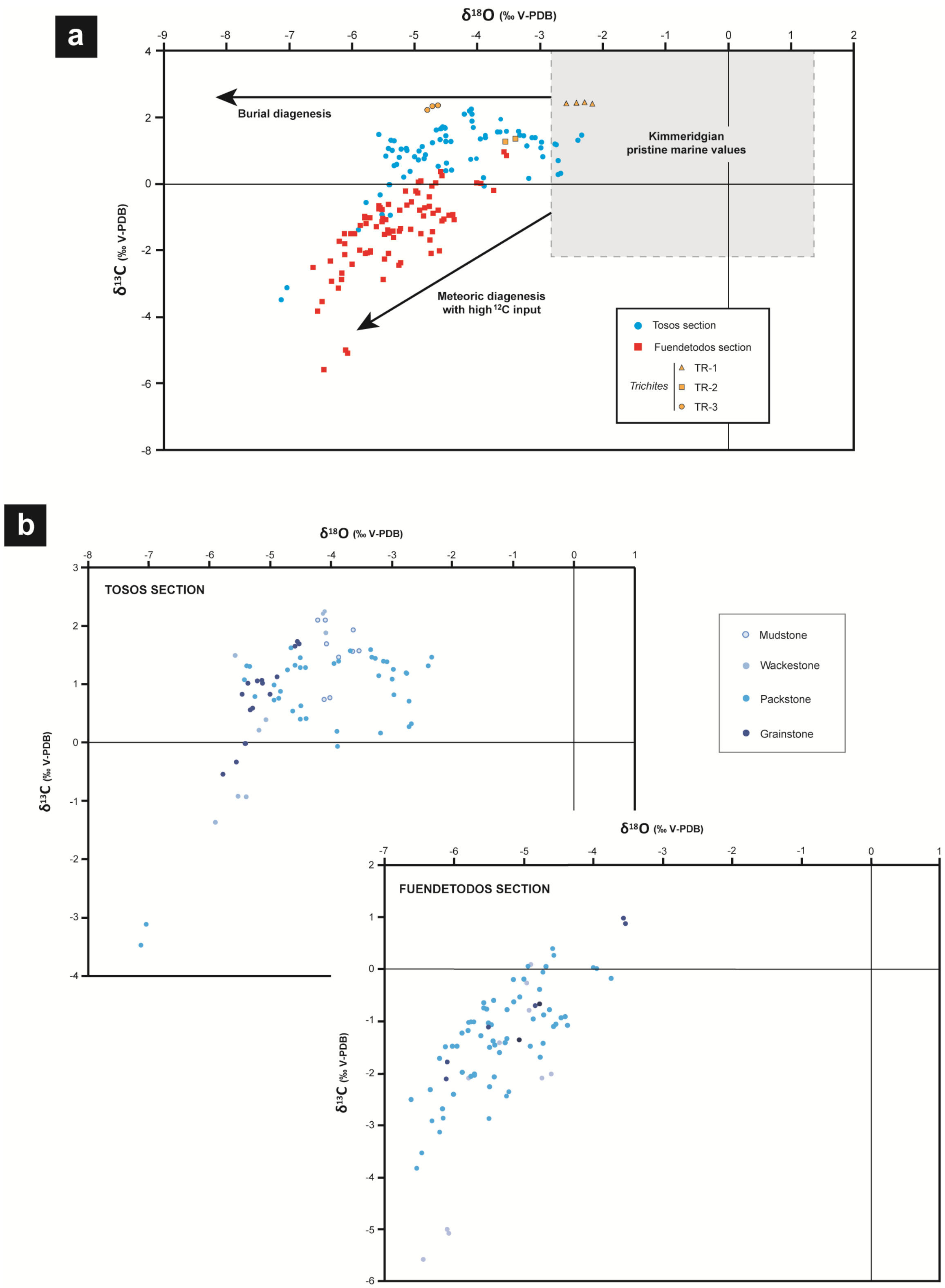
a
δ18O (‰ V-PDB)
δ13C (‰ V-PDB)
Burial diagenesis
Kimmeridgian
pristine marine values
Meteoric diagenesis
with high 12C input
Tosos section
Fuendetodos section
Trichites
TR-1
TR-2
TR-3
b
δ18O (‰ V-PDB)
δ13C (‰ V-PDB)
TOSOS SECTION
Mudstone
Wackestone
Packstone
Grainstone
δ18O (‰ V-PDB)
δ13C (‰ V-PDB)
FUENDETODOS SECTION

8.3.2. Way forward

Rock fabrics address the sum of both primary carbonate components (e.g. carbonate grains, micrite matrix) and diagenetic calcite cements (e.g. Goodner et al., 2020), the latter precipitating in different types of pores (e.g. interparticle porosity, mouldic vugs, fractures) (e.g. Choquette and James, 1987; Tucker and Wright, 1990; Flügel, 2004; Swei and Tucker, 2012; Moore, 2013; San Miguel et al., 2017b; Goodner et al., 2020). The petrographic characteristics of rock fabrics usually differ from those of the depositional fabrics, particularly concerning the pore network. The porosity-type and porosity-volume evolution of carbonates throughout their post-depositional history, which also relates to permeability, would determine the degree of interaction between the diagenetic fluid and the host carbonate rock, being the coarser fabrics more favourable for infiltration of the diagenetic fluids (e.g. Marshall, 1992; Immenhauser et al., 2002; Vincent et al., 2004; Coimbra et al., 2014; Huck et al., 2017; Al-Mojel et al., 2018). During diagenesis, the porosity volume as well as the pores shape and connectivity can be strongly modified (e.g. Hollis et al., 2017), by both porosity occlusion during precipitation of diagenetic calcite cements and/or creating porosity by dissolution of unstable mineralogical phases (e.g. aragonitic shells) (e.g. Swei and Tucker, 2012). Successive events of dissolution and/or precipitation can occur during the post-depositional history of carbonates, also differing concerning the diagenetic processes involved (e.g. burial vs meteoric diagenesis).

A detailed diagenetic analysis of the Higueruelas Fm in both Tosos and Fuendetodos sections is required for evaluating the early vs late diagenetic alteration of these carbonates, regarding the preliminary interpretation of the different post-depositional diagenetic history in each sector. Although the evolution of the porosity and permeability in the studied sections is still unknown, it seems that the fabric type has influenced the magnitude of the diagenetic alteration in those carbonates mainly affected by burial diagenesis (Tosos sector). In this regard, if depositional features has highly determined the porosity and permeability evolution of these carbonate rocks, as reported in previous works (e.g. Goodner et al., 2020), the good control of the internal facies architecture performed in this Thesis would represent a useful tool in predicting porosity-permeability patterns within the potential reservoir-rock bodies, and characterize the diagenetic heterogeneities, resulting in important implications for reservoir characterization.

Further investigations will focus on the relationship between the different types of diagenetic calcite cements recognized (i.e. granular, drusy and blocky; see Chapter 7), distinguishing different diagenetic phases, and the evaluation of other diagenetic features (e.g. stylolites, contact between grains), combined with a complete CL scanning for the total of the samples analysed. Additionally, in order to obtain more information about the origin of the diagenetic fluids, it would be interesting to stain the samples with ferricyanide (an acid solution which reacts in presence of ferrous iron) and/or perform trace elements geochemical analyses (particularly Mn and Fe), and thus stablishing a link with the CL observations. With all of this information, we can reconstruct the succession of diagenetic events affecting these carbonates throughout their post-depositional evolution (*paragenetic sequence*), and the evolution of the porosity and permeability throughout the successive diagenetic events, which have important implications for carbonate reservoir characterization.

In relation to the diagenetic events affecting the Higueruelas Fm, another key aspect to investigate concerns the presence of totally or partially dolomitized tabular dm- to m-thick beds in the studied unit (Fig. 8.9). Previous studies on the Higueruelas Fm in the same region (Aurell, 1990) proposed the existence of dolomitizing fluids circulating through faults acting during the Cenozoic Alpine compression. This hypothesis could be supported by the fact that dolomitized intervals are frequent in areas such as Muel, Jaulín, Valmadrid and Puebla de Albortón sectors (see Fig. 3.1 in Chapter 3 for

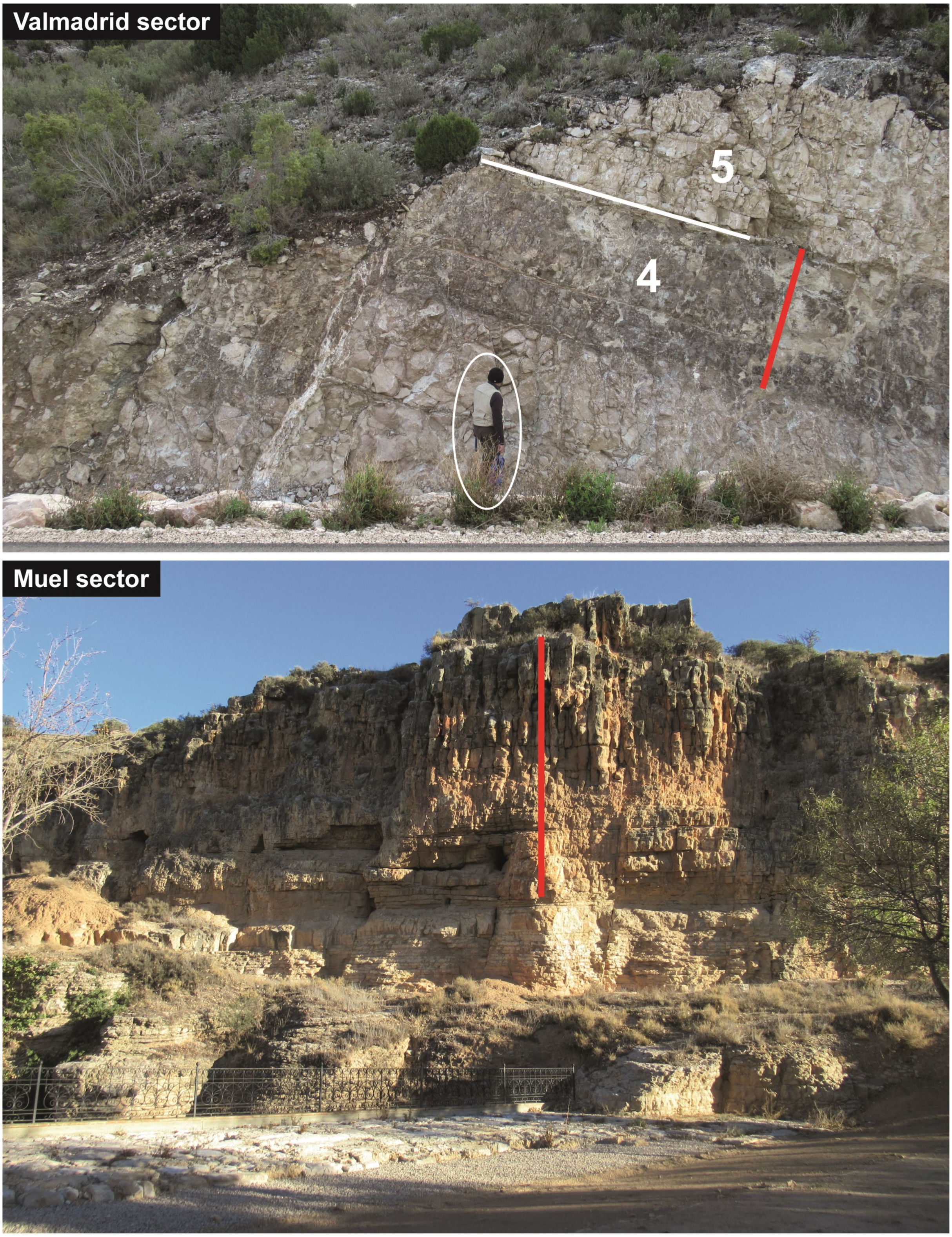

Fig. 8.9. Examples of dolomitized intervals (see red bars) in the Higueruelas Fm from Valmadrid (section V) and Muel sectors (proximal to section MU) (see Chapter 5 for location of the sectors).

location), which form part of the so-called major north-Iberian thrust system (e.g. Vergés and García-Senz, 2001). However, it is also probable that the dolomitization could have occurred during the Early Cretaceous rifting stage, associated to dolomitizing fluids circulating through normal faults (e.g. the Aguilón fault system; see Fig. 2 in Chapter 7), similar as described for the Upper Jurassic-Lower Cretaceous dolomites in eastern areas of the Iberian Basin (i.e. Maestrat Basin; Nadal, 2001; Travé et al., 2019), where dissolution of Triassic and Jurassic carbonates and evaporites represented a potential source of Mg^{2+} for dolomitization. Accordingly, further analyses concerning the diagenetic evolution of the Higueruelas Fm will also address the characterization of dolomitized samples collected in different sections along the study area, by combining petrographic, CL and geochemical analyses, differentiating, if possible, different types of dolomite and their relationship with the described diagenetic calcite cements. It is noteworthy that the characterization of the dolomitization in carbonate reservoir analogues is of particular interest in terms of reservoir quality, as dolomitization has been suggested an important factor controlling the formation and evolution of porosity in carbonate rocks (e.g. Zenger et al., 1980; Roehl and Choquette, 1985; Sun, 1995; Warren, 2000; Tavakoli et al., 2011; Liu et al., 2016).

9. CONCLUSIONS

CONCLUSIONS

This PhD Thesis presents the results obtained of combined stratigraphic, sedimentological and geochemical analyses of the uppermost Jurassic Higueruelas Formation, outcropping in a 20 x 30 km area (south of the city of Zaragoza, NE Spain). The main contributions are:

1) New strontium isotope data combined with the record of key marker foraminifera (lituolids), allowed constraining the age of the Higueruelas Formation at the study area into the latest Kimmeridgian (i.e. upper *eudoxus* and *beckeri* zones). This new age assignment represents a significant advance compared to previous works, in which this unit was discussed to be either early-mid Kimmeridgian or Tithonian.

2) Extensive facies analysis based on the study of 35 logs, 1200 polished slabs and 300 thin sections resulted in the characterization of 19 facies types, formed from inner to mid-domains of a ramp-type platform. Facies were differentiated according to the variable proportions of non-skeletal grains (mainly peloids, ooids and oncoids) and skeletal components, being the detailed analysis of oncoids and the new classification on six oncoid types proposed, a useful tool for sedimentological interpretations. Identification of sedimentary discontinuities allowed the definition of nine high-frequency sequences, whose facies correlation resulted in the precise reconstruction of the vertical and lateral (along strike and down dip) facies distribution and their controlling factors:

    - Two stages of ramp evolution were differentiated. The lower stage (sequences 1 to 4) is characterized by an *oncolitic-peloidal-oolitic-dominated ramp*, which includes: 1) a peloidal intertidal facies belt; 2) a low-energy sheltered lagoon with stromatoporoid carpets and microbial-dominated type IIIb and IVa oncoids; 3) peloidal-oolitic backshoal, shoal-sand blanket and foreshoal deposits with along-strike oncolitic shoal (dominant type II oncoids) and backshoal-foreshoal domains (abundant type IIIa oncoids mainly in the foreshoal), including stromatoporoid carpets in the backshoal; and 3) mid-ramp bioclastic-peloidal packstones to mudstones with chaetetid-stromatoporoid-coral buildups, surrounded by oncolitic (mainly type IVa)-stromatoporoid facies. The second stage of evolution (sequences 5 to 9) is characterized by an *oolitic-peloidal-dominated ramp*, which involves: 1) the development of a wide restricted peloidal-bioclastic-oolitic lagoon without stromatoporoid carpets, 2) peloidal-dominated backshoal, shoal-sand blanket and foreshoal domains, with frequent intraclastic-peloidal storm-related deposits, and 3) the minor development of the oncolitic facies.

    - The combined role of external and internal factors controlled the facies distribution within the two ramp models and the final facies architecture. In the *oncolitic-peloidal -oolitic-dominated ramp*, main factors are: 1) barrier effect of the shoal-sand blankets and low siliciclastic input, favouring the generation of the low-energy sheltered lagoon with microbial-dominated type IIIb and IVa oncoids; 2) lateral variation in energy conditions due to the irregular depositional topography in the backshoal to foreshoal domains, controlling the along-strike change from peloidal-oolitic to oncolitic (type II and IIIa)-dominated facies; and 3) higher tolerance to water energy of stromatoporoids, allowing colonizing from lagoon to backshoal domains, compared to corals that drove in low-energy mid-ramp settings. The transition to an *oolitic-peloidal-dominated ramp* is related to the long-term fall in relative sea level occurring at the end of the Jurassic at basin scale, leading to more restricted conditions and an increase of siliciclastic input in proximal domains, combined with an increment in water energy (i.e. storm-related beds).

- The combined effect of the depositional facies heterogeneities (and their complex controlling factors), and the reduced accommodation space created by both the long-term regional fall in relative sea level and the higher-order sea-level fluctuations (i.e. high-frequency sequences), the latter probably induced by short-eccentricity climate variations, resulted in a complex stratigraphic facies architecture for this unit. The dimension of the sedimentary bodies defined by the different facies types is variable, showing from tens of km to hundreds of m in lateral extent, but only from few dm to several m in thickness. The reconstructed stratigraphic architecture has potential application to further understand the facies heterogeneities of similar carbonate ramp systems, being of particular interest its use for interwell-scale facies pattern predictability in carbonate reservoirs such as the Arab Formation.

3) Carbon and oxygen stable isotopes in two selected sections, representing the proximal (Tosos) and relatively distal (Fuendetodos) areas of the carbonate ramp, are useless for palaeoenvironmental interpretations, but provide significant data to approach the post-depositional evolution of the Higueruelas Formation in each study sector, in particular the variable effect of the burial and meteoric diagenesis: 1) for those deposits mainly affected by burial diagenesis (Tosos), a relationship between the magnitude of the diagenetic alteration and the fabric type has been revealed, being the grainstone texture more diagenetically altered compared to the rest of the fabrics; 2) for those deposits affected by a long-lasting meteoric alteration (Fuendetodos), probably the complexity of the diagenetic events obliterated any differentiated isotopic composition pattern regarding the fabric type. The texture-diagenetic alteration relationship revealed here can be interesting for further investigations concerning the porosity-permeability evolution, with potential implications for reservoir characterization.

CONCLUSIONES

Esta tesis doctoral presenta los resultados que se han obtenido del análisis estratigráfico, sedimentológico y geoquímico en la Formación Higueruelas de edad Jurásico Superior, en concreto en los afloramientos situados en un área de 20 x 30 km situados al sur de la ciudad de Zaragoza (noreste de España). Las principales contribuciones son:

1) La combinación de nuevos datos de isótopos de estroncio y el registro de foraminíferos clave (lituólidos), permitió precisar la edad de la Formación Higueruelas en el área de estudio en el Kimmeridgiense superior (*i.e.* la parte superior de la biozona *eudoxus* y la biozona *beckeri*). Esta nueva asignación de la edad representa un avance significativo respecto a trabajos previos, en los que se discutía que la edad de esta unidad era o bien Kimmeridgiense inferior-medio o bien Titoniense.

2) Un exhaustivo análisis de facies basado en el estudio de 35 perfiles, 1200 secciones pulidas y 300 láminas delgadas ha dado lugar a la caracterización de 19 facies, que representan el depósito desde las zonas internas a medias de una plataforma de tipo rampa. Las facies se han diferenciado en función de las proporciones variables de granos no esqueletales (principalmente peloides, ooides y oncoides) y componentes esqueletales, constituyendo el análisis detallado de los oncoides y la nueva clasificación en seis tipos propuesta, una herramienta útil para interpretaciones paleoambientales. Se han definido nueve secuencias de alto orden, delimitadas por discontinuidades sedimentarias. La correlación de facies llevada a cabo en dichas secuencias permitió reconstruir de manera precisa la distribución de las facies en la vertical y en la lateral (en dirección tanto perpendicular a la línea de pendiente de la rampa o *along strike*, como pendiente abajo o *down dip*), e identificar los factores que controlan dicha distribución:

    - Se han diferenciado dos estadios de evolución de la rampa. El primer estadio (secuencias 1 a 4) corresponde a una *rampa dominada por oncoides, peloides y ooides*, que incluye: 1) un cinturón intermareal dominado por peloides; 2) un *lagoon* protegido de baja energía con desarrollo de praderas de estromatopóridos y oncoides microbiales de tipo IIIb y IVa; 3) una zona de *backshoal*, *shoal-sand blanket* y *foreshoal* dominada por peloides y ooides, que da paso lateralmente (*along strike*) a facies oncolíticas tanto en el *shoal-sand blanket* (donde predominan oncoides de tipo II) como en los dominios de *backshoal* y *foreshoal* (donde abundan oncoides de tipo IIIa, en especial en el *foreshoal*), incluyendo además el desarrollo de praderas de estromatopóridos en la zona de *backshoal*; y 3) una zona de rampa media dominada por facies *packstone* a *mudstone* de peloides y bioclastos, con el desarrollo de bioconstrucciones constituidas por estromatopóridos, chaetétidos y corales que dan paso lateralmente a facies de mezcla de estromatopóridos y oncoides (principalmente de tipo IVa). El segundo estadio de evolución (secuencias 5 a 9) da lugar a una *rampa dominada por ooides y peloides*, que implica: 1) el desarrollo de un *lagoon* restringido dominado por peloides, ooides y bioclastos sin crecimiento de estromatopóridos, 2) el predominio de facies peloidales desde el dominio de *backshoal* al de *foreshoal*, siendo frecuentes los depósitos intraclásticos y peloidales asociados a tormentas, y 3) un menor desarrollo de las facies oncolíticas.

- La acción combinada de diversos factores, tanto externos como internos a la plataforma, controlaron la distribución de facies en los dos modelos de rampa, así como la arquitectura de facies resultante. En la *rampa dominada por oncoides, peloides y ooides*, los principales factores son: 1) el efecto barrera por parte de los *shoal-sand blankets* y la baja tasa de aporte de terrígenos, lo que favoreció el desarrollo del *lagoon* protegido de baja energía con predominio de los oncoides microbiales de tipo IIIb y VIa; 2) las variaciones laterales en las condiciones energéticas debidas a irregularidades en la topografía deposicional que caracterizan desde el dominio de *backshoal* al de *foreshoal*, dando lugar a un cambio lateral (*along strike*) de facies peloidales y oolíticas a facies oncolíticas (oncoides de tipo II y IIIa); y 3) la adaptabilidad de los estromatopóridos a condiciones energéticas variables, permitiendo que estos organismos pudiesen colonizar tanto el *lagoon* como la zona de *backshoal*, en cambio los corales sólo pudieron proliferar en los dominios de baja energía de la rampa media. La transición a la *rampa dominada por ooides y peloides* está relacionada con una caída relativa prolongada del nivel del mar que tuvo lugar a escala de cuenca al final del Jurásico, que dio lugar a condiciones más restringidas y a un aumento del aporte siliciclástico en los dominios proximales de la rampa, y a un incremento en la energía del agua (*i.e.* capas de tormenta).

- La compleja arquitectura de facies que se observa en esta unidad es el resultado de las heterogeneidades de facies observadas en los dos modelos de depósito (y los complejos factores que controlaron dicha distribución), y de la reducción en el espacio de acomodación originada tanto por el contexto regresivo prolongado a escala de cuenca como por variaciones relativas del nivel del mar de alto orden (*i.e.* secuencias de alto orden), en este último caso probablemente ligadas a ciclos de excentricidad de corto término. Los cuerpos sedimentarios representados en los diferentes tipos de facies muestran dimensiones variables, alcanzando desde decenas de kilómetros hasta centenares de metros de extensión lateral, pero sólo desde pocos decímetros hasta varios metros de espesor. La arquitectura de facies reconstruida para esta unidad permite comprender mejor las heterogeneidades de las facies en sistemas de rampa carbonatada similares, siendo de particular interés su uso para predecir heterogeneidades de las facies entre perfiles/sondeos separados varios kilómetros entre sí en reservorios carbonatados como la Formación Arab.

3) Los análisis de isótopos estables de carbono y oxígeno realizados en las dos secciones seleccionadas, en áreas proximales (Tosos) y relativamente distales (Fuendetodos) de la rampa, han resultado no ser apropiados para llevar a cabo interpretaciones paleoambientales. No obstante, dichos registros han proporcionado datos relevantes para abordar la evolución post-deposicional de la Formación Higueruelas en cada sector de estudio, en particular el efecto variable de la diagenesis de enterramiento y meteórica: 1) en aquellos materiales principalmente afectados por la diagenesis de enterramiento (Tosos), se ha puesto de manifiesto una relación entre la magnitud de la alteración diagenética y el tipo de fábrica, siendo los depósitos con textura *grainstone* más afectados por la diagénesis en comparación con el resto de fábricas texturales; 2) en cambio, para aquellos materiales afectados por un largo periodo de alteración meteórica (Fuendetodos), no hay ningún patrón distintivo en la alteración diagenética en relación con el tipo de fábrica, lo que probablemente se deba a la complejidad de los diversos eventos diagenéticos involucrados en dicha alteración meteórica. La relación textura-alteración

diagenética observada aquí puede ser interesante para futuras investigaciones centradas en la evolución de la porosidad y permeabilidad de estos materiales, las cuales pueden tener importantes implicaciones para la caracterización de reservorios.

10. REFERENCES

This Chapter encompasses the references included in chapters 1-4 and 8, in the introductions of chapters 5-7 and in figure captions of Annexe 1.

Ahr, W., 1973. The carbonate ramp: an alternative to the shelf model. Transactions of the Gulf Coast Association of Geological Societies 23, 221-225.

Aigner, T., 1985. Storm Depositional Systems. Dynamic Stratigraphy in Modern and Ancient Shallow-Marine Sequences. Lecture notes in Earth Sciences 3, Springer-Verlag, Berlin, pp. 174.

Ainardi, R., Champetier, Y., 1976. Processus de formation d'intraclastes par dessiccation en milieu margino-littoral: exemple dans le "Purbeckien" du Jura. Bulletin de la Société Géologique de France 18, 159-164.

Al-Awwad, S.F., Collins, L.B., 2013. Arabian carbonate reservoirs: A depositional model of the Arab-D reservoir in Khurais field, Saudi Arabia. The American Association of Petroleum Geologists 97, 1099-1119.

Allan, J.R., Matthews, R.K., 1982. Isotope signatures associated with early meteoric diagenesis. Sedimentology 29, 797-817.

Al-Mojel, A., Dera, G., Razin, P., Le Nindre, Y-M., 2018. Carbon and oxygen isotope stratigraphy of Jurassic platform carbonates from Saudi Arabia: Implications for diagenesis, correlations and global paleoenvironmental changes. Palaeogeography, Palaeoclimatology, Palaeoecology 511, 388-402.

Alnazghah, M.H., Bádenas, B., Pomar, L., Aurell, M., Morsilli, M., 2013. Facies heterogeneity at interwell-scale in a carbonate ramp, Upper Jurassic, NE Spain. Marine and Petroleum Geology 44, 140-163.

Altiner, D., 1991. Microfossil biostratigraphy (mainly foraminifers) of the Jurassic-Lower Cretaceous carbonate successions in north-western Anatolia (Turkey). Geologica Romana 27, 167-213.

Álvaro, M., Capote, R., Vegas, R., 1979. Un modelo de evolución geotectónica para la Cadena Celtibérica. Acta Geológica Hispánica 14, 172-177.

Amour, F., Mutti, M., Christ, N., Immenhauser, A., Agar, S.M., Benson, G.S., Tomás, S., Always, R., Kabiri, L., 2011. Capturing and modelling metre-scale spatial facies heterogeneity in a Jurassic ramp setting (Central High Atlas, Morocco). Sedimentology 59 (4), 1158-1189.

Amour, F., Mutti, M., Christ, N., Inmenhauser, A., Benson, G.S., Agar, S.M., Tomás, S., Kabiri, L., 2013. Outcrop analog for an oolitic carbonate reservoir: A scale-dependent geologic modeling approach based on stratigraphic hierarchy. The American Association of Petroleum Geologists 97 (5), 845-871.

Anderson, T.F., Arthur, M.A., 1983. Stable isotopes of oxygen and carbon and their application to sedimentologic and paleoenvironmental problems. In: Arthur, M.A., Anderson, T.F., Kaplan, I.R., Veizer, J., Land, L.S. (Eds.), Stable Isotopes in Sedimentary Geology. SEPM Short Course 10, Tulsa, pp. 1-151.

Arthaud, F., Matte, P., 1977. Late Paleozoic strike-slip faulting in southern Europe and northern Africa: Result of a right-lateral shear zone between Appalachians and the Urals. Geological Society of America Bulletin 88, 1305-1320.

Arthur, M.A., Dean, W.E., Schlanger, S.O., 1985. Variations in the global carbon cycle during the Cretaceous related to climate, volcanism, and changes in atmospheric CO_2. In: Sundquist, E.T., Broecker, W.S. (Eds.), The carbon cycle and atmospheric CO_2: Natural variations Archean to Present. Geophysical Monograph series 32. American Geophysical Union, Washington, DC, pp. 504-529.

Atrops, F., Meléndez, G., 1984. Kimmeridgian and Lower Tithonian from the Calanda-Berge area (Iberian Chain, Spain): Some biostratigraphic remarks. In: Zeiss, A. (Ed.), Proceedings 1st International Symposium on Jurassic Stratigraphy 2. Erlangen, pp. 377-392.

Aurell, M., 1990. El Jurásico Superior en la Cordillera Ibérica Central (provincias de Zaragoza y Teruel). Análisis de cuenca. PhD Thesis, Universidad de Zaragoza, Spain, pp. 534.

Aurell, M., 1991. Identification of system tracts in low-angle carbonate ramps: examples from the Upper Jurassic of the Iberian Chain (Spain). Sedimentary Geology 73, 101-115.

Aurell, M., Meléndez, A., 1986. Sedimentología de la Formación Calizas con oncolitos de Higueruelas (Malm) en la región de Muel-Belchite (Provincia de Zaragoza). Acta Geológica Hispánica 21-22, 307-312.

Aurell, M., Meléndez, A., 1987. Las bioconstrucciones de corales y sus facies asociadas durante el Malm en la Cordillera Ibérica Central (prov. De Zaragoza). Estudios Geológicos 43, 261-269.

Aurell, M., Meléndez, A., 1993. Sedimentary evolution and sequence stratigraphy of the Upper Jurassic in the central Iberian Chain, northeast Spain. In: Posamentier, H.W., Summerhayes, C.P., Haq, B.U., Allen, G.P. (Eds.), Sequence Stratigraphy and Facies Associations. International Association of Sedimentologists, Special Publications 18, pp. 343-368.

Aurell, M., Bádenas, B., 1994. Factors controlling the sedimentary evolution of the Kimmeridgian ramp in the north Iberian Basin (NE Spain). Estudios Geológicos 50 (1-2), 91-101.

Aurell, M., Bádenas, B., 2004. Facies and depositional sequence evolution controlled by high-frequency sea-level changes in a shallow-water carbonate ramp (late Kimmeridgian, NE Spain). Geological Magazine. 141 (6), 717-733.

Aurell, M., Mas, R., Meléndez, A., Salas, R., 1994. El tránsito Jurásico-Cretácico en la Cordillera Ibérica: relación tectónica-sedimentación y evolución paleogeográfica. Cuadernos de Geología Ibérica 18, 369-396.

Aurell, M., Bosence, D., Waltham, D., 1995. Carbonate ramp depositional systems from a late Jurassic epeiric platform (Iberian Basin, Spain): a combined computer modelling and outcrop analysis. Sedimentology 42 (1), 75-94.

Aurell, M., Bádenas, B., Bosence, D., Waltham, D., 1998. Carbonate production and offshore transport on a Late Jurassic carbonate ramp (Kimmeridgian, Iberian Basin, NE Spain): evidence from outcrops and computer modelling. In: Wright, V., Burchette, T. (Eds.), Carbonate Ramps. vol. 149. Geological Society Special Publications, London, pp. 137-161.

Aurell, M., Meléndez, G., Bádenas, B., Pérez-Urresti, I., Ramajo, J., 2000. Sequence Stratigraphy of the Callovian-Berriasien (Middle Jurassic - Lower Jurassic) of the Iberian Range (NE. Spain). GeoResearch Forum 5, 281-292.

Aurell, M., Robles, S., Bádenas, B., Rosales, I., Quesada, S., Meléndez, G., García-Ramos, J.C., 2003. Transgressive-regressive cycles and Jurassic palaeogeography of northeast Iberia. Sedimentary Geology 162, 239-271.

Aurell, M., Bádenas, B., Ipas, J., Ramajo, J., 2010. Sedimentary evolution of an Upper Jurassic epeiric carbonate ramp, Iberian Basin, NE Spain. In: Van Buchem, F.S.P., Gerdes, K.D., Esteban, M. (Eds.), Mesozoic and Cenozoic Carbonate Systems of the Mediterranean and the Middle East: Stratigraphic and Diagenetic Reference Models. Geological Society, London, Special Publications 329, pp. 89-111.

Aurell, M., Ipas, J., Bádenas, B., Muñoz, A., 2012. Distribución de facies con corales y estromatopóridos en el dominio interno de una plataforma carbonatada (Titónico, Cordillera Ibérica). Geogaceta 51, 67-70.

Aurell, M., Bádenas, B., Gasca, J.M., Canudo, J.I., Liesa, C.L., Soria, A.R., Moreno-Azanza, M., Najes, L., 2016. Stratigraphy and evolution of the Galve sub-basin (Spain) in the middle Tithonian-early Barremian: Implications for the setting and age of some dinosaur fossil sites. Cretaceous Research 65, 138-162.

Aurell, M., Fregenal-Martínez, M., Bádenas, B., Muñoz-García, M. B., Élez, J., Meléndez, N., de Santisteban, C., 2019a. Middle Jurassic–Early Cretaceous tectono-sedimentary evolution of the southwestern Iberian Basin (central Spain): Major palaeogeographical changes in the geotectonic framework of the Western Tethys. Earth-Science Reviews 199, 102983.

Aurell, M., Bádenas, B., Canudo, J.I., Castanera, D., García-Penas, A., Gasca, J.M., Martín-Closas, C., Moliner, L., Moreno-Azanza, M., Rosales, I., Santas, L., Sequero, C., Val, J., 2019b. Kimmeridgian-Berriasian stratigraphy and sedimentary evolution of the central Iberian Rift System (NE Spain). Cretaceous Research 103, 104153.

Baccelle, L., Bosellini, A., 1965. Diagrammi per la stima visiva della composizione percentuale nelle rocce sedimentarie. Annali dell'Università di Ferrara (N.S.), Sez. IX., Scienze Geologiche e Paleontologiche 1, 59-62.

Bádenas, B., 1999. La sedimentación en las rampas carbonatadas del Kimmeridgiense en las cuencas del Este de la Placa Ibérica. PhD Thesis, Universidad de Zaragoza, Spain, pp. 256.

Bádenas, B., 2019. Facies architecture in carbonate ramps: learned lessons from Jurassic cases studies in the Iberian Basin. In: Boughdiri, M., Bádenas, B., Selden, P., Jaillard, E., Bengtson, P., Granier, B.R. (Eds.), Paleobiodiversity and Tectono-Sedimentary Records in the Mediterranean Tethys and Related Eastern Areas. Advances in Science, Technology and Innovation, pp. 7-10.

Bádenas, B., Aurell, M., 2001a. Kimmeridgian palaeogeography and basin evolution of northeastern Iberia. Palaeogeography, Palaeoclimatology, Palaeoecology 168, 291-310.

Bádenas, B., Aurell, M., 2001b. Proximal–distal facies relationships and sedimentary processes in a storm dominated carbonate ramp (Kimmeridgian, northwest of the Iberian Ranges, Spain). Sedimentary Geology 139 (3-4): 319-340.

Bádenas, B., Aurell, M., 2003. Análisis comparado y controles en la sedimentación de dos arrecifes de la zona media de una rampa carbonatada del Jurásico Superior de la Cordillera Ibérica. Revista de la Sociedad Geológica de España 16 (3-4), 151-166.

Bádenas, B. Aurell, M., 2008. Kimmeridgian epeiric sea deposits of northeast Spain: sedimentary dynamics of a storm dominated carbonate ramp. In: Holmden, C., Pratt, B.R. (Eds.), Dynamics of Epeiric Seas. Geological Association of Canada, Special Publication 48, pp. 55-72.

Bádenas, B., Aurell, M., 2010. Facies models of a shallow-water carbonate ramp based on distribution of non-skeletal grains (Kimmeridgian, Spain). Facies 56, 89-110.

Bádenas, B., Aurell, M., 2018. The down-dip preferential sequence record of orbital cycles in greenhouse carbonate ramps: Examples from the Jurassic of the Iberian Basin (NE Spain). In: Montenari, M. (Ed.), Stratigraphy and Timescales 3, Academic Press, pp. 285-325.

Bádenas, B., Aurell, M., Pérez-Urresti. I., Delvene, G., 1998. Estratigrafía y Evolución sedimentaria del Oxfordiense superior-Titónico inferior en Ricla (Zaragoza). Geogaceta 24, 35-38.

Bádenas, B., Aurell, M., Rodríguez-Tovar, F.J., Pardo-Igúzquiza, E., 2003. Sequence stratigraphy and bedding rhythms of an outer ramp limestone succession (Late Kimmeridgian, Northeast Spain). Sedimentary Geology 161, 153-174.

Bádenas, B., Salas, R., Aurell, M., 2004. Three orders of regional sea level changes control facies and stacking patterns of shallow platform carbonates in the Maestrat Basin (Tithonian-Berriasian, NE Spain). International Journal of Earth Sciences 93 (1), 144-162.

Bádenas, B., Aurell, M., Gröcke, D.R., 2005. Facies analysis and correlation of high-order sequences in middle-outer ramp successions: variations in exported carbonate in basinwide $\delta^{13}C$ (Kimmeridgian, NE Spain). Sedimentology 52, 1253-1276.

Bádenas, B., Aurell, M., Bosence, D., 2010. Continuity and facies heterogeneities of shallow carbonate ramp cycles (Sinemurian, Lower Jurassic, North-east Spain). Sedimentology 57, 1021-1048.

Bádenas, B., Aurell, M., Gasca, J.M., 2018. Facies model of a mixed clastic-carbonate, wave-dominated open-coast tidal flat (Tithonian-Berriasian, north-east Spain). Sedimentology 65, 1631-1666.

Bahamonde, J.R., Della Porta, G., Merino-Tomé, O.A., 2017. Lateral variability of shallow-water facies and high-frequency cycles in foreland basin carbonate platforms (Pennsylvanian, NW Spain). Facies 63 (6).

Bartolini, A., Pittet, B., Mattioli, E., Hunziker, J.C., 2003. Shallow-platform palaeoenvironmental conditions recorded in deep-shelf sediments: C and O stable isotopes in Upper Jurassic sections of southern Germany (Oxfordian–Kimmeridgian). Sedimentary Geology 160 (1-3), 107-130.

Basilone, L., Sulli, A., 2016. A facies distribution model controlled by a tectonically inherited sea bottom topography in the carbonate rimmed shelf of the Upper Tithonian–Valanginian Southern Tethyan continental margin (NW Sicily, Italy). Sedimentary Geology 342, 91-105.

Bassant, P., 1999. The high-resolution stratigraphic architecture and evolution of the Burdigalian carbonate-siliciclastic sedimentary systems of the Mut Basin, Turkey. PhD Thesis, Université de Fribourg, pp. 277.

Bassant, P., Van Buchem, F.S.P., Strasser, A., Görür, N., 2005. The stratigraphic architecture and evolution of the Burdigalian carbonate-siliciclastic sedimentary systems of the Mut Basin, Turkey. Sedimentary Geology 173 (1-4), 187-232.

Bassoullet, J.P., 1997. Les grands foraminiferes. Bulletin du Centre de Recherches Elf Exploration Production Mémoires 17, 293-304.

Benson, D.J., 1988. Depositional history of the Smackover Formation in southwest Alabama. Gulf Coast Association of Geological Societies Transactions 38, 197-205.

Betzler, C., Brachert, T.C., Nebelsick, J., 1997. The warm temperate carbonate province-a review of facies, zonations, and delimitations. Courier Forschungs-Institut Senckenberg 201, 83-99.

Bosence, D.W.J., Pomar, L., Waltham, D.A., Lankester, T.G., 1994. Computer modelling of a Miocene carbonate platform, Spain. American Association of Petroleum Geologists Bulletin 78 (2), 247-266.

Bosence, D.W.J., Procter, E., Aurell, M., Bel Kahla, A., Boudagher-Fadel, M., Casaglia, F., Cirilli, S., Mehdie, M., Nieto, L., Rey, J., Scherreiks, R., Soussi, M., Waltham, D., 2009. A dominant tectonic signal in high-frequency, peritidal carbonate cycles? A regional analysis of Liassic platforms from western Tethys. Journal of Sedimentary Research 79, 389-415.

BouDagher-Fadel, M.K., 2008. The Mesozoic larger benthic foraminifera: the Jurassic. In: Wignall, P.B. (Ed.), Evolution and geological significance of larger benthic foraminifera. Development in Palaeontology and Stratigraphy 21, pp. 157-213.

Bover-Arnal, T., Moreno-Bedmar, J.A., Salas, R., Skelton, P.W., Bitzer, K., Gili, E., 2010. Sedimentary evolution of an Aptian syn-rift carbonate system (Maestrat Basin, E Spain): effects of accommodation and environmental change. Geologica Acta 8, 249-280.

Brand, U. and Veizer, J., 1980. Chemical diagenesis of a multicomponent carbonate system -1: trace elements. Journal of Sedimentary Petrology 50, 1219-1236.

Brand, U. and Veizer, J., 1981. Chemical diagenesis of a multicomponent carbonate system -2: Stable isotopes. Journal of Sedimentary Petrology 51, 987-997.

Brandano, M., Corda, L., Tomassetti, L., Testa D.V., 2015. On the peritidal cycles and their diagenetic evolution in the Lower Jurassic carbonates of the Calcare Massiccio Formation (Central Apennines). Geologica Carpathica 66 (5), 393-407.

Brandley, R.T., Krause, F.F., 1997. Upwelling, thermoclines and wave-sweeping on an equatorial carbonate ramp: Lower Carboniferous strata of western Canada. In: James, N.P., Clarke, J.A.D. (Eds.), Cool-Water Carbonates. SEPM (Society for Sedimentary Geology) Special Publication 56, pp. 365-390.

Broecker, W.S., Peng, T.H., 1982. Tracers in the Sea. Eldigio Press, New York, pp. 690.

Bulard, P.F., 1972. Le Jurassique moyen et supérieur de la Chaine Ibérique sur la bordure du bassin de l'Ebre (Espagne). PhD Thesis, Université Nice Sophia Antipolis, France, pp. 702.

Burchette, T.P., Wright, V.P., 1992. Carbonate ramp depositional systems. Sedimentary Geology 79, 3-57.

Caers, J., Zhang, T., 2004. Multiple-point Geostatistics: A Quantitative Vehicle for Integrating Geologic Analogues into Multiple Reservoir Models. AAPG Memoir 80, 383-394.

Callomon, J.H., Dietl, G., 2000. On the proposed basal boundary stratotype (GSSP) of the Middle Jurassic Callovian Stage. GeoResearch Forum 6, 41-54.

Campos-Soto, S., Benito, M.I., Cobos, A., Caus, E., Quijada, E.I., Suarez- González, P., Mas, R., Royo-Torres, R., Alcalá, L., 2019. Revisiting the age and palaeoenvironments of the Upper Jurassice-Lower Cretaceous? dinosaur-bearing sedimentary record of eastern Spain: implications for Iberian palaeogeography. Journal of Iberian Geology, 1-40.

Canérot, J., 1974. Recherches géologiques aux confins des Chaînes Ibérique et Catalane (Espagne). PhD Thesis, Toulouse, Université Paul-Sabatier, Enadimsa, France, pp. 517.

Capote, R., Muñoz, J.A., Simón, J.L., Liesa, C.L., Arlegui, L.E., 2002. Alpine Tectonics I: The Alpine system north of the Betic Cordillera. In: Gibbons, W., Moreno, T. (Eds.), Geology of Spain. The Geological Society, London, pp. 367-400.

Carpenter, S.J., Lohmann, K.C., 1995. $\delta^{18}O$ and $\delta^{13}C$ values of modern brachiopod valves. Geochimica et Cosmochimica Acta 59, 3749-3764.

Chatellier, J.Y., 1988. Carboniferous carbonate ramp, the Banff Formation, Alberta, Canada. Bulletin des Centres de Recherches Exploration-Production Elf-Aquitaine 12, 569-599.

Choquette, P.W., James, N.P., 1987. Diagenesis in limestones-3, the deep burial environment. Geoscience Canada 14, 3-35.

Clarke, L.J., Jenkyns, H.C., 1999. New oxygen isotope evidence for long-term Cretaceous climatic change in the Southern Hemisphere. Geology 27 (8), 699-702.

Coimbra, R., Immenhauser, A., Olóriz, F., 2014. Spatial geochemistry of Upper Jurassic marine carbonates (Iberian subplate). Earth-Science Reviews 139, 1-32.

Colombié, C., Strasser, A., 2005. Facies, cycles, and controls on the evolution of a keep-up carbonate platform (Kimmeridgian, Swiss Jura). Sedimentology 52, 1207-1227.

Colombié C., Lécuyer C., Strasser A., 2011. Carbon- and oxygen-isotope records of palaeoenvironmental and carbonate production changes in shallow-marine carbonates (Kimmeridgian, Swiss Jura). Geological Magazine 148 (1), 133-153.

Cortés Gracia, A.L., Casas Sainz, A.M., 1996. Deformación alpina de zócalo y cobertera en el borde norte de la Cordillera Ibérica (Cubeta de Azuara-Sierra de Herrera). Revista de la Sociedad Geológica de España 9 (1-2), 51-66.

Dahanayake, K., 1977. Classification of oncoids from the Upper Jurassic carbonates of the French Jura. Sedimentary Geology 18, 337-353.

Dahanayake, K., 1978. Sequential position and environmental significance of different types of oncoids. Sedimentary Geology 20, 301-316.

Dahanayake, K., Gerdes, G., Krumbein, W.E., 1985. Stromatolites, oncolites and oolites biogenically formed in situ. Naturwissenschaften 7, 513-518.

Dercourt, J., Ricou, L., Vrielynck, B., 1993. Atlas: Tethys palaeoenvironmental Maps. Gauthier-Villars, Paris, pp. 14.

Díaz-Molina, M., Yébenes, A., 1987. La sedimentación litoral y continental durante el Cretácico Inferior. Sinclinal de Galve, Teruel. Estudios Geológicos 43 (Extra), 3-21.

Dickens, G.R., O'Neil, J.R., Rea, D.K., Owen, R.M., 1995. Dissociation of oceanic methane hydrate as a cause of the carbon isotope excursion at the end of the Paleocene. Paleoceanography 10, 965-971.

Dunham, R.J., 1962. Classification of carbonate rocks according to depositional texture. American Association Petroleum Geology Memoir 1, 108-121.

Dupraz, C., Strasser, A., 1999. Microbialites and micro-encrusters in shallow coral bioherms (Middle to Late Oxfordian, Swiss Jura mountains). Facies 40, 101-129.

Egger, J.G., 1902. Der Bau der Orbitolinen und verwandter Formen. Abhandlungen der königlich bayerischen Akademie der Wissenschaften. Mathematisch-Physikalische Classe 21 (3), 577-600.

Einsele, G., 1985. Response of sediments to sea-level changes in differing subsiding storm-dominated marginal and epeiric basins. In: Bayer, U., Seilacher, A. (Eds.), Sedimentary and Evolutionary Cycles. Lecture Notes in Earth Sciences 1, pp. 68-97.

Elderfield, H., 1986. Strontium isotope stratigraphy. Palaeogeography, Palaeoclimatology, Palaeoecology 57, 71-90.

Eltom, H.A., Gonzalez, L.A., Hasiotis, S.T., Rankey, E.C., Cantrell, D.L., 2018. Paleogeographic and paleo-oceanographic influences on carbon isotope signatures: Implications for global and regional correlation, Middle-Upper Jurassic of Saudi Arabia. Sedimentary Geology 364, 89-102.

Emiliani, C., 1955. Pleistocene temperatures. Journal of Geology 63 (6), 538-578.

Esteban, M., Robles, S., 1979. Periodo preorogénico, el Mesozoico. Acta Geológica Hispánica 11 (3), 73-78.

Fallatah, M.I., Kerans, C., 2018. Stratigraphic evolution of the Late Jurassic Hanifa Formation along the Tuwaiq Escarpment, Saudi Arabia: Evidence for a carbonate ramp system. Sedimentary Geology 363, 152-180.

Fezer, R., Geyer, O.F., 1988. Der Oberjura von Calanda im nordöslichen Keltibericum (Provinz Teruel, Spanien). I Stratigrphie. Arbeiten aus dem Institut für Geologie und Paläontologie der Universität. Sttutgart 84, 207-237.

Finkel, R., 1992. Eine Ammoniten-Fauna aus dem Kimmeridgium des nord-östlichen Keltibericums (Spanien). Profil 3, 227-297.

Fischer, A.G., D'Argenio, B., Silva, I.P., Weissert, H., Ferreri, V., 2004. Cyclostratigraphic approach to Earth's history: an introduction. In: D'Argenio, B., Fischer, A.G., Premoli Silva, I., Weissert, H., Ferreri, V. (Eds.), Cyclostratigraphy Approaches and Case Histories, SEPM, Special Publication 81, pp. 5-16.

Flügel, E., 1974. Fazies-Interpretation der *Cladocoropsis*-Kalke (Malm) auf Karaburun, W-Anatolien. Arch Lagerstätt-Forsch Ostalpen Sd-Bd 2, 79-94.

Flügel, E., 1977. Fossil algae: Recent results and developments. Springer-Verlag, Germany, pp. 375.

Flügel, E., 1982. Microfacies analysis of limestones. Springer-Verlag, Germany, pp. 633.

Flügel, E., 2004. Microfacies of Carbonate Rocks. Analysis, Interpretation and Application. Springer-Verlag, Germany, pp. 976.

Folk, R.L., 1959. Practical petrographic classification of limestones. American Association of Petroleum Geologists Bulletin 43 (1), 1-38.

Föllmi, K.B., Weissert, H., Bisping, M., Funk, H., 1994. Phosphogenesis, carbon-isotope stratigraphy, and carbonate-platform evolution along the Lower Cretaceous northern Tethyan margin. Geological Society of America Bulletin 106, 729-746.

García-Ramos, J.C., 1985. Cretácico Inferior. In: IGME (Ed.), Mapa Geológico de España 1: 200.000 (primera edición), nº 47 (Teruel). Madrid, pp. 81-105.

Gautier, P.W., 1980. Memoria explicativa de la Hoja núm. 543 (Villarluengo). In: Mapa geológico de España 1:50.000, segunda serie. Instituto Geológico de España (IGME), Madrid.

Gautier, P.W., 1981. Memoria explicativa de la Hoja núm. 568 (Alcala de la Selva). In: Mapa geológico de España 1:50.000, segunda serie. Instituto Geológico de España (IGME), Madrid.

Geyer, O., Pelleduhn, R., 1979. Sobre la Estratigrafía y la facies espongiolítica del Kimmeridgiense de Calanda (provincia de Teruel). Cuadernos de Geología Ibérica 10, 67-72.

Giner, J., 1980. Estudio sedimentológico y diagenético de las facies carbonatadas del Jurásico de las Catalánides, Maestrazgo y Rama Aragonesa de la Cordillera Ibérica. PhD Thesis, Universidad de Barcelona, Spain, pp. 315.

Ginsburg, R.N., 1956. Environmental relationships of grains size and constituent particles in some south Florida carbonate sediments. American Associations of Petroleum Geologists Bulletin 40, 2384-2427.

Ginsburg, R.N., 1971. Landward movement of carbonate mud: new model for progressive cycles in carbonates. American Associations of Petroleum Geologists Bulletin 55, pp. 340.

Ginsburg, R.N., 1975. Tidal deposits. Springer-Verlag, Dordrecht, pp. 428.

Ginsburg, R.N., Lowenstam, H.A., 1958. The influence of marine bottom communities on the depositional environments of sediments. Journal of Geology 66, 310-318.

Given, R.K., Lohmann, K.C., 1985. Derivation of the original isotopic composition of Permian marine carbonates. Journal of Sedimentary Petrology 55, 430-439.

Glumac, B., Walker, K., 1998. A Late Cambrian positive carbon-isotope excursion in the southern Appalachians: relation to biostratigraphy, sequence stratigraphy, environments of deposition, and diagenesis. Journal of Sedimentary Research 68 (6), 1212-1222.

Gómez, J.J., 1979. El Jurásico en facies carbonatadas del sector levantino de la Cordillera Ibérica. PhD Thesis. Universidad Complutense de Madrid, Spain, pp. 683.

Gómez, J.J., Goy, A., 1979. Las unidades litoestratigráficas del Jurásico medio y superior del sector levantino de la Cordillera Ibérica. Estudios Geológicos 35, 569-598.

González, A., Pardo, G., Villena, J., 1991. Análisis tectosedimentario del Terciario de la cubeta de Berge. Revista de la Sociedad Geológica de España 4, 369-369.

Goodner, H.M., Rankey, E.C., Zhang, C., Watney, W.L., 2020. Rock fabric controls on pore evolution and porosity-permeability trends in oolitic grainstone reservoirs and reservoir analogs. American Association of Petroleum Geologists Bulletin 104 (7), 1501-1530.

Gradstein, F., Ogg, J., Schmitz, M., Ogg, G., 2012. The Geologic Time Scale 2012. Elsevier, Boston, pp. 1176.

Granier, B., 2019. Dual biozonation scheme (benthic foraminifera and "calcareous" green algae) over the Jurassic-Cretaceous transition. Another plea to revert the system boundary to its historical Orbigny's and Oppel's definition. Cretaceous Research 93, 245-274.

Granier, B., Bucur, I.I., 2011. Stratigraphic ranges of some Tithonian-Berriasian benthic foraminifers and Dasycladales. Re-evaluation of their use in identifying this stage boundary in carbonate platform settings. In: Grosheny, D., Granier, B., Sander, N. (Eds.), Platform to basin correlations in Cretaceous times. Boletín del Instituto de Fisiografía y Geología 9-10, pp. 79-81.

Gröcke, D.R., Price, G.D., Ruffell, A.H., Mutterlose, J., Baraboshkin, E., 2003. Isotopic evidence for Late Jurassic–Early Cretaceous climate change. Palaeogeography, Palaeoclimatology, Palaeoecology 202, 97-118.

Grötsch, H.J., Billing, I., Vahrenkamp, V., 1998. Carbon-isotope stratigraphy in shallow-water carbonates: implications for Cretaceous black-shale deposition. Sedimentology 45, 623-634.

Grötsch, J., Suwaina, O., Ajlani, G., Taher, A., El-Khassawneh, R., Lokier, S., Coy, G., van der Weerd, E., Masalmeh, S., van Dorp, J., 2003. The Arab Formation in central Abu Dhabi: 3-D reservoir architecture and static and dynamic modelling. GeoArabia, Gulf PetroLink, Bahrain 8 (1), 47-86.

Grotzinger, J.P., Fike, D.A. Fischer, W.W., 2011. Enigmatic origin of the largest-known carbon isotope excursion in Earth's history. Nature Geoscience 4, 285-292.

Guimerà, J., 1984. Paleogene evolution of deformation in the northeastern Iberian Peninsula. Geological Magazine 121 (5), 413-420.

Guimerà, J., Álvaro, M., 1990. Structure et évolution de la compression alpine dans la Chaîne Ibérique et la Chaîne côtière catalane (Espagne). Bulletin de la Societé géologique de France 6 (2), 339-348.

Hägele, D., Leinfelder, R., Grau, J., Burmeister, E.G., Struck, U., 2006. Oncoids from the river Alz (southern Germany): tiny ecosystems in a phosphorus-limited environment. Palaeogeography, Palaeoclimatology, Palaeoecology 237, 378-395.

Handford, C.R. Loucks, R.G., 1993. Carbonate depositional sequences and systems tracts-responses of carbonate platforms to relative sea-level changes. In: Loucks, B., Sarg, R.J. (Eds.), Carbonate Sequence Stratigraphy: Recent Developments and Applications. American Associations of Petroleum Geologists Bulletin 57, pp. 3-41.

Hanken, N.M., Bjørlykke, K., Nielsen, J.K., 2015. Carbonate Sediments. In: Bjørlykke K. (Eds.), Petroleum Geoscience. Springer, Berlin, Heidelberg, pp. 151-216.

Hardenbol, J., Thierry, J., Farley, M.B., Jacquin, T., De Gracianski, P.C., Vail, P.R., 1998. Mesozoic and Cenozoic sequence chronostratigraphic framework of European basins. In: De Gracianski, P.C., Hardenbol, J., Jacquin, T., Vail, P.R. (Eds.), Mesozoic and Cenozoic sequence stratigraphy of European basins. SEPM (Society for Sedimentary Geology) Special Publications 60, charts 1-8.

Hardie, L.A., Shinn, E.A., 1986. Carbonate Depositional Environments, Modern and Ancient, Part 3, Tidal Flats: Colorado School of Mines Quarterly 81, pp. 74.

Hiatt, E.E., Pufahl, P.K., 2014. Cathodoluminescence petrography of carbonate rocks: a review of applications for understanding diagenesis, reservoir quality, and pore system evolution. In: Coulson, I.M. (Ed.), Cathodoluminescence and its application to geoscience. Mineralogical Association of Canada Short Course 45, pp. 75-96.

Hillgärtner, H., Strasser, A., 2003. Quantification of high-frequency sea-level fluctuations in shallow-water carbonates: an example from the Berriasian-Valanginian (French Jura). Palaeogeography, Palaeoclimatology, Palaeoecology 200, 43-63.

Hodell, D.A., Mueller, P.A., McKenzie, J.A., Mead, G.A., 1989. Strontium isotope stratigraphy and geochemistry of the late Neogene ocean. Earth and Planetary Science Letters 92, 165-178.

Hodell, D.A., Mead, G.A., Mueller, P.A., 1990. Variation in the strontium isotopic composition of seawater (8 Ma to present). Implications for chemical weathering rates and dissolved fluxes to the ocean. Chemical Geology 80, 291-307.

Hofmann, A., Dirks, P.H.G.M., Jelsma, H.A., 2004. Shallowing-upward carbonate cycles in the Belingwe Greenstone Belt, Zimbabwe: a record of Archean sea-level oscillations. Journal of Sedimentary Research 74 (1), 64-81.

Hollis, C., Lawrence, D.A., Deville de Perière, M., Al Darmaki, F., 2017. Controls on porosity preservation within a Jurassic oolitic reservoir complex, UAE. Marine and Petroleum Geology, 88, 888-906.

Hottinger, L., 1967. Foraminiferes imperforés du Mésozoique marocain, Notes et Mémoires du Service Géologique du Maroc 209. Editions du Service Geologique du Maroc, Rabat, pp. 168.

Hottinger, L., 2006. The "face" of benthic foraminifera. Bollettino della Società Paleontologica Italiana 45 (1), 75-89.

Huck, S., Wohlwend, S., Coimbra, R., Christ, N., Weissert, H., 2017. Disentangling shallow-water bulk carbonate carbon isotope archives with evidence for multi-stage diagenesis: An in-depth component-specific petrographic and geochemical study from Oman (mid-Cretaceous). The Depositional Record 3, 233-257.

Hudson, J.D., 1977. Stable isotopes and limestone lithification. Journal of the Geological Society 133 (6), 637-660.

Hughes, G.W., 1996. A new bioevent stratigraphy of Late Jurassic Arab-D carbonates of Saudi Arabia. GeoArabia 1 (3), 417-434.

Hughes, G.W., 2004. Middle to Upper Jurassic Saudi Arabian carbonate petroleum reservoirs: biostratigraphy, micropaleontology and paleoenvironments. GeoArabia 9 (3), 79-114.

Hughes, G.W., 2005. Complex-walled agglutinated foraminiferal biostratigraphy and palaeoenvironmental significance from the Jurassic supercycle-associated carbonates of Saudi Arabia. Abstracts 7th Int. Workshop Agglutinated Foraminifera, Urbino, Italy, pp. 19-20.

Immenhauser, A., Kenter, J.A.M., Ganssen, G., Bahamonde, J.R., Van Vliet, A., Saher, M.H., 2002. Origin and significance of isotope shifts in Pennsylvanian carbonates (Asturias, NW Spain). Journal of Sedimentary Research 72 (1), 82-94.

Immenhauser, A., Della Porta, G., Kenter, J.A., Bahamonde, J.R., 2003. An alternative model for positive shifts in shallow-marine carbonate $\delta^{13}C$ and $\delta^{18}O$. Sedimentology 50 (5), 953-959.

Ipas, J., 2003. Análisis de facies y estratigrafía secuencial de la Formación Higueruelas (Jurásico Superior) en la Cordillera Ibérica septentrional (provincia de Zaragoza). Bachelor's Thesis, Universidad de Zaragoza, Spain, pp. 115.

Ipas, J., Aurell, M., Bádenas, B., 2004. Ambientes sedimentarios y secuencias en la Fm. Higueruelas (Jurásico Superior) en la Cordillera Ibérica Septentrional. Geogaceta 35, 7-10.

Ipas, J., Aurell, M., Bádenas, B., 2005. Las unidades del tránsito Jurásico-Cretácico del Maestrazgo Septentrional (NE de Teruel). Geogaceta 36, 7-10.

Ipas, J., Aurell, M., Bádenas, B., Canudo, J.I., Liesa, C., Mas, J.R., Soria, A.R., 2007. Caracterización de la Formación Villar del Arzobispo al sur de Zaragoza (Titónico, Cordillera Ibérica). Geogaceta 41, 111-114.

James, N.P., 1984. Shallowing-upward sequences in carbonates. In: Walker, R.G. (Ed.), Facies models: Geological Association of Canada Reprint Series 2, pp. 213-229.

James, N.P., Bone, Y., 1994. Paleoecology of cool-water, subtidal cycles in mid-Cenozoic limestones, Eucla platform, southern Australia. Palaios 9, 457-476.

James, N.P., Dalrymple, R.W., 2010. Facies models 4. Canada: Geological Association of Canada, pp. 586.

James, N.P., Jones, B., 2015. Origin of carbonate sedimentary rocks. First Edition. American Geophysical Union, pp. 464.

James, N.P., Reid, C.M., Bone, Y., Levings, A., Malcolm, I., 2013. The macroalgal carbonate factory at a cool-to-warm temperate marine transition, Southern Australia. Sedimentary Geology 291, 1-26.

Jenkyns, H.C., Clayton, C.J., 1986. Black shales and carbon isotopes in pelagic sediments from the Tethyan Lower Jurassic. Sedimentology 33, 87-106.

Jenkyns, H.C., Jones, C.E., Gröcke, D.R., Hesselbo, S.P., Parkinson, D.N., 2002. Chemostratigraphy of the Jurassic System: applications, limitations and implications for palaeoceanography. Journal of the Geological Society, London, 159, 351-378.

Jervey, M.T., 1988. Quantitative geological modeling of siliciclastic rock sequences and their seismic expression. In: Wilgus, C.K., Hasting, B.S., Kendall, C.G.St.C., Posamentier, H.W., Ross, C.A., Van Wagoner, J.C. (Eds.), Sea-Level Changes: An Integrated Approach. SEPM, Special Publication 42, pp. 47-69.

Jones, B., Renaut, R.W., 1997. Formation of silica oncoids around geysers and hot springs at El Tatio, Chile. Sedimentology 44, 287-304.

Jones, C.E., Jenkyns, H.C., 2001. Seawater strontium isotopes, oceanic anoxic events, and seafloor hydrothermal activity in the Jurassic and Cretaceous. American Journal of Science 301, 112-149.

Jones, C.E., Jenkyns, H.C., Coe, A.L., Hesselbo, S.P., 1994a. Strontium isotopic variations in Jurassic and Cretaceous seawater. Geochimica et Cosmochimica Acta 58, 3061-3074.

Jones, C.E., Jenkyns, H.C., Hesselbo, S.P., 1994b. Strontium isotopes in Early Jurassic seawater. Geochimica et Cosmochimica Acta 58, 1285-1301.

Kendall, C.G.S.C., Schlager, W., 1981. Carbonates and relative changes in sea level. Marine Geology 44 (1-2), 181-212.

Kiessling, W., 2009. Geologic and biologic controls on the evolution of reefs. Annual Review of Ecology, Evolution, and Systematics 40, 173-192.

Kiessling, W., Flügel, E., 2002. Paleoreefs – A database on Phanerozoic reefs. In: Kiessling, W., Flügel, E., Golonka, J. (Eds.), Phanerozoic Reef Patterns. SEPM Society for Sedimentary Geology, Special Publication 72, pp. 77-92.

Kiessling, W., Flügel, E., Golonka, J., 2000. Fluctuations in the carbonate production of Phanerozoic reefs. In: Insalaco, E., Skelton, P.W., Palmer, T.J. (Eds.), Carbonate Platform Systems: Components and Interactions. Geological Society Special Publication 178, pp. 191-215.

Kiessling, W., Flügel, E., Golonka, J., 2003. Patterns of Phanerozoic carbonate platform sedimentation. Lethaia 36 (3), 195-225.

Kleypas, J.A., McManus, J.W., Menez, L.A.B., 1999. Environmental limits to coral reef development: where do we draw the line? American Zoologist 39, 146-159.

Korte, C., Hesselbo, S.P., 2011. Shallow marine carbon and oxygen isotope and elemental records indicate icehouse-greenhouse cycles during the Early Jurassic. Paleoceanography, 26 (4), 1-18.

Kroopnick, P.M., Margolis, P.M., Wong, C.S., 1977. $\delta^{13}C$ variations in marine carbonate sediments as indicators of the CO_2 balance between the atmosphere and oceans. In: Anderson, N.R., Malahoff, A. (Eds.), The Fate of Fossil Fuel CO2 in the Oceans, Plenum Press, New York, pp. 295-321.

Lanés, S., Palma, R.M., 1998. Environmental implications of oncoids and associated sediments from the Remoredo Formation (Lower Jurassic) Mendoza, Argentina. Palaeogeography, Palaeoclimatology, Palaeoecology 140, 357-366.

Lavastre, V., Ader, M., Buschaert, S., Petit, E., Javoy, M., 2011. Water circulation control on carbonate- $\delta^{18}O$ records in a low permeability clay formation and surrounding limestones: the Upper Dogger–Oxfordian sequence from the eastern Paris basin, France. Applied Geochemistry 26 (5), 818-827.

Lavoie, D., Bourque, P.A., 1993. Marine burial and meteoric diagenesis of early Silurian carbonate ramps, Quebec Appalachians, Canada. Journal of Sedimentary Petrology 63 (2), 233-247.

Lees, A., and Miller, J., 1995. Waulsortian banks. In: Monty, C.L.V., Bosence, D.W.J., Bridges, P.H., Pratt, B. R. (Eds.), Carbonate Mud-Mounds – Their Origin and Evolution. International Association of Sedimentologists, Oxford-London (UK), pp. 191-271.

Lehmann, C.T., Al Hosany, K.I., Matarid, T., Ibrahim, M.S., 2010. Addressing reservoir heterogeneities in the development of Upper Jurassic carbonate reservoirs, offshore Abu Dhabi. Abu Dhabi International Petroleum Exhibition and Conference. Society of Petroleum Engineers, SPE 137888.

Leinfelder, R.R., 1987. Formation and significance of black pebbles from the Ota limestone (Upper Jurassic, Portugal). Facies 17 (1), 159-169.

Leinfelder, R.R., 1993. Upper Jurassic reef types and controlling factors. A preliminary report. Profil 5, 1-45.

Leinfelder, R.R., 2001. Jurassic reef ecosystems. In: Stanley, G.D.J. (Ed.), The history and sedimentology of ancient reef systems. Kluwer Academic/Plenum Publishers, New York, pp. 251-302.

Leinfelder, R.R., Nose, M., Schmid, D., Werner, M., 1993. Microbial Crusts of the Late Jurassic: Composition, Palaeoecological Significance and Importance in Reef Construction. Facies 29, 195-230.

Leinfelder, R.R., Krautter, M., Laternser, R., Nose, M., Schmid, D.U., Schweigert, G., Werner, W., Keupp, H., Brugger, H., Herrmann, R., Rehfeld-Kiefer, U., Schroeder, J.H., Reinhold, C., Koch, R., Zeiss, A., Schweizer, V., Christmann, H., Menges, G., Luterbacher, H., 1994. The origin of Jurassic reefs: current research developments and results. Facies 31, 1-56.

Leinfelder, R.R., Schmid D.U., Nose, M., Werner, W., 2002. Jurassic reef patterns-The expression of a changing globe. In: Kiessling, W., Flügel, E., Golonka, J. (Eds), Phanerozoic Reef Patterns. SEPM Special Publications 72, pp. 465-520.

Leinfelder, R.R., Schlagintweit, F., Werner, W., Ebli, O., Nose, M., Schmid, D., Hughes, G., 2005. Significance of stromatoporoids in Jurassic reefs and carbonate platforms-concepts and implications. Facies 51, 287-325.

Li, C., Jones, B., Blanchon, P., 1997. Lagoon-shelf sediment exchange by storms – Evidence from foraminiferal assemblages, east coast of Grand Caiman, British West Indies. Journal of Sedimentary Research 67, 17-25.

Liesa, C.L., Simón, J.L., 2009. Evolution of intraplate stress fields under multiple remote compressions: The case of the Iberian Chain (NE Spain). Tectonophysics 474 (1-2), 144-159.

Liesa, C.L., Soria, A.R., Meléndez, N., Meléndez, A., 2006. Extensional fault control on the sedimentation patterns in a continental rift basin: El Castellar Formation, Galve sub-basin, Spain. Journal of the Geological Society 163, 487-498.

Liesa, C.L., Soria, A.R., Casas, A., Aurell, M., Meléndez, N., Bádenas, B., Fregenal-Martínez, M., Navarrete, R., Peropadre, C., Rodríguez-López, J.P., 2019. The South Iberian, Central-Iberian and Maestrazgo basins. In: Quesada, C., Oliveira, J.T. (Eds.), The Geology of Iberia: A Geodynamic Approach Vol. 3. Springer Nature Switzerland AG, Alpine Cycle, pp. 214-228.

Lindsay, R.F., Cantrell, D.L., Hughes, G.W., Keith, T.H., Mueller H.W. III, Russel, D., 2006. Ghawar Arab-D reservoir: widespread porosity in shoaling-upward carbonate cycles, Saudi Arabia. American Association of Petroleum Geologists, Memoir 88, 97-138.

Lisiecki, L.E., Raymo, M.E., 2005. A Pliocene-Pleistocene stack of 57 globally distributed benthic $\delta^{18}O$ records. Paleoceanography 20 (1), PA1003.

Liu, C., Xie, Q., Wang, G., Song, Y., Qi, K., 2016. Dolomite origin and its implication for porosity development of the carbonate gas reservoirs in the Upper Permian Changxing Formation of the eastern Sichuan Basin, Southwest China. Journal of Natural Gas Science and Engineering 35, 775-797.

Logan, B.W., Davies, G.R., Read, J.F. and Cebulski, D., 1970. Carbonate sedimentation and environments, Shark Bay, Western Australia. American Association of Petroleum Geologists, Memoir 13, Tulsa, pp. 223.

Lohmann, K.C., 1976. Lower Dresbachian (Upper Cambrian) platform to deep-shelf transition in eastern Nevada and western Utah: An evaluation through lithologic cycle correlation. Brigham Young University Geological Studies 23, 111-122.

Lohmann, K.C., 1988. Geochemical patterns of meteoric diagenetic systems and their application to studies of paleokarst. In: James, N.P., Choquette, P.W. (Eds.), Paleokarst. Springer-Verlag, Berlin, pp. 50-80.

Machel, H.G., 1985. Cathodoluminiscence in calcite and dolomite and its chemical interpretation. Geoscience Canada 12 (4), 139-147.

Madden, R., Wilson, M.E., 2013. Diagenesis of a SE Asian Cenozoic carbonate platform margin and its adjacent basinal deposits. Sedimentary Geology 286-287, 20-38.

Madhavaraju, J., Sial, A.N., León, C.M.G., Nagarajan, R., 2013. Carbon and oxygen isotopic variations in early Albian limestone facies of the Mural Formation, Pitaycachi section, northeastern Sonora, Mexico. Revista Mexicana de Ciencias Geológicas 30 (3), 526-539.

Magaritz, M., Holser, W.T., 1990. Carbon isotope shifts in Pennsylvanian seas. American Journal of Science, 290 (9), 977-994.

Marchionda, E., Deschamps, R., Gobianchi, M., Nader, F.H., Di Giulio, A., Morad, D.J., Al Darmaki, F., Ceriani, A., 2018. Field-scale depositional evolution of the Upper Jurassic Arab Formation (onshore Abu Dhabi, UAE). Marine and Petroleum Geology 89, 350-369.

Markello, J.R., Read, J.F., 1982. Upper Cambrian Intrashelf Basin, Nolichucky Formation, Southwest Virginia Appalachians. American Associations of Petroleum Geologists Bulletin 66, 860-878.

Marsaglia, K.M., Klein, G.deV., 1983. The palaeogeography of Paleozoic and Mesozoic storm depositional systems. The Journal of Geology 91, 117-142.

Marshall, J.D., 1992. Climatic and oceanographic isotopic signals from the carbonate rock record and their preservation. Geological Magazine 129, 143-160.

Martín-Closas, C., 1989. Els caròfits del Cretaci inferior de les conques periferiques del Bloc de l'Ebre. PhD Thesis. Universitat de Barcelona, Spain, pp. 581.

Mas, R., Alonso, A., Meléndez, N., 1984. La formación Villar del Arzobispo: un ejemplo de llanuras de mareas siliciclásticas asociadas a plataformas carbonatadas. Jurásico terminal (NW de Valencia y E de Cuenca). Publicaciones de Geología 20, 175-188.

McArthur, J.M., 1994. Recent trends in strontium isotope stratigraphy. Terra nova 6 (4), 331-358.

McArthur, J.M., Morton, N., Thirlwall, M.F., 2000. Strontium isotope startigraphy of the Aalenian/ Bajocian auxiliary stratotype point at Bearreraig, Isle of Skye, NW Scotland. GeoResearch Forum 6, 137-144.

McArthur, J.M., Janssen, N.M.M., Reboulet, S., Leng, M.J., Thirlwall, M.F., van de Schootbrugge, B., 2007. Palaeotemperatures, polar ice-volume, and isotope stratigraphy (Mg/Ca, $\delta^{18}O$, $\delta^{13}C$, $^{87}Sr/^{86}Sr$): the Early Cretaceous (Berriasian, Valanginian, Hauterivian). Palaeogeography, Palaeoclimatology, Palaeoecology 248, 391-430.

McArthur, J.M., Howarth, R. J., Shields, G. A., 2012. Strontium isotope stratigraphy. In: Gradstein, F.M., Ogg, J.G., Schmitz, M., Ogg, G. (Eds.), The geologic time scale 2012. ElSevier, Amsterdam, Boston, Heidelberg, London, New York, Oxford, Paris, San Diego, San Francisco, Singapore, Sydney, Tokyo, pp. 127-144.

McConnaughey, T.A., 1989a. ^{13}C and ^{18}O isotopic disequilibrium in biological carbonates: I. Patterns. Geochimica et Cosmochimica Acta, 53, 151-162.

McConnaughey, T.A., 1989b. ^{13}C and ^{18}O isotopic disequilibrium in biological carbonates: II. *In vitro* simulation of kinetic isotope effects. Geochimica et Cosmochimica Acta 53, 163-171.

Meléndez, A., Pardo, G., Pendón, J.G., Villena, J., 1979. Las facies terminales del Jurásico en el sector central de la Cordillera Ibérica. Cuadernos de Geología 10, 137-148.

Meléndez, G., Aurell, M., Atrops, F., 1990. Las unidades del Jurásico superior en el sector noroccidental de la Cordillera Ibérica: nuevas subdivisiones litoestratigráficas. Cuadernos de Geología Ibérica 14, 225-246.

Meléndez N, Liesa C.L., Soria A.R., Meléndez, A., 2009. Lacustrine System Evolution during Early Rifting: El Castellar Formation (Galve Sub-Basin, Central Iberian Chain). Sedimentary Geology 222 (1–2), 64-77.

Michel, J., Laugié, M., Pohl, A., Lanteaume, C., Masse, J.-P., Donnadieu, Y., Borgomano, J., 2019. Marine carbonate factories: a global model of carbonate platform distribution. International Journal of Earth Sciences 108, 1773-1792

Mitchum, R.M., Van Wagoner, J.C., 1991. High-frequency sequences and their stacking patterns: sequence-stratigraphic evidence of high-frequency eustatic cycles. Sedimentary Geology 70 (2), 131-160.

Mohseni, H., Al-Aasm, I.S., 2004. Tempestite deposits on a storm-influenced carbonate ramp: an example from the Pabdeh Formation (Paleogene), Zagros Basin, SW Iran. Journal of Petroleum Geology 27 (2), 163-178.

Moliner, L., 2009. Ataxioceratinae (ammonitina) del Kimmeridgiense inferior en el NE de la provincia de Teruel (cordillera Ibérica oriental y Maestrazgo). PhD Thesis. Universidad de Granada, Spain, pp. 548.

Moore, C.H., 1989. Carbonate Diagenesis and Porosity. Developments in Sedimentology Vol. 46, Amsterdam, Elsevier, pp. 337.

Moore, C.H., 2001. Carbonate Reservoirs: Porosity evolution and diagenesis in a sequence stratigraphic framework. Elsevier, pp. 460.

Moore, C.H., 2013. Carbonate Reservoirs: Porosity Evolution and Diagenesis in a Sequence Stratigraphic Framework. Elsevier, Amsterdam, pp. 370.

Nadal, J., 2001. Estudi de la dolomitització del Juràssic superior-Cretaci inferior de la Cadena Ibérica oriental y la Cadena Costanera Catalana: relació amb la segona etapa de rift mesozoica (Unpublished PhD thesis). Universitat de Barcelona, pp. 447.

Nelson, C.S., Smith, A.M., 1996. Stable oxygen and carbon isotope compositional fields for skeletal and diagenetic components in New Zealand Cenozoic nontropical carbonate sediments and limestones: a synthesis and review. New Zealand Journal of Geology and Geophysics 39, 93-107.

Nunn, E.V., Price, G.D., 2010. Late Jurassic (Kimmeridgian-Tithonian) stable isotopes ($\delta^{18}O$, $\delta^{13}C$) and Mg/Ca ratios: New paleoclimate data from Helmsdale, northeast Scotland. Palaeogeography, Palaeoclimatology, Palaeoecology 292, 325-335.

Ogg, J.G., Ogg, G., Gradstein, F.M., 2016. A Concise Geologic Time Scale. Elsevier B.V., pp. 240.

Olivier, N., Colombié, C., Pittet, B., Lathuilière, B., 2011. Microbial carbonates and corals on the marginal French Jura platform (Late Oxfordian, Molinges section). Facies 57, 469-492.

Olszewska, B., 2010. Microfossils of the Upper Jurassic-Lower Cretaceous formations of the lublin upland (SE Poland) based on thin section studies. Polish Geological Institute Special Papers 26, 1-56.

O'Neil, J.R., 1986. Theoretical and experimental aspects of isotopic fractionation. In: Valley, J.W., Taylor Jr., H.P., O'Neil, J.R. (Eds.), Stable Isotopes in High Temperature Geological Processes, 1 ed. Mineralogical Society of America, Chelsea, pp. 1-40.

O'Neil, J.R., 1987. Preservation of H, C, and O isotopic ratios in the low temperature environment. In: Kyser, T.K. (Ed.), Stable Isotope Geochemistry of Low Temperature Fluids. Mineralogical Association of Canada, Saskatoon, pp. 85-128.

Osleger, D., 1991. Subtidal carbonate cycles: Implications for allocyclic vs. autocyclic controls. Geology 19, 917-920.

Osleger, D.A., J. Read, J.F., 1991. Relation of Eustasy to Stacking Patterns of Meter-Scale Carbonate Cycles, Late Cambrian, U.S.A. SEPM Journal of Sedimentary Research 61, 1225-1252.

Page, K.N., Meléndez, G., Hart, M.B., Price, G.D., Wright, J.K., Bown, P., Bello, J., 2009. Integrated stratigraphical study of the candidate Oxfordian Global Stratotype Section and Point (GSSP) at Redcliff Point, Weymouth, Dorset, UK. Volumina Jurassica 7, 101-111.

Patterson, W.P. and Walter, L.M., 1994. Depletion of ^{13}C in seawater ΣCO2 on modern carbonate platforms: Significance for the carbon isotopic record of carbonates. Geology 22, 885-888.

Pélissié, T., Peybernès, B., Rey, J., 1984. Les grands foraminifères benthiques du Jurassique moyen/supérieur du sud-ouest de la France (Aquitaine, Causses, Pyrénées). Intérêt biostratigraphique, paléoécologique et paléobiogeographique. Bulletin des Centres de Recherches Exploration-Production Elf-Aquitaine 6, 479-489.

Pérez, A., 1989. Estratigrafia y sedimentologia del Terciario del borde meridional de la Depresión del Ebro (sector riojano- aragones) y cubetas de Muniesa y Montalban. PhD Thesis, Universidad de Zaragoza, Spain, pp. 525.

Pérez, A., Azanza, B., Cuenca, G., Pardo, G., Villena, J., 1985. Nuevos datos estratigráficos y paleontológicos sobre el Terciario del borde meridional de la depresión del Ebro (provincia de Zaragoza). Estudios Geológicos 41, 405-411.

Pérez-López, A., Pérez-Valera, F., 2012. Tempestite facies models for the epicontinental Triassic carbonates of the Betic Cordillera (southern Spain). Sedimentology 59, 646-678.

Pérez-Urresti, I., Delvene, G., Meléndez, G., Ramajo, J., 1998. El Oxfordiense Superior y la posición del límite Oxfordiense-Kimmeridgiense en el sector de Tosos-Aguilón (Rama Aragonesa de la Cordillera Ibérica, España). Geogaceta 24, 251-254.

Peropadre, C., 2012. El Aptiense del margen occidental de la cuenca del Maestrazgo: controles tectónico, eustático y climático en la sedimentación. PhD Thesis, Universidad Complutense de Madrid, Spain, pp. 649.

Peropadre, C., Liesa, C.L., Meléndez, N., 2013. High-frequency, moderate to high amplitude sea-level oscillations during the late early Aptian: insights into the mid-Aptian event (Galve sub-basin, Spain). Sedimentary Geology 294, 233-250.

Peryt, T.M., 1981. Phanerozoic oncoids—an overview. Facies 4, 197-213.

Petrovic, A., Aigner, T., 2017. Are shoal reservoirs discrete bodies? A coquina shoal outcrop analogue from the Mid-Triassic Upper Muschelkalk, SW Germany. Journal of Petroleum Geology 40 (3), 249-275.

Petrovic, A., Aigner, T., Montiggia, M., 2018. Facies heterogeneities in a ramp carbonate reservoir analogue: a new high-resolution approach for 3D facies modelling. Journal of Petroleum Geology 41 (2), 155-174.

Peybernès, B., 1998. Larger benthic foraminifera. Columns for Jurassic chart of Mesozoic and Cenozoic sequence chronostratigraphic framework of European basins, by Hardenbol J, Thierry J, Farley MB, Jacquin T, De Gracianski PC, Vail PR (coordinators) Mesozoic and Cenozoic sequence chronostratigraphic framework of European basins. In: Gracianski, P.C. de, Hardenbol, J., Jacquin, T., Vail, P.R. (Eds.), Mesozoic and Cenozoic Sequence Stratigraphy of European Basins. SEPM Special Publication 60, charts 7.

Pleş, G., Bucur, I.I., Păcurariu, A., 2015. Foraminiferal assemblages and facies associations in the Upper Jurassic carbonates from Ardeu unit (Metaliferi Mountains, Romania). Acta Palaeontologica Romaniae 11 (2), 43-57.

Plunkett, J.M., 1997. Early Diagenesis of Shallow Platform Carbonates in the Oxfordian of the Swiss Jura Mountains. Unpublished PhD Thesis, Université de Fribourg, Switzerland, pp. 166.

Pomar, L., 2001a. Types of carbonate platforms: a genetic approach. Basin Research 13, 313-334.

Pomar, L., 2001b. Ecological control of sedimentary accommodation: evolution from a carbonate ramp to rimmed shelf, Upper Miocene, Balearic Islands. Palaeogeography, Palaeoclimatology, Palaeoecology 175 (1-4), 249-272.

Pomar, L., 2018. Carbonate factories through the Earth History. EGU General Assembly Conference Abstracts 20, 3861.

Pomar, L., Ward, W.C., 1994. Response of a late Miocene Mediterranean reef platform to high-frequency eustasy. Geology 22, 131-134.

Pomar, L., Ward, W.C., 1999. Reservoir-Scale heterogeneity in depositional packages and diagenetic patterns on a reef-rimmed platform, Upper Miocene, Mallorca, Spain. American Associations of Petroleum Geologists Bulletin 83 (11), 1759-1773.

Pomar, L., Hallock, P., 2008. Carbonate factories: a conundrum in sedimentary Geology. Earth-Science Reviews 87, 134-169.

Pomar, L., Kendall, C.S.C., 2008. Architecture of carbonate platforms: a response to hydrodynamics and evolving ecology. In: Lukasik, J., Simo, J.A. (Eds.), Controls on Carbonate Platform and Reef Development 89. SEPM Special Publications, Tulsa, OK, pp. 187-216.

Pomar, L., Haq, B.U., 2016. Decoding depositional sequences in carbonate systems: Concepts vs experience. Global and Planetary Change 146, 190-225.

Pomar, L., Obrador, A., Westphal, H., 2002. Sub-wavebase cross-bedded grainstones on a distally steepened carbonate ramp, Upper Miocene, Menorca, Spain. Sedimentology 49 (1), 139-169.

Pomar, L., Brandano, M., Westphal, H., 2004. Environmental factors influencing skeletal grain sediment associations: a critical review of Miocene examples from the western Mediterranean. Sedimentology 51 (3), 627-651.

Pomar, L., Gili, E., Obrador, A., Ward, W.C., 2005. Facies architecture and high-resolution sequence stratigraphy of an Upper Cretaceous platform margin succession, Southern Central Pyrenees, Spain. Sedimentary Geology 175 (1-4), 339-365.

Pomar, L., Aurell, M., Bádenas, B., Morsilli, M., Al-Awwad, S.F., 2015. Depositional model for a prograding oolitic wedge, Upper Jurassic, Iberian basin. Marine and Petroleum Geology 67, 556-582.

Pop, G., Bucur I.I., 2001. Upper Jurassic and Lower Cretaceous sedimentary formations from the Vîlcan Mountains (South Carpathians). Studia UBB Geologia 46 (2), 77-94.

Posamentier, H.W., James, D.P., 1993. An overview of sequence-stratigraphic concepts: uses and abuses. In: Posamentier, H.W., Summerhayes, C.P., Haq, B.U., Allen, G.P. (Eds.), Sequence Stratigraphy and Facies Associations. International Association of Sedimentologists, Special Publication 18, pp. 3-18.

Pratt, B.R., James, N.P., 1986. The St. George Group (Lower Ordovician) of western Newfoundland: tidal flat island model for carbonate sedimentation in shallow epeiric seas. Sedimentology 33, 313-343.

Price, G.D., Gröcke, D.R., 2002. Strontium-isotope stratigraphy and oxygen- and carbon-isotope variation during the Middle Jurassic–Early Cretaceous of the Falkland Plateau, South Atlantic. Palaeogeography, Palaeoclimatology, Palaeoecology 183 (3-4), 209-222.

Price, G.D., Sellwood, B.W., Valdes, P.J., 1995. Sedimentological evaluation of general circulation model simulations for the "greenhouse" Earth: Cretaceous and Jurassic case studies. Sedimentary Geology 100, 159-180.

Pueyo, E.L., Izquierdo-Llavall, E., Rodríguez-Pintó, A., Rey-Moral, C., Oliva-Urcia, B., Casas, A.M., Calvín, P., Ayala, C., Ramajo, J., del Rio, P., Rubio, F.M., García-Lobón, J.L., 2015. Petrophysical properties in the Iberian Range and surrounding areas (NE Spain): 1-density. Journal of Maps 12 (5), 836-844.

Purkis, S.J., Rowlands, G.P., Kerr, J.M., 2015. Unravelling the influence of water depth and wave energy on the facies diversity of shelf carbonates. Sedimentology 62, 541-565.

Ramajo, J., Aurell, M., 2008. Long-term Callovian–Oxfordian sea-level changes and sedimentation in the Iberian carbonate platform (Jurassic, Spain): possible eustatic implications. Basin Research 20, 163-184.

Ramalho, M., 1971. Contribution à l'étude micropaléontologique et stratigraphique du Jurassique supérieur et du Crétacé inférieur des environs de Lisbonne (Portugal). Serviços Geologicos de Portugal, Memoria 19 (Nova serie), pp. 212.

Ramalho, M., 1981. Note préliminaire sur le microfacies du Jurassique supérieur portugais. Communicações Serviços Geológicos de Portugal 67, 41-45.

Rameil, N., 2005. Carbonate sedimentology, sequence stratigraphy, and cyclostratigraphy of the Tithonian in the Swiss and French Jura Mountains. A high-resolution record of changes in sea level and climate. PhD Thesis, Université de Fribourg, pp. 246.

Rameil, N., Immenhauser, A., Warrlich, G., Hillgaertner, H., Droste, H.J., 2010. Morphological patterns of Aptian Lithocodium–Bacinella geobodies: relation to environment and scale. Sedimentology 57 (3), 883-911.

Ramírez del Pozo, J., 1971. Bioestratigrafía y microfacies del Jurásico y Cretácico del Norte de España (Región Cantábrica). Memorias del Instituto Geológico y Minero de España, Madrid, Spain, pp. 357.

Rankey, E.C., 2004. On the interpretation of shallow shelf carbonate facies and habitats: how much does water depth matter? Journal of Sedimentary Research 74 (1), 2-6.

Rankey, E.C., 2016. On facies belts and facies mosaics: Holocene isolated platforms, South China Sea. Sedimentology 63, 2190-2216.

Rankey, E.C., Reeder, S.L., 2010. Controls on platform-scale patterns of surface sediments, shallow Holocene platforms, Bahamas. Sedimentology 57, 1545-1565.

Read, J.F., 1985. Carbonate platform facies models. American Associations of Petroleum Geologists Bulletin 69, 1-21.

Redmond, C.D., 1964. Lituolid Foraminifera from the Jurassic and Cretaceous of Saudi Arabia. Micropaleontology 10 (4), 405-414.

Rees, P.M., Ziegler, A.M., Valdes, P.J., 2000. Jurassic phytogeography and climates: new data and model comparisons. In: Huber, B.T., Macleod, K.G., Wing, S.L. (Eds.), Warm climates in Earth history. Cambridge University Press, pp. 297-318.

Reijmer, J.J.G., 2014. Carbonate factories. In: Harff, J., Meschede, M., Petersen, S., Thiede, J. (Eds.), Encyclopedia of Marine Geosciences. Springer Science-Business Media, Dordrecht, pp. 80-84.

Reolid, M., Rodríguez-Tovar, F.J., Nagy, J., Olóriz, F., 2008. Benthic foraminiferal morphogroups of mid to outer shelf environments of the Late Jurassic (Prebetic Zone, southern Spain): Characterization of biofacies and environmental significance. Palaeogeography, Palaeoclimatology, Palaeoecology 261 (3-4), 280-299.

Riboulleau, A., Baudin, F., Daux, V., Hantzpergue, P., Renard, M., Zakharov, V., 1998. Evolution de la paléotempératures des eaux de la plateforme russe au cours du Jurassique supérieur. Comptes Rendus de l'Académie des Sciences de Paris, Sciences de la Terre et des Planètes 326, 239-246.

Richter, D.K., Götte, T., Götze, J., Neuser, R.D., 2003. Progress in application of cathodoluminescence (CL) in sedimentary geology. Mineral Petrology 79, 127-166.

Riding, R., 2000. Microbial carbonates: the geological record of calcified bacterial–algal mats and biofilms. Sedimentology 47, 179-214.

Rodríguez-López, J.P., Meléndez, N., De Boer, P.L., Soria, A.R., 2008. Aeolian sand sea development along the Mid-Cretaceous Western Tethyan Margin (Spain): Erg sedimentology and palaeoclimate implications. Sedimentology 55 (5), 1253-1292.

Rodríguez-López, J.P., Meléndez, N., De Boer, P.L., Soria, A.R., 2012. Controls on marine-erg margin cycle variability: Aeolian-marine interaction in the mid-Cretaceous Iberian Desert System, Spain. Sedimentology 59 (2), 466-501.

Roehl, P.Q., Choquette, P.W., 1985. Carbonate Petroleum Reservoirs. Springer Verlag, New York, pp. 622.

Salas, R., 1987. El Malm y el Cretaci inferior entre el Massis del Garraf i la Serra d'Espadà. Analisi de Conca. PhD Thesis. Universitat de Barcelona, Spain, pp. 345.

Salas, R., Casas, A., 1993. Mesozoic extensional tectonics, stratigraphy and crustal evolution during the Alpine cycle of the eastern Iberian basin. Tectonophysics 228, 33-55.

Salas, R., Guimerà, J., 1996. Rasgos estructurales principales de la cuenca cretácica inferior del Maestrazgo (Cordillera Ibérica oriental). Geogaceta 20 (7), 1704-1706.

Salas, R., Guimerà, J., Mas, R., Martín-Closas, C., Meléndez, A., Alonso, A., 2001. Evolution of the Mesozoic central Iberian Rift System and its Cainozoic inversion (Iberian chain). In: Ziegler, P.A., Cavazza, W., Robertson, A.H.F., Crasquin-Soleau, S. (Eds.), Peri-Tethys Memoir 6: Peri-Tethyan Rift/Wrench and Passive Margins. Mémoires du Museum National d'histoire naturelle 186, pp. 145-185.

San Miguel, G., Aurell, M., Bádenas, B., Martínez, V., Caline, B., Pabian-Goyheneche, C., Rolando, J.P., Grasseau, N., 2013. Facies heterogeneity of a Kimmeridgian carbonate ramp (Jabaloyas, eastern Spain): a combined outcrop and 3D geomodelling analysis. Journal of Iberian Geology 39 (2), 233-252.

San Miguel, G., Aurell, M., Bádenas, B., 2017a. Occurrence of high-diversity metazoan- to microbial-dominated bioconstructions in a shallow Kimmeridgian carbonate ramp (Jabaloyas, Spain). Facies 63, 13.

San Miguel, G., Aurell, M., Bádenas, B., 2017b. Diagenetic evolution of a shallow marine Kimmeridgian carbonate ramp (Jabaloyas, NE Spain): implications for hydrocarbon reservoir quality. Arabian Journal of Geosciences 10, 376.

Santos, A.A., Villanueva-Amadoz, U., Royo-Torres, R., Sender, L.M., Cobos, A., Alcala, L., Diez, J.B., 2018. Palaeobotanical records associated with the first dinosaur defined in Spain: Palynostratigraphy, taxonomy and palaeoenvironmental remarks. Cretaceous Research 90, 318-334.

Saúl, S., 2014. Sedimentología de la Formación Higueruelas en Mezalocha (Zaragoza). Análisis de facies de una plataforma somera de finales del Jurásico. Bachelor's Thesis, Universidad de Zaragoza, pp. 28.

Savard, M.M., Veizer, J., Hinton, R.H., 1995. Cathodoluminescence at low Fe and Mn concentrations: A SIMS study of zones in natural calcites. Journal of Sedimentary Research 65 (1a), 208-213.

Schlager, W., 1981. The paradox of drowned reefs and carbonate platforms. Geological Society of America Bulletin 92 (4), 197-211.

Schlager, W., 2000. Sedimentation rates and growth potential of tropical, cool water and mud mound carbonate factories. In: Insalaco, E., Skelton, P.W., Palmer, T.J. (Eds.), Carbonate Platform Systems: components and interactions. Geological Society of London Special Publications 178, pp. 217-227.

Schlager, W., 2003. Benthic carbonate factories of the Phanerozoic. International Journal of Earth Sciences 92, 445-464.

Schlager, W., 2005. Carbonate sedimentology and sequence stratigraphy (No. 8). SEPM Concepts in Sedimentology and Paleontology, Tulsa, Oklahoma, pp. 200.

Schmid, D.U., 1996. Marine Mikrobolithe und Mikroinkrustierer aus dem Oberjura. Profil 9, 101-251.

Schobben, M., Ullmann, C.V., Leda, L., Korn, D., Struck, U., Reimold, W.U., Ghaderi, A., Algeo, T.J., Korte, C., 2015. Discerning primary versus diagenetic signals in carbonate carbon and oxygen isotope records: An example from the Permian–Triassic boundary of Iran. Chemical Geology 422, 94-107.

Schrodt, F., 1894. Das Vorkommen der Foraminiferen-Gattung Cyclammina im oberen Jura. Zeitschrift der Deutschen Geologischen Gesellschaft 45, 733-735.

Scotese, C.R. (2014). Atlas of Jurassic Paleogeographic Maps, PALEOMAP Atlas for ArcGIS, volume 3, The Jurassic and Triassic, Maps 32-42, Mollweide Projection, PALEOMAP Project, Evanston, IL. Researchgate Academia. http://www.scotese.com/ljurclim.htm (accessed 10 March 2020).

Septfontaine, M., 1988. Vers une classification évolutive des Lituolidés (Foraminifères) jurassiques en milieux de plate-forme carbonatée. Revue de Paléobiologie, spécial nr. 2 (Benthos 1986), 229-256.

Septfontaine, M., Arnaud-Vanneau, A., Bassoullet, J.P., Gusic, Y., Ramalho, M., Velic, I., 1991. Les foraminifères imperforés des plates-formes carbonatées jurassiques: état des connaissances et perspectives d'avenir. Bulletin de la Société vaudoise des sciences naturelles 80, 255-277.

Sequero, C., Bádenas, B., Aurell, M., 2018. Facies mosaic in the inner areas of a shallow carbonate ramp (Upper Jurassic, Higueruelas Fm, NE Spain). Facies 64 (9).

Sequero, C., Bádenas, B., Aurell, M., 2019a. Factors controlling oncoid distribution in the inner areas of a Late Kimmeridgian carbonate ramp (Northeast Spain). In: Boughdiri, M., Bádenas, B., Selden, P., Jaillard, E., Bengtson, P., Granier, B.R.C. (Eds), Paleodiversity and Tectono-Sedimentary Records in the Mediterranean Tethys and Related Eastern Areas. Proceedings of the 1st Arabian Journal of Geosciences (CAJG-1), Tunisia, Springer, pp. 171-174.

Sequero, C., Aurell, M., Bádenas, B., 2019b. Sedimentary evolution of a shallow carbonate ramp (Kimmeridgian, NE Spain): Unravelling controlling factors for facies heterogeneities at reservoir scale. Marine and Petroleum Geology 109, 145-174.

Sequero, C., Aurell, M., Bádenas, B., 2020. Oncoid distribution in the shallow domains of a Kimmeridgian carbonate ramp (Late Jurassic, NE Spain). Sedimentary Geology 398, 105585.

Shapiro, R.S., Fricke, H.C., Fox, K., 2009. Dinosaur-bearing oncoids from ephemeral lakes of the Lower Cretaceous Cedar Mountain Formation, Utah. Palaios 24, 51-58.

Shi, G.R., Chen, Z.Q., 2006. Lower Permian oncolites from South China: implications for equatorial sea-level responses to Late Palaeozoic Gondwanan glaciation. Journal of Asian Earth Sciences 26, 424-436.

Shinn, E.A., Lloyd, R.M. and Ginsburg, R.N., 1969. Anatomy of a modern carbonate tidal flat, Andros Island, Bahamas. Journal of Sedimentary Petrology 39, 1202-1228.

Shiraishi, F., Kano, A., 2004. Composition and spatial distribution of microencrusters and microbial crusts in upper Jurassic-lowermost Cretaceous reef limestone (Torinosu Limestone, southwest Japan). Facies 50, 217-227.

Shurygin, B.N., Dzyuba, O.S., Izokh, O.P., Kosenko, I.N., Kuznetsov, A.B., 2015. Isotope markers (C, O, Sr) of the Jurassic–Cretaceous boundary beds in Boreal regions (Maurynya section, Western Siberia). In: Zakharov, V.A., Rogov, M.A., Ippolitov, A.P. (Eds.), Jurassic System of Russia: Problems of stratigraphy and paleogeography. Sixth All Russian Meeting. September 15-20, 2015, Scientific Materials, Makhachkalapp, pp. 318-320.

Simón, J.L., 1989. Late Cenozoic stress field and fracturing in the Iberian Chain and Ebro Basin (Spain). Journal of Structural Geology 11 (3), 285-294.

Soria, A.R., 1997. La sedimentación en las cuencas marginales del surco Ibérico durante el Cretácico Inferior y su control tectónico. PhD Thesis, Universidad de Zaragoza, Spain, pp. 363.

Soria, A.R., Martín Closas, C., Meléndez, A., Meléndez, M.N., Aurell, M., 1995. Estratigrafía del Cretácico inferior continental de la Cordillera Ibérica Central. Estudios Geológicos 51 (3-4), 141-152.

Spencer, G.H., Tucker, M.A., 2007. A proposed integrated multisignature model for peritidal cycles in carbonates. Journal of Sedimentary Research 77, 797-808.

Strasser, A., 1986. Ooids in Purbeck limestones (Lowermost Cretaceous) of the Swiss and French Jura. Sedimentology 33, 711-727.

Strasser, A., 2018. Cyclostratigraphy of Shallow-Marine Carbonates-Limitations and Opportunities. In: Montenari, M. (Ed.), Stratigraphy and Timescales 3, pp. 151-187.

Strasser, A., Védrine, S., 2009. Controls on facies mosaics of carbonate platforms: a case study from the Oxfordian of the Swiss Jura. In: Swart, P., Eberli, G., McKenzie, J. (Eds.), Perspectives in Carbonate Geology: a Tribute to the Career of Robert Nathan Ginsburg. vol. 41 IAS Special Publications, pp. 199-213.

Strasser, A., Pittet, B., Hillgärtner, H., Pasquier, J.B., 1999. Depositional sequences in shallow carbonate-dominated sedimentary systems: concepts for a high-resolution analysis. Sedimentary Geology 128, 201-221.

Sun, S.Q., 1995. Dolomite reservoirs: porosity evolution and reservoir characteristics. American Association of Petroleum Geologists Bulletin 79 (2), 186-204.

Swart, P.K., Eberli, G., 2005. The nature of the $\delta^{13}C$ of periplatform sediments: implications for stratigraphy and the global carbon cycle. Sedimentary Geology 175, 115-129.

Swei, G.H., Tucker, M.E., 2012. Impact of diagenesis on reservoir quality in ramp carbonates: Gialo Formation (Middle Eocene), Sirt Basin, Libya. Journal of Petroleum Geology 35 (1), 25-48.

Swift, D. J. P., Thorne, J. A., 1991. Sedimentation on continental margins, I: a general model for shelf sedimentation. In: Swift, D.J.P., Oertel, G.F., Tillman, R.W., Thorne, J.A. (Eds.), Shelf sand and sandstone bodies: Geometry, facies and sequence stratigraphy. International Association of Sedimentologists, Special Publication 14, pp. 3-31.

Tavakoli, V., Rahimpour-Bonab, H., Esrafili-Dizaji, B., 2011. Diagenetic controlled reservoir quality of South Pars gas field, an integrated approach. Comptes Rendus Geoscience, 343 (1), 55-71.

Taylor, P.D., Allison, P.A., 1998. Bryozoan carbonates through time and space. Geology 26, 459-462.

Taylor, A.M., Gowland, S., Leary, S., Keogh, Kevin J., Martinius, A.W., 2013. Stratigraphical correlation of the Late Jurassic Lourinhã Formation in the Consolação Sub-basin (Lusitanian Basin), Portugal. Geological Journal 49 (2), 143-162.

Teichert, C., 1958. Cold- and deep-water coral banks. American Association of Petroleum Geologists Bulletin, 42 (5), 1064-1082.

Tomás, S., Aurell, M., Bádenas, B., Bjorge, M., Duaso, M., Mutti, M., 2019. Architecture and Paleoenvironment of Mid-Jurassic Microbial–Siliceous Sponge Mounds, Northeastern Spain. Journal of Sedimentary Research, 89 (2), 110-134.

Travé, A., Nadal, J., Playà, E., Salas, R., Martín-Martín, J.D., Gomez-Rivas, E., 2019. Fracture-related dolomitization affecting Late Jurassic-Lowermost Cretaceous syn-rift deposits (Maestrat Basin, Southern Iberian Chain, Eastern Spain). In: Doronzo, D.M., Schingaro, E., Armstrong-Altrin, J.S., Zoheir, B. (Eds.), Petrogenesis and Exploration of the Earth's Interior. Advances in Science, Technology and Innovation, pp. 163-165.

Tucker, M.E., Wright, V.P., 1990. Carbonate Sedimentology. Wiley-Blackwell, Oxford pp. 482.

Turnsek, D., Buser, S., Ogorelec, B., 1981. An Upper Jurassic reef complex from Slovenia, Yugoslavia. In: Toomey, D.F. (Ed.), European fossil reef models. SEPM Special Publications 30, pp. 361-369.

Urey, H.C., Lowenstam, H.A., Epstein, S., McKinney, C.R., 1951. Measurement of paleotemperatures and temperatures of the upper Cretaceous of England, Denmark, and the southeastern United States. Geological Society of America Bulletin 62, 399-416.

Vail, P.R., Audemard, F., Bowman, S.A., Eisner, P.N., Pérez-Cruz, C., 1991. The stratigraphic signatures of tectonics, eustasy and sedimentology – an overview. In: Einsele, G., Ricken, W., and Seilacher, A. (Eds.), Cycles and Events in Stratigraphy. Berlin, Springer-Verlag, pp. 617-659.

Val, J., 2019. Sedimentology and cyclostratigraphy of three Jurassic shallow platforms (Central Iberian Basin): the interplay of internal and external factors. PhD Thesis, Universidad de Zaragoza, Spain, pp. 283.

Val, J., Bádenas, B., Aurell, M., 2018. Sedimentary architecture of a prograding oolitic-siliciclastic wedge: Response to changes in wave-base oscillation (Kimmeridgian, Iberian Basin). Marine and Petroleum Geology 96, 113-127.

Val, J., Aurell, M., Bádenas B., Castanera, D., Subías, S., 2019. Cyclic carbonate-siliciclastic sedimentation in a shallow marine to coastal environment (latest Kimmeridgian–early Tithonian, Galve sub-basin, Spain). Journal of Iberian Geology 45, 195-222.

van de Schootbrugge, B., Föllmi, K.B., Bulot, L.G., Burns, S. J., 2000. Paleoceanographic changes during the early Cretaceous (Valanginian–Hauterivian): evidence from oxygen and carbon stable isotopes. Earth and Planetary Science Letters 181 (1-2), 15-31.

van der Kooij, B., Immenhauser, A., Csoma, A., Bahamonde, J., Steuber, T., 2009. Spatial geochemistry of a Carboniferous platform-margin-to-basin transect: balancing environmental and diagenetic factors. Sedimentary Geology 219, 136-150.

Védrine, S., Strasser, A., 2009. High-frequency palaeoenvironmental changes on a shallow carbonate platform during a marine transgression (Late Oxfordian, Swiss Jura Mountains). Swiss Journal of Geosciences 102 (2), 247-270.

Védrine, S., Strasser, A., Hug, W., 2007. Oncoid growth and distribution controlled by sea-level fluctuations and climate (Late Oxfordian, Swiss Jura Mountains). Facies 53 (4), 535-552.

Vegas, R., Banda, E., 1982. Tectonic framework and Alpine evolution of the Iberian Peninsula. Earth Evolution Sciences 4, 320-343.

Veizer, J. Fritz, P, Jones, P., 1986. Geochemistry of brachiopods: Oxygen and carbon isotopic records of Paleozoic oceans. Geochimica et Cosmochimica Acta 50, 1679-1696.

Veizer J., Ala D., Azmy, K., Bruckschen P., Buhl D., Bruhn F., Carden G.A.F., Diener A., Ebneth S., Godderis Y., Jasper T., Korte C., Pawelleck F., Podlaha O.G., Strauss H., 1999. $^{87}Sr/^{86}Sr$, $\delta^{13}C$ and $\delta^{18}O$ evolution of Phanerozoic seawater. Chemical Geology 161, 59-88.

Vergés, J., García-Senz, J., 2001. Mesozoic evolution and Cenozoic inversion of the Pyrenean Rift. In: Ziegler, P.A., Cavazza, W., Robertson, A.H.F., Crasquin-Soleau, S. (Eds.), Peri-Tethys Memoir 6: Peri-Tethyan Rift/Wrench Basins and Passive Margins. Mémoires du Muséum national d'Histoire naturelle 186, pp. 187-212.

Veron, J.E.N., 1995. Corals in space and time: the biogeography and evolution of the Scleractinia. Cornell University Press (Comstock), Ithaca, London, pp. 321.

Vincent, B., Emmanuel, L., Loreau, J.P., 2004. Significance of the isotopic signal ($\delta^{18}O$, $\delta^{13}C$) of neritic carbonates: diagenetic component and original component (Upper Jurassic of the East of the Paris Basin, France). Comptes Rendus Geoscience 336 (1), 29-39.

Walsh, J., 1996. No second chance? New perspectives on biotic interactions in post-Paleozoic brachiopod history. In: Cooper, P., Jin, J. (Eds.), Brachiopods. Proceedings of the Third International Brachiopod Congress, Balkema, Rotterdam, pp. 281-288.

Warren, J., 2000. Dolomite: occurrence, evolution and economically important associations. Earth-Science Reviews 52 (1), 1-81.

Weissert, H., Mohr, H., 1996. Late Jurassic climate and its impact on carbon cycling. Palaeogeography, Palaeoclimatology, Palaeoecology 122, 27-43.

Weissert, H., Lini, A., Föllmi, K.B., Kuhn, O., 1998. Correlation of Early Cretaceous carbon isotope stratigraphy and platform drowning events: a possible link? Palaeogeography, Palaeoclimatology, Palaeoecology 137, 189-203.

Wender, L.E., Bryant, J.W., Dickens, M.F., Neville, A.S., Al-Moqbel, A.M., 1998. Paleozoic (pre-Khuff) hydrocarbon geology of the Ghawar area, eastern Saudi Arabia. GeoArabia 3, 273-301.

Wendt, J., Belka, Z., Kaufmann, B., Kostrewa, R., and Hayer, J., 1997. The world's most spectacular carbonate mud mounds (Middle Devonian, Algerian Sahara). Journal of Sedimentary Research 67 (3), 424-436.

Whisonant, R.C., 1987. Paleocurrent and petrographic analysis of imbricate intraclasts in shallow-marine carbonates, Upper Cambrian, southwestern Virginia. SEPM Journal of Sedimentary Research, 57 (6), 983-994.

Wierzbowski H., 2004. Carbon and oxygen isotope composition of Oxfordian-Early Kimmeridgian belemnite rostra: palaeoenvironmental implications for Late Jurassic seas. Palaeogeography, Palaeoclimatology, Palaeoecology 203, 153-168.

Wierzbowski, H., Anczkiewicz, R., Bazarnik, J., Pawlak, J., 2012. Strontium isotope variations in Middle Jurassic (Late Bajocian-Callovian) seawater: implications for Earth's tectonic activity and marine environments. Chemical Geology 334, 171-181.

Wierzbowski, H., Anczkiewicz, R., Pawlak, J., Rogov, M.A., Kuznetsov, A.B., 2017. Revised Middle-Upper Jurassic strontium isotope stratigraphy. Chemical Geology 466, 239-255.

Wieser, M.E., Brand, W.A., 1999. Isotope ratio studies using mass spectrometry. In: Lindon, J.C. (Ed.), Encyclopedia of Spectroscopy and Spectrometry. Academic Press, London, ElSevier, pp. 1224-1236.

Wilkinson, B.H., 1979. Biomineralization, paleoceanography and the evolution of calcareous marine organisms. Geology 7 (11), 524-527.

Wilson, J.L., 1975. Carbonate Facies in Geologic History. Springer-Verlag, New York, pp. 471.

Winland, H.D., Matthews, R.K., 1974. Origin and significance of grapestone, Bahama Islands. SEPM Journal of Sedimentary Research 44 (3), 921-927.

Wright, V.P., Faulkner, T.J., 1990. Sediment dynamics of Early Carboniferous ramps: a proposal. Geological Journal 25, 139-144.

Wright, V.P., Burgess, P.M., 2005. The carbonate factory continuum, facies mosaic and microfacies: an appraisal of some of the key concepts underpinning carbonate sedimentology. Facies 51, 17-23.

Yabe, H., Hanzawa, S., 1926. Choffatella Schlumberger and Pseudocyclammina, a new genus of arenaceous foraminifera. Science Reports of the Tôhoku University, Sendai, ser. 2, Geology 9, 9-11.

Zachos, J., Pagani, M., Sloan, L., Thomas, E., Billups, K., 2001. Trends, rhythms, and aberrations in global climate 65 Ma to present. Science 292 (5517), 686-693.

Zakrevsky, K.E., 2011. Geological 3D Modelling. EAGE Publications, DB Houston, pp. 261.

Zenger, D.H., Dunham, J.B., Ethington, R.L., 1980. Concepts and models of dolomitization. SEPM Special Publication 28, pp. 320.

Zhang, W., Shi, X., Jiang, G., Tang, G., Wang, X., 2015. Mass-occurrence of oncoids at the Cambrian Series 2-Series 3 transition: Implications for microbial resurgence following an Early Cambrian extinction. Gondwana Research 28, 432-450.

Zuo, F., Heimhofer, U., Huck, S. Bodin, S., Erbacher, J., Bai, H., 2018. Coupled $\delta^{13}C$ and $^{87}Sr/^{86}Sr$ chemostratigraphy of Kimmeridgian shoal-water deposits: A new composite record from the Lower Saxony Basin, Germany. Sedimentary Geology 376, 18-31.

ANNEXE 1: DATABASE OF THE SEDIMENTOLOGICAL WORK

The following section includes field pictures of the Higueruelas Fm in each study sector, detailed sedimentological information of the studied logs, the mapping of facies, units and key surfaces in continuous outcrops, and the location of the collected samples for petrographic descriptions. The image below illustrates the situation of the Jurassic outcrops and studied sections (stars) from Muel to Aguilón sectors (a) and in Mezalocha sector (b; black square in a).

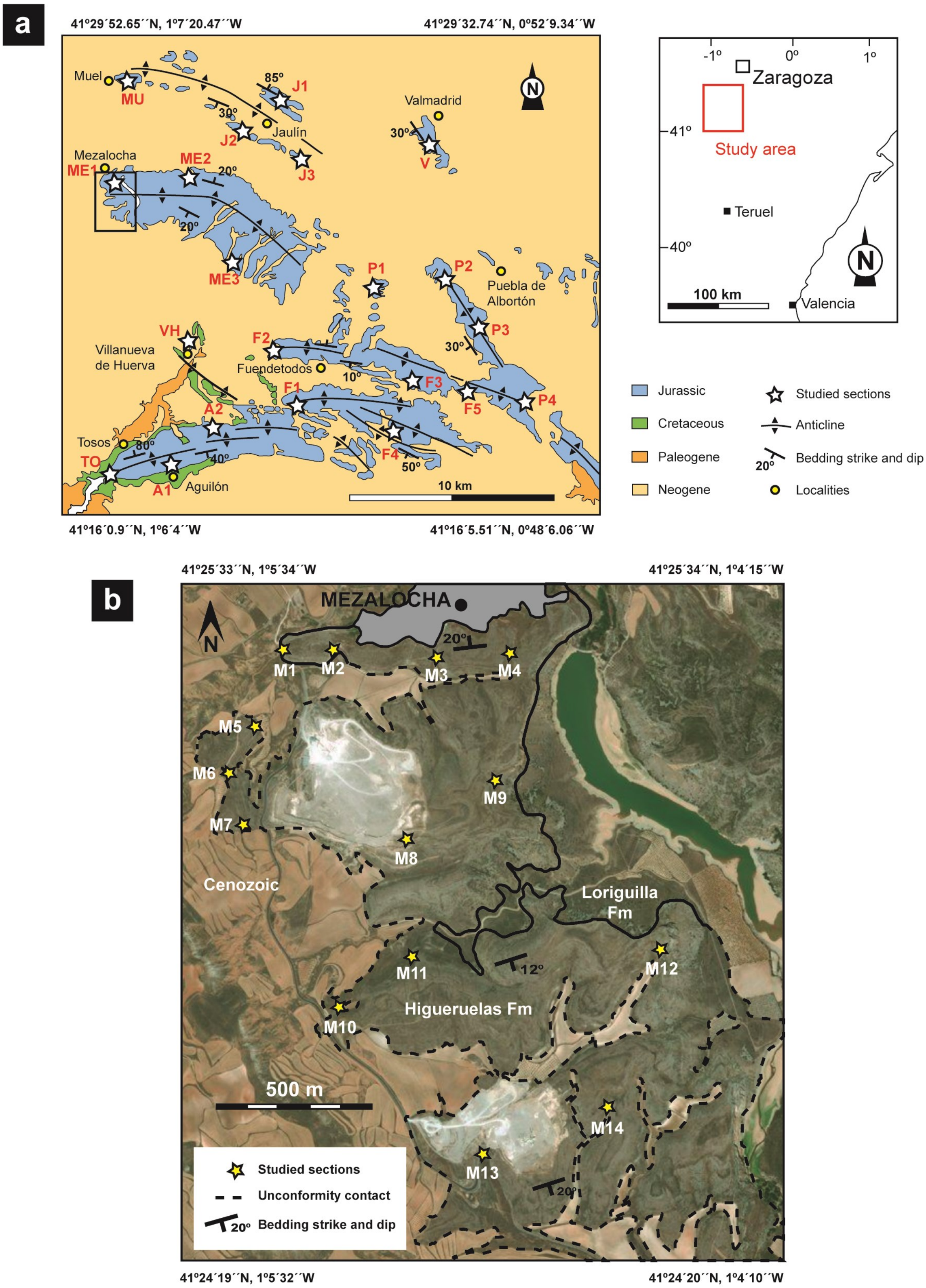

NORTHERN CROSS-SECTION (Muel-Valmadrid sector)

Sections situated around the localities of Muel (MU), Jaulín (J1 to J3) and Valmadrid (V). The field pictures included in this section are representative of the Higueruelas Fm in each sector. Below, the position of the northern cross-section in the study area, and the legend for the information included in the sedimentary logs (the names of the backshoal to foreshoal oncolitic-dominated P to G facies is modified from those originally defined in Chapter 5, due to deeper analysis concerning the oncoid types and their distribution presented in Chapter 6).

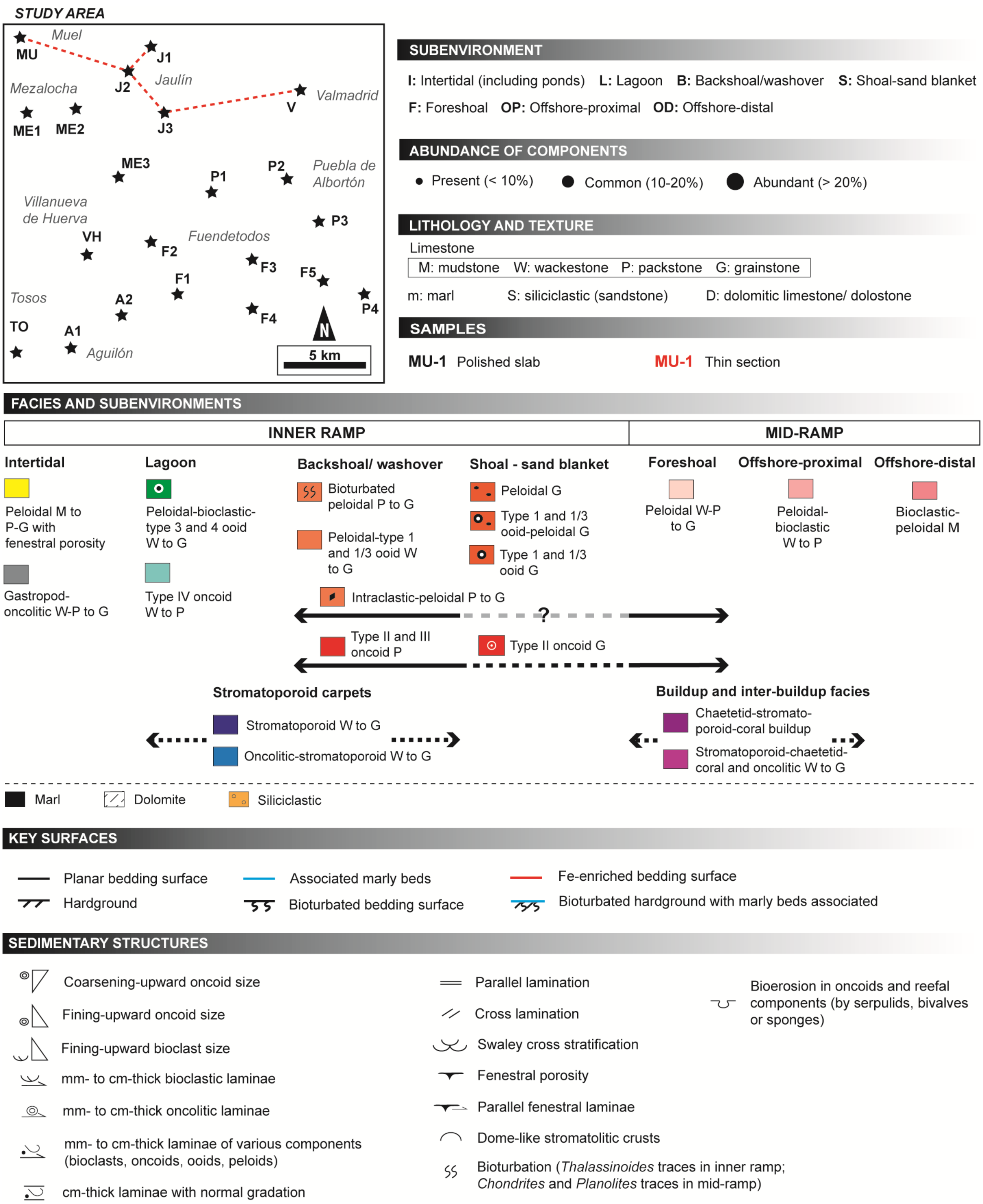

Field pictures

Muel sector

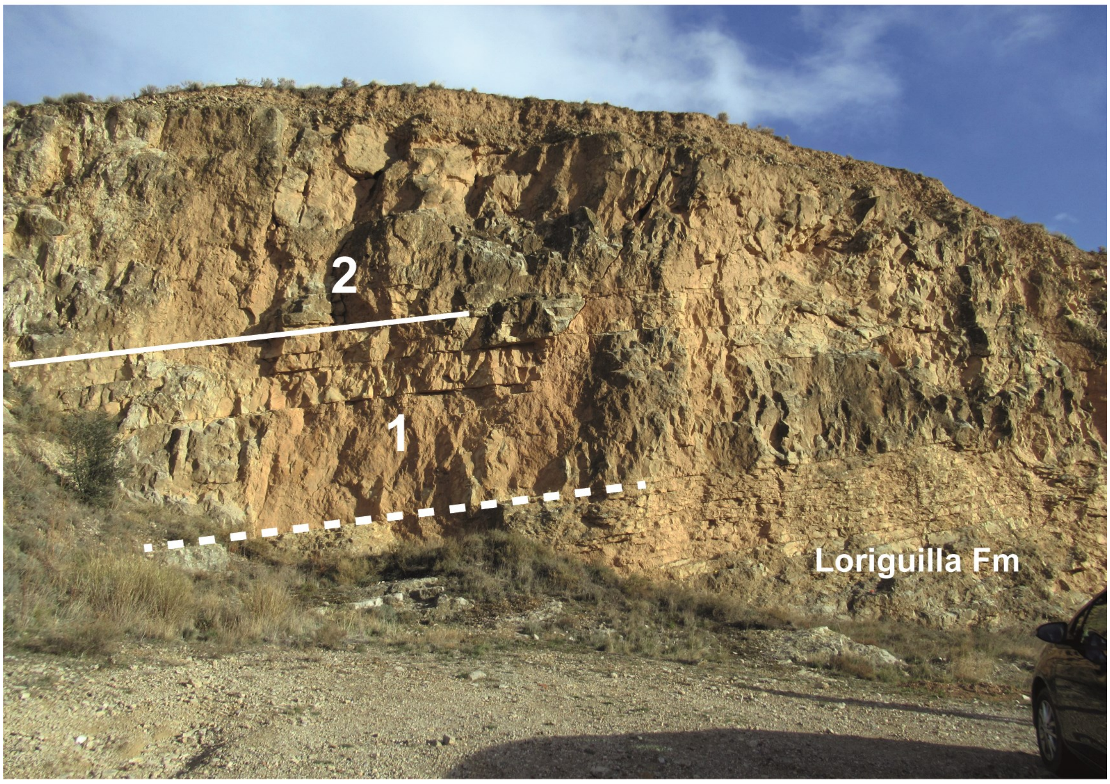

The Higueruelas Fm in Muel sector (section MU), with the recognition of 6 sequences (1-6). The boundary with the overlying coastal-siliciclastic unit (top) and the underlying Loriguilla Fm (bottom) are indicated (dashed lines).

Jaulín sector

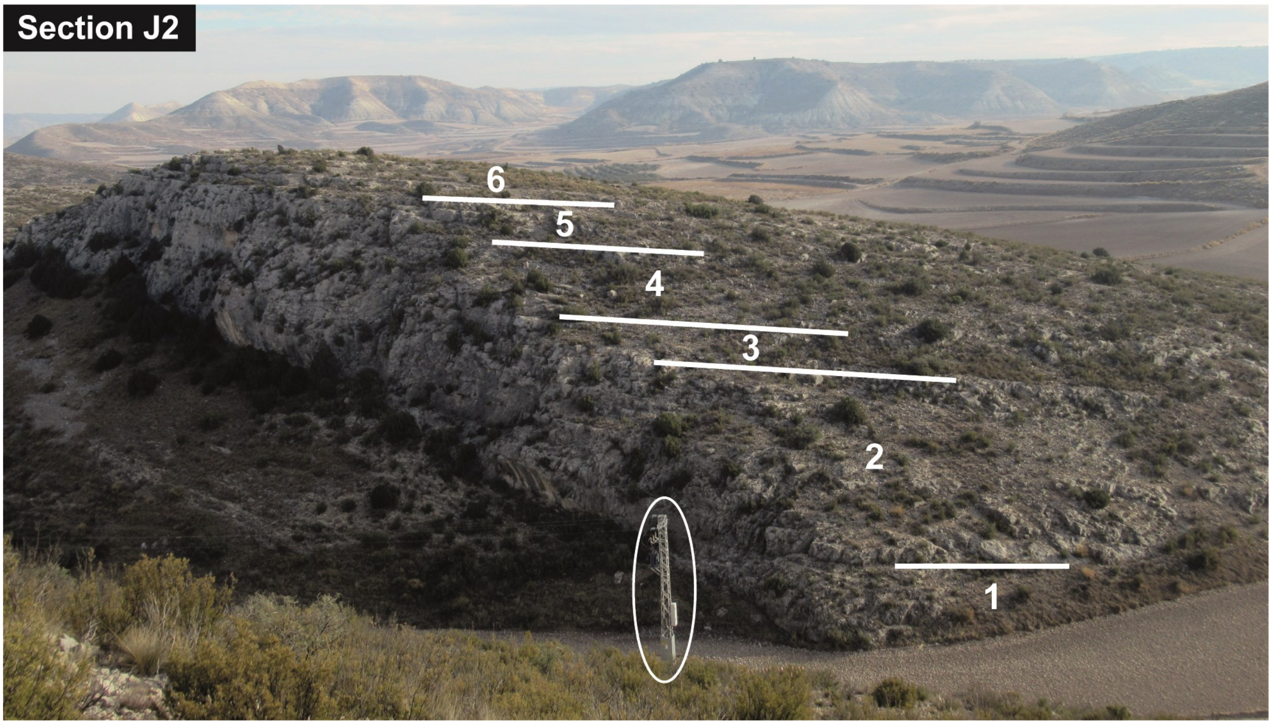

The Higueruelas Fm in Jaulín sector, for the sections J1 (sequences 6-7) and J2 (sequences 1-6). In section J1, the boundary with the overlying coastal-siliciclastic unit is indicated (dashed line).

Valmadrid sector

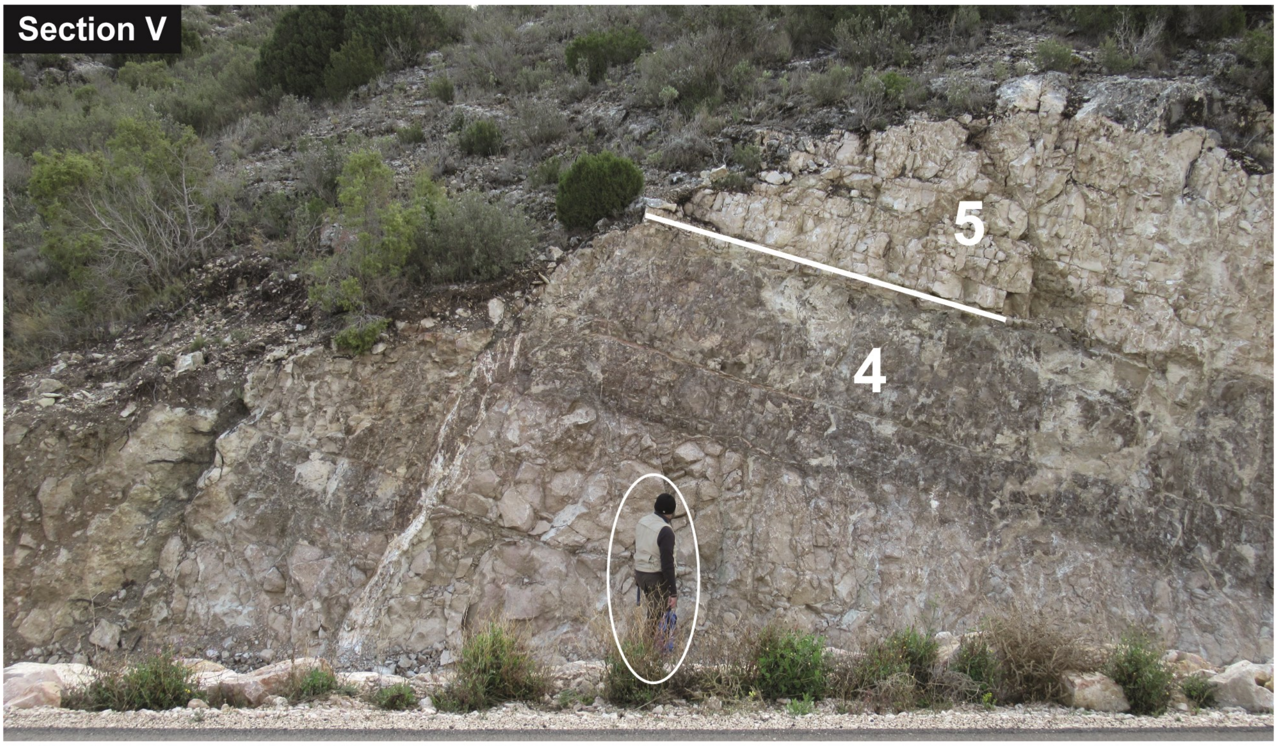

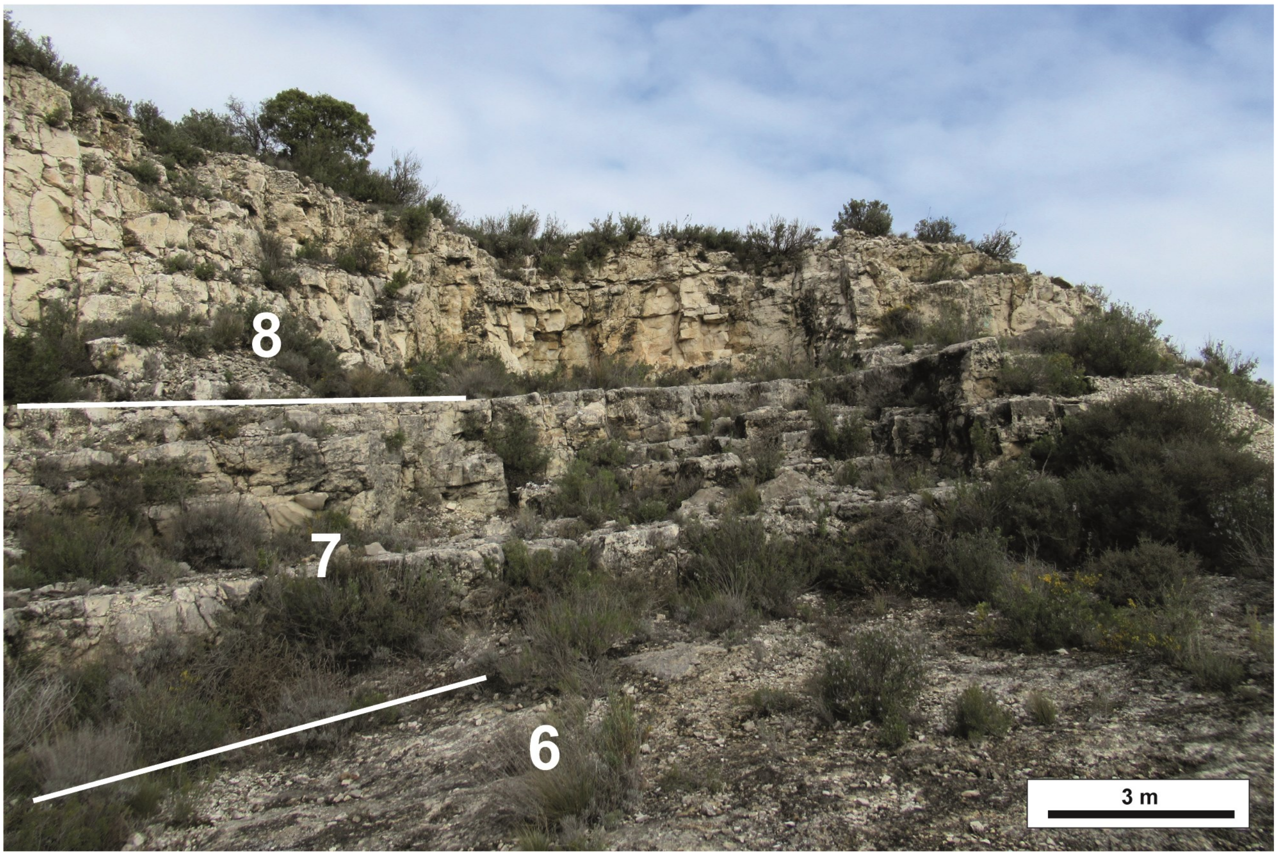

Sequences 4-5 (top) and 6-8 (bottom) recognized in the Higueruelas Fm in Valmadrid sector (section V).

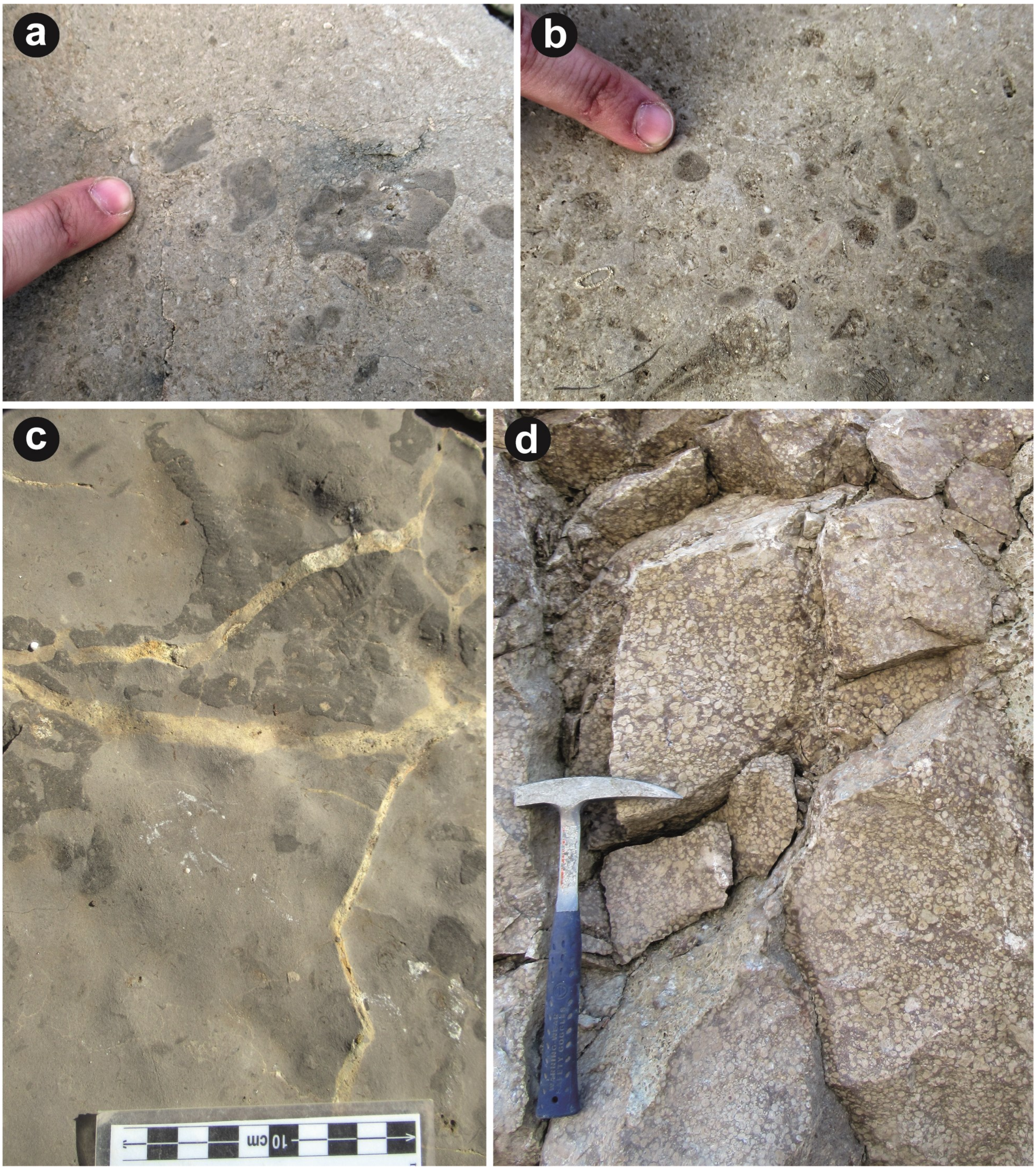

a-c) Field view of backshoal stromatoporoid-rich facies in Jaulín sector, showing cm-sized fragments of broken stromatoporoids and a high diversity of bioclasts (a-b: sequence 6 in section J2; c: sequence 3 in section J3). d) Field view of foreshoal type II and III oncoid facies in Valmadrid sector (sequence 4), showing an oncolitic-supported texture.

Logs and sample location

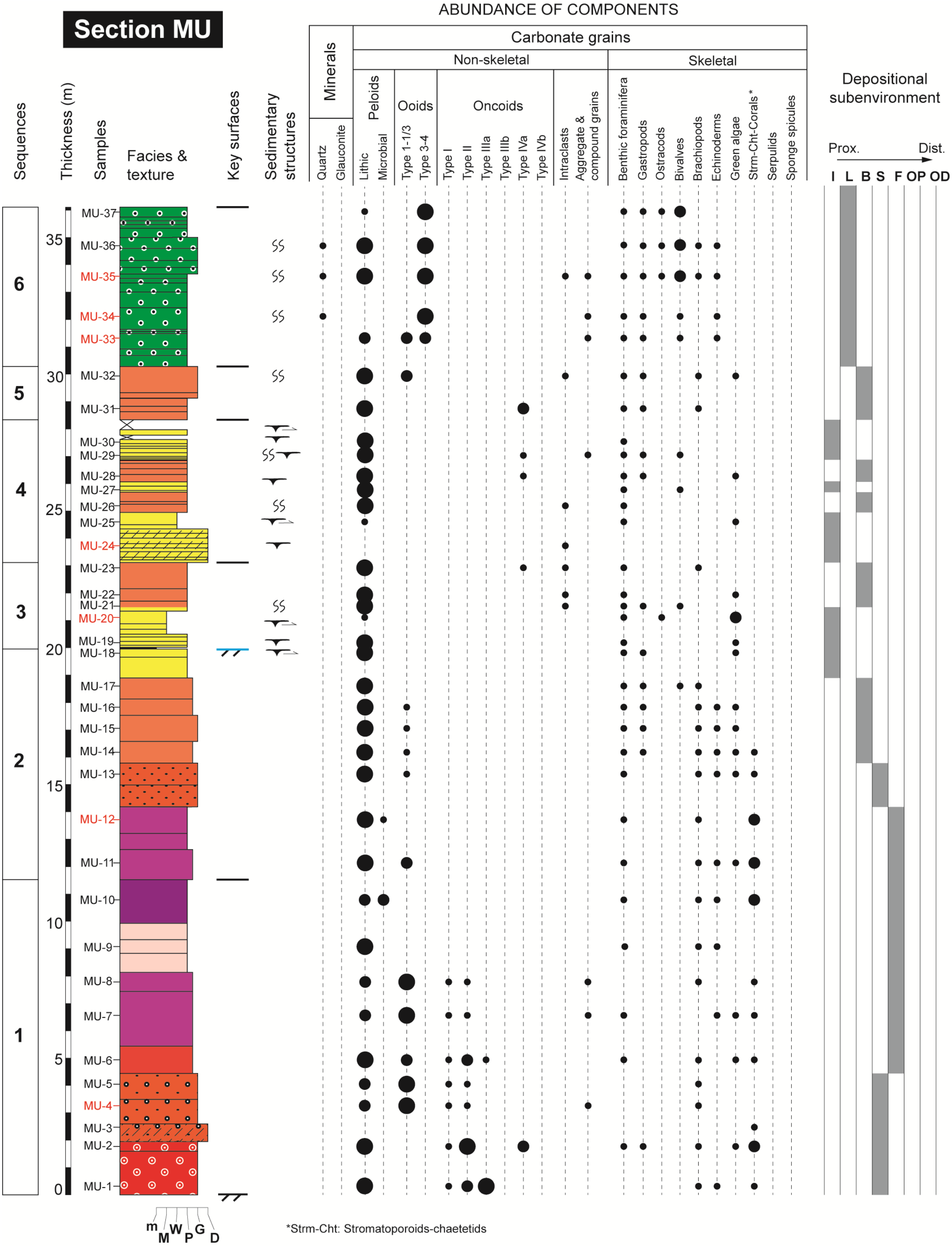

*Strm-Cht: Stromatoporoids-chaetetids

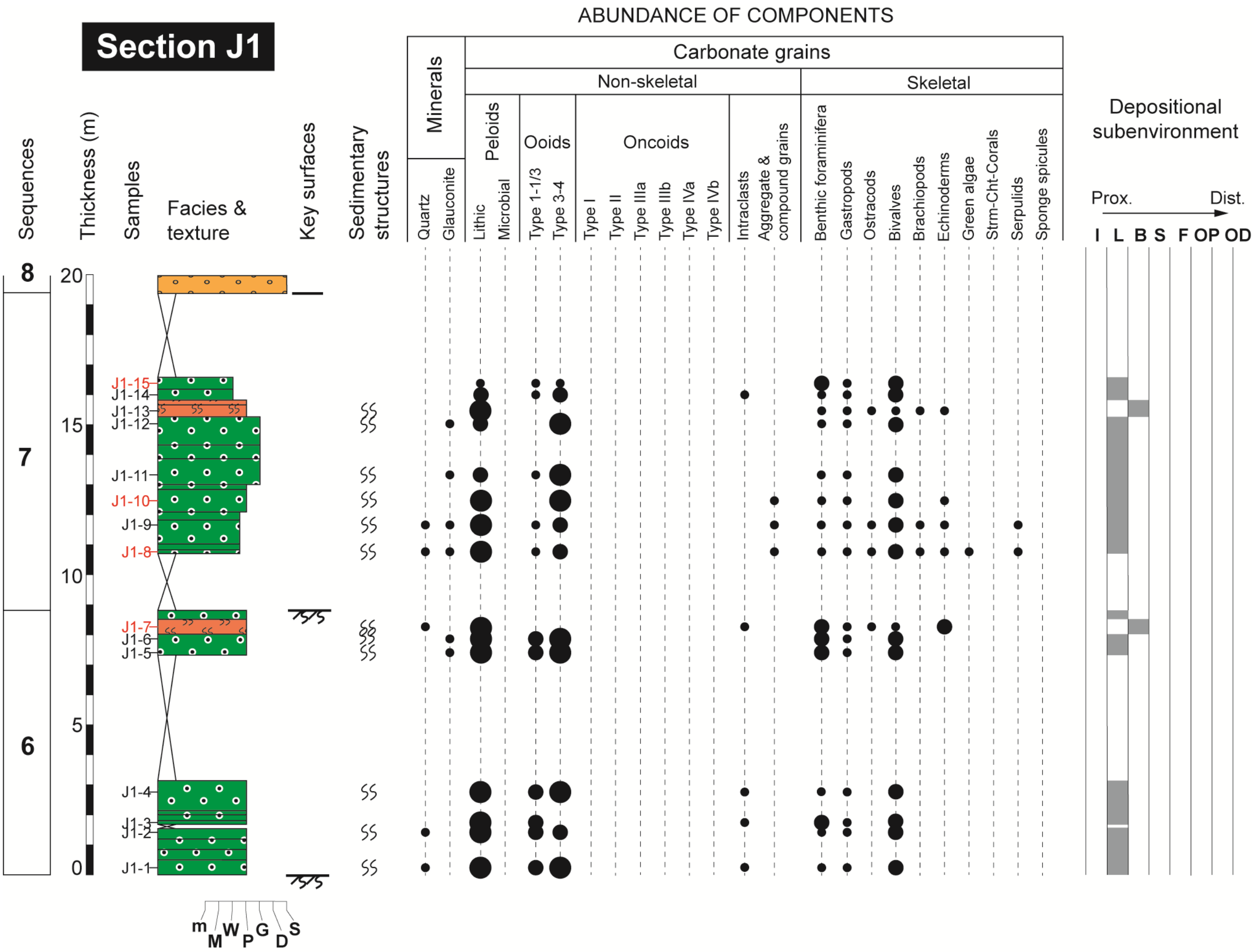
ABUNDANCE OF COMPONENTS
Section J1
Sequences
Thickness (m)
Samples
Facies & texture
Key surfaces
Sedimentary structures
Minerals
Quartz
Glauconite
Carbonate grains
Non-skeletal
Skeletal
Peloids
Lithic
Microbial
Ooids
Type 1-1/3
Type 3-4
Oncoids
Type I
Type II
Type IIIa
Type IIIb
Type IVa
Type IVb
Intraclasts
Aggregate & compound grains
Benthic foraminifera
Gastropods
Ostracods
Bivalves
Brachiopods
Echinoderms
Green algae
Strm-Cht-Corals
Serpulids
Sponge spicules
Depositional subenvironment
Prox.
Dist.
I L B S F OP OD
8
7
6
20
15
10
5
0
J1-15
J1-14
J1-13
J1-12
J1-11
J1-10
J1-9
J1-8
J1-7
J1-6
J1-5
J1-4
J1-3
J1-2
J1-1
m M W P G D S

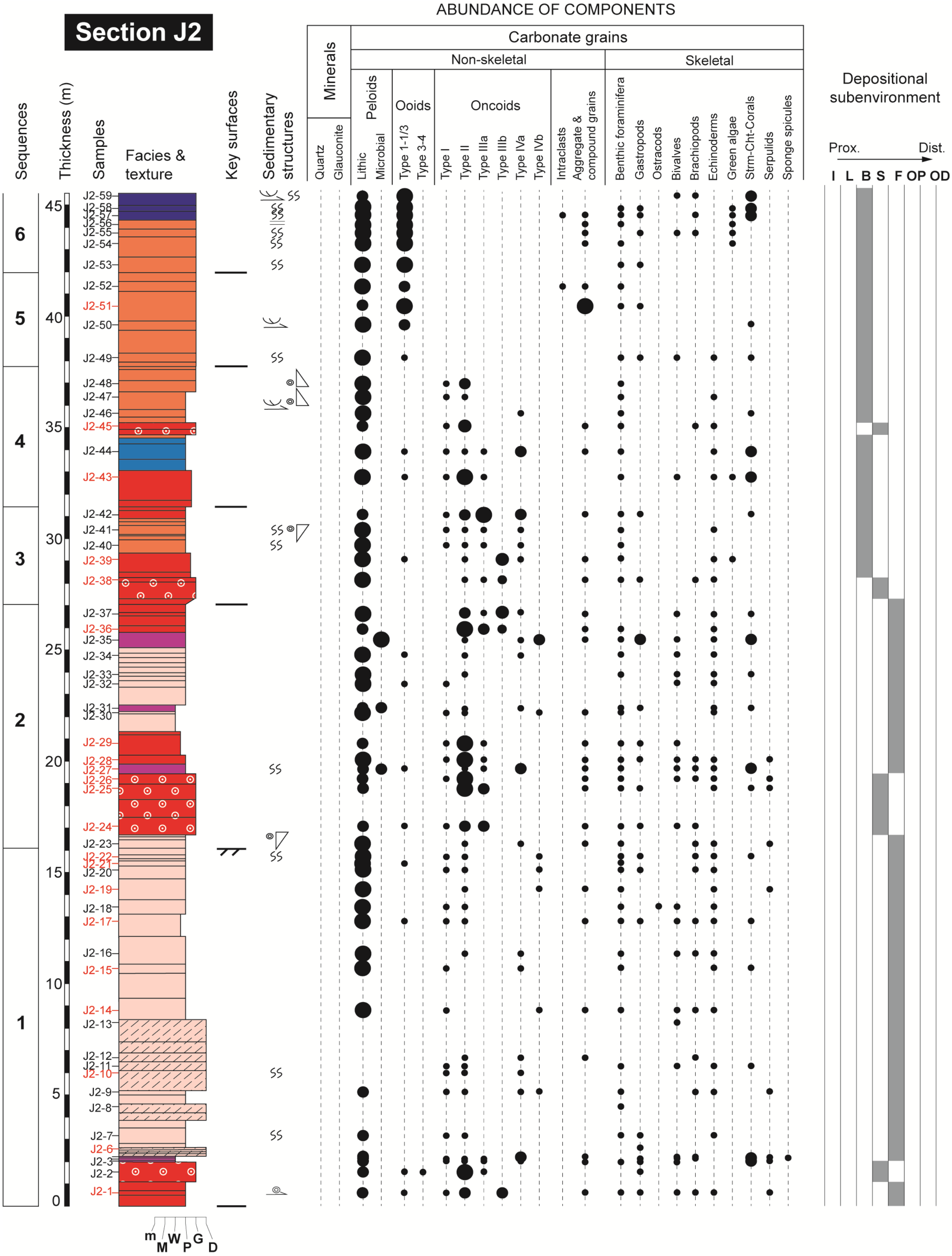
Section J2
ABUNDANCE OF COMPONENTS
Minerals
Carbonate grains
Non-skeletal
Skeletal
Sequences
Thickness (m)
Samples
Facies & texture
Key surfaces
Sedimentary structures
Quartz
Glauconite
Peloids
Lithic
Microbial
Ooids
Type 1-1/3
Type 3-4
Oncoids
Type I
Type II
Type IIIa
Type IIIb
Type IVa
Type IVb
Intraclasts
Aggregate & compound grains
Benthic foraminifera
Gastropods
Ostracods
Bivalves
Brachiopods
Echinoderms
Green algae
Strm-Cht-Corals
Serpulids
Sponge spicules
Depositional subenvironment
Prox.
Dist.
I L B S F OP OD
m M W P G D

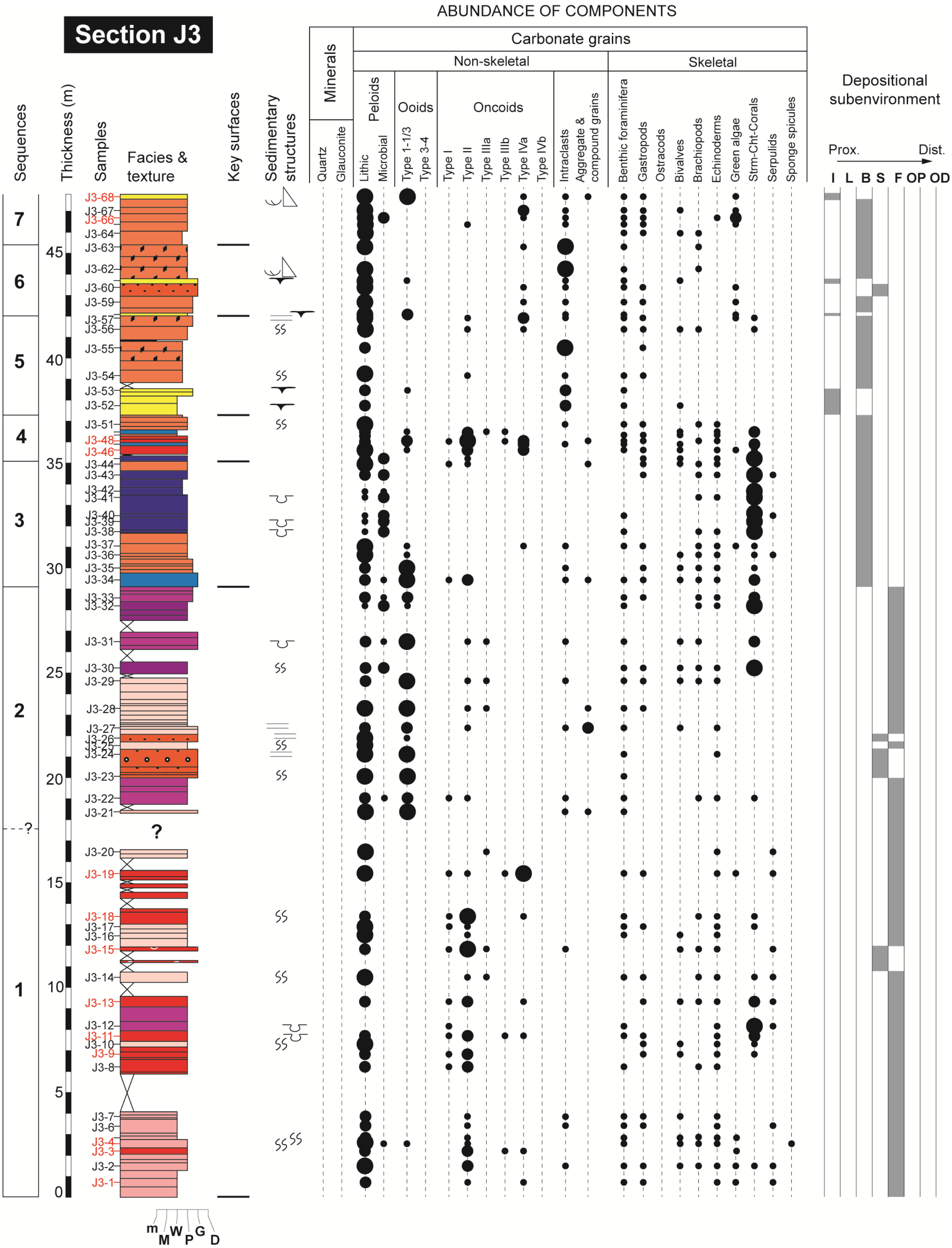
Section J3
ABUNDANCE OF COMPONENTS
Minerals
Carbonate grains
Non-skeletal
Skeletal
Sequences
Thickness (m)
Samples
Facies & texture
Key surfaces
Sedimentary structures
Quartz
Glauconite
Peloids
Lithic
Microbial
Ooids
Type 1-1/3
Type 3-4
Oncoids
Type I
Type II
Type IIIa
Type IIIb
Type IVa
Type IVb
Intraclasts
Aggregate & compound grains
Benthic foraminifera
Gastropods
Ostracods
Bivalves
Brachiopods
Echinoderms
Green algae
Strm-Cht-Corals
Serpulids
Sponge spicules
Depositional subenvironment
Prox.
Dist.
I L B S F OP OD
m M W P G D

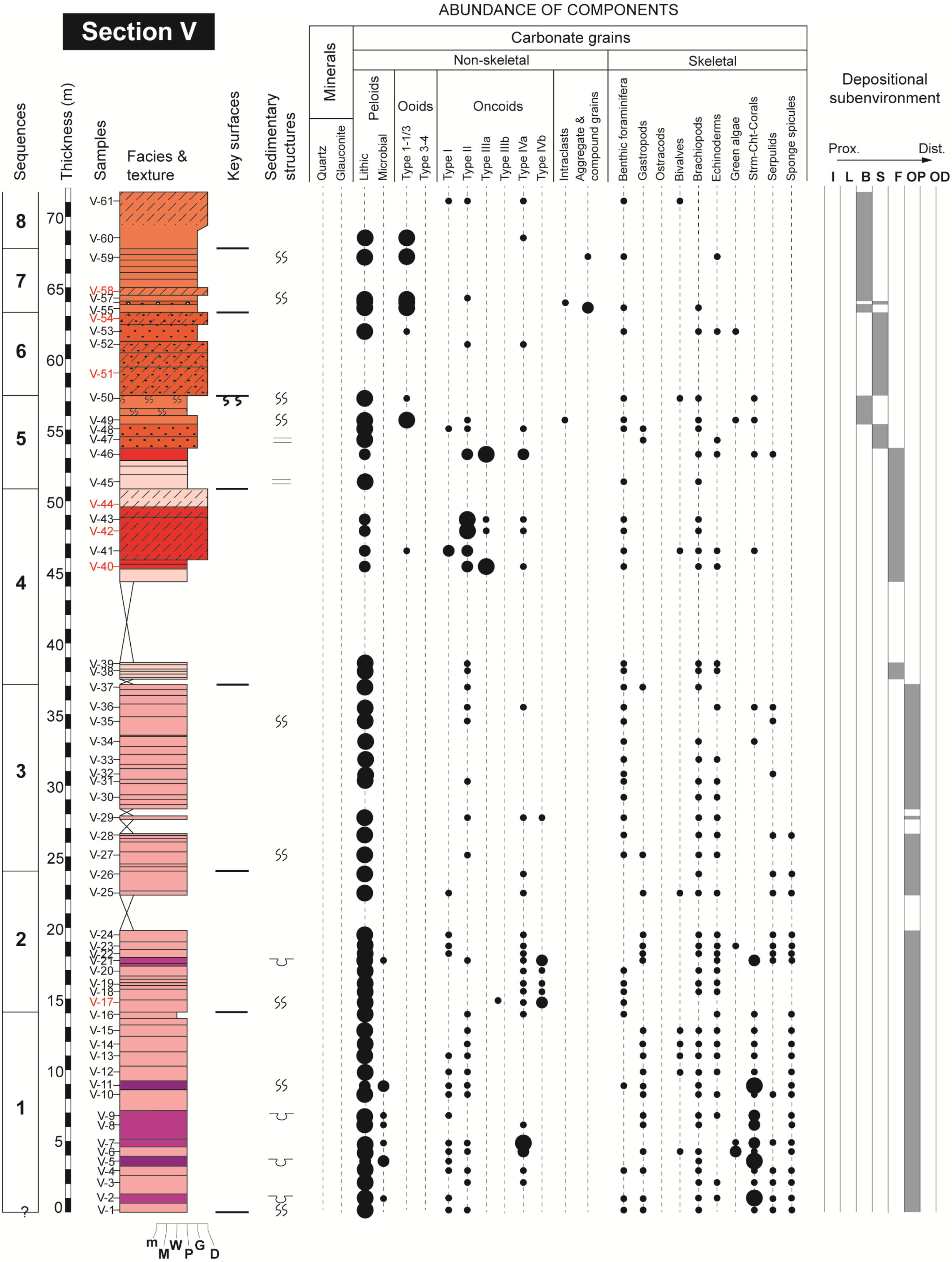
Section V
ABUNDANCE OF COMPONENTS
Minerals
Quartz
Glauconite
Carbonate grains
Non-skeletal
Peloids
Lithic
Microbial
Ooids
Type 1-1/3
Type 3-4
Oncoids
Type I
Type II
Type IIIa
Type IIIb
Type IVa
Type IVb
Intraclasts
Aggregate & compound grains
Skeletal
Benthic foraminifera
Gastropods
Ostracods
Bivalves
Brachiopods
Echinoderms
Green algae
Strm-Cht-Corals
Serpulids
Sponge spicules
Depositional subenvironment
Prox.
Dist.
I L B S F OP OD
Sequences
Thickness (m)
Samples
Facies & texture
Key surfaces
Sedimentary structures
m M W P G D

CENTRAL CROSS-SECTION (Mezalocha-Puebla de Albortón sector)

Sections situated around the localities of Mezalocha (ME1 to ME3), Fuendetodos (F2 and F3) and Puebla de Albortón (P1 to P3). The field pictures included in this section are representative of the Higueruelas Fm in each sector. Below, the position of the central cross-section in the study area, and the legend for the information included in the sedimentary logs.

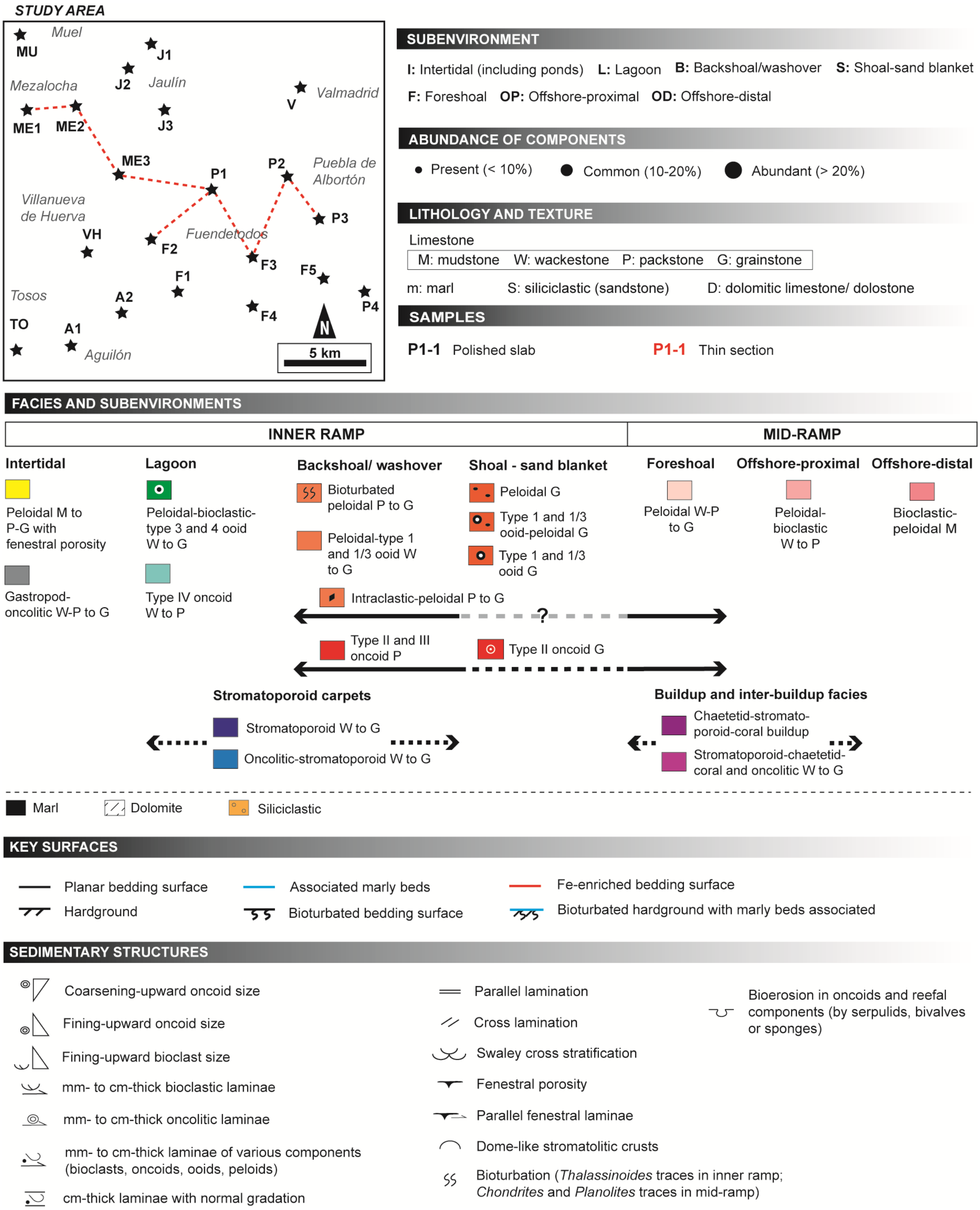

Field pictures

Mezalocha sector

Sequences 1-3 in section ME1 (top) and 2-4 in section ME3 (bottom) of the Higueruelas Fm in Mezalocha sector. In section ME1, the boundary with the underlying Loriguilla Fm is indicated (dashed line).

Fuendetodos sector

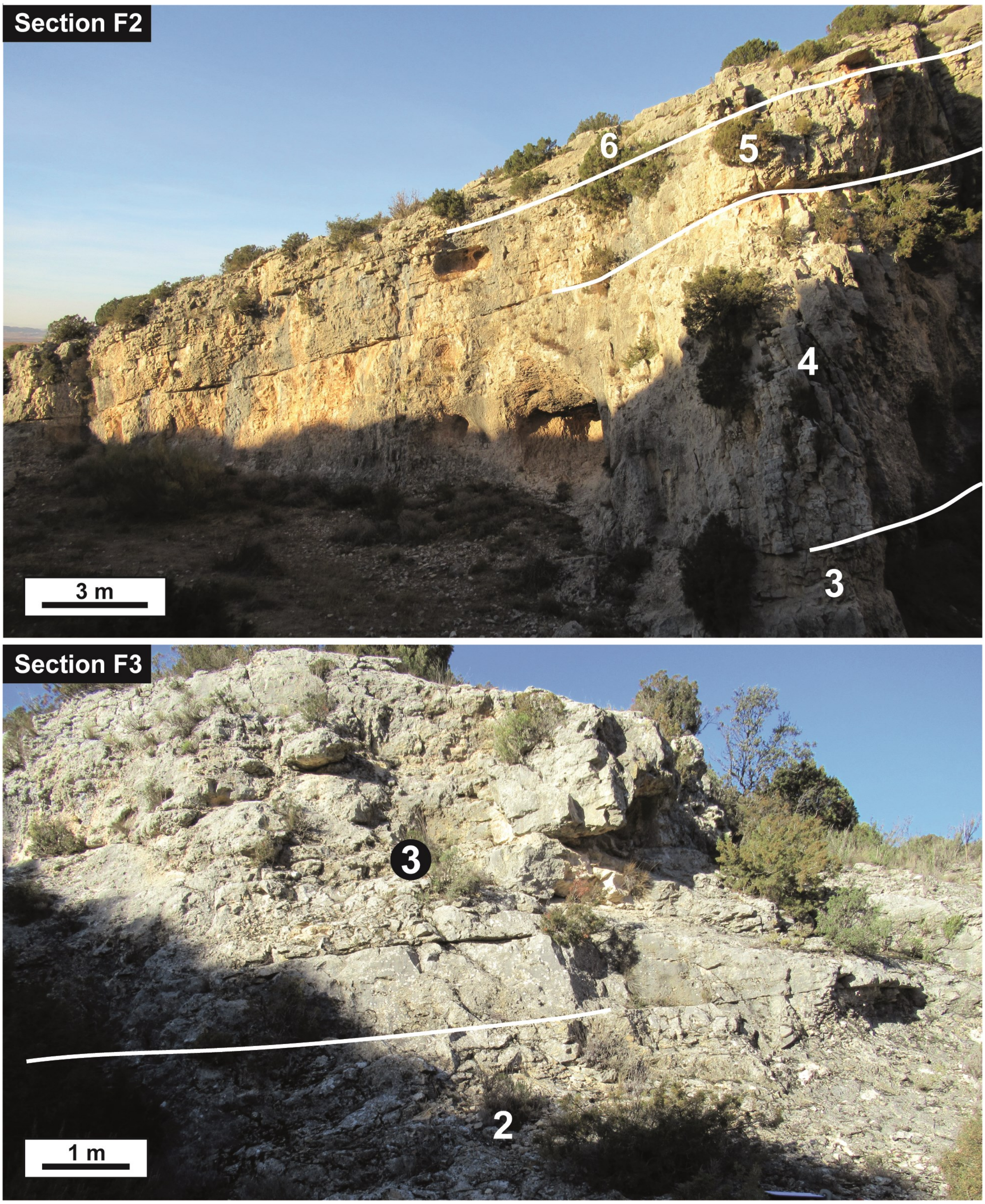

Sequences 3-6 in section F2 (top) and 2-3 in section F3 (bottom) of the Higueruelas Fm in Fuendetodos sector.

Puebla de Albortón sector

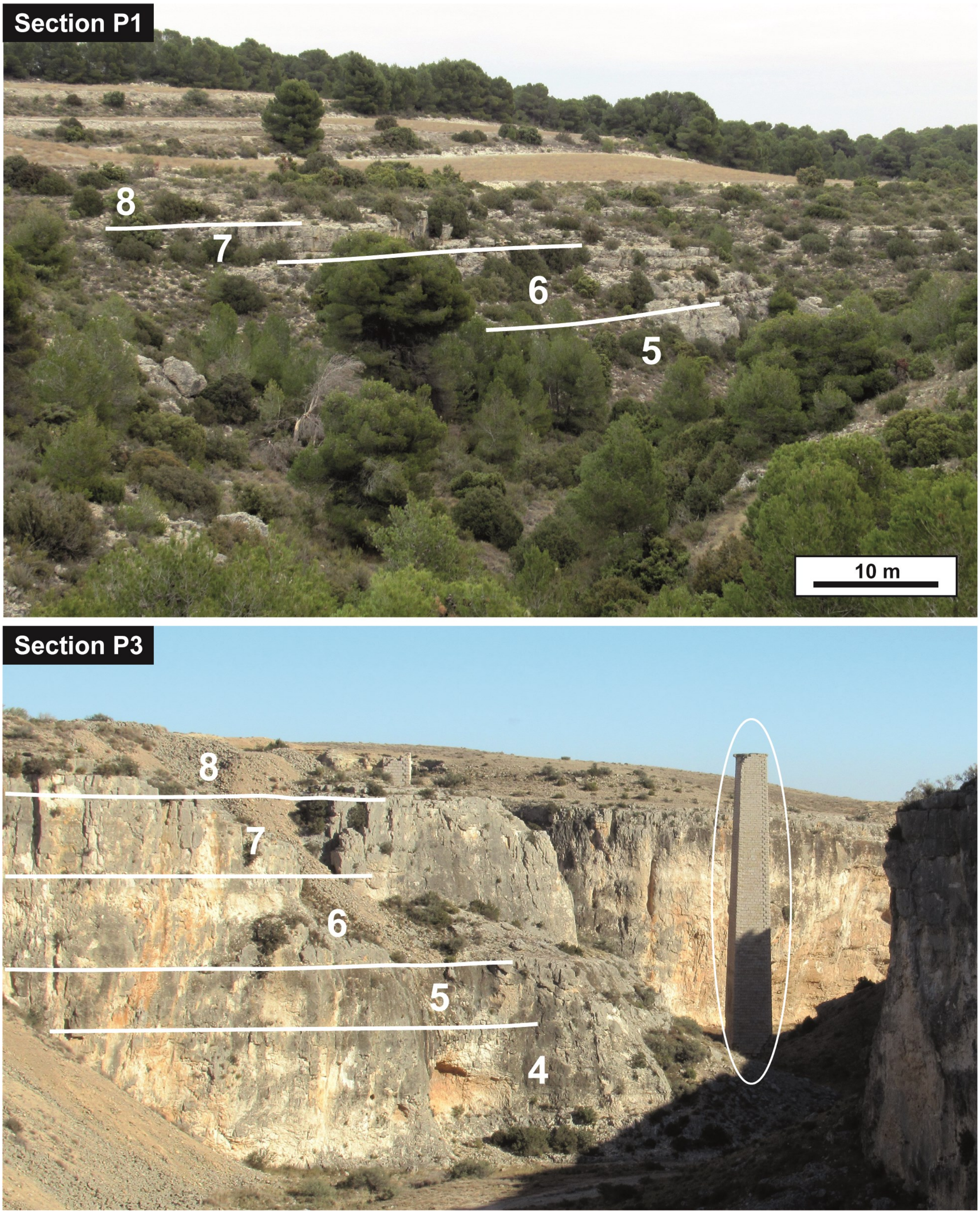

The Higueruelas Fm in Puebla de Albortón sector, for sections P1 (top, sequences 5-8) and P3 (bottom, sequences 4 -8; for scale, the column within the circle is around 30 m high).

Logs and sample location

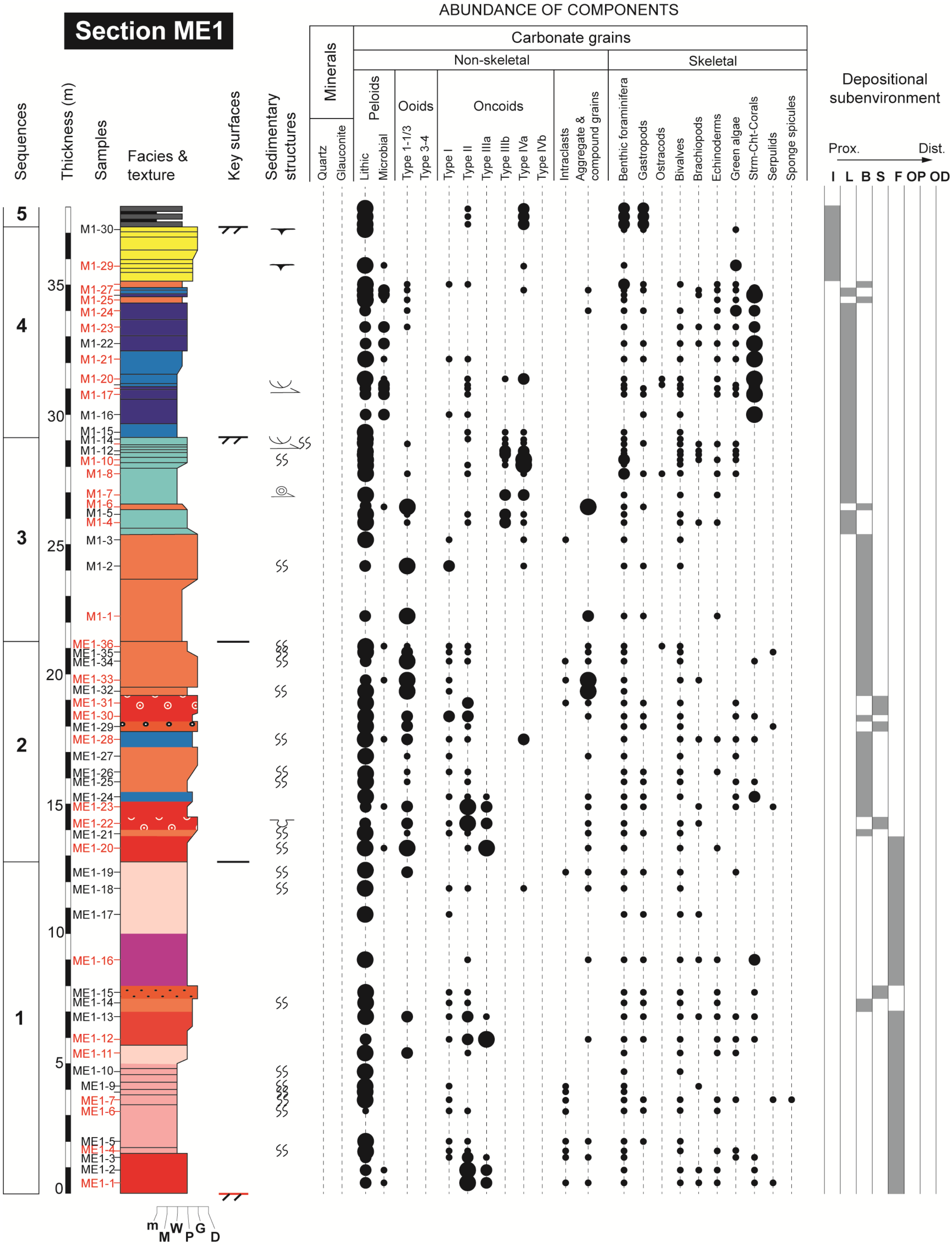

Sequences 3-5 of this section correspond to sequences A to F of the sections M1 (A-E) and M2 (F) of the upper 10-16 m thick of the succession outcropping in Mezalocha sector.

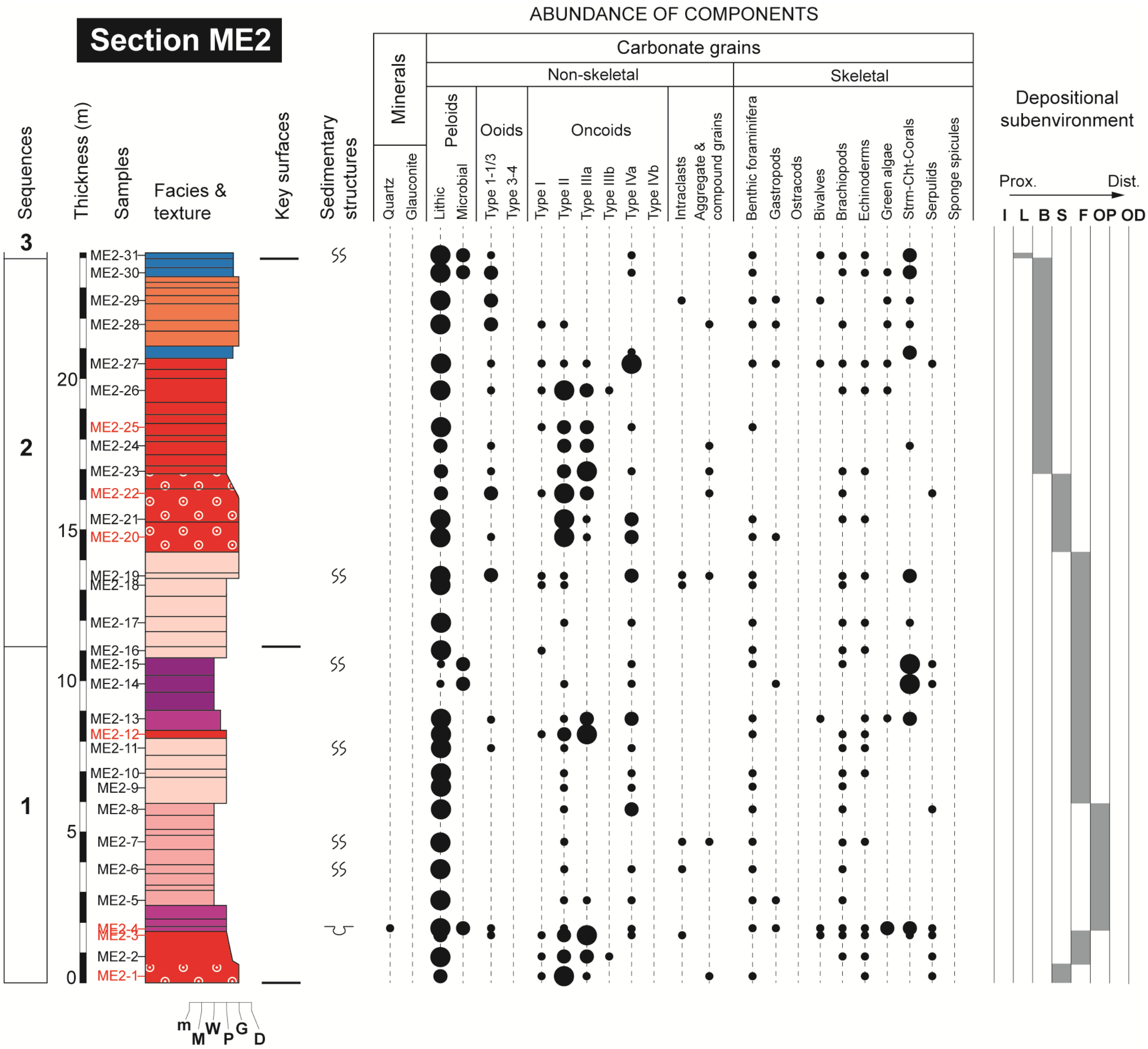
Section ME2
ABUNDANCE OF COMPONENTS
Minerals
Carbonate grains
Non-skeletal
Skeletal
Sequences
Thickness (m)
Samples
Facies & texture
Key surfaces
Sedimentary structures
Quartz
Glauconite
Peloids
Lithic
Microbial
Ooids
Type 1-1/3
Type 3-4
Oncoids
Type I
Type II
Type IIIa
Type IIIb
Type IVa
Type IVb
Intraclasts
Aggregate & compound grains
Benthic foraminifera
Gastropods
Ostracods
Bivalves
Brachiopods
Echinoderms
Green algae
Strm-Cht-Corals
Serpulids
Sponge spicules
Depositional subenvironment
Prox.
Dist.
I L B S F OP OD
3
2
1
0
5
10
15
20
ME2-31
ME2-30
ME2-29
ME2-28
ME2-27
ME2-26
ME2-25
ME2-24
ME2-23
ME2-22
ME2-21
ME2-20
ME2-19
ME2-18
ME2-17
ME2-16
ME2-15
ME2-14
ME2-13
ME2-12
ME2-11
ME2-10
ME2-9
ME2-8
ME2-7
ME2-6
ME2-5
ME2-4
ME2-3
ME2-2
ME2-1
m M W P G D

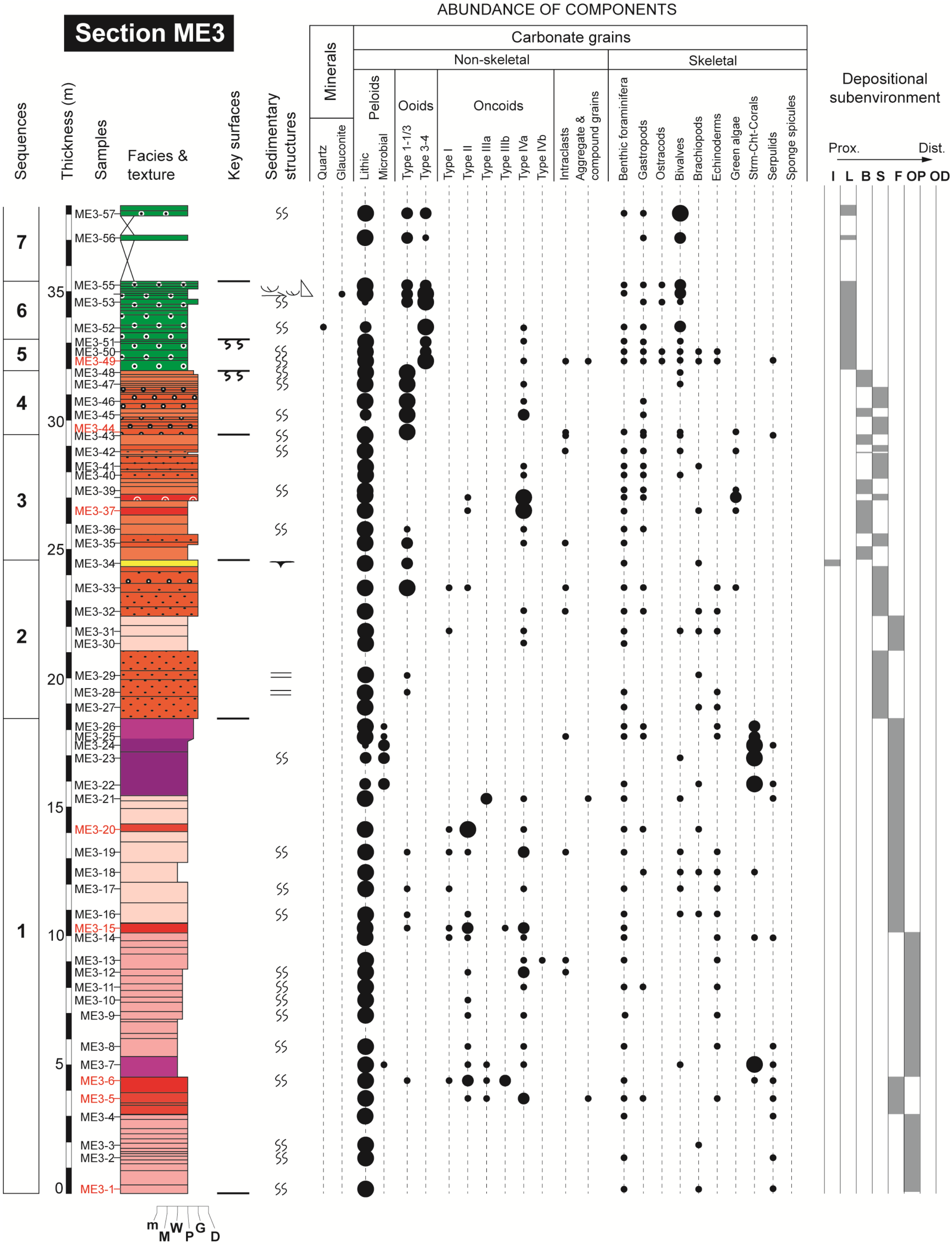
Section ME3
ABUNDANCE OF COMPONENTS
Minerals
Carbonate grains
Non-skeletal
Skeletal
Sequences
Thickness (m)
Samples
Facies & texture
Key surfaces
Sedimentary structures
Quartz
Glauconite
Peloids
Lithic
Microbial
Ooids
Type 1-1/3
Type 3-4
Oncoids
Type I
Type II
Type IIIa
Type IIIb
Type IVa
Type IVb
Intraclasts
Aggregate & compound grains
Benthic foraminifera
Gastropods
Ostracods
Bivalves
Brachiopods
Echinoderms
Green algae
Strm-Cht-Corals
Serpulids
Sponge spicules
Depositional subenvironment
Prox.
Dist.
I L B S F OP OD
m M W P G D

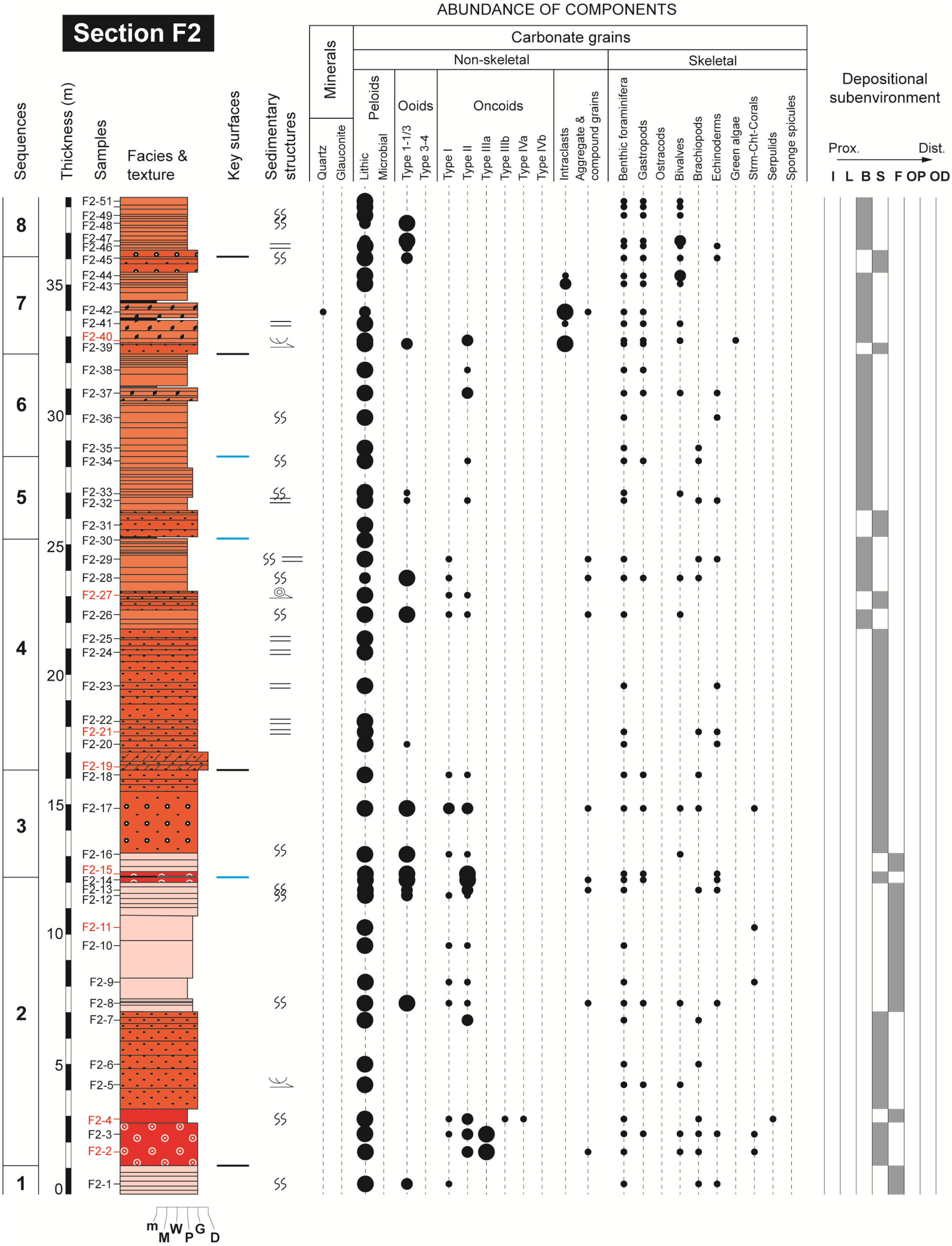

Section F2
ABUNDANCE OF COMPONENTS
Minerals
Carbonate grains
Non-skeletal
Skeletal
Sequences
Thickness (m)
Samples
Facies & texture
Key surfaces
Sedimentary structures
Quartz
Glauconite
Peloids
Lithic
Microbial
Ooids
Type 1-1/3
Type 3-4
Oncoids
Type I
Type II
Type IIIa
Type IIIb
Type IVa
Type IVb
Intraclasts
Aggregate & compound grains
Benthic foraminifera
Gastropods
Ostracods
Bivalves
Brachiopods
Echinoderms
Green algae
Strm-Cht-Corals
Serpulids
Sponge spicules
Depositional subenvironment
Prox.
Dist.
I L B S F OP OD
m M W P G D

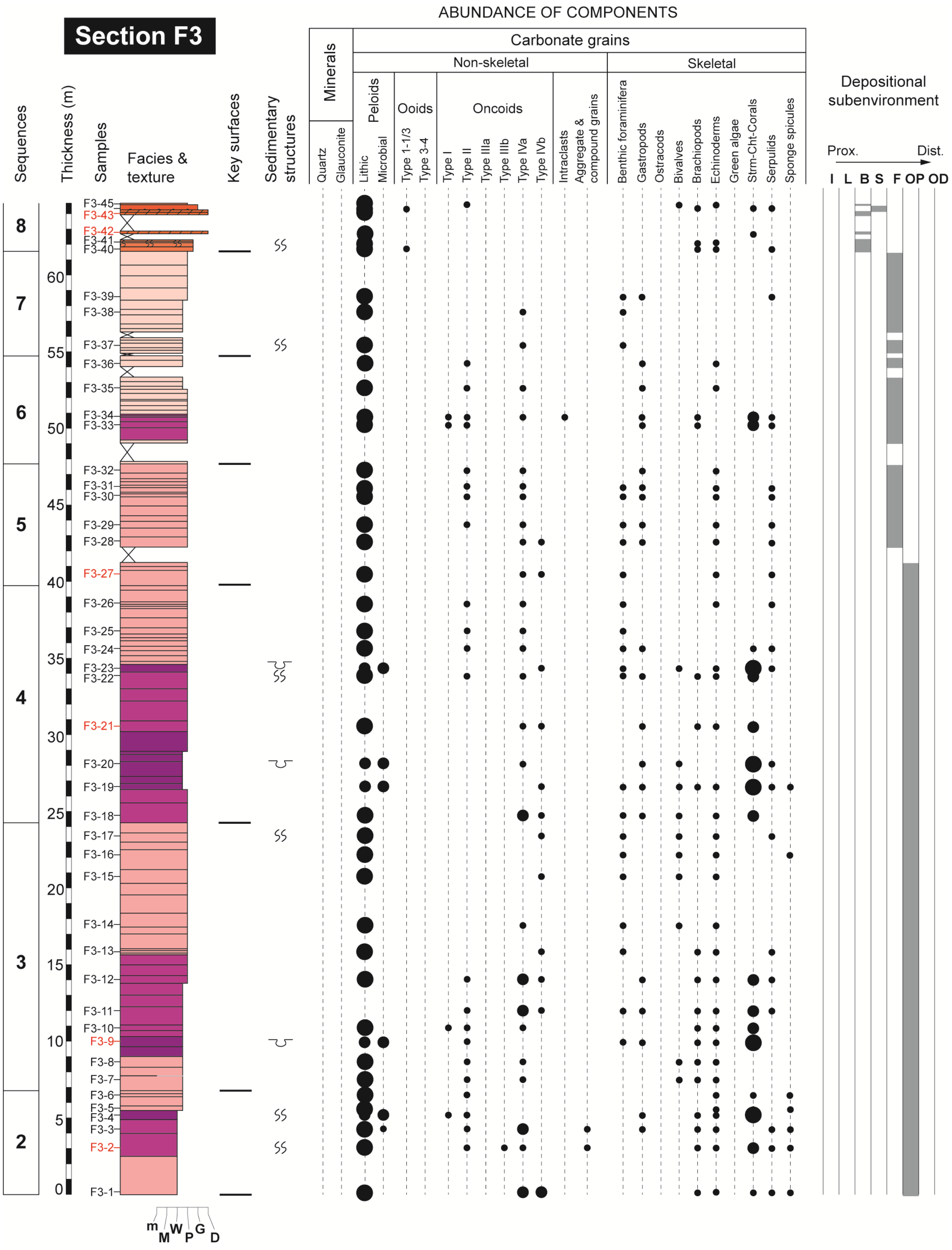
Section F3
ABUNDANCE OF COMPONENTS
Minerals
Carbonate grains
Non-skeletal
Skeletal
Sequences
Thickness (m)
Samples
Facies & texture
Key surfaces
Sedimentary structures
Quartz
Glauconite
Peloids
Lithic
Microbial
Ooids
Type 1-1/3
Type 3-4
Oncoids
Type I
Type II
Type IIIa
Type IIIb
Type IVa
Type IVb
Intraclasts
Aggregate & compound grains
Benthic foraminifera
Gastropods
Ostracods
Bivalves
Brachiopods
Echinoderms
Green algae
Strm-Cht-Corals
Serpulids
Sponge spicules
Depositional subenvironment
Prox.
Dist.
I L B S F OP OD
m M W P G D

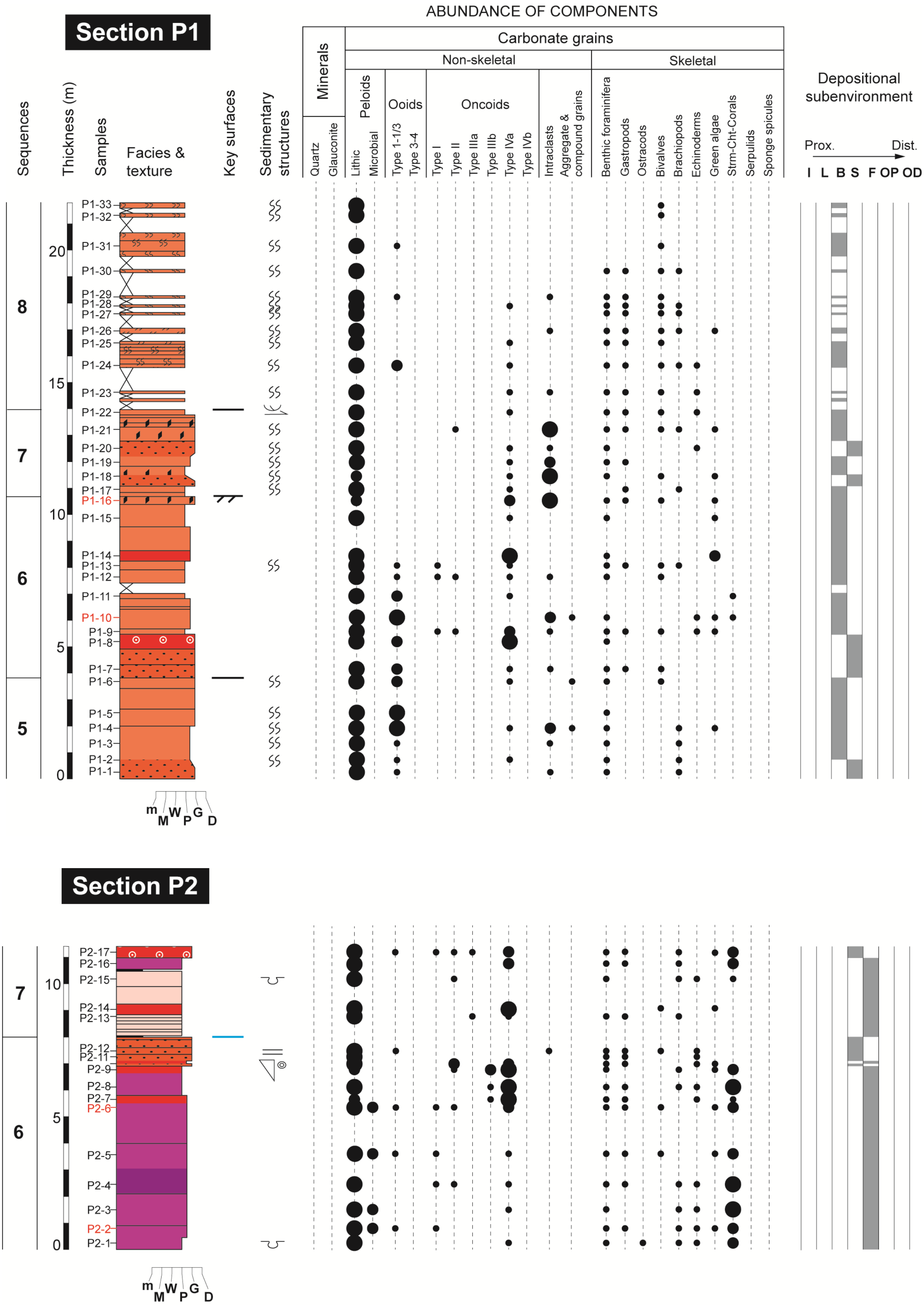
Section P1
ABUNDANCE OF COMPONENTS
Minerals
Carbonate grains
Non-skeletal
Skeletal
Sequences
Thickness (m)
Samples
Facies & texture
Key surfaces
Sedimentary structures
Quartz
Glauconite
Peloids
Lithic
Microbial
Ooids
Type 1-1/3
Type 3-4
Oncoids
Type I
Type II
Type IIIa
Type IIIb
Type IVa
Type IVb
Intraclasts
Aggregate & compound grains
Benthic foraminifera
Gastropods
Ostracods
Bivalves
Brachiopods
Echinoderms
Green algae
Strm-Cht-Corals
Serpulids
Sponge spicules
Depositional subenvironment
Prox.
Dist.
I L B S F OP OD
8
7
6
5
0
5
10
15
20
P1-33
P1-32
P1-31
P1-30
P1-29
P1-28
P1-27
P1-26
P1-25
P1-24
P1-23
P1-22
P1-21
P1-20
P1-19
P1-18
P1-17
P1-16
P1-15
P1-14
P1-13
P1-12
P1-11
P1-10
P1-9
P1-8
P1-7
P1-6
P1-5
P1-4
P1-3
P1-2
P1-1
m M W P G D
Section P2
7
6
0
5
10
P2-17
P2-16
P2-15
P2-14
P2-13
P2-12
P2-11
P2-9
P2-8
P2-7
P2-6
P2-5
P2-4
P2-3
P2-2
P2-1
m M W P G D

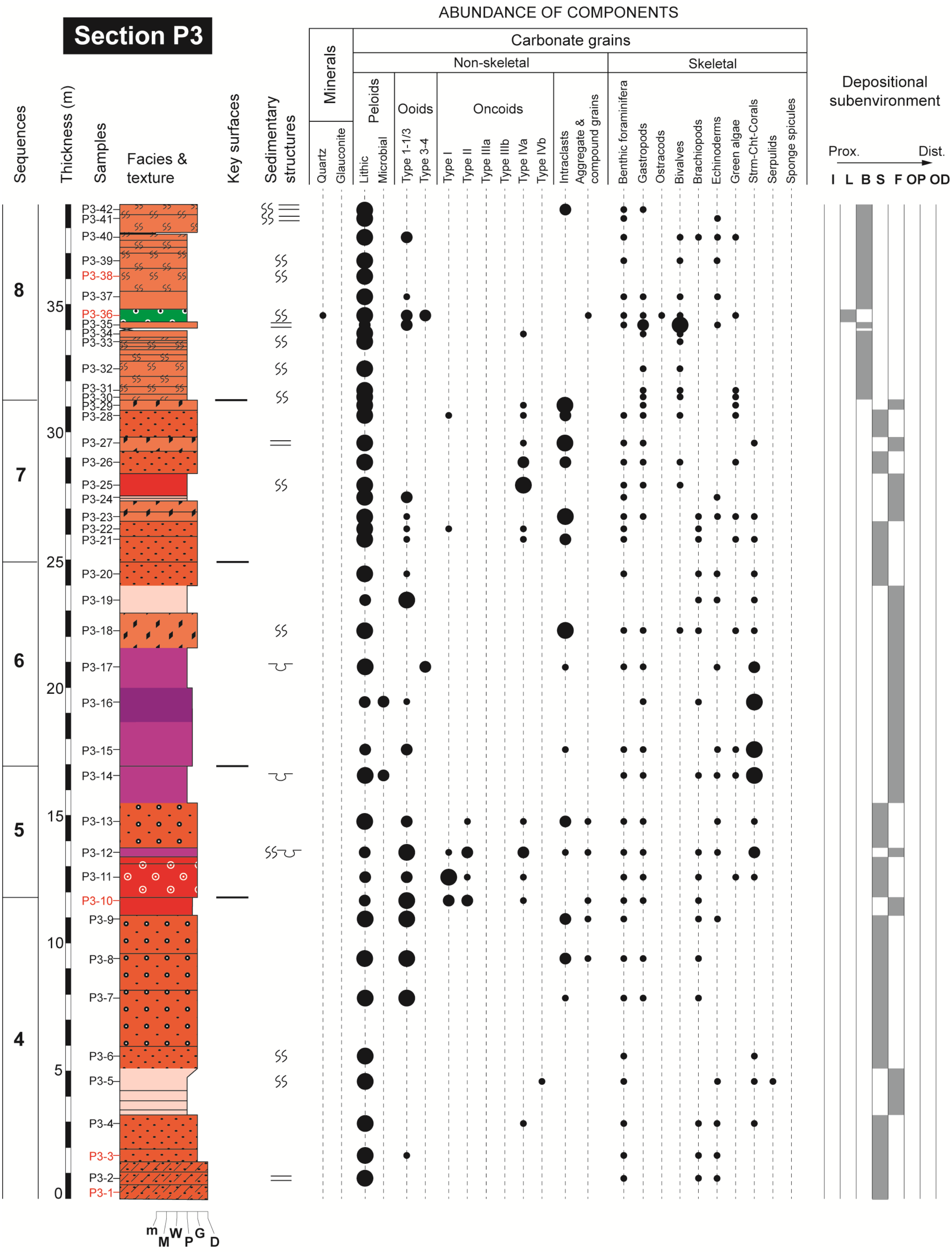
Section P3
ABUNDANCE OF COMPONENTS
Minerals
Carbonate grains
Non-skeletal
Skeletal
Depositional subenvironment
Sequences
Thickness (m)
Samples
Facies & texture
Key surfaces
Sedimentary structures
Quartz
Glauconite
Peloids
Lithic
Microbial
Ooids
Type 1-1/3
Type 3-4
Oncoids
Type I
Type II
Type IIIa
Type IIIb
Type IVa
Type IVb
Intraclasts
Aggregate & compound grains
Benthic foraminifera
Gastropods
Ostracods
Bivalves
Brachiopods
Echinoderms
Green algae
Strm-Cht-Corals
Serpulids
Sponge spicules
Prox.
Dist.
I L B S F OP OD
m M W P G D

SOUTHERN CROSS-SECTION (Tosos-Puebla de Albortón sector)

Sections situated around the localities of Tosos (TO), Aguilón (A1 and A2), Villanueva de Huerva (VH), Fuendetodos (F1, F4 and F5) and Puebla de Albortón (P4). The field pictures included in this section are representative of the Higueruelas Fm in each sector. Below, the position of the southern cross-section in the study area, and the legend for the information included in the sedimentary logs.

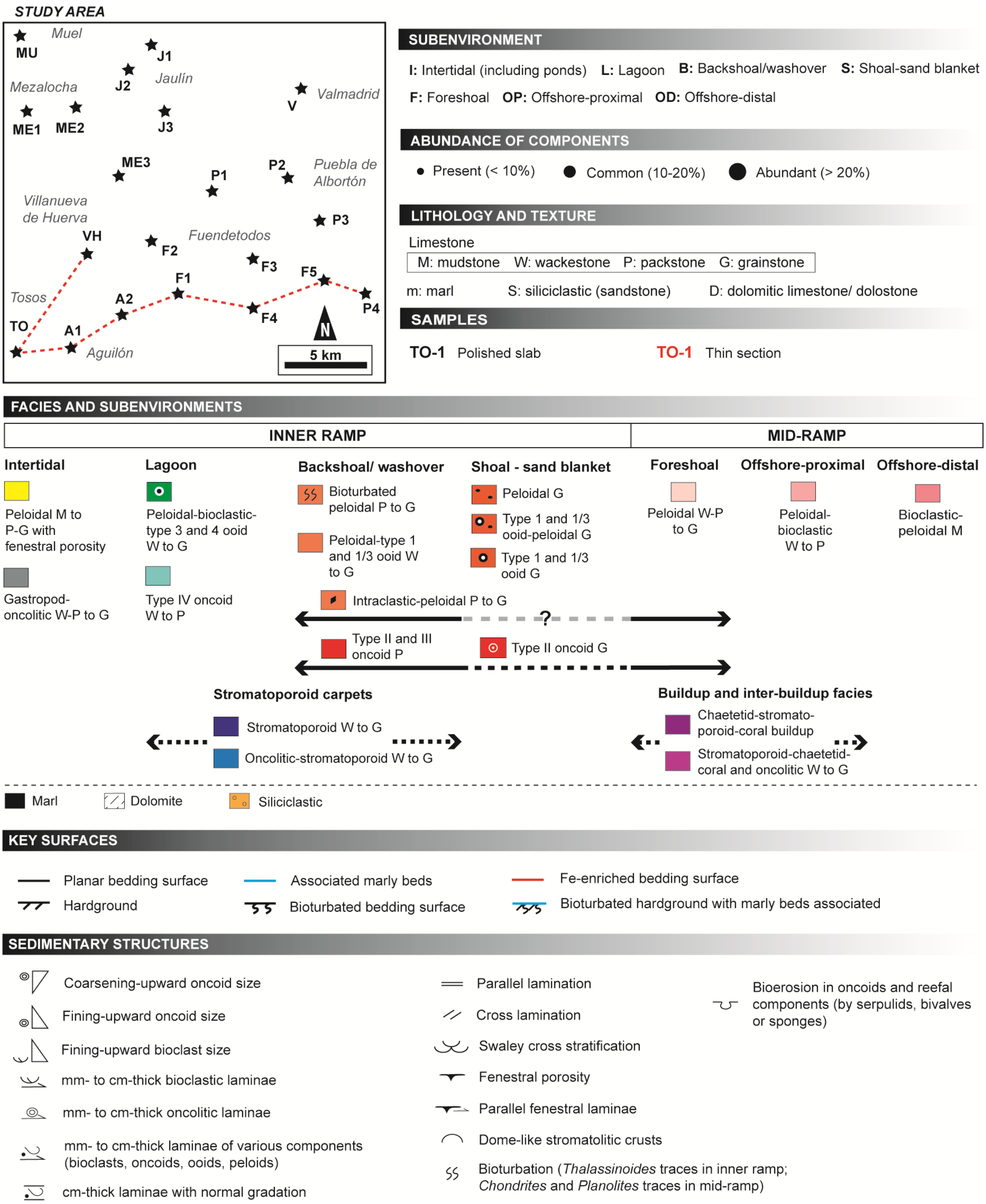

Field pictures

Tosos sector

The Higueruelas Fm in Tosos sector (section TO), with the identification of 7 sequences (top, sequences 1-5; bottom, sequences 3-7). The boundary with the overlying coastal-siliciclastic unit is indicated (bottom, dashed line).

Aguilón sector

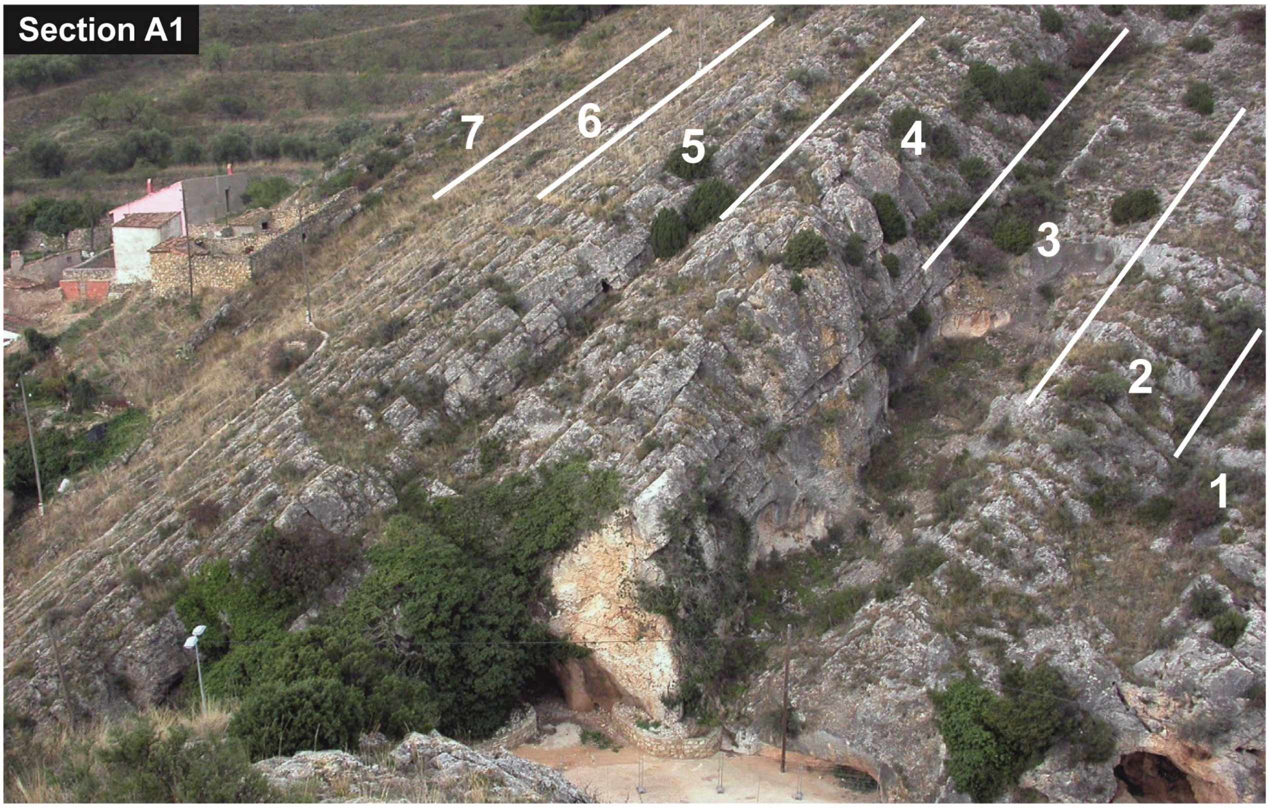

The Higueruelas Fm in sections A1 (top) and A2 (bottom) in Aguilón sector, with in both the recognition of 7 sequences (1-7).

Fuendetodos sector

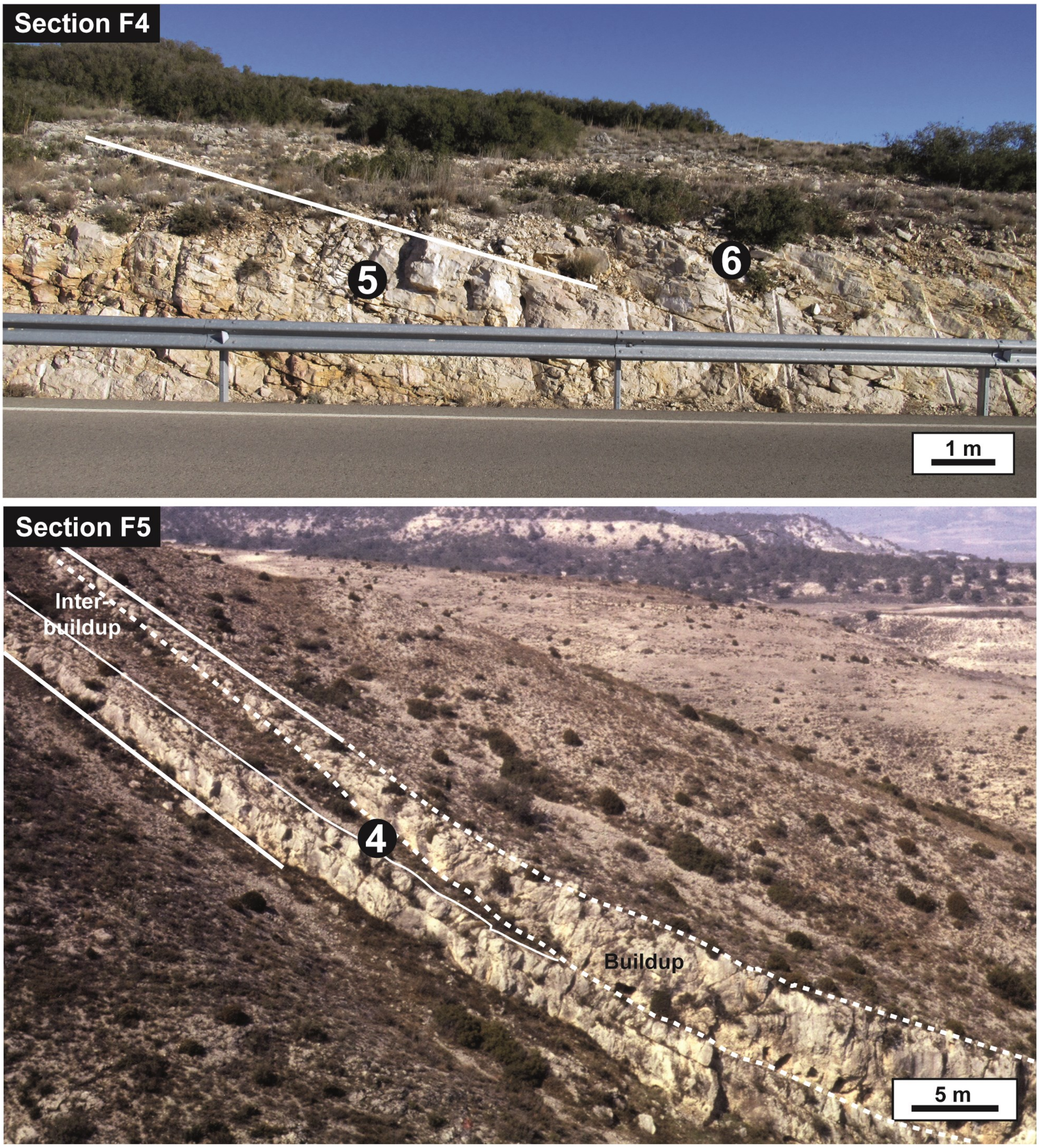

Sequences 5-6 in section F4 (top) and sequence 4 in section F5 (bottom) from Fuendetodos sector. The upper part of sequence 4 in section F5 records the development of buildup (dashed lines) and inter-buildup facies, showing the buildup a low-angle lenticular geometry (picture of section F5 is modified from Bádenas and Aurell, 2003).

Puebla de Albortón sector

The Higueruelas Fm in section P4 from Puebla de Albortón sector, recording sequences 2 to 9. Note the lenticular geometry of buildups in sequence 7 (dashed line).

Villanueva de Huerva sector

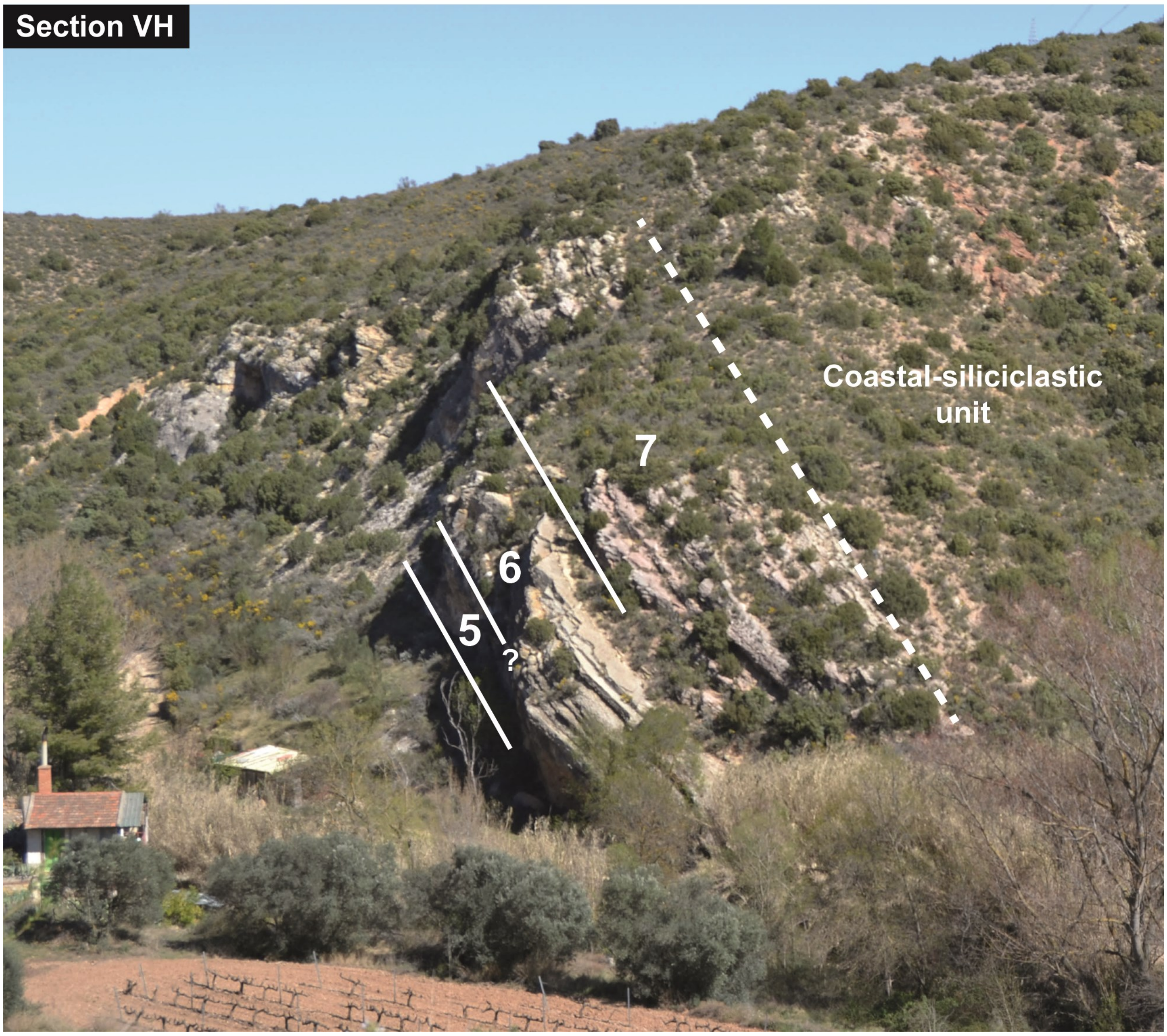

The Higueruelas Fm in Villanueva de Huerva sector (section VH, sequence 5 to 7). The boundary with the overlying coastal-siliciclastic unit is indicated (dashed line).

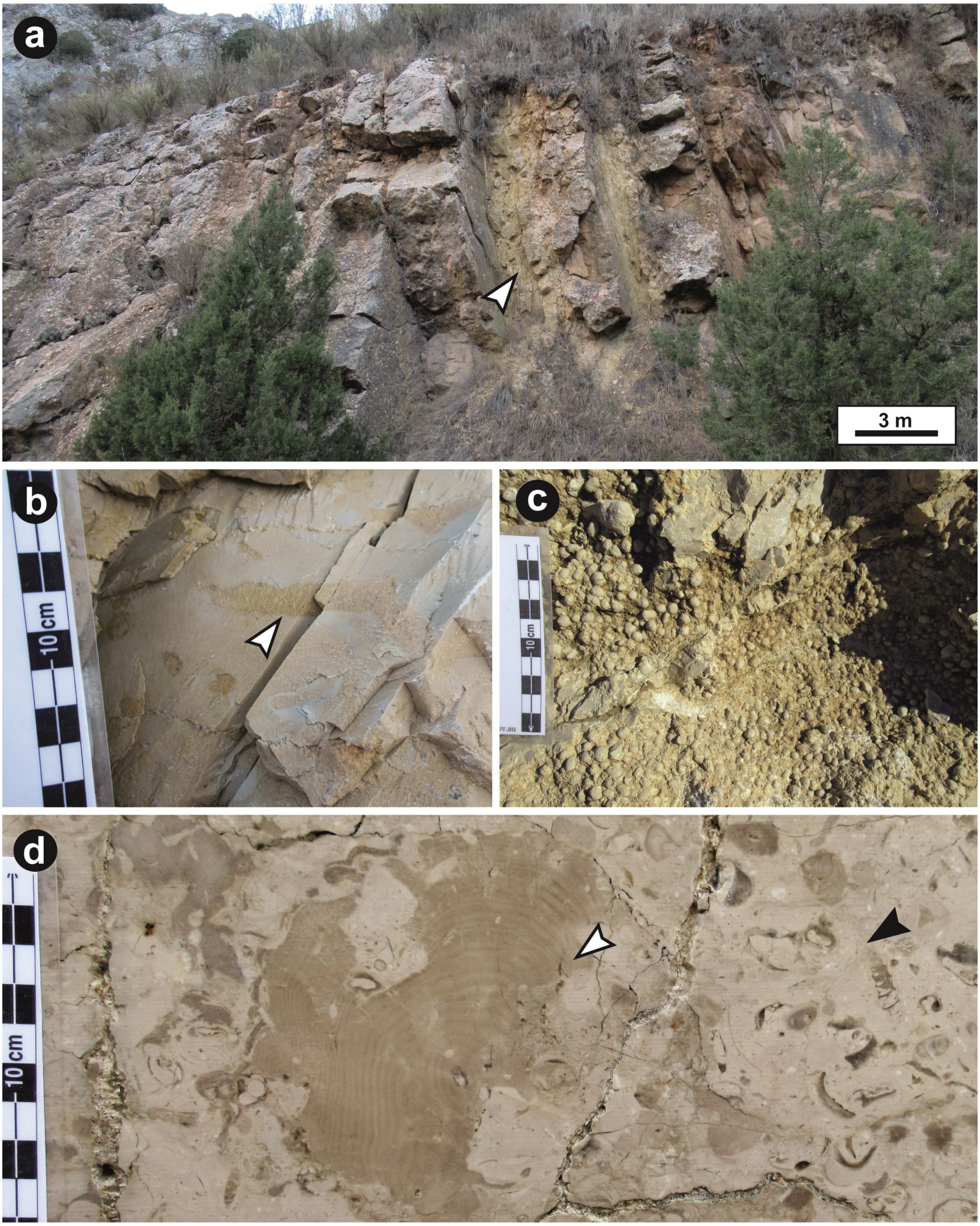

a) Field view of restricted lagoon facies on top of section TO (sequence 7), with intercalations of siliciclastic deposits (arrow). b) Planolites *traces (arrow) in offshore-proximal peloidal-bioclastic facies in section F4 (sequence 2). c) Field view of foreshoal type II and III oncoid facies in section F4 (sequence 6), with well-rounded oncoids constituting an oncolitic-supported texture. d) Field view of foreshoal inter-buildup facies in section P4 (laterally to buildup facies in sequence 7), showing large fragments of chaetetids (white arrow) within a matrix composed of oncoids and a high diversity of bioclasts (black arrow).*

Logs and sample location

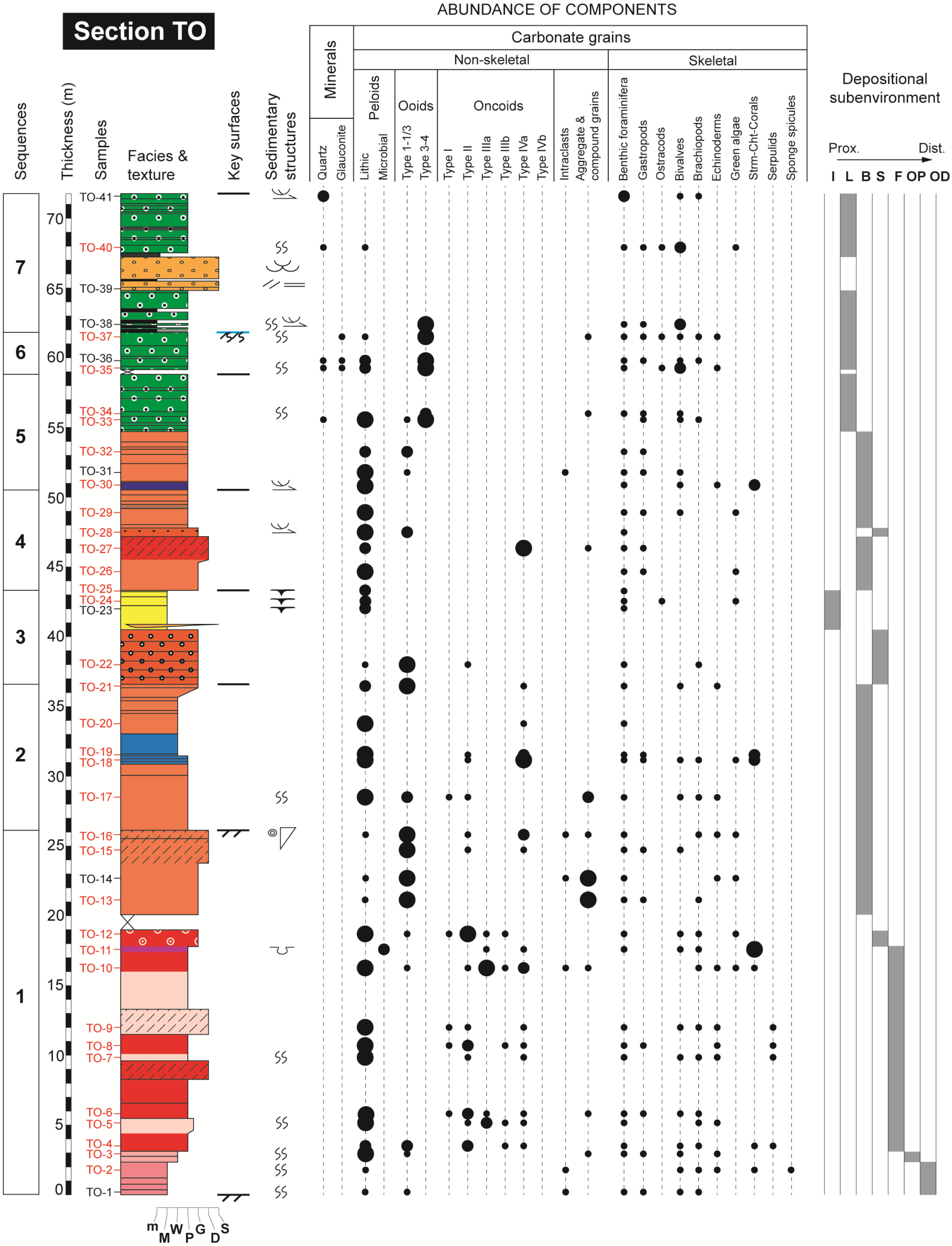

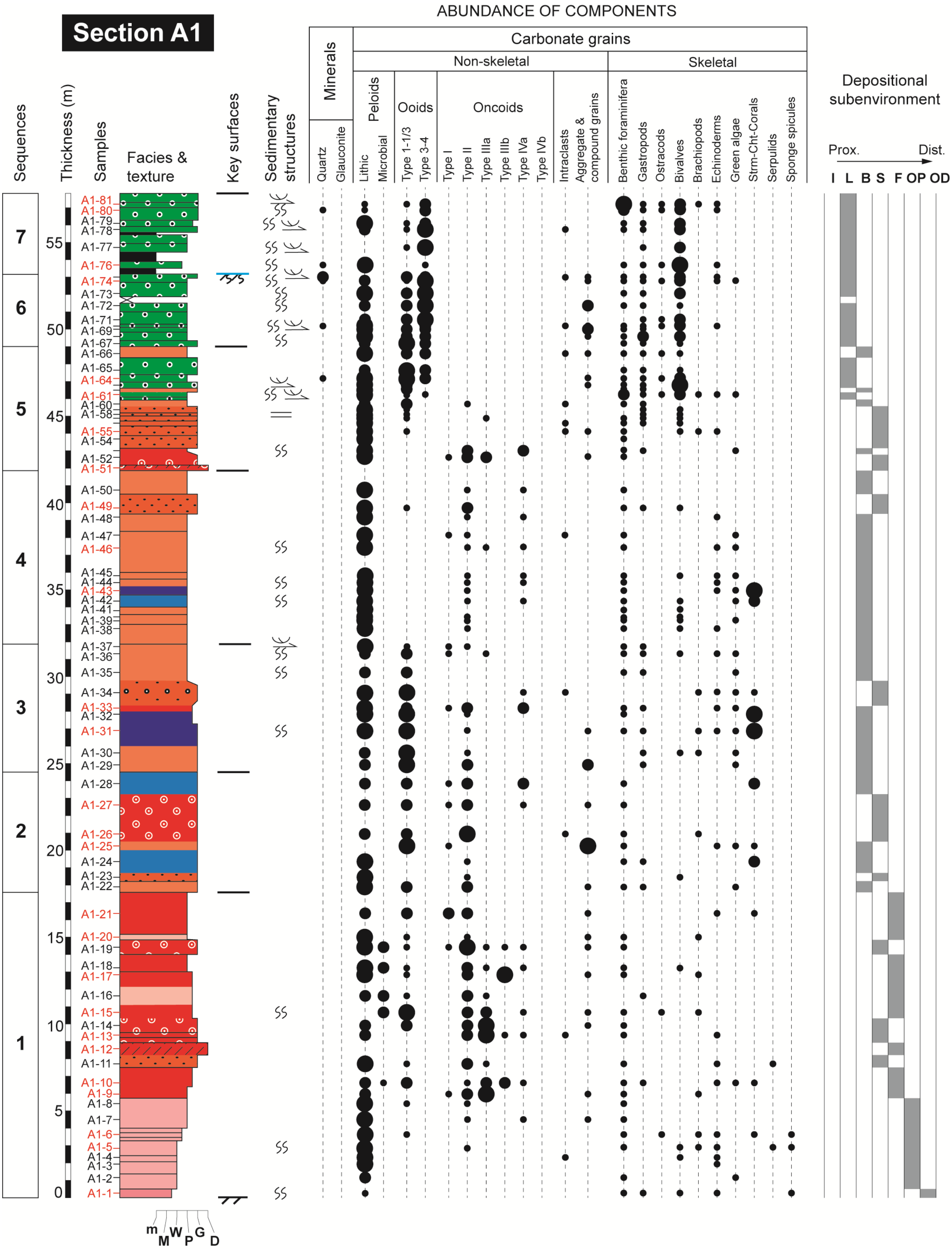
Section A1
ABUNDANCE OF COMPONENTS
Sequences
Thickness (m)
Samples
Facies & texture
Key surfaces
Sedimentary structures
Minerals
Quartz
Glauconite
Carbonate grains
Non-skeletal
Skeletal
Peloids
Lithic
Microbial
Ooids
Type 1-1/3
Type 3-4
Oncoids
Type I
Type II
Type IIIa
Type IIIb
Type IVa
Type IVb
Intraclasts
Aggregate & compound grains
Benthic foraminifera
Gastropods
Ostracods
Bivalves
Brachiopods
Echinoderms
Green algae
Strm-Cht-Corals
Serpulids
Sponge spicules
Depositional subenvironment
Prox.
Dist.
I L B S F OP OD
m M W P G D

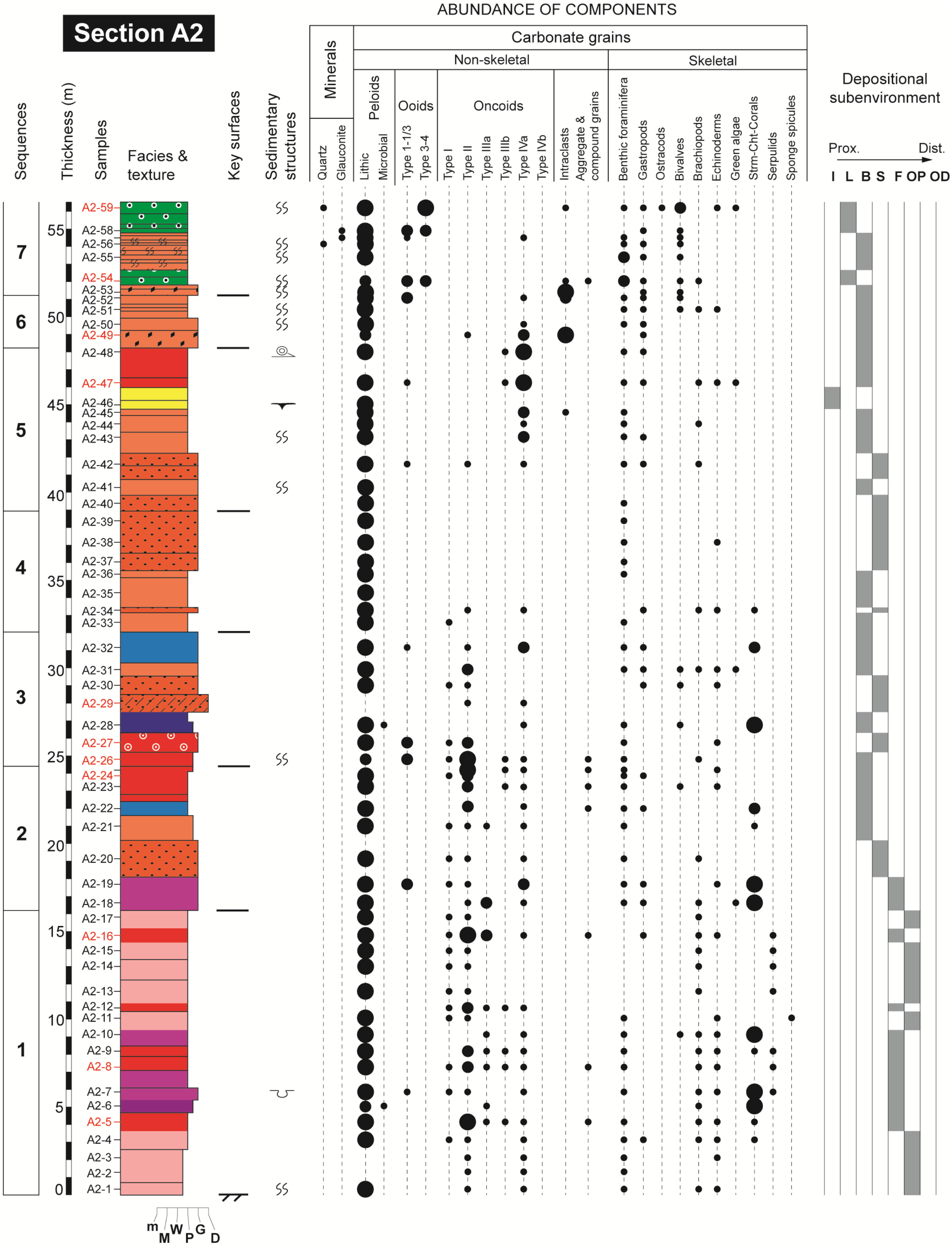
Section A2
ABUNDANCE OF COMPONENTS
Minerals
Carbonate grains
Non-skeletal
Skeletal
Sequences
Thickness (m)
Samples
Facies & texture
Key surfaces
Sedimentary structures
Quartz
Glauconite
Peloids
Lithic
Microbial
Ooids
Type 1-1/3
Type 3-4
Oncoids
Type I
Type II
Type IIIa
Type IIIb
Type IVa
Type IVb
Intraclasts
Aggregate & compound grains
Benthic foraminifera
Gastropods
Ostracods
Bivalves
Brachiopods
Echinoderms
Green algae
Strm-Cht-Corals
Serpulids
Sponge spicules
Depositional subenvironment
Prox.
Dist.
I L B S F OP OD
7
6
5
4
3
2
1
55
50
45
40
35
30
25
20
15
10
5
0
A2-59
A2-58
A2-56
A2-55
A2-54
A2-53
A2-52
A2-51
A2-50
A2-49
A2-48
A2-47
A2-46
A2-45
A2-44
A2-43
A2-42
A2-41
A2-40
A2-39
A2-38
A2-37
A2-36
A2-35
A2-34
A2-33
A2-32
A2-31
A2-30
A2-29
A2-28
A2-27
A2-26
A2-24
A2-23
A2-22
A2-21
A2-20
A2-19
A2-18
A2-17
A2-16
A2-15
A2-14
A2-13
A2-12
A2-11
A2-10
A2-9
A2-8
A2-7
A2-6
A2-5
A2-4
A2-3
A2-2
A2-1
m M W P G D

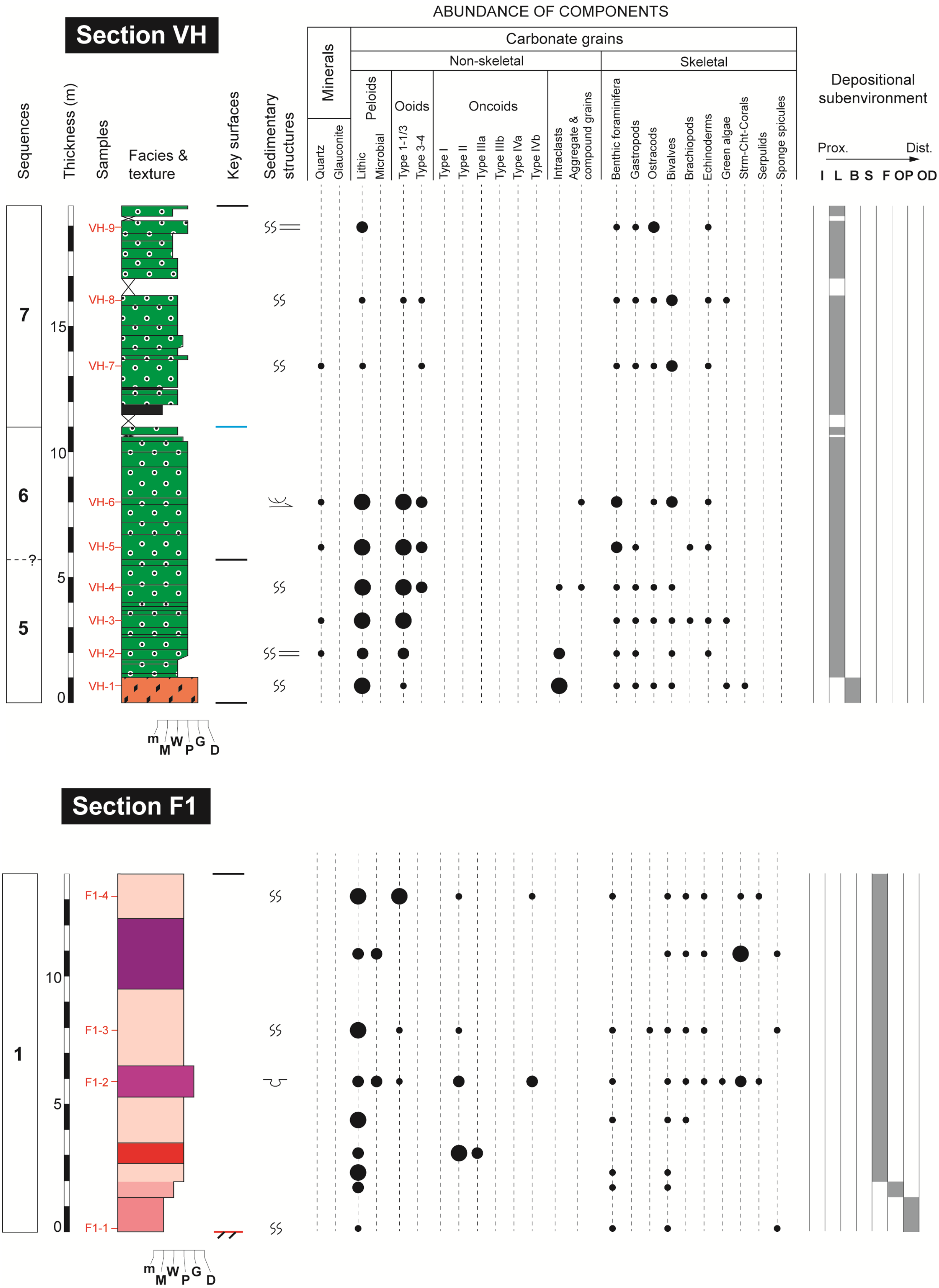

Section VH
ABUNDANCE OF COMPONENTS
Minerals
Carbonate grains
Non-skeletal
Skeletal
Sequences
Thickness (m)
Samples
Facies & texture
Key surfaces
Sedimentary structures
Quartz
Glauconite
Peloids
Lithic
Microbial
Ooids
Type 1-1/3
Type 3-4
Oncoids
Type I
Type II
Type IIIa
Type IIIb
Type IVa
Type IVb
Intraclasts
Aggregate & compound grains
Benthic foraminifera
Gastropods
Ostracods
Bivalves
Brachiopods
Echinoderms
Green algae
Strm-Cht-Corals
Serpulids
Sponge spicules
Depositional subenvironment
Prox.
Dist.
I L B S F OP OD
7
6
5
15
10
5
0
VH-9
VH-8
VH-7
VH-6
VH-5
VH-4
VH-3
VH-2
VH-1
m M W P G D
Section F1
1
10
5
0
F1-4
F1-3
F1-2
F1-1
m M W P G D

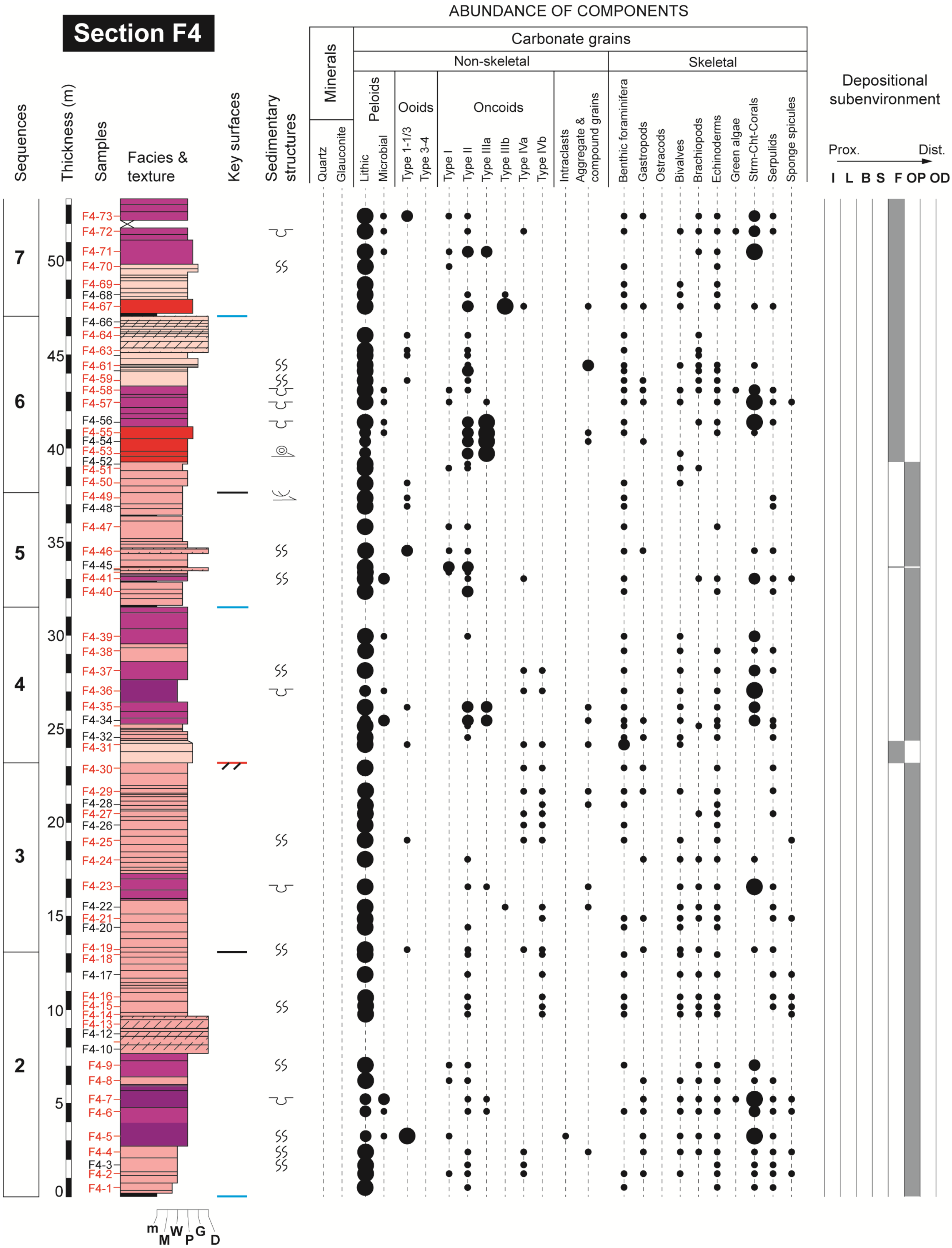
Section F4
ABUNDANCE OF COMPONENTS
Minerals
Carbonate grains
Non-skeletal
Skeletal
Sequences
Thickness (m)
Samples
Facies & texture
Key surfaces
Sedimentary structures
Quartz
Glauconite
Peloids
Lithic
Microbial
Ooids
Type 1-1/3
Type 3-4
Oncoids
Type I
Type II
Type IIIa
Type IIIb
Type IVa
Type IVb
Intraclasts
Aggregate & compound grains
Benthic foraminifera
Gastropods
Ostracods
Bivalves
Brachiopods
Echinoderms
Green algae
Strm-Cht-Corals
Serpulids
Sponge spicules
Depositional subenvironment
Prox.
Dist.
I L B S F OP OD
m M W P G D

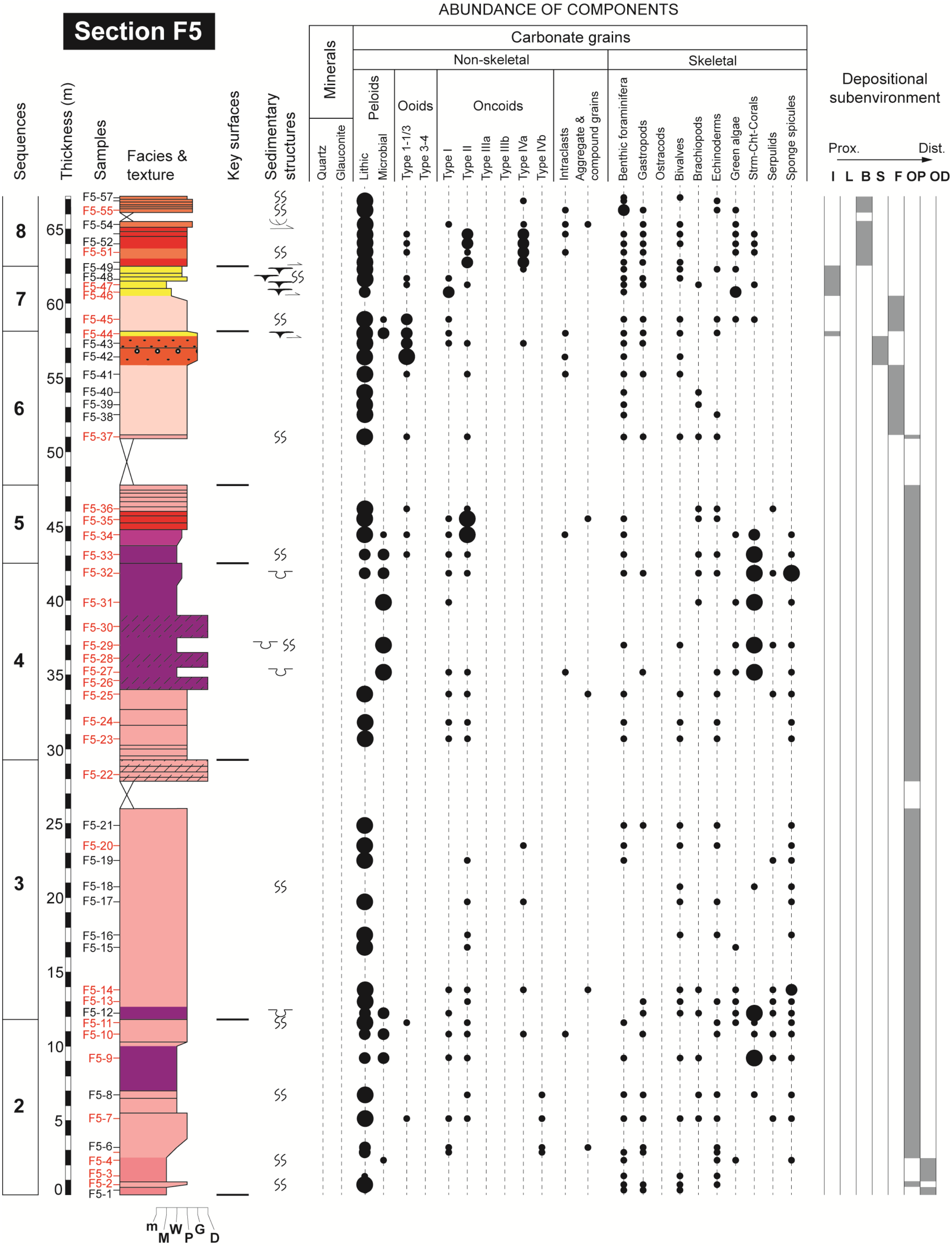

Section F5
ABUNDANCE OF COMPONENTS
Minerals
Carbonate grains
Non-skeletal
Skeletal
Sequences
Thickness (m)
Samples
Facies & texture
Key surfaces
Sedimentary structures
Quartz
Glauconite
Peloids
Lithic
Microbial
Ooids
Type 1-1/3
Type 3-4
Oncoids
Type I
Type II
Type IIIa
Type IIIb
Type IVa
Type IVb
Intraclasts
Aggregate & compound grains
Benthic foraminifera
Gastropods
Ostracods
Bivalves
Brachiopods
Echinoderms
Green algae
Strm-Cht-Corals
Serpulids
Sponge spicules
Depositional subenvironment
Prox.
Dist.
I L B S F OP OD
m M W P G D

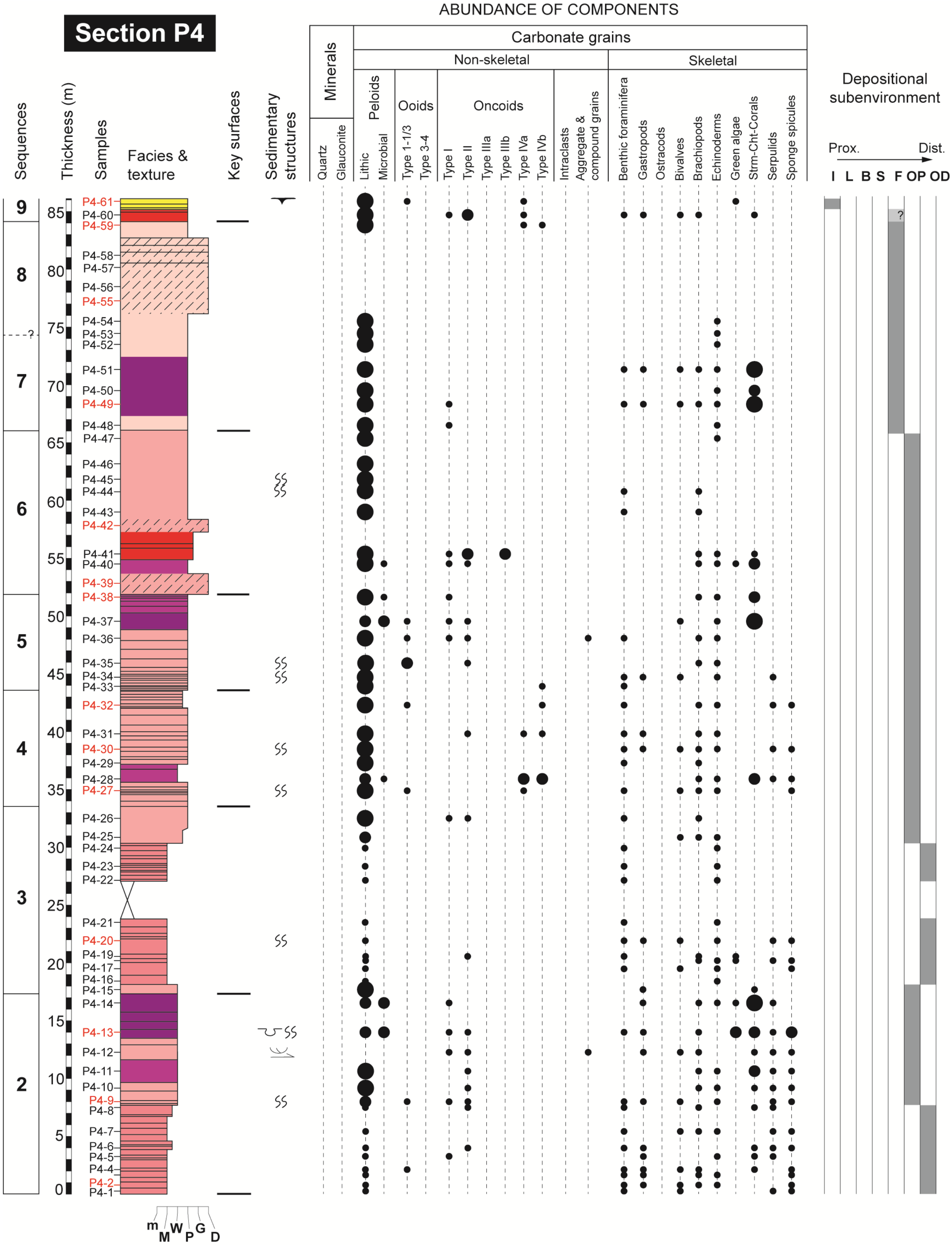

Section P4
ABUNDANCE OF COMPONENTS
Minerals
Carbonate grains
Non-skeletal
Skeletal
Sequences
Thickness (m)
Samples
Facies & texture
Key surfaces
Sedimentary structures
Quartz
Glauconite
Peloids
Lithic
Microbial
Ooids
Type 1-1/3
Type 3-4
Oncoids
Type I
Type II
Type IIIa
Type IIIb
Type IVa
Type IVb
Intraclasts
Aggregate & compound grains
Benthic foraminifera
Gastropods
Ostracods
Bivalves
Brachiopods
Echinoderms
Green algae
Strm-Cht-Corals
Serpulids
Sponge spicules
Depositional subenvironment
Prox.
Dist.
I L B S F OP OD
m M W P G D

MEZALOCHA SECTOR

Sections situated around the locality of Mezalocha (M1 to M14), and the mapping of facies, units and key surfaces in continuous outcrops, which correspond to transects M1-M4, M5-M7 and M10-M11. The field pictures included in this section correspond to the most representative images of the upper 10-16 m thick succession of the Higueruelas Fm in this sector. Below, the location of the studied sections in this area, and the legend for the information included in the logs.

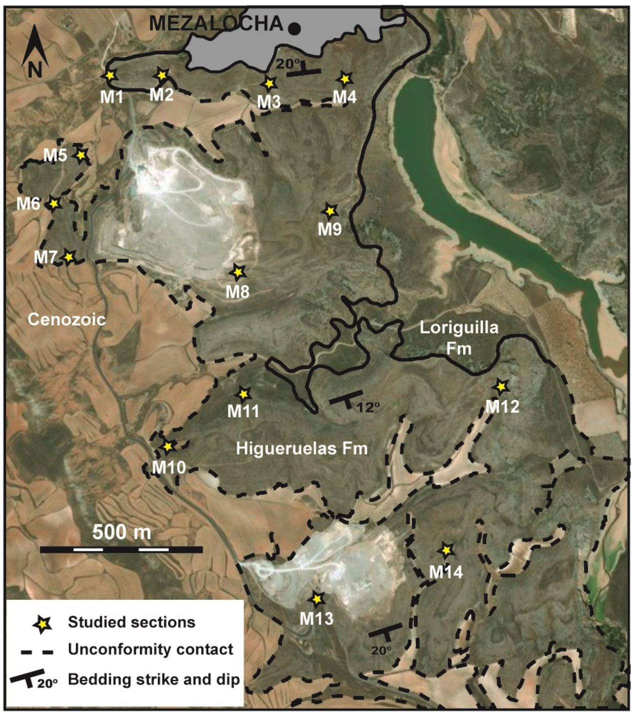

SUBENVIRONMENT

I: Intertidal (including ponds)
L: Lagoon
B: Backshoal/washover
S: Shoal-sand blanket
F: Foreshoal
OP: Offshore-proximal
OD: Offshore-distal

ABUNDANCE OF COMPONENTS

● Present (< 10%) ● Common (10-20%) ● Abundant (> 20%)

LITHOLOGY AND TEXTURE

Limestone
M: mudstone W: wackestone P: packstone G: grainstone
m: marl D: dolomitic limestone/ dolostone

SAMPLES

M1-1 Polished slab **M1-1** Thin section

FACIES AND SUBENVIRONMENTS

Sheltered lagoon
- Oncolitic W
- Oncolitic P
- Oncolitic-stromatoporoid W
- Oncolitic-stromatoporoid P
- Stromatoporoid W
- Stromatoporoid P

Backshoal/washover
- Peloidal W-P
- Peloidal G

Intertidal
- Peloidal M with fenestral porosity
- Peloidal P-G with fenestral porosity

Pond
- Gastropod-oncolitic W-P
- Gastropod-oncolitic G

- Marl
- Dolomite

KEY SURFACES

- Planar bedding surface
- Hardground
- Associated marly beds
- Bioturbated bedding surface
- Fe-enriched hardground

SEDIMENTARY STRUCTURES

- Coarsening-upward oncoid size
- Fining-upward oncoid size
- mm- to cm-thick bioclastic laminae
- mm- to cm-thick oncolitic laminae
- mm- to cm-thick laminae of various components (bioclasts, oncoids, ooids, peloids)
- cm-thick laminae with normal gradation
- Parallel lamination
- Cross lamination
- Fenestral porosity
- Parallel fenestral laminae
- Dome-like stromatolitic crusts
- Bioturbation (*Thalassinoides* traces in inner ramp; *Chondrites* and *Planolites* traces in mid-ramp)
- Bioerosion in oncoids and reefal components (by serpulids, bivalves or sponges)

Field pictures

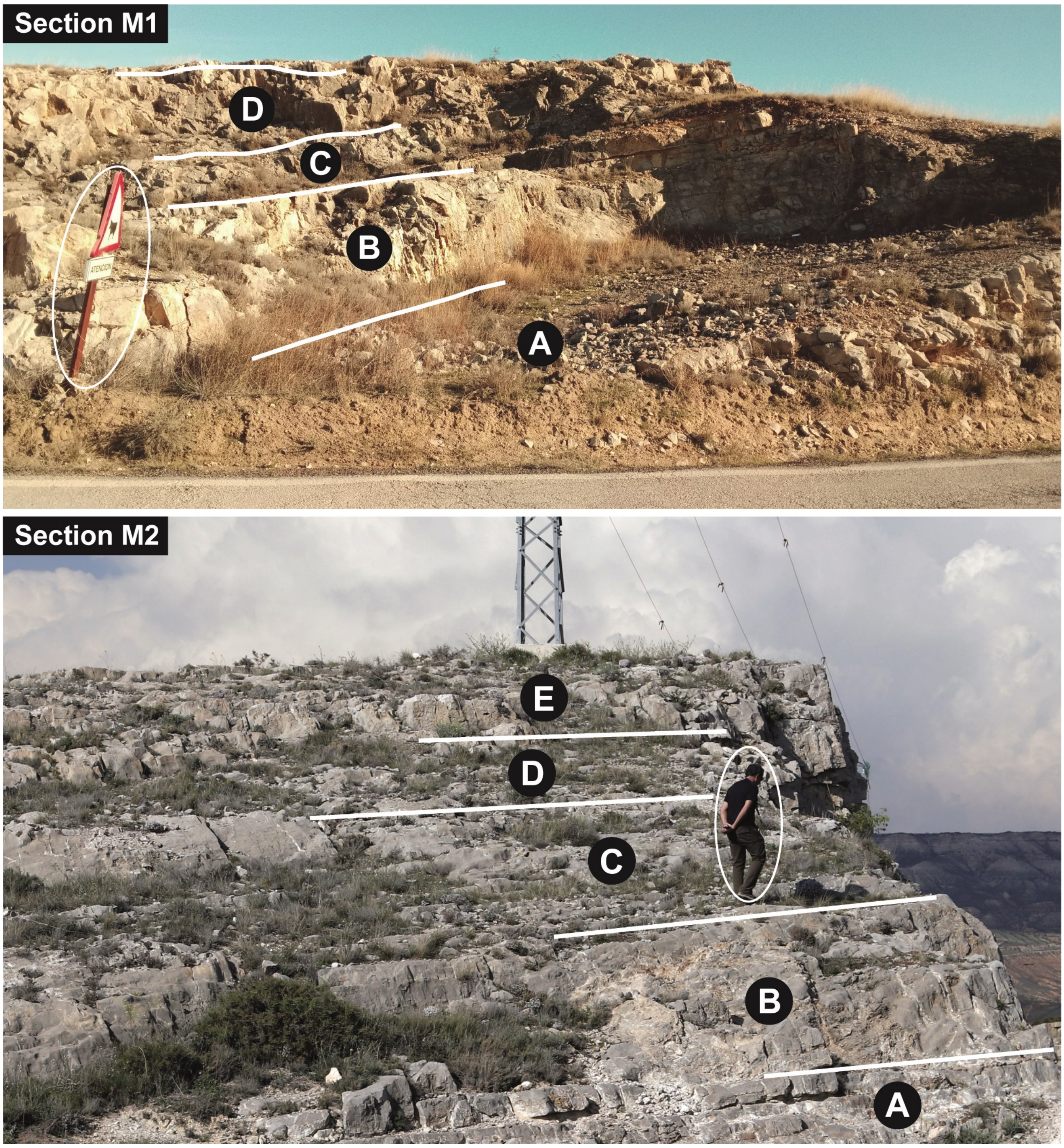

Sequences A to D in section M1 (top) and A to E in section M2 (bottom) identified in the upper part of the Higueruelas Fm in Mezalocha sector.

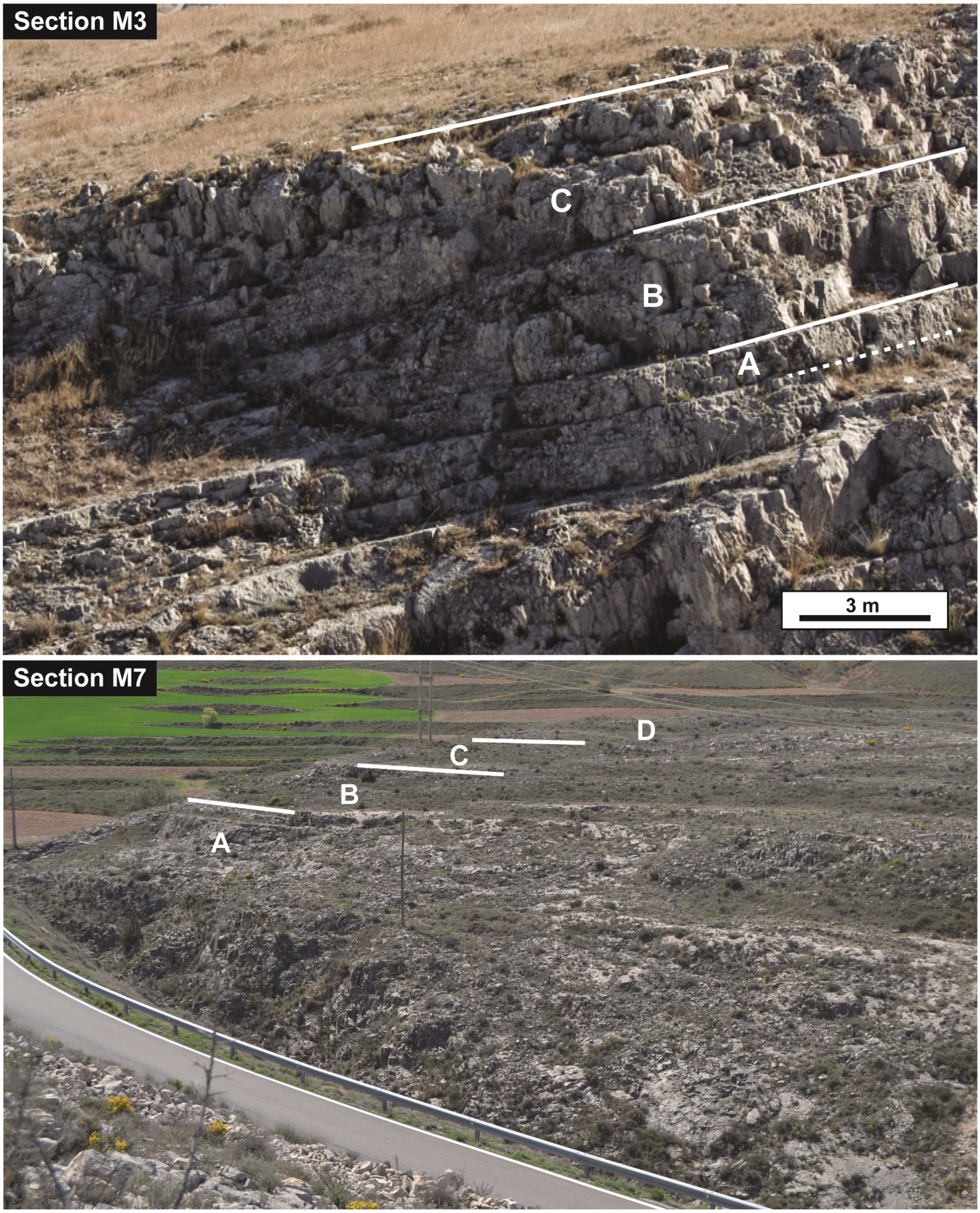

Sequences A to C in section M3 (top) and A to D in section M7 (bottom; for scale, the hill is 13 m high). In section M3, the dashed line in sequence A indicates the lower limit of this log (the image of this section is modified from Saúl, 2014).

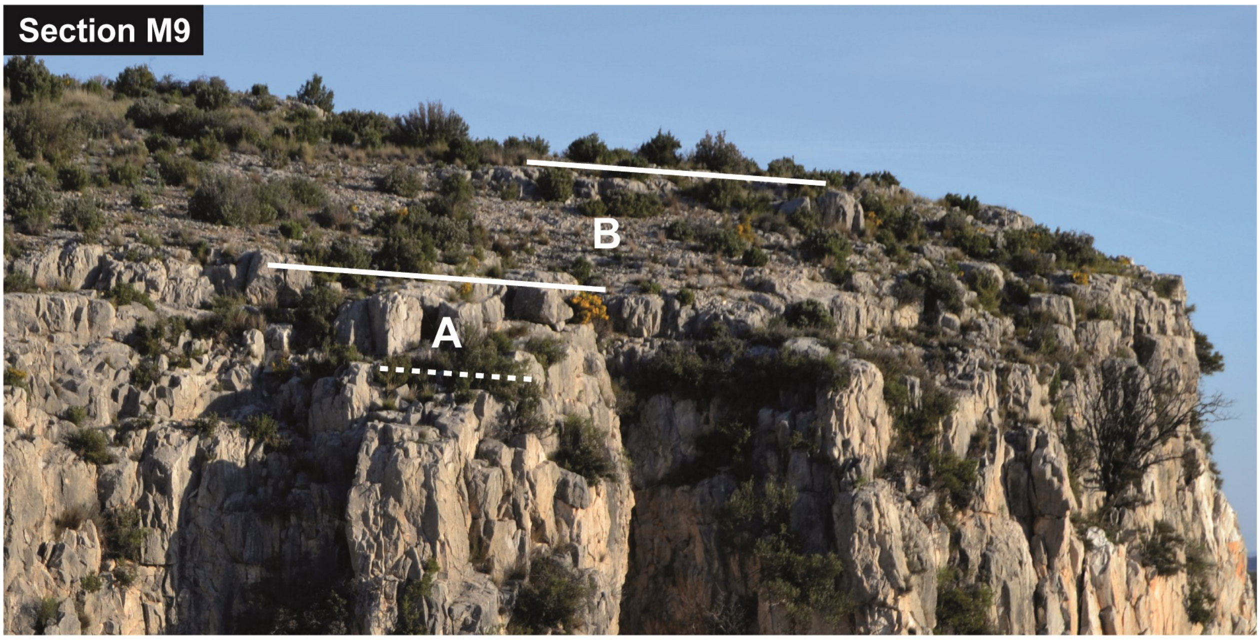

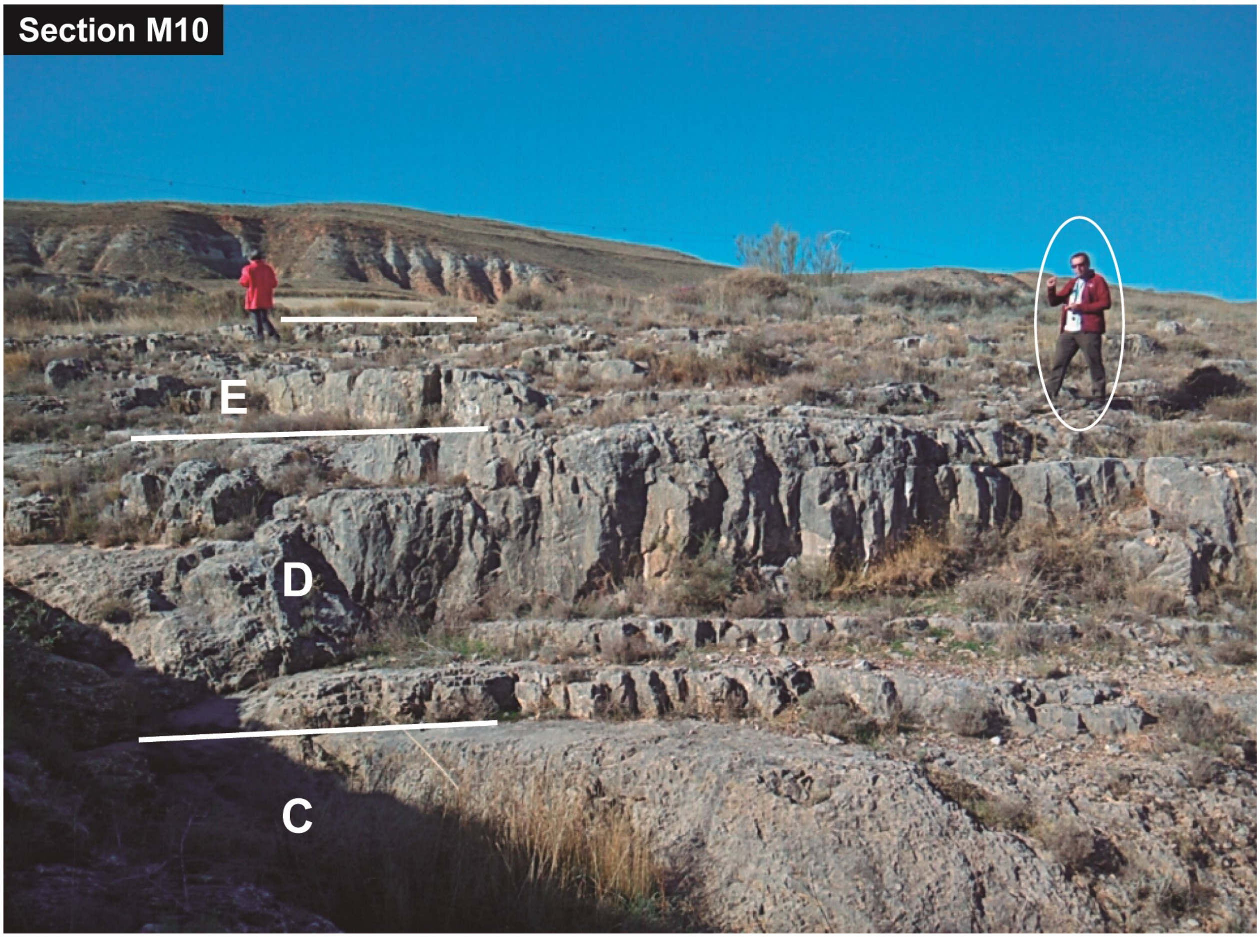

Sequences A and B in section M9 (top; for scale, from the dashed line to the top of sequence B is about 5 m high) and sequences C to E in section M10 (bottom). In section M9, the dashed line indicates the lower limit of the log.

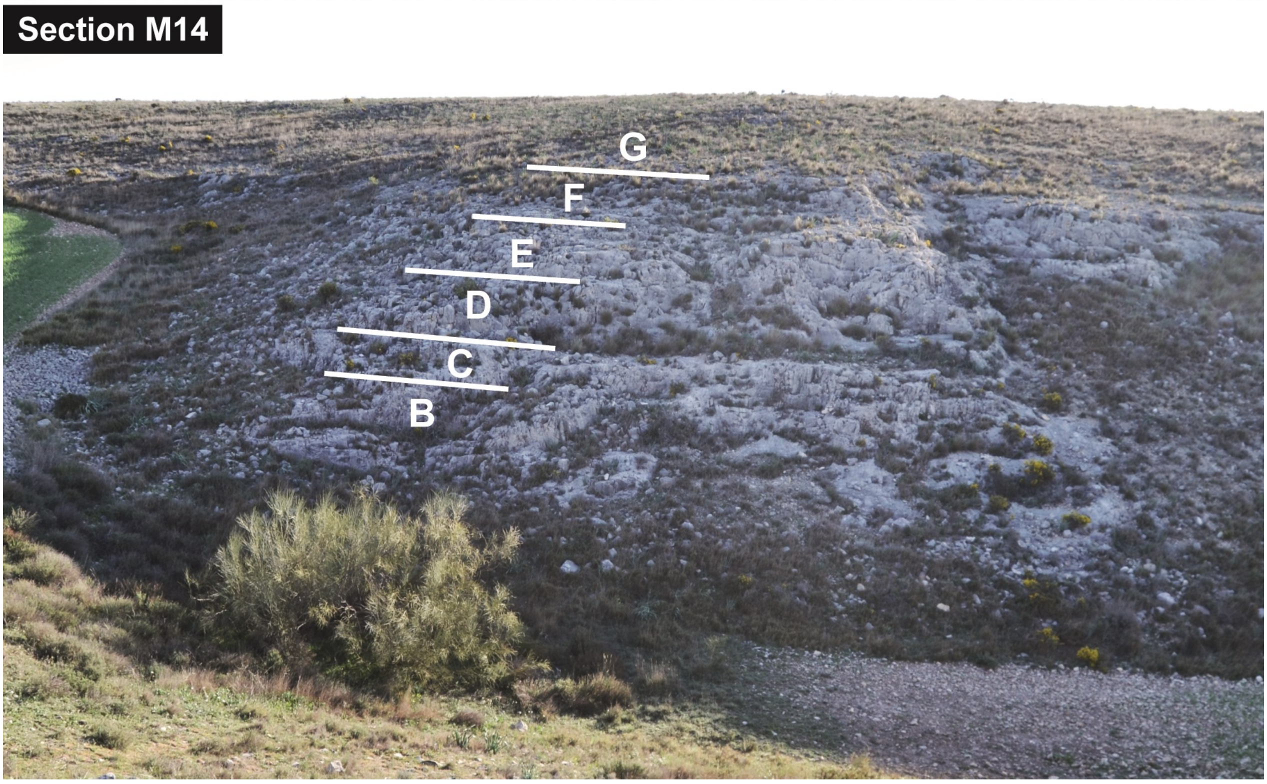

Sequences E to G in section M13 (top) and sequences B to G in section M14 (bottom; for scale, the hill is about 11 m high).

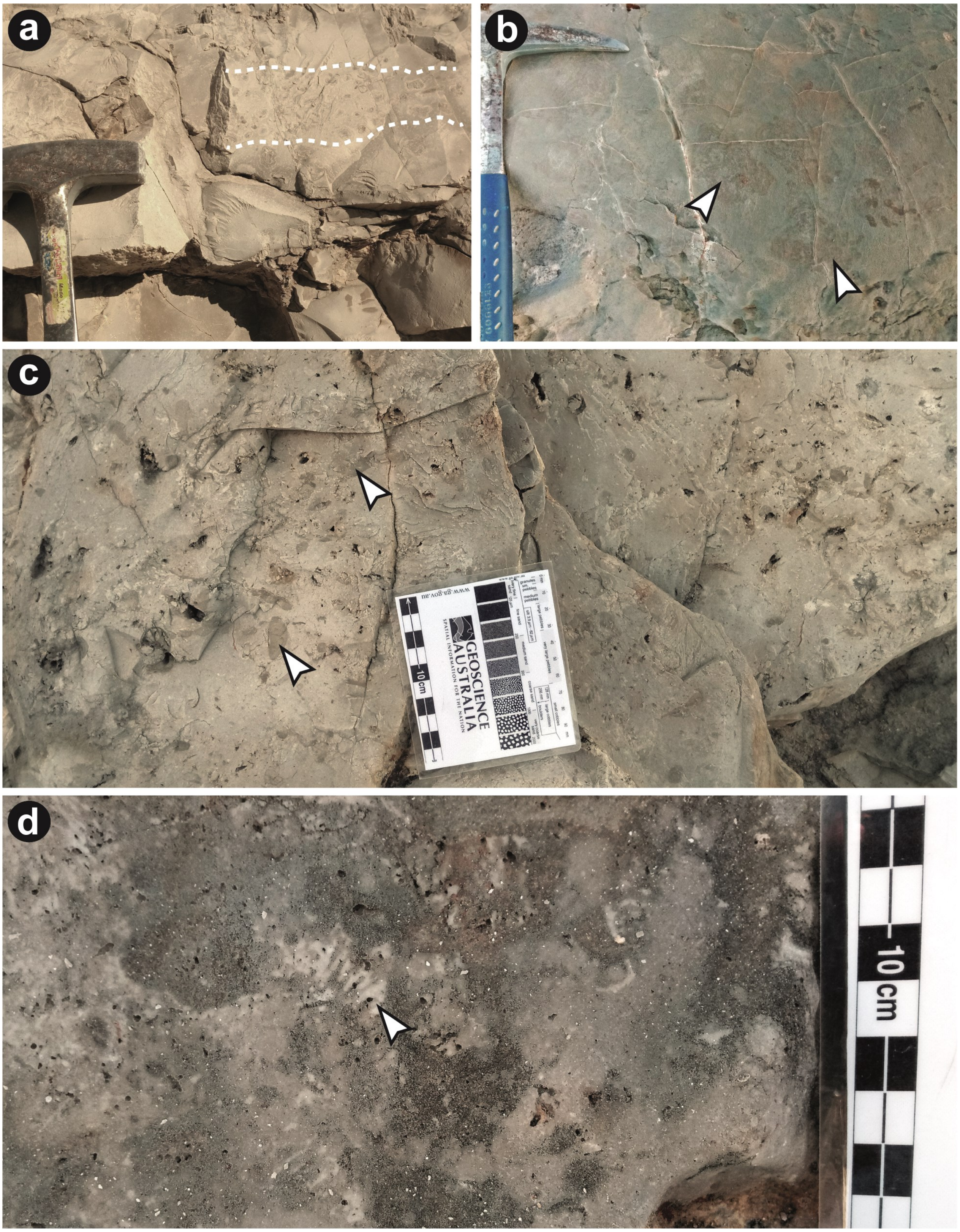

a-b) Field view of sheltered lagoon type IV oncoid facies in section M1 (sequence B), showing large and irregular microbial-dominated type IVa oncoids (arrows in b) and storm-related cm-thick accumulations of oncoids (dashed lines in a). c-d) Field view of sheltered lagoon stromatoporoid facies in section M1 (sequence D), showing cm-sized fragments of broken stromatoporoids (arrows in c), commonly associated with Tubiphytes *encrustations (arrow in d).*

a-b) Field view of pond gastropod-oncolitic facies in section M6 (sequence D). c) Field view of dome-like stromatolitic structures in intertidal peloidal with fenestral porosity facies (section M7, sequence E).

Mapping of units and key surfaces in continuous outcrops

Physical tracing of key surfaces delimiting the sequences A to G between sections M1 and M2, and towards section M3 to the east.

Physical tracing of key surfaces delimiting the sequences A to E between sections M3 and M4.

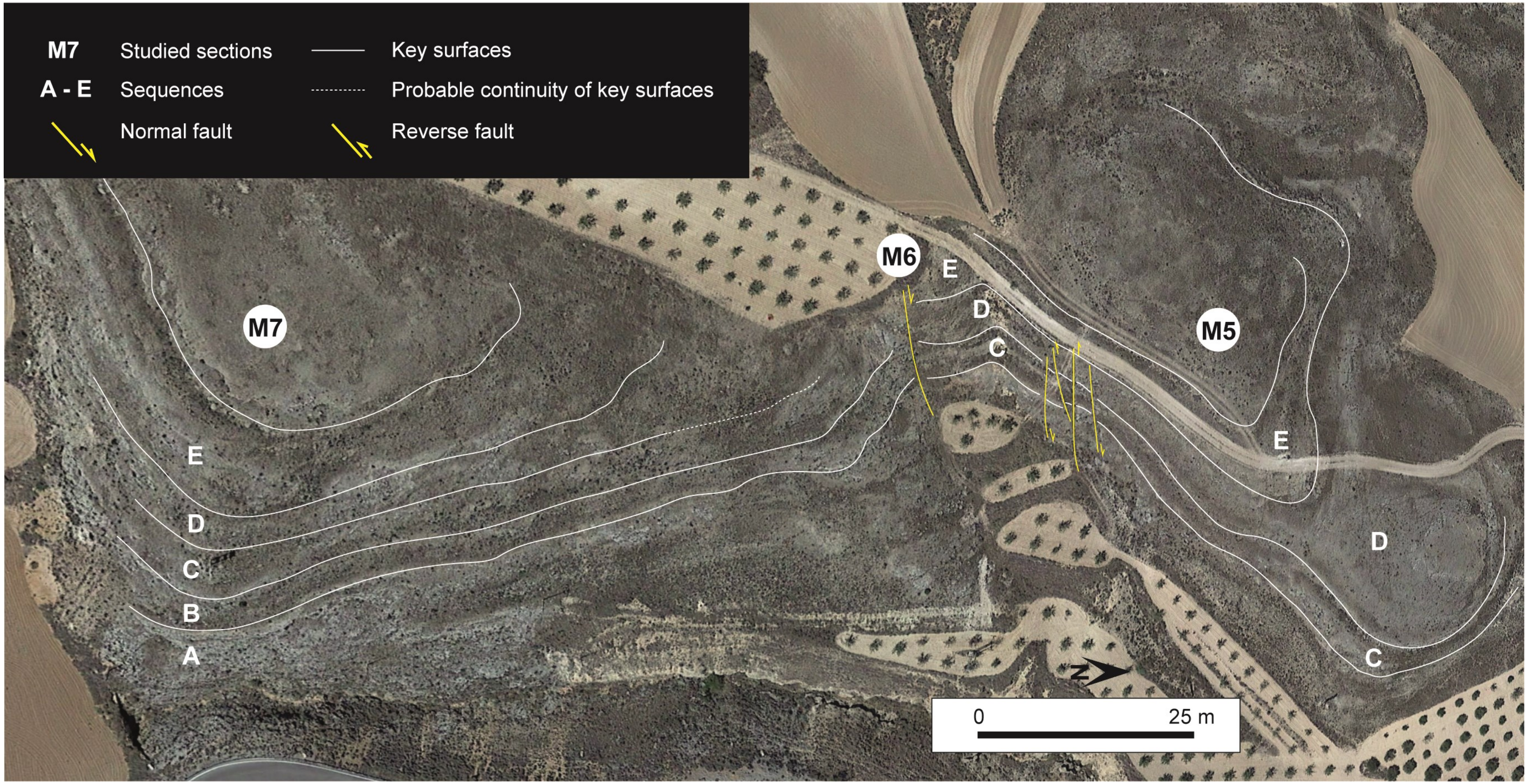

Physical tracing of key surfaces delimiting the sequences A to E between sections M5 to M7. The position of normal and reverse faults is also indicated (yellow lines).

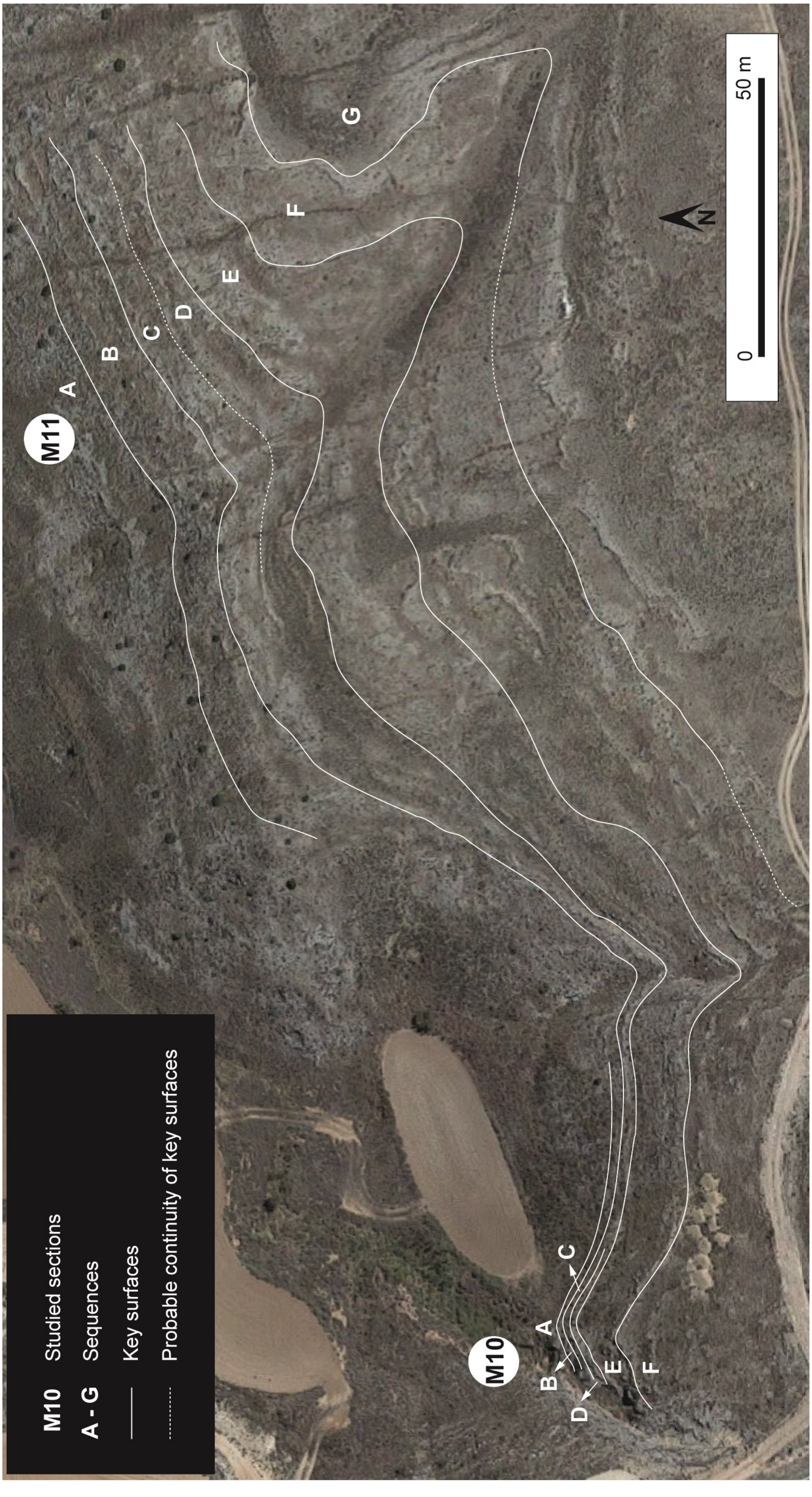

Physical tracing of key surfaces delimiting the sequences A to G between sections M10 and M11.

Logs and sample location

The depositional subenvironment of some of the backshoal/washover peloidal G facies defined in these sections has been re-interpreted as shoal-sand blanket deposits, after further analyses reporting on their similar characteristics with those shoal-sand blanket peloidal facies described in the sedimentary logs from Muel to Aguilón sectors. The legend for the logs presented here remains as shown in the corresponding scientific paper in Chapter 5.

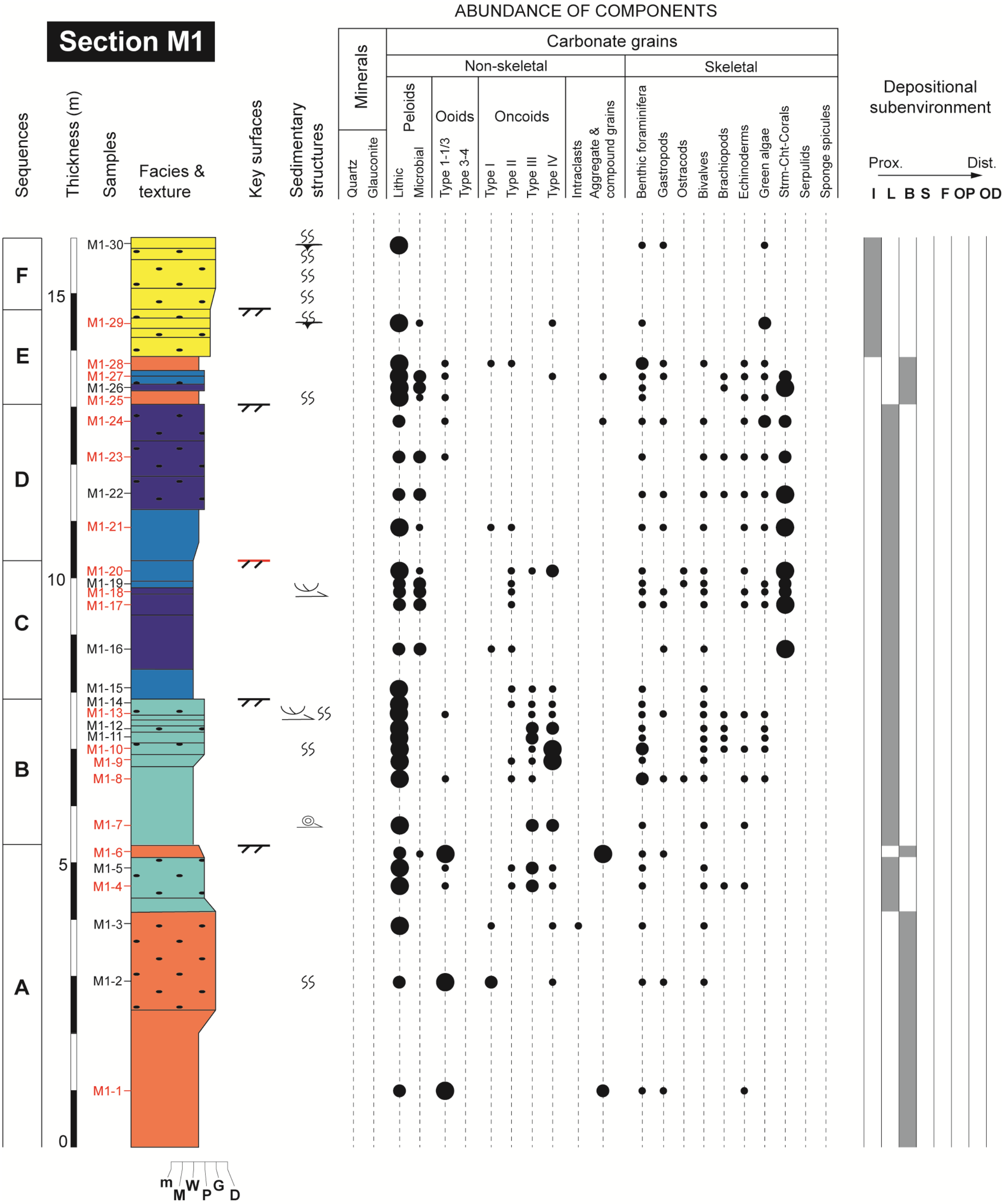

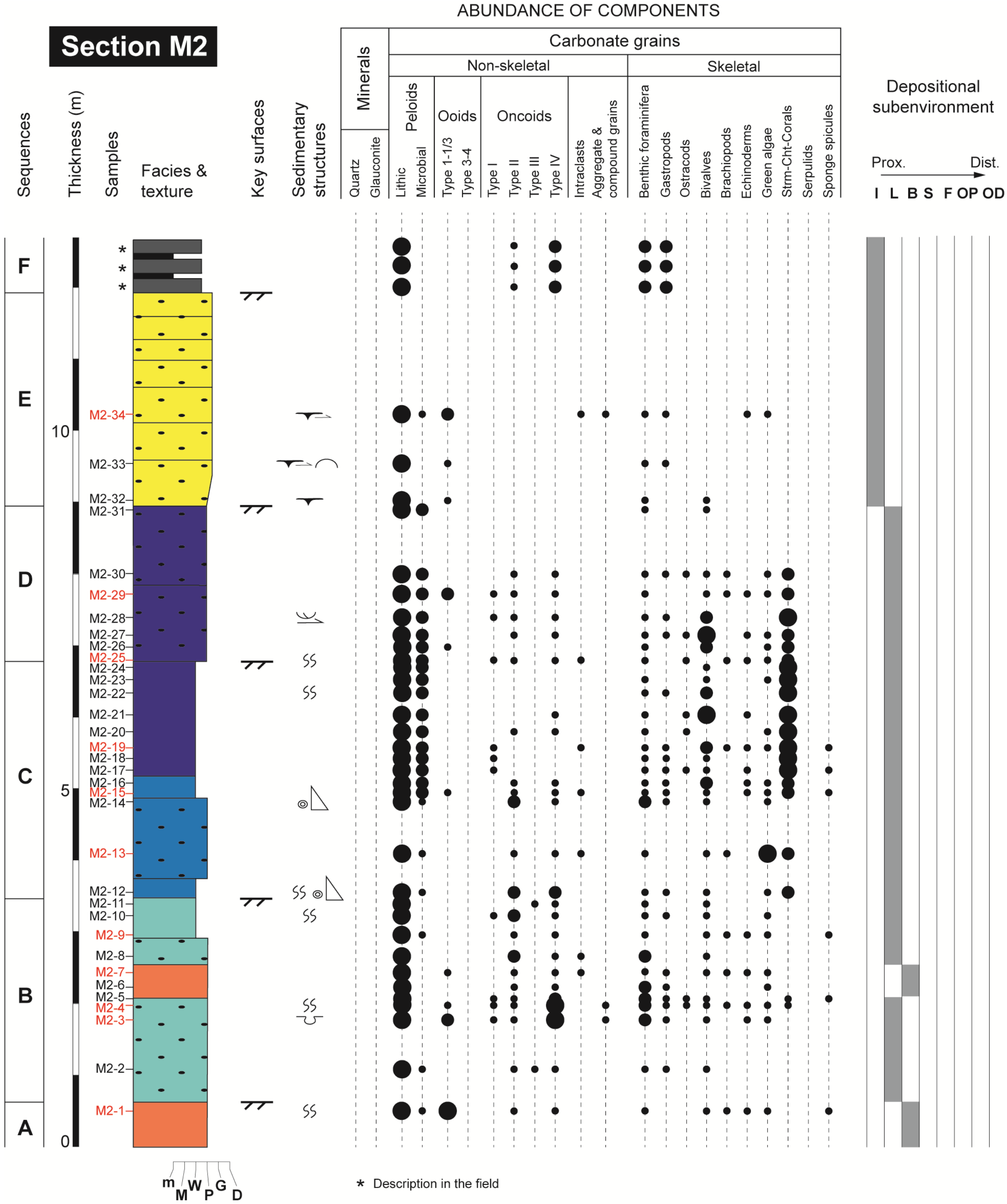
Section M2
ABUNDANCE OF COMPONENTS
Sequences
Thickness (m)
Samples
Facies & texture
Key surfaces
Sedimentary structures
Minerals
Quartz
Glauconite
Carbonate grains
Non-skeletal
Peloids
Lithic
Microbial
Ooids
Type 1-1/3
Type 3-4
Oncoids
Type I
Type II
Type III
Type IV
Intraclasts
Aggregate & compound grains
Skeletal
Benthic foraminifera
Gastropods
Ostracods
Bivalves
Brachiopods
Echinoderms
Green algae
Strm-Cht-Corals
Serpulids
Sponge spicules
Depositional subenvironment
Prox.
Dist.
I L B S F OP OD
F
E
D
C
B
A
10
5
0
M2-34
M2-33
M2-32
M2-31
M2-30
M2-29
M2-28
M2-27
M2-26
M2-25
M2-24
M2-23
M2-22
M2-21
M2-20
M2-19
M2-18
M2-17
M2-16
M2-15
M2-14
M2-13
M2-12
M2-11
M2-10
M2-9
M2-8
M2-7
M2-6
M2-5
M2-4
M2-3
M2-2
M2-1
m M W P G D
* Description in the field

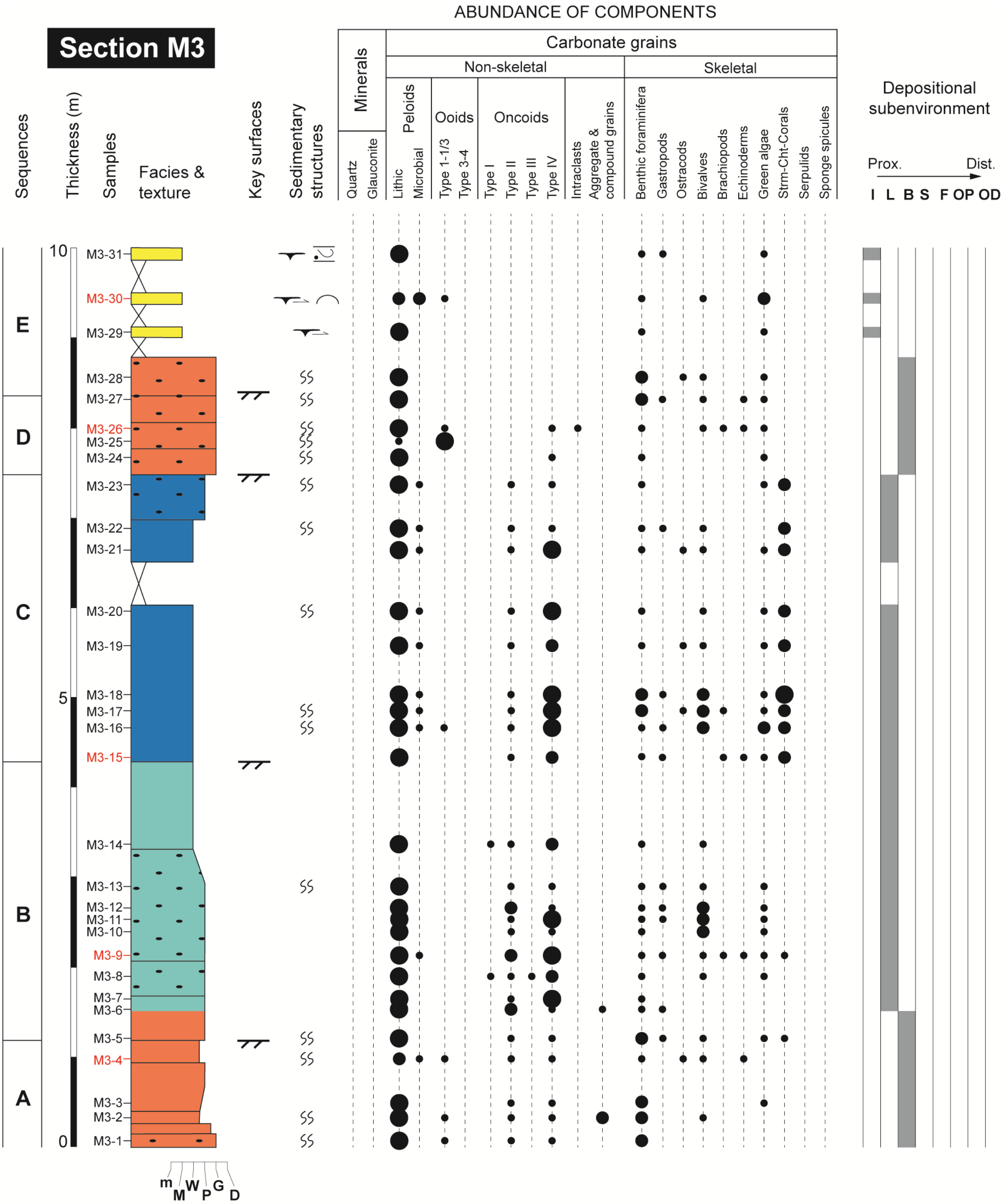
Section M3
ABUNDANCE OF COMPONENTS
Minerals
Carbonate grains
Non-skeletal
Skeletal
Sequences
Thickness (m)
Samples
Facies & texture
Key surfaces
Sedimentary structures
Quartz
Glauconite
Peloids
Lithic
Microbial
Ooids
Type 1-1/3
Type 3-4
Oncoids
Type I
Type II
Type III
Type IV
Intraclasts
Aggregate & compound grains
Benthic foraminifera
Gastropods
Ostracods
Bivalves
Brachiopods
Echinoderms
Green algae
Strm-Cht-Corals
Serpulids
Sponge spicules
Depositional subenvironment
Prox.
Dist.
I L B S F OP OD
E
D
C
B
A
10
5
0
M3-31
M3-30
M3-29
M3-28
M3-27
M3-26
M3-25
M3-24
M3-23
M3-22
M3-21
M3-20
M3-19
M3-18
M3-17
M3-16
M3-15
M3-14
M3-13
M3-12
M3-11
M3-10
M3-9
M3-8
M3-7
M3-6
M3-5
M3-4
M3-3
M3-2
M3-1
m M W P G D

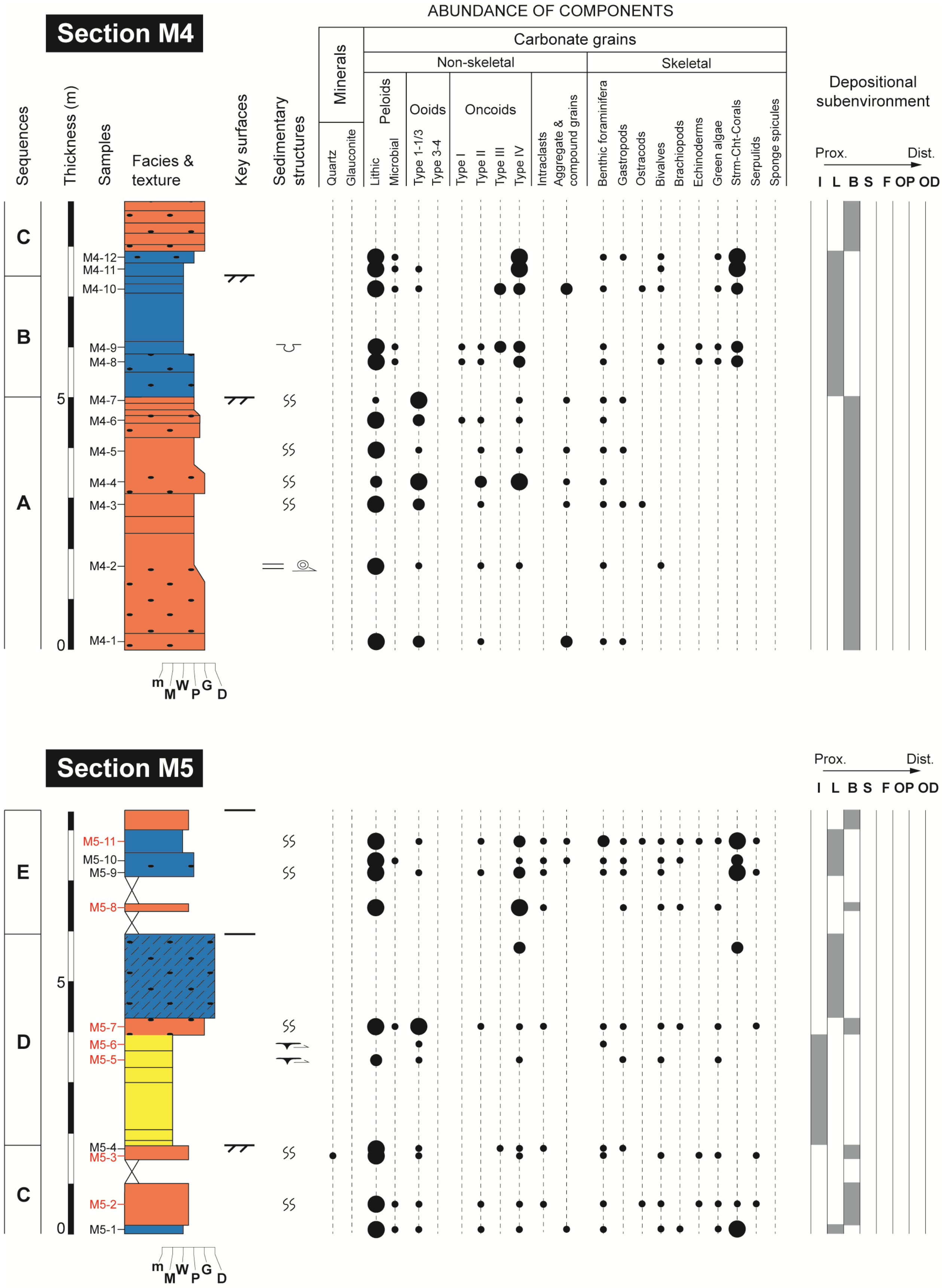
Section M4
ABUNDANCE OF COMPONENTS
Minerals
Quartz
Glauconite
Carbonate grains
Non-skeletal
Peloids
Lithic
Microbial
Ooids
Type 1-1/3
Type 3-4
Oncoids
Type I
Type II
Type III
Type IV
Intraclasts
Aggregate & compound grains
Skeletal
Benthic foraminifera
Gastropods
Ostracods
Bivalves
Brachiopods
Echinoderms
Green algae
Strm-Cht-Corals
Serpulids
Sponge spicules
Depositional subenvironment
Prox.
Dist.
I L B S F OP OD
Sequences
Thickness (m)
Samples
Facies & texture
Key surfaces
Sedimentary structures
C
B
A
5
0
M4-12
M4-11
M4-10
M4-9
M4-8
M4-7
M4-6
M4-5
M4-4
M4-3
M4-2
M4-1
m M W P G D
Section M5
Prox.
Dist.
I L B S F OP OD
E
D
C
5
0
M5-11
M5-10
M5-9
M5-8
M5-7
M5-6
M5-5
M5-4
M5-3
M5-2
M5-1
m M W P G D

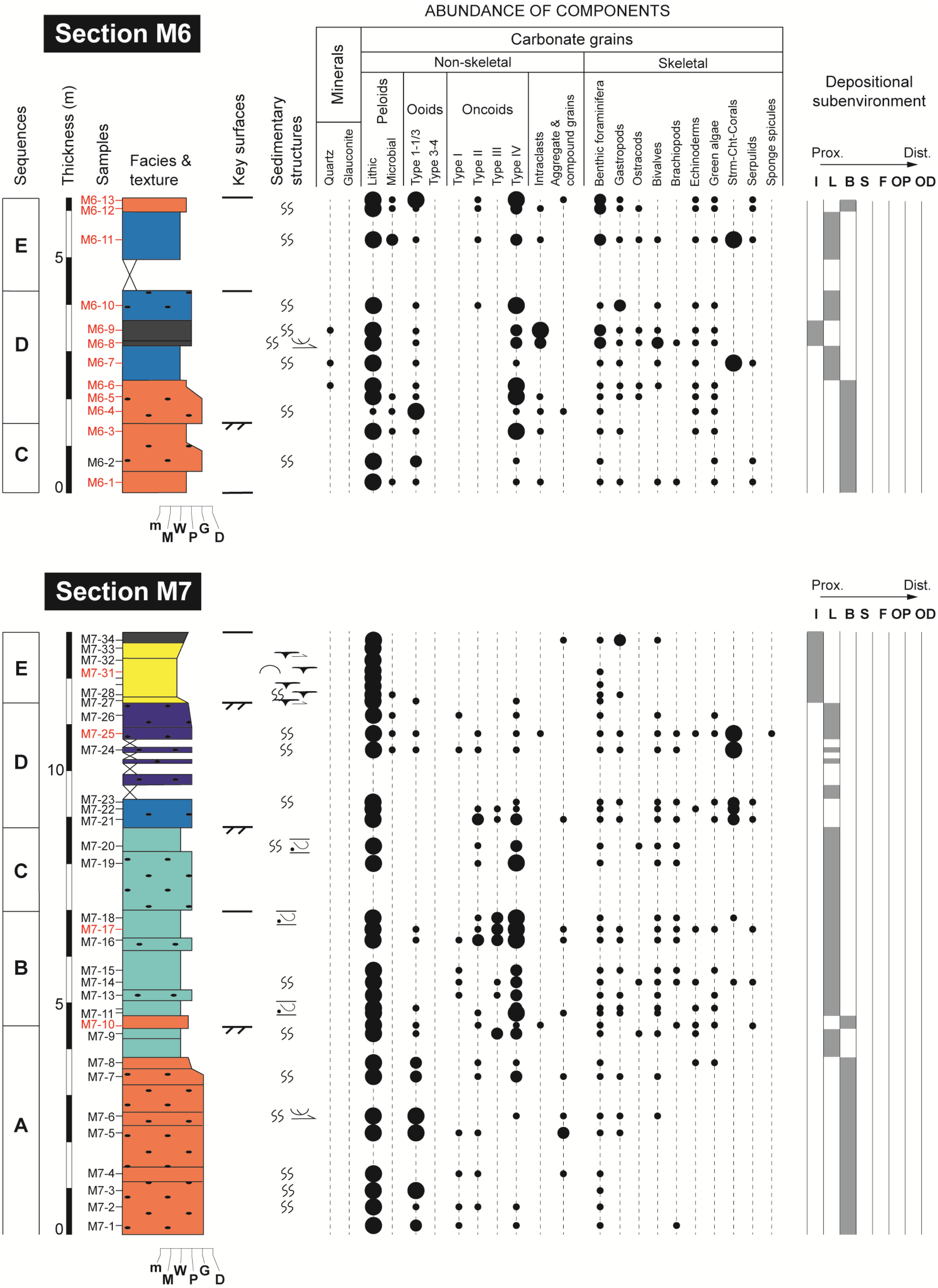
ABUNDANCE OF COMPONENTS
Section M6
Section M7
Sequences
Thickness (m)
Samples
Facies & texture
Key surfaces
Sedimentary structures
Minerals
Quartz
Glauconite
Carbonate grains
Non-skeletal
Skeletal
Peloids
Lithic
Microbial
Ooids
Type 1-1/3
Type 3-4
Oncoids
Type I
Type II
Type III
Type IV
Intraclasts
Aggregate & compound grains
Benthic foraminifera
Gastropods
Ostracods
Bivalves
Brachiopods
Echinoderms
Green algae
Strm-Cht-Corals
Serpulids
Sponge spicules
Depositional subenvironment
Prox.
Dist.
I L B S F OP OD
m M W P G D

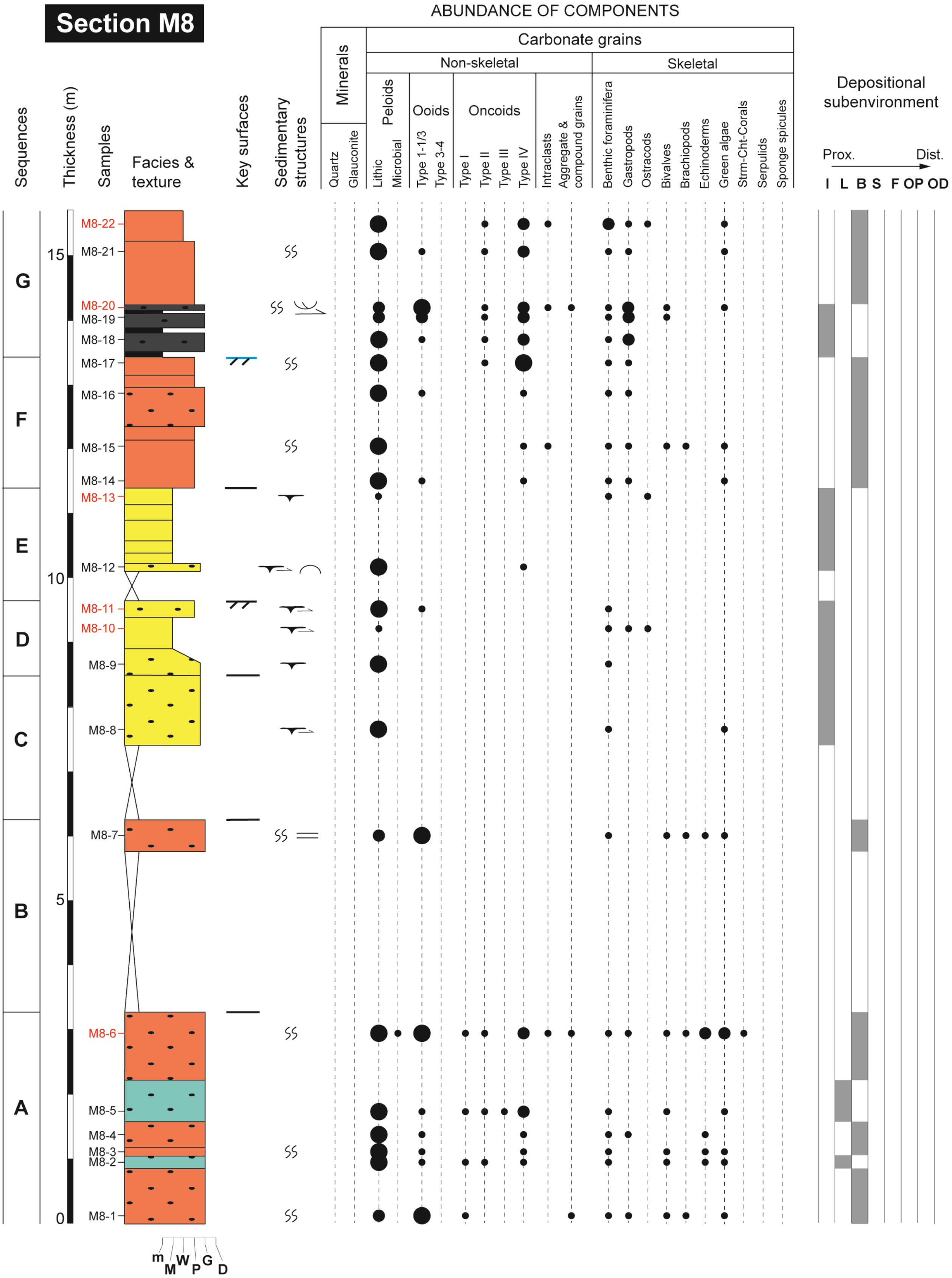
Section M8
ABUNDANCE OF COMPONENTS
Minerals
Quartz
Glauconite
Carbonate grains
Non-skeletal
Skeletal
Peloids
Lithic
Microbial
Ooids
Type 1-1/3
Type 3-4
Oncoids
Type I
Type II
Type III
Type IV
Intraclasts
Aggregate & compound grains
Benthic foraminifera
Gastropods
Ostracods
Bivalves
Brachiopods
Echinoderms
Green algae
Strm-Cht-Corals
Serpulids
Sponge spicules
Depositional subenvironment
Prox.
Dist.
I L B S F OP OD
Sequences
Thickness (m)
Samples
Facies & texture
Key surfaces
Sedimentary structures
G
F
E
D
C
B
A
15
10
5
0
M8-22
M8-21
M8-20
M8-19
M8-18
M8-17
M8-16
M8-15
M8-14
M8-13
M8-12
M8-11
M8-10
M8-9
M8-8
M8-7
M8-6
M8-5
M8-4
M8-3
M8-2
M8-1
m M W P G D

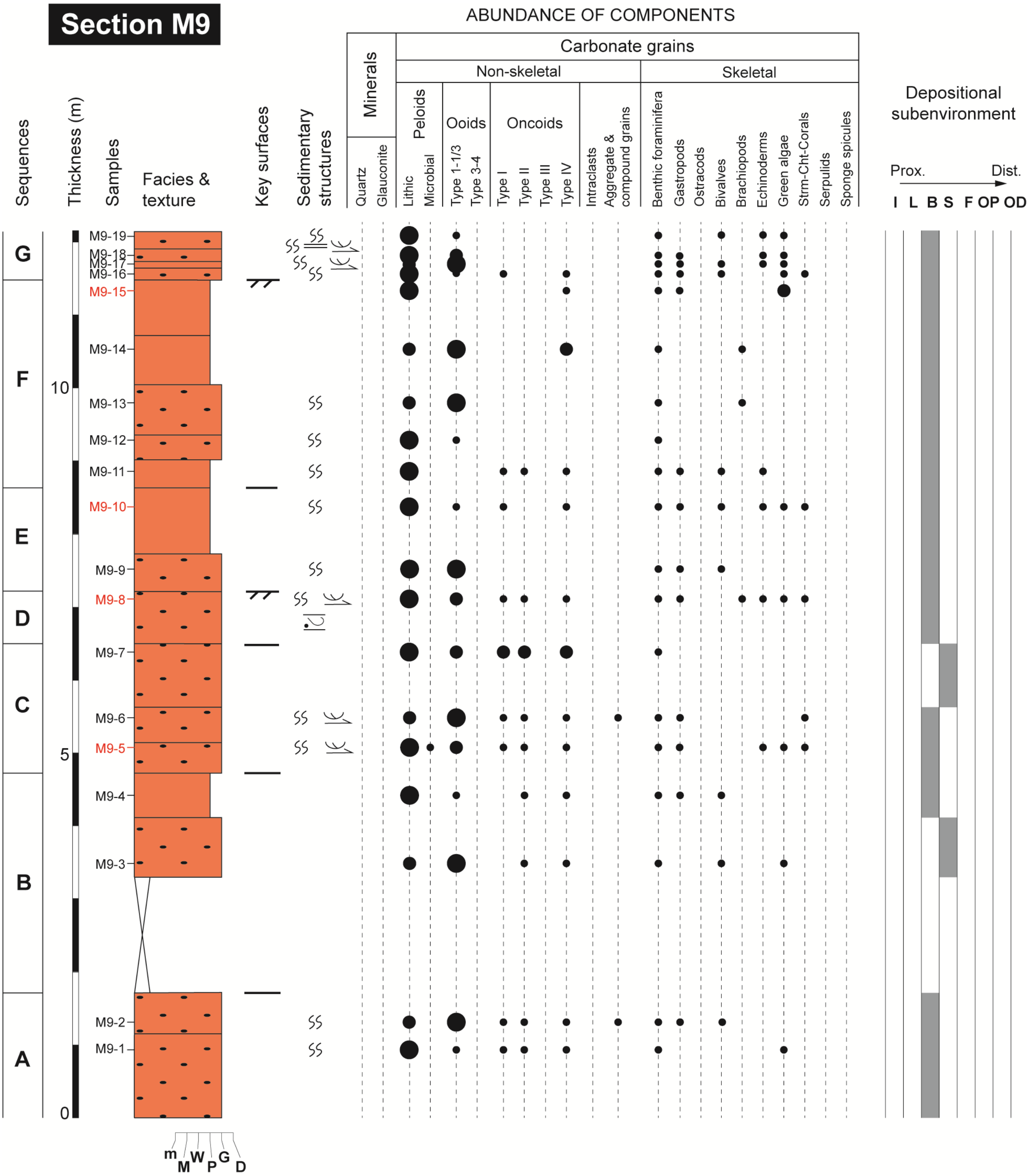

Section M9
ABUNDANCE OF COMPONENTS
Minerals
Carbonate grains
Non-skeletal
Skeletal
Sequences
Thickness (m)
Samples
Facies & texture
Key surfaces
Sedimentary structures
Quartz
Glauconite
Peloids
Lithic
Microbial
Ooids
Type 1-1/3
Type 3-4
Oncoids
Type I
Type II
Type III
Type IV
Intraclasts
Aggregate & compound grains
Benthic foraminifera
Gastropods
Ostracods
Bivalves
Brachiopods
Echinoderms
Green algae
Strm-Cht-Corals
Serpulids
Sponge spicules
Depositional subenvironment
Prox.
Dist.
I L B S F OP OD
G
F
E
D
C
B
A
10
5
0
M9-19
M9-18
M9-17
M9-16
M9-15
M9-14
M9-13
M9-12
M9-11
M9-10
M9-9
M9-8
M9-7
M9-6
M9-5
M9-4
M9-3
M9-2
M9-1
m M W P G D

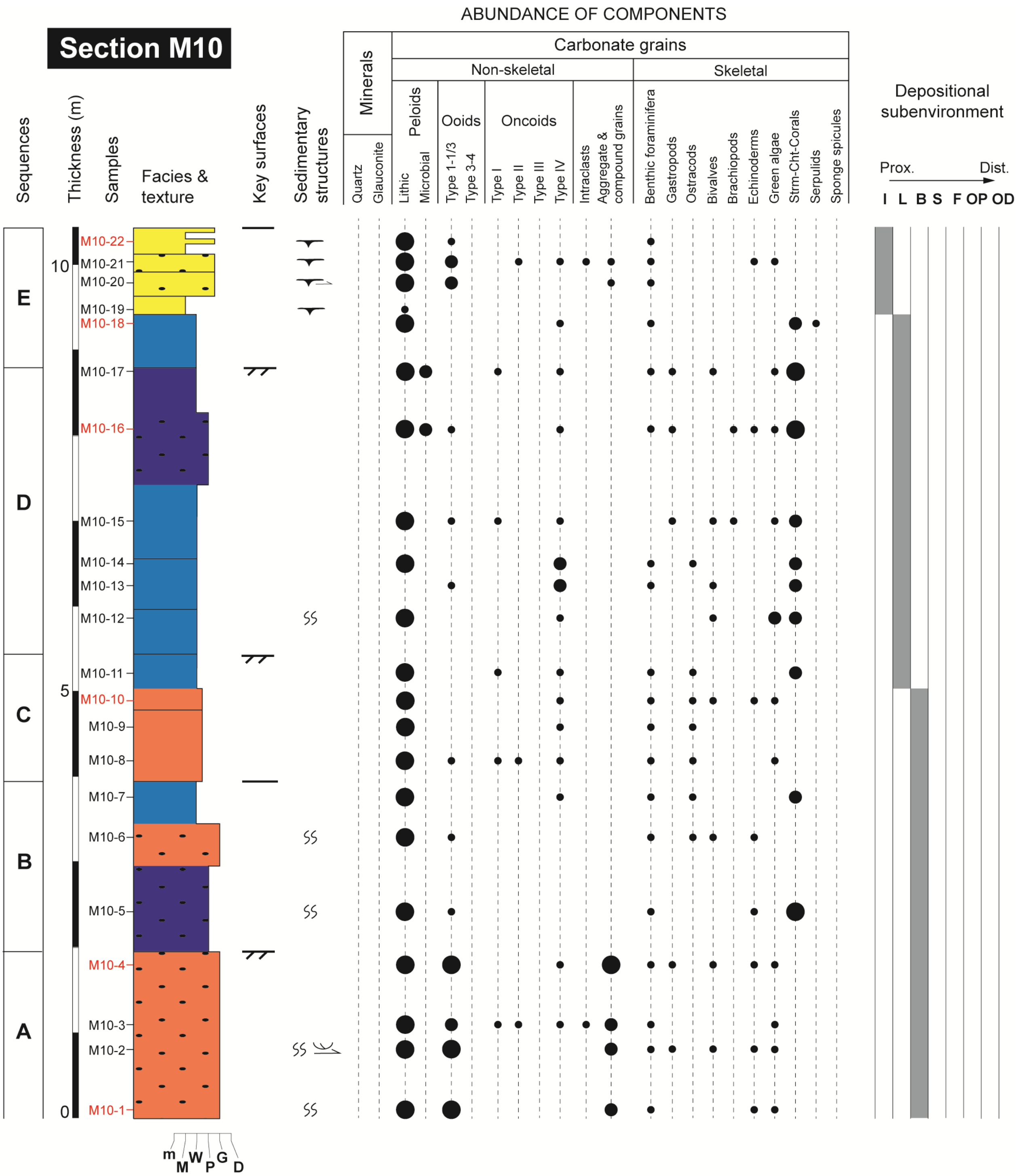
Section M10
ABUNDANCE OF COMPONENTS
Sequences
Thickness (m)
Samples
Facies & texture
Key surfaces
Sedimentary structures
Minerals
Quartz
Glauconite
Carbonate grains
Non-skeletal
Skeletal
Peloids
Lithic
Microbial
Ooids
Type 1-1/3
Type 3-4
Oncoids
Type I
Type II
Type III
Type IV
Intraclasts
Aggregate & compound grains
Benthic foraminifera
Gastropods
Ostracods
Bivalves
Brachiopods
Echinoderms
Green algae
Strm-Cht-Corals
Serpulids
Sponge spicules
Depositional subenvironment
Prox.
Dist.
I L B S F OP OD
E
D
C
B
A
10
5
0
M10-22
M10-21
M10-20
M10-19
M10-18
M10-17
M10-16
M10-15
M10-14
M10-13
M10-12
M10-11
M10-10
M10-9
M10-8
M10-7
M10-6
M10-5
M10-4
M10-3
M10-2
M10-1
m M W P G D

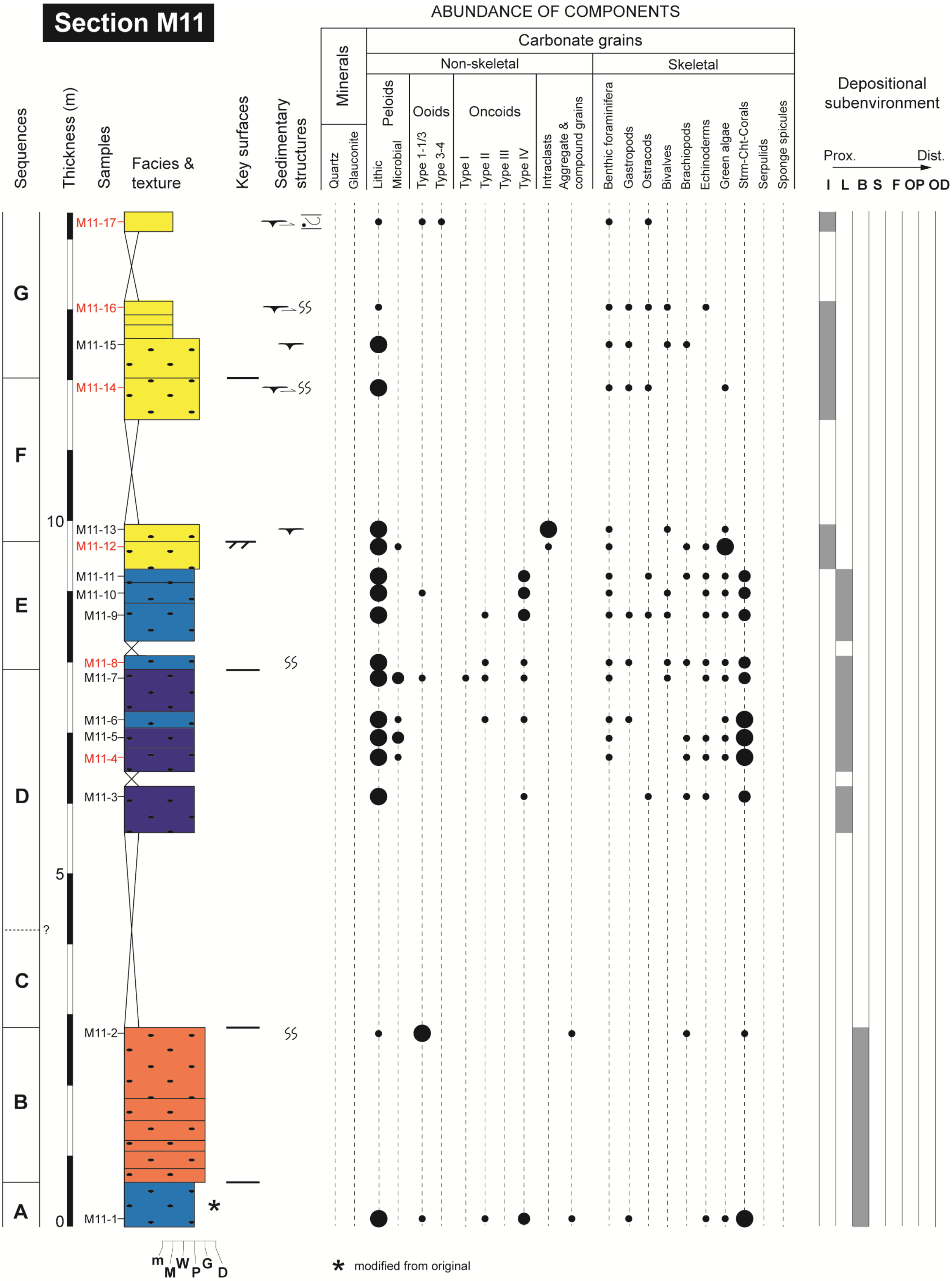
Section M11
ABUNDANCE OF COMPONENTS
Minerals
Carbonate grains
Non-skeletal
Skeletal
Depositional subenvironment
Sequences
Thickness (m)
Samples
Facies & texture
Key surfaces
Sedimentary structures
Quartz
Glauconite
Peloids
Lithic
Microbial
Ooids
Type 1-1/3
Type 3-4
Oncoids
Type I
Type II
Type III
Type IV
Intraclasts
Aggregate & compound grains
Benthic foraminifera
Gastropods
Ostracods
Bivalves
Brachiopods
Echinoderms
Green algae
Strm-Cht-Corals
Serpulids
Sponge spicules
Prox.
Dist.
I L B S F OP OD
G
F
E
D
C
B
A
10
5
0
?
M11-17
M11-16
M11-15
M11-14
M11-13
M11-12
M11-11
M11-10
M11-9
M11-8
M11-7
M11-6
M11-5
M11-4
M11-3
M11-2
M11-1
*
m M W P G D
* modified from original

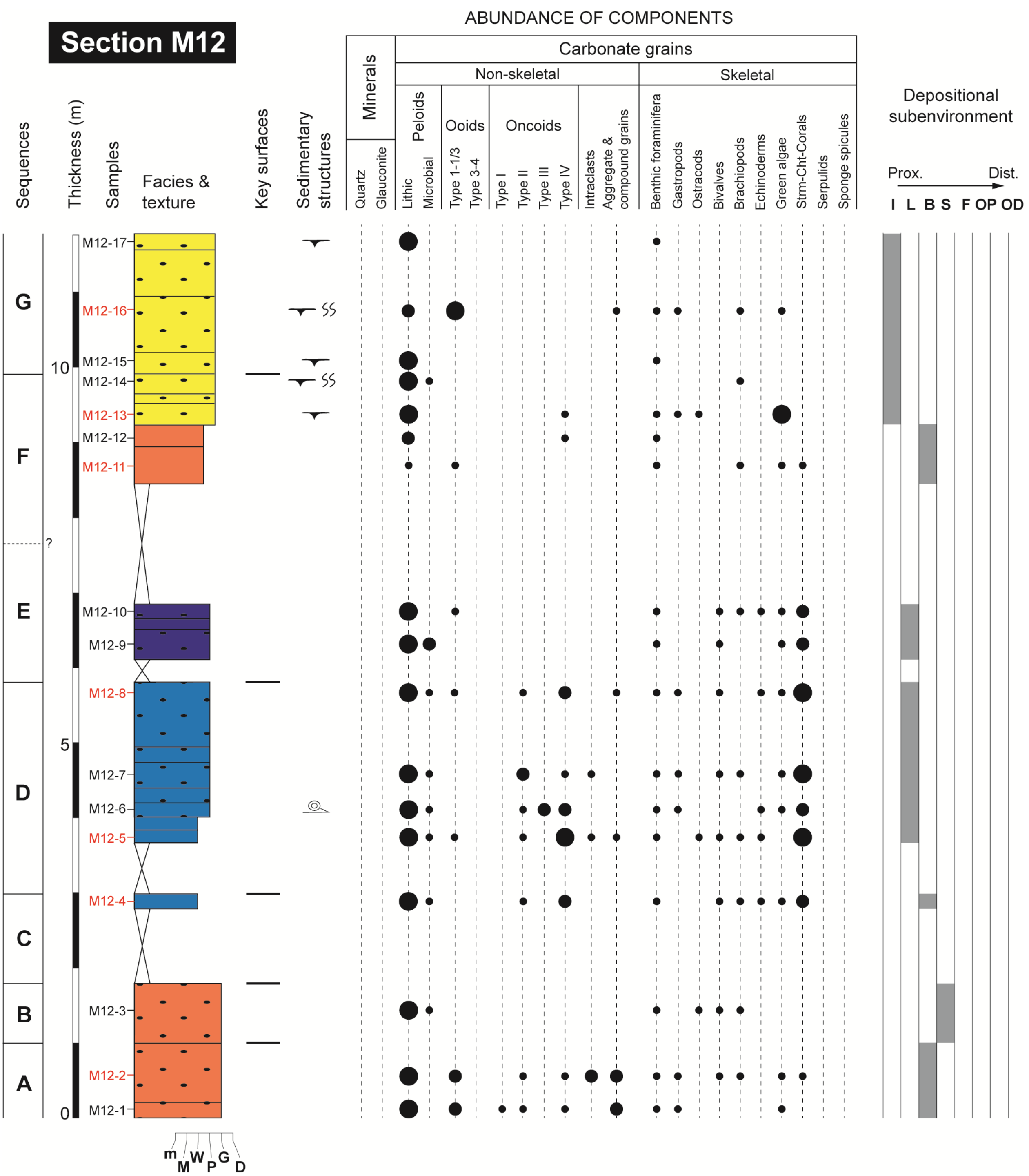
Section M12
ABUNDANCE OF COMPONENTS
Minerals
Carbonate grains
Non-skeletal
Skeletal
Sequences
Thickness (m)
Samples
Facies & texture
Key surfaces
Sedimentary structures
Quartz
Glauconite
Peloids
Lithic
Microbial
Ooids
Type 1-1/3
Type 3-4
Oncoids
Type I
Type II
Type III
Type IV
Intraclasts
Aggregate & compound grains
Benthic foraminifera
Gastropods
Ostracods
Bivalves
Brachiopods
Echinoderms
Green algae
Strm-Cht-Corals
Serpulids
Sponge spicules
Depositional subenvironment
Prox.
Dist.
I L B S F OP OD
G
F
E
D
C
B
A
?
10
5
0
M12-17
M12-16
M12-15
M12-14
M12-13
M12-12
M12-11
M12-10
M12-9
M12-8
M12-7
M12-6
M12-5
M12-4
M12-3
M12-2
M12-1
m M W P G D

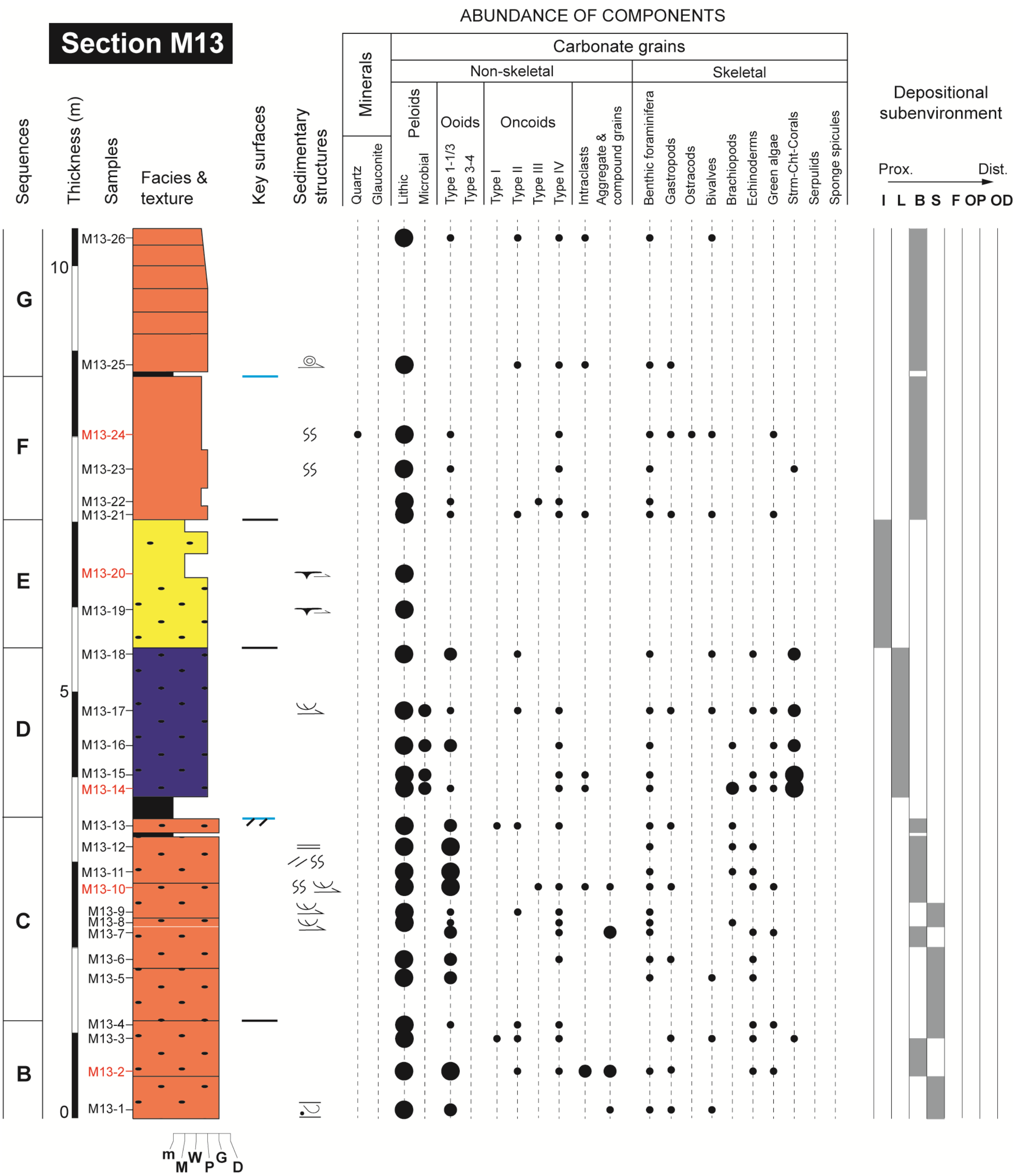
Section M13
ABUNDANCE OF COMPONENTS
Carbonate grains
Non-skeletal
Skeletal
Minerals
Quartz
Glauconite
Peloids
Lithic
Microbial
Ooids
Type 1-1/3
Type 3-4
Oncoids
Type I
Type II
Type III
Type IV
Intraclasts
Aggregate & compound grains
Benthic foraminifera
Gastropods
Ostracods
Bivalves
Brachiopods
Echinoderms
Green algae
Strm-Cht-Corals
Serpulids
Sponge spicules
Depositional subenvironment
Prox.
Dist.
I L B S F OP OD
Sequences
Thickness (m)
Samples
Facies & texture
Key surfaces
Sedimentary structures
G
F
E
D
C
B
10
5
0
M13-26
M13-25
M13-24
M13-23
M13-22
M13-21
M13-20
M13-19
M13-18
M13-17
M13-16
M13-15
M13-14
M13-13
M13-12
M13-11
M13-10
M13-9
M13-8
M13-7
M13-6
M13-5
M13-4
M13-3
M13-2
M13-1
m M W P G D

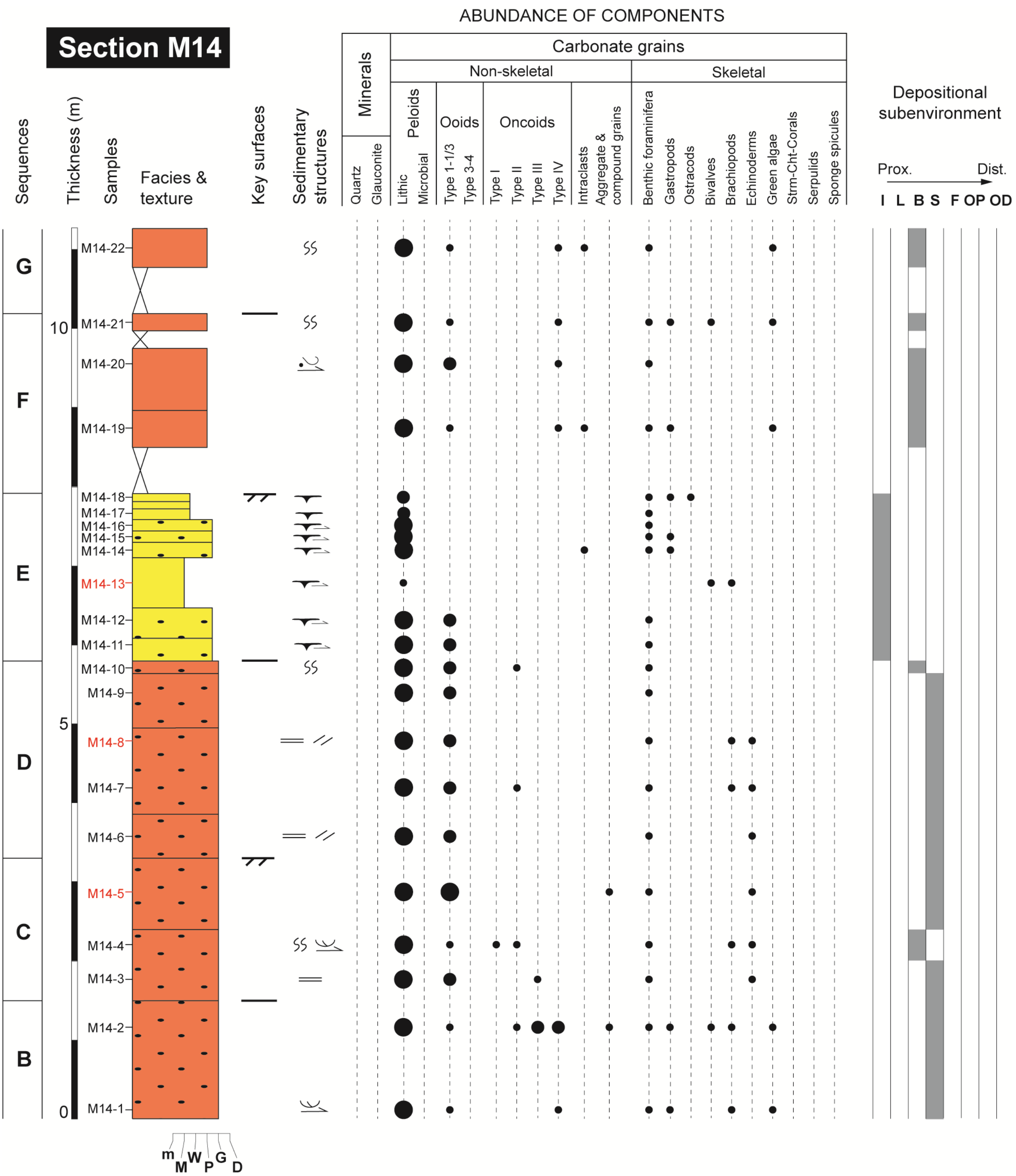
Section M14
ABUNDANCE OF COMPONENTS
Minerals
Carbonate grains
Non-skeletal
Skeletal
Sequences
Thickness (m)
Samples
Facies & texture
Key surfaces
Sedimentary structures
Quartz
Glauconite
Peloids
Lithic
Microbial
Ooids
Type 1-1/3
Type 3-4
Oncoids
Type I
Type II
Type III
Type IV
Intraclasts
Aggregate & compound grains
Benthic foraminifera
Gastropods
Ostracods
Bivalves
Brachiopods
Echinoderms
Green algae
Strm-Cht-Corals
Serpulids
Sponge spicules
Depositional subenvironment
Prox.
Dist.
I L B S F OP OD
G
F
E
D
C
B
10
5
0
M14-22
M14-21
M14-20
M14-19
M14-18
M14-17
M14-16
M14-15
M14-14
M14-13
M14-12
M14-11
M14-10
M14-9
M14-8
M14-7
M14-6
M14-5
M14-4
M14-3
M14-2
M14-1
m M W P G D

Facies mapping in continuous outcrops

Lateral and vertical facies distribution observed within the sequences A to G in continuous outcrops corresponding to the transects M1-M4, M5-M7 and M10-M11. The location of the collected samples for petrographic descriptions (on polished slabs and thin sections in the laboratory, or descriptions in the field) are indicated.

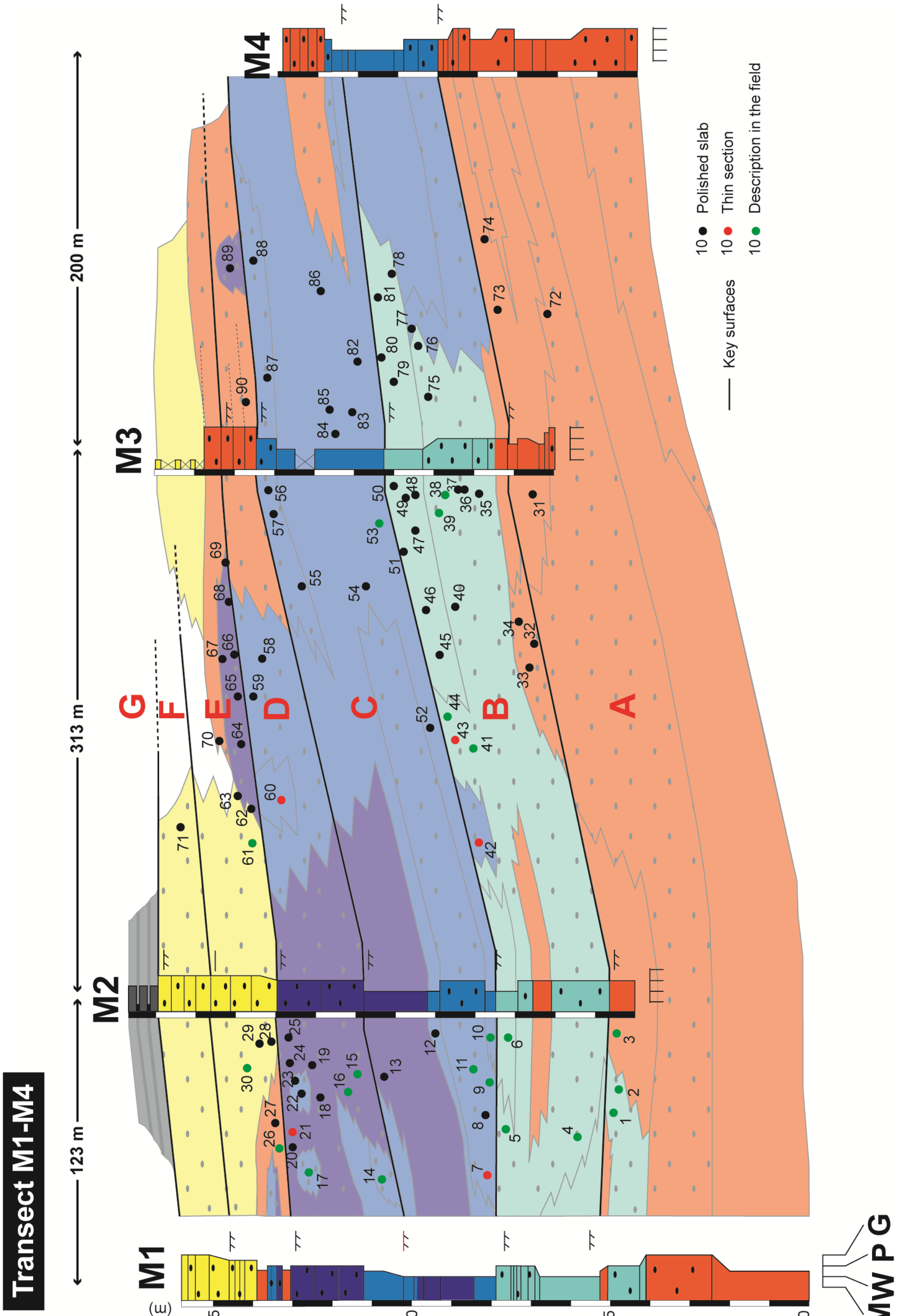

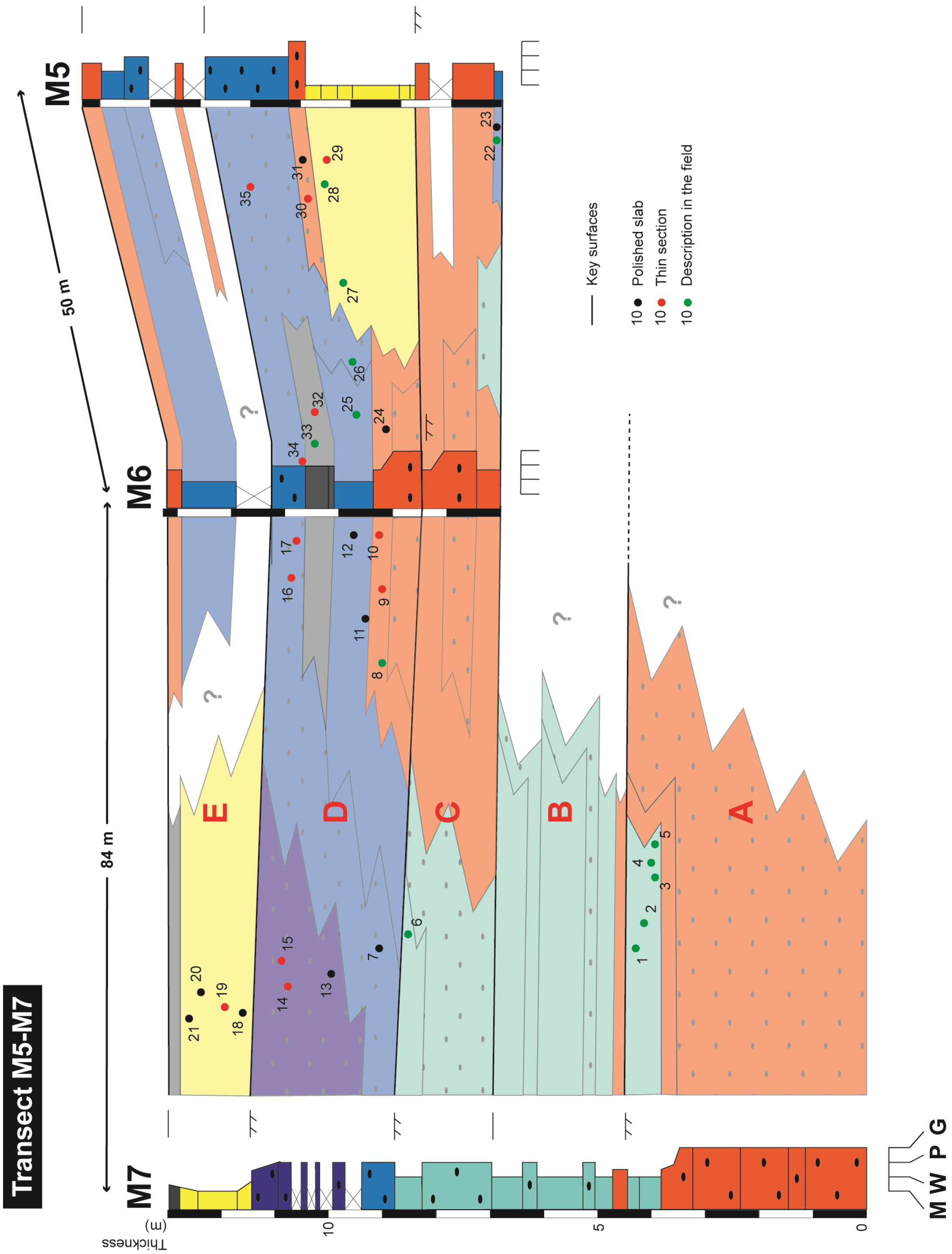

Transect M5-M7
M7
M6
M5
84 m
50 m
A
B
C
D
E
Key surfaces
Polished slab
Thin section
Description in the field
Thickness (m)
M W P G

Transect M10-M11

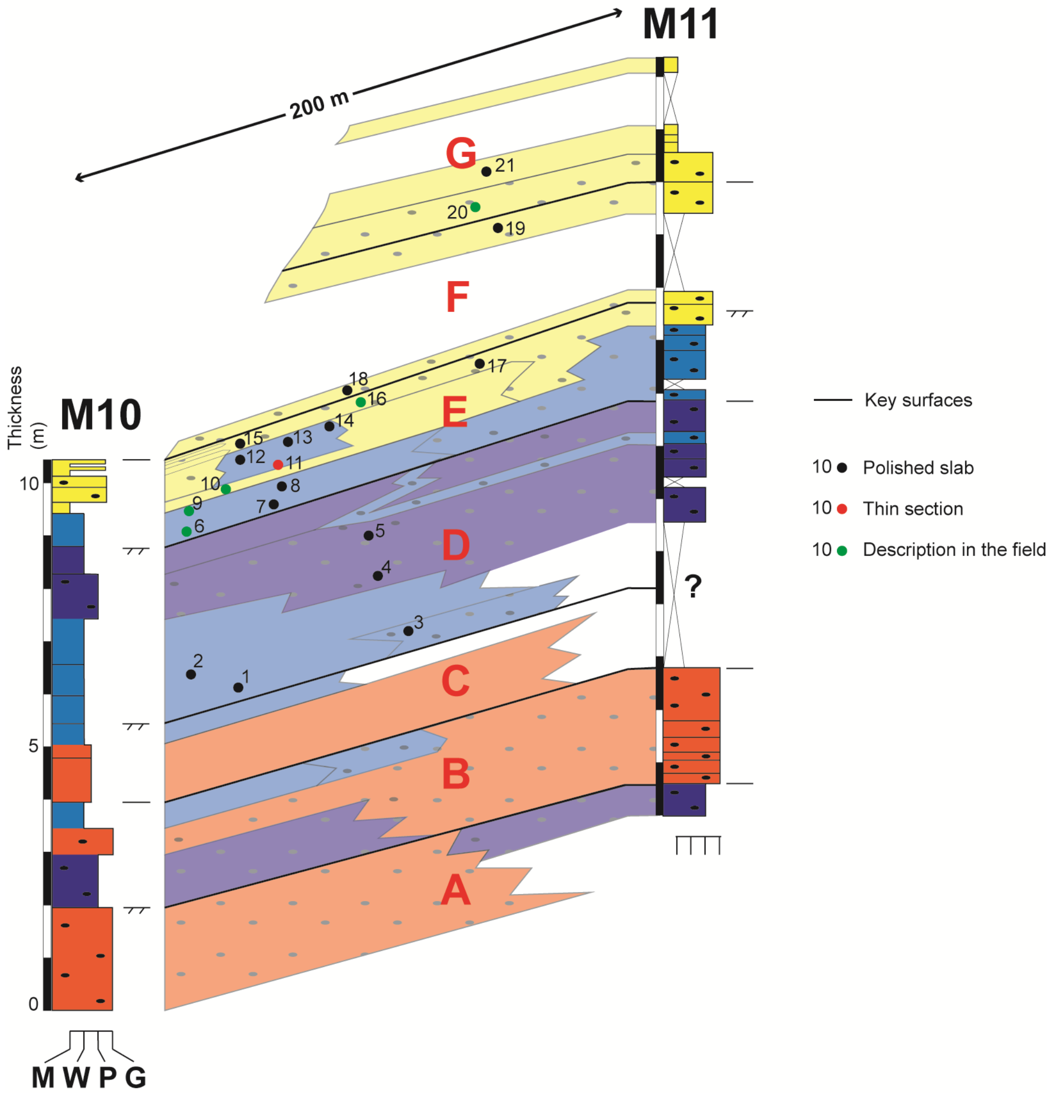

<u>ANNEXE 2</u>: SAMPLE PICTURES

This section includes some of the petrographic thin sections and polished slabs used in this Thesis to characterize the different facies of the Higueruelas Formation, which are grouped regarding the corresponding facies association. Sample references (see Annexe 1 for location), colour codes for facies (equivalent to those shown in the figures of the scientific papers in Chapter 5), and the location of each facies in a 2D schematic profile of the carbonate ramp are indicated.

PELOIDAL AND OOLITIC-DOMINATED FACIES ASSOCIATION

Intertidal domain

Peloidal M to P-G with fenestral porosity

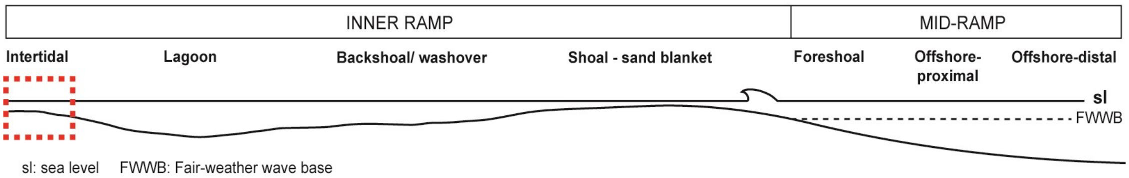

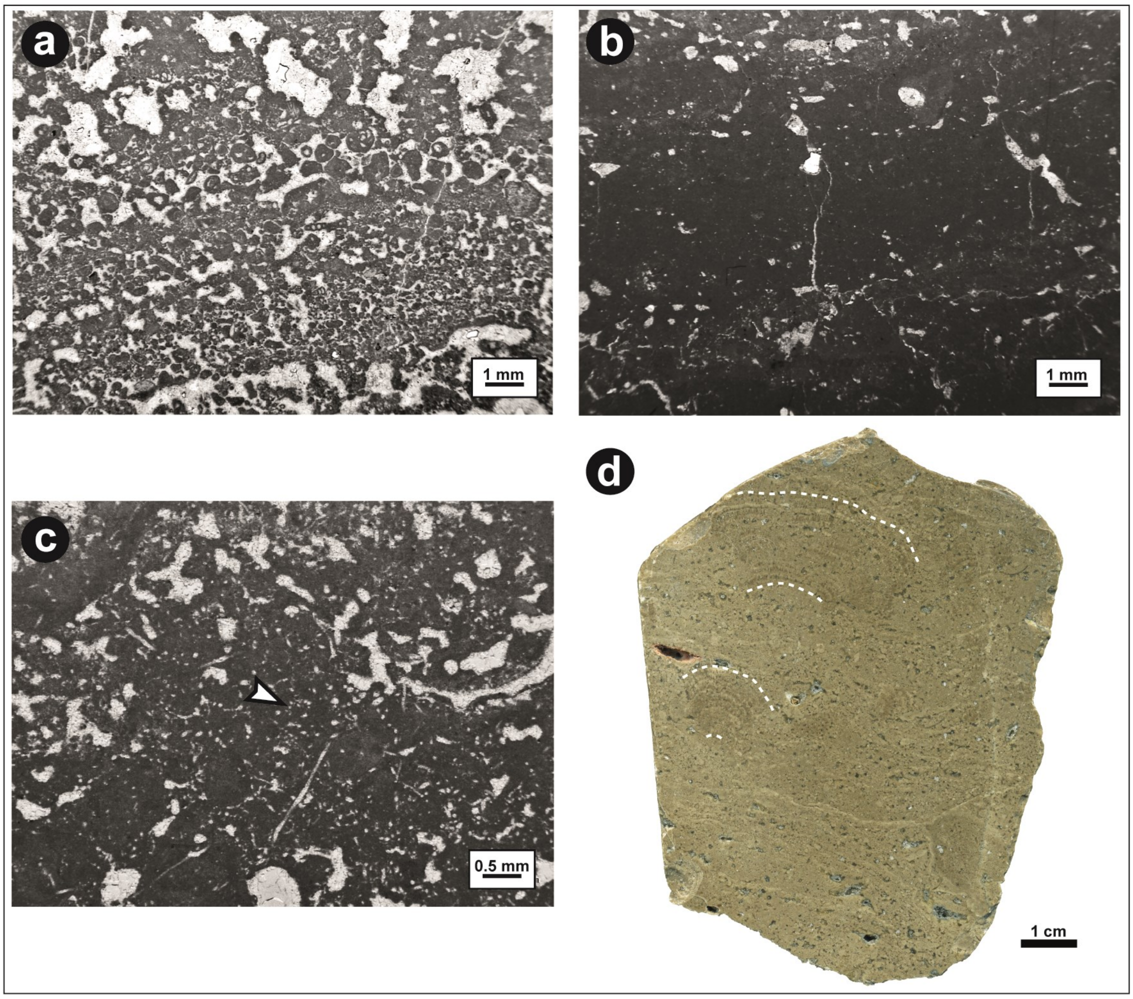

Microphotographs (a-c) and macro-scale example (d) of intertidal peloidal with fenestral porosity facies, showing parallel fenestral laminae (a, b) or a chaotic distribution of fenestral pores (c), and filaments probably associated with cyanobacterial structures (arrow in c). Dome-like stromatolitic structures (dashed lines in d) can also occur. Samples M2-34 (a), M5-5 (b), F5-46 (c) and M2-33 (d).

Restricted lagoon domain

Peloidal-bioclastic-type 3 and 4 ooid W to G

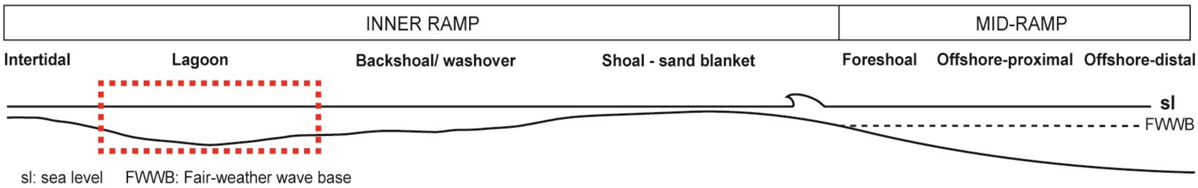

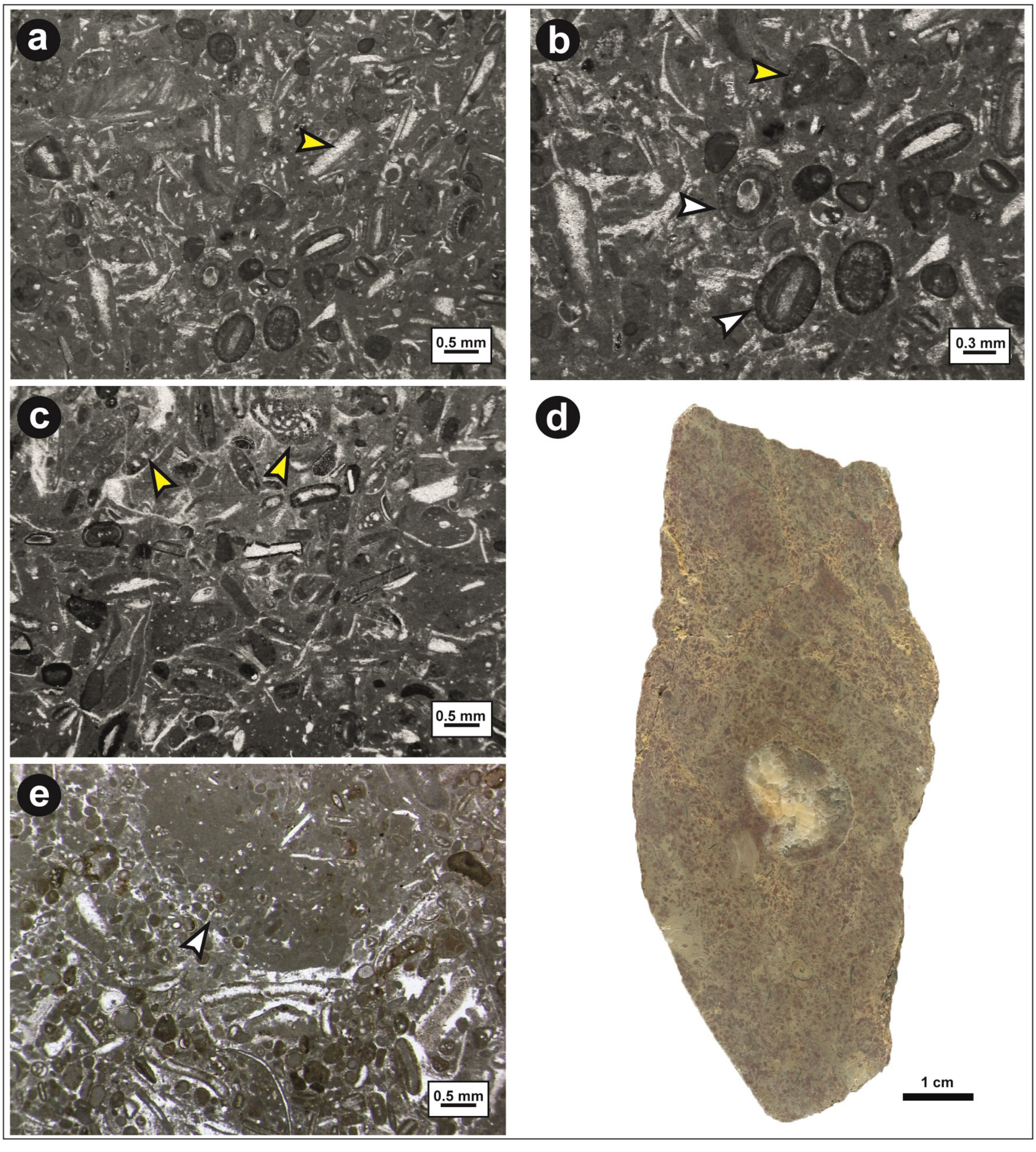

Microphotographs (a-c, e) and macro-scale example (d) of restricted lagoon peloidal-bioclastic-type 3 and 4 ooid facies, showing bivalve fragments and lituolids as main bioclasts (yellow arrows in a and c, respectively; c: Alveosepta jaccardi*). A close view of the fibrous-radial ooids is shown in b (white arrows), some of them aggregated (yellow arrow). Bioturbation galleries (*Thalassinoides *traces) are also common in this facies (arrow in e), and also ferruginization (d, e). Samples A1-74 (a, b, d), A1-80 (c) and A2-59 (e).*

Backshoal/ washover domain

Peloidal-type 1 and 1/3 ooid W to G

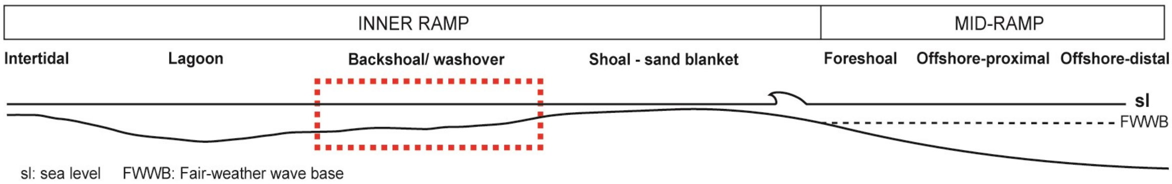

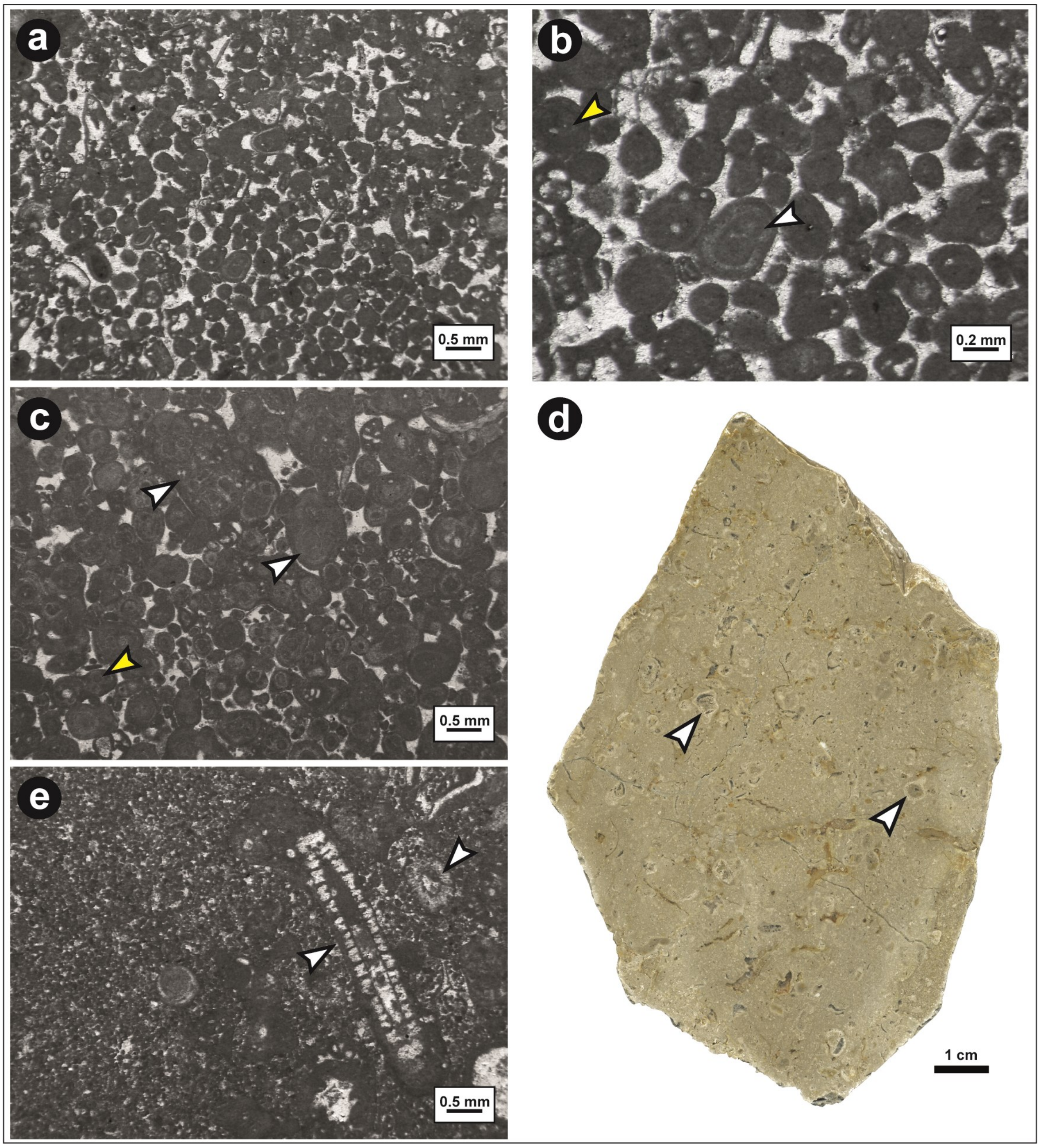

Microphotographs (a-c, e) and macro-scale example (d) of backshoal/washover peloidal-oolitic facies, showing poorly to well-sorted lithic peloids, type 1 and 1/3 ooids (yellow and white arrows in b, respectively) and bioclasts (miliolids and textulariids in a; dasyclad green algae in e (arrows); e: Salpingoporella pygmaea*). Compound and aggregate grains (white and yellow arrows in c, respectively) are also common, as well as mm- to cm-sized oncoids in variable abundance (arrows in d). Samples M6-4 (a, b), ME1-33 (c), sample nº 10 in transect M5-M7 (d) and M9-10 (e).*

Bioturbated peloidal P to G

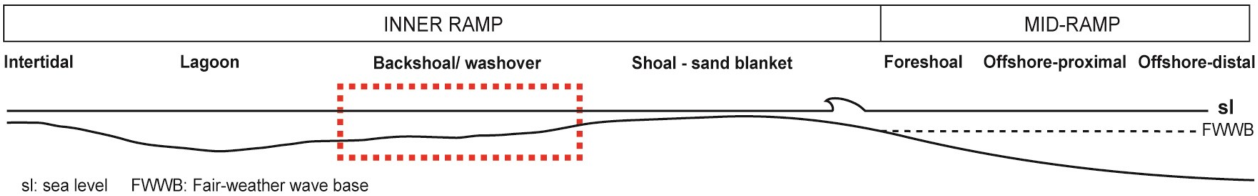

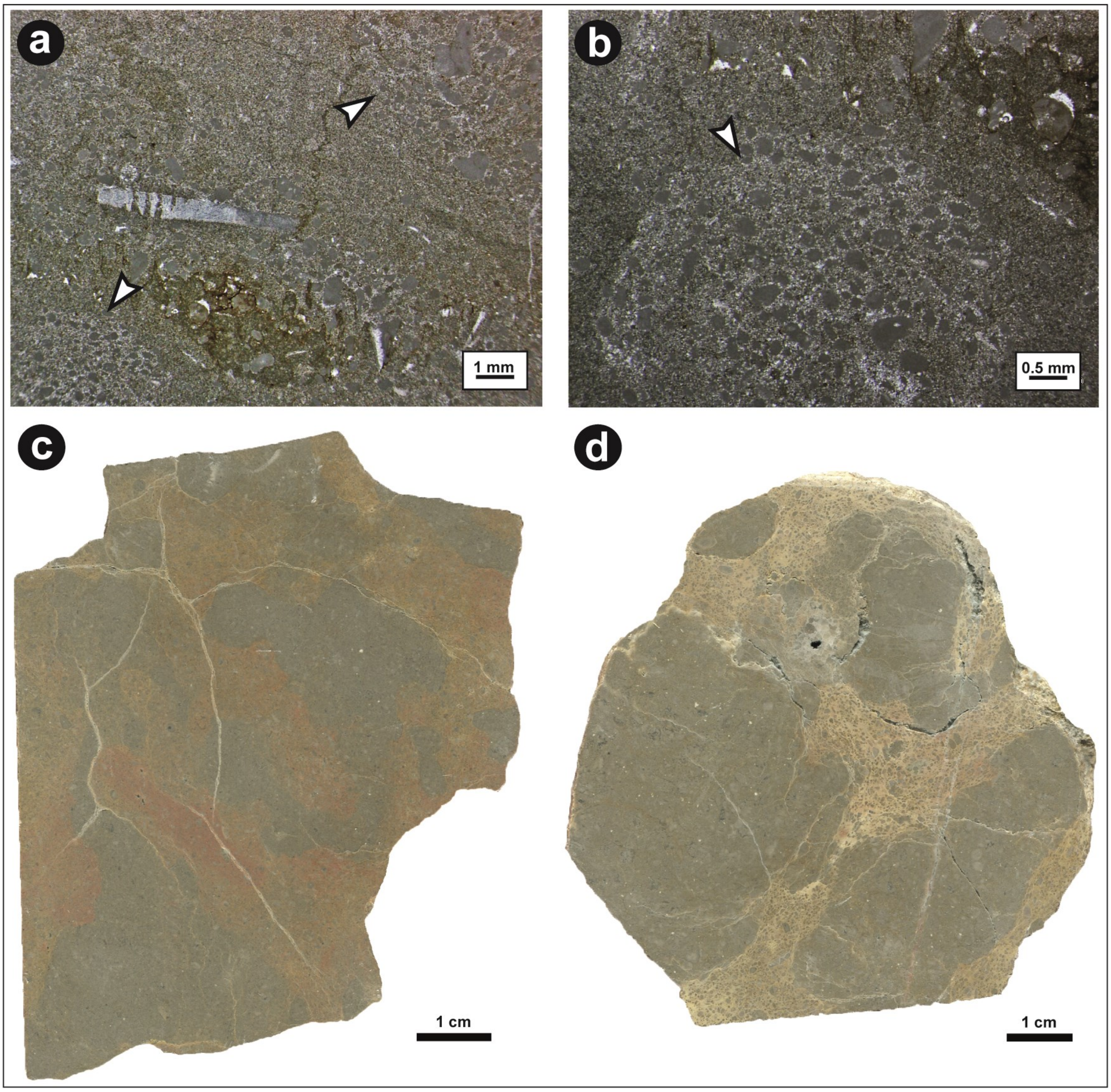

Microphotographs (a, b) and macro-scale examples (c, d) of backshoal/washover bioturbated peloidal facies, with abundant Thalassinoides *traces (indicated with arrows in a and b, and with a different colour in c and d). This facies commonly appears partially dolomitized (a, b, d) and/or ferruginized (c). Samples P3-38 (a, b), P1-25 (c) and P1-32 (d).*

Shoal-sand blanket domain

Peloidal G

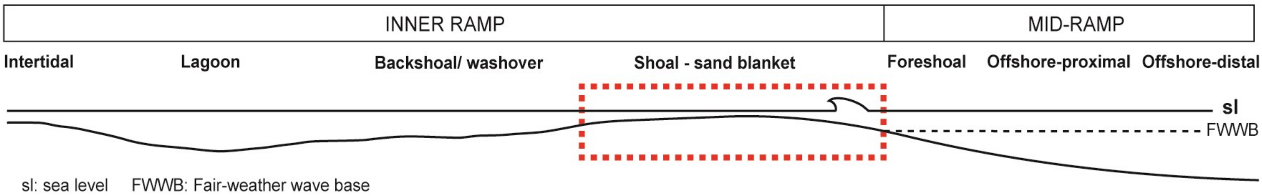

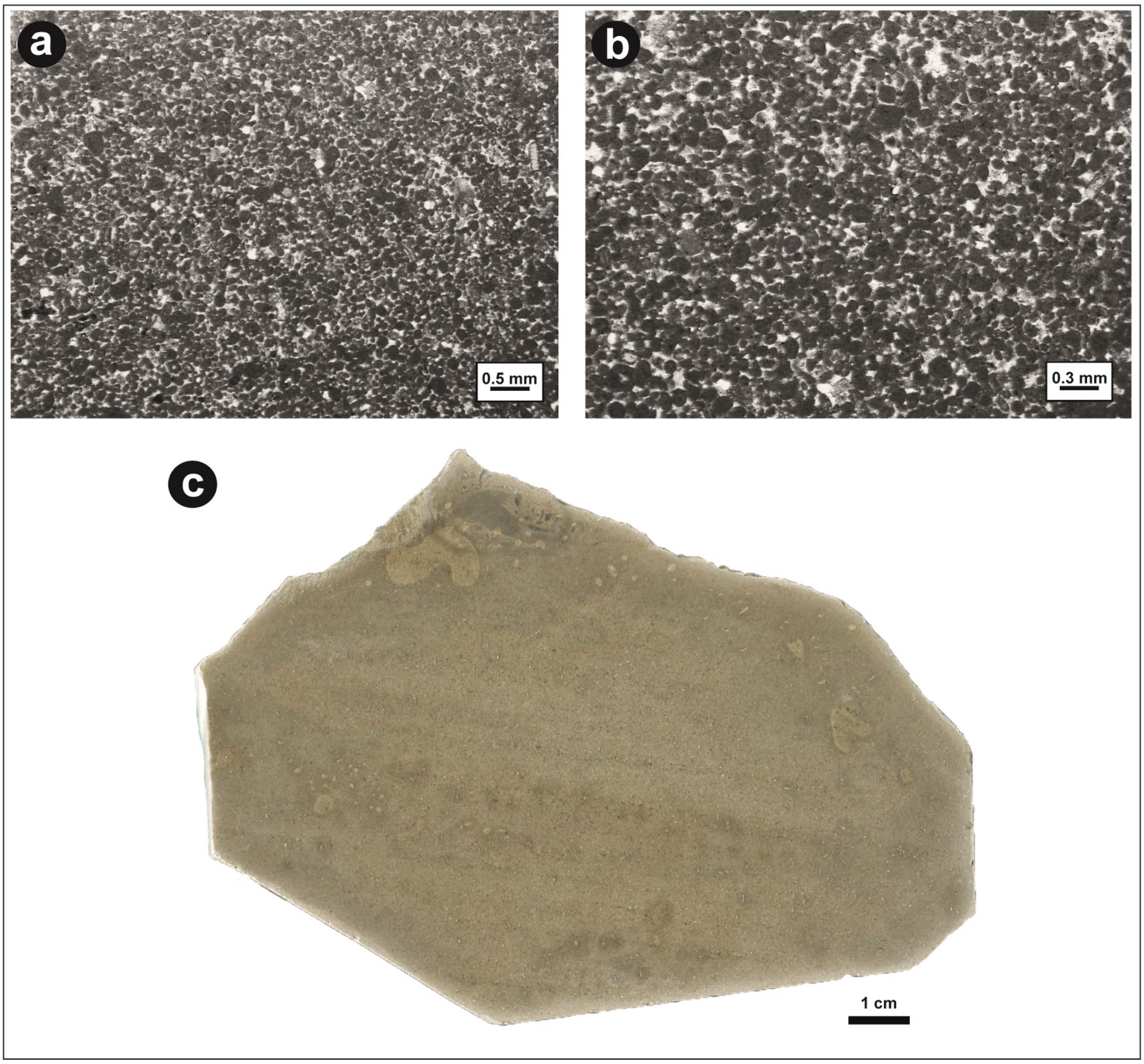

Microphotographs (a, b) and macro-scale example (c) of shoal-sand blanket peloidal facies, showing well-sorted and rounded lithic peloids (a, b) and scarce bioclasts (mainly foraminifera). Parallel lamination is common in this facies (c). Samples P3-3 (a, b) and M14-3 (c).

Type 1 and 1/3 ooid-peloidal G

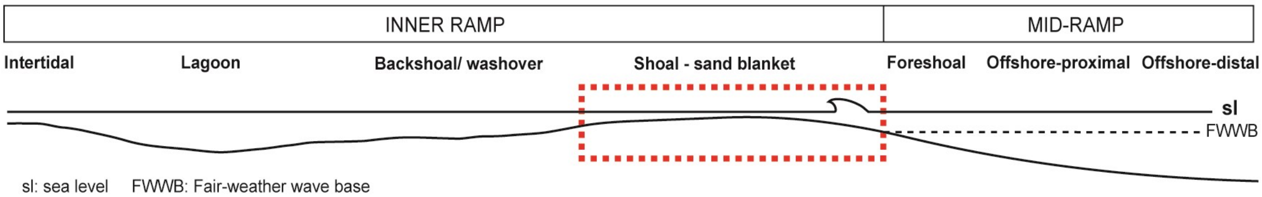

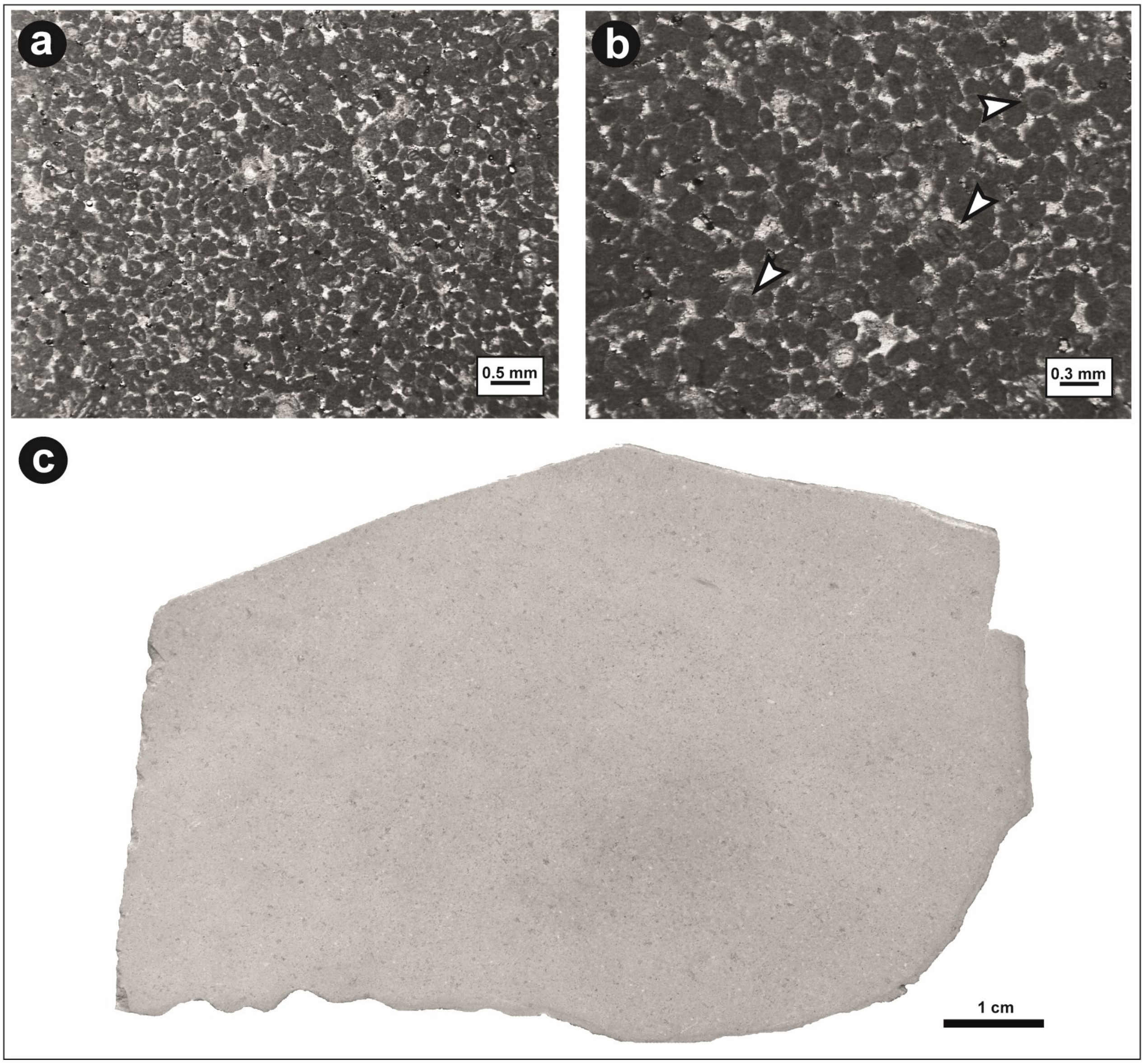

Microphotographs (a, b) and macro-scale example (c) of shoal-sand blanket peloidal-oolitic facies, with well-sorted lithic peloids, type 1 and 1/3 ooids (arrows in b indicate type 1/3 ooids) and scarce bioclasts (mainly foraminifera). Most of these ooids show a thin cortex (b). Sample M14-5.

Type 1 and 1/3 ooid G

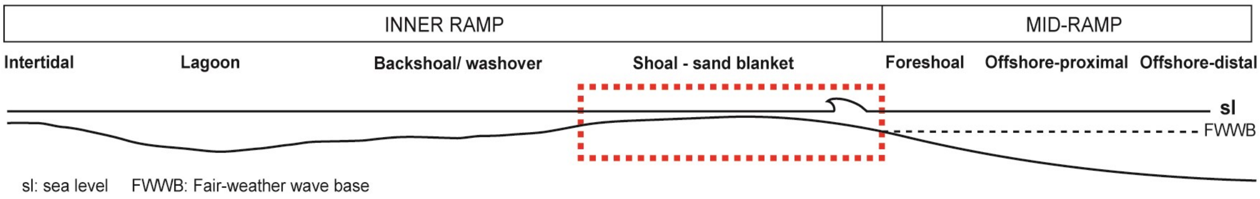

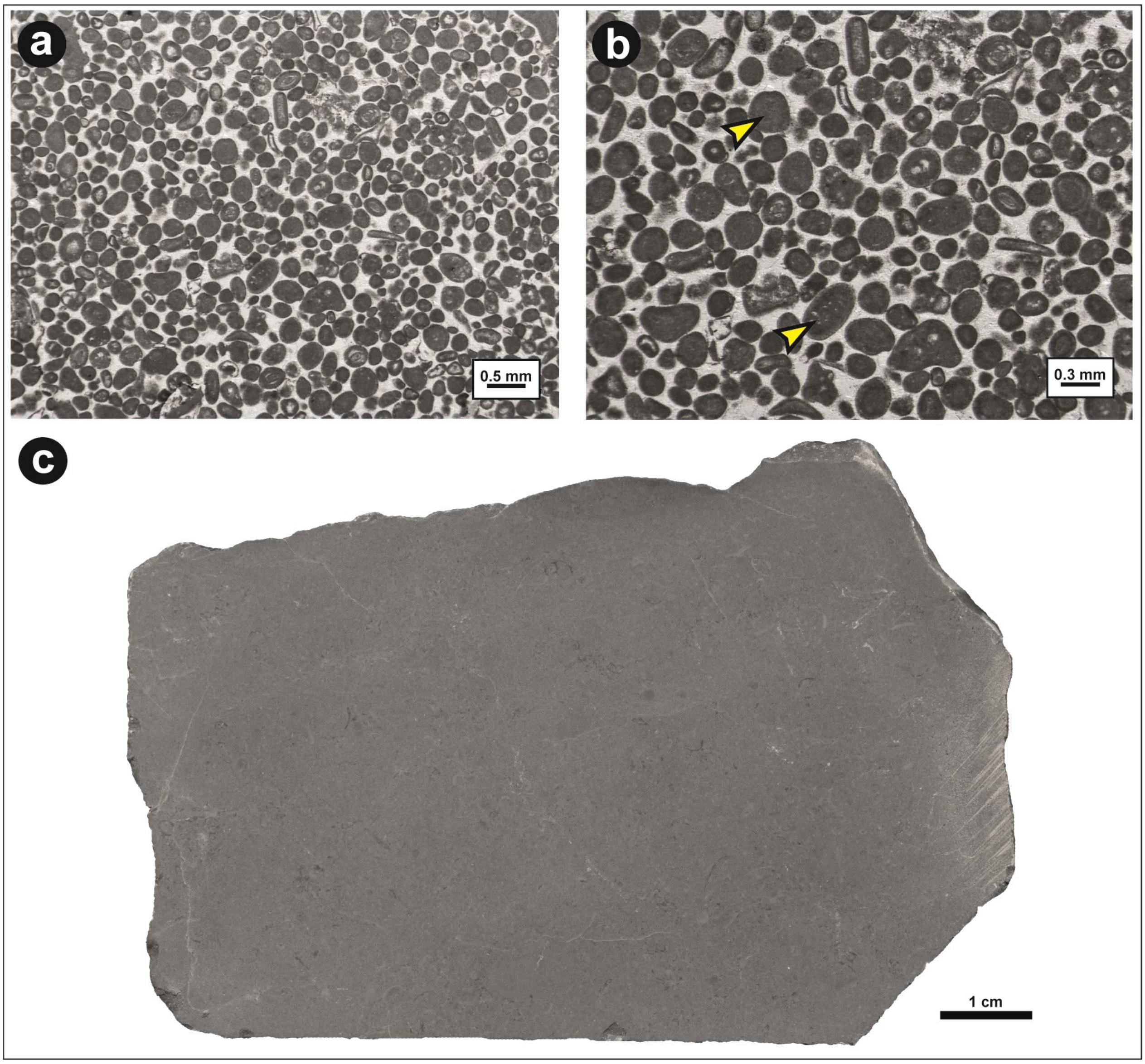

Microphotographs (a, b) and macro-scale example (c) of shoal-sand blanket oolitic facies, mainly composed of well-sorted and rounded type 1 and 1/3 ooids (arrows in b indicate type 1/3 ooids). Lithic peloids are also common in minor proportion, and bioclasts (mainly foraminifera) are scarce. Samples ME3-44 (a, b) and ME3-46 (c).

Foreshoal domain

Peloidal W-P to G

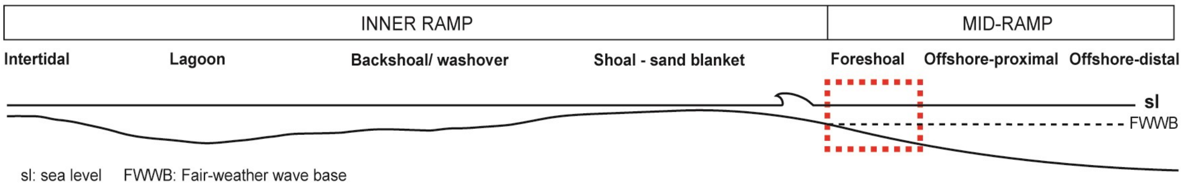

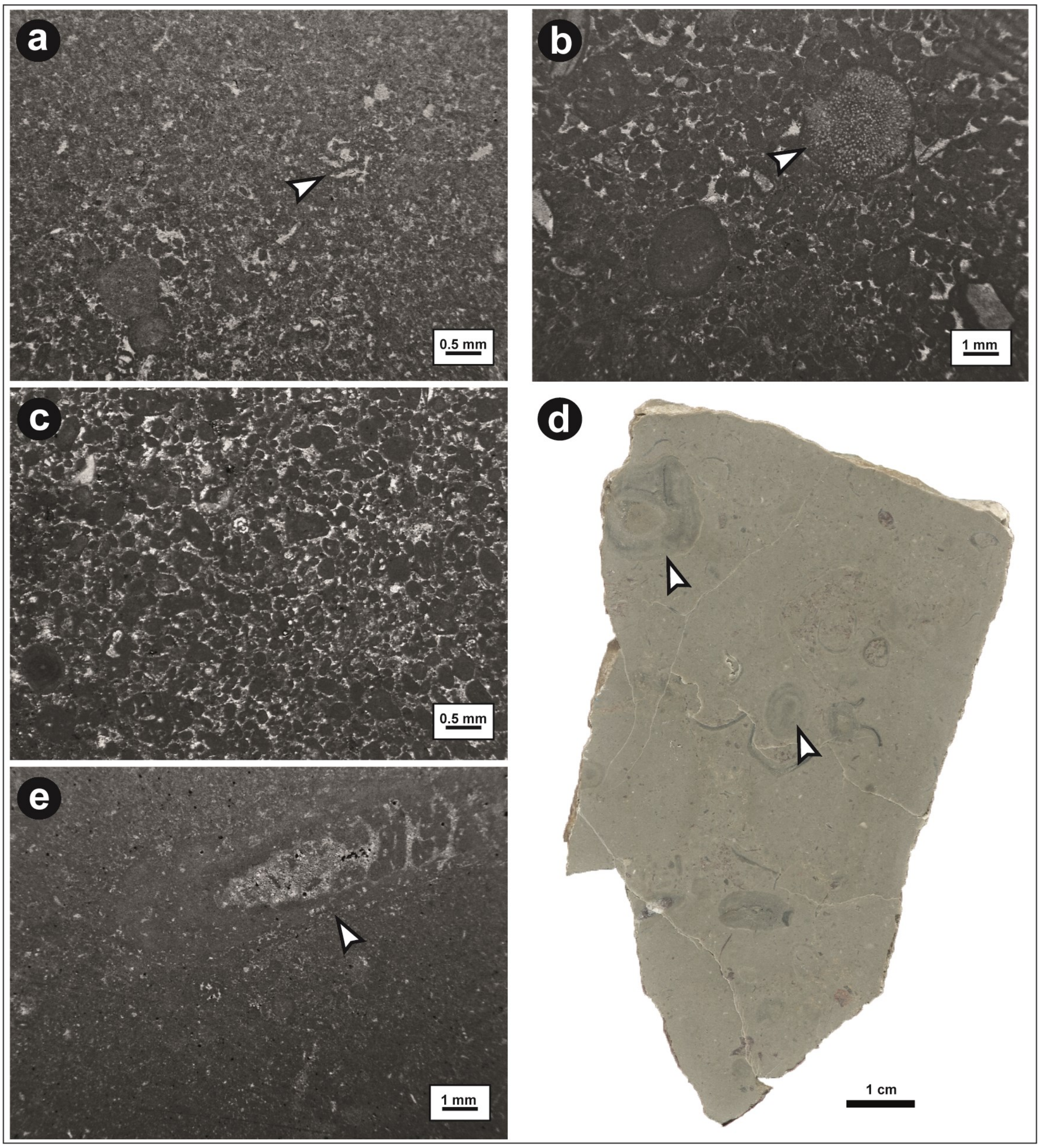

Microphotographs (a-c, e) and macro-scale example (d) of foreshoal peloidal facies, mainly composed of poorly to well-sorted lithic peloids. Bioclasts are also common, such as lituolids (arrow in a) or cyanobacteria (arrow in b: Cayeuxia-Ortonella*). Oncoids can also appear in less abundance, from few millimetres to several centimetres in size (arrows in d, e; e: type II oncoid with a gastropod as nucleus). Samples F1-4 (a), F5-45 (b), F4-59 (c), ME3-19 (d) and J2-15 (e)***.**

Storm lobes in backshoal and foreshoal domains

Intraclastic-peloidal P to G

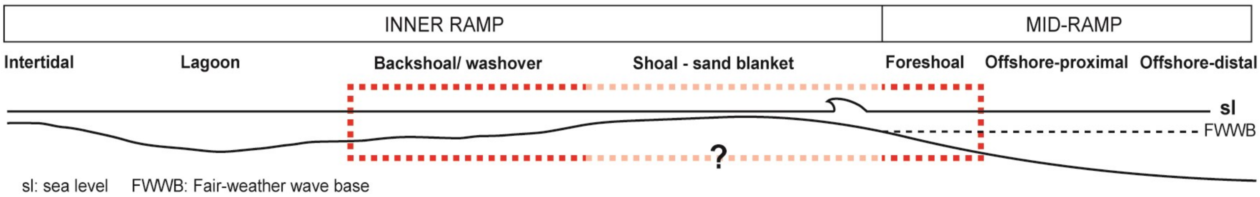

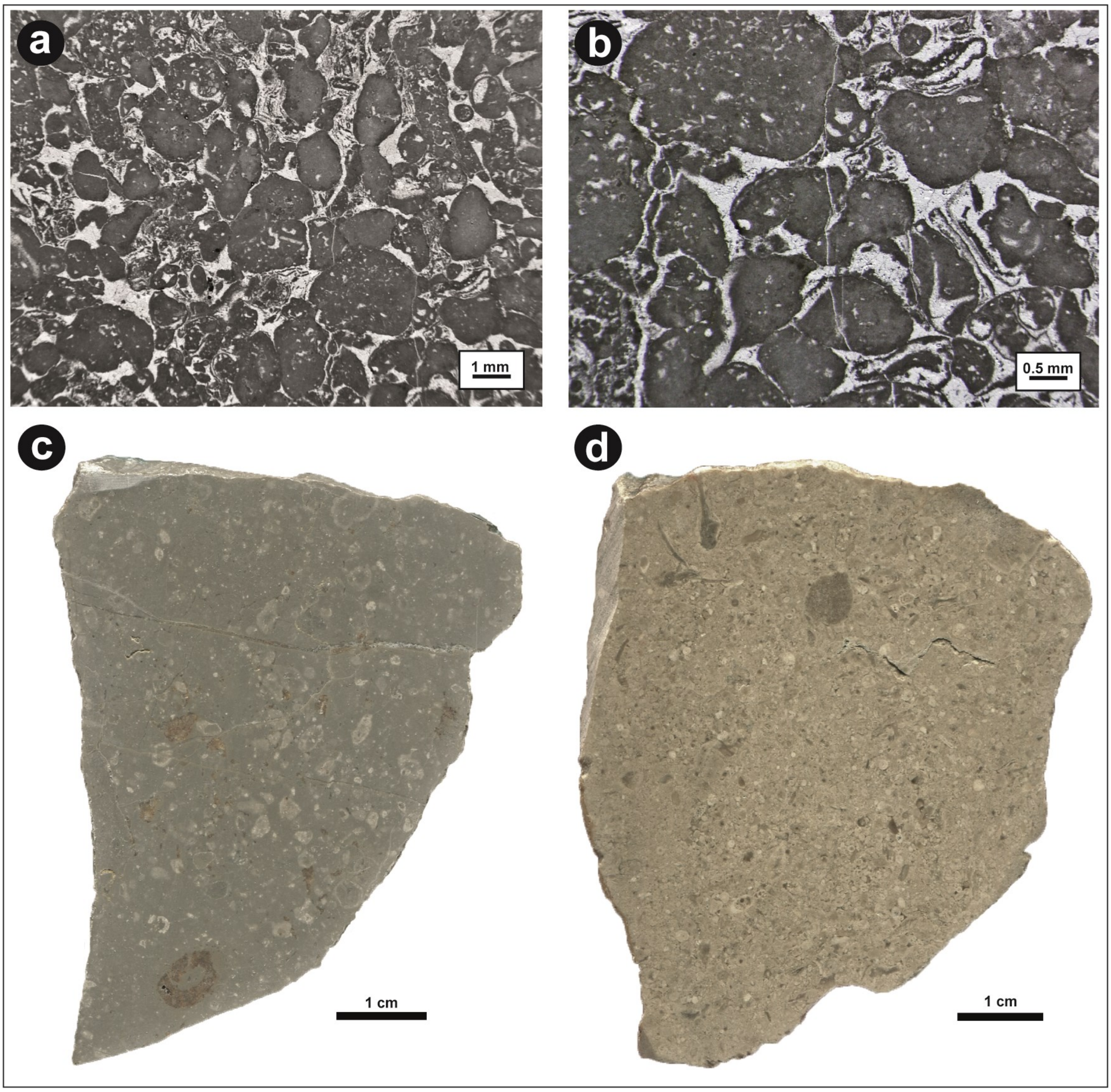

Microphotographs (a, b) and macro-scale examples (c, d) of storm-related intraclastic-peloidal facies, showing poorly sorted (mm to cm in size) and poorly rounded fragments of micritic (with bioclasts) and grain-supported facies (with peloids, ooids and bioclasts), grading into rounded lithic peloids. Samples P1-16 (a, b), J3-55 (c) and P3-18 (d).

Offshore-proximal domain

Peloidal-bioclastic W to P

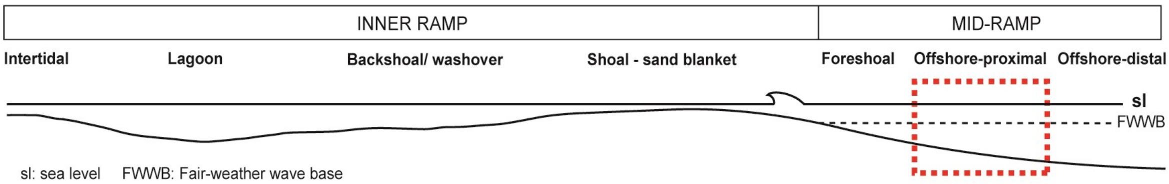

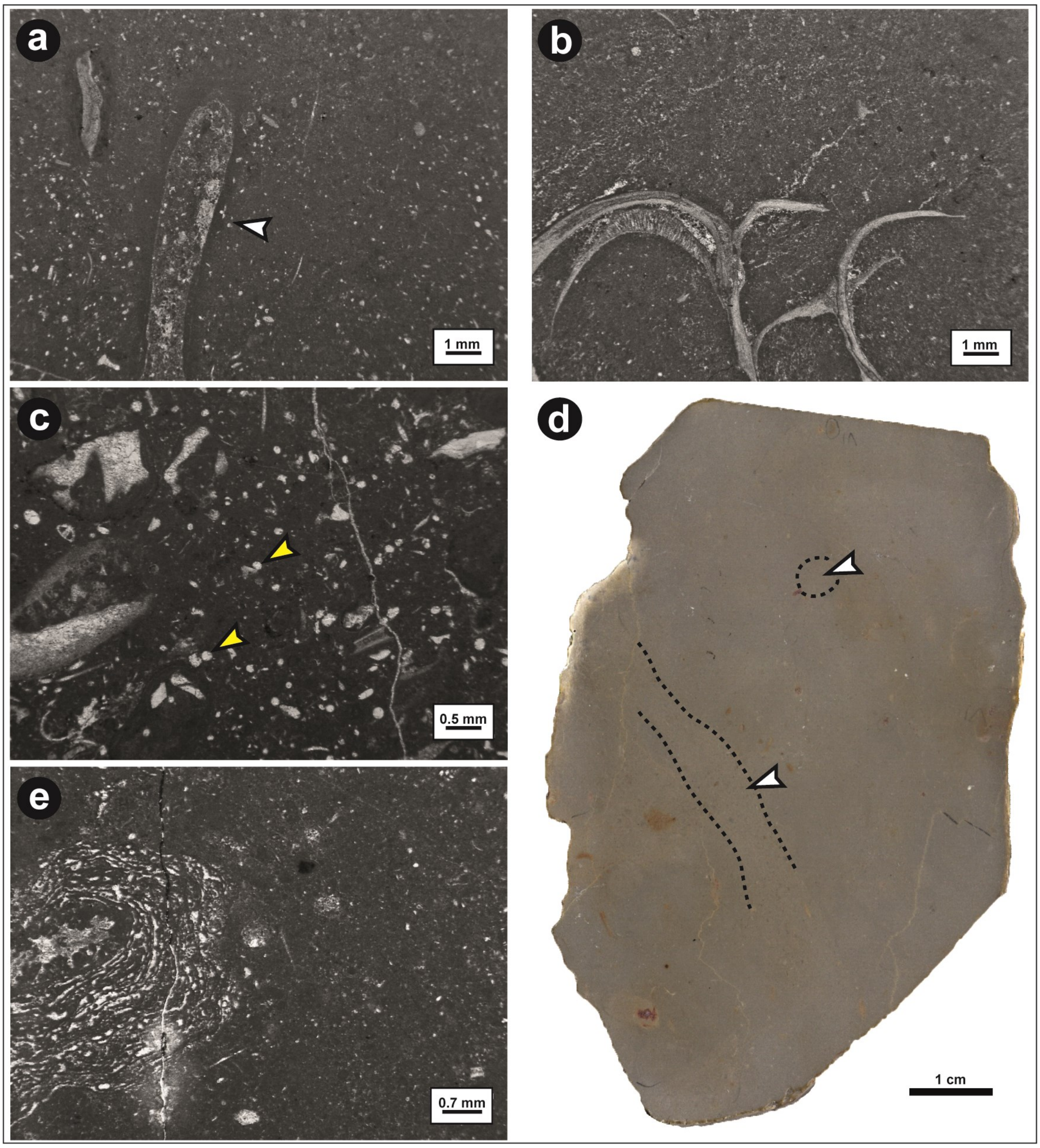

*Microphotographs (a-c, e) and macro-scale example (d) of offshore-proximal peloidal-bioclastic facies, with poorly to well-sorted lithic peloids and bioclasts as main components (arrow in a: serpulids; b: brachiopods; arrows in c: sponge spicules). Bioturbation (*Planolites *traces in d, white arrows) are frequent.* Lithocodium*-dominated type IVb oncoids (e) commonly appear in this facies. Samples F5-14 (a), P4-30 (b), F5-10 (c), ME3-11 (d) and F3-27 (e).*

Offshore-distal domain

Bioclastic-peloidal M

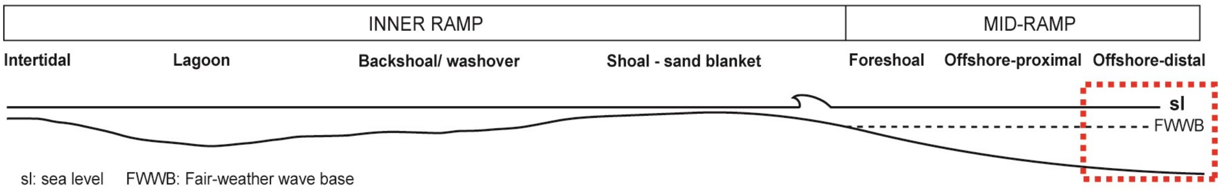

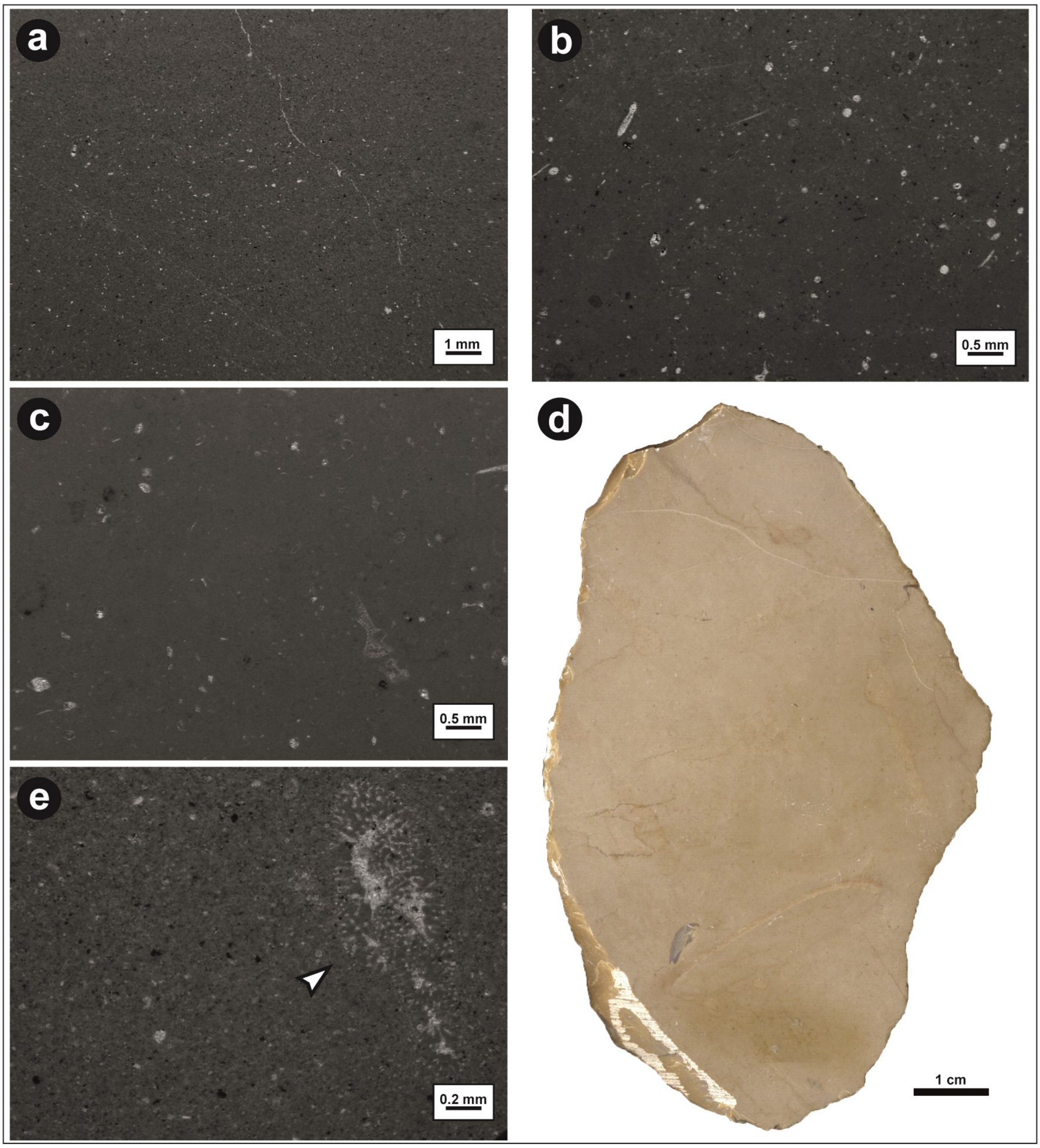

Microphotographs (a-c, e) and macro-scale example (d) of offshore-distal bioclastic-peloidal facies. Sponge spicules (a-c) and lituolids (arrow in e) are common in this facies. Samples F1-1 (a, e), A1-1 (b), P4-2 (c), P4-3 (d).

ONCOLITIC-DOMINATED FACIES ASSOCIATION

Ponds in the intertidal domain

Gastropod-oncolitic W-P to G

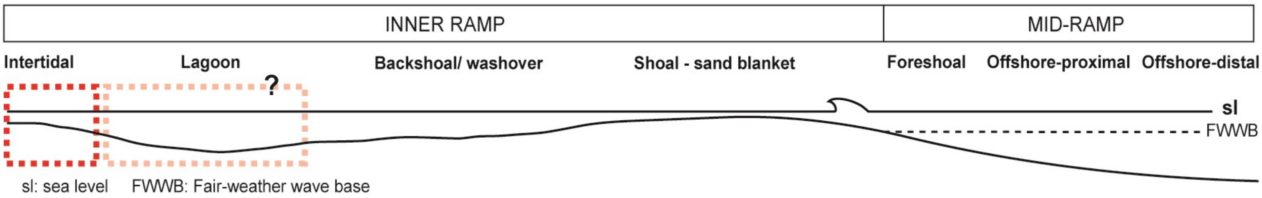

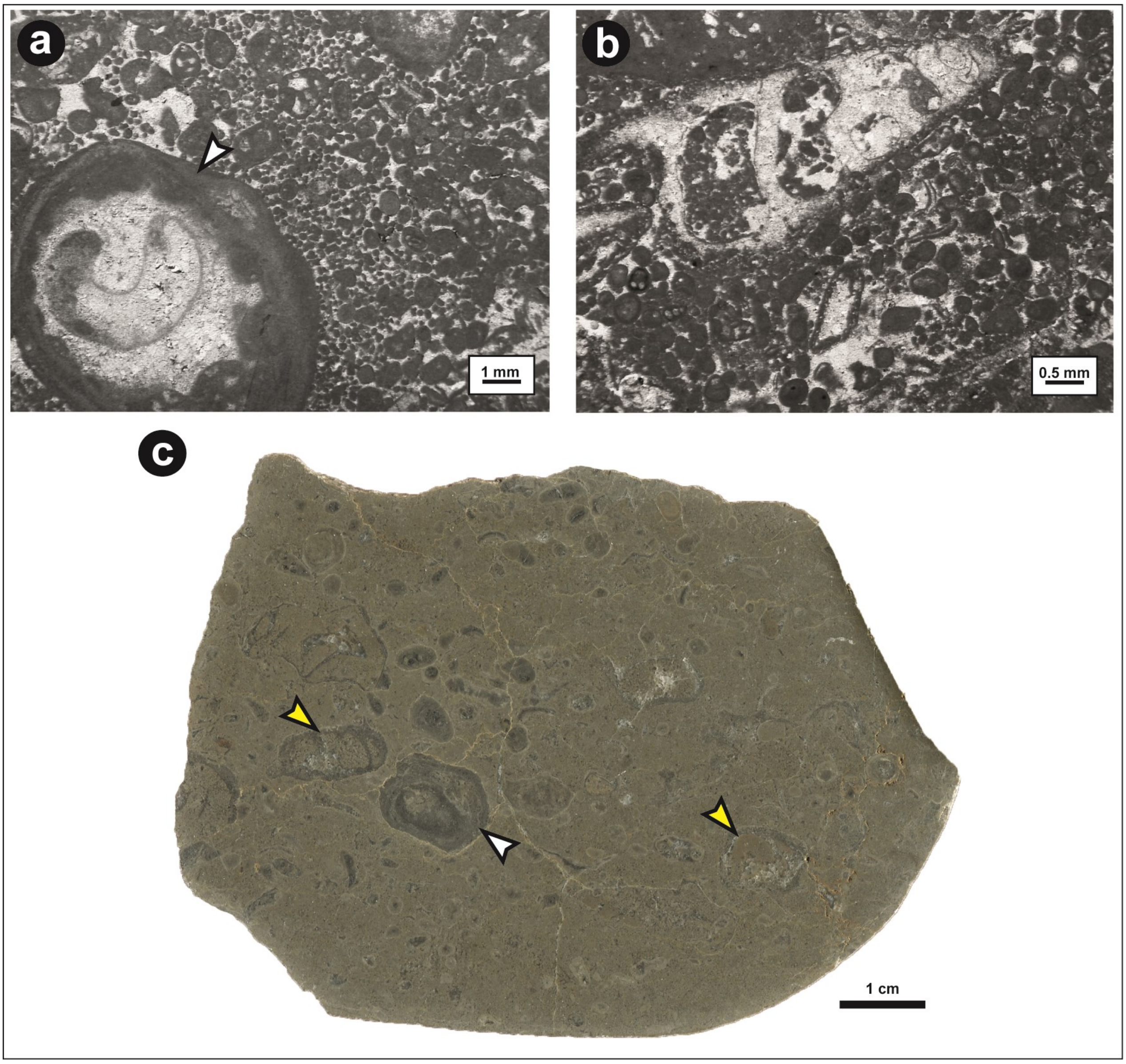

Microphotographs (a, b) and macro-scale example (c) of gastropod-oncolitic facies, representing ponds in the intertidal domain, showing mm- to cm-sized oncoids (white arrows in a and c) and gastropods (b, yellow arrows in c) as main components, surrounded by irregular to well-rounded lithic peloids and some type 1 and 1/3 ooids. Gastropods usually constitute oncoids nuclei (a). Sample M8-20.

Sheltered lagoon domain

Type IV oncoid W to P

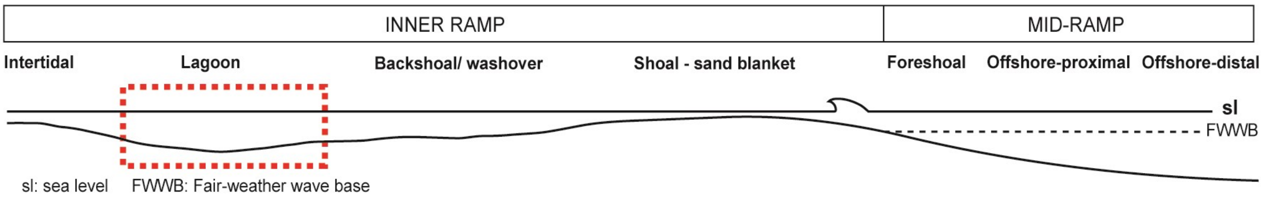

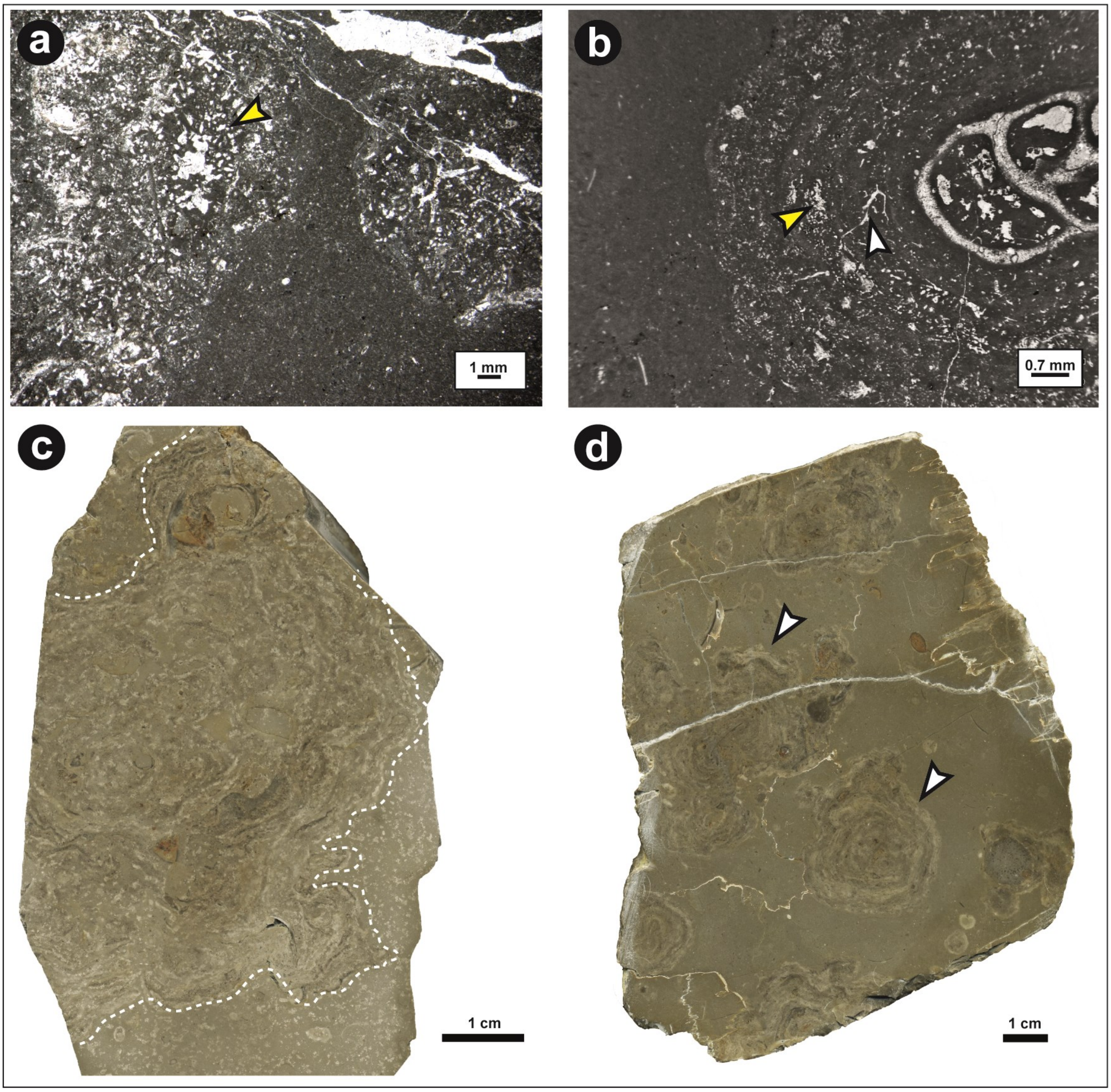

Microphotographs (a, b) and macro-scale examples (c, d) of sheltered lagoon type IV oncoid facies. a) Type IVa oncoids showing Bacinella irregularis *as main micro-encruster, also* Bacinella irregularis-Lithocodium aggregatum *association (arrow). b) Type IIIb oncoid showing* B. irregularis *and* Girvanella *(yellow and white arrows, respectively) within the organism-bearing laminae, alternating with thinner micritic laminae. (c, d) Macro-scale view of large and irregular type IVa oncoids (dashed line in c, arrows in d), showing up to 7 cm in diameter (c). Samples M1-10 (a, c), M7-17 (b) and M3-9 (d).*

Backshoal and foreshoal domains

Type II and III oncoid P

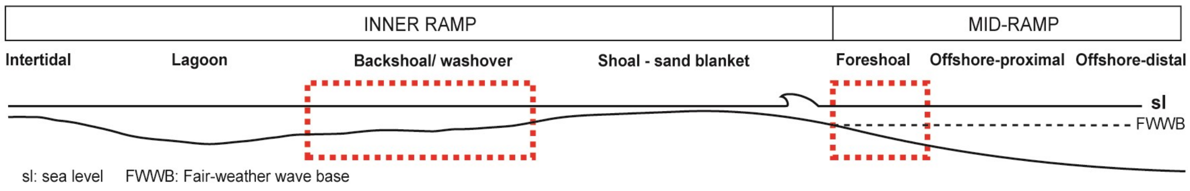

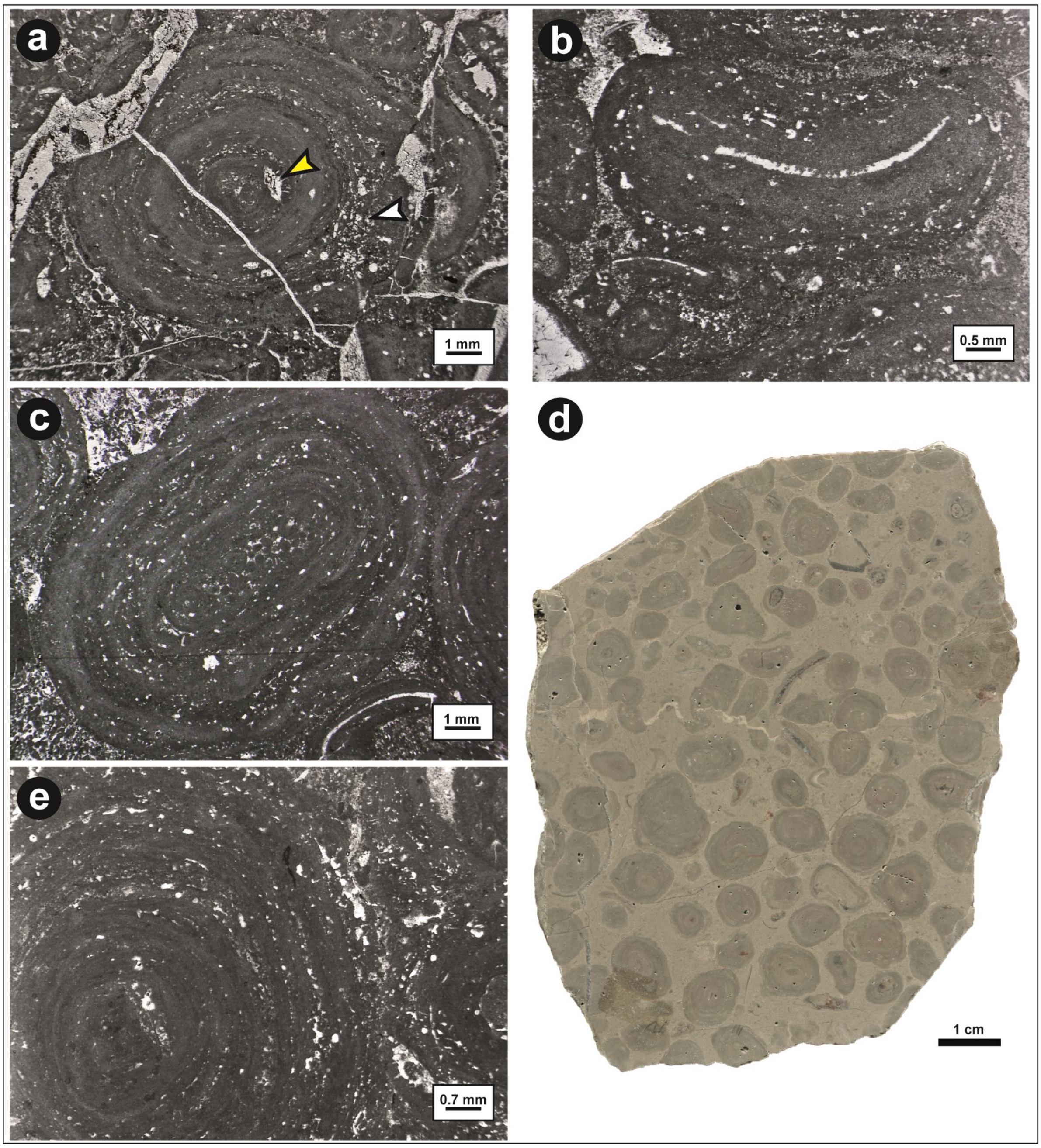

Microphotographs (a-c, e) and macro-scale example (d) of backshoal (a, b) and foreshoal (c-e) type II and III oncoid facies, showing Bacinella irregularis *and* Bacinella-Lithocodium *association (white and yellow arrows in a, respectively) as main micro-encrusters (type II oncoid in b; type IIIa oncoids in a, c, e). Samples A2-26 (a), J3-48 (b), TO-10 (c), A2-16 (d) and ME2-3 (e).*

Shoal-sand blanket domain

Type II oncoid G

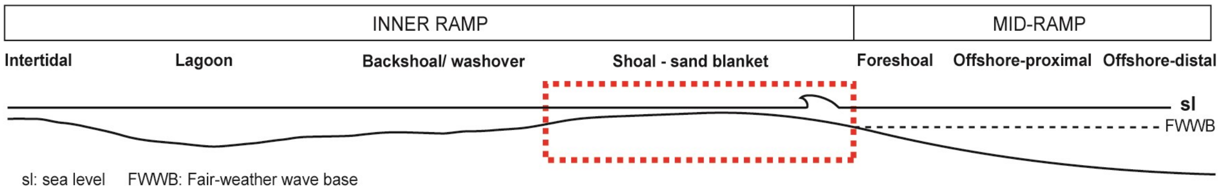

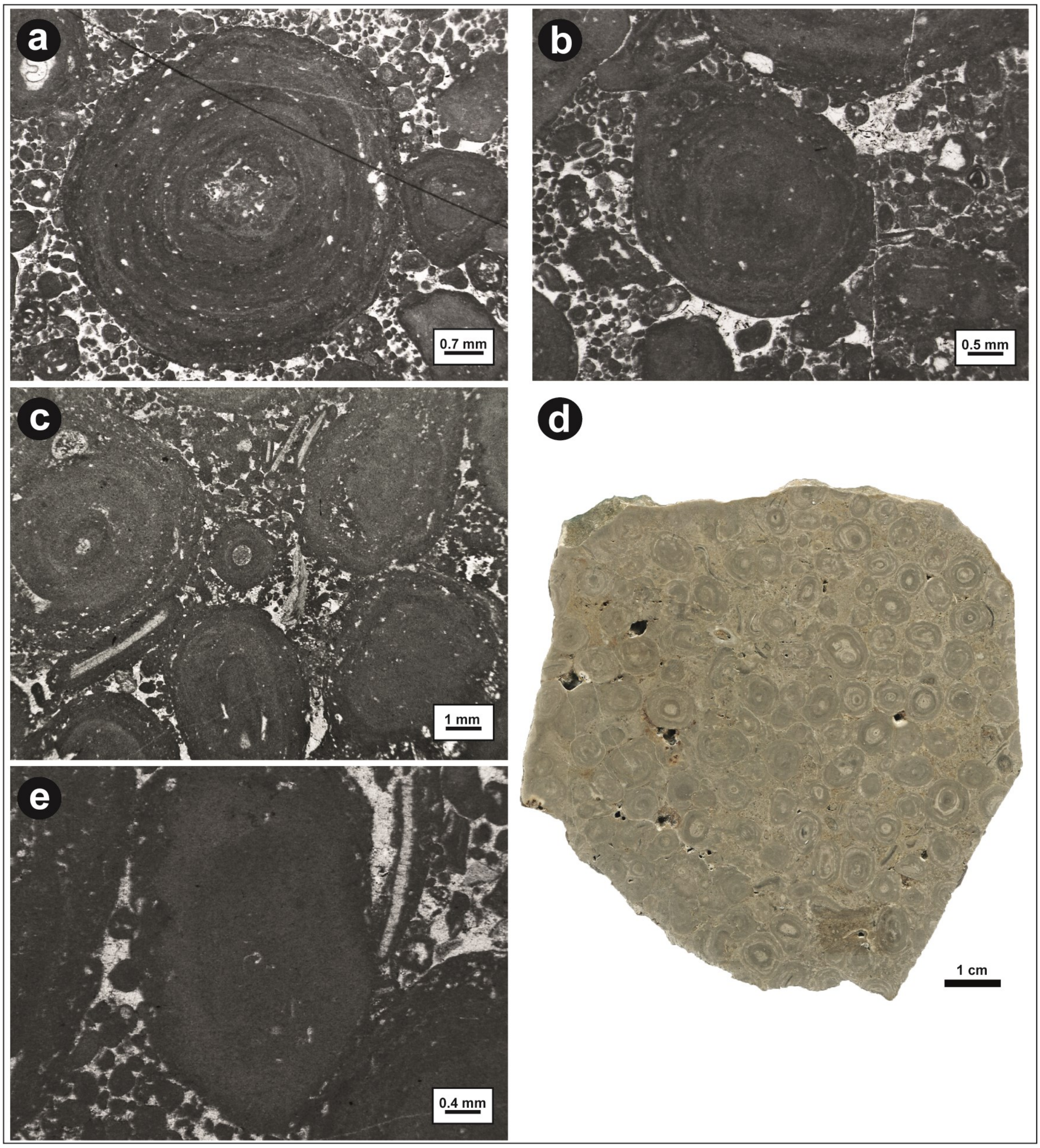

Microphotographs (a-c, e) and macro-scale example (d) of shoal-sand blanket type II oncoid facies. Note the smaller size of oncoids compared to the other oncolitic-dominated facies, and the oncolitic-supported texture in macro-scale view (d). Samples A2-27 (a, b), J2-24 (c, e) and ME2-22 (d).

STROMATOPOROID/CHAETETID/CORAL-RICH FACIES ASSOCIATION

Sheltered lagoon to backshoal domains

Stromatoporoid W to G

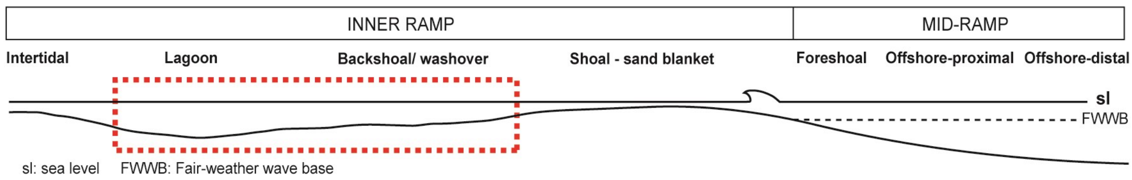

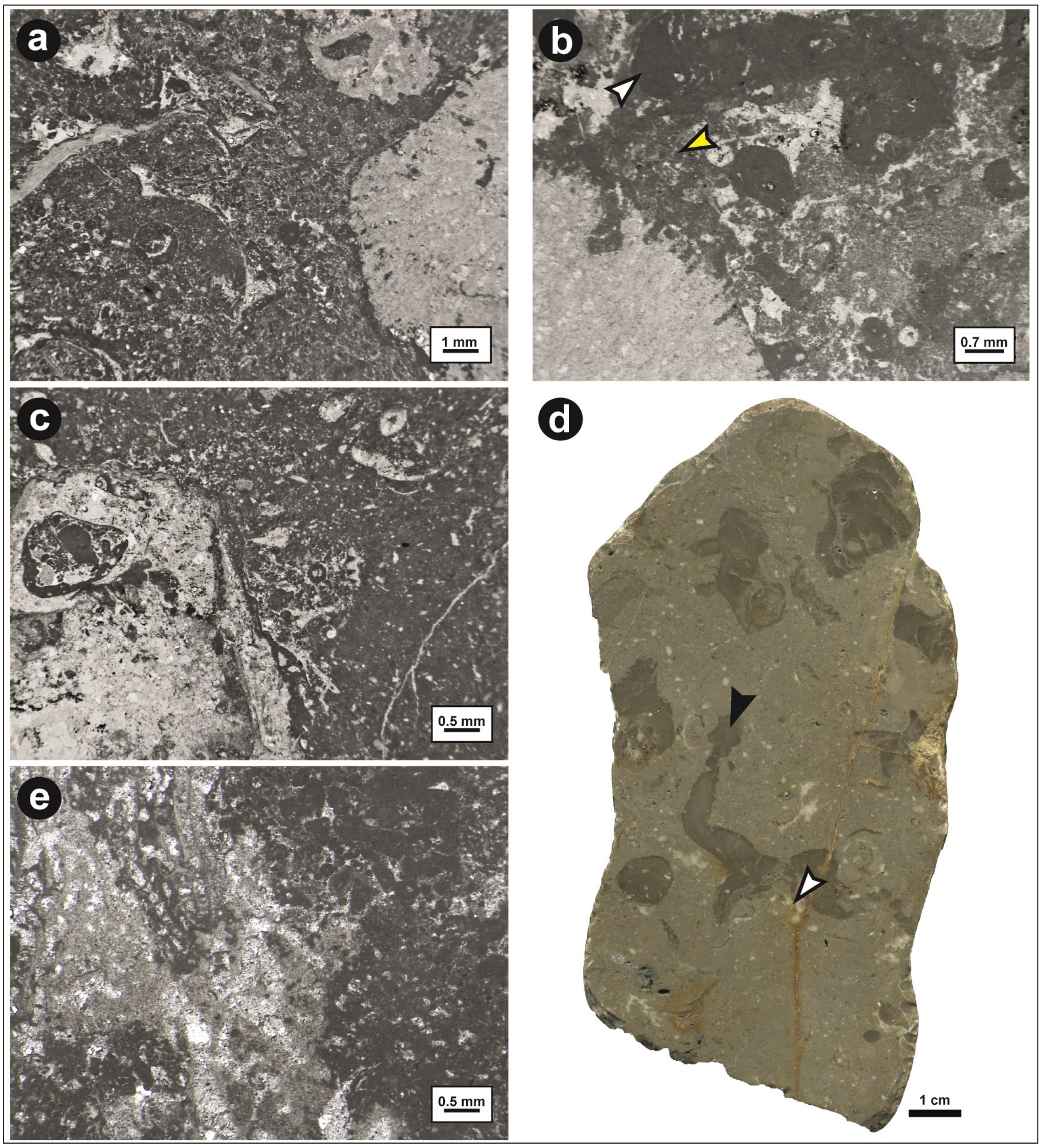

Microphotographs (a-c, e) and macro-scale example (d) of sheltered lagoon to backshoal stromatoporoid facies, with cm-sized stromatoporoid fragments (mainly Cladocoropsis mirabilis*; macro-scale view of these fragments in d (black arrow)) surrounded by microbial (yellow arrow in b) and lithic peloids, bioclasts and showing common* Tubiphytes *encrustations (white arrows in b and d). Samples M2-25 (a, e), M7-25 (b), M2-19 (c) and M2-24 (d).*

Oncolitic-stromatoporoid W to G

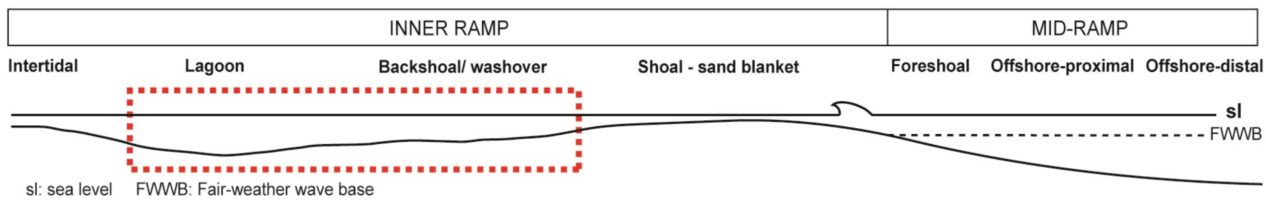

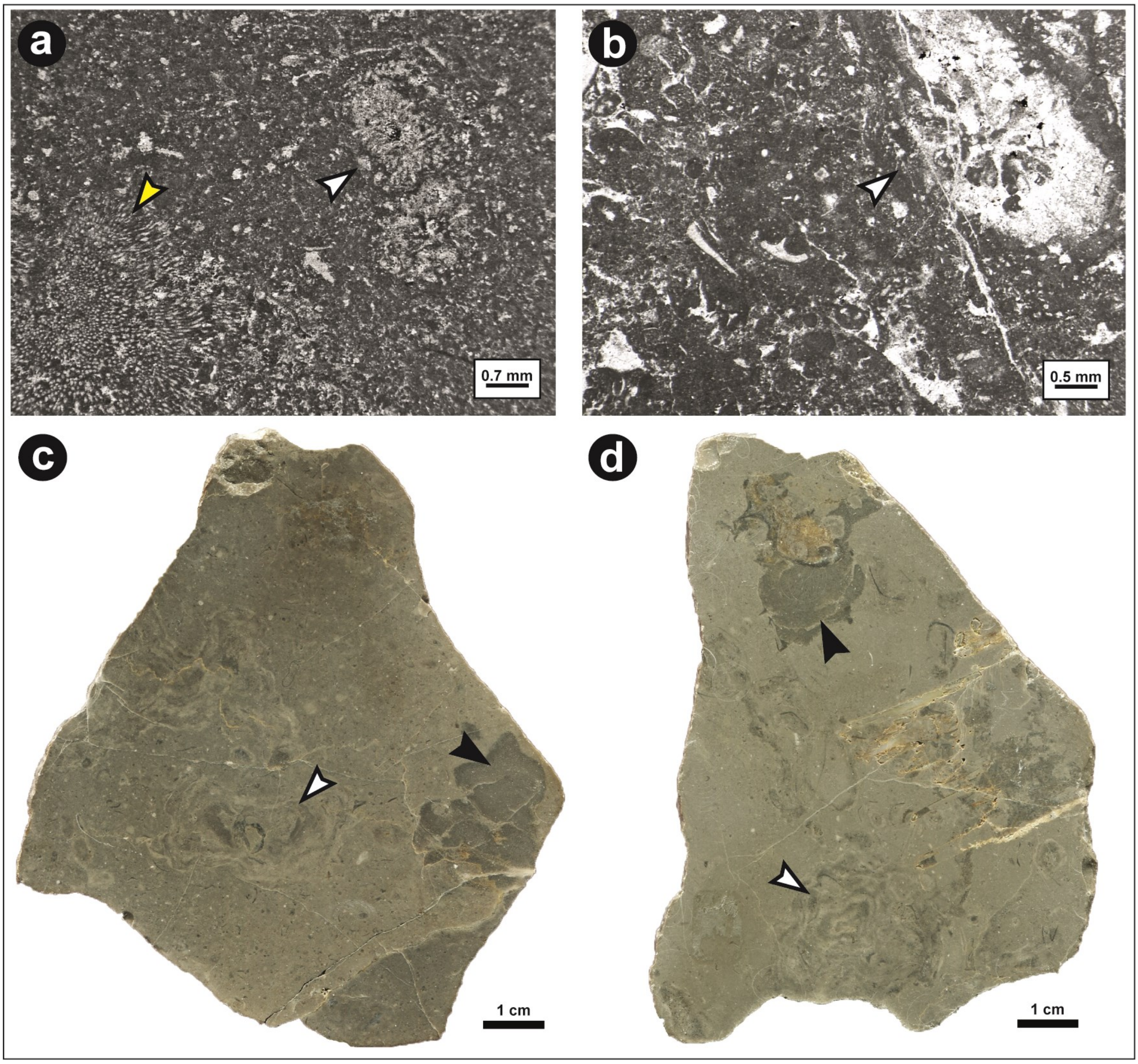

Microphotographs (a, b) and macro-scale examples (c, d) of sheltered lagoon to backshoal oncolitic-stromatoporoid facies. (a, b) Type II oncoids showing stromatoporoid and coral fragments as nuclei (white arrows in a and b, respectively). Growths of Cayeuxia-Ortonella *(yellow arrow in a) are also common. (c, d) Macro-scale view of the oncoids (white arrows) and stromatoporoid fragments (black arrows) in this facies. Samples M12-8 (a), M2-15 (b), sample nº 58 in transect M1-M4 (c) and M10-13 (d).*

Foreshoal to offshore-proximal domains

Chaetetid-stromatoporoid-coral buildup

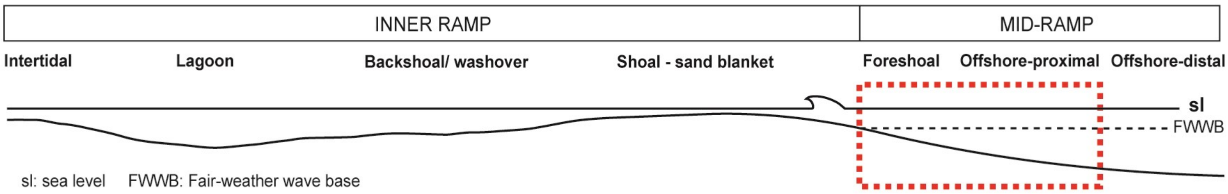

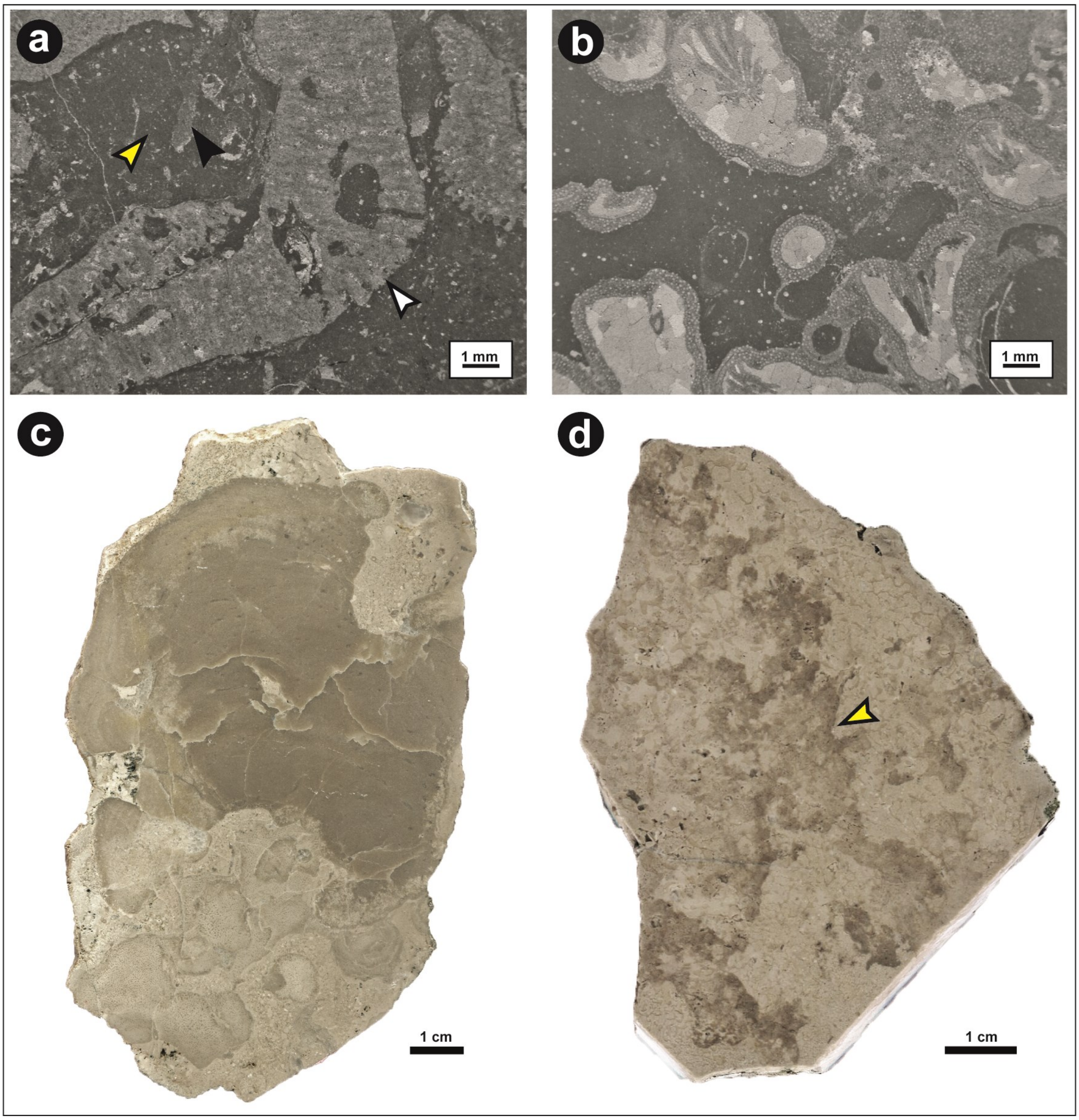

Microphotographs (a, b) and macro-scale examples (c, d) of foreshoal to offshore-proximal chaetetid-stromatoporoid-coral buildup facies, showing cm-sized fragments of chaetetids as main metazoan builder (white arrow in a), in some cases also dominating corals (b); and microbial crusts with internal cavities (yellow and black arrows in a, respectively). c, d) Macro-scale view of large-sized chaetetid fragments (c) and the microbial crust (yellow arrow in d). Samples F5-32 (a), F5-29 (b) and P3-16 (c, d).

Stromatoporoid-chaetetid-coral and oncolitic W to G

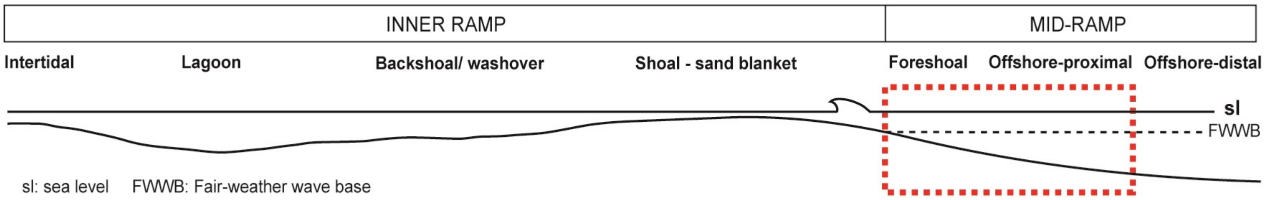

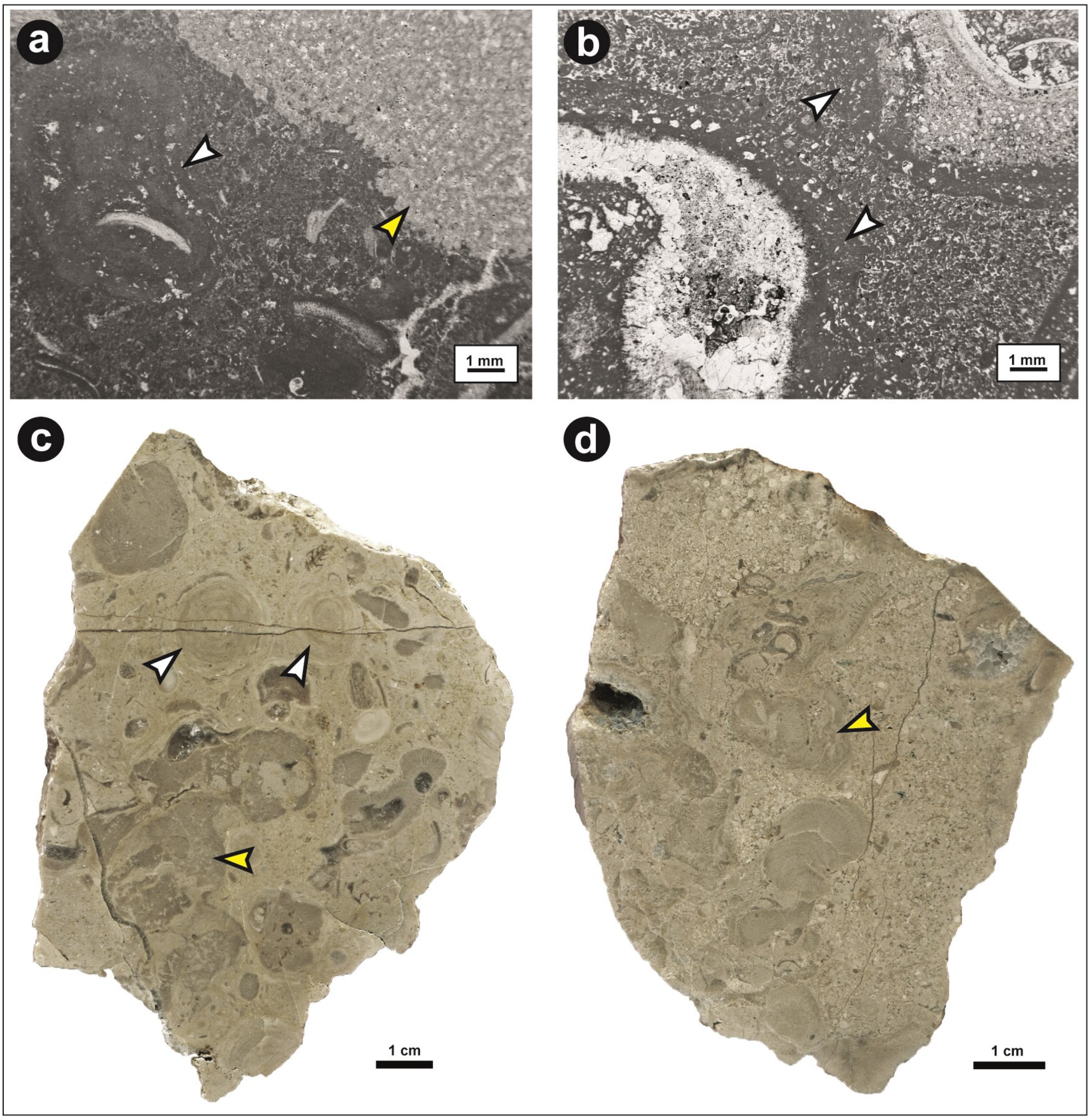

Microphotographs (a, b) and macro-scale examples (c, d) of foreshoal to offshore-proximal stromatoporoid-chaetetid-coral and oncolitic facies, showing cm-sized fragments of mainly stromatoporoids (yellow arrows in a and c) and chaetetids (yellow arrow in d), and variable proportions of mm- to cm-sized oncoids (white arrows in a-c). Stromatoporoids and chaetetids usually constitute the nuclei of these oncoids (b). Samples J2-27 (a), P2-6 (b), F4-56 (c) and P3-15 (d).

<u>ANNEXE 3</u>: PETROGRAPHIC AND CATHODO-LUMINESCENCE CHARACTERISTICS

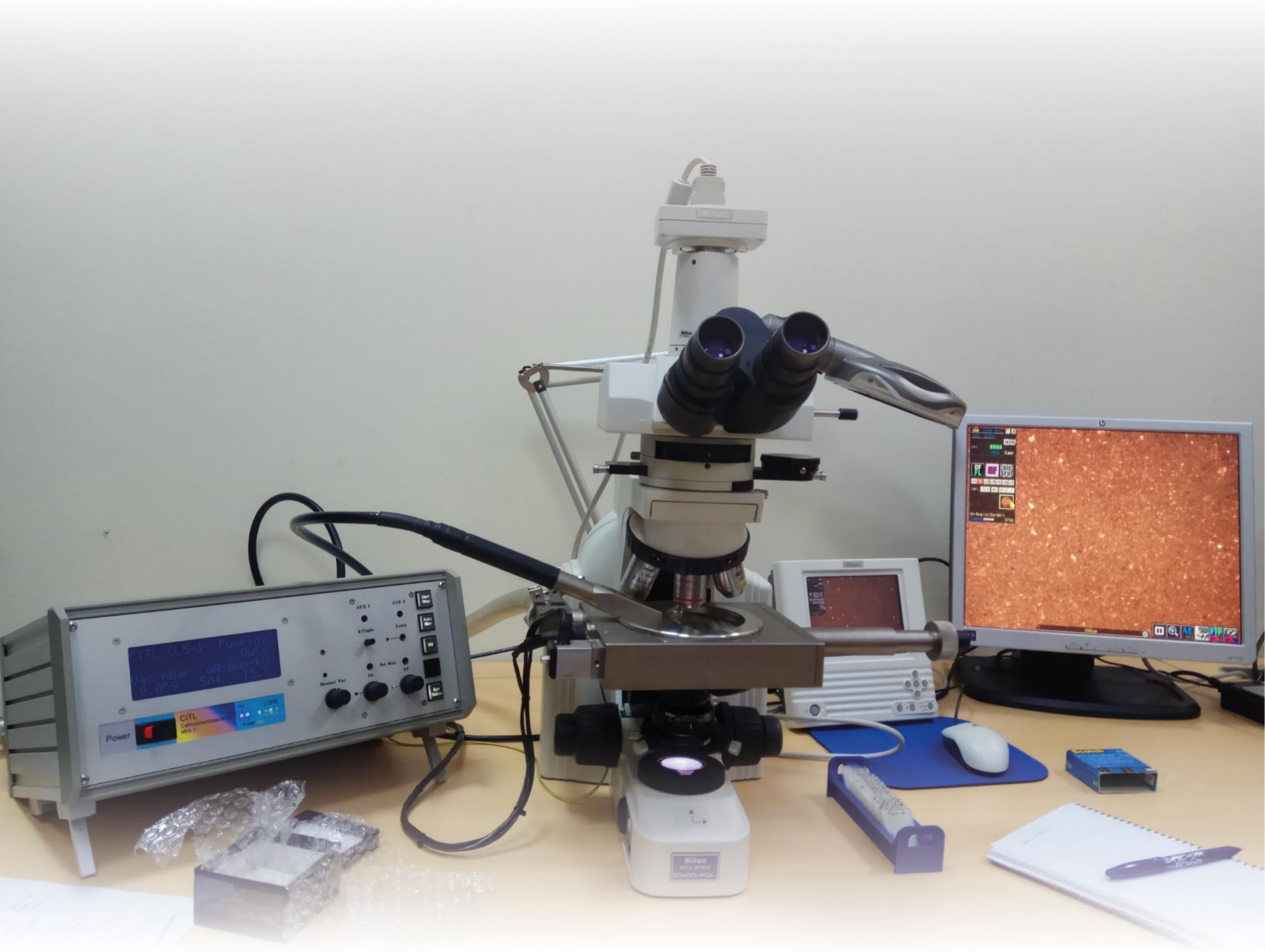

This section includes additional information concerning the petrographic and cathodoluminescence characteristics of the carbonate samples selected in Tosos and Fuendetodos sections for the carbon and oxygen stable isotope analyses. The references of the samples correspond to those of Chapter 7.

TOSOS SECTION

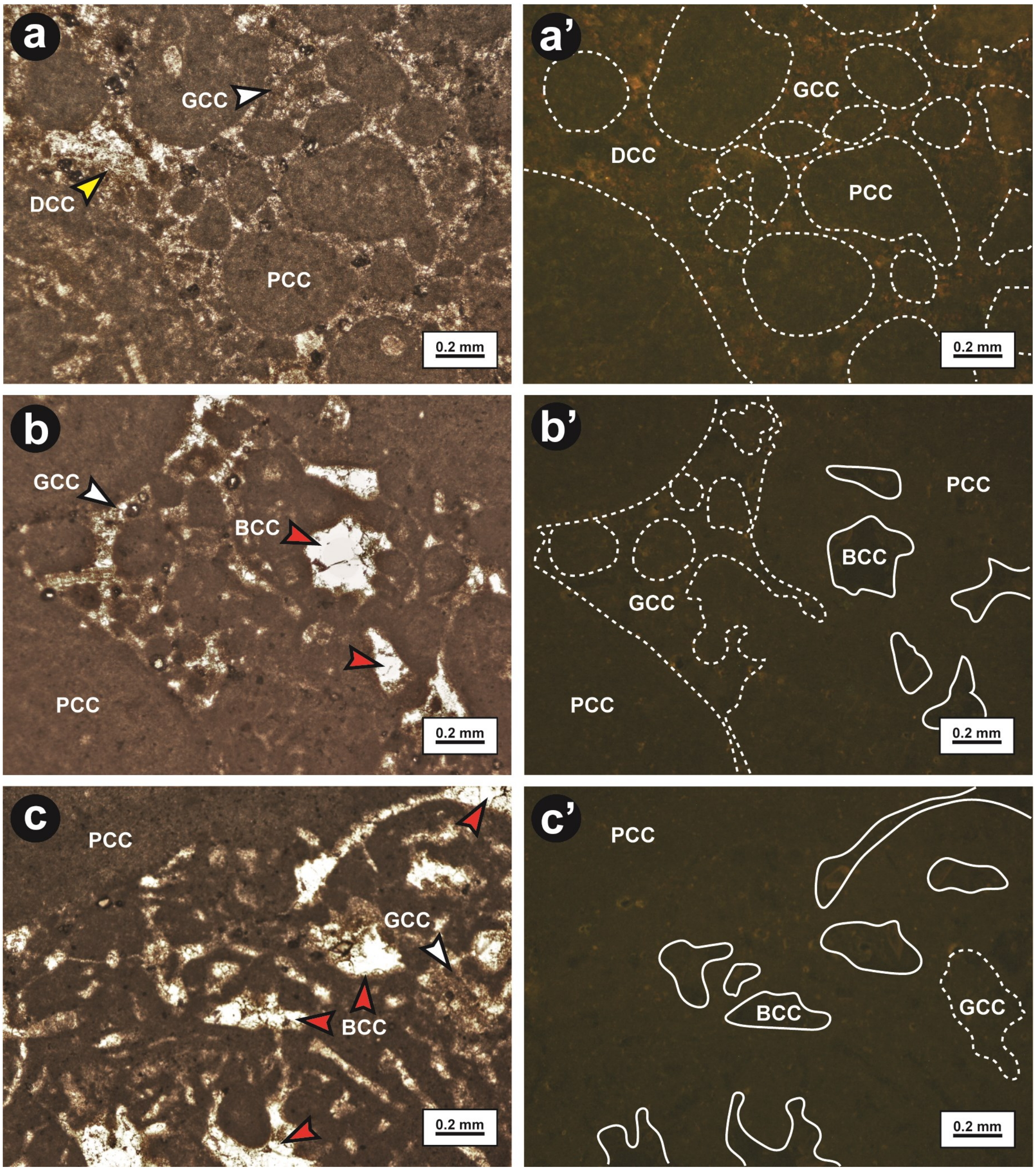

Plain-light (a-c) and cathodoluminescence (a'-c') microphotographs of primary carbonate components (PCC) and diagenetic calcite cements (GCC: granular calcite cement; DCC: drusy calcite cement; BCC: blocky calcite cement) from the samples 6 (a, b) and 8 (c) analysed in the Tosos section, corresponding to foreshoal type II and III oncoid packstone facies. The micrite matrix and carbonate grains (mainly peloids and ooids) show no luminescence (a'-c'; main PCC bordered with dashed lines in a' and b'), whereas the diagenetic calcite cements display from non- to dull (red) luminescence: GCC (white arrows in a-c) and DCC (yellow arrow in a), filling interparticle pores, show non- to dull (red) luminescence (a'-c'); and BCC (red arrows in b, c), filling mouldic vugs, shows no luminescence (solid lines in b' and c').

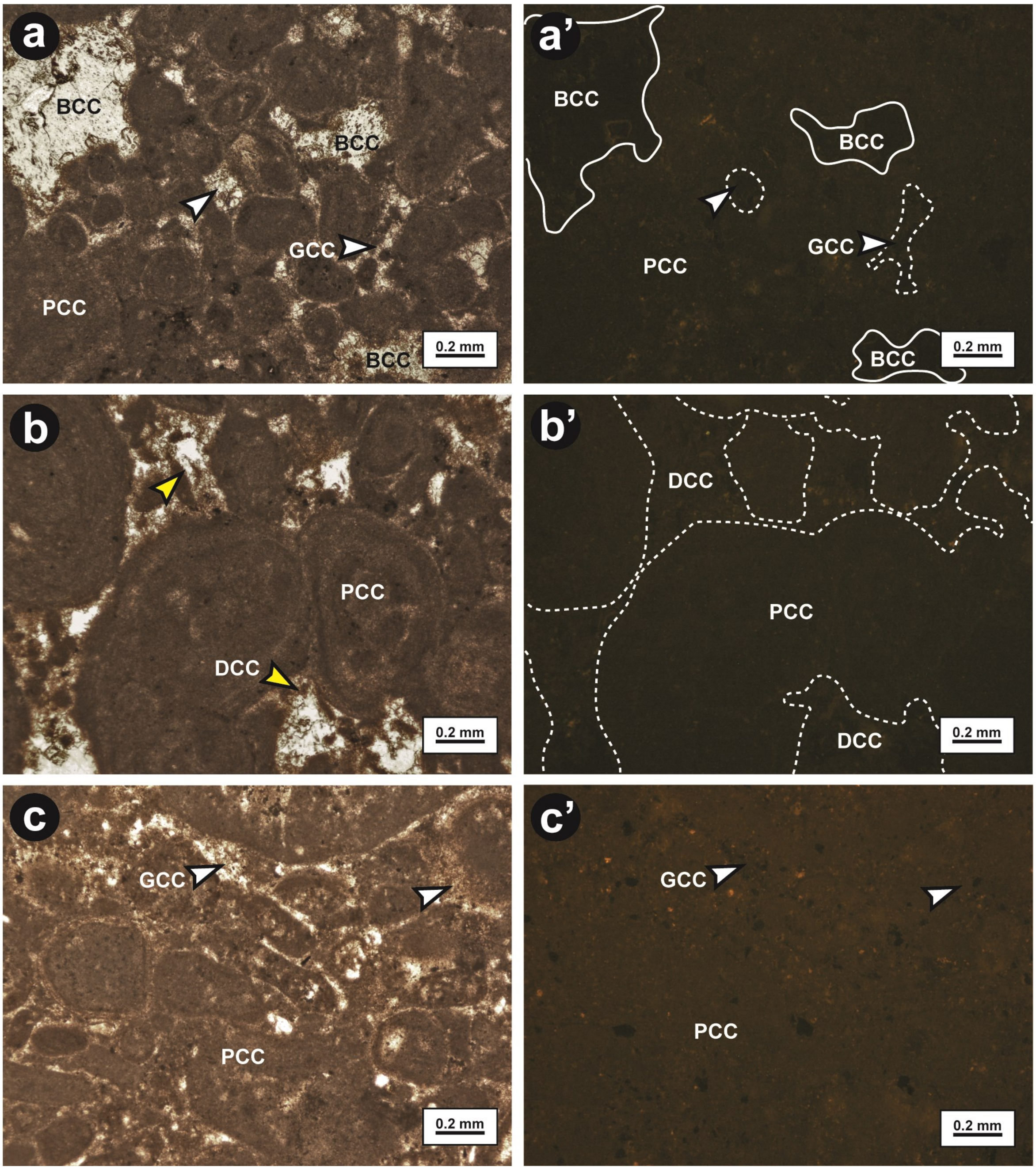

Plain-light (a-c) and cathodoluminescence (a'-c') microphotographs of primary carbonate components (PCC) and diagenetic calcite cements (GCC: granular calcite cement; DCC: drusy calcite cement; BCC: blocky calcite cement) from the samples 11 (a, b) and 27 (c) analysed in the Tosos section, corresponding to backshoal peloidal -type 1 and 1/3 ooid grainstone and packstone facies, respectively. The micrite matrix and carbonate grains (mainly peloids and ooids) show no luminescence (a'-c'; main PCC bordered with dashed lines in b'), whereas the diagenetic calcite cements display from non- to dull (red) luminescence: GCC (white arrows) and DCC (yellow arrows), filling interparticle pores, show non- to dull (red) luminescence (a'-c'); and BCC (a), also filling interparticle spaces, shows no luminescence (solid lines in a').

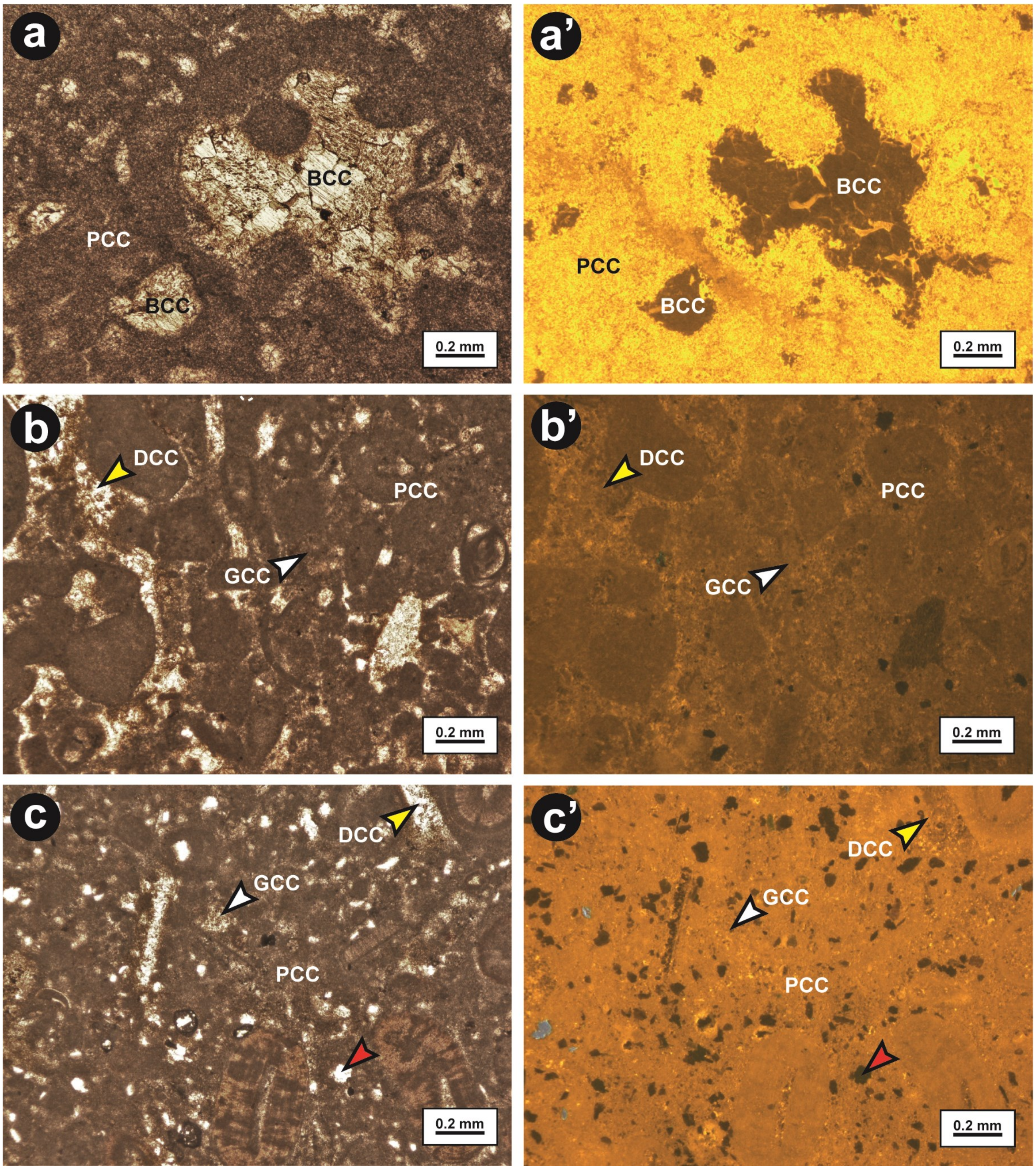

Plain-light (a-c) and cathodoluminescence (a'-c') microphotographs of primary carbonate components (PCC) and diagenetic calcite cements (GCC: granular calcite cement; DCC: drusy calcite cement; BCC: blocky calcite cement) from the three particular intervals in the Tosos section, where both primary carbonate components and diagenetic calcite cements show bright (yellow to orange) luminescence (a: sample 22, backshoal peloidal-type 1 and 1/3 ooid grainstone facies; b: sample 24, backshoal peloidal-type 1 and 1/3 ooid packstone facies; c: sample 29, restricted lagoon peloidal-bioclastic-type 3 and 4 ooid packstone facies). Concerning the diagenetic calcite cements, BCC shows no luminescence (a-a'), whereas GCC and DCC (white and yellow arrows, respectively) show orange luminescence (b-b', c-c'). Note the non-luminescent appearance for the quartz grains (red arrows in c-c').

FUENDETODOS SECTION

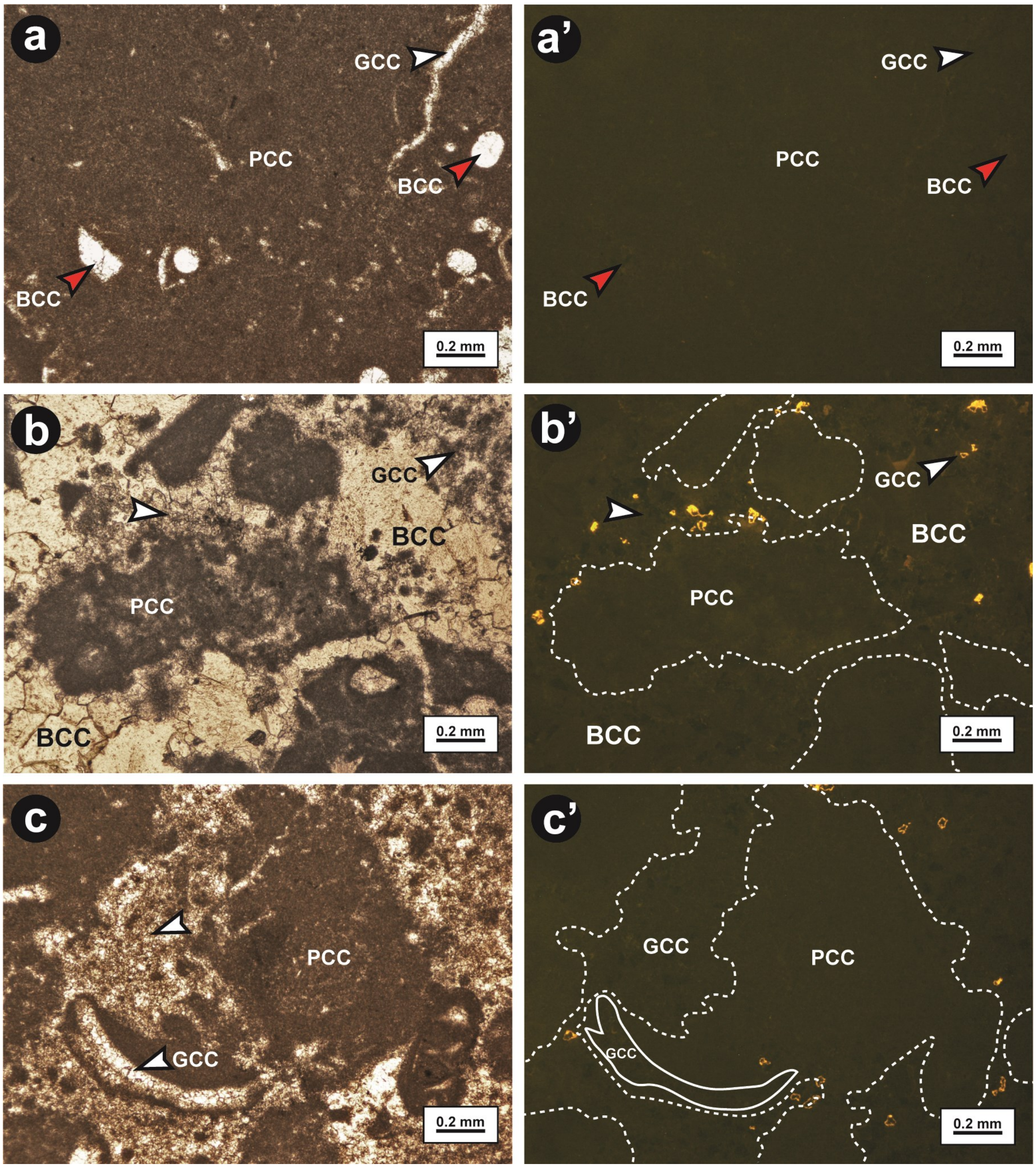

Plain-light (a-c) and cathodoluminescence (a'-c') microphotographs of primary carbonate components (PCC) and diagenetic calcite cements (GCC: granular calcite cement; BCC: blocky calcite cement) from the sample 2 analysed in the Fuendetodos section, corresponding to offshore-proximal peloidal-bioclastic packstone facies. The micrite matrix and carbonate grains (mainly peloids and ooids) show no luminescence (a'-c'; the main carbonate grains are bordered with dashed lines in b' and c'), whereas the diagenetic calcite cements display from non- to dull (red) and locally bright-yellow luminescence: GCC (white arrows), filling calcite veins (a), mouldic vugs (c) or replacing part of the sample (b, c), shows non- to locally yellow-bright luminescence (a'-c'); whereas BCC (b and red arrows in a), filling moudic vugs (a) or replacing part of the sample (b), shows non- to dull (red) luminescence (a' and b').

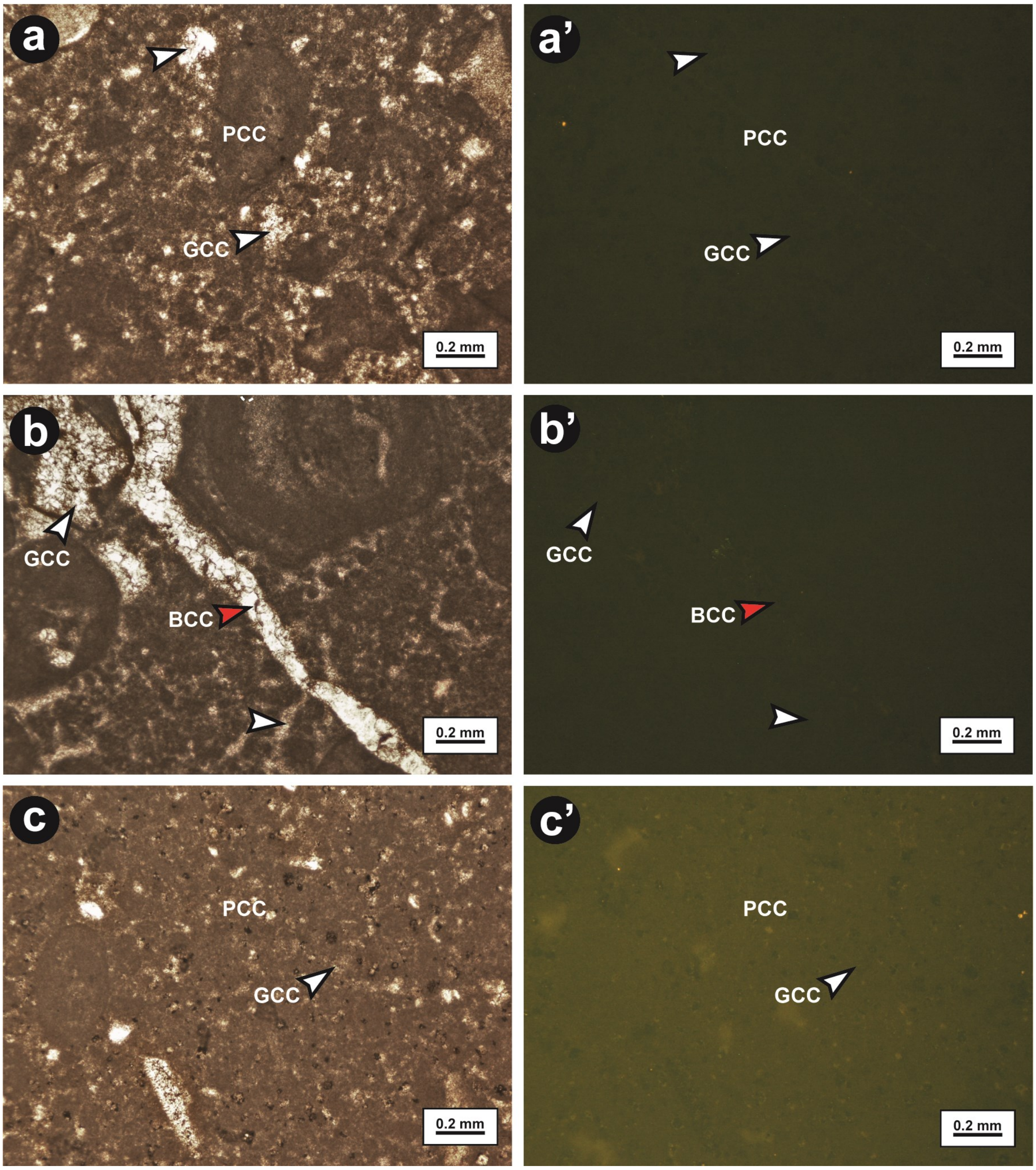

Plain-light (a-c) and cathodoluminescence (a'-c') microphotographs of primary carbonate components (PCC) and diagenetic calcite cements (GCC: granular calcite cement; BCC: blocky calcite cement) from the samples 4 (a, b) and 8 (c) analysed in the Fuendetodos section, corresponding to offshore-proximal chaetetid-stromatoporoid-coral buildup and inter-buildup stromatoporoid-chaetetid-coral and oncolitic packstone facies, respectively. In this case, both primary carbonate components and diagenetic calcite cements (GCC mainly filling interparticle pores (a-c), also mouldic vugs (b), white arrows; and BCC filling calcite veins (red arrow in b)) show no luminescence (a' and b'), locally slightly orange luminescence (PCC and GCC in c').

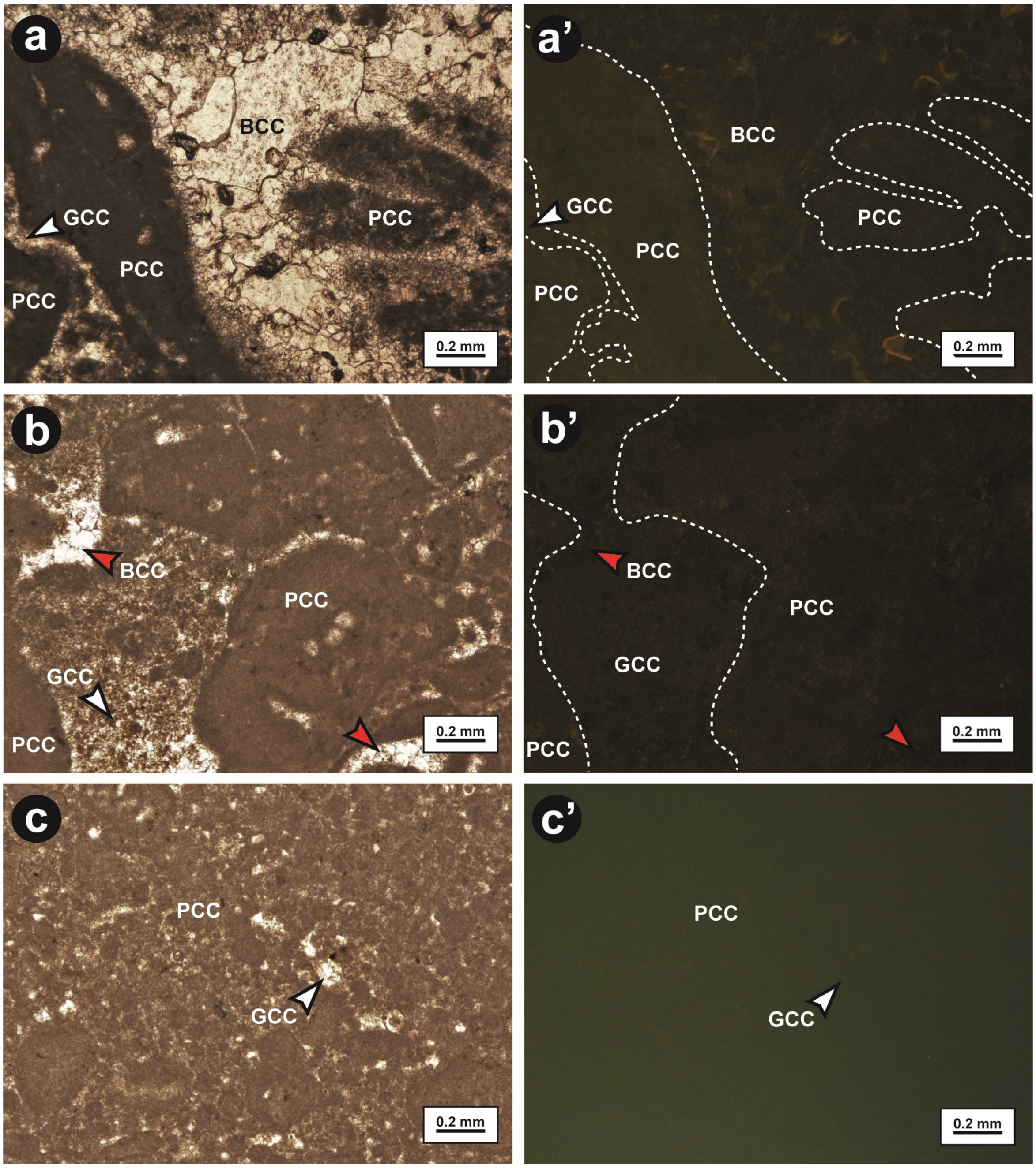

Plain-light (a-c) and cathodoluminescence (a'-c') microphotographs of primary carbonate components (PCC) and diagenetic calcite cements (GCC: granular calcite cement; BCC: blocky calcite cement) from the sample 13 (a, b) and 16 (c) analysed in the Fuendetodos section, corresponding to offshore-proximal peloidal-bioclastic packstone facies. The micrite matrix and carbonate grains (mainly peloids and ooids) show no luminescence (a'-c', main PCC bordered with dashed lines in a' and b'), whereas the diagenetic calcite cements display from non- to dull (red) luminescence: GCC (white arrows), filling interparticle pores, shows no luminescence (a'-c'); whereas BCC (a and red arrows in b), filling mouldic vugs (a, b) and interparticle pores (b), shows non- to dull (red) luminescence (a' and b').

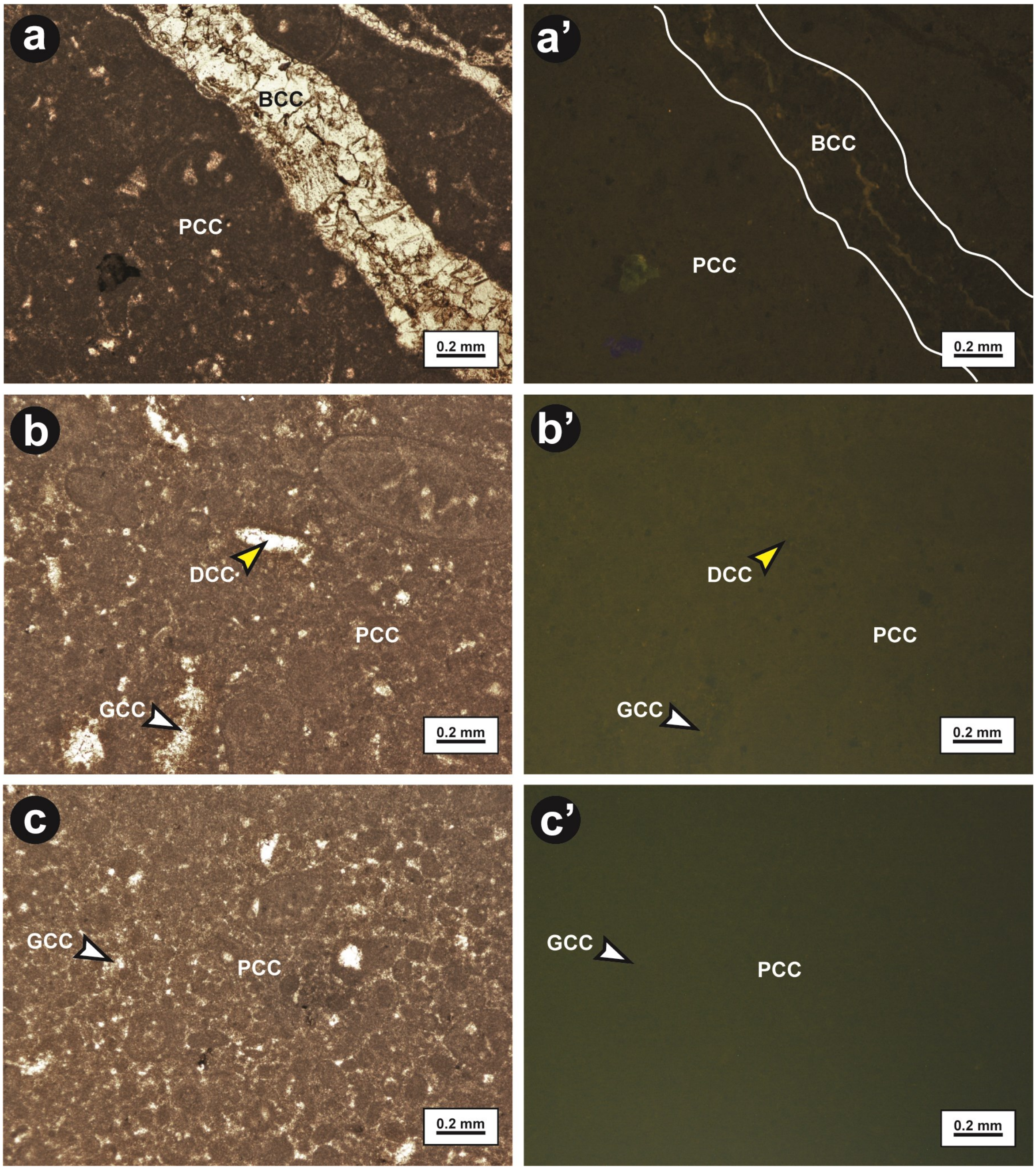

Plain-light (a-c) and cathodoluminescence (a'-c') microphotographs of primary carbonate components (PCC) and diagenetic calcite cements (GCC: granular calcite cement; DCC: drusy calcite cement; BCC: blocky calcite cement) from the sample 22 (a, b) and 25 (c) analysed in the Fuendetodos section, corresponding to offshore-proximal peloidal-bioclastic wackestone-packstone and stromatoporoid-chaetetid-coral and oncolitic packstone facies, respectively. The primary carbonate components (micrite matrix, peloids and ooids) and diagenetic calcite cements generally show no luminescence (a'-c'), the latter filling calcite veins (BCC in a-a'; slightly dull (red) luminescence appears towards the centre of the vein), mouldic vugs and interparticle pores (GCC and DCC, white and yellow arrows, respectively, in b-b' and c-c').

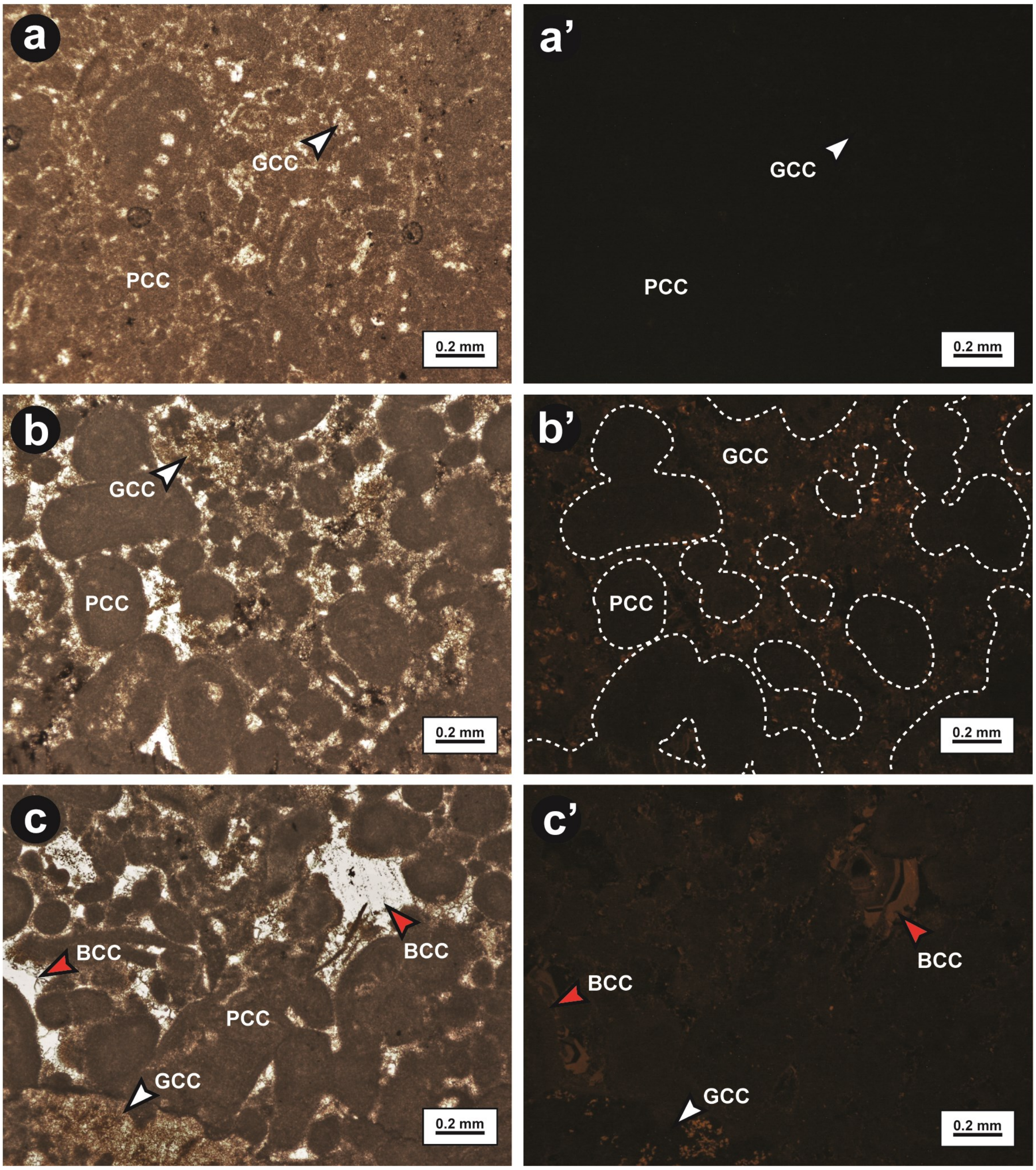

Plain-light (a-c) and cathodoluminescence (a'-c') microphotographs of primary carbonate components (PCC) and diagenetic calcite cements (GCC: granular calcite cement; BCC: blocky calcite cement) from the samples 32 (a) and 33 (b, c) analysed in the Fuendetodos section, corresponding to foreshoal peloidal packstone and grainstone facies, respectively. The primary carbonate components (micrite matrix, peloids and ooids) show no luminescence (a'-c'; main PCC bordered with dashed lines in b'), whereas the diagenetic calcite cements display from non- to dull (red) or zoned luminescence: GCC (white arrows), filling interparticle pores (a, b) or replacing bioclasts, (c) shows non- (a') to dull (red) luminescence (b' and c'); BCC (red arrows) shows zoned luminescence (c': dark nuclei evolving to dull (red) rims).

ANNEXE 4: STABLE ISOTOPE ANALYSES

This section includes tables gathering the chemostratigraphic data which have been obtained by the stable isotope analyses performed in this work, and whose interpretations support the research exposed by this Thesis.

STRONTIUM STABLE ISOTOPES

Sample	Section	Sequence	Type of sample	$^{87}Sr/^{86}Sr$
H1	TO	1	Brachiopod	0.706974
H2	F4	2	*Trichites*	0.706962
H3	P4	4	Brachiopod	0.706981
H4	TO	7	Oyster	0.707083
H5	MU	1	Brachiopod	0.707036
H6	ME3	1	Brachiopod	0.706995
H7	J3	2	Brachiopod	0.706907
H8	J3	2	Brachiopod	0.706922
H9	F3	4	Brachiopod	0.706915
H10	ME3	7	Oyster	0.706951
H11	ME3	7	Oyster	0.706929
H12	TO	7	Oyster	0.707005

Average given by the standard: 0.710 +/-0.000014 (2σ, n=9)

Analytical error: 0.01%, referred to 2σ

Location and results of strontium stable isotopes analysed on 12 samples from brachiopods, oysters and Trichites shells. The samples H1 to H4 (rowed in grey colour) correspond to those used for the age calibration of the Higueruelas Fm in the study area. The rest of the samples were not considered as they show significant deviations due to diagenesis.

CARBON AND OXYGEN STABLE ISOTOPES

Sample	δ18O	δ13C	Sample	δ18O	δ13C	Sample	δ18O	δ13C		δ18O	δ13C
Tosos section											
TO-1-A	-4.1	2.3	TO-13-A	-4.9	1.0	TO-24-B	-3.7	1.6			
TO-1-B	-4.1	2.2	TO-13-B	-5.3	0.8	TO-25-A	-3.9	1.4			
TO-2-A	-4.2	2.1	TO-14-A	-4.9	0.7	TO-25-B	-3.9	1.4			
TO-2-B	-4.1	2.1	TO-14-B	-4.9	0.8	TO-26-A	-3.3	1.5			
TO-3-A	-4.1	1.9	TO-15-A	-5.5	-0.9	TO-26-B	-3.2	1.2			
TO-3-B	-5.6	1.5	TO-15-A-r	-5.4	-0.9	TO-27-A	-4.5	0.4			
TO-4-A	-5.4	1.1	TO-15-B	-5.9	-1.4	TO-27-B	-4.4	0.4			
TO-4-B	-5.4	1.3	TO-16-A	-5.1	0.4	TO-28-A	-3.3	1.5			
TO-4-B-r	-5.3	1.3	TO-16-B	-5.2	0.2	TO-28-B	-3.1	1.4			
TO-5-A	-5.1	1.1	TO-17-A	-5.6	-0.3	TO-28-B-r	-3.1	1.4	Minimum	-7.1	-3.5
TO-5-B	-5.1	1.0	TO-17-B	-5.8	-0.6	TO-29-A	-4.6	0.5	Maximum	-2.4	2.3
TO-6-A	-4.5	1.3	TO-18-A	-5.4	-0.0	TO-29-B	-4.5	0.6	Mean	-4.4	0.8
TO-6-B	-4.8	0.9	TO-18-B	-5.4	-0.0	TO-30-A	-2.8	1.2			
TO-7-A	-4.6	1.3	TO-19-A	-4.0	0.8	TO-30-B	-3.0	1.1			
TO-7-B	-4.7	1.3	TO-19-B	-4.1	0.7	TO-31-A	-2.4	1.5			
TO-8-A	-4.5	1.5	TO-20-A	-3.5	1.6	TO-31-B	-2.4	1.3			
TO-8-B	-4.4	1.3	TO-20-A-r	-3.6	1.6	TO-32-A	-2.9	1.3			
TO-9-A	-4.7	1.6	TO-20-B	-3.9	1.5	TO-32-B	-2.8	1.2			
TO-9-B	-4.5	1.7	TO-21-A	-3.6	1.9	TO-33-A	-2.7	0.7			
TO-10-A	-5.1	1.1	TO-21-B	-4.1	1.7	TO-33-B	-2.9	0.8			
TO-10-B	-5.4	1.0	TO-22-A	-7.0	-3.1	TO-34-A	-2.7	0.3			
TO-11-A	-4.9	1.1	TO-22-B	-7.1	-3.5	TO-34-A-r	-2.7	0.3			
TO-11-B	-5.0	0.8	TO-23-A	-4.6	1.7	TO-34-B	-3.2	0.2			
TO-12-A	-5.5	0.8	TO-23-B	-4.6	1.7	TO-35-A	-3.9	-0.1			
TO-12-B	-5.3	0.6	TO-23-B-r	-4.5	1.7	TO-35-B	-3.9	0.2			
TO-12-B-r	-5.3	0.6	TO-24-A	-3.4	1.6						
Fuendetodos section											
FU-1-A	-6.5	-5.6	FU-12-B	-4.7	-1.4	FU-24-B	-4.9	-0.3			
FU-1-B	-6.1	-5.1	FU-13-A	-4.8	-1.7	FU-25-A	-5.2	-1.3			
FU-1-B-r	-6.1	-4.9	FU-13-B	-4.5	-1.1	FU-25-B	-5.3	-1.4			
FU-2-A	-4.6	-2.0	FU-14-A	-6.2	-1.7	FU-26-A	-4.7	0.0			
FU-2-A-r	-4.7	-2.1	FU-14-B	-6.1	-1.5	FU-26-B	-4.9	-0.2	Minimum	-6.6	-5.6
FU-2-B	-5.8	-2.1	FU-15-A	-5.4	-0.6	FU-27-A	-5.2	-0.8	Maximum	-3.5	1
FU-3-A	-4.9	-0.8	FU-15-A-r	-5.6	-0.7	FU-27-B	-5.1	-0.6	Mean	-5.3	-1.4
FU-3-B	-5.4	-1.4	FU-15-B	-5.6	-0.8	FU-28-A	-4.7	-0.1			
FU-4-A	-5.5	-2.3	FU-15-B-r	-5.5	-0.8	FU-28-B	-4.9	0.1			
FU-4-B	-4.9	-0.9	FU-16-A	-5.9	-1.5	FU-29-A	-4.6	0.3			
FU-5-A	-4.8	-0.4	FU-16-B	-6.0	-1.5	FU-29-B	-4.6	0.4	***Trichites***		
FU-5-B	-5.1	-0.5	FU-17-A	-6.3	-2.3	FU-30-A	-5.5	-1.1	TR-1-A	-2.4	2.4
FU-6-A	-4.6	-1.1	FU-17-B	-6.6	-2.5	FU-30-B	-4.8	-0.7	TR-1-A-r	-2.6	2.4
FU-6-B	-3.7	-0.2	FU-18-A	-5.7	-2.0	FU-31-A	-5.3	-2.5	TR-1-B	-2.3	2.5
FU-7-A	-4.5	-0.9	FU-18-B	-5.7	-2.0	FU-31-B	-5.2	-2.4	TR-1-B-r	-2.2	2.4
FU-7-A-r	-4.4	-0.9	FU-19-A	-5.9	-1.9	FU-32-A	-4.0	0.0	TR-2-A	-3.4	1.4
FU-7-B	-4.4	-1.1	FU-19-B	-5.8	-2.1	FU-32-B	-3.9	0.0	TR-2-B	-3.6	1.3
FU-8-A	-5.4	-1.5	FU-20-A	-5.4	-2.1	FU-33-A	-3.5	0.9	TR-3-A	-4.8	2.2
FU-8-B	-5.4	-1.4	FU-20-B	-5.3	-1.6	FU-33-B	-3.6	0.9	TR-3-B	-4.7	2.3
FU-8-B-r	-5.5	-1.5	FU-21-A	-5.1	-1.4	FU-34-A	-6.1	-2.1	TR-3-B-r	-4.6	2.4
FU-9-A	-5.5	-1.1	FU-21-B	-4.8	-0.7	FU-34-B	-6.1	-1.8			
FU-9-B	-5.2	-0.2	FU-22-A	-5.8	-1.0	FU-35-A	-6.6	-3.8			
FU-10-A	-6.0	-2.4	FU-22-A-r	-5.8	-1.0	FU-35-B	-6.5	-3.5			
FU-10-B	-6.2	-2.7	FU-22-B	-5.5	-1.0	FU-36-A	-6.3	-2.9			
FU-11-A	-5.6	-1.3	FU-22-B-r	-5.7	-1.0	FU-36-B	-6.2	-2.9			
FU-11-B	-4.7	-0.9	FU-23-A	-5.8	-1.2	FU-37-A	-6.2	-3.1			
FU-11-B-r	-4.6	-0.8	FU-23-B	-5.9	-1.2	FU-37-B	-5.5	-2.9			
FU-12-A	-4.9	-1.5	FU-24-A	-4.9	0.1						

Carbon and oxygen stable isotope values (‰ V-PDB) from Tosos and Fuendetodos sections. Samples TO and FU refer to bulk-carbonate samples in Tosos and Fuendetodos sections, respectively, whereas samples TR refer to the calcitic bivalve shells of the three specimens of Trichites collected in the lower part of the Fuendetodos section. A, B: double measure per sample; A-r, B-r: repeated measures every 10 analyses (the position of these repeated analyses does not appear consecutively in the table, as the isotopic measurements were not taken following the order of sample number).

Instituto Universitario de Investigación
en Ciencias Ambientales
de Aragón
Universidad Zaragoza

Facultad de Ciencias
Universidad Zaragoza